
21 January 2005
Science
Vol. 307 No. 5708
Pages 301–464 $10
TYPE 2
DIABETES
125
YEARS OF GLOBAL
Science
AAAS

BE FIRST TO DISCOVER

Explore Phosphorylation with BioSource

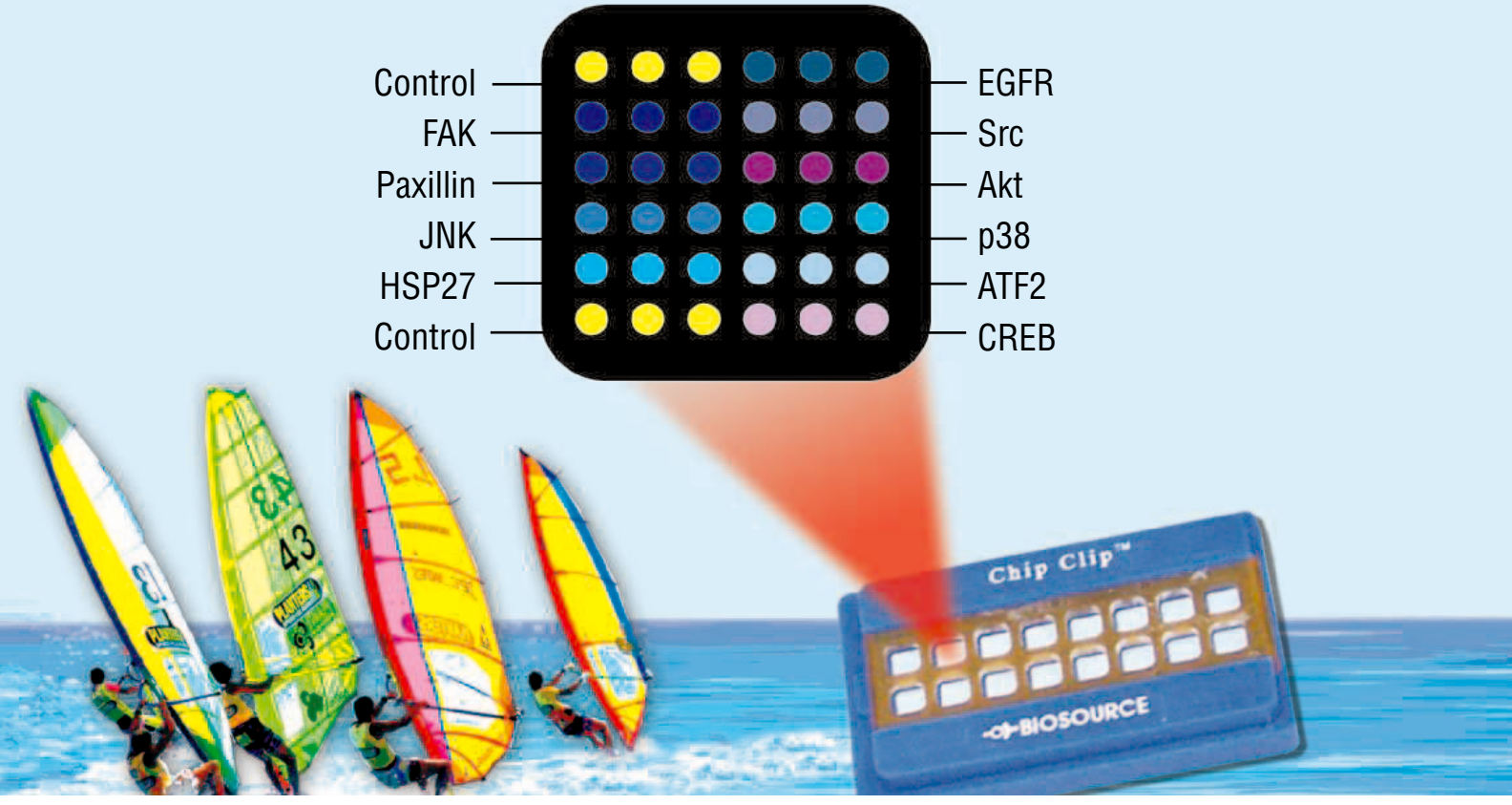

Explore Kinase pathways with easy-to-use Mercator™ PhosphoArray

Mercator™ PhosphoArray

Using a patented technology to achieve increased binding capacity, this glass-slide array is a great complement to Western blotting. After sample addition, the phosphorylation status of key regulatory sites is measured using a panel of phosphorylation site-specific antibodies. The use of in-house manufactured antibodies, and recombinant protein standards allows accurate, reproducible and quantitative measurements.

Glass Slide Array Reader unavailable?
BioSource provides scanning services.

For research use only.

Features and Advantages

- Simultaneously measure phosphorylation of 10 intracellular proteins
- Rapid results in 5 hours
- Available in 1- and 4-slide kits (up to 16 samples per slide)
- Quantitative multiplexed standards available separately
- Compatible with most glass slide array readers
- High precision (CV <8%)
- High specificity

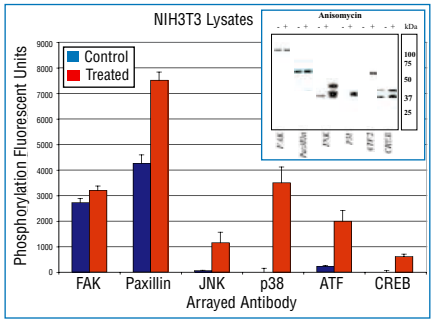

BioSource USA
800.242.0607

BioSource Europe
+32.67.88.99.99

For a complete list of products visit us at
www.biosource.com

BIOSOURCE
Explore Cytokines & Cellular Signaling

SCI0105

Welcome to your own personal world of QPCR.

Personally priced at $24,995*, Stratagene's Mx3000P™ Real-Time PCR System is designed just for you.

Don't give up system features and quantitative PCR (QPCR) performance because of your budget. Our Mx3000P™ Real-Time PCR System** is designed for your research applications, your QPCR experience level, and your budget. Because we take a personal interest in the success of your research, we've designed the system for your personal requirements.

- Easy to use
- Obtain reliable data the first time
- 4-color multiplex, supports all fluorescent chemistries
- Comprehensive training, support, and service program

Need More Information? Give Us A Call:

Stratagene USA and Canada
Order: (800) 424-5444 x3
Technical Services: (800) 894-1304

Stratagene Europe
Order: 00800-7000-7000
Technical Services: 00800-7400-7400

Stratagene Japan K.K.
Order: 03-5159-2060
Technical Services: 03-5159-2070

www.stratagene.com

* Based on comparison of full-featured instruments, price in USD. Price available in US only. Call for pricing in other regions.

** Practice of the patented polymerase chain reaction (PCR) process requires a license. The Mx3000P™ real-time PCR system is an Authorized Thermal Cycler and may be used with PCR licenses available from Applied Biosystems. Its use with Authorized Reagents also provides a limited PCR license in accordance with the label rights accompanying such reagents.

STRATAGENE®

Amersham Biosciences

Part of GE Healthcare

GE03-04

madetoworktogether

Hybond™-N+, Hyperfilm™ MP, Rapid-hyb™ Buffer, Rediprime™ II and RedivueTip™ are just a few of the integrated products in our nucleic acid labeling and detection range. They are designed to work together, because the reliability of your research results ultimately depends on the quality of the research tools you use. Our wide range of innovative, quality kits and reagents is trusted by thousands of demanding scientists worldwide, and backed by outstanding technical support, so you are assured of accurate, reproducible results every time.

And it's now even easier to get what you need, when you need it. Simply go to our website. It's easy to use, and you have 24-hour access to technical support. Shop online today or give us a call to get the best results.

www.madetoworktogether.com

GE imagination at work

Special Issue

Science

Type 2 Diabetes

Polarized light micrograph of glucose, the body's major source of energy. In diabetes, glucose is not properly metabolized and accumulates to dangerously high levels in the blood. A special section in this issue examines the molecular pathogenesis of the most common form of diabetes (type 2), which is projected to soon reach epidemic proportions worldwide. [Image: Eye of Science/Photo Researchers Inc.]

Volume 307
21 January 2005
Number 5708

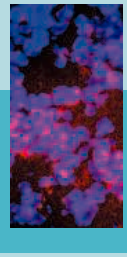

For related online content, see page 311 or go to www.sciencemag.org/sciext/diabetes

Departments

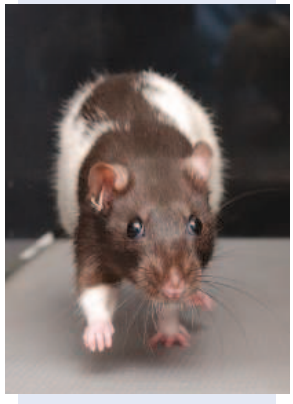

334 & 418

News of the Week

356

News Focus

Letters

Books *et al.*

Policy Forum

Contents continued

HUMAN FRONTIER SCIENCE PROGRAM (HFSP)

12 quai St. Jean, 67080 STRASBOURG Cedex, FRANCE

E-mail:grant@hfsp.org
Web site: http://www.hfsp.org

OPPORTUNITIES FOR INTERDISCIPLINARY RESEARCH

The Human Frontier Science Program (HFSP) supports **international** collaborations in basic research with emphasis placed on novel, **innovative** and **interdisciplinary** approaches to fundamental investigations in the life sciences. Applications are invited for grants to support projects on **complex mechanisms of living organisms**.

CALL FOR LETTERS OF INTENT FOR RESEARCH GRANTS: AWARD YEAR 2006

The HFSP research grant program aims to stimulate novel, daring ideas by supporting collaborative research involving biologists together with scientists from other disciplines such as chemistry, physics, mathematics, computer science and engineering. Recent developments in the biological and physical sciences and new disciplines such as bioinformatics and nanoscience open up new approaches to understanding the complex mechanisms underlying biological functions in living organisms. Preliminary results are not required in research grant applications. Applicants are expected to develop new lines of research through the collaboration; projects must be distinct from applicants' other research funded by other sources. HFSP supports only international, collaborative teams, with an emphasis on encouraging scientists early in their careers.

International teams of scientists interested in submitting applications for support must first submit a letter of intent online via the HFSP web site. The guidelines for potential applicants and further instructions are available on the HFSP web site (www.hfsp.org).

Research grants provide 3 years support for teams with 2 – 4 members, with not more than one member from any one country, unless more members are absolutely necessary for the interdisciplinary nature of the project, which is an essential selection criterion. Applicants may also establish a local interdisciplinary collaboration as a component of an international team (see below). The principal applicant must be located in one of the member countries* but co-investigators may be from any other country. Clear preference is given to **intercontinental** teams.

TWO TYPES OF GRANT ARE AVAILABLE:

Young Investigators' Grants are for teams of scientists who are all within 5 years of establishing an independent laboratory and within 10 years of obtaining their PhDs. Successful teams will receive up to $450,000 per year for the whole team. Scientists involved in a local interdisciplinary collaboration are considered as 1.5 team members for budgetary purposes.
Program Grants are for independent scientists at all stages of their careers, although the participation of younger scientists is especially encouraged. Program grants provide up to $450,000 per year for the whole team. Scientists involved in a local interdisciplinary collaboration are considered as a single team member for budgetary purposes.

Important Deadlines:
Compulsory pre-registration for password: 21 MARCH 2005
Submission of Letters of Intent: 31 MARCH 2005

**Members are Australia, Canada, the European Union (including the 10 new member countries), France, Germany, Italy, Japan, the Republic of Korea, Switzerland, the United Kingdom and the United States.*

New full member countries for award year 2006 are **Australia** and the **Republic of Korea**

Perspectives

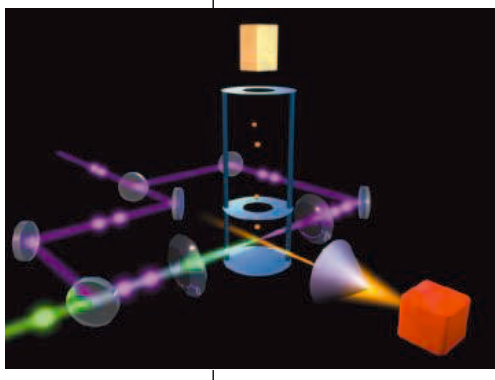

364 & 400

Science Express www.sciencexpress.org

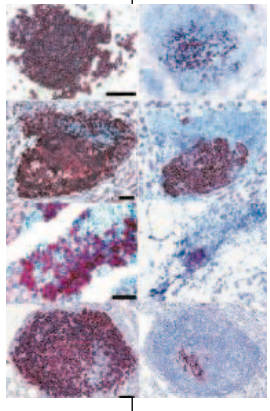

Brevia

Research Article

Reports

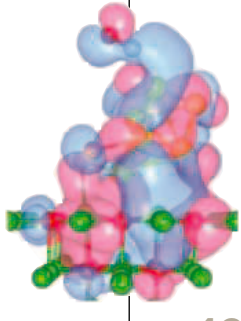

403

Contents continued

Now! Real-time PCR results in under 40 minutes!

Real Affordable
Applied Biosystems
7300 Real-Time PCR System

Real Versatile
Applied Biosystems
7500 Real-Time PCR System

Real Fast
Applied Biosystems
7500 Fast Real-Time PCR System

Looking for faster real-time PCR results? Our new Applied Biosystems 7500 Fast Real-Time PCR System, the choice for labs in a hurry, is the latest addition to the innovative family of real-time PCR systems from Applied Biosystems. It enables 96-well format high-speed thermal cycling, easily integrating into your lab's workflow. Whichever system you choose, you'll get the gold standard combination of TaqMan® assays and the proven performance of the industry leader—plus unbeatable real-time chemistry choices, powerful software, and a comprehensive selection of reagents and consumables. For the real deal in real-time PCR, visit http://info.appliedbiosystems.com/realtimepcr

iScience. Applied Biosystems provides the innovative products, services, and knowledge resources that are enabling new, integrated approaches to scientific discovery.

Applied Biosystems

REPORTS CONTINUED

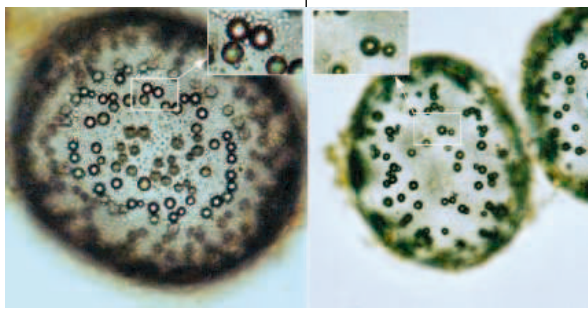

416

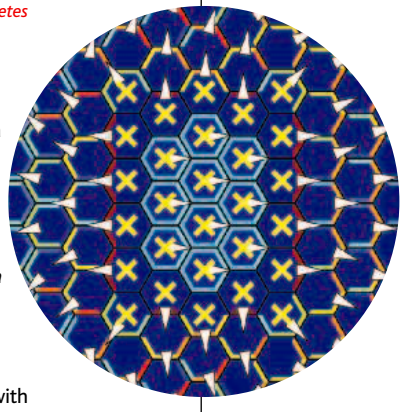

423

AAAS
ADVANCING SCIENCE, SERVING SOCIETY

SCIENCE (ISSN 0036-8075) is published weekly on Friday, except the last week in December, by the American Association for the Advancement of Science, 1200 New York Avenue, NW, Washington, DC 20005. Periodicals Mail postage (publication No. 484460) paid at Washington, DC, and additional mailing offices.

Domestic individual membership and subscription (51 issues): $135 ($74 allocated to subscription). Domestic institutional subscription (51 issues): $550; Foreign postage extra: Mexico, Caribbean (surface mail) $55; other countries (air assist delivery) $85. First class, airmail, student, and emeritus rates on request. Canadian rates with GST available upon request, GST #1254 88122. Publications Mail Agreement Number 1069624. **Printed in the U.S.A.**

Change of address: allow 4 weeks, giving old and new addresses and 8-digit account number. **Postmaster:** Send change of address to *Science*, P.O. Box 1811, Danbury, CT 06813–1811. **Single copy sales:** $10.00 per issue prepaid includes surface postage; bulk rates on request. **Authorization to photocopy** material for internal or personal use under circumstances not falling within the fair use provisions of the Copyright Act is granted by AAAS to libraries and other users registered with the Copyright Clearance Center (CCC) Transactional Reporting Service, provided that $15.00 per article is paid directly to CCC, 222 Rosewood Drive, Danvers, MA 01923. The identification code for *Science* is 0036-8075/83 $15.00. *Science* is indexed in the *Reader's Guide to Periodical Literature* and in several specialized indexes.

Contents continued ▶

Knockout Performance

Powerful siRNA delivery starts with siLentFect™ lipid reagent for RNAi, the most efficient, flexible transfection reagent available.

1 delivery → 2 RNA isolation → 3 reverse transcription → 4 knockdown analysis

- Low cytotoxicity reduces bias
- Excellent gene-specific knockdown obtained using as little as 5 nM siRNA
- Achieve >90% knockdown of both high- and low-abundance gene targets
- Simultaneously deliver siRNA and DNA for cotransfection applications

RNAi: A Bio-Rad pathway from delivery to detection. For more information, visit us on the Web at **www.bio-rad.com/ad/siLentFect/**

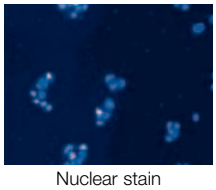

Nuclear stain

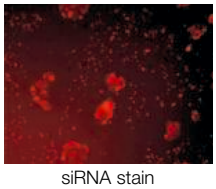

siRNA stain

Delivery of siRNA in MCF-7 cells. Cells were transfected with 10 nM siGLO siRNA using 0.5 µl siLentFect. After 24 hr, cells were imaged to show nuclear staining by Hoechst 33342 dye (top) or the location of fluorescent siRNA (bottom).

sciencenow www.sciencenow.org Daily News Coverage

What, Me Worry?
Carefree people may compromise their health by delaying medical treatment.

Pulsars Aplenty
Astronomers find the densest concentration of rapidly whirling neutron stars.

Galaxies Surf on Cosmic Waves
Astronomers verify that ripples from the big bang control the distribution of galaxies.

Preparing for International Polar Year.

science's next wave www.nextwave.org Career Resources for Young Scientists

Canada: Science on Ice—Canada Readies for International Polar Year *A. Fazekas*
Canada calls for preproposals for research projects aimed at understanding the world's polar regions.

Germany: Uncovering the Situation of Ph.D. Students in Germany *A. Forde*
The first thorough survey of the plight of German Ph.D. students is published.

Europe: European Science Bytes *Next Wave Staff*
Read about the latest funding, training, and job market news from Europe.

MiSciNet: NOAA Program Impacts Minority Serving Institutions *C. Parks*
An educational partnership program is designed to recruit more minorities with quantitative backgrounds.

MiSciNet: Investing in the Future of Science *E. Francisco*
A program sponsored by Oak Ridge National Lab offers math and science research opportunities for minority students.

US: Careers in Science Web Log *J. Austin*
Breaking news and observations related to science careers are updated throughout the week.

science's sage ke www.sageke.org Science of Aging Knowledge Environment

▶ **Perspective: Diabetes and Stem Cell Researchers Turn to the Lowly Spleen** *S. Kodama, M. Davis, D. L. Faustman*
Splenic stem cells might offer hope for the treatment of aging-related disease. *related Type 2 Diabetes section page 369*

News Focus: Pay at the Pump *R. J. Davenport*
Scans of failing hearts in patients reveal an energy crisis.

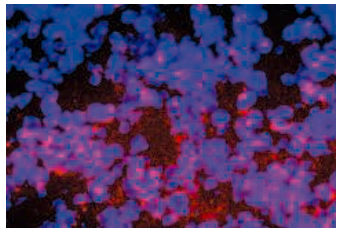

The spleen—a fountain of youth?

Targets of insulin action.

science's stke www.stke.org Signal Transduction Knowledge Environment

Related Type 2 Diabetes section page 369

▶ **Editorial Guide: Diabetes—Fighting Fat on Multiple Fronts** *E. M. Adler*
Mechanisms of insulin resistance and pathways for stimulation of β-cell growth are highlighted.

▶ **Perspective: Diabetes Outfoxed by GLP-1?** *G. G. Holz*
GLP-1 stimulates multiple pathways to stimulate pancreatic β-cell growth.

▶ **Perspective: Lipid Microdomains and Insulin Resistance—Is There a Connection?** *E. Ikonen and S. Vainio*
Alterations in plasma membrane lipid composition may alter insulin signaling.

▶ **Perspective: Ser/Thr Phosphorylation of IRS Proteins—A Molecular Basis for Insulin Resistance** *Y. Zick*
S6K1 participates in homeostatic negative feedback mechanisms that can also lead to insulin resistance.

Separate individual or institutional subscriptions to these products may be required for full-text access.

catch the wave

2005/06 NEB catalog & technical reference is now available.

catalog highlights:

- 15 new Restriction Enzymes (not to mention 225 old favorites)
- Antarctic Phosphatase – the only commercially available phosphatase that is 100% heat inactivated in 5 minutes at 65°C; it's a better enzyme than SAP
- ShortCut siRNA Mixes – highly potent siRNA mixes that can be used at low (1-20 nM) concentration
- TransPass Transfection Reagents for siRNA and DNA
- Peptide-Carrier Kit – ligate your peptide of interest to a carrier protein for detection on Western blots or peptide arrays
- Updated Reference Appendix
- Environmental Theme – the impact of non-governmental organizations (NGOs) on the well-being of our planet

www.neb.com

The new NEB website complements our catalog and features access to an extensive library of product technical literature as well as computer tools such as Enzyme Finder and NEBcutter. The improved interface provides greater functionality when ordering products online, including customer-specific pricing, order history and shipment tracking.


1975/76


1978


1979

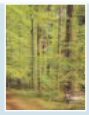
1980/81

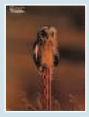
1981/82


1982/83


1983/84

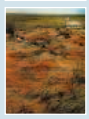
1985/86

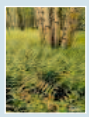
1986/87


1988/89


1990/91


1992

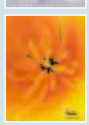
1993/94

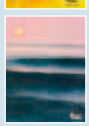
1995


1996/97


1998/99


2000/01


2002/03

www.neb.com

New England Biolabs Inc.
32 Tozer Road • Beverly • MA 01915 USA • 1-800-NEB-LABS • Tel. (978) 927-5054 • Fax (978) 921-1350 • info@neb.com
Canada: Tel. (800) 387-1095 • info@ca.neb.com **Germany:** Tel. 0800/246 5227 • info@de.neb.com
UK: Tel. (0800) 318486 • info@uk.neb.com **China:** Tel. 010-82378266 • beijing@neb-china.com
For a complete list of international offices, please visit www.neb.com.

NEW ENGLAND BioLabs® Inc.
the leader in enzyme technology

edited by Stella Hurtley and Phil Szuromi

Semiconducting Aerogels

Aerogels are porous, very low density materials that have the appearance of frozen smoke. They are typically made from oxides and are thus insulators. **Mohanan *et al.*** (p. 397) have made analogous aerogels from metal chalcogenides (sulfides, selenides, and tellurides), which are materials commonly used for making semiconductor quantum dots. As a result, the aerogels retain semiconducting properties such as photoluminescence, and yet have a porous network structure with pores in the 2- to 50-nanometer-size range.

Brittle Boundaries

The addition of sulfur to many metals and alloys causes them to become brittle, but the reason for this weakening is not well understood. **Yamaguchi *et al.*** (p. 393, published online 6 January 2005) modeled the embrittlement of nickel by progressively adding sulfur atoms to a grain boundary. First-principles calculations reveal that the weakening of the boundary is caused by the aggregation of sulfur atoms at the boundary, which repel each other. The sulfur atoms are forced into non-ideal bonding because the nickel-sulfur bonds are stronger than the sulfur-sulfur bonds.

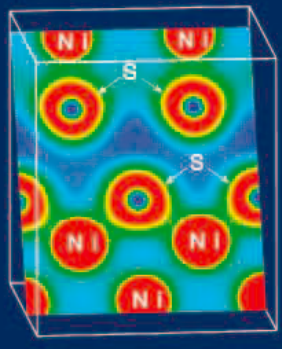

Combing the Ultraviolet

The use of ultrashort, broadband laser pulses, or optical combs, was recently extended from being a reference standard for continuous wave lasers to being a way to probe the energy levels of atoms. The advantage of using the combs is that they combine the high temporal resolution needed to study dynamics with precise frequency measurement. **Witte *et al.*** (p. 400; see the Perspective by **Udem**) have now extended this method to the short-wavelength, deep ultraviolet region of the spectrum by creating a train of the pulses with the fourth harmonic of an optical laser. The authors measured a high-energy transition frequency in Kr atoms with an order of magnitude reduction in uncertainty from prior studies.

Producing Orders Pockets of Spin

The sensitivity of magnetic resonance force microscopy (MRFM) is reaching the point where single spins can be detected. Making measurements on a small ensemble of localized spins created by microwave irradiation of silicon, **Budakian *et al.*** (p. 408) show that that MRFM cannot only detect spin fluctuations but can also be used to manipulate them. Pockets of ordered spin can be formed from a background bath of thermally fluctuating spins in the vicinity of the cantilever tip, and these pockets of ordered spin can be stored and read out. The technique itself should prove useful as a probe of the dynamics of nanoscale magnets, and the ability to create, store, and read out small pockets of ordered spin should prove useful in quantum computing.

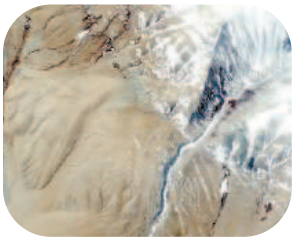

Slips in Slip Rates

The Karakorum fault is a major strike-slip fault trending northwest just north of the western Himalayan Mountain Range. The rate of slip on the fault is difficult to estimate, but these rates are needed to understand the tectonics of the region and the strength of the crust. **Chevalier *et al.*** (p. 411) estimated a rate of slip of about 11 milli-meters per year over about 20,000 to 140,000 years on one branch of the Karakorum based on offset moraines, which is consistent with the extrusion of western Tibet owing to the collision of India with Eurasia. This rate is higher than some geodetic estimates of recent slip over shorter time periods and suggests that slip rates on the fault have varied over time.

Sudden Changes in Lions' Ranges

Population dynamics of social species can be highly complex because of the interplay of group-level factors and population-level factors. **Packer *et al.*** (p. 390; see the Perspective by **Ranta and Kaitala**) present long-term data from the Serengeti plains of East Africa which show how herbivore populations (wildebeest, buffalo, zebra, and gazelle) influence lion populations directly and indirectly through the herbivores' impact on vegetation. The herbivore population changes are smooth and gradual, but the lion populations show sudden shifts between alternative equilibria. A model that constrained the upper and lower limits of pride size gave rise to the observed patterns of sudden shifts. Thus, population trends cannot necessarily be understood solely on the basis of individual survival and reproduction.

Separation and Speciation

Ring species, which are isolated species connected by intergraded populations, have long been thought to exemplify the occurrence of speciation in the presence of gene flow. However, some taxonomic and molecular evidence have cast doubt on this classic model. **Irwin *et al.*** (p. 414) conducted a genome-wide survey for the greenish warbler, whose territory encircles the Tibetan plateau. Two genetically distinct and reproductively isolated forms of the warble are indeed connected by a chain of populations through which genetic patterns change gradually.

Big Bacteria Promote Phosphorite Formation

Thiomargarita namibiensis is a colossus among bacteria (almost 1 millimeter in diameter) found off the Namibian coast. **Schulz and Schulz** (p. 416) show it accumulates intracellular polyphosphates under aerobic conditions and releases phosphate under anoxic conditions, thereby creating pore water supersaturated in phosphate that precipitates as phosphorite. Energy gained by breakdown of polyphosphate under anoxic conditions is used for intracellular accumulation of sulfide and acetate or other organic carbon. The sulfide is oxidized to elemental sulfur by using nitrate as an electron acceptor. The release of phosphate by these organ-

CONTINUED ON PAGE 315

CREDITS: (TOP TO BOTTOM) YAMAGUCHI *ET AL.*; CHEVALIER *ET AL.*

20th ANNUAL New England Biolabs

Molecular Biology Summer Workshops

We are pleased to announce the twentieth annual Molecular Biology Summer Workshops, sponsored by New England Biolabs in conjunction with Smith College. Workshops are held at the Clark Science Center, Smith College, Northampton, MA, USA. Over 2,500 people have graduated from this intensive training program in the past nineteen years.

Learn Molecular Biology in 2 Weeks!

This intensive, two-week course emphasizes hands-on molecular biology laboratory work and covers a wide variety of topics and techniques.

Topics/Techniques:

- **gene cloning (cDNA and genomic)**
- **gene expression analysis**
- **PCR and quantitative RT-PCR**
- **genomics and bioinformatics**
- **DNA sequencing and DNA fingerprinting**
- **and much more – visit our website for a complete list**

Application Information:

No previous experience in molecular biology is required or expected. Fifty participants per session will be selected from a variety of disciplines and academic backgrounds.

FEE: $3900 per participant includes lab manual, use of all equipment and supplies, and room and board (all rooms are singles).

APPLICATION DEADLINE: March 31, 2005.
Payment in full is due by April 29, 2005. Late applications will be accepted! Your application should include a recent resume and one paragraph explaining your reasons for taking the course. Please specify the session to which you are applying (1, 2, or 3) and indicate a second choice from one of the other sessions.

when:

Session 1: June 12 – June 25, 2005
Session 2: July 10 – July 23, 2005
Session 3: July 31 – August 13, 2005

where:

Clark Science Center
Smith College
Northampton, MA USA

to apply:

apply online at
http://www.science.smith.edu/neb
or
Mail a recent resume and one paragraph explaining your interest to:

Molecular Biology Summer Workshops
Dr. Steven A. Williams
Clark Science Center
Smith College
Northampton, MA 01063

apply online!

For additional information,
please call (413) 247-3004
or visit the Summer Workshop web site:
http://www.science.smith.edu/neb

NEW ENGLAND BioLabs® Inc.
the leader in enzyme technology

isms could be sufficient to explain the large accumulations of phosphorite observed in many parts of the world's oceans.

Exercise, Oxygen Metabolism, and Health

Human epidemiological studies have suggested that low aerobic capacity is a strong predictor of mortality. **Wisløff *et al.*** (p. 418; see the news story by **Marx**) compared two lines of rats produced by 11 generations of genetic selection for high or low scores in endurance running. Rats with low aerobic capacity had many of the risk factors that define metabolic syndrome, including high blood pressure, elevated levels of plasma triglycerides, and impaired glucose tolerance. Preliminary expression data were consistent with a decline in mitochondrial function in the unfit rats.

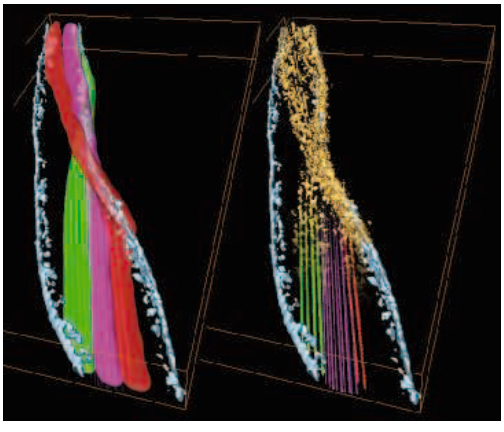

CREDIT: KÜRNER *ET AL.*

Motility in a Mollicute

Mollicutes (Mycoplasma, Acholeplasma, and Spiroplasma) are small prokaryotic cells that have distinct morphologies and that are motile despite their lack of cell walls or appendages such as flagella. Recent studies have identified a fibril protein that forms a cytoskeletal ribbon likely involved in promoting motility. **Kürner *et al.*** (p. 436) have used cryo-electron tomography to visualize the three-dimensional structure of the whole cell for the spiral-shaped mollicute Spiroplasma melliferum. The cytoskeletal structure consists of two outer ribbons, comprising five thick filaments each, joined by an inner ribbon comprising nine thin filaments. The thick filaments are polymers of fibril protein and the thin filaments are polymers of the actin-like protein MreB. Cell motility could be promoted by coordinated length changes of the cytoskeletal ribbons.

An Insulin Mimic Secreted by Visceral Fat

Excessive amounts of abdominal visceral fat, sometimes referred to as "bad fat," significantly increase an individual's risk of developing insulin resistance and other metabolic disorders. These adverse health effects may be mediated in part by fat-derived cytokines that circulate in the blood. **Fukuhara *et al.*** (p. 426, published online 16 December 2004; see the Perspective by **Hug and Lodish**) characterized "visfatin," a cytokine that is highly expressed in visceral fat and whose blood levels correlate with obesity. Surprisingly, functional analyses in mice revealed that visfatin has beneficial, insulin-like activity, causing a lowering of blood glucose levels. Even more surprisingly, visfatin was shown to bind to the insulin receptor and activate the insulin signal transduction pathway. While the precise physiological role of visfatin remains to be established, the discovery of this natural insulin mimetic could open exciting new avenues in diabetes research and therapy.

Transcription Factors and Helper T Cell Lineage Determination

In helper T (Th) cells, cell fate is primarily determined by the transcription factors GATA3, which directs Th2 type cells and T-bet, which regulates Th1 lineage choice. **Hwang *et al.*** (p. 430) found that during the early stages of a T helper precursor's decision to become a Th1 cell, T-bet has an unusual means of repressing the Th2-promoting effects of GATA3. After T cell stimulation and under the right polarizing conditions for Th1 cells, T-bet becomes phosphorylated by the tyrosine kinase, ITK, which allows it to bind GATA3. This process prevents it from interacting with its Th2 cytokine target genes. This study reveals a further means by which transcription factors may directly cross-regulate one another in specifying cell lineage fate.

Roche Applied Science

LightCycler Real-Time PCR System

Insist on More Accurate Quantification of Gene Expression

	Without efficiency correction	Efficiency correction with linear fit function	Efficiency correction with non-linear fit function
	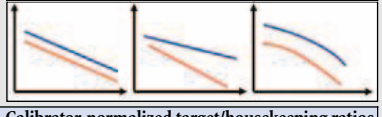		
	Calibrator-normalized target/housekeeping ratios		
40 ng	1.03	1.18	1.41
8 ng	2.21	1.79	1.01
1.6 ng	6.00	4.17	1.17
Mean	3.08	2.38	1.21
S.D.	2.60	1.58	0.22
C.V.	**84.3%**	**66.4%**	**18.0%**

Figure 1: Impact of different PCR efficiency adjustments on accuracy of relative quantification. Total RNA was used for quantitative RT-PCR on the LightCycler System. Sample data were evaluated with the LightCycler Relative Quantification Software, using the efficiency correction functions described above, to generate calibrator-normalized target/housekeeping ratios. The significantly lower Coefficient of Variation (C.V.) demonstrates the greater accuracy made possible by the LightCycler Software's use of efficiency corrections and a non-linear fit function.

Quantify more accurately with the LightCycler Instrument

- Cycle faster to minimize non-specific products that may overestimate copy numbers.
- Analyze all samples in the same thermal chamber to ensure temperature homogeneity and consistent PCR efficiencies.

Analyze data more accurately with LightCycler Relative Quantification Software

- Use calibrator normalization to ensure consistency between PCR runs.
- Within runs, rely on an efficiency-correction feature that accounts for differences in PCR efficiencies between target and reference genes.
- Obtain sample concentrations from non-linear standard curves to more precisely quantify low-copy genes, which often suffer from non-linear PCR efficiencies (Figure 1).

Shouldn't accurate quantification be the primary goal of gene expression studies? Contact your Roche Applied Science representative and visit ***www.lightcycler-online.com*** today!

Roche Diagnostics

Roche Diagnostics GmbH
Roche Applied Science
68298 Mannheim
Germany

Global Chronic Diseases

Chronic diseases, particularly cardiovascular disease (CVD), type 2 diabetes, cancer, and chronic respiratory disease, account for more than 50% of all deaths worldwide. Tobacco use, poor diet, and physical inactivity are among the major risk factors contributing to this disease burden. Yet even as the harmful impact of these diseases on health and economies strengthens and spreads globally, there is still only limited public health, financial, and political support for programs aimed at their prevention.

One reason for this neglect has been the belief by governments and philanthropists that chronic diseases are afflictions of affluent populations who have led a life of sloth. In reality, these diseases are now global problems that have been driven by profound changes in consumption patterns. Ubiquitous marketing of tobacco and unhealthy food introduces children to (and in the case of tobacco, addicts them to) lifestyles that greatly elevate their disease risk. Rapid changes in transport, work, and leisure activities have led to a global collapse in physical activity levels. Overall, unhealthy choices have become the easy choices.

Already, chronic diseases exert a significant negative impact on the health and economies of developing countries. A recent World Bank analysis of how best to improve health in Europe and Central Asia concluded that measures to control CVD would produce more gains in life expectancy than would measures to address the Millennium Development Goals* that focus on selected infectious diseases and maternal and child health. This finding probably applies to many of the 4 billion people living in low- and middle-income countries. About 3 million deaths from CVD occur annually in both India and China. One million tobacco-related deaths occur annually in China and 700,000 in India. With 1 in 5 children in the world now smoking and 1 in 10 classified as overweight or obese, future prospects regarding CVD and type 2 diabetes are grim. Because chronic diseases diminish worker productivity, investor returns in developing countries will be affected, which in turn will likely affect the growth of countries within the Organization for Economic Co-operation and Development. Recent reports by investment banks have raised concerns that transnational corporations and pension funds face future risks from the rise in obesity rates.†

Governments internationally need to act more decisively. The implementation of two major strategies adopted by all governments at World Health Assemblies could make a huge difference in global prevention of the major risk factors driving the chronic disease epidemics: the Framework Convention on Tobacco Control (FCTC), adopted in 2003; and the Global Strategy on Diet, Physical Activity and Health (Global Strategy), adopted in 2004. The FCTC will carry the force of international law when it takes affect on 28 February 2005. Already, it has stimulated increases in tobacco excise taxes, the implementation of marketing bans, and the introduction of smoke-free public places in many countries. These actions have been well documented as effective. In contrast, because there are no long-term best practices against obesity or physical inactivity, applied research is needed to assess the effectiveness of the core educational, legislative, intersectoral, and financial elements of the Global Strategy as it is implemented.

Efforts in chronic disease prevention can often take decades to yield benefits. Potentially, these benefits could be achieved more rapidly by investing in clinically based primary care treatments that focus on people at elevated risk for chronic disease, particularly CVD and diabetes. The recent report by the World Health Organization on Priority Medicines for Europe and the World emphasizes the need to expand access to currently available smoking cessation products, antihypertensives, statins, and aspirin, while investing in research to develop heat-stable insulin and a "polypill" to prevent complications and recurrences in patients with CVD.

At the core, chronic disease prevention and health promotion require a shift in thinking and actions by governments and diverse stakeholders. Each society must decide what it is willing to do and pay to help make healthy choices become the easy choices. The gains for global health and economy could be profound.

Derek Yach, Stephen R. Leeder, John Bell, Barry Kistnasamy

Derek Yach is at the Yale University School of Public Health, New Haven, CT, USA. Stephen R. Leeder is at the University of Sydney, Australia. John Bell is at Oxford University, UK. Barry Kistnasamy is at the Nelson Mandela Medical School, South Africa.

* World Bank, *Millennium Development Goals for Health in Europe and Central Asia. Relevance and Policy Implications* (World Bank, Washington, DC, 2004). † *Too Big to Ignore: The Impact of Obesity on Mortality Trends* (Swiss Reinsurance Company, Zurich, Switzerland, 2004).

10.1126/science.1108656

TrueClone™ Collection

Over 24,000 Authentic Full-Length Human cDNA Clones

Authenticity stands the test of time. Is a copy compromising the value of your research?

The OriGene TrueClone™ Collection includes over 24,000 individual full-length human cDNA clones and comprehensive gene family CloneSets™ including 564 protein kinase genes, 340 non-olfactory G protein-coupled receptors and 70 nuclear hormone receptors.

Directly obtained from human reverse-transcribed cDNA libraries and matched to publicly annotated mRNA reference sequences, the OriGene TrueClone Collection ensures accuracy, avoids the errors that can be introduced with other cloning methods, and ultimately protects downstream experimental results.

Start with the original and preserve the value of your research.

Visit our NEW eCommerce website at www.origene.com to search for a gene or call 800-267-4436 to request a 2005 product catalog.

ORIGENE TECHNOLOGIES, INC.

888-267-4436 • www.origene.com

EDITORS' CHOICE

edited by Gilbert Chin

GENETICS

Parental Contributions in Elephants

African forest elephants and their much larger savanna cousins are now recognized as two distinct species that underwent an evolutionary split some 2.6 million years ago. Still, the two species coexist in narrow transition zones between forest and savanna and can produce forest–savanna hybrids.

In order to study this mixing, Roca *et al.* have analyzed the nuclear and mitochondrial (mt) DNA of the two species across sub-Saharan Africa. The distribution of nuclear alleles is, as expected, distinct between the two elephant species; however, several of the savanna populations have mtDNA typical of their forest counterparts, even though their nuclear DNA is clearly of the savanna. This striking dichotomy between nuclear and maternally inherited mtDNA can best be explained by repeated hydridization between forest/hybrid females and the more aggressive savanna bulls, who presumably out-compete the forest/hybrid males, with each backcross further diluting the forest females' nuclear DNA. The high degree of similarity of the mtDNA in the savanna populations with that of the forest elephants suggests that the mixing is the result of a recent event, and the location of some of these savanna populations provides a clue: Although they are relatively distant from extant forests, they are within the range of the extended forests of the Holocene or, in the case of the Southern African populations, in the region of a large paleo-lake. — GR

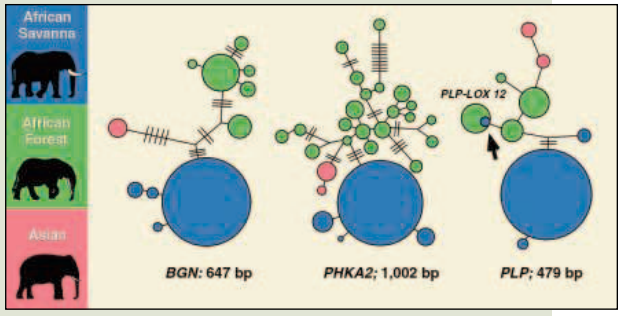

Distinct haplotypes of three nuclear genes.

Nature Genet. **37**, 96 (2005).

MICROBIOLOGY

Breaking and Entering

Malaria begins when an infected Anopheline mosquito injects parasites into a potential host's bloodstream while feeding. The infective stage of the malaria parasite, the sporozoite, then travels to the liver through the bloodstream, where it invades hepatocytes. One of the major sporozoite surface proteins, the circumsporozoite protein (CSP), has been studied as a potential vaccine candidate, but its physiological role for the parasite within the mammalian host is unclear. Coppi *et al.* observed that during the invasion process, when the parasites came into contact with target cells, CSP was proteolytically cleaved by a parasite-derived papain-like cysteine protease. In the presence of inhibitors of CSP processing, invasion was blocked in vitro. Furthermore, when mice were treated with a protease inhibitor specific for papain-like proteases, sporozoite infectivity was also completely inhibited. Thus, a specific proteolytic cleavage event is important in promoting the invasion process, and interfering with this process can prevent malaria infection. — SMH

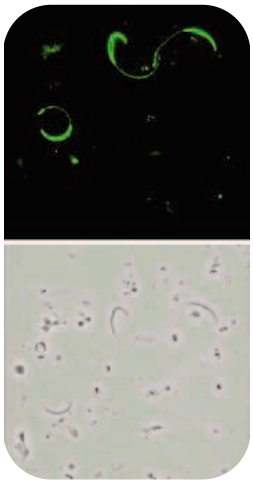

CSP (top, green) on the surface of live sporozoites (bottom).

J. Exp. Med. **201**, 27 (2005).

MATERIALS SCIENCE

Disordered Strain

Many methods exist for the nondestructive measurement of strain in crystalline materials, where the regular ordering of atoms generates a sharp signal when probed with x-rays or neutrons. In amorphous materials, localized strain information can be obtained by using techniques that probe the surface, such as optical or electron microscopy, but behavior at the surface does not typically mimic that in bulk material. Further, the strain fields are usually governed by the behavior around inhomogeneities such as inclusions, voids, and cracks.

Poulsen *et al.* have developed a technique for measuring strain distributions in amorphous materials. They exposed a bulk metallic glass based on magnesium, copper, and yttrium to high-energy x-rays, and then compressed it in situ. Two methods were used to analyze the nearly circular symmetric diffusion patterns, one based on Q space and the other on direct space, and both depend on the shift in the position of the first peak (relative to the uncompressed reading) for determining the strain in the sample. The experiments showed that the macroscopic stiffness of the material was less than one might expect from the nearest-neighbor bonding, due to rearrangement of the atoms on the scale of 4 to 10 Å. For the Q-space method, it is possible that this technique can be applied to polymer glasses using laboratory x-ray sources, where absorption is not an issue. — MSL

Nature Mater. **4**, 33 (2005).

EVOLUTION

A Minimal Set of Folds

The application of technologies that allow the collection of large amounts of data (genomic and proteomic, expression and structure) has generated a demand for methods that can be used to interrogate and systematize these data sets—hence large-scale biology has marched arm in arm with sophisticated (and sometimes bordering on the abstruse) computational analysis. In a refreshing departure from this complexity, Yang *et al.* have used a simple nearest-neighbor kind of approach to overlay a catalog of 174 sequenced genomes with the three-dimensional structures of 1294 protein fold superfamilies.

Surprisingly, they can resurrect the phylogenies of Archaea, Bacteria, and Eukarya quite accurately within each kingdom and pretty well across them. They also find 50 fold superfamilies that are

CONTINUED ON PAGE 321

CREDITS: (TOP) ROCA *ET AL.*, *NATURE GENET.* **37**, 96 (2005); (BOTTOM) COPPI *ET AL.*, *J. EXP. MED.* **201**, 27 (2005)

TaKaRa

Maximum Results, Minimum Effort!

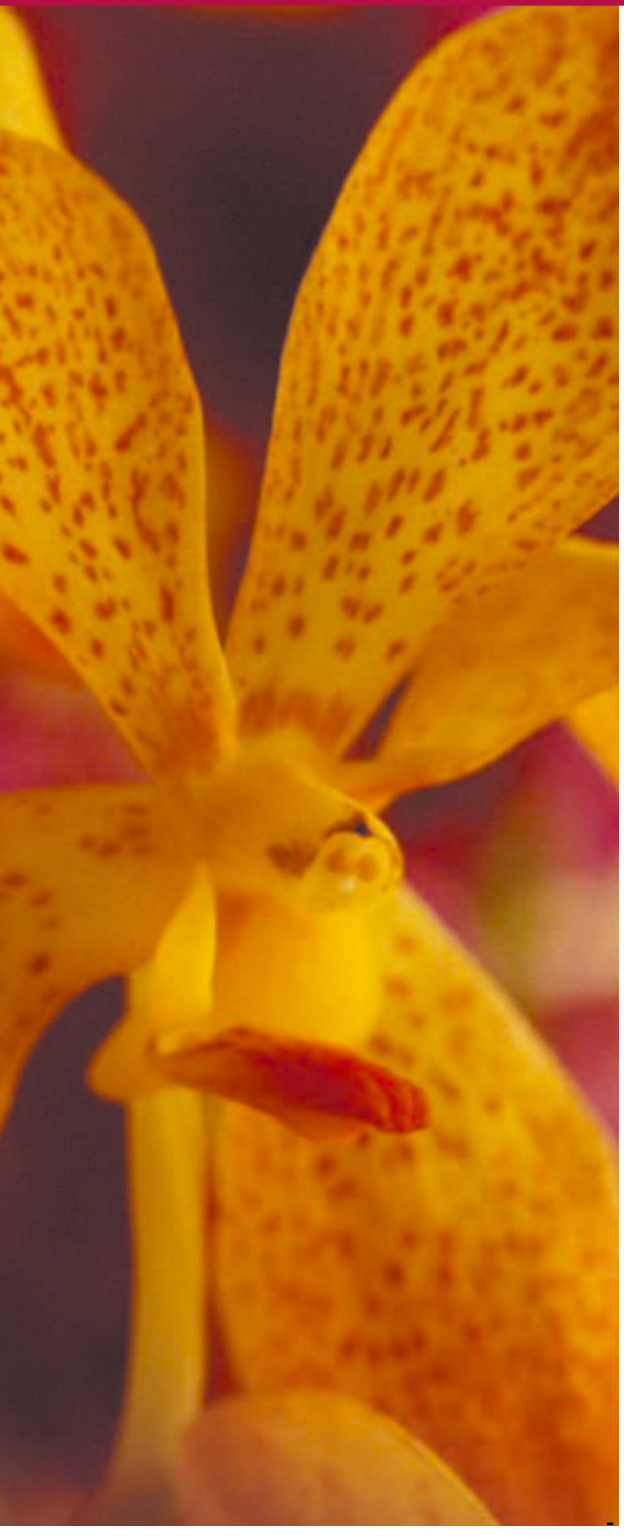

Takara DNA Ligation Kit, Mighty Mix

Takara's DNA Ligation Kit, Mighty Mix, is a new one-solution premix that offers convenient, high efficiency ligations, particularly for blunt-end ligation and TA cloning. The basic reaction can be performed quickly in either 5 minutes at 25°C or 30 minutes at 16°C, depending on the type of DNA ends used. The 2X Ligation Mix Solution also allows small ligation reaction volumes (10 µL), and sufficient reagent is supplied for 75-150 ligation reactions.

- **High Efficiency:** Facilitates high-efficiency ligations for cohesive, blunt-end, and TA cloning.
- **Fast:** Reactions can be performed in either 5 min at 25°C or 30 min at 16°C, depending on DNA ends used.
- **Convenient:** One solution premix eliminates pipetting steps, and the reaction mixture can be used directly in transformations without purification.
- **Small Volumes:** Ten microliter reactions possible to preserve precious DNA samples.

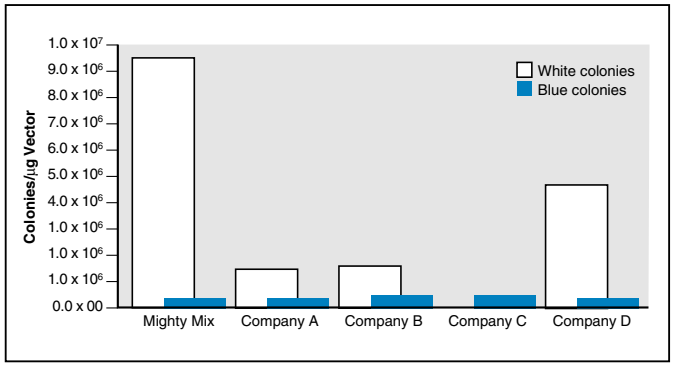

Comparison of Blunt-end Ligation Efficiency with Four Competitors. Each ligation reaction contained 25 fmol of BAP-treated pUC118-Hinc II vector and 75 fmol of a 500 bp insert.

TAKARA BIO INC.
The Biotechnology Company™

Otsu, Shiga, Japan
Phone: +81 77-543-7247 Fax: +81 77-543-9254

USA: **Takara Mirus Bio Inc.** Phone: 888-251-6618 Fax: 608-441-2845
Europe: **Takara Bio Europe S.A.** Phone: +33 1 41 47 23 70 Fax: +33 1 41 47 23 71
Korea: **Takara Korea Biomedical Inc.** Phone: (31)739-3300 Fax: (31)739-3311
China: **Takara Biotechnology (Dalian) Co., Ltd.** Phone: (0411) 8764-1681 Fax: (0411) 8761-9946

For more information and a list of Takara distributors worldwide, please visit our website today!

www.takara-bio.co.jp/english

common to all three kingdoms—many, but not all, of these proteins are involved in translation—which, in the authors' view, represents the fossilized metabolic machinery of the last common ancestor of the three major lineages. — GJC

Proc. Natl. Acad. Sci. U.S.A. **102**, 373 (2005).

CHEMISTRY

Explosive Entropy

Explosive compounds, such as nitroglycerin or trinitrotoluene (TNT), tend to decompose via highly exothermic pathways. The explosion is sustained by the enthalpy released as strong bonds (in the products) form. In contrast, Dubnikova *et al.* suggest that triacetone triperoxide (TATP), which explodes with power comparable to that of TNT, undergoes a nearly thermoneutral decomposition and derives explosive force entirely from the increase in entropy. As its name suggests, this compound incorporates three acetone equivalents: It is a nine-membered ring with three O atom pairs separated by isopropylidene ($>C(CH_3)_2$) groups. The authors used density functional theory to calculate decomposition rates along several pathways, beginning with the structure determined by x-ray diffraction. Comparison with experimental data suggests that exothermic oxidation of the hydrocarbon groups does not play a significant role. Instead, they conclude that the explosion is initiated by cleavage of an O-O bond and is driven by the liberation of four gaseous molecules (one ozone and three acetones) from the harmless-looking solid TATP. — JSY

A trio of peroxide-based explosives.

J. Am. Chem. Soc. 10.1021/ja0464903 (2004).

APPLIED PHYSICS

Seeing Through Fog

Light is scattered and absorbed as it travels through turbid media such as fog, cloud, and dirty water, making it difficult to image objects that may be hidden within. Some light, however, passes through ballistically—that is, without loss—and capturing that ballistic light offers the potential for imaging otherwise hard-to-see objects. Zevallos *et al.* show that combining ultrashort pulses (130 fs) of light with a pulsed detection system (80-ps window) can improve the contrast between the buried object and the noisy background that arises from the diffuse light scattered from the surrounding turbid material; the brief window lets in most of the ballistic light and only a little of the noise, thereby providing a clearer snapshot. The ability to improve the imaging of objects normally hidden from view has a whole host of applications, from the medical imaging of biological tissue to remote sensing and underwater surveillance. — ISO

Appl. Phys. Lett. **86**, 011115 (2005).

HIGHLIGHTED IN *SCIENCE*'S SIGNAL TRANSDUCTION KNOWLEDGE ENVIRONMENT

Science's STKE www.stke.org

Reactivating an Actin Regulator

Control of the actin cytoskeleton is critical for many cellular processes, particularly cell motility, and the actin-depolymerizing factor cofilin is inhibited by phosphorylation. Gohla *et al.* have identified a protein, named chronophin, with phosphatase activity toward phosphorylated cofilin. This enzyme is a member of the haloacid dehalogenase superfamily of phosphotransferases, which have a well-described catalytic mechanism as exemplified by the Ca^{2+}-ATPase of sarco(endo)plasmic reticulum (see Olesen *et al.*, Reports, 24 December 04, p. 2251) but have not previously been implicated in serine dephosphorylation in mammals. Overexpression of chronophin decreased the amount of phosphorylated cofilin in HeLa cells, whereas depletion by RNA interference increased the amounts of phosphorylated cofilin and F-actin, stabilized membrane protrusions and stress fibers, and induced abnormalities in cell division. These findings suggest that chronophin could be a therapeutic target in cases (for instance, chronophin is overexpressed in neuroblastomas) where control of the actin cytoskeleton is disrupted. — LBR

Nature Cell Biol. **7**, 21 (2005).

CREDITS: DUBNIKOVA *ET AL., J. AM. CHEM. SOC.* 10.1021/JA0464903 (2004)

NATO OTAN

Programme for **Security Through Science**

2005 Call for Applications

Overview

Applications are now invited for support under the NATO Programme for Security Through Science. Grants are offered for collaborative activities in Priority Research Topics in the areas of ***Defence Against Terrorism, Countering Other Threats to Security*** and/or ***Partner-Country Priorities***. Collaboration is between scientists in countries of the Euro-Atlantic Partnership Council and countries of the Mediterranean Dialogue, i.e. between scientists in NATO countries on the one hand and scientists in eligible Partner or in Mediterranean Dialogue countries on the other (see countries below). Applications for support are prepared jointly by working scientists in the countries concerned. They are submitted to NATO Headquarters, where they undergo international peer review.

The aim of the NATO Programme on Security Through Science is to contribute to security, stability and solidarity among nations, by applying cutting-edge science to problem solving. Collaboration, networking and capacity-building are means used to accomplish this end. A further aim is to catalyze democratic reform and support economic development in NATO's Partner countries in transition.

Support mechanisms

The aims of the programme are pursued through offering the following types of grant:

- **Collaborative Linkage Grants (CLG):** to pool ideas and resources on research projects, and create specialist networks
- **Expert Visits (EV):** grants to allow the transfer of expertise in an area of research
- **Advanced Study Institutes (ASI):** grants to organize high-level tutorial courses to convey the latest developments in a subject to an advanced-level audience
- **Advanced Research Workshops (ARW):** grants to organize expert workshops where an intense but informal exchange of views at the frontiers of a subject aims at identifying directions for future action
- **Science for Peace projects (SFP):** grants to collaborate on multi-year applied R&D projects in Partner or Mediterranean Dialogue countries.
- **Reintegration Grants (RIG):** to allow young scientists from Partner countries working in NATO countries abroad to return and reintegrate into the research communities of their home countries.

Support for Computer Networking in Partner countries is also available, and further information may be found at the web site.

PHOTO: © ARS/USDA

Priority research topics

The grants support collaboration in the following security-related science topics:

Defence against terrorism

- Rapid detection of Chemical, Biological, Radiological or Nuclear (CBRN) agents, and weapons and rapid diagnosis of their effects on people;
- Novel and rapid methods of detection (e.g. chemical and biosensors, multisensor procesing, gene chips);
- Physical protection against CBRN agents;
- Decontamination of CBRN agents;
- Medical countermeasures (e.g. chemical and vaccine technologies);
- Explosives detection;
- Eco-terrorism countermeasures;
- Computer terrorism countermeasures.

Countering other threats to security

- Environmental security (e.g. desertification, land erosion, pollution, etc.);
- Water resources management;
- Management of non-renewable resources;
- Modeling sustainable consumption (e.g. food, energy, materials, fiscal measures and environmental costings);
- Disaster forecast and prevention;
- Food security;
- Information security;
- Human and societal dynamics (e.g. new challenges for global security, economic impact of terrorist actions, risk studies, management of science, science policy, security-related political science, and international relations in general).

Partner-country priorities

Topics in Partner-country priority areas are also eligible for support. The list of Partner-country priority topics may be found on the programme web site. Applications that fall within both the NATO priority research topics listed above, and the Partner-country priorities, are particularly solicited.

How to apply

Application forms and Notes for Applicants are available for each support mechanism from the NATO science web site - see pull-down menus **Grant Mechanisms** and **Topics Supported.**

Further information on how to participate in a NATO scientific meeting is also given at the NATO science website - see under Calendar of Meetings.

Euro-Atlantic Partnership Council

NATO countries: Belgium, Bulgaria, Canada, Czech Republic, Denmark, Estonia, France, Germany, Greece, Hungary, Iceland, Italy, Latvia, Lithuania, Luxembourg, Netherlands, Norway, Poland, Portugal, Romania, Slovak Republic, Slovenia, Spain, Turkey, United Kingdom, United States.

Eligible Partner countries: Albania, Armenia, Azerbaijan, Belarus, Croatia, Georgia, Kazakhstan, Kyrgyz Republic, Moldova, Russian Federation, Tajikistan, the former Yugoslav Republic of Macedonia [1], Turkmenistan, Ukraine, Uzbekistan

Other Partner countries: Austria, Finland, Ireland, Sweden, Switzerland

Mediterranean Dialogue countries

Algeria, Egypt, Israel, Jordan, Mauritania, Morocco, Tunisia

[1] Turkey recognises the Republic of Macedonia with its constitutional name.

NATO
Security Through Science Programme

Public Diplomacy Division
1110 Brussels, Belgium

www.nato.int/science

www.sciencemag.org

Science

1200 New York Avenue, NW
Washington, DC 20005
Editorial: 202-326-6550, FAX 202-289-7562
News: 202-326-6500, FAX 202-371-9227

Bateman House, 82-88 Hills Road
Cambridge, UK CB2 1LQ
+44 (0) 1223 326500, FAX +44 (0) 1223 326501

SUBSCRIPTION SERVICES For change of address, missing issues, new orders and renewals, and payment questions: 800-731-4939 or 202-326-6417, FAX 202-842-1065. Mailing addresses: AAAS, P.O. Box 1811, Danbury, CT 06813 or AAAS Member Services, 1200 New York Avenue, NW, Washington, DC 20005

INSTITUTIONAL SITE LISCENCES please call 202-326-6755 for any questions or information

REPRINTS Ordering/Billing/Status 800-635-7171; Corrections 202-326-6501

PERMISSIONS 202-326-7074, FAX 202-682-0816

MEMBER BENEFITS Bookstore: AAAS/Barnes&Noble.com bookstore www.aaas.org/bn; Car purchase discount: Subaru VIP Program 202-326-6417; Credit Card: MBNA 800-847-7378; Car Rentals: Hertz 800-654-2200 CDP#343457, Dollar 800-800-4000 #AA1115; AAAS Travels: Betchart Expeditions 800-252-4910; Life Insurance: Seabury & Smith 800-424-9883; Other Benefits: AAAS Member Services 202-326-6417 or www.aaasmember.org.

science_editors@aaas.org (for general editorial queries)
science_letters@aaas.org (for queries about letters)
science_reviews@aaas.org (for returning manuscript reviews)
science_bookrevs@aas.org (for book review queries)

Published by the **American Association for the Advancement of Science (AAAS)**, *Science* serves its readers as a forum for the presentation and discussion of important issues related to the advancement of science, including the presentation of minority or conflicting points of view, rather than by publishing only material on which a consensus has been reached. Accordingly, all articles published in *Science*—including editorials, news and comment, and book reviews—are signed and reflect the individual views of the authors and not official points of view adopted by the AAAS or the institutions with which the authors are affiliated.

AAAS was founded in 1848 and incorporated in 1874. Its mission is to advance science and innovation throughout the world for the benefit of all people. The goals of the association are to: foster communication among scientists, engineers and the public; enhance international cooperation in science and its applications; promote the responsible conduct and use of science and technology; foster education in science and technology for everyone; enhance the science and technology workforce and infrastructure; increase public understanding and appreciation of science and technology; and strengthen support for the science and technology enterprise.

INFORMATION FOR CONTRIBUTORS

See pages 135 and 136 of the 7 January 2005 issue or access www.sciencemag.org/feature/contribinfo/home.shtml

EDITOR-IN-CHIEF **Donald Kennedy**
EXECUTIVE EDITOR **Monica M. Bradford**
DEPUTY EDITORS **R. Brooks Hanson, Katrina L. Kelner**
NEWS EDITOR **Colin Norman**

EDITORIAL SUPERVISORY SENIOR EDITORS Barbara Jasny, Phillip D. Szuromi; SENIOR EDITOR/PERSPECTIVES Orla Smith; SENIOR EDITORS Gilbert J. Chin, Pamela J. Hines, Paula A. Kiberstis (Boston), Beverly A. Purnell, L. Bryan Ray, Guy Riddihough (Manila), Linda R. Rowan, David Voss; ASSOCIATE EDITORS Lisa D. Chong, Marc S. Lavine, H. Jesse Smith, Valda Vinson, Jake S. Yeston; ONLINE EDITOR Stewart Wills; ASSOCIATE ONLINE EDITOR Tara S. Marathe; BOOK REVIEW EDITOR Sherman J. Suter; ASSOCIATE LETTERS EDITOR Etta Kavanagh; INFORMATION SPECIALIST Janet Kegg; EDITORIAL MANAGER Cara Tate; SENIOR COPY EDITORS Jeffrey E. Cook, Harry Jach, Barbara P. Ordway; COPY EDITORS Cynthia Howe, Sabrah M. n'haRaven, Jennifer Sills, Trista Wagoner, Alexis Wynne; EDITORIAL COORDINATORS Carolyn Kyle, Beverly Shields; PUBLICATION ASSISTANTS Chris Filiatreau, Joi S. Granger, Jeffrey Hearn, Scott Miller, Jerry Richardson, Tunisia L. Riley, Brian White, Anita Wynn; EDITORIAL ASSISTANTS Ramatoulaye Diop, E. Annie Hall, Lisa Johnson, Patricia M. Moore, Jamie M. Wilson; EXECUTIVE ASSISTANT Sylvia S. Kihara; ADMINISTRATIVE SUPPORT Patricia F. Fisher

NEWS SENIOR CORRESPONDENTS Jean Marx; DEPUTY NEWS EDITORS Robert Coontz, Jeffrey Mervis, Leslie Roberts, John Travis; CONTRIBUTING EDITORS Elizabeth Culotta, Polly Shulman; NEWS WRITERS Yudhijit Bhattacharjee, Jennifer Couzin, David Grimm, Constance Holden, Jocelyn Kaiser, Richard A. Kerr, Eli Kintisch, Andrew Lawler (New England), Gregory Miller, Elizabeth Pennisi, Charles Seife, Robert F. Service (Pacific NW), Erik Stokstad; Amitabh Avasthi (intern); CONTRIBUTING CORRESPONDENTS Marcia Barinaga (Berkeley, CA), Barry A. Cipra, Adrian Cho, Jon Cohen (San Diego, CA), Daniel Ferber, Ann Gibbons, Robert Irion, Mitch Leslie (NetWatch), Charles C. Mann, Evelyn Strauss, Gary Taubes, Ingrid Wickelgren; COPY EDITORS Linda B. Felaco, Rachel Curran, Sean Richardson; ADMINISTRATIVE SUPPORT Scherraine Mack, Fannie Groom BUREAUS: Berkeley, CA: 510-652-0302, FAX 510-652-1867, New England: 207-549-7755, San Diego, CA: 760-942-3252, FAX 760-942-4979, Pacific Northwest: 503-963-1940

PRODUCTION DIRECTOR James Landry; SENIOR MANAGER Wendy K. Shank; ASSISTANT MANAGER Rebecca Doshi; SENIOR SPECIALISTS Vicki J. Jorgensen, Jessica K. Moshell, Amanda K. Skelton; SPECIALIST Jay R. Covert

PREFLIGHT DIRECTOR David M. Tompkins; MANAGER Marcus Spiegler

ART DIRECTOR Joshua Moglia; ASSOCIATE ART DIRECTOR Kelly Buckheit; ILLUSTRATOR Katharine Sutliff; SENIOR ART ASSOCIATES Holly Bishop, Laura Creveling, Preston Huey, Julie White; ASSOCIATE Nayomi Kevitiyagala; PHOTO RESEARCHER Leslie Blizard

***SCIENCE* INTERNATIONAL**

EUROPE (science@science-int.co.uk) EDITORIAL: INTERNATIONAL MANAGING EDITOR Andrew M. Sugden; SENIOR EDITOR/PERSPECTIVES Julia Fahrenkamp-Uppenbrink; SENIOR EDITORS Caroline Ash, Stella M. Hurtley, Ian S. Osborne, Peter Stern; ASSOCIATE EDITOR Stephen J. Simpson; EDITORIAL SUPPORT Cheryl Sharp, Emma Westgate; ADMINISTRATIVE SUPPORT Janet Clements, Phil Marlow, Jill White; NEWS: INTERNATIONAL NEWS EDITOR Eliot Marshall DEPUTY NEWS EDITOR Daniel Clery; CORRESPONDENT Gretchen Vogel (Berlin: +49 (0) 30 2809 3902, FAX +49 (0) 30 2809 8365); CONTRIBUTING CORRESPONDENTS Michael Balter (Paris), Martin Enserink (Amsterdam and Paris); INTERN Mason Inman

ASIA Japan Office: Asca Corporation, Eiko Ishioka, Fusako Tamura, 1-8-13, Hirano-cho, Chuo-ku, Osaka-shi, Osaka, 541-0046 Japan; +81 (0) 6 6202 6272, FAX +81 (0) 6 6202 6271; asca@os.gulf.or.jp JAPAN NEWS BUREAU: Dennis Normile (contributing correspondent, +81 (0) 3 3391 0630, FAX 81 (0) 3 5936 3531; dnormile@gol.com); CHINA REPRESENTATIVE Hao Xin, + 86 (0) 10 6307 4439 or 6307 3676, FAX +86 (0) 10 6307 4358; haoxin@earthlink.net; SOUTH ASIA Pallava Bagla (contributing correspondent +91 (0) 11 2271 2896; pbagla@vsnl.com); CENTRAL ASIA Richard Stone (+7 3272 6413 35, rstone@aaas.org)

EXECUTIVE PUBLISHER **Alan I. Leshner**
PUBLISHER **Beth Rosner**

FULFILLMENT & MEMBERSHIP SERVICES (membership@aaas.org) DIRECTOR Marlene Zendell; FULFILLMENT SYSTEMS: MANAGER Waylon Butler; MEMBER SERVICES: MANAGER Michael Lung; SENIOR SPECIALIST Pat Butler; SPECIALIST Laurie Baker, Tamara Alfson; REPRESENTATIVE Karena Smith; MARKETING ASSOCIATE Deborah Stromberg

BUSINESS OPERATIONS AND ADMINISTRATION DIRECTOR Deborah Rivera-Wienhold; BUSINESS MANAGER Randy Yi; SENIOR FINANCIAL ANALYSTS Lisa Donovan, Jason Hendricks; ANALYST Jessica Tierney, Farida Yeasmin; RIGHTS AND PERMISSIONS: ADMINISTRATOR Emilie David; ASSOCIATE Elizabeth Sandler; MARKETING: DIRECTOR John Meyers; MEMBERSHIP MARKETING MANAGER Darryl Walter; MARKETING ASSOCIATES Karen Nedbal, Julianne Wielga; RECRUITMENT MARKETING MANAGER Allison Pritchard; ASSOCIATES Mary Ellen Crowley, Amanda Donathen, Catherine Featherston; DIRECTOR OF INTERNATIONAL MARKETING AND RECRUITMENT ADVERTISING Deborah Harris; INTERNATIONAL MARKETING MANAGER Wendy Sturley; MARKETING/MEMBER SERVICES EXECUTIVE: Linda Rusk; JAPAN SALES AND MARKETING MANAGER Jason Hannaford; SITE LICENSE SALES: DIRECTOR Tom Ryan; SALES AND CUSTOMER SERVICE Mehan Dossani, Catherine Holland, Adam Banner, Yaniv Snir; ELECTRONIC MEDIA: INTERNET PRODUCTION MANAGER Lizabeth Harman; ASSISTANT PRODUCTION MANAGER Wendy Stengel; SENIOR PRODUCTION ASSOCIATES Carla Cathey, Sheila Mackall, Lisa Stanford; PRODUCTION ASSOCIATE Nichele Johnston; LEAD APPLICATIONS DEVELOPER Carl Saffell

PRODUCT ADVERTISING (science_advertising@aaas.org); MIDWEST Rick Bongiovanni: 330-405-7080, FAX 330-405-7081 • WEST COAST/W. CANADA B. Neil Boylan (Associate Director): 650-964-2266, FAX 650-964-2267 • EAST COAST/E. CANADA Christopher Breslin: 443-512-0330, FAX 443-512-0331 • UK/SCANDINAVIA/FRANCE/ITALY/BELGIUM/NETHERLANDS Andrew Davies (Associate Director): +44 (0)1782 750111, FAX +44 (0) 1782 751999 • GERMANY/SWITZERLAND/AUSTRIA Tracey Peers (Associate Director): +44 (0) 1782 752530, FAX +44 (0) 1782 752531 JAPAN Mashy Yoshikawa: +81 (0) 33235 5961, FAX +81 (0) 33235 5852 ISRAEL Jessica Nachlas +9723 5449123 • TRAFFIC MANAGER Carol Maddox; SALES COORDINATOR Deiandra Simms

CLASSIFIED ADVERTISING (advertise@sciencecareers.org); U.S.: SALES DIRECTOR Gabrielle Boguslawski: 718-491-1607, FAX 202-289-6742; INTERNET SALES MANAGER Beth Dwyer: 202-326-6534; INSIDE SALES MANAGER Daryl Anderson: 202-326-6543; WEST COAST/MIDWEST Kristine von Zedlitz: 415-956-2531; EAST COAST Jill Downing: 631-580-2445; LINE AD SALES Emnet Tesfaye: 202-326-6740; SENIOR SALES COORDINATOR Erika Bryant; SALES COORDINATORS Rohan Edmonson, Caroline Gallina, Christopher Normile, Joyce Scott, Shirley Young; INTERNATIONAL: SALES MANAGER Tracy Holmes: +44 (0) 1223 326525, FAX +44 (0) 1223 326532; SALES Christina Harrison; SALES ASSISTANT Claire Griffiths; JAPAN: Jason Hannaford: +81 (0) 52 777 9777, FAX +81 (0) 52 777 9781; PRODUCTION: MANAGER Jennifer Rankin; ASSISTANT MANAGER Deborah Tompkins; ASSOCIATE Amy Hardcastle; SENIOR TRAFFICKING ASSOCIATE Christine Hall; SENIOR PUBLICATIONS ASSISTANT Robert Buck; PUBLICATIONS ASSISTANT Natasha Pinol

AAAS BOARD OF DIRECTORS RETIRING PRESIDENT, CHAIR Mary Ellen Avery; PRESIDENT Shirley Ann Jackson; PRESIDENT-ELECT Gilbert S. Omenn; TREASURER David E. Shaw; CHIEF EXECUTIVE OFFICER Alan I. Leshner; BOARD Rosina M. Bierbaum; John E. Burris; John E. Dowling; Karen A. Holbrook; Richard A. Meserve; Norine E. Noonan; Peter J. Stang; Kathryn D. Sullivan; Lydia Villa-Komaroff

AAAS
ADVANCING SCIENCE, SERVING SOCIETY

Still waiting for a way to analyze **microRNA**?

Come get your tools.

Genisphere introduces two new products that make it a whole lot easier for you to work with small microRNA samples. Our **SenseAmp Plus** universal, high-fidelity RNA amplification kits will give you a lot more microRNA to work with: they increase your sample size by about 1,000-fold, and produce polyadenylated, sense-strand RNA that is compatible with standard labeling protocols. If you're using microarrays to analyze your samples, our ultra-sensitive **Array 900miRNA** labeling kits will let you do more with less: they produce excellent array results with enriched microRNA derived from 1-2 microgram total RNA samples.

Okay, now get to work.

For more information or to purchase a trial kit, call us at 877.888.3DNA or visit our website www.genisphere.com.

Genisphere®

SIGNAL + SAMPLE AMPLIFICATION PRODUCTS

February 27 – March 4th, 2005

www.pittcon.org

PITTCON® 2005 ORLANDO

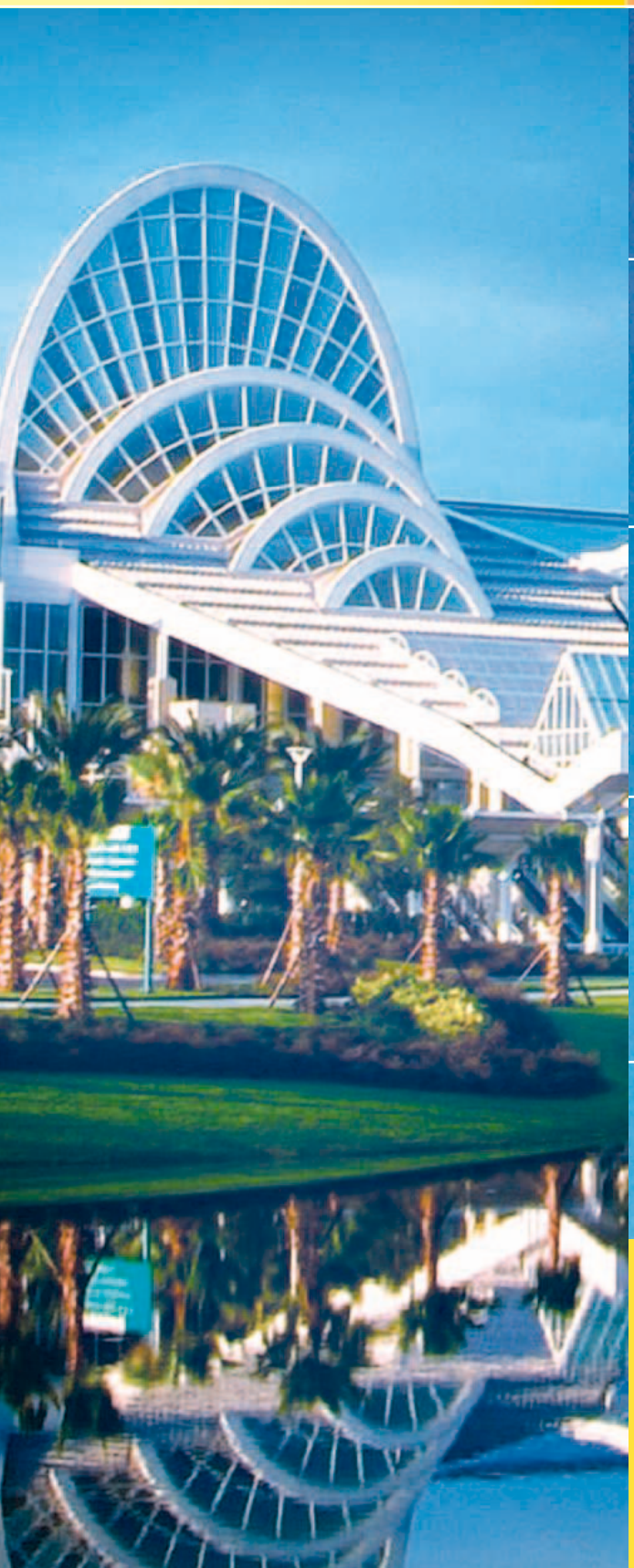

chemistry

nanotechnology

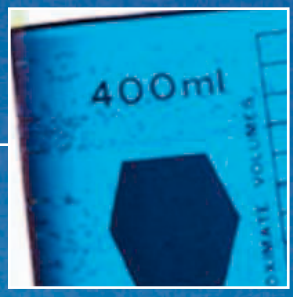

forensics

pharmaceuticals

life sciences

anti-terrorism

food science

environmental

EVERYTHING

SCIENCE

UNDER THE SUN!

Protocol for biomolecular research:

824 experiments (repeatable)

153 skipped lunches

47 I can't talk now honeys

29 missed episodes of "Celebrity Poker"

The procedure is well-established: Put everything on hold until further notice. As a scientist you understand that personal sacrifice is often the cost of discovery. At USB, we understand that too. So we're committed to providing you with the products and support to help you make the most of your time in the lab. We're responsive. Reachable. And ready to help with a team of experts who are just as passionate about your research as you. To learn more, call 800-321-9322 or visit us at www.usbweb.com. After all, isn't it time your reagent supplier worked as hard as you?

usb
Fueling Innovation™

PCR Tools | Molecular Biology Reagents | Mutation Discovery | Nucleotides | Biochemicals

NetWatch

edited by Mitch Leslie

IMAGES

Sketching Out Past Worlds

For more than 200 years, drawings of fossils and extinct plants and animals have helped paleontologists share their findings with other scientists and the public. A new site from illustrator Mary Parrish of the Smithsonian Institution's National Museum of Natural History in Washington, D.C., explores this corner of paleobiology. An online gallery displays examples, such as this *Triceratops* from the dinosaur collection of late-19th-century paleontologist Othniel Charles Marsh. The site's primer on techniques describes how drawings provide what photos can't: reconstructing a jumble of fossilized bones, putting flesh on a skeleton, or illustrating an ancient landscape. A third section discusses the museum's efforts to preserve its 3500 illustrations, launched in 1995 after staffers discovered a crumbling cache of ink drawings.

www.nmnh.si.edu/paleo/PaleoArt

DATABASES

Decoding the Noncode

Researchers once paid little attention to RNA that doesn't code for or help manufacture proteins, but they now realize that strands of untranslated RNA perform all kinds of tasks that keep a cell humming. A new database called NONCODE,* from the Chinese Academy of Sciences, documents more than 5000 noncoding RNA sequences from hundreds of organisms. Curators pull sequences from GenBank and other sources, then annotate them by consulting the literature. Categories include disease and function, such as DNA repair or protein transport. NONCODE debuted this month in the annual database issue of open-access *Nucleic Acids Research*,† which lists 719 databases of note on everything from immune system genes to the silkworm genome.

* noncode.bioinfo.org.cn

† nar.oupjournals.org/content/vol33/suppl_1

TOOLS

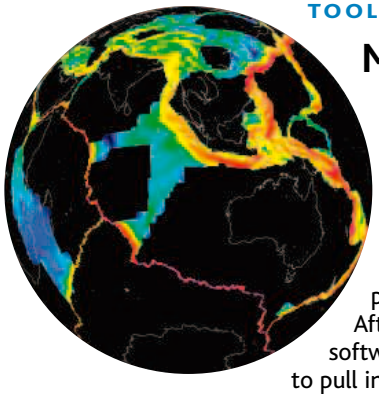

Map-o-Matic

Earth's lithospheric plates (black) meet at geologically active zones in this strain rate map of the world. Red and magenta mark regions with the highest deformation rate, such as south of Sumatra, where a magnitude 9.0 eruption spawned the 26 December tsunami. The image was created with a handy mapping tool from UNAVCO Inc., a nonprofit earth science organization in Boulder, Colorado. After developing the tool 5 years ago for geophysicists, software developer Lou Estey realized it would be a snap to pull in public data sets on the planets, Earth's vegetation, and much more. Users can zoom in, pan out, or download high-resolution maps for printing. A junior version now used by some teachers makes it even easier to create a map of active volcanoes, say, or the world lit up at night. "I've sat down and showed 8-year-olds, and in 5 minutes they're having a blast," says Estey.

jules.unavco.org

RESOURCES

Growth Spurt at Tree of Life

The Tree of Life made a big splash when it debuted in 1994 in the Web's early days. But like many sites, it soon entered a dormant phase. Now the online phylogeny project has gotten new funding and a new educational mission and is seeking more contributors.

The revamped site retains the core of the original tree—now some 3000 pages on beetles, cephalopods, fish, flatworms, and other organisms—but it's now database-driven. That allows visitors to create custom pages on the fly that include, say, an online glossary or more images, notes co-creator David Maddison of the University of Arizona in Tucson. And the tree now invites visitors of all stripes to contribute material linked to the core scientific pages. This supplemental information might include a fruit fly geneticist's data, shots from a professional photographer, or "treehouses" created by children.

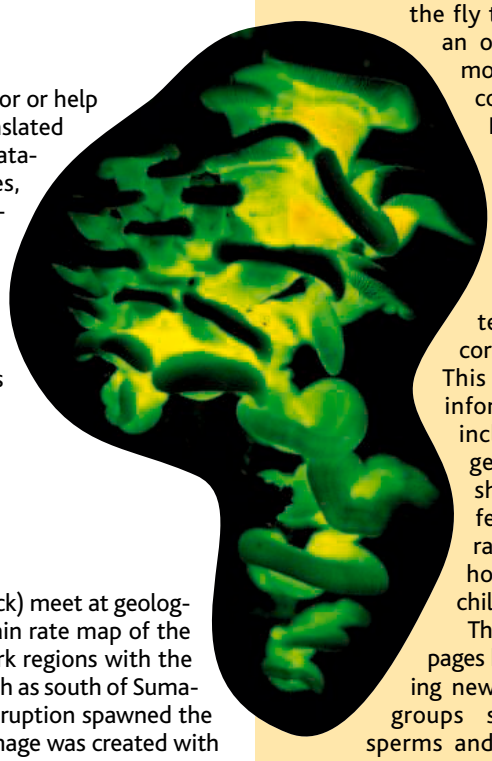

The tree's species pages have been sprouting new shoots, too, on groups such as angiosperms and fungi (above, a bioluminescent mushroom, *Panellus stypticus*). Other sections—such as those on mammals and birds—are still mostly blank. But with revisions to the site's architecture and tools now complete, says managing editor Katja Schulz, "this is the year we hope the content takes off."

tolweb.org

Send site suggestions to netwatch@aaas.org. Archive: www.sciencemag.org/netwatch

CREDITS (TOP TO BOTTOM): NMNH, SMITHSONIAN; D. HIBBETT/CLARK UNIVERSITY; L. ESTEY/UNAVCO, DATA FROM GLOBAL STRAIN RATE MAP PROJECT

This Week

PAGE 333
Upheaval at Pasteur

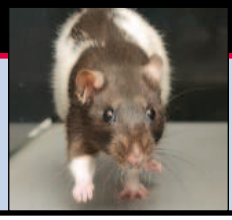

334
Active rats, strong hearts

PLANETARY SCIENCE

Titan, Once a World Apart, Becomes Eerily Familiar

The praise was polyglot, but the sense of it was clear enough: incredible, magnificent, astonishing. The European probe Huygens had blazed into the upper atmosphere of Saturn's big moon Titan, floated down by parachute for two-and-a-half hours—as it snapped pictures, sniffed the air, and checked the weather—and almost miraculously survived a hard landing to taste the surface and return a "wish you were here" view of a truly alien world.

The mission was more than simply a brilliant engineering success. "I was blown away by what I saw," said European Space Agency (ESA) science director David Southwood. "I had wanted to know that there was complexity down there." And complexity he got. What had frustratingly remained an unrecognizable world of broad smears of light and dark, veiled even from the passing Cassini spacecraft by Titan's hazy atmosphere, exploded into sharp details of canyons, riverbeds, plains, rocks, mud, and possible lakes and seas.

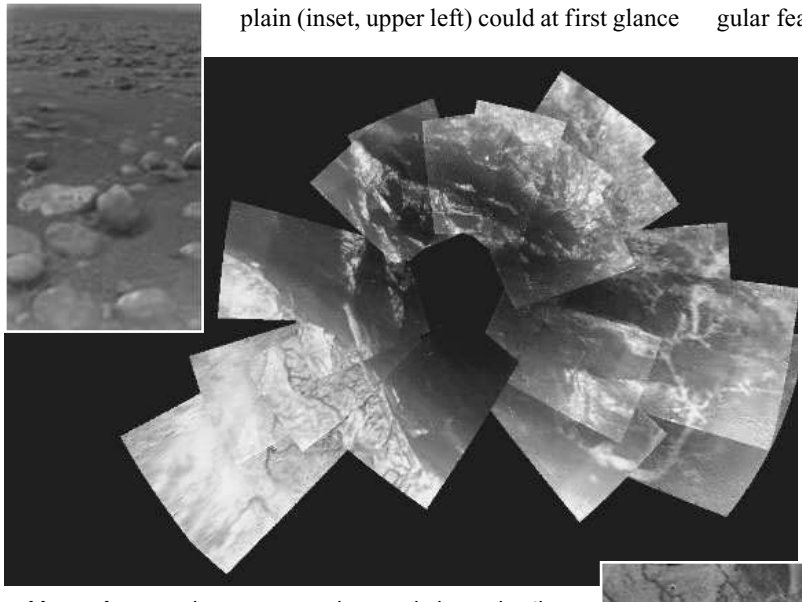

A blur no longer. The Huygens probe revealed new detail on Titan (center, 60 kilometers across), including drainage channels (inset, lower right) and surface rocks (inset, upper left).

Perhaps most astonishing was how familiar it all looked. "I was struck by how similar it looks to what we've seen on a variety of planets," said Huygens descent imager principal investigator Martin Tomasko of the University of Arizona (UA) in Tucson. In particular, this moon of rock-hard ice, organic goo, and liquefied natural gas bears a striking resemblance to deserts like the Mojave and to Mars.

The shock of the familiar crept up on icy-satellite geologist Robert Pappalardo of the University of Colorado, Boulder. "When I first saw the image from the surface," he recalls, "I scrolled right by it because I thought it was Mars. I was amazed." The rusty orange color later added by the imager team is the cast that sunlight gives the surface as it leaks through Titan's hazy atmosphere; Mars, on the other hand, takes its color from the yellow-brown of oxidized iron. But the "rocks" strewn into the distance of a flat plain (inset, upper left) could at first glance easily be taken for martian. In fact, they are probably water ice, as suggested by spectra taken by Huygens. The 10- to 30-centimeter cobbles are well rounded, as if they've been tumbled in a streambed, and are scattered across the scene as if a powerful current had debouched nearby, spread across a broad valley floor, and dropped the rocks where they're now found. On Earth geologists call that a playa.

Huygens's view of the surface on its way down made it plain that powerful currents have indeed carved the surface of Titan. With 20 times the resolution of Cassini and a view from beneath the obscuring haze, the Huygens descent imager returned a picture (inset, lower right) that screams fluid flow. The view from 16 kilometers up "looks very much like drainage channels," said Tomasko, with signs of seepage from canyon walls familiar from both Earth and Mars. Collected fluids would run down the dark-floored channels "out to what looks very much like a shoreline" of a dark sea. This and other Huygens images now add credibility to earlier Cassini observations. "We saw what we called 'dark meandering lines' " in Cassini images, says imaging team member Alfred McEwen of UA, but "we weren't ready to call them channels." And Huygens radar team member Ralph Lorenz of UA had pointed out bright, triangular features in the radar images and suggested—boldly at the time—that they could be rough, bouldery fans of debris dumped where channeled flows opened onto valley floors.

With so many signs of erosion, "the big question is, are the liquids there now?" McEwen asks. Theoreticians had invoked liquid methane—liquefied natural gas—on the surface to explain the presence of methane in the atmosphere. But Cassini observations had failed to reveal any clear sign of a dark methane ocean, sea, or even lake (*Science*, 3 December 2004, p. 1676). As much as the canyon-riddled highland draining to a dark, "shore"-lined plain suggested a sea, Huygens found no obvious sign of standing fluids either. It landed in a generally dark area, said Tomasko, that turns out to be a flat plain.

Even so, Huygens may have found the predicted reservoir of liquid methane. Atmospheric chemist Sushil Atreya of the University of Michigan, Ann Arbor, and the gas chromatograph/mass spectrometer team reported that when they gently heated their instrument's sampling inlet after it was driven into the surface on landing, methane was released. And John Zarnecki of the University of Kent, U.K., principal investigator of the surface science package, said that the penetrometer encountered a thin crust before passing through 15 cen-

CREDIT: ESA/NASA/JPL/UNIVERSITY OF ARIZONA

338 Rough sailing for U.S. researchers

345 Watching for epidemics

346 How cockroaches elude you

timeters of something the consistency of wet sand or clay. His most colorful analogy was a crème brûlée.

Methane seas may yet turn up, but Titan already would seem to have all the parts of a "methylogical cycle" that is analogous—in sometimes strange ways—to the hydrologic cycles of Earth and ancient Mars. Titan's atmosphere contains methane and photochemically produced ethane—analogous to Earth's water vapor—that condense into hydrocarbon clouds. Some clouds must rain onto the surface to erode the channels, although just how hydrocarbons would erode the highly insoluble water ice remains to be worked out. The rain would presumably also pick up the many meters of dark photochemical goo that settles from the haze layer over the eons. That would explain the dark stain on canyon floors and outwash plains. Once the hydrocarbon rivers spread across the wide, flat plains, they would drop any heavy sediment in fans. If the fluids mostly evaporated away to complete the cycle, they would leave their load of organic goo the way water leaves its dissolved salts on a salt flat. Some fluid would likely soak into the plain to become "ground hydrocarbons."

All this sounds to Pappalardo like a desert environment on Earth. It doesn't rain often in deserts, but when it does, the rain can be torrential. That could well be the case on Titan, notes Jonathan Lunine of UA, a Huygens interdisciplinary scientist. Cassini has found few if any clouds outside the south pole region, but ground-based astronomers have seen one cloud outburst at mid latitudes in recent years. That level of activity could be all that's needed to shape a familiar-looking world.

–RICHARD A. KERR

DISASTER PREPAREDNESS

Global Tsunami Warning System Takes Shape

The Bush Administration last week announced a new plan to protect American citizens from tsunamis, bolstering efforts both in wave detection and public readiness.

Unveiling of the proposed $37.5 million effort came a day after Koichiro Matsuura, director-general of the United Nations Educational, Scientific, and Cultural Organization (UNESCO), announced that his organization would build a global tsunami warning system, starting with a $30 million network in the Indian Ocean. White House science adviser John Marburger, speaking at a press conference on 14 January, said the enlarged U.S. network could be part of the worldwide UNESCO effort.

The Administration is proposing to expand the number of wave detectors in the Pacific from six to about 24 and to deploy another seven in the Atlantic and Caribbean. U.S. Geological Survey seismometers are also set for an upgrade. "It's [the] initial straw man plan," said oceanographer Eddie Bernard, director of the National Oceanic and Atmospheric Administration's (NOAA's) Pacific Marine Environmental Laboratory in Seattle, Washington. In the coming months, tsunami experts at NOAA will work with volcano and landslide specialists to finalize the proposal.

The current network of six American wave detectors, which measure water pressure on the sea floor, warns officials on the West Coast and Hawaii of long-ranging tsunamis heading south from Alaska. Ringing Pacific coasts on both sides of the ocean with some 18 new detectors will dramatically improve the network's capabilities. It will also provide crucial early warning to Asian and South American nations.

More warning. NOAA's Conrad Lautenbacher says extending the Pacific tsunami network will make "a significant contribution to a global system."

The expanded detection system would be part of the American-led Global Earth Observation System of Systems (GEOSS), a linking of existing networks for global studies, which is set for formal approval in Brussels on 16 February. Asked if the proposed U.N. and U.S. systems were connected, Marburger noted that UNESCO's Intergovernmental Oceanographic Commission has endorsed GEOSS. And officials hope to coordinate the placement of wave and seismic gauges in international waters. "We want to work it out with our global partners," said NOAA administrator Navy Vice Admiral Conrad Lautenbacher.

Even the upgraded network would give little time to alert coastal communities if a massive earthquake were to strike just offshore. To prepare the public for that, the plan calls for an expansion of the Tsunami Ready program, which prepares local communities to seek higher ground after tremors, among other things. "It's not just a question of putting some buoys out there," Marburger said.

Bolstering defenses—especially for Atlantic shores—only became a priority after the destruction in South Asia. "Even though we haven't experienced an earthquake-tsunami off the East Coast doesn't mean it can't happen," said Bernard, noting that although Atlantic coasts face lower risks from earthquakes, tsunamis can be caused by rare events such as landslides above ground or under water, as well as meteor strikes.

The White House is pressing Congress to approve much of the funds for the new program as part of a supplemental tsunami-relief funding measure for this fiscal year. The House science committee will review the new plan in a hearing 26 January.

–ELI KINTISCH

CREDIT: CHRIS MADDALONI

Get remarkably robust DNA amplification. Again and again and again.

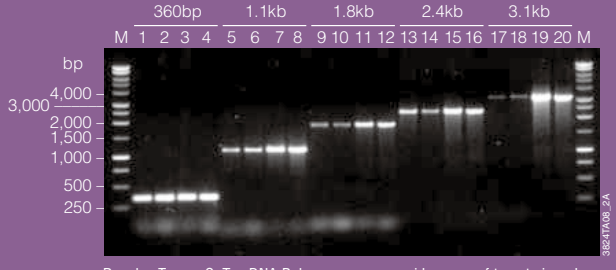

Regular *Taq* vs. GoTaq DNA Polymerase over a wide range of target sizes. In each set the left two lanes are *Taq* DNA Polymerase and the right two lanes are GoTaq DNA Polymerase.

Reap the benefits of consistent, robust performance every time you amplify with GoTaq® Polymerases.

- Harvest spectacular yields with optimal enzyme and buffer
- See faster results with the all-in-one reaction buffer that doubles as a gel loading buffer
- Perform perfect gel tracking with the GoTaq Green buffer – tracks small fragments and bumper products
- Enjoy the Promega PCR Performance Guarantee

Prove it to yourself...again and again and again.

To learn more, visit **www.promega.com/gotaq**

PROMEGA CORPORATION • www.promega.com

Promega

RESEARCH POLICY

Facing a Revolt, Pasteur Board Members Offer to Resign

PARIS—Almost the entire board of directors of the Pasteur Institute offered to step down in an unprecedented mass resignation on 12 January. The disaffected members say they hope the move will calm a long-simmering battle between Pasteur's president Philippe Kourilsky and other scientists and staff—particularly over a plan to relocate some Pasteur labs and offices from central Paris to an unpopular suburban site.

The troubles had been escalating at Pasteur for months. Rumors and anonymous screeds have made the rounds via e-mail and the Web, and the crisis had eaten away at the institute's scientific mission, says Antoine Danchin, head of the Genetics of Bacterial Genomes unit and a member of the board. "People are no longer working. Everybody is upset," he says. "It's very bad for Pasteur."

Under pressure. Pasteur's president Philippe Kourilsky encounters dissent.

Since taking the helm in 2000, Kourilsky, a renowned immunologist, has pushed ahead with an aggressive reform package aimed at revitalizing the institute. When Kourilsky was chosen, many scientists said the fabled but sclerotic research center desperately needed a change (*Science*, 15 October 1999, p. 382). Younger researchers especially have welcomed Kourilsky's efforts to give them a chance to create their own laboratories or direct international research programs, says Ralf Altmeyer, director of the Hong Kong University–Pasteur Research Centre in Hong Kong.

But Kourilsky's "tough, abrasive" management style and indifferent communication skills have wiped out most of his credit, says Pasteur chief of molecular retrovirology Simon Wain-Hobson. "I'm all in favor of strong leadership," he says. "But you can't lead if you're beating up your own troops."

The main irritant has been a plan to move some units out of central Paris—at least temporarily during a renovation—to a building donated by the drug company Pfizer and located 12 kilometers away in the town of Fresnes. Researchers questioned the move's rationale and the brusque way it was pushed through. The criticism has targeted not only Kourilsky but the board of directors, a 20-member body, 14 of them from outside the institute, which appointed him. During a meeting of the board in December, hundreds of *pasteuriens* clad in lab coats voiced their discontent outside. John Skehel, director of the Medical Research Council's National Institute for Medical Research in London, has been appointed a mediator; the mass resignation has delayed his interim report, scheduled to be delivered next week.

Initially, some board members sought only the resignation of the chair, former France Telecomn CEO Michel Bon, a staunch supporter of Kourilsky. But when he refused to step down, a majority opted for a mass resignation that may "help clear the air," says one member who requested anonymity, by giving the institute a chance to choose a new board more to its liking. The new board will be elected by the institute's General Meeting, a parliament-style body of about 100 members, more than half of them from outside the institute, that will meet on 15 March. (Four statutory members representing government agencies will remain.)

Kourilsky, in an interview with *Science*, admitted that the Fresnes plan could have been handled more tactfully. "I don't deny that I have become somewhat controversial," he says. But he vigorously defends his track record and chalks up the criticism in part to the fact that he threatened privileges. "Changing things in France is often very difficult," he says. Last week, Kourilsky also sent all staffers a 47-page document outlining his management accomplishments.

Whether Kourilsky will be eligible for a second term when his 6-year mandate ends in December—or whether he might even be asked to step down before that—will be decided by the new board. Kourilsky declined to say whether he's interested in staying on.

Peace is unlikely to return to Pasteur's labs anytime soon. As one scientist notes, Kourilsky will continue to draw lightning, and jockeying over candidates for the new board is widely expected to be intense. Few are looking forward to it. Pascale Cossart, who heads Pasteur's Bacteria–Cell Interactions Unit, says, "We just want to work in a quiet place without always talking about politics."

—MARTIN ENSERINK

CREDIT: INSTITUT PASTEUR

ScienceScope

NIH Revises Public Access Policy

The National Institutes of Health (NIH) plans to ask its grantees to send their research articles to a public database, which would post them 1 year after they're published in a journal. That's double the length of time it proposed last year in the wake of congressional pressure to give the public greater access to such research (*Science*, 26 November 2004, p. 1451).

Scientific societies are "pleased" with the extension, says Martin Frank, executive director of the American Physiological Society, noting that it conforms to the policies of many nonprofit journals (including *Science*). But he maintains that the archive isn't necessary and that having both the archived manuscript and the published article on the Web will be confusing. Groups that had pushed for quicker public access also had a mixed reaction: "NIH punted," says Rick Johnson, director of the Scholarly Publishing and Academic Research Coalition. But he thinks the policy's impact "could be positive."

NIH was set to unveil its policy on 11 January. But the briefing was cancelled the evening before, prompting speculation that Bush Administration officials didn't want the issue to complicate hearings this week on the confirmation of Health and Human Services Secretary Michael Leavitt.

—JOCELYN KAISER

Korea OK's Work Under New Stem Cell Law

TOKYO—The Korean group that produced the first embryonic stem cell line from cloned human cells has gotten the green light to resume its research.

Woo Suk Hwang of Seoul National University and colleagues did their initial work (*Science*, 12 March 2004, p. 1669) before there were any national rules about embryonic stem cell work. On 1 January, South Korea's Bioethics and Biosafety Act took effect, and 2 days later, Hwang applied to the Ministry of Health and Welfare for permission. The work involves so-called therapeutic cloning, which promises stem cell therapies with genetic material that matches that of a patient and could avoid immune rejection problems. "I'm hoping we can get some results within 2 or 3 months," Hwang says.

Meanwhile, a long-delayed National Bioethics Review Committee will soon review the legislation. Any recommendations could end up extending the approval process.

—DENNIS NORMILE

MEDICINE

Low-Power Mitochondria May Raise Risk of Cardiovascular Problems

Try as we might, only an elite few will ever win the Tour de France or even the local 10-K foot race. People simply vary widely in their ability to perform aerobic exercise. New work with rats now suggests that individuals with a low tolerance for aerobic exercise may have a lot more to worry about than just their inability to run fast and long. The same underlying defect that reduces aerobic capacity may also predispose a person to a witch's brew of medical problems that could increase the possibility of heart attacks and strokes.

On page 418, a research team including Ulrik Wisløff of the Norwegian University of Science and Technology in Trondheim, Sonia Najjar of the Medical College of Ohio in Toledo, and Steven Britton of the University of Michigan, Ann Arbor, reports that rats that have been selectively bred to have reduced capacity for aerobic exercise show obesity, resistance to the hormone insulin (a sign of type II diabetes), and high blood pressure, all symptoms of the so-called metabolic syndrome that raises the risk of cardiovascular disease. The researchers also provide evidence that impaired function of the mitochondria, small structures that produce most of a cell's energy, underlies the metabolic problems of the rats with low aerobic capacity.

Previous work had implicated poor mitochondrial function with individual components of metabolic syndrome, but this is the first time researchers have linked it to all of them at once. "This is an incredibly provocative study," says Vamsi Mootha of Massachusetts General Hospital in Boston, whose own work has linked mitochondrial malfunction to type II diabetes. "They linked metabolic syndrome to mitochondria in a way that hasn't been done before."

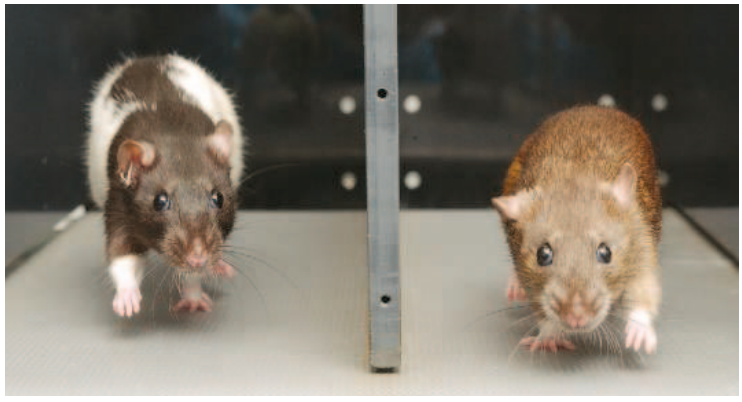

Running for their lives. These rats, bred to have high aerobic capacity, appear to have fewer cardiovascular risk factors than their couch-potato cousins.

The rat-breeding experiments began in 1996, motivated mainly, Britton recalls, by dissatisfaction with existing animal models for diabetes and cardiovascular disease. Most of those models were created by very nonphysiological means, such as tying off the arteries of the heart or administering a drug that destroys the insulin-producing cells of the pancreas, far removed from the way the conditions develop naturally.

To produce animals whose diseases more closely mimic those in humans, the researchers selectively bred rats to have either high or low capacity for aerobic exercise. They identified rats with a high capacity to run on a treadmill and mated them with one another, and they did the same for animals with a low running capacity. "Since oxygen metabolism is such a large part of biology, defects in it should underlie our pathology," explains Britton.

The animals described in the current report, the products of 11 generations of selective breeding, have a 350% difference in their running abilities. And by every measure tested, the couch-potato rats rank high on the cardiovascular risk factor scale: Compared to high-capacity runners, they are more obese, have higher blood pressures and higher levels of blood fats, and have increased insulin resistance.

Although obesity itself can decrease aerobic running capacity, a statistical analysis showed that it accounts for no more than 20% of the decreased aerobic capacity. Indeed, studies of very young rats who were poor exercisers showed that metabolic changes, such as increased blood concentrations of fat and the sugar glucose, occurred before any weight differences became apparent.

Because mitochondria provide the energy for exercise, Britton and his colleagues examined whether these organelles exhibited signs of reduced function in the low–aerobic-capacity rats. The researchers found that muscle from those rats had much lower concentrations of a number of key mitochondrial proteins than did muscle from the high-capacity animals. This indicates that they had either fewer mitochondria or less effective ones.

The work provides "a strong link ▶

TEACHING EVOLUTION

Judge Orders Stickers Removed From Georgia Textbooks

A federal district judge in Atlanta, Georgia, last week ordered a county school board to remove stickers from textbooks that question the validity of evolutionary theory. Even as defenders of Darwin were hailing the victory, however, the school board voted to appeal the order.

In 2002, the school board of suburban Cobb County ordered stickers pasted on high school biology textbooks. The labels describe evolution as "a theory, not a fact, regarding the origin of living things" and advise that the material should be "critically considered." A suit by parents claimed that the stickers violated the First Amendment of the U.S. Constitution that mandates separation of church and state. On 13 January, the U.S. District Court for the Northern District of Georgia noted that describing evolution "as a theory rather than a fact" clearly identifies the school board as being on the side of "religiously motivated individuals."

Wes McCoy, chair of the science department at North Cobb High School in Kennesaw, says he's "thrilled" with the court's decision (www.gand.uscourts.gov). The disclaimer created confusion about the meanings of fact and theory, he says, and led to requests from some students that "we simply not teach evolution anymore, 'since so many people disagree with it.'"

Eugenie Scott of the National Center for Science Education in Oakland, California, says she is "encouraged" by the ruling and hopes it "should at least discourage 'theory, not fact'–type disclaimers." She also sees it as a boon to plaintiffs in Dover, Pennsylvania, who have sued local school officials over a requirement that students be apprised that there are "problems" with Darwinism and that they may consider "other theories of evolution including … intelligent design."

–CONSTANCE HOLDEN

CREDIT: MARTIN VLOET/UNIVERSITY OF MICHIGAN PHOTO SERVICES

between aerobic capacity, mitochondrial function, and the full range of cardiovascular symptoms," says Jeffrey Flier, an obesity and metabolism expert at Beth Israel Deaconess Medical Center in Boston. "If you happen to have drawn the wrong genes, you may be subject to not only not being a long-distance runner but also to diabetes and cardiovascular disease."

All the researchers stress that the results should not be cause for despair among people who suspect that their own aerobic capacity may be on the low side. Wisløff's team is testing whether regular exercise can reduce the various risk factors in the low–aerobic-capacity rats, and early results look promising, Britton says. So rather than providing an excuse for sticking to the couch, the new data could well be yet another reason to hit the bike trail or aerobic floor.

–JEAN MARX

PALEONTOLOGY

Fossil Count Suggests Biggest Die-Off Wasn't Due to a Smashup

If an asteroid or comet impact wiped out the dinosaurs 65 million years ago, unleashing mammal evolution, then might a similar impact have triggered the even bigger extinction 251 million years ago that gave the ancestors of the dinosaurs their start? Evidence for an impact at the boundary between the Permian and Triassic periods (P-T) has yet to convince most researchers (*Science*, 14 May 2004, p. 941). Now, the latest fossil evidence argues that the die-off resulted from a protracted crisis, one that built over tens of thousands or hundreds of thousands of years before pushing Earth over an ecological precipice. The fossil record of large animals in South Africa looks more consistent with extinction by, say, a millennia-long volcanic eruption than by impact.

A goner. This gorgonopsian carnivore disappeared as extinction accelerated in the late Permian, well before the main extinction event.

CREDIT: P. WARD *ET AL.*

In a paper published online this week by *Science* (www.sciencemag.org/cgi/content/abstract/1107068), paleontologist Peter Ward of the University of Washington, Seattle, and colleagues report on 126 fossil reptile and mammal-like reptile skulls they collected during the past 7 years across the P-T boundary in the Karoo Basin of South Africa. There the sand and mud of ancient meandering rivers entombed multitudes of animal skeletons in stone. To pinpoint the relative ages of the fossils from five different collecting sites, the researchers had to find "labels" in the rocks that held them. They used the rocks' changing carbon isotopic composition and Earth's flip-flopping magnetic field frozen into the rocks.

Analyzing the newly found and ordered skulls as well as previously reported fossils, Ward and his colleagues found that after 10 million years or more of relative stability, Permian creatures suffered more rapid extinction in the time during which the last 50 meters or so of Permian rock were deposited before Triassic rocks appear. Time is hard to gauge in the Karoo sediments, but Ward guesses that the extinction-driven decline of Permian taxa might have gone on for as long as 1 million years or as little as 10,000 years. Then a burst of extinctions occurred at the P-T boundary, lasting perhaps 10,000 years, says Ward.

The pattern on land of accelerating decline punctuated by a P-T pulse of extinction "is staggeringly similar" to the P-T pattern in the sea recorded at Meishan, China, says Ward. "Things [in the environment] were bad, and then they were really bad," he says. "We can definitely see it's different from the [dinosaur extinction]. I think there was no impact at all" at the P-T.

Paleontologist Desmond Maxwell of the University of the Pacific in Stockton, California, agrees that the previously proposed foreshadowing of the mass extinction on land—which the new Karoo data strongly support—points to a noncatastrophic cause. Not that life would have been comfortable late in the Permian. In one scenario, eruption of the lavas of the great Siberian Traps at the time of the P-T boundary (*Science*, 21 November 2003, p. 1315) would have poisoned the air and water with acid and alternately chilled the world with a sun-screening haze and baked it with the greenhouse gas carbon dioxide. Hard times indeed.

–RICHARD A. KERR

ScienceScope

EPA Asks for Advice on PFOA

The Environmental Protection Agency (EPA) has asked experts to help it assess the health dangers of a common chemical called perfluorooctanoic acid (PFOA).

PFOA and related chemicals are used to make nonstick and stain-resistant coatings, including Teflon. The chemicals apparently do not break down in the environment and have been widely found in people and wildlife (*Science*, 10 December 2004, p. 1887). Little is known, however, about how people are exposed. EPA officials trying to assess PFOA's risks also face a host of technical issues, says Charles Auer, director of EPA's Office of Pollution Prevention and Toxics, including how to compare blood levels in humans and animals.

So last week, the agency turned to its Science Advisory Board for guidance on how to address these problems. "We're trying to assess the science issues," Auer says. "We're not attempting to make a critical judgment of the risks." But toxicologist Timothy Kropp of the Environmental Working Group, an advocacy organization in Washington, D.C., says that EPA has left important issues off the table, such as the potential for breast and testicular cancers. "This is one of the largest reviews that EPA has embarked on in a long time," he says. "They need to give it a really thorough and fair review."

The advisory board will meet next month in Washington, D.C., to begin a review of EPA's proposed approaches that is expected to take several months.

–ERIK STOKSTAD

NASA's $800 Million Gamble

NASA is keeping mum on how it plans to finance $800 million in projects approved last month by Congress.

The agency's plan for spending what appears to be a robust $16.24 billion budget this year does not include some $300 million needed to get the space shuttle flying again this summer, more than $100 million to repair the Hubble Space Telescope, or $400 million–plus in legislative earmarks. Any realistic spending plan will have to include most, if not all, of that money, which means agency managers must eventually make huge cuts.

Congressional sources worry that much of the squeeze ultimately will defer or even cancel a host of science projects. NASA officials say the agency will reveal the details when the 2006 budget request comes out on 7 February.

–ANDREW LAWLER

iCON™
PROTEIN CONCENTRATORS

Concentrate for Success

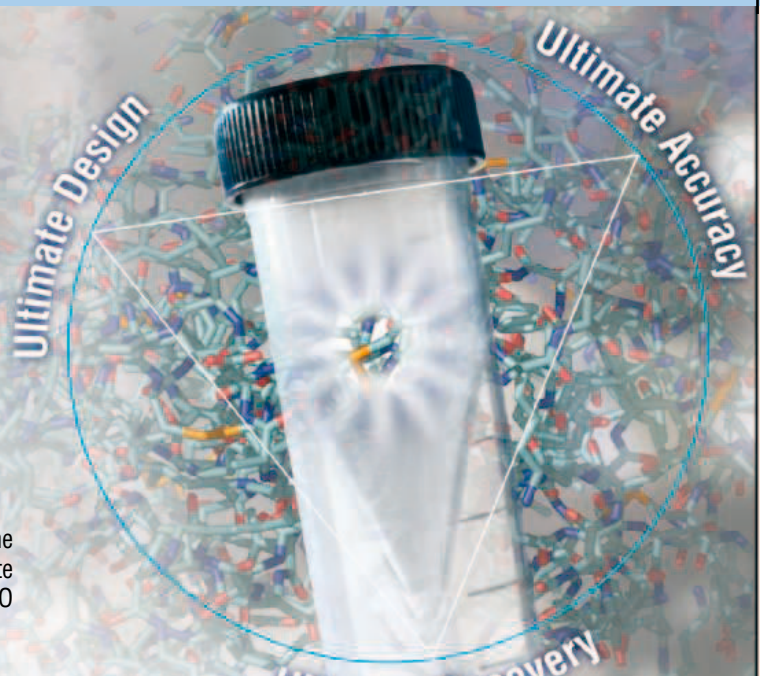

iCON™ Concentrators are advanced disposable ultrafiltration centrifugal devices for concentration and diafiltration/buffer-exchange of biological samples such as enzymes, antigens or antibodies. The innovative conical design* and high-performance regenerated cellulose membrane provide excellent protein concentration and recovery from dilute protein samples. iCON™ Concentrators are available with MWCO of 9K and 20K in 7 and 20 ml volume sizes.

Highlights:

- Achieve 150- to 400-fold protein concentrations in less than 30 minutes
- Accommodate concentration volumes over a wide working range (7 ml = 1-7 ml and 20 ml = 5-20 ml ranges)
- Desalt and exchange buffers
- Uses the maximum membrane surface area, providing unsurpassed protein concentration
- Compatible with swinging-bucket or fixed-angle rotors
- No invert spin required
- Excellent recovery of dilute proteins

Ordering Information

Product #	Description	Pkg. Size	U.S. Price
89884	iCON™ Concentrators, 7 ml, 9K MWCO	25/pkg.	$125
89885	iCON™ Concentrators, 20 ml, 9K MWCO	25/pkg.	$225
89886	iCON™ Concentrators, 7 ml, 20K MWCO	25/pkg.	$125
89887	iCON™ Concentrators, 20 ml, 20K MWCO	25/pkg.	$225

www.piercenet.com/icon

PIERCE

Tel: 815-968-0747 or 800-874-3723 • Fax: 815-968-7316
Customer Assistance E-mail: CS@piercenet.com

Outside the United States, visit our web site or call 815-968-0747 to locate your local Perbio Science branch office (below) or distributor

Belgium & Dist.:	China:	France:	Germany:	Hong Kong:	The Netherlands:	United Kingdom:	Switzerland:
Tel +32 (0)53 83 44 04	Tel (8610)8048 9552	Tel 0800 50 82 15	Tel 0228 9125650	Tel 852 2753 0686	Tel 076 50 31 880	Tel 0800 252185	Tel 0800 56 31 40
euromarketing@perbio.com	support@perbio.com.cn	euromarketing@perbio.com	de.info@perbio.com	SalesHK@perbio.com	euromarketing@perbio.com	uk.info@perbio.com	euromarketing@perbio.com

PERBIO

PATENT LAW

Inventor Knocks Japan's System After Settlement

TOKYO—Shuji Nakamura may be $8 million richer. But his new wealth doesn't seem to have bought much happiness.

Last week the Japanese-born engineer blasted his native country's attitude toward innovation and told colleagues they should join him in the United States if they want to be rewarded for their creative talents. His comments followed a court-mediated, $8 million settlement of a suit against his former employer for a share of the enormous profits generated by his breakthrough development of a blue light-emitting diode (LED) and work on blue semiconductor lasers.

Nakamura, now a professor of materials science at the University of California, Santa Barbara, spent 20 years at Nichia Corp. in Anan, Tokushima. The LEDs are now used in giant outdoor displays and traffic signals and could eventually replace ordinary light bulbs, and blue lasers will be at the heart of next-generation DVD players.

In Japan, patents are awarded to individuals, who may cede rights to their employers in exchange for "fair compensation." Nakamura claims to have gotten just $190 for relinquishing a key patent covering a new chemical vapor deposition method used in producing both the blue LEDs and blue lasers. The privately owned Nichia dominates the LED market, with total sales in 2004 topping $2 billion and profits estimated at $950 million.

In 2001, Nakamura sued the company for a share of those profits. In January 2004, the Tokyo District Court awarded him $190 million (*Science*, 6 February 2004, p. 744). Nichia appealed to the Tokyo High Court, which in a statement recommending a settlement said fair compensation "should be sufficient to motivate employees but at the same time allow the company to survive international competition."

Nichia hailed the settlement, which covers all of Nakamura's patent claims. "Our position was well understood by the court, especially the point that the blue LED was not invented by a single individual," Nichia President Eiji Ogawa wrote in a statement posted on the company's Web site. The business community breathed a huge sigh of relief, with Toyota chair Hiroshi Okuda, head of the Keidanren, Japan's leading business group, calling the amount "appropriate in light of common sense."

The court's concern for the company's bottom line is uniquely Japanese, says Robert Kneller, a U.S. intellectual-property lawyer on the faculty of the University of Tokyo. "I don't think any U.S. court would have said, 'According to the law, damages should be X, but that might hurt the competitiveness of the company; therefore we have to make a judgment ourselves.' " But he noted that the issue of fair compensation is so fuzzy in Japan that it creates problems for judges.

Regardless of the amount, the case may already have improved conditions for Japan's legions of engineers. "Engineers, like myself, think it was very good that this suit has prompted discussion about the low status of engineers," says Hiroyuki Yoshikawa, a former president of the University of Tokyo who is now president of Japan's National Institute of Advanced Industrial Science and Technology. AIST now awards researchers 25% of the royalties from their patents, Yoshikawa says, and many companies have modified their policies to give scientists a bigger bite of the fruits of their research.

–DENNIS NORMILE

Shuji Nakamura Speaks Out

Appearing at a press conference in Tokyo on 12 January, Shuji Nakamura had strong words about the settlement of his lawsuit against his former employer and what it represents:

On Japan's court system: "U.S. courts really try to get down to the principles involved in a case. In Japan, hearings are over in 5 or 10 minutes! The court said that paying huge amounts of money to inventors would hinder industrial development. Who can be satisfied with such a system? If we don't change this kind of approach, [circumstances for inventors] in Japan can never be improved."

On the size of the award: "We've been fighting this trial on the idea of sharing 'excess' profits between the inventor and the company, based on their respective contributions. [In two other recent cases, courts awarded 10% and 20% of "excess" profits, judged as being above "normal" profit levels, to the inventors.] In my case, the district court determined that by 2003, Nichia had earned 'excess' profits of 160 billion yen. The high court set an award of 600 million yen. That means my contribution to this patent was not even 0.5%."

On conditions for researchers: "Basically, Japanese society doesn't value the contributions of individuals. In Japan, the world is centered on big companies. The underlying principle is the concept of sacrificing yourself for big companies. In Japan we have a saying that the nail that sticks up gets hammered down. ... I can only say that competent researchers should come to America. It may be tough, but it is a country with a merit system. You'll be rewarded according to what you do."

On Japan's educational system: "One good point about Japan is its educational system. But it is geared toward turning out production workers. In America, inventors are educated, beginning in childhood, to dream of starting their own companies. American society values individuals, not companies; Japanese society values companies, not individuals."

On the impact of the award: "After paying taxes, attorney fees, etc., very little will be left. I might be able to pay off my mortgage. But that's about it. ... I hate legal battles, they're such a waste of energy. I want to get back to the world of research, where I belong."

CREDIT: D. NORMILE

Unless the government takes action, aging vessels, tight budgets, and rising demand could mean rough weather for U.S. marine scientists who need to go to sea

Grim Forecast for a Fading Fleet

Early this month, one of the world's most powerful ice breakers reached the U.S. research station at McMurdo Bay after smashing its way through the Antarctic ice pack. It's a familiar task for the candy-red, 122-meter-long *Polar Star*, which has been opening essential supply lanes to McMurdo for more than 30 years. But this year she's had to plow through some 200 kilometers of pack ice—nearly five times the usual distance—to reach the logistical hub of the U.S. Antarctic program. And she's done it without help from her customary companion, the twin icebreaker *Polar Sea*, which is idled indefinitely with age-related mechanical ailments.

Much more work, with fewer resources. Things aren't quite that bad for the U.S. science fleet as a whole—yet. But oceangoing scientists don't like what they see when they look out at the fiscal horizon. Over the next decade, a combination of aging vessels and scant funds for replacements could dramatically shrink the number of ships available for marine science just as new, large-scale research programs are expected to greatly boost demand. The mismatch "is making the ocean science community very nervous," says Robert Knox, an associate director of the Scripps Institution of Oceanography in La Jolla, California. "Unless we start building some new ships soon, the fleet will wither away."

Crunch time. Two U.S. Coast Guard icebreakers clear a path through Antarctic sea ice.

Down to the sea

Ships have long played a central role in marine science, allowing researchers to do everything from track currents critical to understanding Earth's climate to sample life on the deep sea floor. For years observers have predicted that new technologies, from satellites to robotic submarines, will ultimately make ships obsolete. "But for the moment, if you want to do good science, there is no alternative to going to sea," says Dave Hebert, an oceanographer at the University of Rhode Island, Kingston.

To keep researchers sailing, the United States has funded the construction of a small armada of research ships. They range from nimble day-trippers that carry just a few researchers to massive floating laboratories able to sustain dozens of scientists for months at a time (see table, p. 340). Today, the loose-knit fleet boasts about 60 major ships (those longer than 20 meters). Many are owned and operated by the U.S. Navy, the National Oceanic and Atmospheric Administration (NOAA), the National Science Foundation (NSF), and other agencies.

Throughout the Cold War, the Navy was the most reliable source of funding for new research vessels. In return, it expected scientists to help predict conditions its ships would face at sea and find new ways to spot threats, such as Soviet submarines. But after the fall of the Berlin wall, the military's interest in marine science began to fade. Although other agencies have tried to fill the gap, none have had deep enough pockets to build many new ships, which can cost up to $100 million each, depending on their size and capabilities.

For most academic researchers, the key component of the fleet is the 27 ships that are operated by the University-National Oceanographic Laboratory System (UNOLS). A coalition of 60-plus research institutions, UNOLS was formed in 1971 to help share ship time and costs. NSF provides about two-thirds of the $65 million needed each year to operate the UNOLS ships, with the Navy and NOAA supplying the balance.

Without a formal capital improvements budget, the UNOLS fleet is showing its age. Twelve of the 17 largest UNOLS ships, for instance, are due to be removed from service by 2020, and several could retire as early as the end of this decade. And given the 10 years needed to design, fund, and build replacement ships, researchers don't have much time to spare. "The clock is ticking," says Knox.

Exactly what a new fleet should look like, however—and who should pay for it—has become an increasingly hot topic. Four years ago, a government body called the Federal Oceanographic Facilities Committee (FOFC) recommended building nine new large ships in three size classes by 2020 for the academic fleet. But it didn't specify who should pay for them. Academic scientists weren't entirely pleased with the recommendations, noting that even if the blueprint were followed, scheduled retirements would cause the fleet to shrink. UNOLS officials successfully argued for including three more "potential"

CREDIT: U.S. COAST GUARD

ships in the group's final report. Insiders dubbed the added UNOLS vessels the "gray ships," corresponding to the color used for them in one key chart that displayed the FOFC-backed ships in black.

Whatever their shades, few of the recommended ships have acquired the most important color of all: green. "Unfortunately, [the plan] has not yet been funded or implemented," notes a congressionally mandated report on U.S. ocean policy that came out last fall (oceancommission.gov). The pending lack of ships, the U.S. Commission on Ocean Policy added, threatens to "hinder the conduct of research."

It's not for lack of interest. NSF is hoping to make room in its budget over the next few years for three smaller "regional class" vessels, at a cost of about $30 million each. The schedule, however, will most likely be disrupted if NSF's budget, which Congress cut this year, fails to rebound. NSF has already stretched out its timetable to refit an ocean drilling vessel after receiving only $15 million of the $40 million it requested to start the work, which will cost an estimated $100 million. At the same time, Senate appropriators reminded NSF last summer that they expect it to ask for $50 million in 2006 to start building a new flagship for Arctic marine science.

Other agencies are also trying to stand up for the fleet. The Navy's Office of Naval Research is trying to scare up funds to build one of the plan's biggest ships, a $75 million "global" ship capable of staying at sea for months. But the ongoing cost of the Iraq War has slowed their progress, Navy officials say. Still, there have been some successes: The National Marine Fisheries Service is buying up to four new trawlers for fisheries surveys, and the Navy recently donated one of its ships to NOAA for its Ocean Exploration program. Columbia University's Lamont-Doherty Earth Observatory and the University of Delaware are also getting new research ships, drawing on a mix of government funding and other sources.

Pleas for more additions could get a boost in the fall, when FOFC is due to issue updated recommendations for the entire spectrum of federally funded ships. "We're considering the whole national fleet, not just the academic ships," says FOFC chief Robert Winokur of the Navy. But Winokur has already warned researchers that they may not like everything the committee will say about the UNOLS fleet. "The message I gave UNOLS is that we need to develop a plan that is tied to realistic budgets," he says. Knox, meanwhile, predicts that the UNOLS response will be guided by "what the science requires. … The community won't be asking for Cadillacs and gold faucets."

One key issue will be predicting how many "ship days" researchers will need. The current annual number of 3600 could grow significantly if Congress funds current proposals to build several major ocean observing systems, including one that aims to cover an entire tectonic plate with cabled sensors. Contrary to predictions that such robotic sensors could reduce the demand for ships, deploying and maintaining these systems will actually increase demand for large ships able to operate in deep seas and handle heavy equipment, a recent UNOLS report concluded. And even if ship use doesn't grow, a separate UNOLS analysis suggests that retirements could eat away at available ship time in just 5 years if no new ships are built (see graph, left).

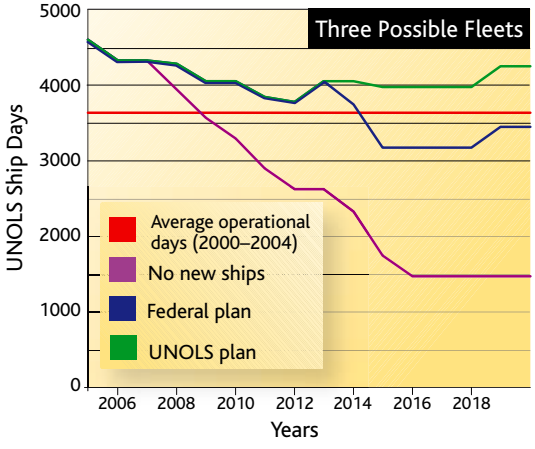

Sinking slowly. Studies project fewer days at sea unless the research fleet is renovated.

The best way to avoid the crunch, it concludes, is to build all 12 of FOFC's black and gray ships. A less costly alternative would be to upgrade vessels or delay their retirement dates, UNOLS and Navy officials note. Extending by 5 years the life of 11 UNOLS ships over 40 meters long, for instance, would cost just $1 million to $5 million per ship, the group estimates.

But there's a price to pay for that penury. Aging ships are generally more expensive to maintain and often can't be equipped with the state-of-the-art sonars, submersibles, and navigation systems that are becoming must-haves for marine scientists. They are also more likely to break down. "What happened with the icebreakers is a lesson we don't want to repeat," says Knox.

Chilling costs

The icebreakers also offer a warning about the high cost of ship repairs and the need to plan as far ahead as possible. White House officials are pondering the fate of the 3-decade-old *Polar Sea*, now moored alongside a pier in its home port of Seattle, Washington. Coast Guard officials say that years of battling ice up to 5 meters thick have taken their toll. Two of its three massive engines are worn out and have been condemned.

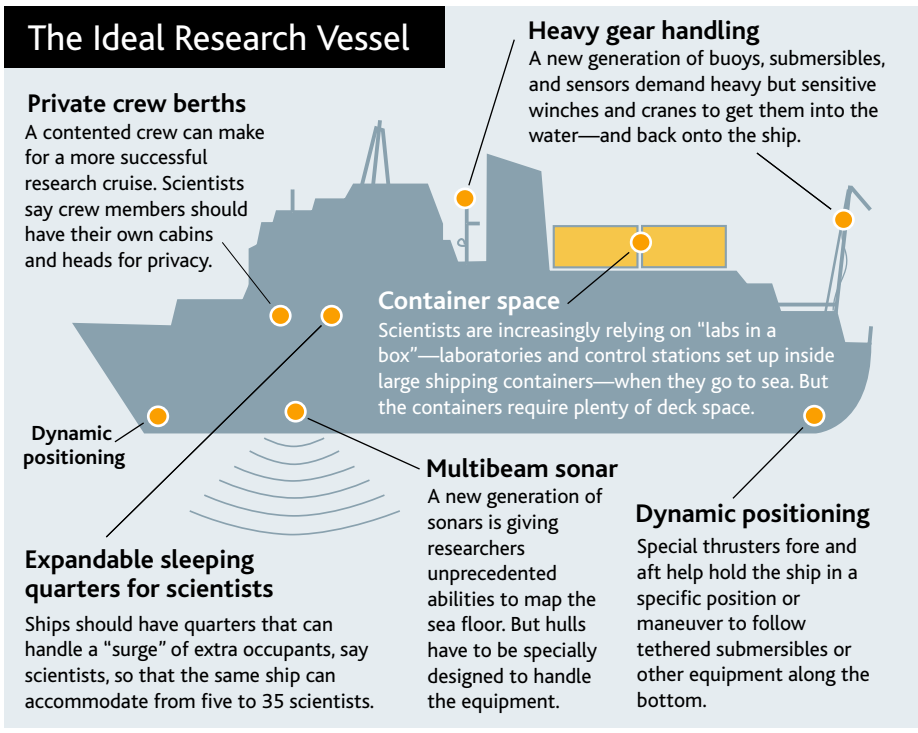

Making waves. The science of going to sea is always evolving.

CREDITS (TOP TO BOTTOM): K. BUCKHEIT/*SCIENCE*; SOURCE: UNOLS

Replacing them, however, could require cracking open the hull and inserting new hardware—at a possible cost exceeding $200 million. "It's a very big ticket item," said Karl Erb, head of polar research programs at NSF, at a recent meeting of the Polar Research Board of the National Academies. Even that price tag, however, is smaller than the cost of an entirely new ship, which could run as high as $1 billion.

Those eye-popping numbers prompted Congress last year to ask the polar board to examine the scientific need for the icebreakers, which spend a large fraction of their time supporting research in the Southern Ocean. The Coast Guard, meanwhile, has commissioned its own studies, and the White House Office of Science and Technology Policy is pondering the problem. A decision on what to do could come as early as next month as part of the president's 2006 budget request. But final action will be up to Congress.

The U.S. Research Fleet
(longer than 20 meters)

Agency	No. of Ships
Navy*	9
NOAA	18
Coast Guard	3
UNOLS †	27

** Owns other ships operated by UNOLS*
† Operates ships owned by others

Note: USGS and EPA operate a number of vessels under 20 meters

In the meantime, NSF is hoping that the *Polar Star* can keep open the path to McMurdo for ships carrying critical cargoes of fuel oil, food, and other supplies for the 1200 scientists and support staff who work at NSF's two mainland Antarctic stations each austral summer. Erb is confident that the *Star* can do the job. But just to be safe, the agency has hired the Russian icebreaker *Krasin*, which this week was due to arrive at the edge of the ice after making the trip from Vladivostok. It's not the best way to run a research fleet, say polar researchers. But in the current era of constrained spending, just-in-time icebreaking may be the best option for U.S. officials.

The same is true for the U.S. research fleet as a whole. With overall U.S. research funding facing its biggest political challenge in a decade, the preferred alternative—an orderly replacement schedule made possible by long lead times and expansive budgets—may have to be abandoned and replaced by a strategy that gives marine scientists at least a chance to keep their heads above water.

–DAVID MALAKOFF

David Malakoff, a former staff writer for *Science*, is now a correspondent and editor at National Public Radio in Washington, D.C.

Profile Fred Kavli

A New Benefactor Takes Aim at Basic Scientific Questions

Norwegian-born industrialist Fred Kavli is dedicating his wealth to fundamental research in fields that have fascinated him since childhood

SANTA BARBARA, CALIFORNIA—As a child in Norway, Fred Kavli skied under the clear shimmer of the Northern Lights, wondering about the universe beyond and our place within it. Today, Kavli still wonders, and in the past few years he has spent tens of millions of dollars to bring answers within reach.

Kavli eased into academic philanthropy after 2000, when he sold the precision-sensor company he founded and ran for more than 40 years. Two physics institutes, at the University of California here (UCSB) and at Stanford University, took his name after receiving $7.5 million grants from his Kavli Foundation. Last year, the foundation crossed state and disciplinary borders with a flourish: It endowed eight more institutes at major universities, featuring top-rank scientists in Kavli's chosen fields of astrophysics, nanoscience, and neuroscience.

With gifts surpassing $100 million and more to come, Kavli is making an impact at a time of unsteady federal funding. And he is doing it out of curiosity. "He is interested in deeply fundamental questions," says neuroscientist and Nobel laureate Eric Kandel of Columbia University in New York City, director of the Kavli Institute for Brain Science. "He is absolutely distinctive because of this. It's just a spectacular impetus for universities."

It's a whirlwind retirement for a lifelong industrialist, but Kavli is having a grand time. "I always felt strongly that I wanted to do something of value for mankind," he says. "To start a business and be successful, it's good. But that was not my goal at all."

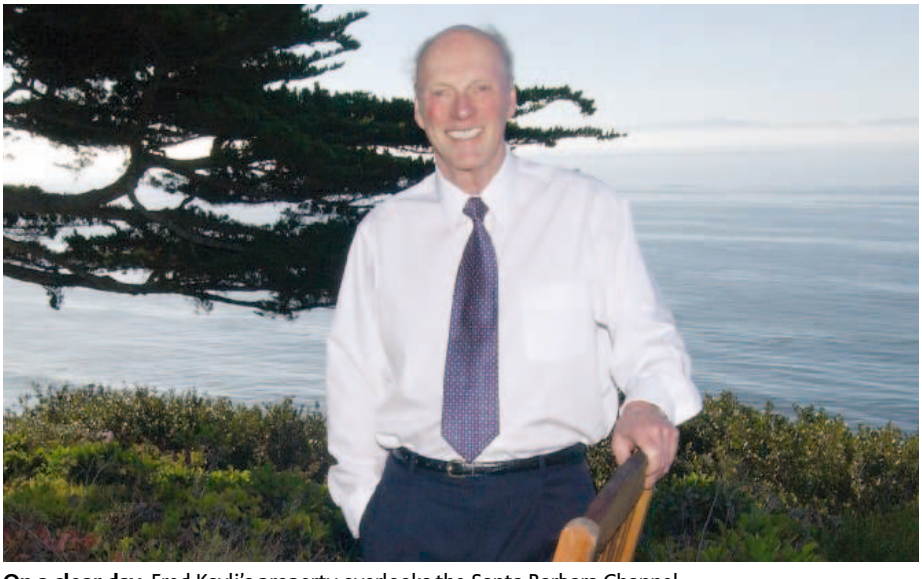

On a clear day. Fred Kavli's property overlooks the Santa Barbara Channel.

CREDIT (BOTTOM): BOB ELLIOT

Paneling and presidents

During a walk through his oceanfront home a few kilometers from UCSB—a stunning house, much of which he designed—Kavli apologizes for a towel on his bedroom floor. "I was stretching there this morning," he explains. Tall and lean, with thin tufts of white hair and an angular face, Kavli resembles the late Francis Crick without the unruly eyebrows. A treadmill, tennis court, and 50-meter stairway to the beach keep him spry and sharp at age 77, as does his favored diet of fruit, fish, sushi and sashimi, and soymilk.

As Kavli climbs a stairway, he passes an array of framed photos without pausing. The faces are familiar: Gerald Ford, Ronald Reagan and Mikhail Gorbachev, Margaret Thatcher, George and Barbara Bush, Dan and Marilyn Quayle. Kavli appears in every image, dashing in a tuxedo. Those were boom times for the military-industrial complex, and he was every bit the politically attuned CEO. "I've met all the presidents, but not [Jimmy] Carter," he observes.

Upstairs, in a simply outfitted study, Kavli slows his pace. High-powered binoculars are fixed upon the orange-hued Kohn Hall at UCSB, home of the Kavli Institute for Theoretical Physics (KITP). He lingers over pictures of his children Ingrid and Eric, adopted with his former wife, Helen; an ultrafast SR-71 reconnaissance jet, for which his company was the sole supplier of flight-control sensors; and a joyous photo from the 1940s with his older brother Aslak. The two blond hotshots sprawl in a field near motorcycles, amid a rapt cluster of three Norwegian girls.

Aslak and Fred, 7 years younger, were inseparable on their family farm near the town of Molde, about 180 kilometers southwest of Trondheim and 5 kilometers inland from the Norwegian Sea. The boys ran a profitable business cutting trees to make planks for furniture factories, as well as wood briquettes that fueled cars and buses during World War II gasoline shortages.

Fred was just as precocious at school, one of which was seven bus and ferry rides from home. He dove headlong into extracurricular life and served as student body president. "Leadership came naturally to me," he says. "More than anything, those activities gave me the confidence to go to America, completely alone, and start my business."

He earned a degree in engineering physics from the Norwegian Institute of Technology (now the Norwegian University of Science and Technology) in Trondheim. Two days later, he boarded the *S.S. Stavangerfjord* in Oslo to steam for Halifax, Nova Scotia. It was 1955, he had $300, and no sure prospects awaited him.

Kavli's quiet voice catches and his eyes well up as he mentions leaving a dear school friend at the port in Oslo, never to see her again. Later, he remembers how much he loved the farm's horses—how gently they responded to kindness, how they looked at him when they grew angry. Conversations with Kavli combine these Old World manners and emotions with dispassionate business acumen, and the fusion draws people in. "He's a shrewd but simple man," says one UCSB physicist. "His heart is in the right place."

Engineer seeks funding

After a year of making ammunition and explosives for a Canadian firm, Kavli got his U.S. visa. His first job, in southern California, was designing flight-control transducers for the Atlas missile. "I had only been out of college 1 year, and they made me chief engineer," he marvels. "I discovered very soon that in America you didn't need to know anything. You just needed to ask the right questions."

Kavli soon itched to step out on his own. He did so in 1958 with a two-line ad in the *Los Angeles Times*: "Engineer seeking financial backing to start own business." "Surprisingly enough, I got several responses," he says with a laugh. The company, soon called Kavlico, was born.

Throughout the 1960s and 1970s, Kavlico grew into a major supplier of pressure, position, and force sensors for commercial airplanes and military jets, bombers, and missiles. In 1976, Kavlico outcompeted 41 companies to land a contract with Ford Motor Co. for automotive sensors. Kavli found that the transition to producing cheap but reliable sensors for cars was excruciatingly difficult. "I wouldn't have done it if I had known. Ignorance is bliss," he says. But ultimately, the automotive contracts made Kavlico's value soar. A Canadian conglomerate bought the company from Kavli in 2000 for $340 million.

"I had no doubt I would succeed," says Kavli, "but I could not have been as successful anywhere else."

Building the foundation

For years, Kavli repaid his gratitude by donating to civic causes in Ventura County and Santa Barbara County, such as the Fred Kavli Theatre for the Performing Arts in Thousand Oaks. But his company's sale enabled him to set up his Kavli Foundation and leave his mark upon science. His themes of astrophysics, nanoscience, and neuroscience—"from the largest, to the smallest, to the most complex," in Kavli's words—reflect both his industrial expertise with micromachinery and his deeply held fascination about the extremes of nature (see table, above).

To run the foundation's programs, Kavli recruited physicist David Auston from the presidency of Case Western Reserve University in Cleveland, Ohio. A member of both the National Academy of Sciences and the National Academy of Engineering, Auston shares and enacts Kavli's philosophy.

"I have a real concern about the argument that many scientists and universities promulgate these days, that science is good for the economy," Auston says. "If that is your only short-term goal, you'll be disappointed in most cases. Our foundation is really distinct in that regard. We are dedicated to long-term—and in some cases high-risk—basic research that advances knowledge as its goal."

The Kavli Family

Kavli Institute for Theoretical Physics (December 2001)
University of California, Santa Barbara
Astrophysics, condensed matter physics, string theory, biophysics

Kavli Institute for Particle Astrophysics and Cosmology (January 2003)
Stanford University/Stanford Linear Accelerator Center
Astrophysics, high-energy physics, cosmology

Kavli Institute for Brain Science (March 2004)
Columbia University
Neural circuitry and plasticity, mediation of complex behaviors

Kavli Institute for Brain and Mind (March 2004)
University of California, San Diego
Origins, evolution, and mechanisms of human cognition

Kavli Institute of Nanoscience (March 2004)
Delft University of Technology, Netherlands
Protein nanomachinery, molecular electronics, quantum information

Kavli Nanoscience Institute (March 2004)
California Institute of Technology
Nanobiotechnology, nanophotonics, integration of nanosystems

Kavli Institute for Nanoscale Science (March 2004)
Cornell University
Signal communication of cells, collective behaviors of nanostructures

Kavli Institute for Cosmological Physics (March 2004)
University of Chicago
Dark matter and energy, cosmology, neutrinos, and cosmic rays

Kavli Institute for Neuroscience (March 2004)
Yale University
Development, cellular organization, and function of the cerebral cortex

Kavli Institute for Astrophysics and Space Research (August 2004)
Massachusetts Institute of Technology
Space science, gravitational physics, dark matter and energy

SOURCE: ADAPTED FROM KAVLI FOUNDATION

A Physics Home Away From Home

The peach, orange, and mango tones are clues that Kohn Hall isn't your typical academic building. Then there are the light maple furniture and green carpeting, the wall-size Vermont slate blackboards, and the giant round windows in a hexagonal tower that glows like a lighthouse at night. In the New Age words of a promotional article, it is "a warm, inviting environment that simultaneously relaxes and alerts the visitor's mind." However, funding constraints are casting a chill inside the hall's cozy womb.

The building houses the Kavli Institute for Theoretical Physics (KITP), formerly known as ITP. Established in 1979 after a national competition, ITP was created for the community to use. "This was the first institute in physics based on visitors," says University of California, Santa Barbara, physicist Robert Sugar, part of the proposal team. "It was very controversial at the time."

But in its 25 years, the institute has grown to play a central role in the intellectual lives of most theoretical physicists. Scientists come by the dozens for "programs" on emerging topics that last from a few weeks to several months. They leave classes and committees behind to think and talk within the building's residential atmosphere. Recent programs ranged from the physics, chemistry, and mineralogy of Earth's interior to the intersection between string theory and strong nuclear interactions.

Warm retreat. Nobelist David Gross oversees a national physics institute housed in striking Kohn Hall.

"When people are here, they're in a different state," says astrophysicist Lars Bildsten, one of KITP's five permanent members. "You really see them get refreshed." Or in the words of astrophysicist Kip Thorne of the California Institute of Technology in Pasadena: "Thank god for the KITP."

With 1000 visitors each year, it's common to see cosmologists, string theorists, biophysicists, condensed matter physicists, particle theorists, and others forge new ties, Bildsten says. "Everyone higher up in the [academic] food chain talks about the importance of interdisciplinary research, and we say, 'Indeed. We have a model for that.'"

Fred Kavli entered the picture in 2001, when the Kavli Foundation awarded a $7.5 million grant to ITP. Now, Kohn Hall features more offices and dramatic new spaces thanks to a $6 million expansion funded out of the grant. Designed by the building's original architect, Princeton-based Michael Graves, the hexagonal tower is proving a popular meeting place. A newly enclosed outdoor courtyard—with the Vermont slate—has led to open-air chats. "Theoretical physicists are incredibly collaborative and interactive," says KITP director David Gross. "They don't need labs; they just need a blackboard."

The staff also webcasts and archives talks from a striking new auditorium, which seats 50 within tightly curved rows so that everyone can see everyone else. Fifteen ceiling microphones pick up every word, so some physicists have stifled their nasty asides, Bildsten jokes.

But Kohn Hall's new spaciousness also frustrates Gross, for he lacks the budget to take full advantage of it. Flat funding from the National Science Foundation has eroded KITP's abilities to support visitors and run programs. "We built this for the community," says Gross, "but now we are funds limited. I regard it as an outrageous, scandalous tragedy."

–R.I.

With just Auston and Kavli at the helm and a couple of support staffers, the foundation does not respond to unsolicited proposals. Rather, the two conduct dozens of site visits in search of what Kavli calls "winning science teams with the very best supporting organizations." From the leading candidates, they ask for simple proposals that strip basic mysteries to their essence: the links between cosmology and string theory, the nanomachinery of proteins in cells, the evolution of thought.

"If you applied for [federal] grants asking these questions, you would be laughed off," says neuroscientist Pasko Rakic of Yale University, director of the Kavli Institute for Neuroscience. "They want to know which subunit of which channel you want to study for the next 3 years. But [Kavli] wants to ask the big questions."

Auston and Kavli ask the host universities to support the institutes with more funds, infrastructure, faculty recruitments, and the like. Moreover, they expect researchers within each of the three themes to collaborate. In the near future, a grand assembly may involve all 10 institutes—soon to be 12, with the expected addition of others in Europe and Asia.

By all accounts, there is no pressure to do science in a "Kavli way." "Our initial reaction [to the new institutes] was a loss of uniqueness," says UCSB physicist Joseph Polchinski. "We all wondered, 'Are we now part of a chain?' But no, each of these Kavlis retains its unique identity." Indeed, Kavli seeks independent and strong-willed scientists who won't hesitate to plunge in unforeseen directions. In return, he asks only for periodic reports and occasional invitations to special programs.

The researchers are not as sanguine about the foundation's plan to bestow three $1 million Kavli Prizes, one within each theme, biennially starting in 2007. Auston and Kavli feel that a grand ceremony, possibly conducted in Oslo, eventually could rival the Nobel Prizes in public impact. But several at UCSB worry that the effort will land with a thud in the prize-heavy fields.

To the recipients of Kavli's largess, it's a minor point. "As a donor, he's a jewel," says physicist David Gross, KITP's director and one of the latest set of Nobel laureates. "He doesn't interfere. You hear a lot of horror stories with other donors. They give money and then lots and lots and lots of advice."

Ever the businessman, Kavli trusts his investments. His only advice is to keep working at the frontier toward a future he will not see and cannot imagine. "Fred wants this foundation to exist in perpetuity," says Auston. "He will dedicate his entire wealth to that goal."

–ROBERT IRION

CREDIT: BOB ELLIOT

Twisted Parasites From "Outer Space" Perplex Biologists

A bizarre group of parasitic insects challenges the biological rule book

The odd group of insects called twisted-wing parasites, or more formally Strepsiptera, is easily overlooked. Spending most of their lives hidden inside other insects, the majority of the 596 known species have been identified only from adult males caught during their brief mate-seeking flight. "These are really, truly enigmatic insects," says David Grimaldi, entomology curator at the American Museum of Natural History in New York City. "They break all the rules."

The differences between males and females of the same strepsipteran species are extreme. Adult males are small, flylike creatures, whereas most adult females resemble grubs and remain inside their host, merely protruding their fused heads and thoraces when ready to receive a male's sperm. In one strepsipteran family, males and females actually parasitize different kinds of insects. "Everything you find about them is like they came from outer space," says population geneticist J. Spencer Johnston of Texas A&M University in College Station.

Unlocking the secrets of how these strange parasites originated and how they maintain their bizarre lifestyle promises to deliver new insights in evolutionary and developmental biology, says Jeyaraney Kathirithamby, an insect evolutionary taxonomist at Oxford University in the United Kingdom. She and Johnston have recently turned up oddities in the strepsipteran genome and begun to tease out how the parasites survive within their hosts. Kathirithamby and researchers in Papua New Guinea have even enlisted Strepsiptera in the battle against important insect pests.

Quirky physical characteristics and lifestyle have made Strepsiptera tough to place in the insect family tree, notes Grimaldi. Some systematists group them with the beetles, others with flies. Grimaldi, however, has recently analyzed a primitive strepsipteran found in Cretaceous amber and says it doesn't resemble either flies or beetles. Meanwhile, he adds, molecular analyses of strepsipteran phylogeny have been "at best controversial."

The sequencing of a strepsipteran genome could resolve its phylogeny, but no organization has stepped forward so far to fund such an effort. Last month, however, a team led by Kathirithamby and Johnston reported online in *Insect Molecular Biology* that the strepsipteran *Caenocholax fenyesi* has the smallest documented genome of any insect. In still-unpublished work with graduate student Joseph Gillespie of Texas A&M, they also discovered that the ribosomal DNA of this species has a unique structure. "They're just so different from everything else," says Johnston.

Strepsipterans parasitize 34 families across 7 of the 32 orders of insects, most commonly wasps, bees, and Hemiptera (true bugs). The discovery last year that the larvae of one species, *Stichotrema dallatorreanum*, wrap themselves in a bag created from their katydid host's epidermis, thereby eluding an immune response, may explain how strepsipterans are able to parasitize such a wide range of hosts. But Kathirithamby and Johnston think it's possible that this strategy only evolved in the family Myrmecolacidae to which *S. dallatorreanum* belongs.

For most parasites, males and females prey upon the same host. Myrmecolacids are an exception: They are the only group of parasitic insects in which male and female larvae enter completely different hosts, notes Kathirithamby. The males parasitize ants, whereas females take up residence in crickets or grasshoppers. An intriguing question, says Kathirithamby, is whether myrmecolacid larvae start life sexless and only become male or female once they enter an ant or cricket. "To date, there is no organism that determines its sex by its host, but it makes sense to me," says Johnston. It's possible that a signal from the host sets off a cascade of sex-determining genes, he adds.

Studying sex determination in myrmecolacids is no easy task. The differences between the sexes have made it difficult to find the females and match them to males of the same species. Kathirithamby and Johnston scored a first last year when they used DNA analyses to match male and female specimens of *C. fenyesi* from Mexico.

At the same time, they discovered that there are significant differences between the DNA sequences of two genes in *C. fenyesi* males from Texas (which parasitize red imported fire ants) and identical-looking males from Mexico (which parasitize other ants). That suggests that these insects are actually separate species, or are on the verge of becoming so, because they have different hosts. "What is puzzling us is how this speciation is going on," says Kathirithamby.

Strange pair. Strepsipteran males (left) and females (right) look very different and, in one family, parasitize completely different hosts.

Understanding the basic biology of strepsipterans may prove useful in controlling insect pests, such as those ravaging coffee, rice, and oil palm crops. *S. dallatorreanum* is already a hit with oil palm growers in the Papua New Guinean island of West New Britain; since its introduction in 2000, it seems to have reduced katydid numbers and lessened oil palm damage.

Whether strepsipterans could also control U.S. red imported fire ants remains an open question. Jerry Cook, an entomologist at Sam Houston State University in Huntsville, Texas, has estimated that *C. fenyesi* is unlikely to be effective because it parasitizes only 1% to 2% of ants. Kathirithamby and Johnston think that this is an underestimate; in large fire ants, parasitism rates run as high as 55%, they say.

Still, Johnston acknowledges that the "funny biology" of strepsipterans may create a hitch. Fire ants naturally eat any insect in sight, including crickets, the most probable hosts of *C. fenyesi* females.

–FIONA PROFFITT

CREDITS: J. KATHIRITHAMBY

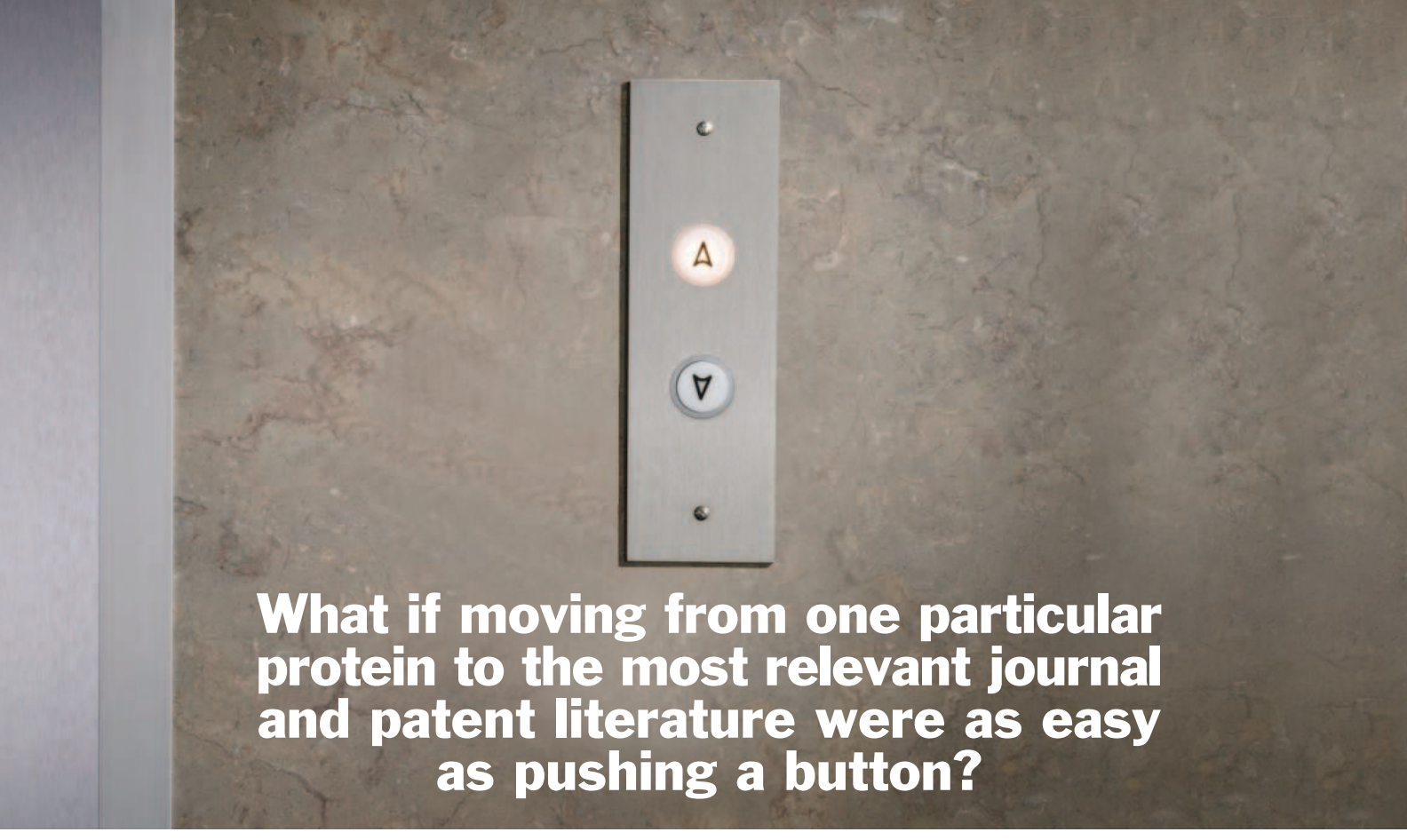

What if moving from one particular protein to the most relevant journal and patent literature were as easy as pushing a button?

It is.

Not only does SciFinder provide access to more proteins and nucleic acids than any publicly available source, but they're a single click away from their referencing patents and original research.

Coverage includes everything from the U.S. National Library of Medicine's (NLM) MEDLINE® and much more. In fact, SciFinder is the only single source of patents and journals worldwide.

Once you've found relevant literature, you can use SciFinder's powerful refinement tools to focus on a specific research area, for example: biological studies such as target organisms or diseases; expression microarrays; or analytical studies such as immunoassays, fluorescence, or PCR analysis. From each reference, you can link to the electronic full text of the original paper or patent, plus use citation tools to track how the research has evolved and been applied.

Visualization tools help you understand results at a glance. You can categorize topics and substances, identify relationships between areas of study, and see areas that haven't been explored at all.

Comprehensive, intuitive, seamless—SciFinder directs you. It's part of the process. To find out more, call us at 1-800-753-4227 (North America) or 1-614-447-3700 (worldwide) or visit www.cas.org/SCIFINDER.

SciFinder®

Part of the process.℠

CAS®

Using Scientific Assessments to Stave Off Epidemics

In devastated villages and refugee camps, aid workers are racing to stay ahead of and systematically block microbes that could prove as deadly as the tsunami

At least one early-warning system in Indonesia is in place and working. On the morning of 8 January, World Health Organization (WHO) officials in Banda Aceh received a call from a relief worker reporting a case of measles—one of the biggest potential killers of children during humanitarian disasters. The team confirmed it within hours; by afternoon, health officials and aid workers were able to vaccinate more than 1000 people in the sick child's village.

The danger is far from over: WHO estimates that only a quarter of the children in the Aceh area have received a measles vaccination. But the quick and effective response to this case—and another a few days later—is one example of the kind of science-based approaches that relief organizations are bringing to the region devastated by the tsunami, says Ronald Waldman of Columbia University, who helped coordinate WHO's team in Banda Aceh.

As soon as the extent of the tsunami's devastation became clear, WHO and relief agencies went into overdrive to try to prevent what all too often occurs in the aftermath of natural or human-made disasters: killer outbreaks of communicable diseases that can sometimes claim more lives than the original disaster itself. Ten years ago such efforts were well meaning but often ineffective and were considered secondary to providing food and housing. But a better understanding of the epidemiology of so-called complex emergencies has changed relief agencies' priorities. "The question is determining what can cause a large amount of death quickly and then ensuring that we prioritize our efforts accordingly," says Peter Salama, an epidemiologist and relief expert who works with UNICEF and USAID.

Paul Spiegel, a physician and relief expert with the United Nations High Commissioner for Refugees, credits Waldman with helping pioneer the use of epidemiology and other science-based assessments in disaster relief efforts. Waldman and Michael Toole, now of the Burnet Institute in Melbourne, Australia, published a 1990 study showing that vaccine-preventable measles infections had helped push the mortality rate of children in Ethiopian and Sudanese refugee camps to 60 times the normal rate. Even though measles is well known as a major child killer, the finding surprised many public health and aid agency workers, Spiegel says: "Before that, people just weren't looking that closely."

Now they are looking. Indeed, WHO identified disease surveillance, along with water and sanitation, as one of the top priorities for the tsunami-affected region. "The key issue here is to make sure we hear about the first 10 or 20 suspected cases" instead of the 200th, says Máire Connolly, who heads the Communicable Diseases in Complex Emergencies program at WHO. Aid workers need to be able to recognize the signs of the major killers and confirm a diagnosis as soon as possible, she says. One of the most notorious examples of a relief effort that failed is the 1994 epidemic of cholera and dysentery in a camp sheltering Rwandan refugees in Goma, Democratic Republic of Congo. The outbreak killed an estimated 50,000 people in 3 weeks. "If we had had [these techniques] in 1994," Connolly says, "it is possible we could have prevented that major outbreak."

The measles report in Aceh came the first morning after Waldman and his colleagues met with nearly two dozen relief organizations to hand out and explain the agency's standardized form—tailored to local conditions—for recording and reporting epidemic-prone diseases.

The forms ask workers to notify authorities of signs of potential killers in 10 categories: measles, cholera, dysentery, meningitis, malaria, acute respiratory infections, jaundice, hemorrhagic fevers, any fever of unknown origin, and any acute clusters of disease that can't be explained. Such surveillance will also pick up tetanus, Japanese encephalitis, and hepatitis A and E—as well as unknown killers that could emerge, Connolly says.

Many of the affected areas already had disease surveillance teams in place, says Aberra Bekele, medical director for UNICEF in Sri Lanka. In India, workers trained to immediately report any signs of polio are being tapped to watch for diseases such as cholera, typhoid, and malaria. In Sri Lanka too, Bekele says, efforts are focused on supporting the existing disease monitoring system and expanding it to include possible disaster-related epidemics. Ideally, he says, the efforts will leave behind a stronger system for the long term.

Preventive medicine. Health workers hope that mass vaccination campaigns will block any spread of measles in the Aceh region.

A crucial part of that system will be diagnostic labs that can quickly tell the difference between diarrhea caused by relatively benign viruses and that caused by deadly cholera, Connolly says, as well as perform immunological tests for hepatitis, Japanese encephalitis, and leptospirosis—a major concern following floods.

"We are better prepared than we would have been 5 years ago," Connolly says. "We now have refined tools for the early-warning systems. We have access to standard protocols for dealing with cholera. We have recommendations for what should be in a stockpile, what field workers should have in an investigation kit."

But to use those tools, relief workers must reach the people in need. In spite of intense efforts, the tsunami's destruction prevented aid workers from reaching the northwest coast of Aceh for nearly 3 weeks, leaving officials worried that preventable disease—especially malaria and leptospirosis—may be spreading. "I won't be satisfied until 100% of the population is reached," Waldman says. "There was a blind spot" along the coast, agrees David Nabarro, head of WHO Crisis Operations. But he is cautiously optimistic. "You can have an epidemic of an infectious disease anytime … until you have improved sanitation and a safe water supply," he says. But with the surveillance system now in place, "it would be very hard for a major outbreak to take root and cause mass mortality."

–GRETCHEN VOGEL

With reporting by Martin Enserink.

CREDIT: GETTY IMAGES

SAN DIEGO, CALIFORNIA—From 4 to 8 January, agile roaches, swimming robots, and digging reptiles demonstrated the synergy between robotics and biology.

Scurrying Roaches Outwit Without Their Brains

To an urbanite, it's a depressingly familiar scene: You flip on the light, and there's a cockroach, zipping across the cluttered countertops, scooting along a wall, and disappearing behind the sofa. Cockroaches are master escape artists. Two studies combining math, engineering, neurobiology, and biomechanics have begun to tease out the secret of this pest's success: conservative use of brainpower. According to the new research, a cockroach taps the brain when sticking close to walls but skips nervous system control during excursions across countertops and other uneven surfaces. "It can go on its own without a lot of sensory input," says Robert Full of the University of California, Berkeley, who led the work.

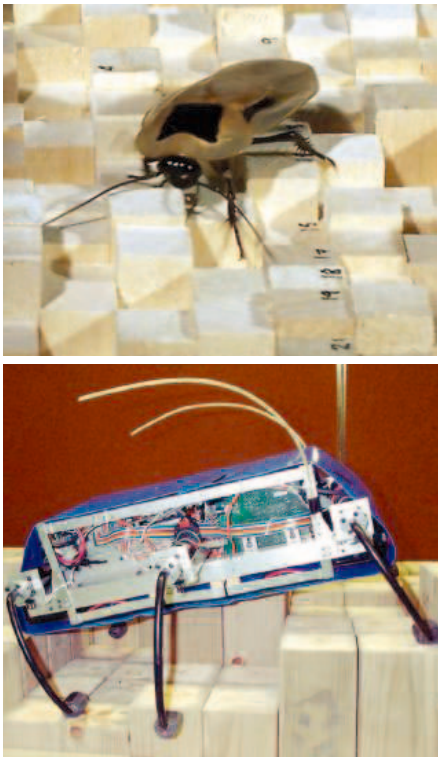

To think or not. On obstacle courses, cockroaches are on autopilot (upper). But this antennaed robot (lower) has shown that running along walls takes brains.

In 2002, as part of their effort to understand cockroach locomotion over flat surfaces, Full and his colleagues tied miniature cannons onto cockroaches' backs. When they fired the cannon to knock the treadmill-running insects off balance, the researchers discovered that the bugs seemed to recover too fast for their muscles to be controlled by nerves (*Science*, 6 September 2002, p. 1643).

To follow up, Simon Sponberg, a graduate student in Full's lab, tracked the neuromuscular activity of cockroaches as they scrambled through an insect-scale obstacle course. "We usually think about these complicated leg movements as being coordinated neuromuscular interactions," says John Bertram, a biomechanicist at the University of Calgary in Canada.

But that proved not to be the case. Sponberg's colleagues first used mathematical modeling to show that an insect relying on the natural springiness of its legs could run the obstacle course without peripheral nervous system guidance. Next, they modified the control program of a cockroach-inspired robot so that it ran without such guidance; it did fine on an obstacle course. Sponberg then monitored the electrical activity of cockroach leg muscles and the nerves working them as the insects sprinted across both flat and rough terrain. The pattern of electrical activity was the same on both terrains, indicating that no additional neural control is used to navigate complex environments, he reported at the meeting. The work "has revealed that the mechanical system [legs, etc.] is a complex, dynamic system with a mind of its own," says Devin Jindrich, a comparative physiologist at the University of California, Los Angeles.

Such independence simplifies locomotion, as the brain doesn't have to keep track of either the legs or the obstacles. If designed properly, robots too could conserve brainpower, adds Jindrich. "That allows you to free up control for other things that might be more difficult," he notes.

However, brainpower is crucial to running next to a wall, another typical behavior for cockroaches, says Noah Cowan, now an engineer at Johns Hopkins University in Baltimore, Maryland. Cowan recently blindfolded cockroaches, forcing them to use just their antennae for guidance. Using high-speed video of roaches running next to walls, he concluded that the insects monitor the bend of an antenna as it touches a wall. If the antenna bends back too much, the body is heading too close; when the antenna is straight, the insect is too far away. Sensing these differences, the brain signals muscles and adjusts the insect's orientation to the wall accordingly. When he gave an antenna-laden robot that capability, however, it didn't stay close to the wall at all.

After more observations of the live specimens, Cowan realized that a cockroach also factors in its speed. It determines velocity based on how quickly the antenna bends and unbends, input that adds another degree of control for the behavior. With that added feature, the robot excelled as a wall runner. "A combination of these two control systems was absolutely necessary," says Bertram. If only such understanding of how roaches use—or don't use—their brains would make us smarter about catching them.

With Flippers, Two Can Equal Four

Researchers trying to model how a beast that vanished millions of years ago swam through oceans have discovered that more isn't always better when it comes to flippers.

Intuitively, two pair of fins—as in those used by the large, extinct reptiles called plesiosaurs—would be faster than one pair. But then why do many modern aquatic animals usually use just two, with the other two limbs reduced in size or eliminated all together? Seals, for example, evolved from a four-legged terrestrial ancestor but now depend on just modified hind feet for locomotion. Similarly, sea lions use mainly their front flippers.

Using a robot, a team of engineers and biologists has begun to resolve not just how plesiosaurs swam but also the pros and cons of two versus four flippers. Their preliminary conclusion: Two limbs are good for a steady swimmer, and four are better for starts and stops, John Long, a vertebrate physiologist at Vassar College in Poughkeepsie, New York, reported at the meeting.

Long's colleagues Charles Pell, Brett Hobson, and Matthew Kemp of Nekton Research LLC in Durham, North Carolina, designed and built their robot over the past 9 months, dubbing it "Madeleine." She looks a little like a turtle and can swim forward or backward. Each side has a front and back "flipper"—flexible flaps that can move in sync or independently. The robot can roll and wiggle side to side as well as tilt its body up and down. "By simply turning on various combinations [of the fins], they can get different kinds of locomotion,"

CREDITS (TOP TO BOTTOM): SIMON SPONBERG; MARTIN BUEHLER/BOSTON DYNAMICS

Hang 10. Researchers are using this surf-swimming robot to learn about underwater locomotion.

says Frank Fish, a functional morphologist at West Chester University in Pennsylvania.

A computer onboard Madeleine lets the researchers determine the efficiency of locomotion in a way not yet possible in living organisms, says Adam Summers, a comparative physiologist at the University of California, Irvine: "It's not a good mimic of a truly biological system, but it provides a platform to understanding the mechanics of multiple [limbs]."

Long has now looked at the possible mechanics of swimming plesiosaurs, which plied the oceans between 248 million and 65 million years ago. Researchers have had different ideas about how these creatures' four flippers worked. To begin to characterize a plesiosaur's stroke, Long's team has varied the speed of the robot's flapping, the time between each stroke, and whether the fins worked independently or together as a twosome or foursome. "We asked the robot how might the [plesiosaur's] four limbs interact," says Long. They also compared those interactions against the dynamics of using just two limbs.

When Madeleine was swimming steadily, two fins were as good as four. "Adding fins did not produce faster [motion]," Long explains. Water swirling off the front fins interfered with the thrust provided by the second set, preventing any boost from the extra fins.

Four fins came in handy for starting and stopping, though. When the robot begins to swim, its front fins have not yet created any turbulence, enabling the back fins to work efficiently. And four fins were better at stopping than two, thanks to the added resistance created by the extra pair. Long suggests that plesiosaurs, with their four limbs, "may have been good starters and stoppers" who ambushed prey rather than chasing them down.

Robert Full, an integrative biologist at the University of California, Berkeley, worries that Long, Pell, and their colleagues' approach is too simplistic to reveal how plesiosaurs swam or even that two fins are better than four. He suggests that they need to do more mathematical modeling and make more of an effort to incorporate biological data into the robot's design.

But even with the robot's shortcomings, Summers has high hopes for Madeleine. "I'm very impressed," he says. "I think there are many more interesting questions ahead for this robot."

CREDITS (TOP TO BOTTOM): BRETT HOBSON/NEKTON RESEARCH LLC; A. DEUFEL/MINOT STATE UNIVERSITY

More Than One Way to Dig a Tunnel

Digging with one's nose is no small feat. Snakes and other legless animals do just that, typically relying on tough skulls, long slender heads, and strong trunk muscles to pound their way through soil. But researchers have recently found surprising exceptions, including a snake that tunnels by "wiggling" its nose and another reptile that uses its head but not its body to push forward. "We've had a lot of traditional ideas about how limbless animals burrow," says James O'Reilly, a functional morphologist at the University of Miami, Florida. "They all have to be revised."

Most legless burrowers are small, with tiny eyes and a narrow, pointy snout fused to the skull to form a battering ram. The shield-nosed cobra (*Aspidelaps scutatus*) doesn't fit that mold. It's small, about 50 centimeters long, but its eyes are large, its head is broad, and its snout is just loosely connected to the rest of the skull. In addition, it has a large, flat scale—the shield—at the tip of its nose. None of this hints at the snake's talent: "It doesn't look like it would be able to burrow," says Adam Summers, a comparative physiologist at the University of California, Irvine.

It digs quite well, however, just not the way people would have thought, Alexandra Deufel, a functional morphologist at Minot University in North Dakota, reported in San Diego. She put the shield-nosed cobra into an aquarium filled with moist sand and videotaped the snake's progress as it tunneled along the bottom.

The cobra's shield can move independently of the head, she found. To begin, the snake arches its neck, lays the shield flat on the ground, and moves its head from side to side, throwing the shield back and forth. The shield wiggles just slightly—about 10 degrees off center—but enough that it can shove a little dirt out of the way with each nod of the head. "That's a completely novel mechanism," says O'Reilly. Adds Summers: "It's awesome to see a snake that can wiggle its nose."

O'Reilly found a different digging strategy in a worm lizard, a reptile that is neither a snake nor a true lizard. Unlike most worm lizards, *Leposternon microcephalum* uses its head, with little help from its body, when traveling underground. "We were really surprised," O'Reilly says.

Normally an elusive study subject, hundreds of these worm lizards were recently captured by O'Reilly's Brazilian colleague Nelson Jorge da Silva of the Catholic University of Goiás as the creatures tried to escape the rising waters behind newly constructed dams. That allowed O'Reilly to study their digging habits more closely. For example, he set up a test tank where the reptile pushed against a force sensor as it tunneled through the soil. The worm lizard pounded its head against the soil around it, presumably to pat the soil down and make a clear path for the rest of the body. In most other legless dirt dwellers, the body provides the momentum that drives the animal forward. Typically, muscles along the body contract, bracing it against the sides of the burrow and enabling the head to ram into the dirt ahead. But *L. microcephalum* doesn't really have those muscles, O'Reilly and his colleagues found.

Instead, as researchers discovered when the worm lizard was placed in a very short artificial tunnel, the work is done by using muscles in the head. In such a setting, most limbless animals lose traction because their body needs walls to brace against—but not the worm lizard, which braces its skull against the burrow and thrusts forward and upward. "One of the most surprising [findings] is that these guys could generate all this force with virtually none of their body," says Summers. Now that's using your head.

–ELIZABETH PENNISI

Nosing along. Shield-nosed snakes depend on their "shields" to dig.

The Way Ahead™

in custom expression

Arabidopsis to Zebrafish.

Custom Array Solutions

Flexible, fast, affordable expression arrays as unique as your research. Let Affymetrix help you design custom microarrays for your #1 organism. We offer arrays with content ranging from 500 to 61,000 genes and new flexible formats so you can design experiments with as few as 10 custom arrays. With hundreds of completed designs, from prokaryotic gene expression to human genome tiling, we can deliver your custom product in 4-6 weeks. We've earned our stripes with the custom array program so you can focus on experiments, not microarray production.

www.affymetrix.com/genechip/custom • 1-888-DNA-CHIP (362-2447)
Europe: +44 (0) 1628 552550 • Japan: +81-(0)3-5730-8200

AFFYMETRIX®

Edited by Constance Holden

Scientists' Personalities

The results of the "first-ever psychological profile of life science researchers" indicate that most of them tend to be assertive ("leader") and data-oriented ("organizer"). Many are highly creative ("explorer"), but few belong in the "enthusiast" category, which seems to be a catchall for unambitious team players. Based on the usual polarities personality tests favor—that is, with many items revealing whether you are a logical versus intuitive thinker—the survey used a series of questions cooked up by the Science Advisory Board, a virtual community of biomedical researchers. (Take the test at scienceboard.net/s/s151/?u=99156290&p=3933EEC0)

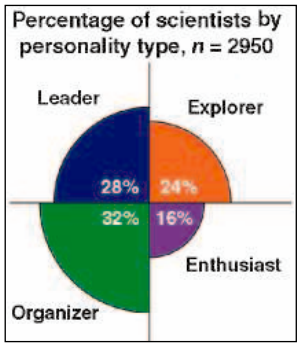

Unloading Biosphere

The Texas-based company that owns Biosphere 2 intends to sell the glass-enclosed facility designed to simulate Earth's environment. According to Martin Bowen, vice president of Decisions Investments Corp. (DIC), "we are seeking a right buyer who can keep the project going for the long term."

Built in the 1980s by Texas billionaire Edward Bass, Biosphere 2, located in Oracle, Arizona, was supposed to replicate in a closed environment various ecosystems found on Earth. Problems such as oxygen leaks frustrated those plans even after Columbia University took over managing the project in 1996. The school decided to walk away in 2003.

DIC won't reveal its asking price for the facility but says it is open to a joint venture. This spring the company and the National Academy of Sciences are hosting a meeting in Washington, D.C., with experts from the government and academia to discuss the future of the 1.27-hectare technological marvel. "We don't know what uses Biosphere 2 can have in the future," says Bowen. "That is something we want to explore."

Ring Around a Moon?

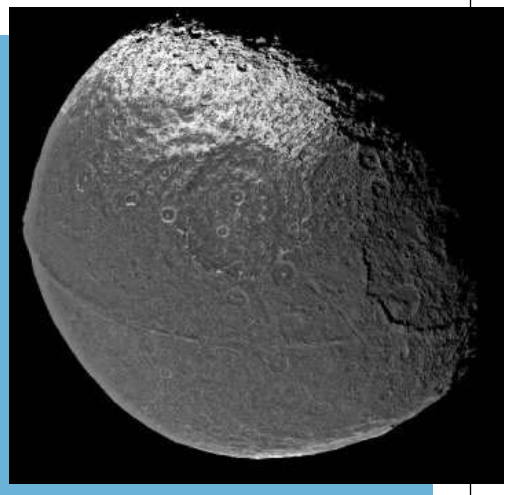

This is the closest picture ever taken of Saturn's moon Iapetus—a composite of images caught on New Year's Eve by the Huygens-Cassini mission to Saturn and its big moon Titan. It reveals for the first time a striking feature: a 20-kilometer-wide ridge, rising as high as 13 kilometers, that appears to girdle the planet almost exactly along its equator. It could be a mountain belt or it could be a crack through which subsurface material has welled up, according to NASA officials. But no one has an explanation for its regularity.

Iapetus, 1436 kilometers in diameter, holds other mysteries. Almost half the moon is a heavily cratered region called Cassini Regio that is covered with dark material that scientists haven't been able to identify—it could have erupted out of the moon's interior, but it also might be debris from impact events on other, dark satellites. Because the darkness gets spottier at the poles, the new image supports the notion that it's from fallout.

Gambling as Addiction

A new study lends support to what many experts believe—that compulsive gambling is like drug addiction.

Gamblers and drug addicts describe similar cravings and highs. To see if each group's brains have similar abnormalities, a team led by Christian Büchel, a neurologist at the University Medical Center Hamburg-Eppendorf in Hamburg, Germany, used functional magnetic resonance imaging to compare the brains of 12 compulsive slot machine players and 12 controls while both groups engaged in a simple gamble: choosing one of two face-down playing cards. They gained or lost a euro depending on whether the card was red or black.

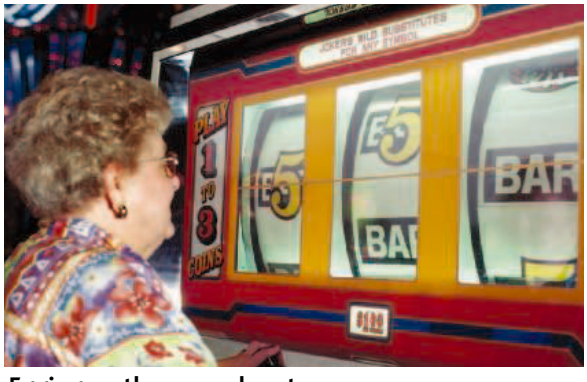

Egging on the reward system.

Büchel's team found that winners showed increased blood flow to the ventral striatum, a key part of the brain's reward system that involves the neurotransmitter dopamine. But the gamblers exhibited significantly less blood flow than did the controls, indicating a more sluggish reward system, the researchers report online 9 January in *Nature Neuroscience*.

The result fits with the notion that gamblers compensate for deficiencies in their brain reward systems by overdoing and getting hooked. Addiction researcher Eric Nestler, a psychiatrist at the University of Texas Southwestern Medical Center in Dallas, says this looks like the "tolerance" to reward seen in drug addicts that leads to the need for increasingly higher doses. But he says it would be useful to determine whether gamblers also experience "sensitization"—which involves greater responses to rewarding effects of the drug and which "may be the more critical feature" in addiction.

CREDITS (TOP TO BOTTOM): NASA/JPL/SPACE SCIENCE INSTITUTE; SCIENCE ADVISORY BOARD; ROYALTY-FREE/CORBIS

BRISTOL-MYERS SQUIBB

FREEDOM TO DISCOVER™

BRISTOL-MYERS SQUIBB SALUTES THE WINNERS OF THE FREEDOM TO DISCOVER™ AWARDS FOR DISTINGUISHED ACHIEVEMENT IN BIOMEDICAL RESEARCH

Winners from left to right are:

John Mendelsohn, M.D., *University of Texas M. D. Anderson Cancer Center, winner of the 27th annual Cancer Award;* **C. Ronald Kahn, M.D.**, *Joslin Diabetes Center and Harvard Medical School, winner of the 5th annual Metabolics Award;* **Hiroshi Nikaido, M.D.**, *University of California, Berkeley, winner of the 14th annual Infectious Diseases Award;* **Shaun R. Coughlin, M.D., Ph.D.**, *University of California, San Francisco, winner of the 14th annual Cardiovascular Award;* **Jan-Åke Gustafsson, M.D., Ph.D.**, *Novum, Karolinska Institutet, Stockholm, Sweden, winner of the 24th annual Nutrition Award; and* **Thomas C. Südhof, M.D.**, *University of Texas Southwestern Medical Center at Dallas, winner of the 17th annual Neuroscience Award*

In October 2004, the Bristol-Myers Squibb Freedom to Discover Awards for Distinguished Achievement in Biomedical Research were presented at the American Museum of Natural History in New York City. The winners were awarded $50,000 and a silver commemorative medallion. Awards are given each year to researchers who have made outstanding contributions to biomedical research in each of six areas: cancer, cardiovascular diseases, infectious diseases, metabolic diseases, neuroscience and nutrition.

Freedom to Discover is a philanthropic program of the Bristol-Myers Squibb Company and Bristol-Myers Squibb Foundation. The program provides no-strings-attached funding for biomedical research in six scientific fields in the form of unrestricted grants and distinguished achievement awards. Since its inception in 1977, Bristol-Myers Squibb has committed more than $110 million in support of the Freedom to Discover program, awarding 260 grants to more than 155 academic and medical research institutions in 23 countries.

For information about the Freedom to Discover program visit: www.bms.com/freedomtodiscover

Bristol-Myers Squibb Company

Hope, Triumph, and the Miracle of Medicine™

Edited by Yudhijit Bhattacharjee

AWARDS

Japan Prizes. Masatoshi Takeichi, director of the RIKEN Center for Developmental Biology in Kobe, Japan, and Erkki Ruoslahti of the Burnham Institute in La Jolla, California, will split this year's Japan Prize for cell biology. Makoto Nagao, president of Japan's National Institute of Information and Communications Technology in Tokyo, will receive the Information and Media Technology prize.

Takeichi (above, left inset) and Ruoslahti (right inset) made fundamental contributions toward elucidating the molecular mechanisms of cell adhesion, which could lead to new therapies for treating malignant tumors. Nagao (center left) is honored for his contributions to natural language processing, which paved the way for advances in machine translation of languages. Each prize is worth $475,000, an amount Takeichi and Ruoslahti will share.

JOBS

Adios. Two years after being fired as head of Spain's premier agency for basic research, theoretical physicist Rolf Tarrach has become rector of the University of Luxembourg.

Tarrach says his decision to join the 2-year-old institution was driven in part by his frustration with the Spanish bureaucracy, which he says stifles innovative research. "I never had sufficient freedom" to reform the archaic structures of the Spanish Higher Research Council, says Tarrach, who was fired from the agency in January 2003 after the government was criticized for its handling of the *Prestige* oil spill (*Science*, 31 January 2003, p. 637).

Tarrach hopes things will be different at the University of Luxembourg, a government-owned institution that he says is run like a private corporation. That should provide "more flexibility and ease" to execute new ideas, he says. Tarrach will be on unpaid leave from the University of Barcelona until the end of his 5-year term.

PIONEERS

Support group. Meeting other women at scientific conferences helped Maria Klawe get through graduate school in the male-dominated field of mathematics. Now, as dean of Princeton's engineering school, Klawe hopes that an exchange program starting in the spring of 2006 with the all-women's Smith College in Northampton, Massachusetts, will serve as a similar confidence booster for Princeton co-eds.

The initiative is part of a broader effort to increase the number of women in science and engineering at Princeton. Klawe hopes that some of Smith's undergraduates will want to go to engineering graduate school at Princeton after completing the semester-long exchange.

"When you meet lots and lots of people like you," she says, "it makes you feel that you are not weird."

CELEBRATING HISTORY

Vietnam's friend. Few people in France know his name. But French microbiologist Alexandre Yersin, who discovered the plague bacterium, is still revered in Vietnam, where he was sent by Louis Pasteur in 1891 and where he remained until his death in 1943. A new documentary film about Yersin's life that premiered this month in Paris depicts his devotion to public health and the simple life he led in the fishing village of Nha Trang. Those values make Yersin a "hero" and a "great humanitarian," says director Alain Tyr.

Change at AAMC. One of the top jobs in medical research and education policy will open up next year when nephrologist Jordan Cohen steps down as president of the Association of American Medical Colleges (AAMC). Cohen, who has led AAMC since 1994, completes his current term in June 2006.

Got any tips for this page? E-mail people@aaas.org

CREDITS (TOP TO BOTTOM): TOP INSET, THE BURNHAM INST.; SCIENCE AND TECHNOLOGY FOUNDATION OF JAPAN; UNIVERSITY OF LUXEMBOURG; CRAIG R. TERRY/PRINCETON UNIVERSITY

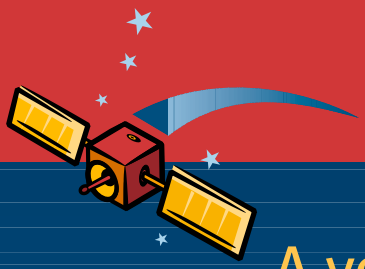

Thank you!

A very special "thank you" to all of the sponsors and supporters of the 2005 AAAS Annual Meeting.

SPONSORS

SUBARU

Premier Sponsor

National Science Foundation

L'ORÉAL USA

World Year of Physics 2005
www.physics2005.org

AFFYMETRIX

Pacific Northwest National Laboratory
Operated by Battelle for the U.S. Department of Energy

SUPPORTERS

- Apple Computer, Inc.
- Burroughs Wellcome Fund
- CommCore Consulting Group
- European Commission
- Merck/AAAS Undergraduate Science Research Program
- Monsanto
- Sandia National Laboratories
- SEED Magazine

AAAS
ADVANCING SCIENCE, SERVING SOCIETY

Letters to the Editor

Letters (~300 words) discuss material published in *Science* in the previous 6 months or issues of general interest. They can be submitted through the Web (www.submit2science.org) or by regular mail (1200 New York Ave., NW, Washington, DC 20005, USA). Letters are not acknowledged upon receipt, nor are authors generally consulted before publication. Whether published in full or in part, letters are subject to editing for clarity and space.

Revisiting the Taxonomic Impediment

WE READ WITH SOME FRUSTRATION THE RECENT Editorial and Letters concerning the "taxonomic impediment" (Q. D. Wheeler *et al.*, "Taxonomy: Impediment or expedient?", Editorial, 16 Jan. 2004, p. 285; "Taxonomists and the CBD," R. Geeta *et al.*, Letters, 20 Aug. 2004, p. 1105; "Museum collections and taxonomy," D. Causey *et al.*, Letters, 20 Aug. 2004, p. 1106). Geeta *et al.*'s claim that "developing nations… produce far fewer taxonomists than developed countries" is not true in much of Latin America, where a large proportion of research biologists are systematists. For example, Brazil has more systematic ichthyologists, entomologists, and botanists than most countries, due to a federal directive in the 1980s that trained new generations of specialists in cladistics. Undergraduate biology courses in Brazil emphasize not only zoology and botany but also cladistics and biogeography, more so than in American universities, which consequently produce fewer new systematists. But with meager employment prospects in morphological systematics in U.S. institutions and in the developed world generally, how could this be otherwise? This bleak prognosis has also affected U.S. collections (*1*), representing a "broader trend away from organismal biology" (*2*); the number of doctorates awarded yearly in botany and zoology is decreasing in the United States.

Unfazed, Geeta *et al.* further suggest that the United States must help overcome the taxonomic ignorance and "dearth of taxonomists" in biodiversity-rich countries. A globalization of taxonomy, like its economic cousin, may negatively affect taxonomic research where it is most needed—in developing nations, which should have a greater stake in biodiversity-related profits. This, in turn, depends on an efficient legal framework that discriminates basic research from biopiracy (*3, 4*). Developing countries should take the lead in funding research on their biodiversity (*5*); it will be their burden to protect it.

Wheeler *et al.*'s argument that taxonomists are not capable of efficiently providing species "identities" for ecologists, conservationists, and politicians is fallacious. This static, atheoretical view of species ignores their phylogeny and biogeography, and thus fails to consider relevant conservation priorities (*6*). Our notions of species and their relationships (taxa) are based on scientific theories subject to change; the identification of a species is also open to falsification. This is trivialized by conservationists, some molecular systematists (*7, 8*), and even by Wheeler *et al.*, who affirm that current taxonomic practices "are clearly inadequate for the challenge at hand." Descriptions of new taxa require theoretical, empirical, and epistemological rigor and seldom follow a time-frame judged appropriate to curtail the biodiversity crisis. This is not a "failure" of systematists but of those who regard taxonomy as only a "biodiversity-naming" service.

> **"A globalization of taxonomy, like its economic cousin, may negatively affect taxonomic research where it is most needed—in developing nations, which should have a greater stake in biodiversity-related profits."**
>
> –DE CARVALHO ET AL.

A disregard for long-established taxonomic practice, not considered cyber-enhanced enough (*7–10*), underscores our angst. We concur that "informatics… is not a substitute for science" (*11*), and that the "Big Machine" of molecular taxonomy will "do little to address the real problem" (*12*). Speeding up the pace of taxonomy through the Internet and technology, although desirable, is not enough to stimulate a growing taxonomic foundation. For this, systematics needs theoretical training, more professionals, a lasting commitment to collections, and recognition as a robust science by peers and policy-makers, without which taxonomy itself may fall victim to extinction.

MARCELO R. DE CARVALHO,[1] FLÁVIO A. BOCKMANN,[1] DALTON S. AMORIM,[1] MÁRIO DE VIVO,[2] MÔNICA DE TOLEDO-PIZA,[3] NAÉRCIO A. MENEZES,[2] JOSÉ L. DE FIGUEIREDO,[2] RICARDO M. C. CASTRO,[1] ANTHONY C. GILL,[4] JOHN D. MCEACHRAN,[5] LEONARD J. V. COMPAGNO,[6] ROBERT C. SCHELLY,[7] RALF BRITZ,[8] JOHN G. LUNDBERG,[9] RICHARD P. VARI,[10] GARETH NELSON [11]

[1]Departamento de Biologia (FFCLRP), Universidade de São Paulo, Avenida dos Bandeirantes 3900, Ribeirão Preto, SP 14040-901, Brazil. [2]Museu de Zoologia, Universidade de São Paulo, Avenida Nazaré 481, São Paulo, SP 04263-000, Brazil. [3]Departamento de Zoologia, Instituto de Biociências, Universidade de São Paulo, São Paulo, SP 05508-900, Brazil. [4]School of Life Sciences, Post Office Box 874501, Arizona State University, Tempe, AZ 85287–4501, USA. [5]Department of Wildlife & Fisheries Sciences, Texas A&M University, College Station, TX 77843–2258, USA. [6]Shark Research Center, South African Museum, 25 Queen Victoria Street, Post Office Box 61, Cape Town, 8000, South Africa. [7]Department of Ichthyology, American Museum of Natural History, Central Park West at 79th Street, New York, NY 10024–5192, USA. [8]Department of Zoology, The Natural History Museum, Cromwell Road, London, SW7 5BD, UK. [9]Department of Ichthyology, The Academy of Natural Sciences, 1900 Benjamin Franklin Parkway, Philadelphia, PA 19103, USA. [10]Division of Fishes, National Museum of Natural History, Post Office Box 37012, Washington, DC 20013–7012, USA. [11]School of Botany, University of Melbourne, Parkville, Victoria, 3052, Australia.

References

1. A. V. Suarez, N. T. Tsutsui, *BioScience* **54**, 1 (2004).
2. R. E. Gropp, *Systematics Biodiversity* **1**, 285 (2004).
3. A. C. Revkin, "Biologists sought a treaty; now they fault it," *N.Y. Times*, 7 May 2002, p. F1.
4. P. Rebêlo, "Brazilian officials destroy rare fish specimens," *SciDev.Net* (www.scidev.net), 25 Aug. 2004.
5. See www.fapesp.br (e.g., Programa Biota/FAPESP).
6. M. L. J. Stiassny, M. C. C. de Pinna, in *Systematics and Conservation Evaluation*, P. L. Forey, C. J. Humphries, R. I. Vane-Wright, Eds. (Clarendon, Oxford, UK, 1994), pp. 235–249.
7. D. Tautz, P. Arctander, A. Minelli, R. H. Thomas, A. P. Vogler, *Trends Ecol. Evol.* **18**, 70 (2003).
8. J. Mallat, K. Willmott, *Trends Ecol. Evol.* **18**, 57 (2003).
9. E. O. Wilson, in *Assembling the Tree of Life*, J. Cracraft, M. J. Donoghue, Eds. (Oxford Univ. Press, Oxford, 2004), pp. 539–544.
10. H. C. J. Godfray, *Nature* **417**, 17 (2002).
11. S. Knapp *et al.*, *Nature* **419**, 559 (2002).
12. R. Scotland, C. Hughes, D. Bailey, A. Wortley, *Systematics Biodiversity* **1**, 139 (2003).

A Clue to the Origin of the Bilateria?

IN THEIR REPORT "ORIGINS OF BILATERAL symmetry: *Hox* and *Dpp* expression in a sea anemone" (28 May 2004, p. 1335), J. R. Finnerty *et al.* deduce from expression patterns of *Hox* genes during development of the planula larva (their fig. 3) that the oral-aboral axis in the adult sea anemone *Nematostella vectensis* is homologous to the anterior-posterior axis (A-P axis) of adult arthropods and craniates. In his accompanying Perspective, "The ups and downs of a sea anemone" (p. 1255), P. Holland points out that a homolog of an "anteriorly" expressed *Hox* gene in the

anthozoan *Nematostella* is expressed posteriorly in the planula of the hydrozoan *Podocoryne* (*1*). This conflicting evidence may be resolved by assuming a "developmental reversal of spatial polarity" during hydrozoan metamorphosis (Finnerty *et al*. SOM).

Concerning this discrepancy, we want to point out that in acoel flatworms, which are regarded by some to represent the most basal extant bilaterians (*2*–*4*), the anterior pole of the A-P axis in the developing brain is separate from the developing mouth (*5*), as is the case in most bilaterians (*6*). The developing anterior pole and the A-P axis of the acoel *Convoluta pulchra* can be deduced from the formation of the primary muscle grid consisting of circular and longitudinal fibers (*7*, *8*). The mouth becomes visible after the primary muscle grid is established on the ventral side in the posterior third of the animal. The separate spatial origin of the mouth and anterior pole of the A-P axis is consistent with the planula concept for the origin of the Bilateria, in which triploblasts are derived from larval diploblasts (*9*, *10*), but is in conflict with the co-localization of the mouth and anterior pole as indicated by Finnerty *et al.*

However, the new *Hox* gene information from *Nematostella* brings into focus the opposing hypotheses, in which triploblasts are either derived from larval or from adult diploblasts (*11*–*13*). Spatial expression of homolog *Hox*/*ParaHox* genes (*14*) in embryos of acoel flatworms and similar data on basal scalidophorans (e.g., priapulids) with the brain encircling the mouth may bring us closer to solving the puzzle of the origin of the Bilateria, summarized by Hyman in the closing sentence of her famous "Retrospect": "Anything said on these questions lies in the realm of fantasy" [(*15*), p. 754].

REINHARD M. RIEGER, PETER LADURNER, BERT HOBMAYER

Department of Zoology and Limnology, University of Innsbruck, Technikerstrasse 25, Innsbruck A-6020, Austria. E-mail: reinhard.rieger@uibk.ac.at

References

1. N. Yanze *et al.*, *Dev. Biol.* **236**, 89 (2001).
2. I. Ruiz-Trillo *et al.*, *Proc. Natl. Acad. Sci. U.S.A.* **99**, 11246 (2002).
3. U. Jondelius *et al.*, *Zool. Scripta* **31**, 201 (2002).
4. M. J. Telford *et al.*, *Proc. R. Soc. London B* **270**, 1077 (2003).
5. J. Q. Henry *et al.*, *Dev. Biol.* **220**, 285 (2000).
6. C. Nielsen, *Animal Evolution: Interrelationships of the Living Phyla* (Oxford Univ. Press, New York, 2001).
7. P. Ladurner, R. Rieger, *Dev. Biol.* **222**, 359 (2000).
8. R. Rieger, P. Ladurner, *Belg. J. Zool. Suppl.* **1**, 27 (2001).
9. L. H. Hyman, *The Invertebrates, Vol. II, Platyhelminthes and Rhynchocoela* (McGraw-Hill, New York, 1959).
10. R. Rieger, P. Ladurner, *Belg. J. Zool. Suppl.* **1**, 27 (2001).
11. J. M. Turbeville, E. E. Ruppert, *Zoomorphology* **103**, 103 (1983).
12. G. Balavoine, *Am. Zool.* **38**, 843 (1998).
13. R. M. Rieger, *Am. Zool.* **34**, 484 (1994).
14. C. E. Cook *et al.*, *Evol. Dev.* **6**, 154 (2004).
15. L. H. Hyman, *The Invertebrates, Vol. V, Smaller Coelomate Groups* (McGraw-Hill, New York, 1959).

Response

RIEGER *ET AL.* FOCUS ON TWO QUESTIONS that are not directly addressed by the data in our Report: first, the evolutionary relationship of the mouth to the anterior-posterior axis, and second, the derivation of bilaterians from either a larval or an adult diploblastic ancestor.

On the basis of broad similarities in *Hox* and *TGF-β* expression between *Nematostella* and bilaterian metazoans, we argued that the bilateral symmetry exhibited by anthozoan cnidarians (corals, anemones, and their allies) is homologous to the bilateral symmetry exhibited by bilaterians. Our hypothesis implies a direct correspondence between the oral-aboral axis of cnidarians and the anterior-posterior axis of bilaterians. Furthermore, because *Nematostella* homologs of "anterior" *Hox* and *ParaHox* genes are expressed near the mouth, we suggest a correspondence between the oral end of cnidarians and the anterior end of bilaterians (*1*).

However, as Rieger *et al*. point out, a different relationship is suggested by the expression of an anterior *Hox* gene in the hydrozoan jellyfish *Podocoryne*: *cnox1-Pc* is expressed in a region of the planula larva corresponding to the future aboral end of the adult polyp (*2*). The evolutionary significance of this finding is unclear because (i) the expression patterns of *Hox* and *Hox*-related genes vary among hydrozoans (*1*, *2*), and (ii), in one instance, a *Hox*-related gene undergoes an axial reversal during the course of development in *Podocoryne* itself (*3*). This variability within and between hydrozoan cnidarians makes it difficult to reconstruct the spatial expression of *Hox*-related genes in the ancestral hydrozoan. It is therefore impossible to reliably extrapolate these hydrozoan data to the ancestral cnidarian or the cnidarian-bilaterian ancestor. In contrast, orthologous genes in *Nematostella* and the coral *Acropora*, two anthozoan cnidarians, tend to exhibit highly similar and presumably conserved patterns of spatial expression [our Report, (*4*)].

We argue that the mouth of most bilaterians is formed "in a region" close to the anterior end of the adult body plan. On the basis of paleontological evidence, an anterior terminal mouth is likely to be the ancestral condition for all ecdysozoans (*5*), and a composite circum-oral "brain" is a feature of virtually all invertebrate animals (*6*). With regard to the position of the mouth in acoels, the development of the primary muscle grid may or may not be associated with the position of the anterior pole. The only way to make such a statement about the embryological origin of any structure is to perform a detailed fate map, but such a fate map has been performed only for a single species of acoelomorph (*7*).

Finally, it is not clear if our data can distinguish whether triploblastic bilaterians arose from larval or adult diploblasts. Diploblasts (cnidarians and ctenophores) do not generate feeding larvae and the adult mouth arises only once, at the animal pole (also the site of first cleavage). In cnidarians, the mouth arises at the posterior pole of the swimming stage (planula). If *Nematostella* reflects the ancestral condition for the cnidarian-bilaterian ancestor, then most descendant organisms modified an axial system in which the mouth forms at the anterior pole.

MARK Q. MARTINDALE[1] AND JOHN R. FINNERTY[2]
[1]Kewalo Marine Laboratory, Pacific Biomedical Research Center, University of Hawaii, 41 Ahui Street, Honolulu, HI 96813, USA. [2]Department of Biology, Boston University, 5 Cummington Street, Boston, MA 02215, USA.

References
1. J. R. Finnerty, D. Paulson, P. Burton, K. Pang, M. Q. Martindale, *Evol. Dev.* **5**, 331 (2003).
2. N. Yanze, J. Spring, C. Schmidli, V. Schmid, *Dev. Biol.* **236**, 89 (2001).
3. L. M. Masuda-Nakagawa, H. Gröger, B. L. Aerne, V. Schmid, *Dev. Genes Evol.* **210**, 151 (2000).
4. D. C. Hayward *et al.*, *Proc. Natl. Acad. Sci. U.S.A.* **99**, 8106 (2002).
5. G. E. Budd, S. Jensen, *Biol. Rev.* **75**, 253 (2000).
6. E. E. Ruppert, R. S. Fox, R. D. Barnes, *Invertebrate Zoology. A Functional Evolutionary Approach* (Brooks/Cole-Thompson Learning, Belmont, CA, ed. 7, 2004).
7. J. Q. Henry, M. Q. Martindale, B. C. Boyer, *Dev. Biol.* **220**, 285 (2000).

CORRECTIONS AND CLARIFICATIONS:

Essays: "The scientific consensus on climate change" by N. Oreskes (3 Dec. 2004, p. 1686). The final sentence of the fifth paragraph should read "That hypothesis was tested by analyzing 928 abstracts, published in refereed scientific journals between 1993 and 2003, and listed in the ISI database with the keywords 'global climate change' (*9*)." The keywords used were "global climate change," not "climate change."

News of the Week: "Science agencies caught in postelection spending squeeze" (3 Dec. 2004, p.1662). The article contains an incorrect reference to Michael Marx's institutional affiliation. He is a professor of physics at Stony Brook University in New York.

HISTORY OF MEDICINE

For Many Approaches, Styles, and Aims

Xavier Bosch

Histories of medicine have thoroughly examined the development of medical theories and the treatment of diseases in Western culture. Less known are how different countries and cultures have approached their medical heritages and to what degree accounts of their medical histories have been influenced by social, cultural, and philosophical issues. Such investigation of the history of medical historiography is the main purpose of *Locating Medical History: The Stories and Their Meanings*, a collection of 20 essays developed from an international conference held in Maastricht, The Netherlands, in June 1999. The contributors largely concentrate on how the field of medical history established itself during the 19th and 20th centuries. Some chapters include discussions of such major personalities as Karl Sudhoff (the founding director of the first institute in medical history, at Leipzig) and Henry Sigerist (Sudhoff's successor, who later left Germany for Johns Hopkins, where he worked to professionalize the field of the history of medicine as well as to influence contemporary health policy). The volume also deepens to encompass examinations of the trend for medical histories to adapt social perspectives and the polarization between physicians interested in the development of medicine and Ph.D.'s interested in the social or cultural history of medicine.

Over the last two decades, medical history has thus become increasingly interesting to scholars with backgrounds in history rather than medicine. This development has facilitated the linking of the history of medicine to wider historical concerns, from politics to attitudes about gender within society to popular beliefs about health and the body. It has led to the publication of numerous specialized studies influenced by the new social history. Not surprisingly, some modern historians criticize standard books about the history of medicine on the grounds that these often pluck medicine out of its social and historical context and thus distort rather than explain the past.

The reviewer is in the Department of Internal Medicine, Hospital Clinic, University of Barcelona, Villarroel 170, 08036 Barcelona, Spain. E-mail: xavbosch@ub.edu

Locating Medical History
The Stories and Their Meanings
Frank Huisman and John Harley Warner, Eds.
Johns Hopkins University Press, Baltimore, MD, 2004. 519 pp. $45, £32. ISBN 0-8018-7861-6.

The volume opens with an overview of histories of medicine by the editors, medical historians Frank Huisman (Maastricht University) and John Harley Warner (Yale University). This introduction challenges currently common descriptions of "'traditional' medical history." Chapters in the first of the book's three major sections, "Traditions," examine the history of the field during the 19th and early 20th centuries.

The middle section, "A Generation Reviewed," explores how the history of medicine came to be approached more as a social enterprise than as a purely scientific or celebratory one. In their essay " 'Beyond the Great Doctors' Revisited," Susan Reverby and David Rosner point out that "as more and more of us entered the field in the late 1970s from the periphery, the center of gravity shifted away from traditional centers of research such as Johns Hopkins, the home of…the Institute of the History of Medicine, and spread more widely throughout the historical landscape."

To address such questions as how the professionalization of medical history has been reflected in changes in its literature and whether the discipline has moved closer to general social and cultural history, Olga Amsterdamska and Anja Hiddinga examined articles published between 1960 and 2001 in the four major history-of-medicine journals. Tracking trends in the citations in and of these articles, they conclude that medical history today is being written by historians rather than physicians and that the attention of its scholars has shifted "from heroic tales about individual physicians…to more…contextualized stories of professionalization and the everyday practice of medicine." They argue that professionalization "has taken a long time" and that shifts in topics are better described as a process of diversification than as a dramatic refocusing of attention. Contrary to their expectations, they also found that the audience for medical history is mainly physicians and medical researchers: A third of the citations to the five most highly cited papers from each journal for 1988 to 2000 were from medical journals such as *JAMA* and *The Lancet*. The citations in these journals were slightly more numerous than those in journals of medical history and much more numerous than those in general historical journals.

Detail from Diego Rivera's *The History of Cardiology* (1943–44). A fresco painted for the Instituto Nacional de Cardiologia, Mexico City.

"After the Cultural Turn," the volume's third section, "plunges into the methodological and political swamp of practices and controversies." As a clinician, I found particularly useful Jacalyn Duffin's chapter "A Hippocratic Triangle." Duffin, a clinician-historian, was asked by the editors to consider "history written and read by clinicians…and how it could be used in teaching." She argues that an M.D. degree is not a predictor for subject, method, or style and that there are only the individual fascinations of individual historians that enlighten other people. In contrast to historians' claims that teaching history to medical students is a waste of time because future doctors will never become real historians, she explains that teaching history to medical students "will make them better doctors.… History draws attention to organized reasoning. Learning a second language always enhances understanding of the first. I see no reason to skimp on content or on scholarship. All doctors will become historians of their own patients."

Locating Medical History more than succeeds as, in the editors' words, "an invitation to explore and reflect on a 'field'—one that can include widely disparate senses of what medical history is, should be, and should do." The volume contains several specialized and deeply theoretical essays intended for the medical historian, but any physician or researcher interested in the current status of the history of medicine will also enjoy and learn from it.

10.1126/science.1107232

PUBLIC HEALTH

Cutting World Hunger in Half

Pedro A. Sanchez and M. S. Swaminathan

The Millennium Project was commissioned by the United Nations Secretary-General to recommend the best strategies for meeting the Millennium Development Goals (MDGs) (*1*). In October 2002, the Hunger Task Force was established to determine how to meet the hunger MDG—to reduce the proportion of hungry people in half from 1990 to 2015. Task Force members came from diverse backgrounds in science, policy, the private sector, civil society, U.N. agencies, and government, with broad representation from developed and developing countries (2). After analysis, stakeholder consultations, and observation, the Task Force has just produced its report (*2*), which is summarized here.

Enhanced online at www.sciencemag.org/cgi/content/full/307/5708/357

Diagnosis

There are 854 million people in the world (about 14% of our population) who are chronically or acutely malnourished. Most are in Asia, but sub-Saharan Africa is the only region where hunger prevalence is over 30%, and the absolute numbers of malnourished people are increasing (3). More than 90% are chronically malnourished (*4*), with a constant or recurrent lack of access to sufficient quality and quantity of food, good health care, and adequate maternal caring practices. Acute hunger (the wasting and starvation resulting from famines, war, and natural disaster) represents 10% of the hungry yet receives most of the media coverage and attention. In addition, hidden hunger from micronutrient deficiencies affects more than 2 billion people worldwide. Chronic and hidden hunger deserve much more global attention and support.

Roughly 50% of the hungry are in smallholder farming households; 20% are the landless rural; 10% are pastoralists, fishers, and forest dwellers; and 20% are the urban hungry. The Task Force has identified hunger hot spots, defined as the subnational units where the prevalence of underweight children (*4*) less than 5 years of age is at least 20%. The 313 hunger hot spots identified (see the figure on page 358) indicate priority regions, as they cover 79% of the hungry.

The importance of different causes of hunger varies among regions. Low agricultural productivity is likely to be the primary reason in tropical Africa and remote parts of Asia and Latin America, whereas poverty and unemployment are the main causes in most of South and East Asia, Latin America, Central Asia, and the Middle East.

Economically, hunger results in annual losses of 6 to 10% in foregone Gross Domestic Product (GDP) due to losses in labor productivity. Economic growth alone is insufficient for eliminating hunger, because so many hungry people live in deep poverty traps, beyond the reach of markets (*5*). People affected by HIV/AIDS become unable to grow food or work for a living. Malnourishment weakens their immunity and strength, making them succumb more quickly to disease (*6*). Similarly, nearly 57% of malaria deaths are attributable to malnutrition (*7*). The challenge of halving hunger is, therefore, closely linked with that of achieving other MDGs.

Recommendations

The Task Force calls for simultaneous action at global (recommendation 1), national (recommendation 2), and local levels (recommendations 3 to 7) (see the figure on page 359).

1. *Move from political commitment to action.* A commitment to halving world hunger was made by all member countries of the United Nations at the World Food Summits of 1996 and 2001, the Millennium Summit of 2000, the 2002 World Summit on Sustainable Development, and the 2002 Monterrey Summit on Development Finance. The message for political leaders is that halving hunger is within our means; what has been lacking is action to implement and scale up known solutions.

The Secretary-General of the United Nations reinforced this message when he called for a "uniquely African green revolution for the 21st century" (*8*).

2. *Reform policy and create an enabling environment for hunger reduction.* Government policies in poor countries can make or break efforts to end hunger. Good governance, including the rule of law, low levels of corruption, and respect for human rights, is essential for achieving food security. Policies conducive to ending hunger and poverty need to be put in place at all levels, from the local to the national.

The Task Force proposes that poor countries integrate hunger reduction action plans into their Poverty Reduction Strategies or equivalent national planning process. Poor countries need to adopt a multisectoral approach to hunger reduction. African governments should invest at least 10% of their national budgets specifically in agriculture and nutrition, in addition to making investments in rural energy, infrastructure, health, education, and other sectors. Building capacity at all levels should be the central goal of national government and donor-funded activities. Linking nutritional and agricultural interventions, which are so often implemented separately, would be a powerful means of creating more effective hunger reduction programs.

Clearly assigned and enforceable rights for women to own, inherit, and trade land must be guaranteed. Women and girls need better access to services such as credit, health care, and education, as well as to technologies that will ease the workload of rural women, such as rooftop water harvesting and growing trees for firewood close to home.

Agricultural research has been a major driver of hunger reduction. The Task Force recommends doubling investments in national research to at least 2% of agricultural GDP by 2010. It also recommends that donors increase funding to the Consultative Group on International Agricultural Research to US$1 billion by 2010.

3. *Increase agricultural productivity of food-insecure farmers.* Small-scale farming families represent about half the hungry worldwide and probably three-quarters of the hungry in Africa. Raising the productivity of their crops, livestock, fish, and trees is a major priority.

Restoring soil health is often the first entry point for increasing agricultural productivity, because soil nutrient depletion is extreme in most areas where farmers have small holdings, as in Africa (*9*). Applying appropriate combinations of mineral and organic fertilizers, using leguminous green manures and agroforestry fertilizer trees, returning crop residues to the soil, and using improved methods of soil conservation can

P. A. Sanchez is at the Earth Institute at Columbia University, New York, NY 10964, USA. E-mail: sanchez@iri.columbia.edu; M. S. Swaminathan chairs the M.S. Swaminathan Research Foundation, Taramani, Chennai 600 113, India. E-mail: msswami@mssrf.res.in. The authors cochair the U.N. Millennium Project Task Force on Hunger.

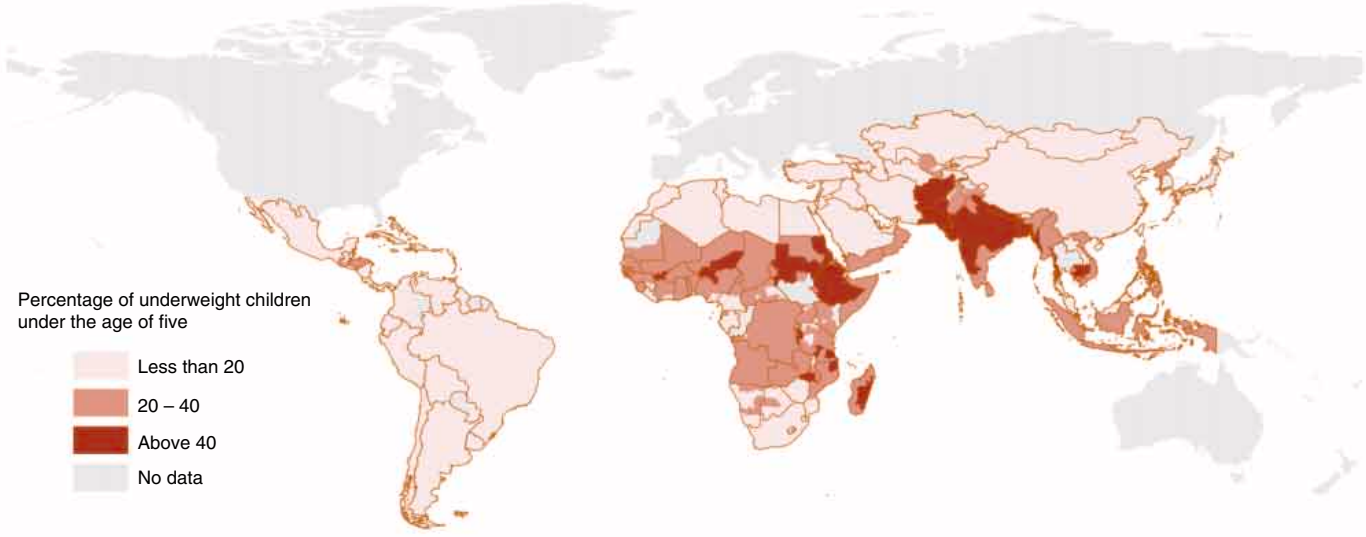

Hot spots of world hunger.

restore soil health and double or triple yields of the cereal staple crop. Making mineral fertilizers available at affordable prices and using them efficiently remain major challenges. As an emergency short-term measure, targeted subsidy programs should be designed to supply mineral and organic fertilizers (as seeds) to farmers. Tamper-proof "smart cards" redeemable at private agrodealers are one promising way of administering targeted subsidies, avoiding many of the pitfalls of past fertilizer subsidy schemes. When combined with similar vouchers for farmers to sell their products to school and community feeding programs, the demand side can be also addressed, avoiding price crashes when production increases.

In subhumid and semiarid areas, improving water management can be at least as important as improving soil fertility. Various water harvesting and small-scale irrigation techniques can be used to transform crop and livestock production in these regions. Investments in small-scale water management can also be financed with targeted subsidies.

The provision of genetically superior crop, pasture, tree, livestock, and fish germ plasm can greatly increase the productivity of small-scale farms. The Task Force supports both conventional breeding and transgenic research with appropriate biosafety measures. The traits that will benefit poor farmers in more marginal areas are tolerance to stresses (drought, salinity, poor soil fertility, pests, and diseases) and improved nutritional value. .

After farmers attain food security, they can begin to diversify their farming systems to produce high-value products. Livestock, farm trees, aquaculture, and vegetables are attractive options for diversifying their diets and sources of income. Increases in milk production, for example, can reduce malnutrition in rural and urban settings. In South Asia and Africa, farming systems integrating crops and livestock are very important in strengthening household nutrition and income. Small-scale farmers could emerge as major timber suppliers of the 21st century in many tropical regions.

Breathing new life into the moribund extension services of many poor countries is vital if the benefits of new knowledge and improved technology are to reach farmers. The Task Force recommends that every village in a hunger hot spot have paraprofessional extension workers trained in agriculture and nutrition, with counterparts in health and energy. They should be supported by professional services and enhanced research institutions.

4. *Improve nutrition for chronically hungry and vulnerable groups.* Adequate nutrition lies at the heart of the fight against hunger. As the primary care providers for children and families, women are particularly important in improving nutrition for vulnerable groups. Particular attention should be focused on children under the age of two and on supplemental feeding for pregnant and lactating mothers. The Task Force recommends that, where possible, locally produced foods be used, rather than imported food aid.

To break the intergenerational cycle of undernutrition, the Task Force recommends supplemental feeding for underweight pregnant women and nursing mothers. Exclusive breastfeeding up to 6 months of age is the best way of ensuring optimum nutrition for babies, although the decision may be complicated by the risk of transmitting HIV through breast milk.

To reduce malnutrition in children under five, the Task Force recommends providing fortified or blended supplementary foods, clean drinking water, and therapeutic care for all seriously malnourished children and women, especially in remote rural areas. Community extension workers should take the lead in raising awareness and implementation.

The Task Force recommends that malnutrition be reduced among school-age children and adolescents by providing free, nutritionally balanced school meals from locally produced foods for all poor children. This will improve learning, attract the 40% of primary school age children who are currently out of school in Africa (mostly girls), empower girls with good nutrition and knowledge before they become mothers, and create a steady demand for local foods. We estimate that if this is practiced in half of the primary schools in Africa, the local demand for maize alone could increase by as much as 25%. Systematic deworming; micronutrient supplementation; education about HIV/AIDS, health, nutrition, and hygiene; and provision of safe drinking water and take-home rations should be part of the program.

Vitamin and mineral deficiencies should be reduced by increasing consumption of micronutrient-rich foods such as fruits and vegetables; improving food fortification; and increasing micronutrient supplementation when necessary. Village extension workers should promote these mutually reinforcing actions.

Parallel health measures are also needed to eliminate the diseases that rob people of nutrients. All children should be fully immunized and receive prompt treatment for common infections such as diarrhea, pneumonia, malaria, and helminthes, as well as appropriate nutritional care provided for people living with or affected by HIV/AIDS.

5. *Reduce vulnerability of the acutely hungry through productive safety nets.*

While investing in agriculture, education, and health remains critical to long-term food security, past gains can be threatened if people's vulnerability to short-term disasters and shocks are not addressed. To address acute hunger, the Task Force recommends strengthening (i) national and local early warning systems to take advantage of advances in climate prediction; (ii) the capacity to respond to emergencies; and (iii) investments in productive safety nets (food for work; cash for work).

The Task Force recommends, whenever possible, the substitution of cash for program food aid, so that governments can invest more flexibly in reducing hunger. The additional resources needed to reduce vulnerability to shocks must not draw funds away from long-term development.

Safety nets should be both an effective protector of last resort during shocks and economically productive in years without crisis. This involves investing in community activities that reduce vulnerability while increasing productive potential. Large injections of cash or food aid can distort the local economy unless they are targeted toward development objectives.

6. *Increase incomes and make markets work for the poor.* Properly functioning markets are critical in ensuring that farmers are able to earn a decent income, obtain the inputs they need to raise crop yields, and sell their produce at fair prices.

The Task Force proposes that major investments be made in developing and maintaining market infrastructure. Markets will not develop without public investment in transport and communications. A major effort is needed to increase road building, including paved roads and all-weather feeder roads, in large parts of Africa where there is high prevalence of malnutrition. Every village should have a vehicle for transporting products to markets and health emergencies. Effective grain storage capacity at the local level would enable farmers to obtain fairer prices for their crop surpluses and would reduce postharvest losses to pests. Investments in small-scale processing should quickly yield benefits in terms of increased employment opportunities.

Networks of trained rural agrodealers are needed to allow essential agricultural inputs to reach remote areas, especially in Africa. Access to credit and other financial services is particularly problematic for food-insecure farmers. Community groups established to take on loans on behalf of their members could mitigate risk and make lending more attractive to financial institutions.

Lack of market information negatively affects the terms of trade for poor farmers. Governments and donors should continue investing in information technology, including combinations of mobile phones, radio, and the Internet to bring information to producers. For example, fishermen in India are now using mobile phones to seek the best price from dealers before deciding where to land their catch.

There are opportunities for increasing on-farm and off-farm income by encouraging farmers to switch part of their farms from staple food crops into higher value livestock, vegetable, and tree products and to add value through processing. Farmers can grow crops for large-scale producers. Supermarkets are becoming dominant buyers in much of the developing world. Governments should encourage them to pursue socially responsible policies and to stimulate local production.

7. *Restore and conserve natural resources essential for food security.* Degradation of natural resources directly threatens the food security and incomes of poor people. Reversing degradation requires both community- and national-level interventions. Local ownership, access, and management rights should be secured for forests, fisheries, and rangelands. Natural resource–based "green enterprises" should be developed. Poor farmers should be paid for environmental services they provide, including biodiversity protection, watershed stability, and carbon sequestration.

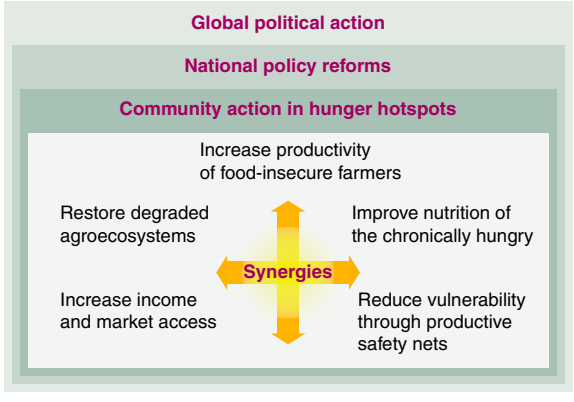

Hunger Task Force recommendations (*2*).

Entry Points

Community nutrition programs, homegrown school feeding programs, and investments in soils and water are local initiatives that can serve as "entry points" in the battle against hunger. A combination may constitute an attractive new integrated program in rural areas facing the dual challenge of high chronic malnutrition and low agricultural productivity. The increased local production will have a ready market in the homegrown feeding programs, and the joint facilitation by community extension workers will create a virtuous cycle. The resulting synergies will open the way for other interventions.

Resources Needed

The Millennium Project estimates that hunger reduction interventions to increase agricultural productivity and address chronic malnutrition will cost about 6 to 10% of the additional development assistance envisioned for attaining all the MDGs (*1*). That amounts to about $8 billion a year for 2005, between $10 and $11 billion a year for 2010–15, or an average of 60 U.S. cents per month for every person living in a developed country.

It Can Be Done

The Task Force concludes that the hunger MDG can be achieved by 2015 and hunger can eventually be eliminated. This will require focused and unprecedented levels of effort that are well within our financial and technological capability. Currently, more than 5.5 million children are dying of malnutrition-related causes each year. The actions outlined here, taken up by a broad coalition of stakeholders and applied in every poor country, can change that.

References and Notes

1. U.N. Millennium Project, *Investing in Development: A Practical Plan to Achieve the Millennium Development Goals: Overview* (Earthscan, London and Sterling, VA, 2005); available at www.unmillenniumproject.org/html/about.shtm.
2. U.N. Millennium Project, *Task Force on Hunger, Halving Hunger: It Can Be Done* (Earthscan, London and Sterling, VA, 2005); available at www.unmillenniumproject.org/html/tf2docs.shtm.
3. Food and Agricultural Organization of the United Nations (FAO), *The State of Food Insecurity in the World* (FAO, Rome, 2004).
4. A child is underweight if his/her weight is more than two standard deviations below the median of the international reference population used for analysis by the World Health Organization, the U.S. National Center for Health Statistics, and the Centers for Disease Control and Prevention.
5. J. D. Sachs *et al.*, *Brookings Pap. Econ. Act.* **1**, 117 (2004).
6. S. Kadiyala, S. Gillespie, *Rethinking Food Aid to Fight HIV/AIDS* (Food Consumption and Nutrition Division Discussion Paper 159, International Food Policy Research Institute, Washington, DC, 2003).
7. D. L. Pelletier *et al.*, *Bull. WHO* **73**, 443 (1995).
8. Secretary-General calls for "Uniquely African green revolution in 21st century to end the Continent's plague of hunger," U.N. Press Release; available at www.unmillenniumproject.org/html/addis/documents.shtm
9. P. A. Sanchez, *Science* **295**, 2019 (2002).
10. We acknowledge dedicated work of Task Force members and secretariat, particularly P. Dobie, N. Yuksel, L. Dreier, and R. Flor; superb leadership of J. Sachs and J. McArthur of the Millennium Project; and financial support from the Millennium Project Trust Fund, Canadian International Development Agency, U.K. Department for International Development, Earth Institute at Columbia University, Irish Development Council, Rockefeller Foundation, Swedish International Development Association, the World Bank, the World Food Program, and the U.N. Development Programme.

10.1126/science.1109057

MEDICINE

Treating Neurodegenerative Diseases with Antibiotics

Timothy M. Miller and Don W. Cleveland

It is difficult to overstate the impact of penicillin and the family of β-lactam antibiotics since their introduction into clinical medicine in the early 1940s. These drugs act by inhibiting assembly of the protective outer wall of bacteria. Their impact on the treatment of a wide variety of infections has been nothing short of miraculous. But this family of wonder drugs from the last century may have yet more untapped therapeutic potential, as Rothstein and colleagues report in a recent issue of *Nature* (*1*). They demonstrate that certain β-lactam antibiotics have potential as neurotherapeutics for treating neurological diseases such as amyotrophic lateral sclerosis (ALS), adult motor neuron disease, and ischemic injury.

The evidence for this remarkable finding has arisen from a unique public-private partnership between the National Institute of Neurologic Disorders and Stroke of the NIH and a consortium of disease-oriented philanthropic organizations, including the ALS Association, the Huntington's Disease Society of America, and the Hereditary Disease Foundation. This consortium sponsored a drug screening effort that ignored the hundreds of thousands of compounds within the traditional chemical libraries mined by pharmaceutical companies. Instead, the consortium screened 1040 bioactive compounds, 750 of which were already approved by the FDA for use in humans. These compounds were then tested for their efficacy in multiple assays associated with one or more neurological diseases by 27 separate academic laboratories.

The first insight to emerge from this approach (see the figure, panel A) was a surprising new function for 15 β-lactam antibiotics, including penicillin and a more modern variant, ceftriaxone, that enters the brain by crossing the blood-brain barrier. These antibiotics selectively induce transcription of the gene encoding the EAAT2 glutamate transporter; other classes of antibiotics do not have these effects. Glutamate is crucial for normal signal transmission between many types of neurons, including the motor neurons whose job is to trigger muscle contraction and whose premature death produces the progressive paralysis characteristic of ALS. Upper motor neurons extend processes from the brain into the spinal cord, where they form synaptic attachments directly with the lower motor neurons or indirectly through intermediate neurons. The axonal processes of the lower motor neurons extend out of the spinal cord and form connections with muscle. These neurons communicate with each other by release from the presynaptic cell of the neurotransmitter glutamate (see the figure, panel B), which then binds to receptors expressed by the lower motor neuron. Glutamate receptor activation triggers local membrane depolarization and generation of an electrical impulse that propagates down the full length of the neuron, where it stimulates release of another neurotransmitter that provokes contraction of the muscle. In the spinal cord, a non-neuronal supporting cell, the astrocyte, provides a key element in this signaling pathway—that is, a rapid off switch for the glutamate signal. It does this by juxtaposing a fingerlike projection adjacent to the synapse between the two motor neurons. On the surface of this projection are EAAT2 glutamate transporters, which are glutamate pumps that allow efficient recovery of released glutamate and hence rapid silencing of the glutamate signal.

Excessive glutamate levels in the synapse and associated repetitive firing of neurons results in excitotoxic injury to neurons, a fea-

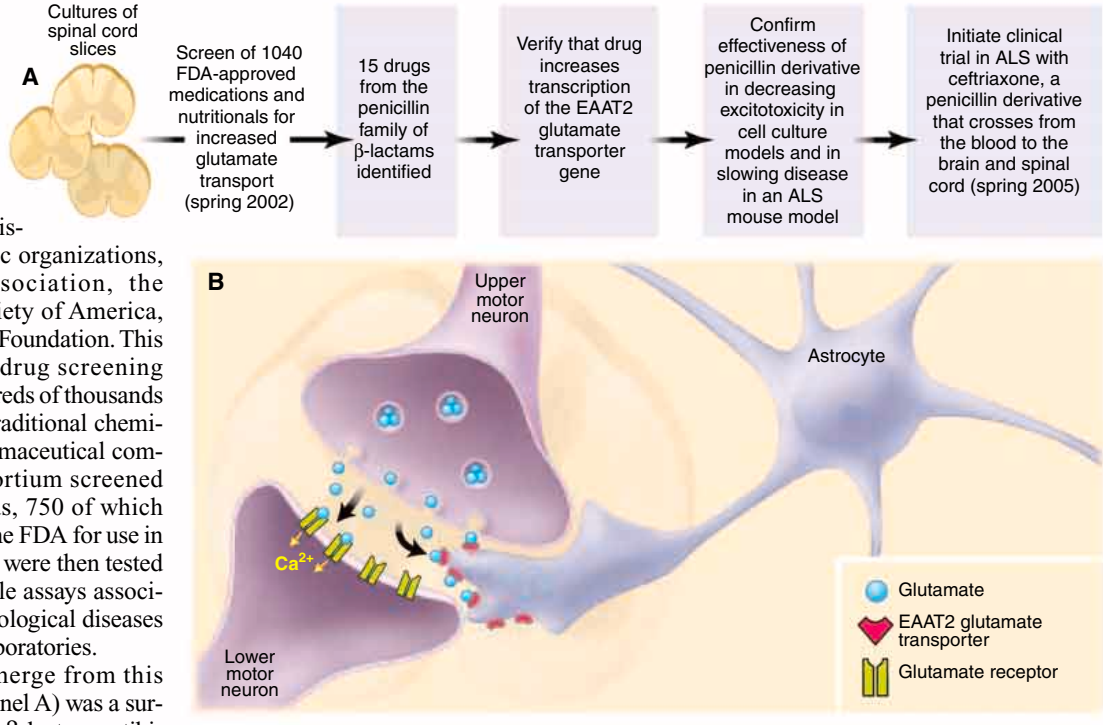

Reinventing the β-lactam heroes of the last century. (**A**) Rapid drug discovery by subjecting compounds already approved by the FDA to a battery of new biological screening assays. (**B**) Communication between motor neurons via the excitatory neurotransmitter glutamate. Glutamate released from the ending of one motor neuron binds to glutamate receptors expressed on the surface of a downstream motor neuron, triggering its activation. Excitotoxic damage results from excessive firing from these receptors, leading to the continued influx of calcium ions and resulting in neuronal injury. The glutamate transporter protein EAAT2 recovers synaptic glutamate such that glutamate neurotransmission is rapidly silenced and the neurons are protected from excess stimulation. Certain β-lactam antibiotics induce expression of the glutamate transporter, reducing the risk of excitotoxic damage to neurons.

The authors are at the Ludwig Institute for Cancer Research and the Department of Medicine and Neurosciences, University of California, San Diego, La Jolla, CA 92093, USA. E-mail: dcleveland@ucsd.edu

ture of many neurological disorders including stroke, spinal cord injury, and ALS (*2*). Excitotoxicity is one of the best links between the rare familial form of ALS (caused by mutations in the gene encoding superoxide dismutase) and the more common sporadic form of this disease (*3*). This realization came from studies in the early 1990s that showed increased glutamate in the fluid surrounding the brain and spinal cord of patients with sporadic ALS (*4*, *5*). Similarly, in a rat model of familial ALS, animals develop focal loss of the EAAT2 glutamate transporter in regions of the spinal cord that house motor neurons (*6*). Indeed, the only approved medication for treating ALS, the drug riluzole, is thought to act by limiting synaptic glutamate release. The effectiveness of this drug, however, has been disappointing, extending survival of ALS patients by a mere 3 months (*7*).

The remarkable discovery by Rothstein and co-workers offers renewed hope for a more effective therapy for ALS and other neurological diseases. A ceftriaxone-induced increase in expression of glutamate transporters by astroctyes enhanced the clearance of glutamate in spinal cord explants and, more important, slowed loss of muscle strength and modestly extended survival of ALS mice. Any benefit from increased glutamate clearance also extends to other types of neuronal damage with an excitotoxic component—for example, the damage that accompanies decreased blood flow typical of stroke (frequently referred to as ischemia). A ceftriaxone-mediated increase in glutamate clearance also decreased neuronal death induced by oxygen deprivation, at least in cell culture.

The encouraging preclinical data from the ALS mouse and other models of neurological disease have prompted a clinical trial combining all three phases. This is expected to begin this spring with a safety and efficacy study of ceftriaxone in the treatment of ALS. The data generated by the consortium represent a phenomenally quick turnaround from initial drug screening (started in early 2002) to actual use in patients. This reflects the major advantage of screening FDA-approved drugs whose safety profiles are already known. Even more encouraging for the Rothstein *et al.* findings are the excellent safety profiles of the β-lactam antibiotics in humans. Drug toxicity is costly and time-consuming to exclude and, in the end, is often the Achilles' heel that sinks the development of promising new therapeutics. In addition, spotting unwanted side effects is challenging even after undertaking multiple preclinical and clinical trials. This lesson was learned most recently with the realization of the increased risk of stroke and heart attack in people taking commonly prescribed anti-inflammatory drugs (*8*). Against this backdrop are the β-lactam antibiotics, first identified with the discovery of penicillin in 1928 and now among the most widely used modern pharmaceuticals. Although data about the safety of long-term ceftriaxone use still need to be collected, the best predictor of safety is a long history of safe use in humans. Our vast experience with short-term β-lactam antibiotic treatment predicts that very few problems should arise over the long term.

The discovery of new modes of action for the β-lactam antibiotic family offers two additional lessons for biomedical researchers. The first is unproven but predictable: A systematic screen of easily accessible chemical compounds already approved by the FDA may reveal common therapeutics with new potential applications. The second is more surprising: Some of these compounds may act by transcriptional induction of key proteins. Searching for transcriptional up-regulation is not an approach generally thought attractive in drug screening. With that in mind, last century's miracle drug, the β-lactams, may well rise to one of the big challenges of this century: slowing the progression of neurological diseases whose treatment has so far evaded the world's best efforts.

References

1. J. D. Rothstein *et al.*, *Nature* **433**, 73 (2005).
2. M. P. Mattson, *Neuromol. Med.* **3**, 65 (2003).
3. P. R. Heath, P. J. Shaw, *Muscle Nerve* **26**, 438 (2002).
4. J. D. Rothstein *et al.*, *Ann. Neurol.* **28**, 18 (1990).
5. J. D. Rothstein *et al.*, *Ann. Neurol.* **30**, 224 (1991).
6. D. S. Howland *et al.*, *Proc. Natl. Acad. Sci. U.S.A.* **99**, 1604 (2002).
7. L. I. Bruijn *et al.*, *Annu. Rev. Neurosci.* **27**, 723 (2004).
8. E. J. Topol, *N. Engl. J. Med.* **351**, 1707 (2004).

10.1126/science.1109027

GEOSCIENCE

The Boon and Bane of Radiocarbon Dating

Tom P. Guilderson, Paula J. Reimer, Tom A. Brown

Radiocarbon (^{14}C) dating (*1*, *2*) is widely used to determine the ages of samples that are less than about 50,000 years old. Natural radiocarbon is mainly formed in Earth's stratosphere through the interaction of neutrons produced by cosmic rays with 14-nitrogen. However, the rate of radiocarbon production is not constant (*3*), nor is its partitioning among the atmosphere, terrestrial biosphere, and oceans. After local corrections [see, for example, (*4*–*6*)], radiocarbon ages must therefore be calibrated to obtain ages on an absolute time scale (*7*). For decades, the radiocarbon community has adopted international calibration standards, most recently IntCal98 (*8*). Here, we discuss the inherent limitations faced when using radiocarbon dates to derive calendar ages.

From modern day to 11,800 years ago, IntCal98 is based on sets of tree-ring chronologies that each cover several thousand years and together provide an annually resolved, nearly absolute time frame. These data set a quality standard against which other proposed calibration datasets can be judged. Prior to 11,800 years ago, IntCal98 is based on marine data and contains additional assumptions and uncertainties associated with the translation of marine data into atmospheric radiocarbon values.

Here we examine how precisely calendar ages can be determined from individual radiocarbon dates. We focus on the tree-ring section of the IntCal98 calibration curve. Between 0 and 8000 years before the present (B.P.), the error in this curve is often less than 20 years, and—except for a few brief intervals—it is less than 30 years over the past 11,800 years. But as we will show, the range of statistically possible calendar ages, or calibrated age ranges, corresponding to any particular radiocarbon date can be larger or smaller, depending on where it falls on the curve.

We have linearly interpolated the IntCal98 curve at intervals of 20 calendar years and determined the radiocarbon dates that correspond to the calendar ages. We then calibrated these resampled radiocarbon ages using CALIB v4.4 (*4*) assuming an uncertainty of ±40 radiocarbon years, which is currently typical of routine dating (calibration 1). We performed a second calibration with a constant uncertainty of ±15 radiocarbon years, which is typical of the IntCal98 tree-ring data (calibration 2).

The calibrated age range waxes and wanes (see the first figure) as a result of variations in the atmospheric $^{14}C/^{12}C$ ratio. On average, the 1σ calibrated age range is 180 years (minimum 30 years, maximum 529 years) for calibration 1 and 140 years

The authors are at the LLNL Center for Accelerator Mass Spectrometry, University of California, Livermore, CA 94550, USA. T. P. Guilderson is also at the Institute of Marine Science and Department of Ocean Sciences, University of California, Santa Cruz, CA 95064, USA. E-mail: tguilderson@llnl.gov

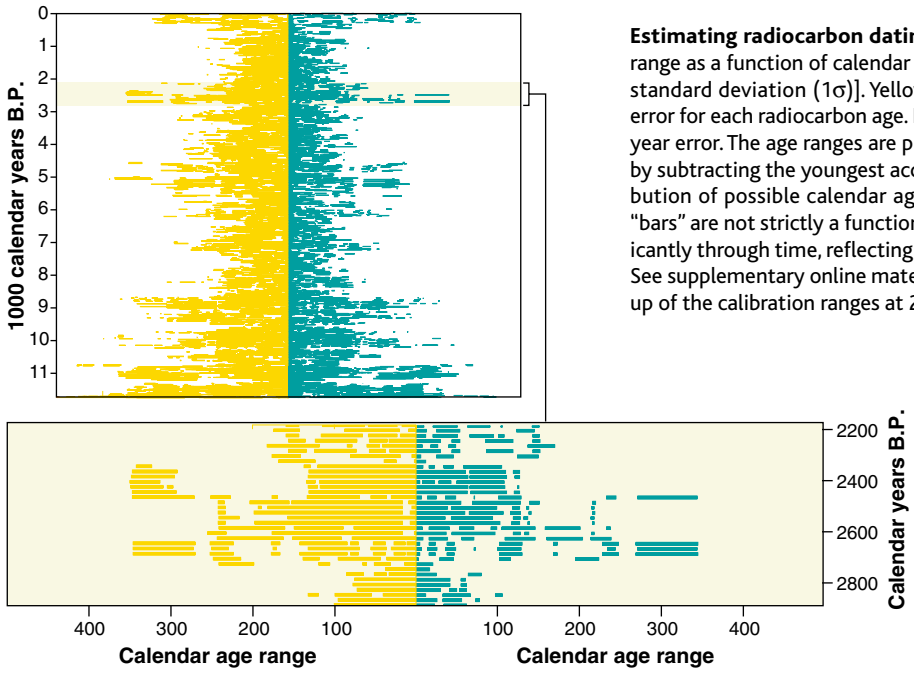

Estimating radiocarbon dating/calibration uncertainty. (**Top**) Calibrated age range as a function of calendar age and the uncertainty in the radiocarbon date [1 standard deviation (1σ)]. Yellow lines: Calibration 1, calculated with a ±40 year error for each radiocarbon age. Blue lines: Calibration 2, calculated assuming a ±15 year error. The age ranges are plotted against true calendar age and are calculated by subtracting the youngest acceptable age (1 standard deviation) from the distribution of possible calendar age ranges. The lengths of the calibrated age-range "bars" are not strictly a function of radiocarbon age/date precision but vary significantly through time, reflecting the strong influence of calibration curve "wiggles." See supplementary online material for the full calibration results. (**Bottom**) Close-up of the calibration ranges at 2200 to 2900 calendar years B.P.

(minimum 4 years, maximum 511 years) for calibration 2. During the most recent 500 years, the calibrated age ranges for calibration 2 are relatively low because single-year calibration data are available for that period, compared to the decadal calibration data for earlier sections.

The IntCal98 curve shows several "age plateaus" caused by variations in the atmospheric radiocarbon content. For the duration of such a plateau, the $^{14}C/^{12}C$ ratio fell at a rate equal to that of radiocarbon decay. For example, the "Golden Age of Greece" from 546 to 404 B.C. coincides with a radiocarbon plateau (~2450 radiocarbon years B.P.) that lasted nearly 350 years (see the second figure). Because of this plateau, the utility of radiocarbon dating in establishing chronologies for events between ~750 and ~400 B.C. is extremely limited. Two radiocarbon plateaus associated with the Younger Dryas (~11,900 to ~13,000 calendar years B.P.) have made it very difficult to determine whether climate change occurred synchronously across the globe during this period.

In fact, instances in which the calibrated age range is equal to or less than the analytical error in the radiocarbon age are relatively rare (<2%). Calibration of radiocarbon dates most often results in calendar age ranges that are much wider than indicated by the radiocarbon date uncertainties, resulting in an often underappreciated shortcoming of many paleoclimate time series: It is very difficult to determine absolute timing of events between independent paleoclimate records at the centennial level. Far too often, the interpretations of leads, lags, or synchronicity of paleoclimate records are not fully supported by the radiocarbon chronology.

Comparison of calibrations 1 and 2 shows that throughout much of the past 10,000 years, increased precision will reduce the calibrated age range by 20 to 50%, at least for high-quality terrestrial samples. For example, the 8200 calendar year age assigned from a Greenland ice core chronology (GISP-2) to a cold event that is widely recognized in circum-North Atlantic records (*9*) corresponds to 7410 radiocarbon years B.P. Calibration 1 then yields a calibrated age range of 8173 to 8325 calendar years B.P. (152 years), whereas calibration 2 gives 8167 to 8284 calendar years B.P. (117 years). The calibrated age ranges exceed one century because of a ~100-year plateau between 8300 and 8200 calendar years B.P.

The decreased calendar year age ranges that could be obtained from chronologies based on more precise radiocarbon dates could help to discern the temporal relationship between abrupt climate change and societal response. The collapse of the Akkadian Empire in Mesopotamia at ~3800 radiocarbon years B.P. (*10*) could then be calibrated to 4149 to 4231 calendar years B.P. (82 years, calibration 2), compared with 4093 to 4241 calendar years B.P. (148 years, calibration 1). Such increased precision could help to show when city-states in northern and in southern Mesopotamia were abandoned and perhaps to distinguish between climatic and societal effects.

But additional precision would not necessarily help to determine the relative roles of climate and society in the Terminal Classic Collapse of the Mayan civilization (*11*). The end of the collapse at ~1000 radiocarbon years B.P. (*12*) can be calibrated to 1003 to 1027 A.D. with calibration 2, but its beginning at 800 A.D. (~1190 radiocarbon years B.P.) yields roughly the same calibrated age range, 780 to 890 A.D., for calibrations 1 and 2.

Before 11,800 years ago, problems and difficulties still exist in deriving an accu-

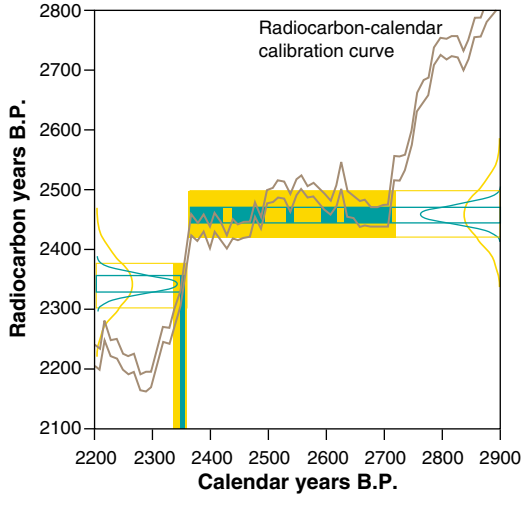

A calibration example. This is an example of the influence of a radiocarbon plateau on radiocarbon calibration. The curves are 1σ Gaussian probabilities of hypothetical radiocarbon ages with ±40 (yellow, calibration 1) and ±15 (blue, calibration 2) year error bars for 2340 (left) and 2460 (right) radiocarbon years B.P. The bars and pattern-fill show the regions of the calibration curve that are intercepted by the radiocarbon ages and their 1σ uncertainties. The intercept regions are projected onto the calendar year axis for the 2340 radiocarbon age to indicate the calendar year age ranges that would be obtained from the calibration process. The variations in the calibration curve dictate that for a 2340 radiocarbon date, it would be possible to derive a decadal-scale calendar year age range. In contrast, for a 2460 radiocarbon date, the derived age range would encompass several centuries irrespective of the uncertainty in the radiocarbon date.

rate radiocarbon year–calendar year calibration curve. This problem is particularly acute prior to the last glacial maximum (about 20,000 years ago). Several data sets from various natural sources have been proposed for calibration use, but no two data sets agree sufficiently to establish a consensus (*13*).

Scientists attempting to take advantage of the available IntCal98 calibration curve to establish subcentennial resolution chronologies must become more familiar with the calibration curve and its inherent limitations. In many circumstances, radiocarbon dates on a series of carefully chosen samples will allow considerable refinement of the derived calendar ages through constraints imposed by a priori information (such as stratigraphy) or by the pattern of the radiocarbon dates relative to calibration curve variations (an approach that is sometimes referred to as "wiggle-matching"). Even with the implementation of such methods, the establishment of reliable chronologies with centennial or better resolution will require substantial diligence and the devotion of appropriate resources to overcome the inherent limitations in the conversion of radiocarbon dates to calendar ages.

References and Notes

1. W. F. Libby, E. C. Anderson, J. R. Arnold, *Science* **109**, 227 (1949).
2. M. Stuiver, H. A. Polach, *Radiocarbon* **19**, 355 (1977).
3. M. Stuiver, P. D. Quay, *Earth Planet. Sci. Lett.* **53**, 349 (1981).
4. M. Stuiver, P. J. Reimer, *Radiocarbon* **35**, 215 (1993).
5. E. S. Deevey *et al.*, *Proc. Natl. Acad. Sci. U.S.A.* **40**, 285 (1954).
6. I. Hutchinson *et al.*, *Quat. Res.* **61**, 193 (2004).
7. M. Stuiver, H. E. Suess, *Radiocarbon* **8**, 534 (1966).
8. M. Stuiver *et al.*, *Radiocarbon* **40**, 1041 (1998).
9. P. M. Grootes, M. Stuiver, *J. Geophys. Res.* **102**, 26455 (1997).
10. H. Weiss *et al.*, *Science* **261**, 995 (1993).
11. D. A. Hodell *et al.*, *Science* **292**, 1367 (2001).
12. This simple exercise uses the tree-ring portion of the IntCal98 calibration curve. This portion is constructed entirely from Northern Hemisphere trees. However, the seasonal migration of the intertropical convergence zone will yield a mixture of Northern Hemisphere and Southern Hemisphere air in the tropics (*14*). The Northern Hemisphere–Southern Hemisphere difference averages 41±14 years between 1850 and 950 A.D. but varies from ~8 to ~80 years for any given decade (*15*).
13. P. J. Reimer, *Radiocarbon* **44**, 653 (2002).
14. J. A. Westbrook, T. P. Guilderson, P. A. Colinvaux, *IAWA Bulletin*, in press.
15. A. G. Hogg *et al.*, *Radiocarbon* **44**, 633 (2002).

16. This manuscript benefited from discussions with the IntCal 2004 and the MESH Abrupt Climate Change working groups. We thank B. Thunell for reviewing an early draft of this manuscript, and the criticisms and comments of two anonymous reviewers. Funding provided by the U.S. National Science Foundation's ESH Program (ATM-0407554) and the University of California's Lawrence Livermore National Laboratory (contract W-7405-Eng-48).

Supplementary Online Material

www.sciencemag.org/cgi/content/full/307/5708/362/DC1
Table S1

10.1126/science.1104164

CHEMISTRY

Short and Sharp—Spectroscopy with Frequency Combs

Thomas Udem

Ever since high-resolution laser spectroscopy was introduced as a way to study atoms and molecules, many experts in the field thought that only continuous ("single-mode") lasers can resolve narrow spectral features. Much work has therefore been devoted to the construction of spectrally pure single-mode lasers. These lasers work well at infrared and visible wavelengths, but they become troublesome in the near-ultraviolet and virtually impossible to realize for even shorter wavelengths, for example in the extreme ultraviolet (10 to 100 nm).

These short wavelengths can easily be accessed with pulsed lasers through the use of nonlinear interactions. The shortest wavelength to date has been achieved with a process called high harmonic generation (HHG). (Harmonics are integer multiples of a laser frequency, that is, integer fractions of its wavelength.) However, nonlinear interactions are efficient only with short laser pulses, which cause spectral broadening of the laser. The spectral width of the laser is roughly equal to the inverse pulse duration, yielding 10^{14} Hz for a 10-femtosecond (10^{-14} s) pulse (a typical pulse duration for HHG). This is far too wide for precision experiments, where a resolution of ~10 Hz has been reached (*1*, *2*).

The author is at the Max-Planck-Institut für Quantenoptik, 85748 Garching, Germany. E-mail: thu@mpq.mpg.de

On page 400 of this issue, Witte *et al.* (*3*) report an experiment that circumvents that limit. The trick is to use not just one pulse but a train of N coherent pulses. (This is similar to the interference of multiple light rays to form the spectrally narrow features of a grating.) The authors are not the first to record spectral lines that are narrower than the spectral width of a single pulse, but they are the first to use harmonics for that purpose.

The spectrum of a pulse train has an "envelope" that is given by the spectrum of a single pulse, but it is divided up into a series of fringes that are separated by the pulse repetition rate f_{rep} of the pulse train (see the first figure). The fringes are perfectly regular in frequency space if the pulses are perfectly regular in the time domain. The pulse train must be coherent, that is, the pulses must have a defined (nonrandom) phase relation to each other. This requirement is almost automatically fulfilled with a mode-locked laser. Such lasers emit pulse trains in which all pulses are copies of a single pulse. In the spectrum of a train of $N > 1$ pulses, the fundamental limit of the width of a single fringe is given approximately by f_{rep}/N. For a typical mode-locked laser, this is much smaller than the spectral width of a single pulse. For $N = 3$ and $f_{rep} \sim 70$ MHz, as used by Witte *et al.* (*3*), we expect a fringe width of 70/3 MHz = 23 MHz. Indeed, that is roughly the linewidth observed by the authors [see figure 3 of (*3*)]. It is still large compared to the requirements of high-resolution spectroscopy, but improvements by many orders of magnitude should be possible.

For these improvements to become a reality, one must shine more pulses on the atoms or molecules. In this case, the fringes turn into sharp spikes that can be as narrow as in a well-stabilized single-mode laser (*4*). Such a series of delta-shaped spikes is usually called a frequency comb and can be used to measure the frequency of any of the spikes relative to an atomic clock (a very

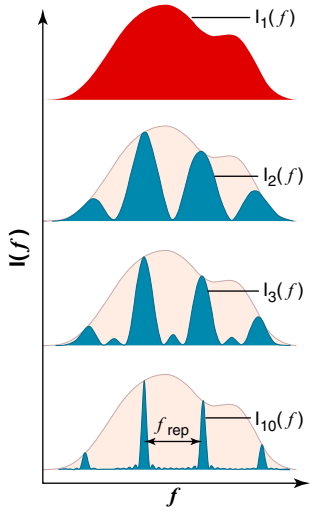

How to narrow the linewidth. The spectrum of a train of N pulses, $I_N(f)$, is shown schematically for some values of N. The single-pulse spectrum (red curve; repeated as a pink "envelope" in the subsequent spectra) is as broad as the inverse pulse duration. Multiple pulsing causes fringes (blue curves) with a linewidth of f_{rep}/N to appear. For a large number of pulses, the spectrum resembles a series of delta-shaped spikes, which are the modes of the frequency comb, that is, the modes of the laser. For a laser with f_{rep} = 100 MHz and a pulse duration of 10 fs, one expects 1 million modes (or fringes) to appear.

precise clock operating in the radio frequency domain).

In principle, it should be possible to apply many pulses in series to an atom or molecule, because a typical mode-locked laser emits ~70 million pulses per second. However, at room temperature, atoms or molecules tend to move out of the laser focus before they can be hit by a large number of pulses. This becomes even more of a problem if a harmonic of a laser is used, because these harmonics are usually of low power and must therefore be focused to a small spot size to obtain a reasonable intensity.

To date, spectroscopy with frequency combs has not reached the resolution of single-mode lasers. In an early experiment, Eckstein *et al.* reached a resolution of 4 MHz for the sodium 4s-4d transition (natural linewidth 1.6 MHz) (*5*). More recently, Marian *et al.* (*6*) and Snadden *et al.* (*7*) have performed comb spectroscopy on the two-photon 5s-5d transition of rubidium. The latter authors laser-cooled and trapped the atoms to keep them within the laser focus. The resulting linewidth approached the natural linewidth of 300 kHz (see the second figure). In contrast to Witte *et al.*, all these authors used the fundamental, not a harmonic, of a frequency comb.

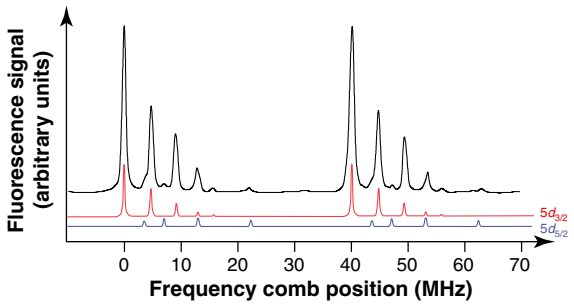

Probing the resonance frequencies with a frequency comb. The two-photon 5s-5d transition in ^{85}Rb breaks up into several components: For the 5s state, only the F = 3 hyperfine state is used. The 5d state first breaks up into two fine structure states, $5d_{3/2}$ and $5d_{5/2}$, which in turn break up into hyperfine components (red and blue curves). The black curve is the resonance fluorescence (shifted up for clarity) that is recorded as the frequency comb is scanned across the line. The two-photon excitation becomes possible whenever the frequency of two modes or twice the frequency of one mode coincides with the atomic transition. As a consequence, the two-photon absorption spectrum repeats at an interval of half the laser repetition rate (80.3 MHz in this experiment). Figure adapted from (*7*).

Despite these advances, single-mode lasers remain more suitable than frequency combs for spectroscopy—unless one uses harmonics of frequency combs where single-mode lasers are not readily available. This is what Witte *et al.* have now demonstrated with a train of three pulses of the fourth harmonic of a Ti:sapphire mode-locked laser (rather than with the femtosecond laser pulses themselves). Hopefully, we can expect the application of much higher harmonics with many more pulses to interesting atomic or molecular species. A whole new window for high-resolution spectroscopy thus opens. It might even become possible to use a single laser system to cover all wavelengths from the near-infrared to soft x-rays; this possibility is out of reach for single-mode lasers.

High-resolution spectroscopy in the extreme-ultraviolet regime would be very useful for investigating hydrogen-like ions. For these ions, the quantum electrodynamic contributions to the energy levels (Lamb shifts) become more important and can be determined more precisely. It might even be possible to create an optical clock that operates in the extreme ultraviolet regime. The stability of such a clock is proportional to the transition frequency in use, and would thus be very high.

References

1. E. Peik *et al.*, *Phys. Rev. Lett.* **93**, 170801 (2004).
2. R. J. Rafac *et al.*, *Phys. Rev. Lett.* **85**, 2462 (2000).
3. S. Witte, R. Th. Zinkstok, W. Ubachs, W. Hogervorst, K. S. E. Eikema, *Science* **307**, 400 (2005).
4. Ye. V. Baklanov, V. P. Chebotayev, *Appl. Phys.* **12**, 97 (1997).
5. J. N. Eckstein, A. I. Ferguson, T. W. Hänsch, *Phys. Rev. Lett.* **40**, 847 (1977).
6. A. Marian, M. C. Stowe, J. R. Lawall, D. Felinto, J. Ye, *Science* **306**, 2063 (2004); published online 18 November 2004 (10.1126/science.1105660).
7. M. J. Snadden, A. S. Bell, E. Riis, A. I. Ferguson, *Opt. Commun.* **125**, 70 (1996).

10.1126/science.1108159

ECOLOGY

A Leap for Lion Populations

Esa Ranta and Veijo Kaitala

There are substantial populations of lions in Africa and Asia. Despite being known as "the king of the jungle," the African lion is principally found on open savannas, with smaller numbers in woodland areas. Since the 1960s, the ecology of lions has been intensively studied in the Serengeti National Park of Tanzania in East Africa (*1*–*3*) (see the figure). Lions live in family groups known as prides. Both woodlands and plains prides of the Serengeti are typically composed of six related females, their cubs, and a few unrelated males who mate with the adult females. The females do most of the hunting for the pride (*1*), and they must hunt in groups to be successful. Most of the daily activity of males concerns maintenance of territory. Packer *et al.* (*4*) have completed a detailed analysis of long-term records of lion populations in a 2000-km^2 area of the Serengeti National Park. As they report on page 390 of this issue, lion population size has remained remarkably stable for long periods (10 to 20 years) punctuated by sudden increases that do not seem to reflect numbers of available prey.

The population dynamics (changes in the population size) of animals obey several key rules (*5*, *6*). Population increases are due to births of new individuals and arrival of immigrants from nearby populations, whereas any decreases are due to individuals dying or leaving their natal population. Often births and deaths are dependent on each other either directly or with an intervening time lag. Population increases also depend on the amount of resources that mature females are able to monopolize. However, Packer *et al.* now reveal an unusual feature of the population dynamics of Serengeti lions (*4*). They discovered that lion numbers, both in the woodlands and on the plains, undergo long periods of stability interrupted by abrupt changes. This is intriguing because no such saltatory changes in population dynamics are reported for lion prey such as wildebeest, Cape buffalo, and gazelle (*4*).

The authors are in the Integrative Ecology Unit of the Department of Biological and Environmental Sciences, University of Helsinki, FIN-00014 Helsinki, Finland. E-mail: esa.ranta@ helsinki.fi

CREDITS: (TOP) A. I. FERGUSON/UNIVERSITY OF STRATHCLYDE, UK; (BOTTOM) PRESTON HUEY/*SCIENCE*

Rather, the populations of these Serengeti prey species have changed without evidence of the dramatic leaps characterizing lion populations since the 1960s, when quantitative censuses began.

A straightforward expectation of predator-prey population dynamics is that a gradual change in resources (prey) would support a corresponding smooth change in predator population size (*6*). However, in Serengeti lions, the population increases have been abrupt often constituting an increase of 20 to 50% of the extant population size. The population records since the end of the 1960s include three saltatory changes (1973, 1983, and 1999) for lions inhabiting Serengeti woodlands and one (1997) for lions inhabiting the plains. In between these leaps, the lion population remained stable, hovering around the number reached during the previous increase.

Packer and his research team (*4*) now provide an explanation for these jerky dynamics by incorporating into their simulation model the social grouping behavior of lions within their prides. Serengeti lion prides have an optimal size: In the smallest prides, females have very low reproductive success, because hunting of their major ungulate prey calls for the cooperation of several individuals. In contrast, in the largest prides, females suffer from intense competition for the prey they have subdued jointly. When resources increase sufficiently to support more offspring and when the size of an extant pride is sufficiently large, the pride splits; several related females disperse together to form a new pride. Packer *et al*. suggest that it is optimal from an evolutionarily standpoint for a group of females to leave their pride and to establish a new pride with a different territory because this behavior ensures greater breeding potential. In this way, a gradual increase in prey population size supports a sequence of continued stability interrupted by abrupt increases in the abundance of lion populations.

The only major decrease (since the 1960s) in the population size of Serengeti lions occurred in 1994. The rapid decline (to 50% of the pre-1994 level) of woodland lions coincided with a decrease in the numbers of wildebeest and Cape buffalo due to a severe drought in that habitat. It is tempting to suggest that the collapse in lion numbers represented a reversal of the social mechanisms that result in punctuated increases in lion population size. A decrease in resources could have affected lion population size by reducing the number of prides in the overall population. However, this possibility cannot be verified because the 1994 decline in lion numbers was in fact due to an epidemic of canine distemper (*4*).

It is worth contrasting the population dynamics of Serengeti lions with the known dynamics of other species where long-term data are available (*6*). Whereas Serengeti lion population dynamics show saltatory changes in size, all other known predator-prey populations follow—with a time lag—a model in which smooth increases in prey availability result in smooth increases in predator population size. The best documented predator-prey populations display characteristic periodic fluctuations (*5*–*7*) that obey the standard models found in any population ecology textbook (*6*, *7*). One feature shared by traditional predator-prey models (*6*, *7*) and the Serengeti lion model of Packer *et al.* (*4*) is the presence of a time lag between changes in the population size of prey and that of predator.

The new data about Serengeti lion population dynamics (*4*) enriches our existing palette of predator-prey population patterns. One recent theory takes as a starting point the idea that individual behavior eventually has repercussions on long-term population ecology (*8*). The findings of Packer and colleagues support this view, although traditional population theories (*5*–*7*) have yet to incorporate the notion of social behavior into their models. The population dynamics of woodland and plains Serengeti lions are largely driven by the social structure of prides: To breed successfully, lionesses must belong to a pride that is sufficiently large (but not too large). Once a pride exceeds the optimal size, it splits with several females leaving to form a new pride. This leads to an increase in the lion population, presuming that sufficient resources are available to support the increase in offspring. We anticipate that behavior-based population models examining social behavior within populations and how these behaviors influence population growth will ultimately find their way into the analytical toolbox of population ecologists. The use of such models will help ecologists to better understand the dynamics of focal animal populations, and to provide more sophisticated management of threatened animal populations such as those of the Serengeti.

References

1. G. B. Schaller, *The Serengeti Lion* (Univ. of Chicago Press, Chicago, 1972).
2. A. R. E. Sinclair, P. Arcese, Eds., *Serengeti Past and Present. Serengeti II: Research, Management and Conservation of an Ecosystem* (Univ. of Chicago Press, Chicago, 1995).
3. Serengeti Park (www.serengeti.org).
4. C. Packer *et al.*, *Science* **307**, 390 (2005).
5. T. Royama, *Analytical Population Dynamics* (Chapman & Hall, London, 1992).
6. P. Turchin, *Complex Population Dynamics: A Theoretical/Empirical Synthesis* (Princeton Univ. Press, Princeton, NJ, 2003).
7. A. Berryman, Ed., *Population Cycles: The Case for Trophic Interactions* (Oxford Univ. Press, Oxford, 2002).
8. W. J. Sutherland, *From Individual Behaviour to Population Ecology* (Oxford Univ. Press, Oxford, 1996).

10.1126/science.1108599

MEDICINE

Visfatin: A New Adipokine

Christopher Hug and Harvey F. Lodish

The developed world has been engulfed by a rapid rise in the incidence of obesity and diabetes. One hypothesis for the marked prevalence of obesity posits that selective evolutionary pressure favored those of our ancestors who were able to store excess food in the form of triglycerides, the primary component of adipose (fat) tissue. Unfortunately, what may have been an advantage eons ago is now manifest as a rapidly expanding waistline. The increased incidence of obesity and diabetes carry many sequelae, collectively known as the metabolic syndrome or syndrome X. Such sequelae include an increased risk of cardiovascular and kidney disorders as well as breast cancer, hepatocellular carcinoma, and Alzheimer's disease. How these and other conditions are related to the multiple defects in energy metabolism associated with diabetes and obesity is a major focus of current research efforts. An emerging theme is that adipose tissue, found in several locations throughout the body and long thought to be primarily a repository for triglycerides, is also important for regulating homeostasis and metabolism. Fat is an endocrine tissue and, indeed, may constitute the largest endocrine organ in the body (*1*, *2*). Several hormones, called adipokines or adipocytokines, are synthesized by adipose tissue. These include adiponectin, tumor necrosis factor–α (TNF-α), leptin, resistin, and adipsin (see the figure). To be added to the list, as Fukuhara *et al*. report on page 426 of this week's issue (*3*), is a presumed new member of the adipokine family, visfatin.

Certain attributes of visceral fat, the adipose tissue surrounding abdominal organs,

The authors are at the Whitehead Institute for Biomedical Research, Cambridge, MA 02142, USA, and the Department of Biology, Massachusetts Institute of Technology, Cambridge, MA 02142, USA. C. Hug is also in the Division of Respiratory Disease, Children's Hospital, Boston, MA 02115, USA.

make its accumulation more worrisome than the accumulation of subcutaneous fat, which resides below the skin. Such concerns include an association of increased visceral fat with the metabolic syndrome, enhanced secretion of TNF-α and other proinflammatory adipokines, and reduced secretion of antidiabetic and anti-inflammatory adipokines relative to those secreted by other fat depots (*4*). Using differential display of expressed genes in visceral fat and subcutaneous fat obtained from two female volunteers, Fukuhara *et al*. (*3*) identified a molecule that is expressed at much higher levels in visceral fat than in subcutaneous fat. This molecule, denoted visfatin to indicate its abundance in visceral fat, turns out to have been already identified as a growth factor for early B cells called pre-B cell colony-enhancing factor (PBEF) (*5*). Adipose tissue and cells of the immune system are known to express many of the same genes; indeed, some researchers have postulated that adipose tissue may serve not only to coordinate metabolic pathways in the body but also to coordinate immunological responses (*6*).

Fukuhara and colleagues analyzed the relationship between serum visfatin levels and the amount of visceral and subcutaneous fat in humans and in several mouse models of obesity and diabetes. They found that visfatin levels in serum increased in parallel with visceral but not subcutaneous fat in both mice and humans. To address the importance of visfatin beyond it's known effect on B cells, Fukuhara *et al*. used recombinant visfatin produced by transfected cultured cells and purified from culture medium. The primary amino acid sequence of visfatin does not include a signal sequence, although Fukuhara *et al*. did detect low serum concentrations of visfatin indicating that this adipokine may be secreted; this observation was also made by the investigators who originally described PBEF (*5*). Other researchers working on PBEF, however, have found this cytokine primarily in the cell nucleus and cytoplasm, which suggests that visfatin's putative role as a secreted protein involved in metabolism should be interpreted with caution (*7*). Rongvaux and colleagues have characterized murine PBEF as an intracellular nicotinamide phosphoribosyl-transferase and have demonstrated that PBEF can rescue a mutant bacterium deficient in this enzymic activity (*8*). Precedent exists for secreted proteins lacking a signal sequence, such as the cytokine interleukin-(IL)-1β, although these examples represent the minority of secreted proteins. Inhibition of the secretory pathway in adipocytes did not seem to affect secretion of visfatin, raising the possibility that this hormone is released during lysis of fat cells rather than being secreted (*8*).

To address the ways in which visfatin could be involved in metabolism, Fukuhara *et al*. injected recombinant visfatin into KKAy obese mice (a model of type II diabetes where the mice become obese at 6 to 12 weeks of age) and mice rendered diabetic by injection of streptozocin. They observed a decrease in the concentration of plasma glucose in both mouse models similar to that induced by injection of insulin, suggesting that visfatin may be an insulin-mimetic. Chronic supplementation of visfatin in these mice (achieved by infecting animals with an adenoviral vector carrying the visfatin gene) resulted in a slightly reduced concentration of plasma glucose and a decrease in insulin levels. These effects were greater in obese KKAy mice than in wild-type mice. Next the investigators showed that mice heterozygous for a targeted mutation in the visfatin gene had elevated plasma glucose levels, both while fasting and after feeding, and exhibited a small defect in a glucose tolerance test. (Mice lacking both copies of the visfatin gene die in utero.)

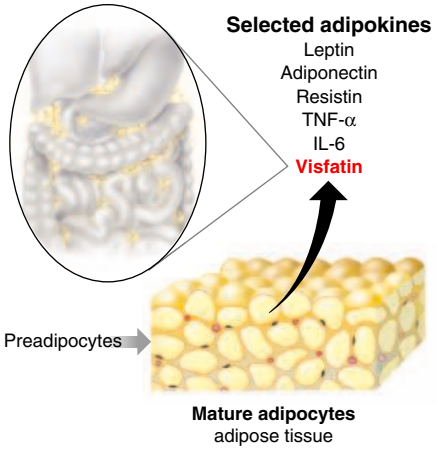

The adipokine family. The differentiation of preadipocytes into mature fat cells is accompanied by the expression of genes encoding hormones that regulate the metabolism of fats and sugars. Three of these hormones—TNF-α, resistin, and IL-6—induce resistance to insulin, the principal hormone that regulates blood glucose levels. TNF-α is a proinflammatory cytokine that suppresses expression of adipocyte-specific genes; resistin maintains blood glucose levels during fasting; and IL-6 production increases in those with obesity and diabetes. Adiponectin and visfatin are adipokines that work synergistically with insulin to enhance glucose uptake and metabolism in muscle and to block glucose formation (gluconeogenesis) in liver. Adiponectin activates AMP-activated protein kinase (AMPK), modulates signaling pathways controlled by the master transcription factor NF-κB, increases β-oxidation of fatty acids by muscle, protects endothelial cells, and is reduced in diabetic or obese individuals. Visfatin, the newly characterized hormone secreted by visceral fat, binds to the insulin receptor at a site separate from insulin and acts as a natural insulin mimetic. Leptin activates AMPK, acts centrally and peripherally to regulate metabolism and to reduce food intake, and is reduced in individuals with rare genetic obesity disorders.

Like insulin, visfatin stimulates glucose uptake by cultured adipocytes and muscle cells and suppresses glucose release by cultured hepatocyes (liver cells). Visfatin, like insulin, also induces phosphorylation of signal transduction proteins that operate downstream of the insulin receptor. Most intriguing of all, Fukuhara *et al*. show that visfatin binds to the insulin receptor but does not compete with insulin, suggesting that the two proteins bind to different sites. That this is the case is confirmed by the observation that visfatin binds tightly to a mutant insulin receptor with reduced affinity for insulin. The 3 nM affinity of visfatin for the wild-type insulin receptor is similar to that of insulin, suggesting that this interaction may have physiological relevance. However, the lower serum levels of visfatin, compared to those of insulin, and the fact that visfatin levels do not change after feeding imply that the hypoglycemic effects of visfatin may not be of physiological importance. There are other noninsulin molecules that activate the insulin receptor, notably membrane-permeable small molecules that bind to intracellular domains of the receptor and stimulate activity (*9*). These findings have spurred development of an orally bioavailable small molecule with insulin-mimicking effects (*10*), which may evolve into an antidiabetic drug in the future. Given that visfatin mimics insulin signaling by binding to the insulin receptor, this adipokine may serve as a valuable model for studying other insulin-mimetic molecules. Further study of the cell biology and physiology of this natural insulin-mimetic should help to determine its role in glucose homeostasis and will boost diabetes research and therapy.

References

1. V. Mohamed-Ali *et al*., *Int. J. Obes. Relat. Metab. Disord.* **22**, 1145 (1998).
2. E. E. Kershaw, J. S. Flier, *J. Clin. Endocrinol. Metab.* **89**, 2548 (2004).
3. A. Fukuhara *et al*., *Science* **307**, 426 (2005); published online 16 December 2004 (10.1126/science.1097243).
4. D. E. Moller, K. D. Kaufman, *Annu. Rev. Med.*, in press.
5. B. Samal *et al*., *Mol. Cell. Biol.* **14**, 1431 (1994).
6. M. W. Rajala, P. E. Scherer, *Endocrinology* **144**, 3765 (2003).
7. T. Kitani *et al*., *FEBS Lett.* **544**, 74 (2003).
8. A. Rongvaux *et al*., *Eur. J. Immunol.* **32**, 3225 (2002).
9. B. Zhang *et al*., *Science* **284**, 974 (1999).
10. M. Z. Strowski *et al*., *Endocrinology* **145**, 5259 (2004).

Published online 16 December 2004;
10.1126/science.1106933
Include this information when citing this paper.

CREDIT: KATHARINE SUTLIFF/*SCIENCE*

IT TAKES BOTH SIDES OF THE BRAIN.

CALL FOR ENTRIES

Science & Engineering Visualization Challenge

When the left brain collaborates with the right brain, science merges with art to enhance communication and understanding of research results—illustrating concepts, depicting phenomena, drawing conclusions.

The National Science Foundation and *Science*, published by the American Association for the Advancement of Science, invite you to participate in the annual *Science and Engineering Visualization Challenge*. The competition recognizes scientists, engineers, visualization specialists, and artists for producing or commissioning innovative work in visual communications.

ENTRY DEADLINE:
May 31, 2005

AWARDS CATEGORIES:
Photos/Still Images, Illustrations, Explanatory Graphics, Interactive Media, Non-interactive media

COMPLETE ENTRY INFORMATION:
www.nsf.gov/od/lpa/events/sevc/

Awards in each category will be published in the September 23, 2005 issue of Science *and* Science Online *and displayed on the NSF website.*

Accept the challenge. Show how you've mastered the art of understanding.

INTRODUCTION

A Surfeit of Suspects

If human diseases were story lines for the popular television drama *CSI*, type 2 diabetes would be one of the toughest cases. The key evidence is elevated blood glucose, but the crime scene encompasses multiple organ sites—the pancreas, liver, skeletal muscle, fat, and brain—each of which supplies a long list of molecular suspects that may or may not be causally involved in the disease. Why is solving this case so important? The numbers say it all: The global incidence of type 2 diabetes is projected to nearly double to 300 million people by the year 2025, and many of those affected will be young adults. Successful strategies to halt this epidemic will require a better mechanistic understanding of how the disease arises.

In a series of Viewpoints, *Science* provides a sampling of the many exciting leads currently being pursued by researchers. O'Rahilly *et al*. (p. 370) discuss the suspects that have emerged from genetic studies of rare inherited forms of diabetes and what this information has revealed about susceptibility to the more common forms of the disease. A major contributing factor in the escalating rates of type 2 diabetes is the global increase in obesity rates. On p. 373, Lazar considers the link between these two epidemics from both evolutionary and biological perspectives, highlighting the important role of fat-derived hormones in glucose metabolism. In a related Report, an intriguing new hormone secreted by visceral fat is described by Fukuhara *et al*. (p. 426). Schwartz and Porte (p. 375) review the mechanisms by which the brain regulates body fat and glucose metabolism, following up on ideas initially proposed by Claude Bernard more than a century ago. Rhodes (p. 380) discusses the important role of pancreatic β-cell mass in glucose homeostasis and postulates that the body's inability to secrete enough insulin in type 2 diabetes may be due in part to an aberrant increase in β-cell apoptosis. Finally, Lowell and Shulman (p. 384) summarize the evidence implicating mitochondrial dysfunction in the pathogenesis of type 2 diabetes. The link between mitochondria and metabolic disease is a theme continued in a Report by Wisløff *et al*. (p. 418).

PAGE 381

Additional molecular suspects are featured in *Science* Online's Signal Transduction Knowledge Environment (STKE) and Science of Aging Knowledge Environment (SAGE KE) (www.sciencemag.org/sciext/diabetes/). In STKE, Zick discusses the mechanisms controlling the phosphorylation of insulin receptor substrate proteins and how these mechanisms could be subverted to cause insulin resistance, whereas Ikonen and Vainio consider the impact of plasma membrane lipid composition on insulin signaling. Holz and Chepurny review the signaling pathways by which the glucose-lowering hormone glucagon-like peptide 1 could stimulate an increase in β-cell mass. In SAGE, Faustman *et al*. discuss the use of spleen-derived stem cells as a possible strategy for regenerating insulin-producing pancreatic islet cells.

Which of these suspects will ultimately be found guilty? Stay tuned.

–PAULA A. KIBERSTIS

CONTENTS

VIEWPOINTS

See also related STKE and SAGE KE material on page 311; Editorial page 317; News story page 334; Perspective page 366; and Reports pages 418 and 426.

CREDITS: C. J. RHODES

Science

VIEWPOINT

Genetic Factors in Type 2 Diabetes: The End of the Beginning?

Stephen O'Rahilly,[1]* Inês Barroso,[2] Nicholas J. Wareham[3]

The intensive search for genetic variants that predispose to type 2 diabetes was launched with optimism, but progress has been slower than was hoped. Even so, major advances have been made in the understanding of monogenic forms of the disease which together represent a substantial health burden, and a few common gene variants that influence susceptibility have now been unequivocally identified. Armed with a better understanding of the tools needed to detect such genes, it seems inevitable that the rate of progress will increase and the relevance of genetic information to the diagnosis, treatment, and prevention of diabetes will become increasingly tangible.

Serious efforts to identify genetic variants that predispose to complex human diseases have been under way for 20 years or more. The birth of the global effort to determine the genetic basis of these diseases was accompanied by a fanfare of optimism, but as time has passed and major successes seem more elusive than was anticipated, notes of discord have been increasingly heard. Where are the personalized medicines and life-style interventions based on genotype? Could research funding have been better deployed? Type 2 diabetes is a complex disease that represents a major international public health threat. Although the current rise in its prevalence is almost certainly driven by life-style changes, the inherent susceptibility to the condition is widely considered to be attributable to complex genetic determinants. It is, therefore, an interesting test case in which to think critically about where we are now and how we might progress. To structure our thoughts, we have posed seven questions, which will be applicable, to varying degrees, to most other common diseases.

How Homogenous Is Type 2 Diabetes?

If type 2 diabetes were a homogenous condition with a common underlying molecular pathogenesis, then tracking down the common genetic variants that underlie susceptibility would be relatively easy. Unfortunately, it is more likely that the disease we call type 2 diabetes is heterogeneous and may result from defects in one or more diverse molecular pathways. The control of plasma glucose within tight limits requires precise, life-long coordination of the function of the pancreatic β cell with the responsiveness to insulin of major metabolic tissues such as muscle, liver, and fat. We have long known that there are multiple ways of producing a disease that looks like type 2 diabetes. Stimuli as diverse as glucocorticoid treatment and iron overload, for example, can result in a state of chronically elevated blood glucose that is hard to distinguish from type 2 diabetes. With the elucidation of the molecular bases of a range of monogenic disorders that result in diabetes, it has become clear that many affected members in these families may be diagnosed in middle life and look, superficially at least, much like patients with common type 2 diabetes. The heterogeneous nature of type 2 diabetes suggests that we may need to focus our attention on more phenotypically homogenous subgroups of individuals. It is possible, however, that classical phenotyping approaches will be too crude to act as a useful guide to etiological subgroups. If so, then a revised classification of diabetes will only be engineered the other way around, with improved nosology emerging from a better understanding of molecular pathogenesis.

How Important Is Heredity in Determining the Risk of Type 2 Diabetes?

This apparently simple question is actually very difficult to answer, because the contribution of heredity appears to differ considerably between different populations and in different environments. The best evidence that heredity plays an important role comes from the following observations: (i) Concordance rates for type 2 diabetes and its predecessor, impaired glucose tolerance, are consistently higher in monozygotic than in dizygotic twin pairs; (ii) sibling recurrence rates are consistently higher than population prevalence rates, although the reported excess is modest; (iii) groups of patients labeled as having type 2 diabetes include individuals suffering from unrecognized monogenic and digenic disorders; and (iv) certain common single-nucleotide polymorphisms (SNPs) appear to influence diabetes risk (*1*).

The influence of environment and lifestyle on risk should not be underestimated, however. Ecological studies, comparisons of migrant populations, cohort studies, and intervention trials clearly demonstrate that factors related to diet and physical activity have a major impact on the development of diabetes (*2*). More recent attention has focused on the possible effects of prenatal and early postnatal environment on diabetes risk (*3*). The correlation between low birth weight and later diabetes is consistent across many populations studied, but could, of course, imply that genetic factors influence both birth weight and diabetes risk. Indeed, Hattersley and colleagues have reported an elegant example of this, illustrating how mutations in the glucokinase gene of a fetus lead to reduced intrauterine growth, presumably as a result of relatively low fetal insulin levels, and also to postnatal diabetes. (*4*). To counter this, however, Beck-Nielsen and colleagues have demonstrated that in a group of middle-aged identical twins discordant for type 2 diabetes, the diabetic twin was much more frequently the lighter of the pair at birth (*5*). This implies that even when genetic factors are held constant, intrauterine factors influencing fetal growth may have long-term implications for metabolic health. The lesson for geneticists interested in this disease is that if they ignore the effects of the pre- and postnatal environment and their capacity to interact with genetic variants, real progress in understanding diabetes may be impeded.

What Have We Learned from Monogenic Disorders?

Over the past 20 years, several Mendelian disorders with diabetes as a major phenotypic feature have been characterized at the molecular level. The largest subgroup of these monogenic diseases is caused by defects in the pancreatic β cell, resulting in a stable or progressive disorder of insulin secretion (*6*). Monogenic disorders that primarily impair insulin action either involve molecules in the insulin signal transduction cascade or result in abnormalities of fat tissue development (lipodystrophy) with secondary metabolic derangements leading to insulin resistance (*7*).

[1]University of Cambridge, Department of Clinical Biochemistry, Addenbrooke's Hospital, Cambridge CB2 2QQ, UK. [2]The Wellcome Trust Sanger Institute, Wellcome Trust Genome Campus, Hinxton, Cambs CB10 1SA, UK. [3]Medical Research Council Epidemiology Unit, Elsie Widdowson Laboratory, Fulbourn Road, Cambridge CB1 9NL, UK.

*To whom correspondence should be addressed. E-mail: so104@medschl.cam.ac.uk

If major mutations (i.e., mutations that cause a substantial functional defect and are normally rare in the population) in these molecules lead to a highly penetrant form of human diabetes, then it seems plausible that more subtle genetic changes affecting the structure or expression of these molecules might play a role in determining susceptibility to type 2 diabetes. Our current state of knowledge regarding genetic variants influencing type 2 diabetes strongly supports this notion (Table 1). Thus, a common missense variant in the γ2 isoform of peroxisome proliferator–activated receptor gamma (PPARγ) [Pro^{12}→Ala^{12} (Pro12Ala)] has shown an association with diabetes in multiple studies, with a meta-analysis suggesting that the common allele is associated with an increased diabetes risk of 25% (*8*). Major missense mutations in this gene result in severe, dominantly inherited insulin resistance, diabetes mellitus, and additional features such as partial lipodystrophy and hypertension (*9*). A common variant (Glu23Lys) in the gene encoding the inwardly rectifying potassium channel KIR 6.2 also seems to increase diabetes risk by about 25%. Again, major mutations in this gene lead to an inherited form of severe diabetes or hypoglycemia depending on whether the mutations cause aberrant opening or closing of the channel. On somewhat less secure ground, common variants in the gene encoding the transcription factor hepatocyte nuclear factor 4α (HNF4α), the insulin receptor, and the mitochondrial genome appear to influence type 2 diabetes risk, whereas major mutations in these genes lead to more overt and early-onset metabolic disturbances. Thus, if past performance is any guide to future success, then any monogenic disorder that impairs glucose homeostasis is worthy of exhaustive study of its causative gene as a candidate for influencing diabetes risk in the general population.

How Helpful Have Animal Models Been?

The power of modern murine genetics means that naturally occurring or induced mutations resulting in a relevant phenotype can be positionally identified and, in addition, targeted mutagenesis can reveal the potential contribution of any gene to glucose homeostasis. The importance of murine genetics has been emphatically shown in the field of energy balance and obesity, a topic of great importance to type 2 diabetes given that most type 2 diabetic humans are obese. The discovery of the leptin and melanocortin pathways controlling energy balance have largely been driven by murine genetics (*10*). The relevance of these pathways to the control of energy balance in humans has been repeatedly demonstrated, although there are some notable exceptions where humans and mice diverge (*11*).

In the case of diabetes, however, the situation is rather different. Thus, when considering the group of human autosomal dominant disorders of insulin secretion, termed maturity-onset diabetes of the young (MODY), it is notable that in no case has the homologous heterozygous murine knockout exhibited hyperglycemia (*6*). Even with something as fundamental as the insulin receptor, there are significant differences between the human and mouse phenotypes. Thus, mice lacking both copies of the insulin receptor are born of normal weight but die rapidly after birth of ketoacidosis (*12*), whereas humans with analogous null mutations are small at birth and rarely if ever develop ketoacidosis (*3*). We have demonstrated (*4*) that humans with the PPARγ Pro467Leu allele develop extreme insulin resistance, diabetes mellitus, and hypertension. Surprisingly, mice with the identical mutation, although they are hypertensive, show completely normal insulin sensitivity and glucose homeostasis (*13*) Thus, when it comes to the control of intermediary metabolism and plasma glucose levels, there may sometimes be important differences between mice and humans. The extent to which mice accurately model human phenotypes may be highly dependent on the particular phenotype under investigation.

Why Do We Want to Discover the Precise Genetic Basis of Type 2 Diabetes Risk?

Given the massive investment of time, money, and energy in the search for genetic determinants for type 2 diabetes, it is reasonable to ask "Why did we bother starting in the first place?" Intellectual curiosity is a respectable motivation, but it would be difficult to justify the required resources on that basis alone. The principal motivation for this venture lies in the potential for improvement of human health. We could take the attitude that we already know about many of the environmental and lifestyle risk factors for type 2 diabetes and that intensive programs targeted at altering those factors can substantially reduce diabetes incidence in at-risk individuals (*2*). The rapid and widespread implementation of life-

Table 1. Human genes in which rare major missense and/or nonsense mutations result in a disorder of glucose homeostasis with a clear Mendelian (or mitochondrial) pattern of inheritance and for which large and/or replicated case-control studies have shown an association between diabetes risk and more common SNPs in or close to the gene. OMIM, Online Mendelian Inheritance in Man; OR, odds ratio of disease in carriers of the susceptibility allele versus noncarriers; VNTR, variable number of tandem repeats.

Gene	Monogenic disease	OMIM	Polygenic type 2 diabetes	Reference
PPARG	Familial partial lipodystrophy (FPLD3)	604367	Pro12Ala, OR = 1.25	(*8*)
KCNJ11	Permanent neonatal diabetes mellitus (PNDM)	606176	Glu23Lys OR = 1.18	(*18–20*)
	Persistent hyperinsulinaemia hypoglycemia of infancy (PHHI)	601820		
HNF4A	MODY1	125850	Thr103Ile late-onset diabetes in Japanese (OR = 4.3), 5′ SNPs increased risk in Finnish (OR = 1.33) and Ashkenazim (OR = 1.4), protective haplotype in UK Caucasian (OR = 0.83)	(*20–23*)
Mitochondrial genome	Diabetes and deafness maternally inherited (MIDD)	520000	Mitochondrial DNA 16189, OR = 1.6	(*24*)
HNF1A	MODY3	600496	Gly319Ser, OR = 1.97 in Oji-Cree	(*25*)
INS	Diabetes-type hyperglycemia with hyperinsulinemia	176730	Excess paternal transmission of class III VNTR (69% versus expected 50%), 3p+9 in UK Caucasian (OR = 2.02 recessive model only)	(*20*, *26*)
INSR	Leprechaunism (Donahue syndrome)	246200	Val985Met in the Netherlands (OR = 1.87), IVS6+43 (OR = 1.32) and haplotype in UK Caucasians (OR = 1.34)	(*20*, *27*)
	Rabson-Mendenhall syndrome	262190		
	"Type A" insulin resistance	147670		

style interventions to reduce diabetes is not, however, incompatible with the desire to improve the effectiveness and precision of treatment and prevention through greater understanding of the genetic and molecular etiology of the disease.

How could genetic information help us? The great hope that inspired most efforts in disease gene discovery is that such genes will then become therapeutic targets and that drugs targeted to molecules that are fundamentally involved in disease causation will be more effective than the cruder therapies we now use. An alternative strategy is to use murine genetics to identify molecules critical for the normal control of metabolism and glucose homeostasis and to infer from that how pharmacological manipulation of such molecules would offer therapeutic benefit. In this scenario, genetics is being used as a tool to aid the discovery of drugs. Perhaps more immediately applicable is the notion that the presence of particular genetic variants in an individual will influence his/her response to particular therapies (''pharmacogenomics''), as in the case of patients with MODY resulting from HNF1α mutations who preferentially respond to sulphonylurea therapy (*6*). In this case, we are looking at genetics as a guide to better drug use in the clinic. Greater understanding of the basis of disease also allows for more accurate provision of prognostic information to patients as the risk of future complications and likely disease trajectory is more accurately determined. Individuals with glucokinase mutations, for example, have stable hyperglycemia with limited risk of the microvascular complications, whereas those with mutations in the HNFs have a more progressive course (*6*).

Perhaps the most exciting future for genetics in type 2 diabetes is not necessarily in pharmacogenomics or provision of prognostic information but in understanding how specific genes interact with diet, exercise, and other lifestyle factors in the control of intermediary metabolism. We look forward to the day when the genetic technology will aid the identification of individuals at high risk and will also help to determine which particular combination and type of diet and exercise program and perhaps pharmacotherapy can be optimally used to prevent the onset of hyperglycemia. In the short term, because we know that family history and obesity interact to increase risk, it might be sensible to target preventive measures at sedentary people with a family history of diabetes (*14*).

How Might We Progress Our Understanding of the Genetic Basis of Diabetes?

It is likely that future progress in the identification of true diabetes susceptibility genes will come from a variety of directions and that it will require synthesis of different types of research evidence. The clearest example of success from family-based linkage studies and positional cloning in complex disease has been the identification of CARD15 variants in inflammatory bowel disease, in which a relatively uncommon variant of large effect was detected by fine mapping of a region underlying a linkage peak (*15*). However, this may not be the case with other variants and other diseases if the effects of the variants are less pronounced and the linkage peaks less distinct. Thus, to detect the effect of the PPARγ2 Pro12Ala polymorphism, which is only associated with a modest risk of diabetes, the use of linkage studies would have required an impracticably large number of families. The only type 2 diabetes susceptibility gene thus far identified with a positional approach is that encoding the protease Calpain 10 (*16*). Although data supporting the proposition that this is a true susceptibility gene are accumulating, it may be too early to conclude that its contribution has been established beyond reasonable doubt. Recognizing the importance of study size, an important characteristic of current positional cloning-based efforts is the establishment of global collaborative consortia.

The continuing study of murine models with both gene targeting and random mutagenesis strategies is very likely to continue to aid the identification of molecules important for the control of glucose homeostasis and thereby provide previously unrecognized therapeutic targets. Extreme human phenotypes will remain a powerful route to finding genes that may be relevant for common human phenotypes. Thus far, we have implied that if major missense or nonsense mutations in a particular gene cause simple Mendelian forms of diabetes, then common SNPs in or around that gene—usually thought to affect gene expression—might alter the risk of the more common form of the disease. The effect on risk would be modest in any one individual but widespread in the population. Recent work by Hobbs and colleagues (*17*) examining genetic determinants of plasma high-density lipoprotein (HDL) concentrations raises the possibility of an alternative model. These authors sequenced genes in which homozygous mutations were known to cause rare dyslipidemic syndromes in subjects from the normal population who were either below the 5th or above the 95th percentile for plasma HDL cholesterol. Remarkably, there was a high frequency of rare missense variants in these genes among subjects in the lowest fifth percentile for plasma HDL, suggesting that major phenotypic effects of multiple different rare alleles contribute substantially to low HDL cholesterol in the general population. If the same is true for the physiological traits that underlie type 2 diabetes (e.g., insulin sensitivity), then strategies relying on common SNPs alone will not be sufficient to find all the important genetic contributors to type 2 diabetes risk.

Case-control studies, combined with confirmation of transmission disequilibrium in family-based studies, are likely to provide the mainstay of future association studies of possible ''diabetogenes.'' However, much more attention will need to be paid to study size and the careful characterization of cases and controls. Examining studies for heterogeneity and in particular biased estimation of the magnitude of effect by study size will be important because of potential publication bias.

Is It Possible to Determine the Genetic Basis of Diabetes Without Considering Key Life-style Factors?

Traditionally genetic investigators have tackled gene-environment interaction as a second-order question, to be examined once susceptibility alleles have been identified. However, in a phenotype such as type 2 diabetes, for which life-style factors are likely to have a major impact, the neglect of environmental exposures may mean that important effects of particular alleles are not only attenuated but even obscured if the effect of genotype differs markedly according to life-style. Our epidemiological methods for measuring dietary factors and physical activity are imprecise, and measurement precision is critical to the ability to detect interaction. The quantitation of environmental exposures is therefore a major challenge but one that should not be ignored. Simple cross-sectional case-control studies of gene-life-style interaction will not work because of biased estimation of life-style in people who have been given the diagnostic label of diabetes. The optimal approach will involve case-control studies nested within major epidemiological cohort studies. These need to be large, have careful measurement of life-style factors at baseline and critically amass sufficient person-years of follow-up before they are of use. Cohorts of this nature are planned but will need many years before sufficient incident cases occur. In the meantime, we can make use of existing opportunities in multicohort studies that were established in the past.

Conclusions

In the hunt for genetic factors that influence susceptibility to type 2 diabetes, no single approach is likely to be successful, and the optimal strategy will involve a variety of different study designs and analytical approaches, including the use of model organisms. Once we are properly positioned to examine the relationship between genetic polymorphisms and responses to different therapies and preventative strategies, the era of personalized, genome-based medicine will have begun in

earnest. To paraphrase Winston Churchill, in the area of common disease genetics we are certainly not at the end, nor are we even at the beginning of the end, but we may, perhaps, be at the end of the beginning.

References and Notes

1. M. I. McCarthy, P. Froguel, *Am. J. Physiol. Endocrinol. Metab.* **283**, E217 (2002).
2. J. Tuomilehto *et al.*, *N. Engl. J. Med.* **344**, 1343 (2001).
3. C. N. Hales, D. J. Barker, *Br. Med. Bull.* **60**, 5 (2001).
4. A. T. Hattersley *et al.*, *Nature Genet.* **19**, 268 (1998).
5. H. Beck-Nielsen, A. Vaag, P. Poulsen, M. Gaster, *Best Pract. Res. Clin. Endocrinol. Metab.* **17**, 445 (2003).
6. A. Stride, A. T. Hattersley, *Ann. Med.* **34**, 207 (2002).
7. S. O'Rahilly, *Eur. J. Endocrinol.* **147**, 435 (2002).
8. D. Altshuler *et al.*, *Nature Genet.* **26**, 76 (2000).
9. I. Barroso *et al.*, *Nature* **402**, 880 (1999).
10. J. M. Friedman, *Nature Med.* **10**, 563 (2004).
11. S. O'Rahilly, I. S. Farooqi, G. S. Yeo, B. G. Challis, *Endocrinology* **144**, 3757 (2003).
12. D. Accili *et al.*, *Nature Genet.* **12**, 106 (1996).
13. Y. S. Tsai *et al.*, *J. Clin. Invest.* **114**, 240 (2004).
14. L. A. Sargeant, N. J. Wareham, K. T. Khaw, *Int. J. Obes. Relat. Metab. Disord.* **24**, 1333 (2000).
15. J. P. Hugot *et al.*, *Nature* **411**, 599 (2001).
16. Y. Horikawa *et al.*, *Nature Genet.* **26**, 163 (2000); erratum in *Nature Genet.* **26**, 502 (2000).
17. J. C. Cohen *et al.*, *Science* **305**, 869 (2004).
18. A. L. Gloyn *et al.*, *Diabetes* **52**, 568 (2003).
19. L. Love-Gregory *et al.*, *Diabetologia* **46**, 136 (2003).
20. I. Barroso *et al.*, *PLoS Biol.* **1**, 41 (2003).
21. Q. Zhu *et al.*, *Diabetologia* **46**, 567 (2003).
22. K. Silander *et al.*, *Diabetes* **53**, 1141 (2004).
23. L. D. Love-Gregory *et al.*, *Diabetes* **53**, 1134 (2004).
24. J. Poulton *et al.*, *Hum. Mol. Genet.* **11**, 1581 (2002).
25. R. A. Hegele, H. Cao, S. B. Harris, A. J. Hanley, B. Zinman, *Diabetes Care* **22**, 524 (1999).
26. S. J. Huxtable *et al.*, *Diabetes* **49**, 126 (2000).
27. L. M. Hart *et al.*, *J. Clin. Endocrinol. Metab.* **84**, 1002 (1999).

28. We thank the Wellcome Trust (S.O'R., I.B., and N.J.W.), the Medical Research Council UK (S.O'R. and N.J.W.), and the European Union Framework Programme (S.O'R., I.B., and N.J.W.) for their continuing support. S.O'R. has a financial relationship with and is a member of the Scientific Advisory Boards of Prosidion Ltd. and Biovitrum AB. He is a member of the Scientific Advisory Boards of Cambridge Antibody Technology, Cambridge Biotechnology Ltd., Paradigm Therapeutics PLC, and Xcellsyz Ltd. He is a consultant for Merck & Co. Inc., Unilever PLC, and Ingenium Pharmaceuticals AG.

10.1126/science.1104346

VIEWPOINT

How Obesity Causes Diabetes: Not a Tall Tale

Mitchell A. Lazar

The epidemic of obesity-associated diabetes is a major crisis in modern societies, in which food is plentiful and exercise is optional. The biological basis of this problem has been explored from evolutionary and mechanistic perspectives. Evolutionary theories, focusing on the potential survival advantages of "thrifty" genes that are now maladaptive, are of great interest but are inherently speculative and difficult to prove. Mechanistic studies have revealed numerous fat-derived molecules and a link to inflammation that, together, are hypothesized to underlie the obesity-diabetes connection and thereby represent prospective targets for therapeutic intervention.

Type 2 diabetes stems from the failure of the body to respond normally to insulin, called "insulin resistance," coupled with the inability to produce enough insulin to overcome this resistant state. This common form of diabetes is often associated with obesity, and the current epidemics of these two conditions are seemingly related (*1*). This is glaringly evident in children, who are increasingly plagued by obesity and in whom the prevalence of type 2 diabetes (formerly termed "adult onset") is approaching that of type 1 diabetes (formerly termed "juvenile onset") (*2*). The epidemic of diabetes has a huge associated cost in terms of healthcare dollars as well as human morbidity and mortality (*3*). Recent studies predict that one in three Americans born in the year 2000 will develop diabetes in their lifetime (*4*), and a similarly ominous future confronts nearly all developed nations. Here, I discuss the relationship between obesity and diabetes, first in terms of the evolutionary forces that might explain their increased incidence in the modern world and then in terms of the pathogenic pathways that link the two conditions and inform rational strategies for prevention and therapy.

Division of Endocrinology, Diabetes, and Metabolism, Department of Medicine, and The Penn Diabetes Center, University of Pennsylvania School of Medicine, Philadelphia, PA 19104–6149, USA. E-mail: lazar@mail.med.upenn.edu

Why We Have Epidemics of Obesity and Diabetes: An Evolutionary Perspective

The evolutionary perspective has successfully guided much of modern biology, yet it is not always definitive. Take, for example, the giraffe's long neck, which would seem to provide a competitive advantage for obtaining food, thus favoring survival and reproduction of the species. However, in his essay ''The Tallest Tale,'' Gould argued that the weight of scientific evidence favors alternative selective pressures as having led to the giraffe's long neck, including combat advantages, sighting of predators, and efficient heat loss (*5*).

There are no known survival advantages of morbid obesity, and increased body fat is associated with increased mortality (*6*). Hence, natural selection is unlikely to have favored obesity per se. On the other hand, during periods of prolonged famine that plagued early human hunter-gatherers, a survival advantage would have been conferred by genes that favor the economical use and storage of energy: so-called ''thrifty'' genes (*7*). The existence of thrifty genes was initially proposed by Neel, who focused on the efficient use of glucose as a biological fuel; he suggested that evolutionary pressure to preserve glucose for use by the brain during starvation led to a genetic propensity toward insulin resistance in peripheral tissues (*8*). Biological systems store energy most efficiently as fat and, hence, another function of thrifty genes is to promote an increase in adipose tissue. In the modern setting of sedentary lifestyles and unrestricted access to high-caloric foods, thrifty genes have been suggested to underlie the twin epidemics of obesity and diabetes (*7*).

Human obesity has a clear genetic component but is rarely monogenic (*9*). Thus, there are likely to be multiple thrifty genes, and the inheritance of several polymorphisms leading to small differences in expression can make populations more or less susceptible to obesity and diabetes (*10*). Several candidate thrifty genes have been proposed and are reviewed elsewhere (*11*). In principle, there could be separate sets of thrifty genes that promote body fat deposition or insulin resistance. Indeed, this concept is supported by a paradox: Insulin actually increases the production and storage of fatty acids in adipose tissue, thereby exacerbating obesity, whereas tissues such as muscle are insensitive to insulin (*12*). Nevertheless, Occam's Razor (the principle that plurality of causes should not be postulated unless absolutely necessary) argues for thrifty genes that both increase energy storage and cause insulin resistance.

Perhaps the best thrifty gene candidate is the gene that encodes leptin, a hormone produced by adipose tissue and the absence of which leads to obesity and insulin resistance in rodents and humans (*13*). Leptin functions physiologically as a signal of energy stores, inhibiting food intake and accelerating energy

metabolism (*13*). During starvation, it is the fall in circulating leptin levels that triggers increased appetite and decreased metabolic rate. Consistent with this, rodents and humans with only one functional copy of the leptin gene have increased body fat (*14*), and leptin deficiency due to lipodystrophy causes insulin resistance (*15*, *16*). Because a reduction in leptin levels appears to be the physiological signal for a thrifty metabolic response, leptin itself must have been evolutionarily selected for another function. Indeed, leptin replacement reverses amenorrhea in leptin-deficient females with low body weight (*17*), providing the mechanistic explanation for the link between body fat and reproductive capacity that was first proposed three decades ago by Frisch on the basis of epidemiological studies of indigenous and modern populations (*18*). This physiological function of leptin thus favors survival of the species by conferring a reproductive advantage to individuals who are nutritionally fit.

An alternative to thrifty genes is the "thrifty phenotype" hypothesis, first proposed by Hales and Barker on the basis of clinical observations that poor fetal and/or postnatal nutrition is associated with obesity and type 2 diabetes later in life (*19*). This hypothesis posits that fetal malnutrition alters metabolic pathways that result in tissue adaptations favoring the thrifty use of nutrients in utero and in postnatal life, thereby leading to obesity and diabetes in the setting of subsequent adequate nutrition. The focus on an inadequate maternal-fetal nutritional environment differs from the focus on thrifty genes. Indeed, the thrifty phenotype hypothesis postulates epigenetic memory of the fetal/neonatal environment. Epigenetic regulation of gene expression involves chemical modification of chromatin by enzymes such as sirtuins, whose activities are linked to cellular energy stores and, in lower organisms, interface with insulin signaling pathways (*20*, *21*).

If fetal adaptations to malnutrition are preserved later in life, as proposed by the thrifty phenotype hypothesis, gene sets that facilitate these epigenetic changes would favor survival and reproduction in adulthood. Thus, in the thrifty phenotype model, there would be ample selective pressure for genes that protect from early malnutrition but promote obesity and diabetes under modern conditions.

How Obesity Causes Diabetes: A Biological Perspective

Although once considered a passive fuel depot, adipose tissue is now recognized to be an endocrine organ that communicates with the brain and peripheral tissues by secreting hormones regulating appetite and metabolism (*22*). These functions appear to be modulated by the location of the adipose tissue (visceral versus subcutaneous) (*23*), by the size of the average adipocyte in the tissue (*24*), and by adipocyte metabolism of glucose (*25*) and corticosteroids (*26*).

Except in rare cases where the leptin gene is defective, leptin levels are elevated in obesity (*13*). This is due to resistance to the actions of leptin at the cellular level, which may be mechanistically related to insulin resistance, as discussed below. Several other adipocyte-derived factors have been shown to contribute to systemic insulin resistance. One such factor is the increased levels of adipocyte-derived free fatty acids that have been shown to contribute to insulin resistance in liver and muscle in obesity (*27*, *28*). Adipose tissue also secretes a large number of proteins in addition to leptin that modulate glucose metabolism and insulin action (*22*, *29*) (Table 1). The causal role of several of these proteins in insulin resistance and diabetes has been established through studies of mouse genetic models. Studies of humans generally suggest that circulating levels of these proteins are elevated in individuals with type 2 diabetes. One exception is adiponectin, which enhances insulin action yet circulates at reduced levels in obesity (*30*). Each of these proteins constitutes a potential target for therapies aimed at uncoupling insulin resistance from obesity.

A subset of these adipose-derived proteins are adipocyte-specific, whereas others are not. Intriguingly, many proteins that are adipose-derived but not adipose-specific play a role in innate immunity, a relatively primitive defense mechanism against infection (*31*). Cytokines such as tumor necrosis factor α and interleukin-6 are produced by macrophages as well as by adipocytes; they act directly on inflammatory cells and also contribute indirectly to inflammation by acting on the liver to produce acute phase proteins. These cytokines also induce suppressor of cytokine signaling-3 (SOCS-3), an intracellular signaling molecule that impairs the signaling of both leptin and insulin. SOCS-3 levels are elevated in obesity and thus may represent a final common pathway of obesity-associated resistance to the actions of both leptin and insulin (*32*).

The similarity between macrophages and adipocytes extends beyond cytokine production. Both cell types express peroxisome proliferator-activated receptor γ, a transcription factor that is the target of insulin-sensitizing therapies (*33*) and that has been dubbed "the ultimate thrifty gene" because of its role in lipid accumulation (*34*). It has also become evident that macrophage infiltration of adipose tissue is characteristic of obesity (*35*, *36*), although the pathophysiological consequences are unknown. The anatomic blurring of the line between adipocytes and macrophages is paralleled by the tissue expression of the polypeptide hormone resistin, whose levels are increased in insulin-resistant mice and humans (*37*, *38*). Resistin is expressed exclusively in adipocytes in mice (*39*) but predominantly in macrophages in humans (*40*). The evolutionary and functional implications of this remain to be determined. Perhaps the commonalities of adipocyte and macrophage function are remnants of an ancestral evolutionary adaptation; indeed, invertebrates concentrate endocrine and immune functions in a single cell type resembling the macrophage (*41*, *42*).

The close relationship between inflammation and diabetes is supported by the observation that stimulation of the innate immune response [by bacterial endotoxin during sepsis, for example (*43*)] results in insulin resistance that contributes to the high mortality of critical illness (*44*). The interaction between inflammation and insulin signaling is also suggested by the ability of aspirin to improve insulin resistance, in part by preventing the antagonistic effects of fatty acids and cytokines (*45*).

Table 1. Proteins secreted by adipose tissue that are also thought to play a role in obesity-associated insulin resistance and diabetes (*22*, *29*, *51*). ASP, acylation stimulatory protein; TNF-α, tumor necrosis factor α; IL-6, interleukin 6; MCP-1, macrophage and monocyte chemoattractant protein 1; PBEF, pre-B cell colony enhancing factor; PAI-1, plasminogen activator inhibitor 1.

Adipose-derived protein	Effect on insulin sensitivity	Other tissue sources
Leptin	Improvement	None
Adiponectin	Improvement	None
Adipsin/ASP	Decline	None
Resistin	Decline	None (rodent) Macrophage (human)
TNF-α	Decline	Macrophage
IL-6	Decline	Macrophage
MCP-1	Decline	Macrophage
Visfatin (PBEF)	Improvement	Liver, lymphocytes
PAI-1	Decline	Liver
Angiotensinogen	Decline	Liver
Serum amyloid A	Not known	Liver
α1-acid glycoprotein	Not known	Liver

Why is obesity an inflammatory state and why does inflammation cause diabetes? The search for answers to these questions takes us again to evolutionary considerations. Perhaps the response to infection is more effective when glucose is shunted from muscle to the inflammatory cells involved in the immune response and tissue repair (*46*). A potentially unifying view is that the body's ability to survive major stress, including infection and starvation, is enhanced by peripheral insulin resistance that preserves the brain's glucose supply (*47*). This hypothesis might explain why cortisol, the major stress hormone, causes insulin resistance and stimulates the innate immune response (*31*), even though chronic cortisol exposure is anti-inflammatory because of down-modulation of the acquired immune response. The stress connection may extend to individual cells, as it has recently been shown that intracellular stress induces insulin resistance in a manner that is exacerbated by obesity, potentially through adipocyte-secreted factors (*48*). Moreover, chronic metabolic stress impairs the ability of pancreatic beta cells to secrete sufficient insulin to overcome insulin resistance, which is a hallmark of type 2 diabetes (*49*).

Not a Tall Tale: How Will it End?

Humanity has been curious about the giraffe's long neck since time immemorial. Although it is very likely that this unusual phenotype contributed to the survival of that species, there is as yet no molecular or genetic explanation for it. We are now curious about the explanation for the dramatic rise in human obesity and diabetes. It is interesting to speculate about the origin of genes that make us particularly susceptible to these metabolic diseases in the setting of modern lifestyles. The theories that emerge may provide clues to the underlying mechanisms, especially if they can be supported by studies in model organisms (*50*). Of course, natural selection itself has the potential to solve these health crises, but only when they threaten the survival of our species. A more optimistic view is that we can turn the tide of these epidemics by focusing on mechanistic questions such as how obesity causes diabetes. It is hoped that harnessing this knowledge will allow us to successfully intervene before natural selection takes over.

References and Notes

1. A. H. Mokdad *et al.*, *JAMA* **289**, 76 (2003).
2. W. H. Dietz, *N. Engl. J. Med.* **350**, 855 (2004).
3. P. Hogan, T. Dall, P. Nikolov, *Diabetes Care* **26**, 917 (2003).
4. K. M. Narayan, J. P. Boyle, T. J. Thompson, S. W. Sorensen, D. F. Williamson, *JAMA* **290**, 1884 (2003).
5. S. J. Gould, *Nat. Hist.* **5**, 18 (1996).
6. E. E. Calle, M. J. Thun, J. M. Petrelli, C. Rodriguez, C. W. Heath Jr., *N. Engl. J. Med.* **341**, 1097 (1999).
7. P. Zimmet, C. R. Thomas, *J. Intern. Med.* **254**, 114 (2003).
8. J. V. Neel, *Am. J. Hum. Genet.* **14**, 353 (1962).
9. S. O'Rahilly, I. S. Farooqi, G. S. Yeo, B. G. Challis, *Endocrinology* **144**, 3757 (2003).
10. J. Diamond, *Nature* **423**, 599 (2003).
11. C. M. Damcott, P. Sack, A. R. Shuldiner, *Endocrinol. Metab. Clin. North Am.* **32**, 761 (2003).
12. R. H. Unger, *Trends Endocrinol. Metab.* **14**, 398 (2003).
13. J. M. Friedman, *Nutr. Rev.* **60**, S1 (2002).
14. I. S. Farooqi *et al.*, *Nature* **414**, 34 (2001).
15. I. Shimomura, R. E. Hammer, S. Ikemoto, M. S. Brown, J. L. Goldstein, *Nature* **401**, 73 (1999).
16. E. A. Oral *et al.*, *N. Engl. J. Med.* **346**, 570 (2002).
17. C. K. Welt *et al.*, *N. Engl. J. Med.* **351**, 987 (2004).
18. R. E. Frisch, J. W. McArthur, *Science* **185**, 949 (1974).
19. C. N. Hales, D. J. Barker, *Diabetologia* **35**, 595 (1992).
20. T. Jenuwein, C. D. Allis, *Science* **293**, 1074 (2001).
21. G. Blander, L. Guarente, *Annu. Rev. Biochem.* **73**, 417 (2004).
22. E. E. Kershaw, J. S. Flier, *J. Clin. Endocrinol. Metab.* **89**, 2548 (2004).
23. M. Das, I. Gabriely, N. Barzilai, *Obes. Rev.* **5**, 13 (2004).
24. C. Weyer *et al.*, *Mol. Genet. Metab.* **72**, 231 (2001).
25. E. D. Abel *et al.*, *Nature* **409**, 729 (2001).
26. H. Masuzaki *et al.*, *Science* **294**, 2166 (2001).
27. R. N. Bergman, M. Ader, *Trends Endocrinol. Metab.* **11**, 351 (2000).
28. G. Boden, G. I. Shulman, *Eur. J. Clin. Invest.* **32** (suppl. 3), 14 (2002).
29. M. W. Rajala, P. E. Scherer, *Endocrinology* **144**, 3765 (2003).
30. M. Haluzik, J. Parizkova, M. M. Haluzik, *Physiol. Res.* **53**, 123 (2004).
31. C. Gabay, I. Kushner, *N. Engl. J. Med.* **340**, 448 (1999).
32. H. Shi, I. Tzameli, C. Bjorbaek, J. S. Flier, *J. Biol. Chem.* **279**, 34733 (2004).
33. S. M. Rangwala, M. A. Lazar, *Trends Pharmacol. Sci.* **25**, 331 (2004).
34. J. Auwerx, *Diabetologia* **42**, 1033 (1999).
35. H. Xu *et al.*, *J. Clin. Invest.* **112**, 1821 (2003).
36. S. P. Weisberg *et al.*, *J. Clin. Invest.* **112**, 1796 (2003).
37. M. W. Rajala *et al.*, *Diabetes* **53**, 1671 (2004).
38. H. Osawa *et al.*, *Am. J. Hum. Genet.* **75**, 678 (2004).
39. C. M. Steppan *et al.*, *Nature* **409**, 307 (2001).
40. L. Patel *et al.*, *Biochem. Biophys. Res. Commun.* **300**, 472 (2003).
41. E. Ottaviani, C. Franceschi, *Domest. Anim. Endocrinol.* **15**, 291 (1998).
42. G. S. Hotamisligil, *Int. J. Obes. Relat. Metab. Disord.* **27** (suppl. 3), S53 (2003).
43. A. O. Agwunobi, C. Reid, P. Maycock, R. A. Little, G. L. Carlson, *J. Clin. Endocrinol. Metab.* **85**, 3770 (2000).
44. G. Van den Berghe, *J. Clin. Invest.* **114**, 1187 (2004).
45. M. Yuan *et al.*, *Science* **293**, 1673 (2001).
46. J. M. Fernandez-Real, W. Ricart, *Diabetologia* **42**, 1367 (1999).
47. P. H. Black, *Brain Behav. Immun.* **17**, 350 (2003).
48. U. Ozcan *et al.*, *Science* **306**, 457 (2004).
49. C. J. Rhodes, *Science*, **307**, 380.
50. V. D. Longo, C. E. Finch, *Science* **299**, 1342 (2003).
51. A. Fukuhara *et al.*, *Science* **307**, 426 (2005).

52. I thank R. Ahima, M. Birnbaum, M. Brown, A. Lazar, S. Mandel, and A. Rubenstein for critical comments on the manuscript and members of my laboratory for helpful discussions. I apologize that many relevant articles could not be cited because of space limitations. Supported by the National Institute of Diabetes, Digestive, and Kidney Diseases.

10.1126/science.1104342

VIEWPOINT

Diabetes, Obesity, and the Brain

Michael W. Schwartz[1,2]* and Daniel Porte Jr.[1,3,4]

Recent evidence suggests a key role for the brain in the control of both body fat content and glucose metabolism. Neuronal systems that regulate energy intake, energy expenditure, and endogenous glucose production sense and respond to input from hormonal and nutrient-related signals that convey information regarding both body energy stores and current energy availability. In response to this input, adaptive changes occur that promote energy homeostasis and the maintenance of blood glucose levels in the normal range. Defects in this control system are implicated in the link between obesity and type 2 diabetes.

More than a century ago, the renowned physiologist Claude Bernard observed that diabetes could be induced in animals by puncture of the floor of the fourth cerebral ventricle ("piqure diabetique") (*1*). Although this striking finding suggested a key role for the brain in glucose homeostasis, its importance was largely neglected after the discovery of insulin in 1923. However, new findings have revived interest in the role played by the brain in both glucose homeostasis and the mechanism linking obesity to type 2 diabetes. As Bernard might have predicted, this new information suggests that a full understanding of the pathogenesis of these disorders must incorporate a role for the brain in metabolic regulation.

[1]Division of Metabolism, Endocrinology and Nutrition, University of Washington, Seattle, WA 98110, USA. [2]Harborview Medical Center, 325 Ninth Avenue, Seattle, WA 98110, USA. [3]Division of Metabolism, Diabetes and Endocrinology, University of California San Diego, San Diego, CA 92161, USA. [4]Division of Metabolism, Diabetes and Endocrinology, VA San Diego Health Care System, 3350 La Jolla Village Drive, San Diego, CA 92161, USA.

*To whom correspondence should be addressed. E-mail: mschwart@u.washington.edu

Evidence now indicates that the brain processes information from "adiposity signals" such as the hormones insulin and leptin, which circulate in proportion to body fat mass, and integrates this input with signals from nutrients such as free fatty acids (FFAs). In response, feeding behavior, autonomic outflow, and substrate metabolism are adjusted in ways that promote homeostasis of both energy stores and fuel metabolism. The overarching hypothesis is that in times of plenty (ample fat stores and food availability), input to key brain areas from these afferent signals leads to inhibition of both energy intake and endogenous glucose production, while simultaneously increasing energy expenditure and mobilizing fat stores (Fig. 1) (*2*, *3*). The net effect is that when the brain senses that body energy content and nutrient availability are sufficient, further increases of stored energy (in the form of fat) and circulating nutrients (such as glucose) are resisted.

Conversely, a decrease in neuronal input from one or more of these afferent signals is proposed to alert the brain to a current or pending deficiency of stored energy or nutrient availability. In turn, the brain activates responses that promote positive energy balance (increased food intake and decreased energy expenditure) and raise circulating nutrient levels (increased hepatic glucose production). As body fat content and plasma glucose levels begin to increase, circulating concentrations of leptin, insulin, and FFAs increase as well. The latter are sensed in the brain, favoring the return of food intake and glucose production to their original values. The central nervous system (CNS) response to these signals is therefore catabolic in nature and is in direct opposition to the anabolic actions of insulin and FFAs on fuel storage and metabolism in peripheral tissues. Should defects arise in the CNS response to these signals, the resulting imbalance in this homeostatic system will result in elevated levels of both body fat content and hepatic glucose production. Accordingly, reduced secretion of, sensing of, or responsiveness to afferent hormonal or nutrient-related signals can be predicted to cause weight gain and insulin resistance: cardinal features that link obesity with type 2 diabetes.

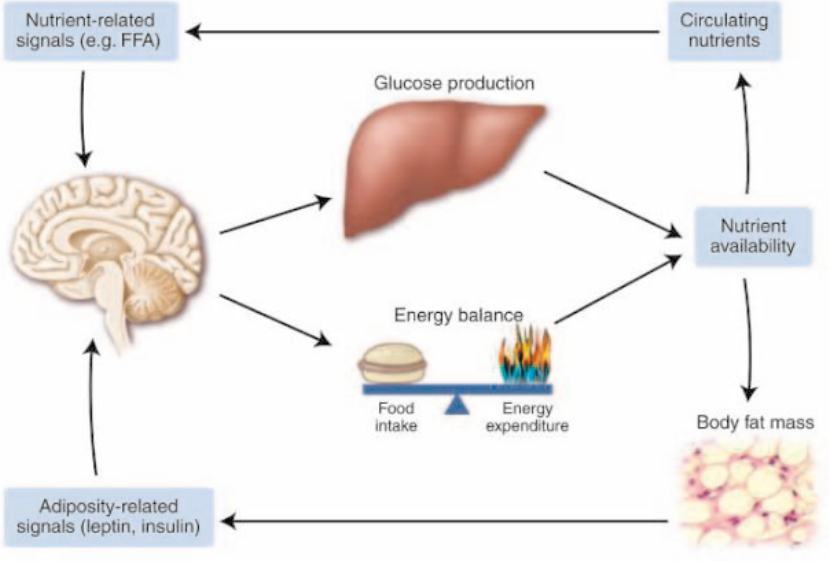

Fig. 1. Model depicting the control of energy homeostasis and hepatic glucose metabolism by adiposity- and nutrient-related signals. Neuronal systems sense and respond to input from hormones such as insulin and leptin that are secreted in proportion to body energy stores and from the metabolism of circulating nutrients (such as glucose and FFAs). In response to this input, adaptive changes occur in energy intake, energy expenditure, and hepatic glucose production.

The Brain as an Insulin-Sensitive Tissue

In contrast to its prominent action in liver, muscle, and fat, insulin is not a major regulator of glucose use by the brain (*4*). This observation, combined with the widespread belief that a peptide the size of insulin would be unable to cross the blood-brain barrier, has led to the perception of the brain as an insulin-insensitive tissue. Recent observations have revealed this presumption to be erroneous and demonstrate that even though the brain is insulin-independent (with respect to glucose use), it clearly is not insulin-insensitive.

Evidence of insulin action in the brain emerged 25 years ago with the demonstration in a primate model that food intake decreases when a low dose of insulin is delivered directly to the brain by continuous intracerebroventricular (icv) infusion (*5*). When this fact was combined with evidence that insulin circulates at levels proportionate to body fat mass, that circulating insulin is transported into the brain, and that insulin receptors are concentrated in brain areas involved in the control of food intake and autonomic function (*6*), insulin emerged as a candidate "adiposity negative feedback" signal in the central control of energy homeostasis. When it was later shown that icv insulin administration also reduces hepatic glucose production (by increasing liver sensitivity to insulin) (*7*), insulin was hypothesized to be a central regulator of both energy homeostasis and glucose metabolism.

The hypothesis that brain insulin action is required for intact glucose homeostasis is supported by a series of recent findings. Studying mice genetically deficient in the insulin receptor, Accili and colleagues showed that selective expression of insulin receptors in only two tissues (liver and pancreas) substantially reduces diabetes severity and prolongs life-span (*8*). Even more surprising is that rescue of insulin receptor expression in the brain, in addition to the liver and pancreas, confers near-complete protection against hyperglycemia. In parallel studies undertaken in normal rats, chronic blockade of hypothalamic insulin receptor signaling was shown to cause hepatic insulin resistance and to increase hepatic glucose production (*7*, *9*). Combined with evidence that mice with neuron-specific insulin receptor deletion are overweight, insulin-resistant, and glucose-intolerant (*10*), these data demonstrate that neuronal insulin signaling is required for intact control of both body fat mass and glucose homeostasis.

A potentially confounding aspect of these studies is that reduced neuronal insulin action increases food intake and body weight, and these effects may also cause insulin resistance. Nevertheless, available data suggest that central insulin action can regulate energy homeostasis and glucose metabolism via neuronal systems that are, at least in part, independent of one another (*9*).

In peripheral tissues, insulin signal transduction involves the insulin receptor substrate–phosphatidylinositol 3-OH kinase (IRS-PI3K) pathway (*11*). The idea that this cellular pathway is a key mediator of neuronal insulin action is supported by evidence that the actions of icv insulin on both food intake and hepatic glucose production are blocked by icv pretreatment with either of two PI3K inhibitors (*7*, *12*). Because defective IRS-PI3K signaling has been implicated in the pathogenesis of insulin resistance in peripheral tissues (*11*, *13*), these observations raise the unanswered question of whether neuronal insulin resistance might also occur by this mechanism. This possibility takes on

heightened significance in view of evidence that IRS-PI3K signal transduction in hypothalamic neurons is also activated by the adipocyte hormone leptin (*14*), and that deletion of IRS2 from hypothalamic neurons results in obesity and insulin resistance (*15*, *16*).

Leptin and Glucose Homeostasis

The neuronal response to leptin receptor activation involves the Janus kinase–signal transducer and activator of transcription (Jak-STAT) pathway (*17*). Among the proteins induced by leptin-mediated STAT signaling is suppressor of cytokine signaling-3 (SOCS3), which inhibits leptin activation of the Jak-STAT pathway (*17*). Interestingly, SOCS3 also potently inhibits signaling by insulin receptors (*18*), and sensitivity to both insulin and leptin is augmented in mice with reduced neuronal expression of SOCS3 (*19*, *20*). That these mice are protected against diet-induced obesity suggests further that SOCS3-mediated attenuation of the neuronal response to adiposity signals is required for weight gain induced by consumption of a highly palatable, energy-rich diet. Combined with evidence that both leptin- and insulin-induced signaling involves the IRS-PI3K pathway, the cellular actions of these two adiposity-related hormones appear to overlap at multiple levels within neuronal systems that are important to both energy homeostasis and glucose metabolism (*21*).

Genetic leptin deficiency in *ob/ob* mice (*22*) is associated not only with pronounced hyperphagia and obesity but with insulin resistance and mild-to-moderate diabetes. Although impaired glucose metabolism in these mice is clearly driven by their severe obesity, leptin deficiency per se appears to make an independent contribution, because the glucose-lowering effect of leptin occurs at doses below those needed to reverse obesity (*23*) and cannot be reproduced by simple caloric restriction (*24*). In addition, the hyperglycemic consequences of impaired leptin signaling are dependent on coexistent defects in insulin secretion that are, at least in part, genetically determined. Background genes that influence endocrine pancreatic function are therefore important determinants of the predisposition to diabetes in genetic models of deficient leptin signaling. The lack of such genes may explain why children with genetic leptin deficiency are not reported to have diabetes, although they are severely obese (*25*).

A variety of gene defects have been identified that disrupt adipogenesis, causing a disorder known as lipodystrophy that is characterized by a loss of body adipose tissue, leptin deficiency, and a unique and severe form of insulin resistance and diabetes (*26*). Mouse models recapitulate the key features of the human disorder and have yielded substantial new insights into both its metabolic basis and its treatment (*27*). Because lipodystrophic mice are lean and, by definition, have reduced or absent fat mass, their body weight phenotype contrasts sharply with the severe obesity of *ob/ob* mice. Yet lipodystrophic and leptin-deficient mice share key features in common, including hyperphagia, insulin resistance, diabetes, and markedly reduced leptin signaling. Because the diabetes phenotype of lipodystrophic and leptin-deficient mice is ameliorated by leptin administration (*28*), a role for leptin deficiency in both diabetes syndromes is suggested (*29*). Moreover, icv administration of leptin at a low dose reversed the metabolic disturbance of lipodystrophic mice as effectively as systemic administration of a much higher dose (*30*), suggesting that the antidiabetic effect of leptin in this setting involves an action in the brain.

Lipodystrophic diabetes also develops in mice that express insulin receptors in the liver and pancreas but otherwise lack the insulin receptor gene (*8*). Surprisingly, this lipodystrophy is prevented by the expression of insulin receptors in the brain, in addition to the liver and pancreas (*8*). How might insulin action in the brain affect the predisposition to lipodystrophy? One possibility is suggested by the recently discovered mutations of the *BSCL2* gene. Although the function of the protein encoded by this gene (termed ''seipin'') remains to be determined, these mutations are responsible for one variant of the Berardinelli-Seip congenital lipodystrophy syndrome associated with mental retardation in humans (*31*, *32*). This gene is highly expressed in the brain but only modestly in adipocytes (*31*), suggesting a role for the CNS in the pathogenesis of lipodystrophy in humans.

Hypothalamic Targets of Insulin and Leptin Action

The arcuate nucleus, situated adjacent to the floor of the third ventricle in the mediobasal hypothalamus, contains neurons that exert potent effects on food intake, energy expenditure, and glucose homeostasis and are regulated by input from both hormonal and nutrient-related signals (*2*, *33*). ''Anabolic'' neurons coexpress neuropeptide Y (NPY) and Agouti-related peptide (AgRP), two peptides that potently stimulate food intake and reduce energy expenditure, and thereby promote weight gain (*34*–*36*). These neurons are inhibited by leptin and insulin (*33*); consequently, reduced neuronal input from these hormones increases hypothalamic signaling by both peptides. Central administration of NPY causes insulin resistance and

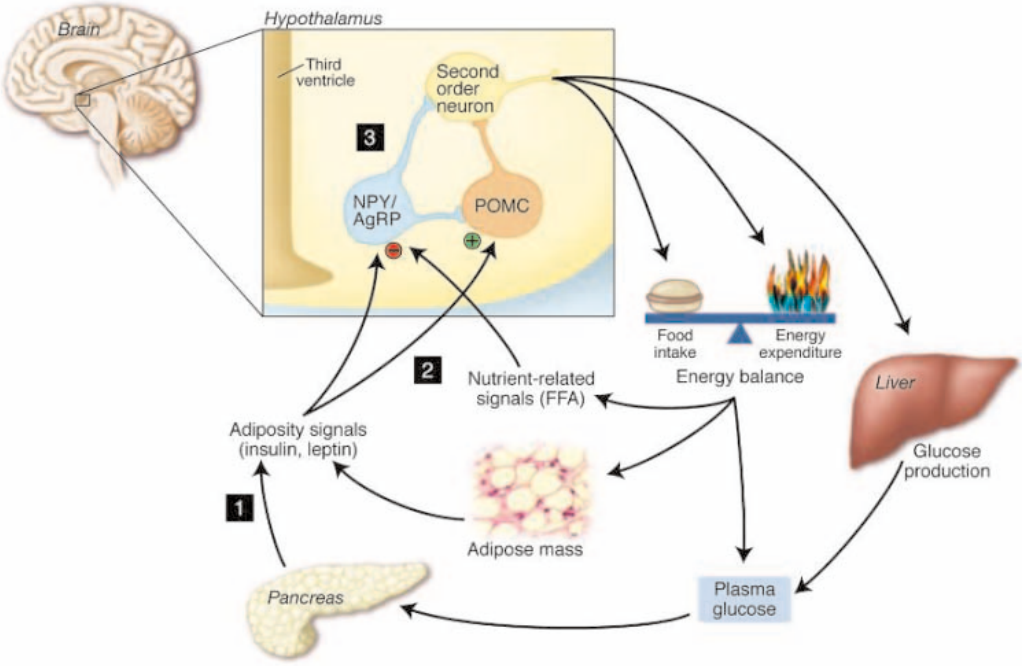

Fig. 2. Neurocentric model depicting sites where defects in the negative feedback regulation of energy balance and glucose production predispose to weight gain and insulin resistance. Defects in the secretion of insulin or leptin (*1*), in the hypothalamic sensing of adiposity- or nutrient related signals (*2*), or in the neuronal responsiveness to these inputs (*3*) predispose to both positive energy balance and increased glucose production. If sustained, these will result in pathological weight gain and insulin resistance.

glucose intolerance, even when its effects on food intake are prevented (*37*, *38*). Under conditions of reduced hypothalamic signaling by insulin and leptin, increased NPY signaling may therefore contribute not only to the resultant hyperphagia and weight gain but to systemic insulin resistance and glucose intolerance as well (Fig. 2).

By comparison, the anabolic effects of AgRP arise from antagonism of neuronal melanocortin receptors (MC3r and MC4r) (*36*, *39*) that serve to limit food intake and body weight. Like the response to NPY administration, chronic blockade of central melanocortin receptors causes weight gain and insulin resistance (*40*), although the extent to which AgRP affects glucose metabolism independently of its effects on body fat mass awaits further study.

Melanocortins are peptides derived from posttranslational processing of the precursor proopiomelanocortin (POMC), and POMC neurons in the arcuate nucleus innervate the same hypothalamic areas supplied by fibers from NPY/AgRP neurons. Unlike NPY/AgRP neurons, however, POMC neurons are stimulated by input from insulin and leptin (*41*, *42*), and the binding of melanocortins to MC3r and MC4r inhibits food intake and promotes weight loss (*43*). When neuronal input from leptin and insulin is reduced, therefore, POMC neurons are inhibited whereas NPY/AgRP neurons are activated, responses that in turn can cause hyperphagia, insulin resistance, and glucose intolerance. Although changes in autonomic outflow to the liver and other tissues have been proposed, the efferent mechanism whereby output from arcuate nucleus neurons is linked to the control of glucose metabolism in peripheral tissues remains uncertain. Moreover, the arcuate nucleus is by no means the only area of the brain that can process input from adiposity- and nutrient-related signals, and an important priority is to clarify the contribution of other brain areas to the control of energy homeostasis and glucose metabolism.

Nutrient Sensing and the Central Control of Glucose Homeostasis

In addition to processing input from leptin and insulin, hypothalamic neurons involved in peripheral glucose metabolism also sense and respond to intracellular signals that reflect ongoing cellular energy status. Like other cell types, neurons possess fuel-sensing mechanisms that not only ensure that cellular energy needs are met but, in specialized cells, influence firing rate, gene expression, or other cellular functions. The enzyme adenosine monophosphate (AMP)–activated protein kinase (AMPK) is activated in response to falling intracellular adenosine triphosphate levels (which are typically accompanied by rising AMP content) and is an example of such a cellular fuel sensor (*44*). In the arcuate nucleus, AMPK activation induces hyperphagia and weight gain resembling the response to reduced hypothalamic input from insulin and leptin (*45*). Further, arcuate nucleus AMPK activity is inhibited by both insulin and leptin, and the ability of leptin to reduce food intake appears to require this inhibition of AMPK (*45*). The extent to which this fuel-sensing mechanism mediates effects of adiposity-related hormones in the central control of glucose metabolism is an active area of study.

In addition to mechanisms for sensing the depletion of cellular energy reserves, the hypothalamus can also respond to an increase of nutrient availability. One example is the intracellular esterification of FFAs into long-chain fatty-acyl–CoA molecules (LCFACoA, derived from both exogenous FFAs and de novo FFA synthesis) (*46*, *47*). Accumulation of LCFACoA in key neurons is hypothesized to constitute a cellular signal of plenty that increases when both glucose and FFAs are in abundant supply. In the hypothalamus, acute increases of FACoA levels can potently inhibit food intake while also increasing hepatic insulin sensitivity (*3*). This area of research was originally inspired by the observation of leptin- and insulin-like effects (reductions of food intake, hypothalamic NPY gene expression, and blood glucose levels) after administration of C75, an inhibitor of fatty acid synthase (*48*). This drug is predicted to increase intracellular FACoA content through the accumulation of malonyl-CoA, a molecule that inhibits FACoA oxidation. The extent to which the accumulation of FACoA [or of malonyl-CoA, also proposed to have signaling properties (*49*)] mediates the actions of C75 is unclear, because this compound also inhibits AMPK (*50*) and has neurotoxic effects (*51*).

The work of Rossetti and colleagues strongly supports a role for FACoA signaling in the central control of both food intake and glucose homeostasis. They found that icv infusion of oleic acid (a long-chain FFA) in rats potently reduces food intake, inhibits *Npy* gene expression, and increases hepatic insulin sensitivity (*52*) (Fig. 2). Similar responses were reported after icv infusion of an inhibitor of CPT-1 (*3*), the mitochondrial transfer protein that controls the rate of fatty acid oxidation. This intervention increased hypothalamic FACoA levels and again triggered behavioral, metabolic, and hypothalamic responses that resemble the central actions of insulin and leptin. Furthermore, central CPT-1 inhibition activated neurons in brainstem areas that control parasympathetic outflow and increased hepatic insulin sensitivity through a mechanism that is blocked by vagotomy (*53*). Thus, hypothalamic lipid sensing is proposed to regulate hepatic glucose metabolism via the activation of vagal efferent fibers that supply the liver (Fig. 2). Remaining challenges include efforts to clarify whether hypothalamic FACoA content is sensitive to changes in plasma FFA levels, how fluctuations of intracellular nutrient metabolism affect neuronal function, how they are integrated with input from insulin and leptin, and how this information is transduced into behavioral, autonomic, and metabolic responses.

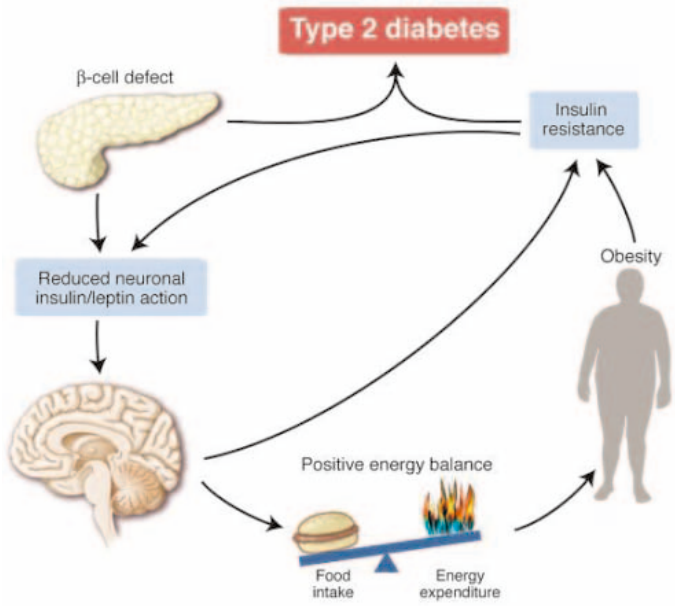

Fig. 3. Neurocentric model linking obesity to the pathogenesis of insulin resistance and type 2 diabetes. Reduced neuronal input from adiposity- or nutrient-related signals favors both positive energy balance and hepatic insulin resistance. As weight gain progresses to obesity, worsening insulin resistance increases the demand for insulin secretion. When combined with a β-cell defect (which reduces insulin action in the brain and periphery), type 2 diabetes ensues.

Obesity, the Brain, and Type 2 Diabetes

Conventional wisdom links type 2 diabetes to obesity by virtue of the insulin resistance that

arises from an excess of body fat. If pancreatic β cells cannot appropriately increase insulin secretion, glucose intolerance and ultimately frank hyperglycemia ensue. These same observations, however, are compatible with an alternative, neurocentric model (Fig. 3). This model is predicated on four key observations highlighted in this essay. First, the brain is not insulin-insensitive; on the contrary, it uses input from insulin, leptin, and nutrient-related signals to regulate both body fat content and hepatic insulin sensitivity (Fig. 2). Second, impaired neuronal signaling by these afferent signals causes hyperphagia, weight gain, and hepatic insulin resistance through mechanisms that are at least partly independent of one another. Third, obesity is strongly associated with biochemical resistance to both insulin and leptin. Fourth, defective insulin secretion (which presumably reduces insulin delivery to the brain as well as to other tissues) is a prerequisite for type 2 diabetes (*54*). Together these observations support a model in which reduced neuronal insulin and leptin signaling contributes to the link between excess body fat and disordered glucose metabolism.

According to this model, obesity and impaired glucose metabolism can be predicted to arise from any of several defects that affect how the brain receives or processes input from key adiposity- or nutrient-related signals. Reduced insulin secretion can be invoked as a primary event, because reduced insulin delivery to the brain favors both weight gain and hepatic insulin resistance. As obesity progresses, a further deterioration of insulin sensitivity occurs (due to increased body fat content) that, together with impaired insulin secretion, will cause plasma glucose levels to increase. Although such increases may initially be limited by a compensatory increase of insulin secretion, the ability of the β cell to meet the demand posed by progressive weight gain and insulin resistance may ultimately reach its limit, leading to overt hyperglycemia. If obesity causes resistance to insulin in neurons as well as in peripheral tissues, a vicious cycle is created that accelerates weight gain and hepatic insulin resistance and thereby hastens diabetes onset (Fig. 3).

Defects in either the neuronal sensing of, or response to, afferent hormonal or nutrient-related signals can also set in motion a pathological cascade that progresses ultimately to obesity and diabetes. Because convergent signal transduction (for example, via the IRS-PI3K signaling pathway) and termination (for example, SOCS3) mechanisms mediate the neuronal actions of insulin and leptin, defects within a single biochemical pathway can potentially cause resistance to the central actions of both hormones (*21*). This in turn can be predicted to induce hyperphagia, weight gain, hepatic insulin resistance, and glucose intolerance. The feasibility of this concept is strengthened by evidence implicating impaired IRS-PI3K signal transduction in the insulin resistance of peripheral tissues in diabetic humans and animal models (*13*). When combined with a β-cell defect, a feed-forward mechanism is again set in motion whereby reduced insulin and leptin action in the brain and periphery initially favors weight gain and insulin resistance, progressing to glucose intolerance and ultimately diabetes. Because functional resistance to both leptin and insulin is common among the obese, this hypothesis warrants careful consideration (*21*) (Fig. 3).

Direct evidence in support of these predictions was recently provided from studies of mice in which IRS2 was selectively deleted from pancreatic β cells and hypothalamic neurons (*15*, *16*). Because IRS-2 is necessary for β-cell survival, a gradual, progressive loss of β-cell mass occurs in these mice and predisposes them to diabetes. Because IRS-2 is also implicated in neuronal signaling by insulin and leptin, deletion of this protein from the hypothalamus impairs afferent input from the two known adiposity signals. Consequently, these animals develop obesity and insulin resistance that, combined with β-cell dysfunction, progress to glucose intolerance and finally to diabetes. Disruption of signaling via the IRS-PI3K pathway is therefore sufficient to cause obesity and diabetes, even when this defect is limited to only the brain and pancreas.

A neurocentric model to explain the link between obesity and diabetes also predicts that the risk of these disorders is strongly increased by environmental factors that favor weight gain (such as an abundance of highly palatable, energy-dense foods combined with a minimal requirement for physical activity). Accordingly, therapies that restore neuronal signaling by key afferent signals may prove beneficial for both obesity and diabetes, especially when combined with adjustments in diet and physical activity. Therefore, as Bernard anticipated in 1854, progress in understanding and treating diabetes will require an improved understanding of brain systems that control body fuel homeostasis and energy storage.

References and Notes

1. C. Bernard, *Leçons de physiologie experimentale appliqués á là medecine* (Baillere et Fils, Paris, 1854).
2. R. J. Seeley, S. C. Woods, *Nature Rev. Neurosci.* **4**, 901 (2003).
3. S. Obici, Z. Feng, A. Arduini, R. Conti, L. Rossetti, *Nature Med.* **9**, 756 (2003).
4. E. R. Seaquist, G. S. Damberg, I. Tkac, R. Gruetter, *Diabetes* **50**, 2203 (2001).
5. S. C. Woods, E. C. Lotter, L. D. McKay, D. Porte Jr., *Nature* **282**, 503 (1979).
6. M. W. Schwartz, D. P. Figlewicz, D. G. Baskin, S. C. Woods, D. Porte Jr., *Endocr. Rev.* **13**, 387 (1992).
7. S. Obici, B. B. Zhang, G. Karkanias, L. Rossetti, *Nature Med.* **8**, 1376 (2002).
8. H. Okamoto, J. Nakae, T. Kitamura, B. C. Park, I. Dragatsis, D. Accili, *J. Clin. Invest.* **114**, 214 (2004).
9. S. Obici, Z. Feng, G. Karkanias, D. G. Baskin, L. Rossetti, *Nature Neurosci.* **5**, 566 (2002).
10. J. C. Bruning *et al.*, *Science* **289**, 2122 (2000).
11. M. F. White, *Science* **302**, 1710 (2003).
12. K. D. Niswender *et al.*, *Diabetes* **52**, 227 (2003).
13. G. I. Shulman, *J. Clin. Invest.* **106**, 171 (2000).
14. K. D. Niswender *et al.*, *Nature* **413**, 794 (2001).
15. N. Kubota *et al.*, *J. Clin. Invest.* **114**, 917 (2004).
16. X. Lin *et al.*, *J. Clin. Invest.* **114**, 908 (2004).
17. S. H. Bates, M. G. Myers, *J. Mol. Med.* **82**, 12 (2004).
18. K. Ueki, T. Kondo, C. R. Kahn, *Mol. Cell Biol.* **24**, 5434 (2004).
19. J. K. Howard *et al.*, *Nature Med.* **10**, 734 (2004).
20. H. Mori *et al.*, *Nature Med.* **10**, 739 (2004).
21. M. W. Schwartz, K. D. Niswender, *J. Clin. Endocrinol. Metab.* **89**, 5889 (2004).
22. Y. Zhang *et al.*, *Nature* **372**, 425 (1994).
23. R. B. Harris *et al.*, *Endocrinology* **139**, 8 (1998).
24. M. W. Schwartz *et al.*, *Diabetes* **45**, 531 (1996).
25. C. T. Montague *et al.*, *Nature* **387**, 903 (1997).
26. B. I. Joffe, V. R. Panz, F. J. Raal, *Lancet* **357**, 1379 (2001).
27. M. L. Reitman, E. Arioglu, O. Gavrilova, S. I. Taylor, *Trends Endocrinol. Metab.* **11**, 410 (2000).
28. K. Ebihara *et al.*, *Diabetes* **50**, 1440 (2001).
29. E. A. Oral *et al.*, *N. Engl. J. Med.* **346**, 570 (2002).
30. E. Asilmaz *et al.*, *J. Clin. Invest.* **113**, 414 (2004).
31. J. Magre *et al.*, *Nature Genet.* **28**, 365 (2001).
32. L. Van Maldergem *et al.*, *J. Med. Genet.* **39**, 722 (2002).
33. M. W. Schwartz, S. C. Woods, D. Porte Jr., R. J. Seeley, D. G. Baskin, *Nature* **404**, 661 (2000).
34. J. T. Clark, P. S. Kalra, S. P. Kalra, *Endocrinology* **117**, 2435 (1985).
35. C. M. Kotz, J. E. Briggs, M. K. Grace, A. S. Levine, C. J. Billington, *Am. J. Physiol.* **275**, R471 (1998).
36. M. M. Ollmann *et al.*, *Science* **278**, 135 (1997).
37. J. L. Marks, K. Waite, *J. Neuroendocrinol.* **9**, 99 (1997).
38. A. M. van den Hoek *et al.*, *Diabetes* **53**, 2529 (2004).
39. J. R. Shutter, M. Graham, A. C. Kinsey, S. Scully, R. Luthy, K. L. Stark, *Genes Dev.* **11**, 593 (1997).
40. T. Adage *et al.*, *J. Neurosci.* **21**, 3639 (2001).
41. M. A. Cowley *et al.*, *Nature* **411**, 480 (2001).
42. M. W. Schwartz *et al.*, *Diabetes* **46**, 2119 (1997).
43. R. D. Cone, *Trends Endocrinol. Metab.* **10**, 211 (1999).
44. D. G. Hardie, *Endocrinology* **144**, 5179 (2003).
45. Y. Minokoshi *et al.*, *Nature* **428**, 569 (2004).
46. J. T. Deeney, M. Prentki, B. E. Corkey, *Semin. Cell Dev. Biol.* **11**, 267 (2000).
47. G. C. Yaney, B. E. Corkey, *Diabetologia* **46**, 1297 (2003).
48. T. M. Loftus *et al.*, *Science* **288**, 2379 (2000).
49. Z. Hu, S. H. Cha, S. Chohnan, M. D. Lane, *Proc. Natl. Acad. Sci. U.S.A.* **100**, 12624 (2003).
50. E. K. Kim *et al.*, *J. Biol. Chem.* **279**, 19970 (2004).
51. K. A. Takahashi, J. L. Smart, H. Liu, R. D. Cone, *Endocrinology* **145**, 184 (2004).
52. S. Obici *et al.*, *Diabetes* **51**, 271 (2002).
53. A. Pocai, S. Obici, G. Schwartz, L. Rosetti, *Cell Metab.*, in press.
54. D. Porte Jr., *Diabetes Metab. Res. Rev.* **17**, 181 (2001).

55. Supported by NIH grants DK52989, DK683840, and NS32273 and by the Diabetes Endocrinology Research Center and Clinical Nutrition Research Unit of the University of Washington.

10.1126/science.1104344

VIEWPOINT

Type 2 Diabetes—a Matter of β-Cell Life and Death?

Christopher J. Rhodes

In type 2 diabetes, the β cells of the pancreas fail to produce enough insulin to meet the body's demand, in part because of an acquired decrease in β-cell mass. In adults, pancreatic β-cell mass is controlled by several mechanisms, including β-cell replication, neogenesis, hypertrophy, and survival. Here, I discuss evidence supporting the notion that increased β-cell apoptosis is an important factor contributing to β-cell loss and the onset of type 2 diabetes. Interestingly, a key signaling molecule that promotes β-cell growth and survival, insulin receptor substrate 2 (IRS-2), is a member of a family of proteins whose inhibition contributes to the development of insulin resistance in the liver and other insulin-responsive tissues. Thus, the IRS-2 pathway appears to be a crucial participant in the tenuous balance between effective pancreatic β-cell mass and insulin resistance.

Concurrent with the obesity epidemic, the incidence of type 2 diabetes is increasing at an alarming rate (*1*). Type 2 diabetes arises when the endocrine pancreas fails to secrete sufficient insulin to cope with the metabolic demand (*2*, *3*), because of acquired β-cell secretory dysfunction and/or decreased β-cell mass. Insulin secretory dysfunction in type 2 diabetes is well documented and has been reviewed elsewhere (*4*, *5*). Whether insulin secretory dysfunction is a cause or consequence of the disease is still debated, but there is mounting evidence that it may be symptomatic of changes in β-cell mass (*3*, *6*). Although proposed nearly 50 years ago (*7*), the hypothesis that β-cell loss plays an important role in the pathogenesis of type 2 diabetes has only recently come to the fore (*3*). β-cell mass in the adult is plastic, and adjustments in β-cell growth and survival maintain a balance between insulin supply and metabolic demand. For example, obese individuals who do not develop diabetes exhibit an increase in β-cell mass that appears to compensate for the increased metabolic load and obesity-associated insulin resistance. However, this β-cell adaptation eventually fails in the subset of obese individuals who develop type 2 diabetes (*2*, *7*–*12*). Indeed, most individuals with type 2 diabetes, whether obese or lean, show a net decrease in β-cell mass (*8*). Thus, type 2 diabetes is a disease of relative insulin deficiency.

Given the pivotal role of β-cell mass in determining whether an individual will progress to type 2 diabetes (*2*, *10*), there is growing interest in understanding the mechanisms that control the life and death of β cells. Here, I outline current concepts of β-cell growth and survival, with an emphasis on one particular cell survival mechanism that is thought to go awry in type 2 diabetes.

Cellular Mechanisms Controlling Adult β-Cell Mass

Pancreatic β-cell mass is regulated by at least four independent mechanisms: (i) β-cell replication (i.e., the mitogenic division of existing β cells), (ii) β-cell size, (iii) β-cell neogenesis [i.e., the emergence of "new β cells" from certain common pancreatic ductal epithelial cells (*8*, *13*, *14*)], and (iv) β-cell apoptosis (*10*, *12*, *13*). The sum of the rates of β-cell replication, size, and neogenesis, minus the rate of β-cell apoptosis gives the net rate of β-cell growth (*12*, *15*). The contribution made by each of these mechanisms is variable and may change at different stages of life or when the β-cell mass adapts to changes in metabolic load. Moreover, the relative contribution of each may be species specific. For example, recent evidence indicates that maintenance of β-cell mass in young adult mice is primarily due to β-cell replication (*16*, *17*), yet in humans both β-cell neogenesis and replication appear to play a role (*8*). Adding further complexity, β-cell neogenesis has been documented in older mice (*18*), an observation that underscores the age dependence of these mechanisms.

Measuring dynamic changes in β-cell mass is technically difficult and subtleties can be overlooked. Markers of cell division, such as Ki-67, correspond to a small transient window in the cell cycle and may underestimate the incidence of β-cell replication. Likewise, apoptotic and necrotic cells are efficiently cleared by macrophages in vivo and so the extent of β-cell apoptosis, especially when analyzed in ex vivo pancreatic sections, may be underappreciated. Pancreatic β-cell neogenesis (often measured as the abundance of insulin-positive cells in the pancreatic ductal epithelium) is relatively rare and its detection requires analysis of multiple pancreatic sections. Moreover, without specific markers for "precursor β cells," it is difficult to judge whether "insulin-positive cells" actually mature into fully differentiated β cells or are alternative cell types that have been misdiagnosed (*19*, *20*). Such studies are particularly challenging in humans, where retrograde analyses from autopsy specimens cannot be done and pancreatic biopsies are difficult to obtain. In addition, pancreatic specimens from patients with type 2 diabetes often represent only the end stages of the disease.

These technical difficulties notwithstanding, a model of postnatal pancreatic β-cell growth in humans is emerging from studies of both humans (*7*–*9*) and rodents (*21*, *22*) (Figs. 1 and 2). Under normal circumstances, there is a transient burst of β-cell replication just after birth, followed by a transitory rise in β-cell neogenesis (*21*) (Fig. 2). In the later phase of this neonatal burst of β-cell replication and neogenesis, there is also a modest amount of apoptosis that parallels pancreatic islet rearrangement. Because this rate of apoptosis is low, the net effect is a marked increase in β-cell growth early in life. It should be noted that the early burst of β-cell growth has been observed primarily in rodent models. This is obviously difficult to substantiate in newborn humans, although it is generally thought that a similar spurt of human postnatal β-cell growth occurs (*21*). Thereafter, through childhood and adolescence the rates of β-cell replication, neogenesis, and apoptosis drop markedly (Fig. 2). In adults, β cells have an estimated life-span of ~60 days (*13*). Under normal conditions, ~0.5% of adult β cells undergo apoptosis, but this is balanced by β-cell replication and, to a lesser extent, β-cell neogenesis (*2*, *21*). Normally, β-cell size stays relatively constant and, as such, β-cell mass is maintained at an optimal level through most of adulthood (Fig. 2). In the senior years of life, β-cell mass may decrease as apoptosis slightly outweighs β-cell replication and neogenesis (Fig. 2). This may partially explain why the elderly have an increased susceptibility to type 2 diabetes.

The Pacific Northwest Research Institute, 720 Broadway, Seattle, WA 98122, USA, and Department of Pharmacology, University of Washington, Seattle, WA 98122, USA. E-mail: cjr@pnri.org

Adaptation of β-Cell Mass to Metabolic Load

During adulthood, the β-cell mass is highly adaptive to changes in metabolic homeostasis. A good example is pregnancy: Rodent studies have shown that the maternal β-cell population can almost double to compensate for the increased metabolic load of a developing fetus (*23*). Although the evidence is limited, a similar adaptation likely occurs in humans (*23*). This is achieved primarily by increased β-cell replication driven by the pregnancy hormones prolactin and placental lactogen (*23*). Postpartum, the rate of β-cell replication decreases and a concomitant increase in β-cell apoptosis ensures a rapid return of β-cell mass to normal levels (*21*).

More pertinent to this article, however, is that β-cell mass adapts to an increased metabolic load caused by obesity and the inherent insulin resistance. In humans, this increased β-cell mass is thought to occur through an increase in β-cell replication and neogenesis, as well as β-cell hypertrophy (Figs. 1 and 2) (*8*, *11*). A small increase in β-cell apoptosis has also been observed in nondiabetic obesity (*8*); however, this is outweighed by increases in β-cell replication, neogenesis, and cell size, resulting in a net increase in β-cell mass (Fig. 2). As previously mentioned, the relative contributions of β-cell replication, neogenesis, and size to this compensatory increase in β-cell mass may vary between species and even between different strains of rats and mice (*12*). Whether humans have a genetically based variability in the adaptive mechanisms that increase β-cell mass remains to be determined.

Failure of β-Cell Mass to Compensate for Metabolic Load

Although there may be an initial compensatory increase in β-cell mass, the onset of type 2 diabetes in both humans and rodent models is accompanied by a progressive decrease in β-cell mass. As a result, the body can no longer adapt to any increases in metabolic load, including insulin resistance associated with obesity. This β-cell loss arises from a marked increase in β-cell apoptosis, which far outweighs modest increases in β-cell replication and neogenesis (Fig. 2) (*2*, *8*, *11*, *22*). As the type 2 diabetic state progresses, the situation worsens; the incidence of β-cell replication decreases and the β-cell population declines (Fig. 2). In humans, the increased β-cell apoptosis in type 2 diabetes is further exacerbated by the formation of amyloid plaque deposits in islets (*24*) (Fig. 1). Eventually, in the most severe cases, a ''point of no return'' in β-cell mass can be reached and a permanent type 2 diabetic state arises that must be treated with insulin replacement therapy (*6*).

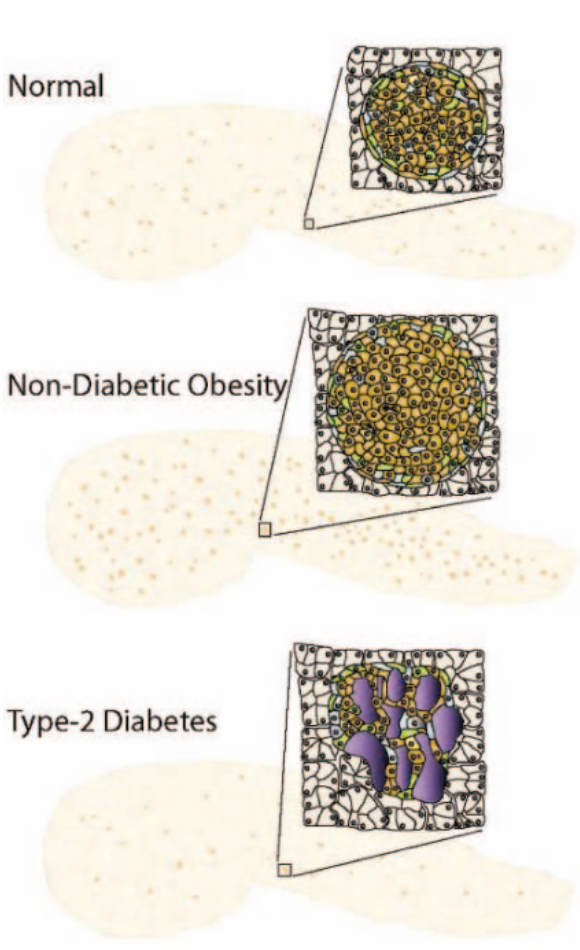

Fig. 1. Adult pancreatic morphology in normal, nondiabetic obesity and type 2 diabetes. The whole pancreas, which is composed primarily of exocrine cells (which produce enzymes that are delivered directly to the gut by way of the pancreatic duct for digestion), retains the same shape and size in all of these conditions. The endocrine islets (which secrete insulin) are more dynamic. Under normal circumstances, these islets are scattered throughout the pancreas and comprise about 1% of the total pancreatic population of cells. In normal islets (inset), the β cells (brown) tend to populate the core of the islet, representing about 70% of the islet endocrine cells. In nondiabetic obesity, the number of islets in the pancreas increases and these islets (inset) tend to be larger, primarily because of increased numbers of β cells per islet or in some instances because of increased β-cell size. As a result, >90% of the islet endocrine cells are β cells. In type 2 diabetes, the number of islets in the pancreas can decrease and these islets (inset) tend to be disorganized and misshapen. There is a marked reduction in the number of β cells per islet and amyloid plaques (purple) can dominate the islet area.

About one-third of obese individuals develop type 2 diabetes. This may be due to a genetic predisposition at the level of the β cell. Consistent with this idea, certain inherited forms of type 2 diabetes, called maturity-onset diabetes of the young (MODY), are caused by mutations in proteins required for normal β-cell function, such as glucokinase and the transcription factor PDX-1 (*25*). However, environmental contributions should also be considered. In humans, low birth weight has been associated with an increased risk of developing type 2 diabetes in adulthood (*26*). In this regard, the surges in β-cell replication and neogenesis early in postnatal life become critical for laying down the baseline population of β cells in adult life (Fig. 2). In a smaller neonate, a proportionally smaller baseline β-cell mass may be acquired in the adult (*12*). A limited adult β-cell mass could compromise the body's capacity to compensate for an increased metabolic load, as in pregnancy or obesity, which in turn may contribute to an increased risk of gestational diabetes or earlier onset of obesity-linked type 2 diabetes (*12*).

The Role of IRS-2 Signaling in β-Cell Survival

Many mechanisms could trigger the increase in β-cell apoptosis that occurs during the pathogenesis of type 2 diabetes (*2*, *3*, *11*, *27*). Among them are the development of endoplasmic reticulum (ER) stress, chronic hyperglycemia, chronic hyperlipidemia, oxidative stress, and certain cytokines (*2*, *3*, *11*, *27*). Here, I consider how certain circulating factors that are elevated in obesity-linked diabetes might disrupt signal transduction pathways that promote normal β-cell turnover and survival. I focus on factors that affect expression levels of IRS-2 because IRS-2 is especially potent in promoting β-cell survival (*28*) and because dampening of IRS-2 signaling leads to insulin resistance as well as β-cell apoptosis.

Members of the IRS protein family are intracellular tyrosine kinase substrates that act as signaling interfaces immediately downstream of cell surface receptors, such as the insulin and insulin-like growth factor-1 (IGF-1) receptors (*29*). Deletion of IRS-1 and IRS-2 leads to marked insulin resistance, indicating that these genes play a key role in insulin action (*30*–*33*). Once an IRS molecule is tyrosine phosphorylated, certain signaling proteins selectively dock by means of their SH2-domains to specific IRS-phosphotyrosine sites, resulting in activation of downstream signaling pathways. Examples include the phosphatidylinositol-3′-kinase (PI3′K)/protein kinase-B (PKB, also known as Akt) pathway and the Ras pathway that leads to activation of

the mitogen-activated protein (MAP) kinases Erk-1 and Erk-2 (*29*). Both IRS-1 and IRS-2 are expressed in pancreatic β-cells. However, IRS-1 is not involved in the control of β-cell mass (*30*), but instead appears to function in cellular Ca^{2+} homeostasis (*34*). In contrast, IRS-2 plays a critical role in regulation of β-cell growth (*30*, *33*, *35*). Increased IRS-2 expression can promote β-cell replication, neogenesis, and survival (*12*, *18*, *28*), whereas decreased IRS-2 expression causes spontaneous β-cell apoptosis (*30*, *35*, *36*). Thus, IRS-2 is critically important for maintaining β-cell mass, especially by promoting β-cell survival (*12*, *28*). It follows then that mechanisms leading to suppression of IRS-2 expression in β-cells may be linked to the increased incidence of β-cell apoptosis and consequently the onset of type 2 diabetes (*29*, *37*).

What mechanisms might contribute to the loss of IRS-2 expression in β cells? Although experimental evidence is limited, some interesting parallels can be drawn to mechanisms by which insulin resistance develops in insulin-responsive tissues, such as skeletal muscle and the liver. Tyrosine phosphorylation of IRS-2 leads to increased β-cell growth and survival (*2*). However, IRS-2 contains multiple sites for serine/threonine phosphorylation, and these, for the most part, have a negative effect on IRS signal transduction by promoting IRS degradation (*37*, *38*). Several mechanisms relevant to the pathogenesis of type-2 diabetes could potentially increase IRS-2 serine/threonine phosphorylation, subsequently resulting in IRS-2 ubiquitination, proteosomal degradation, and ultimately β-cell apoptosis (Fig. 3).

Chronic hyperglycemia can lead to chronic activation of the nutrient-sensing serine/threonine protein kinase, mammalian Target of Rapamycin (mTOR) in β cells. Activated mTOR triggers serine/threonine phosphorylation of IRS-2 and its subsequent proteosomal degradation, leading to increased β-cell apoptosis (*39*). It should be noted, however, that chronic hyperglycemia can also trigger β-cell apoptosis by additional mechanisms, collectively referred to as "glucotoxicity." These mechanisms include the generation of potentially damaging reactive-oxygen species (ROS) as a consequence of chronically increased glucose metabolism in β cells (*40*); chronic elevation of intracellular $[Ca^{2+}]$ to cytotoxic levels (*3*); a marked up-regulation in the synthesis of β-cell secretory granule proteins, including pro-insulin and pro-Islet Amyloid Associated Peptide (proIAPP), which in turn could promote ER stress (*3*, *41*); and a glucose-induced increase in local interleukin-1β (IL-1β) production (*42*). Some of these "metabolic stresses," such as dangerously high levels of ROS and $[Ca^{2+}]$ in the β cell, may activate the Jnk/p38 stress protein kinases in β cells (*43*), in turn leading to serine/threonine phosphorylation of IRS-2 and its degradation (*37*, *44*).

Hyperlipidemia, another feature of obesity-linked type 2 diabetes, can lead to abnormal accumulation of lipids in β cells with detrimental effects, including fatty acid–induced β-cell apoptosis (*11*, *45*). Fatty acids, through the production of intracellular long chain acyl-CoA, can activate a novel class of protein kinase C isoforms (nPKC) independent of $[Ca^{2+}]$ (*46*). Chronic activation of certain nPKCs can lead to serine/threonine phosphorylation of IRS molecules (*38*, *47*) that in β cells would promote IRS-2 degradation and ultimately lead to β-cell apoptosis (*37*) (Fig. 3). As with chronic hyperglycemia, this is only one possible mechanism by which chronic accumulation of lipids in the β cell can contribute to fatty acid–induced β-cell apoptosis, commonly known as "lipotoxicity" (*11*). Other lipotoxic mechanisms include the generation of ceramide from palmitate, which induces a mitochondrial apoptotic pathway (*11*); inhibition of PKB (*45*); and fatty acid/ceramide–induced activation of the c-Jun N-terminal kinase (Jnk)/p38 stress kinase pathway (*48*). Interestingly, Jnk/p38-mediated phosphorylation of IRS-2 may also be induced by hyperglycemia, underscoring a likely interplay between glucotoxicity and lipotoxicity mechanisms in β-cell apoptosis (*49*).

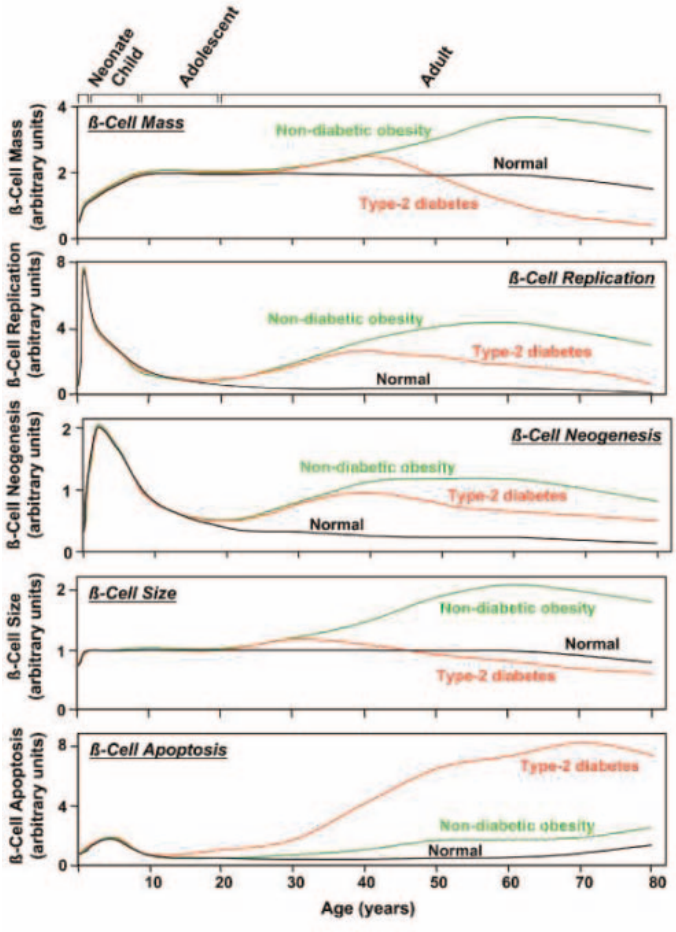

Fig. 2. A hypothetical model for postnatal pancreatic β-cell growth in humans. Three conditions are depicted: normal (black), nondiabetic obesity (green), and type 2 diabetes (red). The upper panel shows changes in the total β-cell mass. This reflects the sum of changes in β-cell replication, β-cell neogenesis, and β-cell size, minus the incidence of β-cell apoptosis, depicted individually in the other four panels. The changes in β-cell mass, replication, neogenesis, size, and apoptosis are in arbitrary units that reflect the magnitude of change from birth onward.

A variety of cytokines play a role in the pathogenesis of type 2 diabetes. The discovery that there is local induction of IL-1β production within islets in response to chronic glucose implies that IL-1β plays a role in inducing β-cell apoptosis in type 2 diabetes (*42*), as well as in type 1 diabetes (*27*, *50*). In obesity-linked diabetes, certain adipocyte-derived cytokines are elevated in the circulation, including leptin, tumor necrosis factor α (TNFα), and IL-6. Intriguingly, leptin has recently been shown to modulate IL-1β–induced apoptosis in human β cells (*51*). Some of these cytokines can induce β-cell apoptosis through induction of signaling pathways that activate the transcription factor NFκB (*27*). However, they may also activate signaling pathways that trigger increased degradation of IRS-2. Certain cytokines, such as leptin, IL-6, and IFN-γ activate the Janus Kinase-2/Signal Transducer and Activator of Transcription (JAK/STAT) post-receptor signaling pathway. This leads to increased expression of Suppressor of Cytokine Signaling-1 (SOCS-1) and SOCS-3 proteins, which normally bind to the leptin, IL-6, and IFN-γ receptors and inhibit JAK-2/STAT signaling. SOCS-1 and SOCS-3 have also been shown to bind to the C terminus of IRS molecules, leading to their ubiquitination and subsequent degradation (*52*, *53*). Thus, it is conceivable that leptin and/or IL-6 may cause β-cell apoptosis by decreasing β-cell IRS-2 levels through a similar mechanism. IL-1β and TNFα promote

activation of the protein kinase IκK (*27*). IκK phosphorylates the cytosolic inhibitory protein IκB, resulting in release and activation of NFκB (*27*). However, IκK has also been shown to phosphorylate IRS molecules on serine/threonine sites, promoting their degradation (*54*). If this occurs with IRS-2 in β cells, it should then trigger apoptosis. In addition, IL-1β and TNFα are known to activate Jnk/p38 "stress protein kinases" as well as the nPKC isoform, PKCδ (*27*). As mentioned previously, Jnk/p38 and PKCδ may also increase the serine/threonine phosphorylation state of IRS-2, leading to IRS-2 degradation and ultimately β-cell apoptosis.

IRS-2 also plays a pivotal role in insulin signal transduction pathways in insulin target tissues, especially the liver (*29*, *37*). A decrease in IRS-2 expression causes insulin resistance in insulin-responsive tissues (*30*, *33*, *37*). Indeed, several of the mechanisms proposed above to explain the loss of IRS-2 expression in β cells have also been proposed to reduce IRS-1 and IRS-2 levels in liver, muscle, and/or fat, thereby contributing to insulin resistance (*29*, *38*, *44*, *52*–*55*). Thus, there are parallels between the molecular mechanisms that control insulin sensitivity and those that promote β-cell survival. If these mechanisms go awry, then the balance between insulin resistance and compensatory β-cell mass will become ever more disrupted as time goes on, accelerating the onset of type 2 diabetes.

Summary

Although there is a tenuous balance between insulin resistance and an effective β-cell mass, for the most part, the β-cell mass adapts adequately to compensate for changes in the metabolic load. However, β cells can be pushed too far in susceptible individuals. Eventually the β-cell mass fails to compensate for insulin resistance, and type 2 diabetes ensues. I have argued here that this failure is caused by a marked increase in β-cell apoptosis, most likely induced by a combination of chronic hyperglycemia, hyperlipidemia, and/or certain cytokines that interfere with the signaling pathways that maintain normal β-cell growth and survival. The net effect is a reduction in functional β-cell mass in the type 2 diabetic state. There are many signal transduction pathways that affect β-cell growth and survival (*2*), and here I have focused only on one component of those pathways, IRS-2, because it is vital to normal maintenance of the adult β-cell population. One can envisage that pharmacological manipulations that increase IRS-2 expression in β cells may be a valuable strategy for promoting β-cell survival and delaying the onset of diabetes (*12*, *28*). Because decreased expression of IRS-2 in insulin-responsive tissues contributes to the insulin-resistant state, such a therapeutic strategy—at least in principle—would not only protect β cells but also help alleviate insulin resistance.

Analyses of the other signaling pathways governing β-cell growth and survival (*2*) will likely identify additional drug targets for preventing β-cell apoptosis. The future holds promise that strategies directed at prolonging the survival of the β cell will be successful in delaying or even preventing the onset of type 2 diabetes.

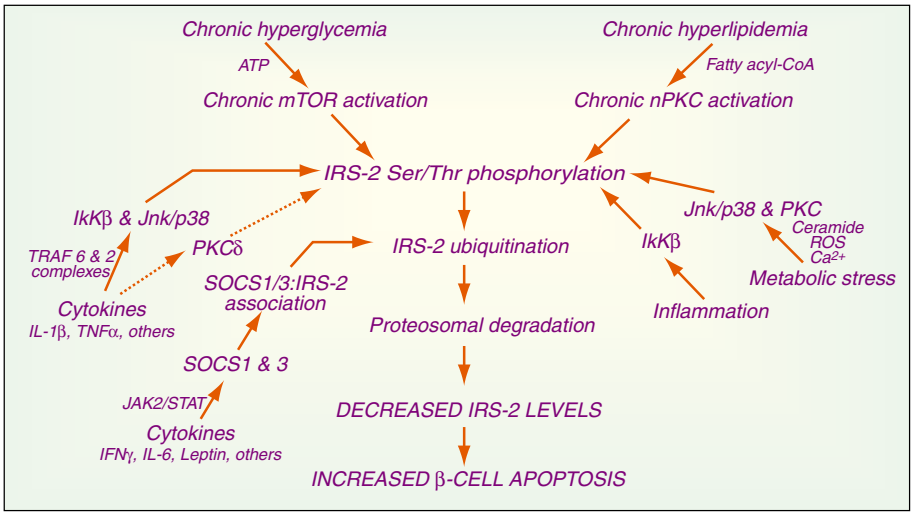

Fig. 3. Potential mechanisms that trigger IRS-2 degradation and apoptosis of pancreatic β cells. IRS-2 expression in β cells is vital for normal β-cell growth, survival, and turnover. Chronic hyperglycemia by means of mTOR activation and hyperlipidemia by means of fatty acyl-CoA–mediated activation of the novel class of PKC isoforms can lead to increased serine/threonine phosphorylation of IRS-2 that then leads to its ubiquitination and subsequent proteosomal degradation. In addition, certain cytokines, including IL-1β and TNF-α, activate IκKβ and Jnk/p38 kinases [by means of TNF-receptor associated factor (TRAF) signaling complexes] and/or PKCδ, which in turn also leads to IRS-2 serine/threonine phosphorylation. Other local inflammatory responses can activate IκKβ, and other metabolic stresses (e.g., increased ROS and ceramide generation, or chronically elevated [Ca^{2+}]) can activate PKC isoforms and/or Jnk/p38 kinases, which can reduce IRS-2 levels by a similar mechanism. Other cytokines (including IL-6 and IFN-γ) can induce expression of SOCS-1 and SOCS-3, which can then bind to IRS-2, leading to its ubiquitination and subsequent proteosomal degradation. This multipronged assault could significantly lower IRS-2 levels in the β cell. The resultant increase in β-cell apoptosis is thought to be a key factor contributing to the loss of β-cell mass in type 2 diabetes.

References and Notes

1. P. Zimmet, K. G. Alberti, J. Shaw, *Nature* **414**, 782 (2001).
2. M. K. Lingohr, R. Buettner, C. J. Rhodes, *Trends Mol. Med.* **8**, 375 (2002).
3. M. Y. Donath, P. A. Halban, *Diabetologia* **47**, 581 (2004).
4. S. E. Kahn, *J. Clin. Endocrinol. Metab.* **86**, 4047 (2001).
5. J. L. Leahy, *Diabetes Care* **13**, 992 (1990).
6. G. C. Weir, S. Bonner-Weir, *Diabetes* **53** (suppl. 3), S16 (2004).
7. N. Mclean, R. F. Ogilvie, *Diabetes* **4**, 367 (1955).
8. A. E. Butler *et al.*, *Diabetes* **52**, 102 (2003).
9. G. Kloppel, M. Lohr, K. Habich, M. Oberholzer, P. U. Heitz, *Surv. Synth. Pathol. Res.* **4**, 110 (1985).
10. G. C. Weir, D. R. Laybutt, H. Kaneto, S. Bonner-Weir, A. Sharma, *Diabetes* **50** (suppl. 1), S154 (2001).
11. R. H. Unger, L. Orci, *FASEB J.* **15**, 312 (2001).
12. L. Dickson, C. J. Rhodes, *Am. J. Physiol.* **287**, E192 (2004).
13. S. Bonner-Weir, *Trends Endocrinol. Metab.* **11**, 375 (2000).
14. L. Bouwens, G. Kloppel, *Virchows Arch.* **427**, 553 (1996).
15. D. T. Finegood, L. Scaglia, S. Bonner-Weir, *Diabetes* **44**, 249 (1995).
16. Y. Dor, J. Brown, O. I. Martinez, D. A. Melton, *Nature* **429**, 41 (2004).
17. S. Georgia, A. Bhushan, *J. Clin. Invest.* **114**, 963 (2004).
18. X. Lin *et al.*, *J. Clin. Invest.* **114**, 908 (2004).
19. J. Rajagopal, W. J. Anderson, S. Kume, O. I. Martinez, D. A. Melton, *Science* **299**, 363 (2003).
20. M. Hansson *et al.*, *Diabetes* **53**, 2603 (2004).
21. S. Bonner-Weir, *Endocrinology* **141**, 1926 (2000).
22. A. Pick *et al.*, *Diabetes* **47**, 358 (1998).
23. R. L. Sorenson, T. C. Brelje, *Horm. Metab. Res.* **29**, 301 (1997).
24. E. T. Jaikaran, A. Clark, *Biochim. Biophys. Acta* **1537**, 179 (2001).
25. G. I. Bell, K. S. Polonsky, *Nature* **414**, 788 (2001).
26. C. N. Hales, D. J. Barker, *Br. Med. Bull.* **60**, 5 (2001).
27. M. Y. Donath, J. Storling, K. Maedler, T. Mandrup-Poulsen, *J. Mol. Med.* **81**, 455 (2003).
28. A. M. Hennige *et al.*, *J. Clin. Invest.* **112**, 1521 (2003).
29. C. J. Rhodes, M. F. White, *Eur. J. Clin. Invest.* **32** (suppl. 3), 3 (2002).
30. D. J. Withers *et al.*, *Nature* **391**, 900 (1998).
31. E. Araki *et al.*, *Nature* **372**, 186 (1994).
32. H. Tamemoto *et al.*, *Nature* **372**, 182 (1994).
33. N. Kubota *et al.*, *Diabetes* **49**, 1880 (2000).
34. P. D. Borge, B. A. Wolf, *J. Biol. Chem.* **278**, 11359 (2003).
35. D. J. Withers *et al.*, *Nature Genet.* **23**, 32 (1999).
36. M. K. Lingohr *et al.*, *Mol. Cell. Endocrinol.* **209**, 17 (2003).
37. M. F. White, *Am. J. Physiol. Endocrinol. Metab.* **283**, E413 (2002).
38. Y. Zick, *Trends Cell Biol.* **11**, 437 (2001).
39. I. Briaud *et al.*, *J. Biol. Chem.* 9 November 2004 (www.jbc.org/cgi/reprint/M412179200v1.pdf).
40. Y. Kajimoto, H. Kaneto, *Ann. N.Y. Acad. Sci.* **1011**, 168 (2004).
41. E. Araki, S. Oyadomari, M. Mori, *Exp. Biol. Med.* **228**, 1213 (2003).
42. K. Maedler *et al.*, *J. Clin. Invest.* **110**, 851 (2002).
43. H. Kaneto *et al.*, *J. Biol. Chem.* **277**, 30010 (2002).
44. E. D. Werner, J. Lee, L. Hansen, M. Yuan, S. E. Shoelson, *J. Biol. Chem.* **279**, 35298 (2004).
45. C. E. Wrede *et al.*, *J. Biol. Chem.* **277**, 49676 (2002).

46. C. Wrede, L. M. Dickson, M. K. Lingohr, I. Briaud, C. J. Rhodes, *J. Mol. Endocrinol.* **30**, 271 (2003).
47. M. W. Greene, N. Morrice, R. S. Garofalo, R. A. Roth, *Biochem. J.* **378**, 105 (2004).
48. S. Willaime-Morawek, K. Brami-Cherrier, J. Mariani, J. Caboche, B. Brugg, *Neuroscience* **119**, 387 (2003).
49. V. Poitout, R. P. Robertson, *Endocrinology* **143**, 339 (2002).
50. T. Mandrup-Poulsen, *Diabetes* **50** (suppl. 1), S58 (2001).
51. K. Maedler *et al.*, *Proc. Natl. Acad. Sci. U.S.A.* **101**, 8138 (2004).
52. L. Rui, M. Yuan, D. Frantz, S. Shoelson, M. F. White, *J. Biol. Chem.* **277**, 42394 (2002).
53. K. Ueki, T. Kondo, C. R. Kahn, *Mol. Cell. Biol.* **24**, 5434 (2004).
54. Z. Gao *et al.*, *J. Biol. Chem.* **277**, 48115 (2002).
55. A. Takano *et al.*, *Mol. Cell. Biol.* **21**, 5050 (2001).
56. I thank S. Bonner-Weir, P. Butler, J. Leahy, and M. White for valuable discussions over the years. Supported by a NIH grant DK-55267. The author is on the β-cell Advisory Board of the Partnership formed by Amylin Pharmaceuticals and Eli Lilly.

10.1126/science.1104345

VIEWPOINT

Mitochondrial Dysfunction and Type 2 Diabetes

Bradford B. Lowell[1] and Gerald I. Shulman[2]

Maintenance of normal blood glucose levels depends on a complex interplay between the insulin responsiveness of skeletal muscle and liver and glucose-stimulated insulin secretion by pancreatic β cells. Defects in the former are responsible for insulin resistance, and defects in the latter are responsible for progression to hyperglycemia. Emerging evidence supports the potentially unifying hypothesis that both of these prominent features of type 2 diabetes are caused by mitochondrial dysfunction.

Type 2 diabetes is the most common metabolic disease in the world. In the United States, it is the leading cause of blindness, end-stage renal disease, and nontraumatic loss of limb, with associated health care costs estimated to exceed $130 billion per year (*1*). Of even greater concern, type 2 diabetes is rapidly becoming a global pandemic and is projected to afflict more than 300 million individuals worldwide by the year 2025, with most of the increase occurring in India and Asia (*2*). Although the primary cause of this disease is unknown, it is clear that insulin resistance plays an early role in its pathogenesis and that defects in insulin secretion by pancreatic β cells are instrumental in the progression to hyperglycemia. Here, we explore the potentially unifying hypothesis that these two prominent features of type 2 diabetes are both attributable to defects in mitochondria, the organelles that provide energy to the cell.

Role of Intracellular Fatty Acid Metabolites in Insulin Resistance

Several lines of evidence indicate that insulin resistance is an early feature of type 2 diabetes. First, virtually all patients with type 2 diabetes are insulin-resistant, and prospective studies have shown that this insulin-resistant state develops 1 to 2 decades before the onset of the disease (*3*–*5*). Second, insulin resistance in the offspring of parents with type 2 diabetes is the best predictor for later development of the disease (*6*). Lastly, perturbations that reduce insulin resistance prevent the development of diabetes (*7*).

[1]Department of Medicine, Beth Israel Deaconess Medical Center, 99 Brookline Avenue, Harvard Medical School, Boston, MA 02215, USA. E-mail: blowell@bidmc.harvard.edu [2]Howard Hughes Medical Institute, Department of Internal Medicine and Department of Cellular and Molecular Physiology, Yale University School of Medicine, 300 Cedar Street, New Haven, CT 06536, USA. E-mail: gerald.shulman@yale.edu

Skeletal muscle and liver are the two key insulin-responsive organs responsible for maintaining normal glucose homeostasis, and their transition to an insulin-resistant state accounts for most of the alterations in glucose metabolism seen in patients with type 2 diabetes. Before considering whether mitochondrial dysfunction contributes to the development of insulin resistance in these organs, it is first important to understand the cellular mechanisms responsible for insulin resistance. As discussed by Lazar (*8*), there is growing evidence that circulating cytokines secreted by fat tissue can modulate the insulin responsiveness of liver and muscle. However, fatty acids (*9*) and/or intracellular fatty acid metabolites such as fatty acyl coenzyme As (fatty acyl CoAs) (*10*, *11*), diacylglycerol (*10*, *11*), or ceramides (*12*) are also thought to play a critical role.

Over 40 years ago, Randle *et al*. demonstrated that fatty acids caused insulin resistance in an in vitro rat muscle preparation, and they hypothesized that this occurred by a substrate competition mechanism (*13*). According to his model, increased oxidation of muscle fatty acids would produce increased levels of intracellular acetyl CoA and citrate, which in turn would inhibit, respectively, two enzymes involved in glucose utilization, pyruvate dehydrogenase and phosphofructokinase. Inhibition of the glycolytic pathway at these steps would increase intracellular glucose and glucose-6-phosphate concentrations, ultimately resulting in reduced insulin-stimulated glucose uptake.

More recent studies using ^{13}C and ^{31}P magnetic resonance spectroscopy (MRS) have shown that this mechanism for fatty acid–induced insulin resistance is untenable in human skeletal muscle (*14*); rather, fatty acids appear to cause insulin resistance by directly inhibiting insulin-stimulated glucose transport activity (*15*). This inhibition is likely because of the accumulation of intracellular fatty acyl CoAs and diacylglycerol, which then activate critical signal transduction pathways that ultimately lead to suppression of insulin signaling (Fig. 1). One might therefore predict that any metabolic perturbation that promotes the accumulation of fatty acids in liver and/or muscle and/or any defect in the ability of these organs to metabolize fatty acids might result in insulin resistance (*10*). Indeed, defects in adipocyte metabolism, which occur in conditions such as severe lipodystrophy (*16*), can result in the former, and it has become increasingly evident that defects in mitochondrial fatty acid oxidation can result in the latter and may be responsible for the more common forms of insulin resistance.

Mitochondrial Dysfunction, Intracellular Fatty Acids, and Insulin Resistance

It is well established that mitochondrial function is required for normal glucose-stimulated insulin secretion from pancreatic β cells. In addition, maternally inherited defects in mitochondrial DNA that disrupt mitochondrial function are known to cause an insulin-deficient form of diabetes resembling type 1 diabetes (*17*). However, recent MRS studies of humans suggest that more subtle defects in mitochondrial function might also play a role in the pathogenesis of insulin resistance and type 2 diabetes. Petersen *et al*. found that in comparison with matched young controls, healthy lean elderly subjects had severe insulin resistance in muscle, as well as significantly higher levels of triglycerides in both muscle and liver (*18*). These changes were accompanied by decreases in both mitochondrial oxidative activity and mitochondrial adenosine triphosphate (ATP) synthesis. These data support the hypothesis that insulin resistance in humans arises from defects in mitochondrial fatty acid oxidation, which in turn lead to increases in intracellular fatty acid metabolites (fatty acyl CoA and diacylglyerol) that disrupt insulin signaling (Fig. 1).

Alterations in mitochondrial DNA (MtDNA) have been correlated with human aging in several previous studies, and a recent study of genetically manipulated mice provided evidence that such alterations may play a causal role in aging (*19*). Whether the mitochondrial

dysfunction detected in the elderly subjects studied by Petersen *et al.* (*18*) is related to age-associated accumulation of MtDNA mutations is not yet clear.

Other studies using the MRS technique have revealed similar decreases in mitochondrial activity and increases in intramyocellular fat content in young insulin-resistant offspring of parents with type 2 diabetes, a group that has a strong tendency to develop diabetes later in life (*20*). In addition, in comparison with insulin-sensitive controls, the insulin-resistant subjects were found to have a lower ratio of type 1 to type 2 muscle fibers. Type 1 fibers are mostly oxidative and contain more mitochondria than type 2 muscle fibers, which are more glycolytic. Conceivably, these individuals may have fewer muscle mitochondria, possibly because of decreased expression of nuclear-encoded genes that regulate mitochondrial biogenesis, such as peroxisome proliferator-activated receptorγ coactivator 1α [PGC-1α (*21*) and PGC-1β (*22*)]. Microarray studies support this idea: PGC-1α–responsive genes are down-regulated in obese Caucasians with impaired glucose tolerance and type 2 diabetes (*23*), and PGC-1α and PGC-1β are themselves down-regulated in both obese diabetic and overweight nondiabetic Mexican-Americans (*24*).

Alternatively, the reduction in mitochondrial oxidative-phosphorylation activity in insulin-resistant individuals could be due not to mitochondrial loss but rather to a defect in mitochondrial function. This hypothesis is supported by muscle biopsy studies. In one study, the activity of mitochondrial oxidative enzymes was found to be lower in type 2 diabetic subjects (*25*), and in another, the activity of mitochondrial rotenone-sensitive nicotinamide adenine dinucleotide oxidoreductase [NADH:O(*2*)] was found to be lower (*26*). However, in contrast to the MRS studies, these studies were performed with isolated mitochondria obtained from diabetic subjects who were also obese. Because obese individuals have also been shown to have smaller mitochondria with reduced bioenergetic capacity compared with lean controls (*26*), the mitochondrial abnormalities in these subjects might be related to obesity rather than to insulin resistance. The role of the obese state in the down-regulated expression of the PGC-1α and PGC-1β genes discussed above (*23*, *24*) is an important question that remains to be answered.

Mitochondrial Dysfunction and Insulin Secretion by Pancreatic β Cells

Many obese individuals with marked insulin resistance do not develop frank diabetes. In these individuals, the pancreatic β cells adapt to meet the body's markedly increased demand for insulin. This adaptation involves expansion of β cell mass, as well as maintenance of normal responsiveness of β cells to glucose. Conversely, in obese individuals destined to develop type 2 diabetes, β cells do not secrete enough insulin to compensate for the increased demand. This β cell failure is likely caused by inadequate expansion of the β cell mass and/or failure of the existing β cell mass to respond to glucose (*27*).

β cell mass is governed by several factors, including β cell size, the rate of β cell replication and/or differentiation, and the rate of β cell apoptotic cell death. Although difficult to quantify, β cell mass appears to be decreased in individuals with type 2 diabetes relative to matched individuals with similar degrees of insulin resistance (*28*, *29*). Although the cause of this relative decrease in β cell mass is unknown, increased rates of apoptosis may play an important role (*27*, *28*, *30*). The signals to and from mitochondria that regulate apoptosis in β cells and the effect of the prediabetic milieu on these signals are incompletely understood (*31*, *32*) but are likely to be a fertile area of future investigation.

Numerous studies have documented that, in individuals with type 2 diabetes, β cells do not sense glucose properly and therefore do not release appropriate amounts of insulin (*33*). Glucose sensing requires oxidative mitochondrial metabolism, leading to the generation of ATP (*34*). This increases the ratio of ATP to adenosine diphosphate (ADP) in the β cell, which then initiates the following chain of events: inhibition of the cell's ATP/ADP-regulated potassium channel (K_{ATP}), plasma membrane depolarization, opening of a voltage-gated calcium channel, calcium

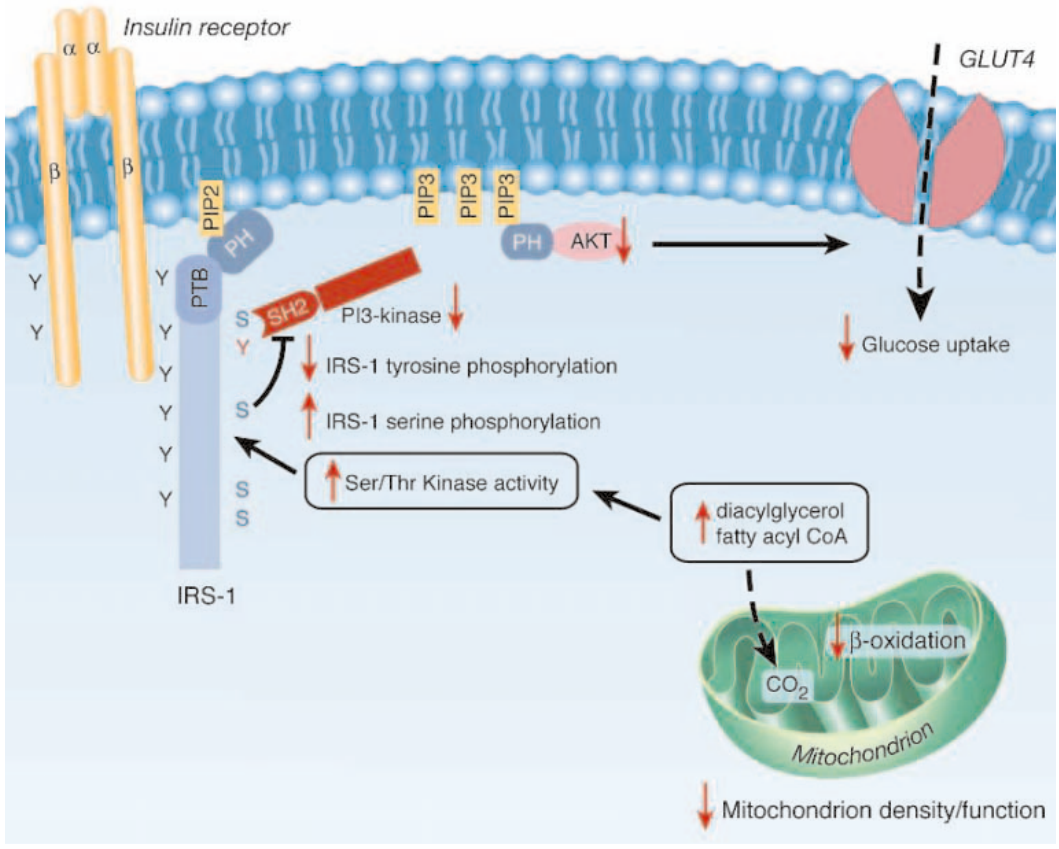

Fig. 1. Potential mechanism by which mitochondrial dysfunction induces insulin resistance in skeletal muscle. In the depicted model, a decrease in mitochondrial fatty acid oxidation, caused by mitochondrial dysfunction and/or reduced mitochondrial content, produces increased levels of intracellular fatty acyl CoA and diacylglycerol. These molecules activate novel protein kinase C, which in turn activates a serine kinase cascade [possibly involving inhibitor of nuclear factor κB kinase (IKK) and c-Jun N-terminal kinase–1], leading to increased serine phosphorylation (pS) of insulin receptor substrate–1 (IRS-1). Increased serine phosphorylation of IRS-1 on critical sites (e.g., IRS-1 Ser^{307}) blocks IRS-1 tyrosine (Y) phosphorylation by the insulin receptor, which in turn inhibits the activity of phosphatidyl inositol 3-kinase (PI 3-kinase). This inhibition results in suppression of insulin-stimulated glucose transport, the process by which glucose is removed from the blood. PIP3 indicates phosphatidylinositol 3,4,5-trisphosphate; PTB, phosphotyrosine binding domain; PH, pleckstrin homology domain; SH2, src homology domain.

influx, and secretion of insulin (Fig. 2). Although insulin secretion is also modulated by a number of stimuli that operate outside this pathway, it is clear that oxidative mitochondrial metabolism is central to glucose-stimulated insulin secretion (*34*).

The critical role of mitochondria is evident from the rare hereditary disorders in which diabetes with β cell dysfunction have been traced to specific mutations in the mitochondrial genome (*34*, *35*). Given the central role of mitochondria in glucose sensing, it is possible that decreased mitochondrial function in β cells, analogous to that observed in skeletal muscle (described above), might predispose individuals to develop β cell dysfunction and type 2 diabetes. However, because of the difficulties in obtaining β cell samples for analyses, this

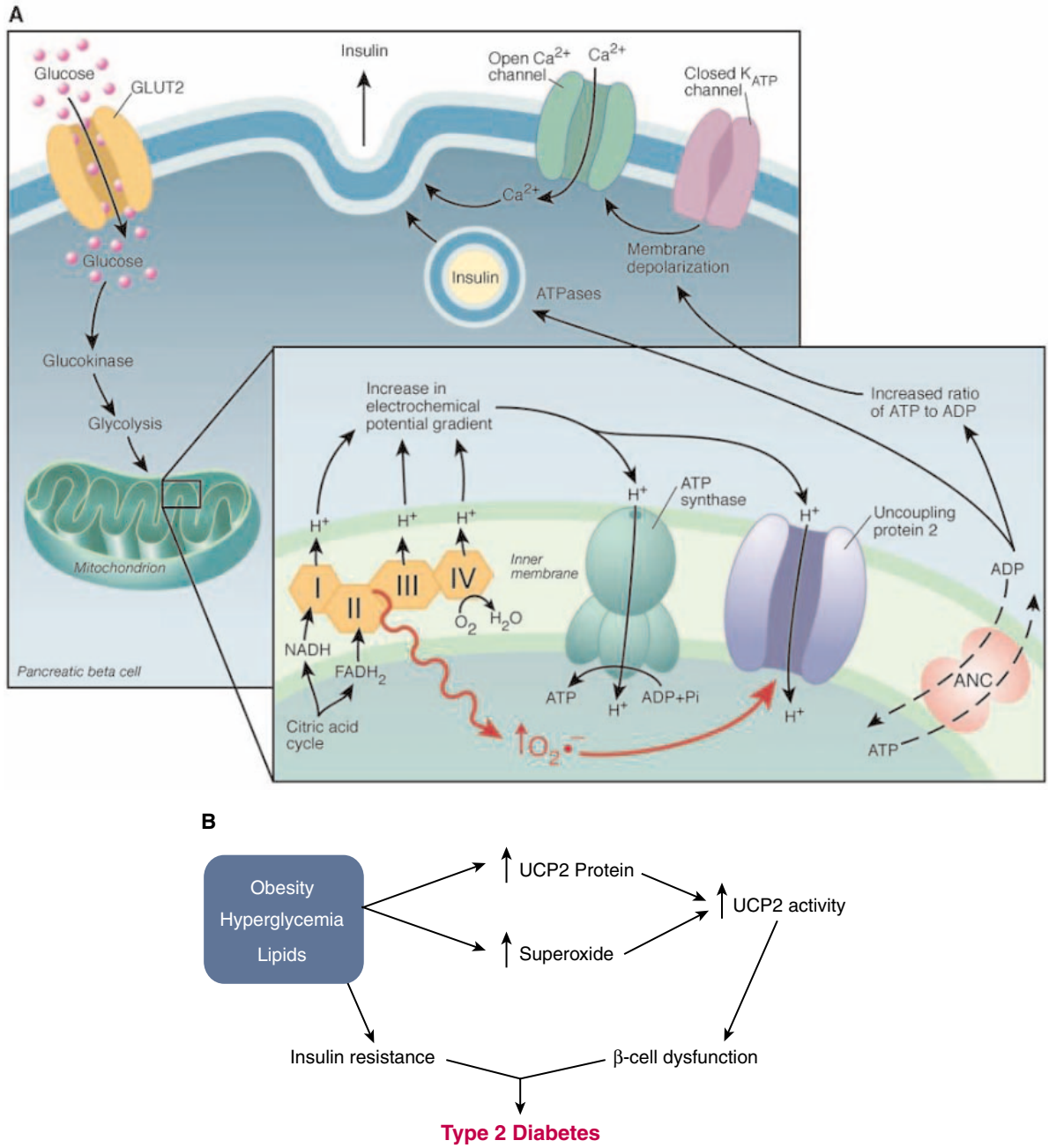

Fig. 2. Potential mechanism by which UCP2-mediated mitochondrial dysfunction disrupts insulin secretion from pancreatic β cells. (**A**) UCP2, superoxide, and glucose-stimulated insulin secretion. Insulin secretion is coupled to glucose metabolism by the subsequent increase in the ATP/ADP ratio arising from glucose oxidation, which closes K^{ATP} channels. This depolarizes the plasma membrane, opening voltage-gated Ca^{2+} channels with the influx of Ca^{2+} stimulating secretion of insulin. UCP2 decreases glucose-stimulated insulin secretion by increasing proton leak across the mitochondrial inner membrane, diverting energy stored within electrochemical potential gradient away from ATP synthase, thereby decreasing the yield of ATP from glucose. Superoxide generated by the electron transport chain stimulates proton leak activity of UCP2 protein, thereby decreasing glucose-stimulated insulin secretion. [Figure adapted with permission from (*58*). Copyright 2001, Massachusetts Medical Society. All rights reserved.] (**B**) The effects of obesity, hyperglycemia, and lipids on UCP2. In the obese state, hyperglycemia, and high lipid levels each induce expression of UCP2 protein in pancreatic β cells. These stimuli also increase production of superoxide by the electron transport chain. As a result, UCP2 is activated, leading to a marked increase in UCP2-mediated proton leak. This proton leak impairs glucose-stimulated insulin secretion, resulting in β cell dysfunction. β cell dysfunction and insulin resistance in muscle, liver, and fat are characteristic features of type 2 diabetes.

interesting hypothesis has not yet been directly tested.

β cell dysfunction in type 2 diabetes is thought to be secondary to increased exposure of β cells to glucose (glucotoxicity) and/or lipids (lipotoxicity), frequently associated with the obese, insulin-resistant state (*36*–*38*). A number of hypotheses have been proposed to explain how these conditions induce β cell dysfunction (*36*–*38*). One of these hypotheses, discussed below, focuses on changes in the expression and function of a mitochondrial inner membrane protein called uncoupling protein–2 (UCP2) (*39*–*42*). To understand the role of UCP2, it is first necessary to review relevant aspects of mitochondrial oxidative metabolism.

Oxidative metabolism of glucose involves the transfer of energy stored within the carbon bonds of glucose to the third phosphate bond of ATP (Fig. 2A). This complex reaction begins as electrons within the carbon bonds are transferred to the dinucleotide electron carriers, NADH and flavin adenine dinucleotide ($FADH_2$). These in turn donate electrons to the mitochondrial electron transport chain, a multiprotein unit grouped into four complexes (I to IV), all located within the mitochondrial inner membrane. Ultimately, the electrons are funneled to their final destination, reduction of oxygen to water. Complexes I, III, and IV are reduction- and oxidation-driven proton pumps that use energy carried by the electrons to pump protons out of the matrix, creating a proton electrochemical potential gradient across the mitochondrial inner membrane (Fig. 2A). These protons then reenter the mitochondrial matrix via ATP synthase with the use of energy stored within the electrochemical gradient to drive synthesis of ATP from ADP. UCP2 is an integral membrane protein that, when activated, leaks protons across the inner membrane (*43*), hence uncoupling glucose oxidative metabolism from ATP production. Because it decreases the amount of ATP generated from glucose, UCP2 is predicted to negatively regulate glucose-stimulated insulin secretion. Experimental evidence has shown that this is indeed the case. Forced overexpression of UCP2 in β cells in cell culture decreases glucose-stimulated insulin secretion (*40*), whereas targeted inactivation of the UCP2 gene in mice has the opposite effect (*39*). Importantly, heterozygosity for a null UCP2 allele produces an effect that is intermediate between those observed in wild-type and homozygous mice, indicating that relatively small changes in UCP2 expression have meaningful effects on glucose-stimulated insulin secretion (*39*). Thus, UCP2 exerts substantial negative control over glucose-stimulated insulin secretion.

Does increased expression of UCP2 have a causal role in β cell dysfunction in type 2 diabetes? This idea is supported by the finding that UCP2 expression is stimulated, in vitro and in vivo, by hyperglycemia (glucotoxicity) and lipid fuels (lipotoxicity), and in animal models with type 2 diabetes (*39*, *41*, *42*, *44*–*47*). Moreover, genetic deficiency of UCP2 has been found to greatly improve β cell function in rodent models of obesity/diabetes (*38*, *40*). Similarly, genetic deficiency of UCP2 prevents β cell dysfunction in in vitro models of glucotoxicity and lipotoxicity (*42*, *48*, *49*). Together, these data from experimental models suggest that UCP2 plays an important pathogenic role. A similar role seems likely in human type 2 diabetes, because UCP2 is expressed in human β cells and its expression is increased by hyperglycemia (*50*). Additionally, a polymorphism in the promoter of the human UCP2 gene that appears to increase UCP2 expression has been linked to reduced insulin secretion and higher frequency and/or earlier onset of type 2 diabetes (*51*–*53*).

It was recently discovered that superoxide, a byproduct of electron transport chain activity, stimulates the proton leak activity of UCP2 when added exogenously to isolated mitochondria (*54*) or when generated in situ within intact β cells (*42*) (Fig. 2A). The mechanism by which superoxide activates UCP2 is unknown but may involve the generation of free radical intermediates (*55*). Stimulation of UCP2 activity by superoxide is relevant to the development of β cell dysfunction, because superoxide production is increased in β cells of rodents with type 2 diabetes (*42*, *56*) and in cultured β cells exposed to hyperglycemia and elevated levels of lipids (*42*, *56*). This increase in superoxide, coupled with the increase in UCP2 protein, results in a large stimulation of proton leak, ultimately leading to β cell dysfunction (Fig. 2B). Indeed, removal of endogenous superoxide in β cells that are unresponsive to glucose, either because of in vitro exposure to hyperglycemia or because of the in vivo obese or diabetic state, acutely inhibits UCP2 activity and restores glucose-stimulated insulin secretion (*42*). Thus, the superoxide-UCP2 proton leak pathway is an important contributor to β cell dysfunction and may play an important role in the pathogenesis of type 2 diabetes (Fig. 2B). These findings raise the possibility that UCP2 inhibitors could be used to prevent or treat type 2 diabetes.

Conclusions

A series of diverse experiments support the proposal that mitochondrial defects play a critical role in two prominent features of type 2 diabetes: insulin resistance and pancreatic β cell dysfunction. Several important questions remain to be answered: (i) Is the reduction in mitochondrial function in vivo due to mitochondrial loss, functional defects in the mitochondria, or both? (ii) Is the down-regulation of PGC-1α/PGC-1β responsive genes a primary or secondary event in the pathogenesis of type 2 diabetes? If it is a primary event, what are the upstream genes responsible for their altered expression? (iii) Does UCP-2 play an important role in β cell dysfunction in patients with type 2 diabetes? Answers to these questions may provide new pharmacologic targets for the prevention and treatment of the world's most common metabolic disease.

References and Notes

1. American Diabetes Association, *Diabetes Care* **26**, 917 (2003).
2. P. Zimmet, K. G. Alberti, J. Shaw, *Nature* **414**, 782 (2001).
3. S. Lillioja *et al.*, *N. Engl. J. Med.* **318**, 1217 (1988).
4. S. Lillioja *et al.*, *N. Engl. J. Med.* **329**, 1988 (1993).
5. R. A. DeFronzo, R. C. Bonadonna, E. Ferrannini, *Diabetes Care* **15**, 318 (1992).
6. J. H. Warram, B. C. Martin, A. S. Krolewski, J. S. Soeldner, C. R. Kahn, *Ann. Intern. Med.* **113**, 909 (1990).
7. S. P. Azen *et al.*, *Controlled Clin. Trials* **19**, 217 (1998).
8. M. A. Lazar, *Science* **307**, 373 (2005).
9. G. Boden, G. I. Shulman, *Eur. J. Clin. Invest.* **32** (suppl. 3), 14 (2002).
10. G. I. Shulman, *J. Clin. Invest.* **106**, 171 (2000).
11. C. Yu *et al.*, *J. Biol. Chem.* **277**, 50230 (2002).
12. E. W. Kraegen, G. J. Cooney, J. M. Ye, A. L. Thompson, S. M. Furler, *Exp. Clin. Endocrinol. Diabetes* **109**, S189 (2001).
13. P. J. Randle, P. B. Garland, C. N. Hales, E. A. Newsholme, *Lancet* **i**, 785 (1963).
14. M. Roden *et al.*, *J. Clin. Invest.* **97**, 2859 (1996).
15. A. Dresner *et al.*, *J. Clin. Invest.* **103**, 253 (1999).
16. K. F. Petersen *et al.*, *J. Clin. Invest.* **109**, 1345 (2002).
17. R. Luft, *Proc. Natl. Acad. Sci. U.S.A.* **91**, 8731 (1994).
18. K. F. Petersen *et al.*, *Science* **300**, 1140 (2003).
19. E. Dufour, N. G. Larsson, *Biochim. Biophys. Acta* **1658**, 122 (2004).
20. K. F. Petersen, S. Dufour, D. Befroy, R. Garcia, G. I. Shulman, *N. Engl. J. Med.* **350**, 664 (2004).
21. Z. Wu *et al.*, *Cell* **98**, 115 (1999).
22. J. St-Pierre *et al.*, *J. Biol. Chem.* **278**, 26597 (2003).
23. V. K. Mootha *et al.*, *Nature Genet.* **34**, 267 (2003).
24. M. E. Patti *et al.*, *Proc. Natl. Acad. Sci. U.S.A.* **100**, 8466 (2003).
25. K. Vondra *et al.*, *Diabetologia* **13**, 527 (1977).
26. D. E. Kelley, J. He, E. V. Menshikova, V. B. Ritov, *Diabetes* **51**, 2944 (2002).
27. C. J. Rhodes, *Science* **307**, 380 (2005).
28. A. E. Butler *et al.*, *Diabetes* **52**, 102 (2003).
29. S. Deng *et al.*, *Diabetes* **53**, 624 (2004).
30. A. Pick *et al.*, *Diabetes* **47**, 358 (1998).
31. L. M. Dickson, C. J. Rhodes, *Am. J. Physiol. Endocrinol. Metab.* **287**, E192 (2004).
32. H. Hui, F. Dotta, U. Di Mario, R. Perfetti, *J. Cell. Physiol.* **200**, 177 (2004).
33. J. E. Gerich, *Mayo Clin. Proc.* **78**, 447 (2003).
34. P. Maechler, C. B. Wollheim, *Nature* **414**, 807 (2001).
35. J. A. Maassen *et al.*, *Diabetes* **53** (suppl. 1), S103 (2004).
36. R. H. Unger, *Diabetes* **44**, 863 (1995).
37. V. Poitout, R. P. Robertson, *Endocrinology* **143**, 339 (2002).
38. M. Prentki, E. Joly, W. El-Assaad, R. Roduit, *Diabetes* **51** (suppl. 3), S405 (2002).
39. C. Y. Zhang *et al.*, *Cell* **105**, 745 (2001).
40. C. B. Chan *et al.*, *Diabetes* **50**, 1302 (2001).
41. J. W. Joseph *et al.*, *Diabetes* **51**, 3211 (2002).
42. S. Krauss *et al.*, *J. Clin. Invest.* **112**, 1831 (2003).
43. S. Krauss, C. Y. Zhang, B. B. Lowell, *Proc. Natl. Acad. Sci. U.S.A.* **99**, 118 (2002).
44. M. S. Winzell *et al.*, *Diabetes* **52**, 2057 (2003).
45. D. R. Laybutt *et al.*, *J. Biol. Chem.* **277**, 10912 (2002).
46. V. Poitout, *Endocrinology* **145**, 3563 (2004).
47. S. Kashyap *et al.*, *Diabetes* **52**, 2461 (2003).
48. T. Yamashita *et al.*, *Endocrinology* **145**, 3566 (2004).
49. J. W. Joseph *et al.*, *J. Biol. Chem.* **279**, 51049 (2004).
50. J. E. Brown, S. Thomas, J. E. Digby, S. J. Dunmore, *FEBS Lett.* **513**, 189 (2002).
51. F. Krempler *et al.*, *Diabetes* **51**, 3331 (2002).
52. G. Sesti *et al.*, *Diabetes* **52**, 1280 (2003).
53. M. Sasahara *et al.*, *Diabetes* **53**, 482 (2004).
54. K. S. Echtay, M. P. Murphy, R. A. Smith, D. A. Talbot, M. D. Brand, *J. Biol. Chem.* **277**, 47129 (2002).
55. M. P. Murphy *et al.*, *J. Biol. Chem.* **278**, 48534 (2003).
56. V. P. Bindokas *et al.*, *J. Biol. Chem.* **278**, 9796 (2003).
57. V. Koshkin, X. Wang, P. E. Scherer, C. B. Chan, M. B. Wheeler, *J. Biol. Chem.* **278**, 19709 (2003).
58. D. Langin, *N. Engl. J. Med.* **345**, 1772 (2001).

59. Funded by grants from the U.S. Public Health Service (G.I.S. and B.B.L.) and by the American Diabetes Association (G.I.S.).

10.1126/science.1104343

Nonvolcanic Tremors Deep Beneath the San Andreas Fault

Robert M. Nadeau* and David Dolenc

We have discovered nonvolcanic tremor activity (i.e., long-duration seismic signals with no clear *P* or *S* waves) within a transform plate boundary zone along the San Andreas Fault (SAF) near Cholame, California, the inferred epicentral region (*1*) of the 1857 Fort Tejon earthquake [moment magnitude (M_w) ~7.8]. The tremors occur at depths between 20 and 40 km, below the seismogenic zone (i.e., the upper ~15 km of Earth's crust where earthquakes occur), and their activity rates may correlate with variations in local earthquake activity.

Analysis of triggered event data from the borehole High Resolution Seismic Network (HRSN) at Parkfield, California, revealed tremorlike signals originating in the vicinity of Cholame (Fig. 1). Seismic data recorded continuously with 20-Hz sampling frequency by two stations of the Southern California Seismic Network (SCSN) (Fig. 1) and with 250-Hz sampling by the HRSN were processed with the methods of Obara (*2*) and used to identify and analyze tremor events within a ~15-km radius centered ~5 km southeast of Cholame (Fig. 1). For the 3-year search period from 23 December 2000 to 22 December 2003, when the M_w 6.5 San Simeon earthquake occurred (*3*), 110 tremor events lasting between 4 and 20 min were identified. Their locations indicate that, within the search radius, the tremors are confined to a ~25-km segment of the SAF and occur at depths of between ~20 and 40 km.

Previously, nonvolcanic tremors have only been observed in subduction zones, which are predominantly thrust fault boundaries. The depth, frequency content (generally 1 to 10 Hz), *S*-wave propagation velocity, and waveform character of the SAF tremors are similar to those of the subduction zone tremors (*2*, *4*). However, the SAF tremors are less frequent (fewer than 5 events detected in any 24-hour period), have shorter durations (less than 20 min), have smaller peak amplitudes (<M_w 0.5 earthquakes), and release less energy (energy equivalents < M_w 1.5).

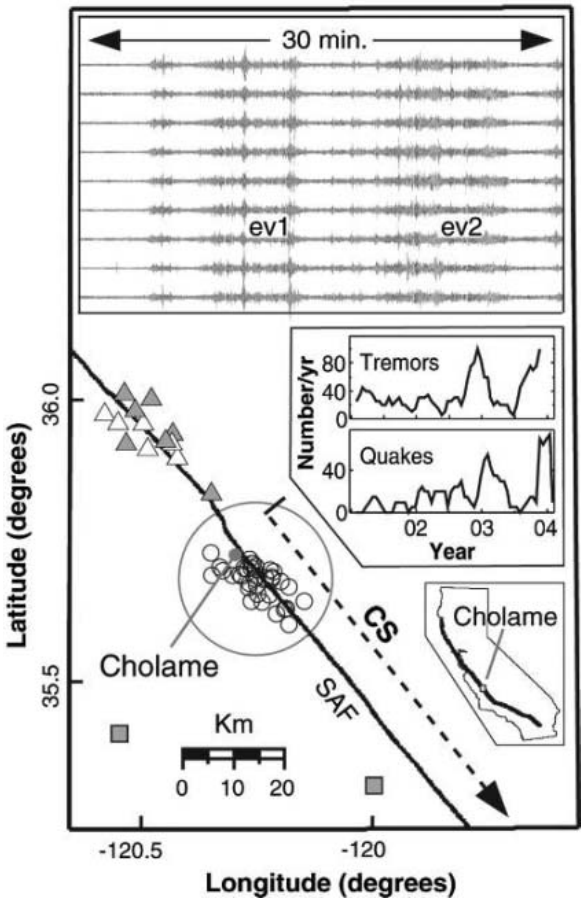

Fig. 1. Thirty-four well-located tremors (small circles) along the northern Cholame segment (CS) of the SAF. Triangles and squares represent seismic stations of the HRSN and SCSN, respectively. The large circle is the ~15-km-radius search zone. (Top inset) Horizontal component velocity seismograms (3- to 8-Hz band-pass filtered) of two tremor events (ev1 and ev2) recorded by the stations shown in gray. (Middle inset) The occurrence rates of 110 tremors and 58 microearthquakes (M_w < 2.1, occurring in a 25-km square box centered on the tremors, oriented N45°W, and including events within 0.2 years after the San Simeon earthquake), computed every 0.05 years with a 0.2-year smoothing window. Correlation of the rates is 0.75 when earthquake rates are delayed 0.15 years and 0.28 with no delay. Randomized tremor and earthquake times produce correlations ≥0.75 less than 1% of the time. (Bottom inset) The location of Cholame, California.

Fluids from subduction processes may be important for generating subduction zone tremors (*2*, *4*). Because subduction does not occur along the central SAF, either fluids are not important for the SAF tremors or an alternative fluid source exists below the seismogenic zone in this area.

In Cascadia, the correlation between subduction zone tremor rates and subseismogenic zone slow slip events is called episodic tremor and slip (ETS) (*4*). Stress changes from ETS events are expected to increase stress and possibly trigger earthquakes on the shallower seismogenic fault (*4*). The apparent correlation between tremor and local earthquake rates at Cholame (Fig. 1, inset), therefore, suggests that ETS may be taking place in this area. The tremor rate changes at Cholame also appear to precede changes in earthquake rate by several weeks (Fig. 1, inset), suggesting a possible causal relationship.

The Cholame segment of the SAF above the tremors last ruptured in, and possibly nucleated (*1*), the great M_w 7.8 Fort Tejon earthquake in 1857. This segment has an estimated earthquake recurrence time of 140 years (+93, –69) (*5*), and it is now more than 140 years since the Fort Tejon event. Because stress changes from ETS events may trigger large earthquakes (*4*), future increases in SAF tremor activity may signal periods of increased probability for the next large earthquake on the Cholame segment.

References and Notes

1. R. E. Wallace, Ed., *U.S. Geol. Surv. Prof. Pap. 1515* (Government Printing Office, Washington, DC, 1990).
2. K. Obara, *Science* **296**, 1679 (2002).
3. For ~3 months after the San Simeon earthquake (located ~60 km to the west), seismic signals from intense aftershock activity frequently mixed with the lower amplitude tremor signals, making accurate analysis of the SAF tremors infeasible.
4. G. Rogers, H. Dragert, *Science* **300**, 1942 (2003).
5. Working Group on California Earthquake Probabilities, *Bull. Seismol. Soc. Am.* **85**, 379 (1995).
6. Supported by U.S. Geological Survey award no. 04HQGR0085 and U.S. Department of Energy Office of Basic Energy Sciences contract no. DE-AC03-76SF00098. This is Berkeley Seismological Laboratory contribution no. 04-13.

4 November 2004; accepted 2 December 2004
Published online 9 December 2004;
10.1126/science.1107142
Include this information when citing this paper.

Berkeley Seismological Laboratory, 211 McCone Hall, University of California, Berkeley, CA 94720–4760, USA.

*To whom correspondence should be addressed. E-mail: nadeau@seismo.berkeley.edu

Ecological Change, Group Territoriality, and Population Dynamics in Serengeti Lions

Craig Packer,[1]* Ray Hilborn,[2] Anna Mosser,[1] Bernard Kissui,[1] Markus Borner,[3] Grant Hopcraft,[3] John Wilmshurst,[4] Simon Mduma,[5] Anthony R. E. Sinclair[6]

Territorial behavior is expected to buffer populations against short-term environmental perturbations, but we have found that group living in African lions causes a complex response to long-term ecological change. Despite numerous gradual changes in prey availability and vegetative cover, regional populations of Serengeti lions remained stable for 10- to 20-year periods and only shifted to new equilibria in sudden leaps. Although gradually improving environmental conditions provided sufficient resources to permit the subdivision of preexisting territories, regional lion populations did not expand until short-term conditions supplied enough prey to generate large cohorts of surviving young. The results of a simulation model show that the observed pattern of "saltatory equilibria" results from the lions' grouping behavior.

To test the effects of ecological changes on population dynamics (*1*–*3*), we rely on long-term records available from the Serengeti National Park, Tanzania (*4*). Lions in a 2,000 km^2 area of the Serengeti have been studied continuously since 1966 (*5*). "Woodlands" prides reside in regions dominated by *Acacia* and *Commiphora* trees, with resident herds of hartebeest, topi, and buffalo. "Plains" prides occupy grasslands consisting primarily of *Sporobolus*, *Themeda*, *Pennisetum*, and *Cynodon* spp., with low densities of resident warthog and Grant's gazelle. Large numbers of migratory wildebeest, zebra, and Thompson's gazelle move through both habitats in response to seasonal rainfall patterns each year. Lion prides consist of 1 to 18 adult females, their dependent offspring, and a resident coalition of 1 to 9 males. Females defend joint territories, and larger prides dominate smaller ones (*6*, *7*). As a result, prides of ≤2 females suffer very low reproductive success; prides of >10 females also fare poorly because of high levels of within-group competition (*5*, *8*). Prides persist for generations, and new prides consist of related females that disperse together from preexisting prides (*9*). Lion territory size varies with overall food availability (*10*) but not with the number of females in the pride (*11*), and a pride territory must also contain permanent water and adequate denning sites (*5*, *12*).

Population stasis and transition. To breed successfully, female lions must have sufficient companions to defend adequate food, water, and denning sites. Thus, an expanding food supply can only cause lion populations to grow when preexisting prides can split to form descendant prides that are large enough to establish themselves successfully. Population size should therefore increase as a direct function of the number of breeding groups in the population. The month-by-month change in population size between the 1960s and 2002 was highly correlated with the corresponding change in the number of prides in that habitat, regardless of whether we defined a pride as containing a minimum of two, three, or four adult females (and whether females were defined as "adults" after reaching 2, 3, or 4 years of age). However, the best statistical fit defined prides as groups containing a minimum of four females of at least 2 years of age (*13*), the age at which young females first participate in territorial defense (*14*).

Figure 1, A and B, shows the monthly population sizes in each study area. Totals fluctuated slightly from month to month; but at a broad time scale, each population showed long periods of stasis ended by a sudden transition to a new equilibrium (*15*), and each change point was associated with a specific ecological change in that habitat. Figure 1C shows the population sizes of the major Serengeti herbivore species over the past 40 years. Wildebeest and buffalo numbers increased dramatically from the early 1960s until the late 1970s because of their release from rinderpest infection in 1963 (*4*). This was by far the most substantial change in prey abundance over the entire study period, and the lion population showed a clear increase over this same span [also see (*16*)]. Most striking, however, is that the woodlands lion population suddenly increased to a new equilibrium in 1973. The plains lions were not monitored between 1969 and 1974, so the precise timing and tempo of its increase are not known.

Lions enjoy higher feeding success in areas with greater vegetative cover (*17*), and each Serengeti habitat has undergone a large-scale increase in cover in the past 20 years. The grazing wildebeest herds remove vast quantities of grass that would fuel wildfires if left to senesce, and the enormous increase in wildebeest numbers led to a striking decrease in grassfires that, in turn, stimulated a regeneration of the Serengeti woodlands during the 1980s (Fig. 2). In November 1983, the woodlands lion population suddenly increased to a new plateau after several years of unprecedented growth of woody vegetation (Fig. 1A). The wildebeest population declined in 1994 (as a result of severe drought); the migration "skipped" the intermediate grass plains in 1995, enabling the tallest species in this community to dominate, and this pattern persisted for the following 5 to 6 years (Fig. 3). The tall grass provided improved cover for the plains lions, and the plains population suddenly increased in February 1997 after remaining at a persistent equilibrium since at least 1975.

The woodland lion population dropped significantly in 1994 because of the canine distemper virus (CDV) epizootic that killed approximately one-third of the Serengeti lions (*18*). Although the die-off caused the lions to drop well below their equilibrium density, the population remained relatively constant for 5 years until suddenly returning to its previous plateau in May 1999.

Determinants of population change. The irruption of the herbivores, the regeneration of the woodlands, and the expansion of the tall grass plains were all processes that continued over several years, yet the lion populations always reached a new equilibrium in a single year. Similarly, the woodland population recovered suddenly but not until 5 years after the CDV outbreak. What determined the precise timing of these changes? The migratory patterns of the dominant herbivores (wildebeest, zebra, and gazelle) are primarily driven by seasonal rains in the Serengeti, and all of the sudden changes in lion population size coincided with years of unusual rainfall: 1973 was the first in a series of unusually "wet" dry seasons [which attracted the migratory herds to the woodlands study area

[1]Department of Ecology, Evolution, and Behavior, University of Minnesota, 1987 Upper Buford Circle, Saint Paul, MN 55108, USA. [2]School of Aquatics and Fishery Science, University of Washington, Seattle, WA 98105, USA. [3]Frankfurt Zoological Society, Post Office Box 14935, Arusha, Tanzania. [4]Parks Canada, Ecosystem Services, Winnipeg, MB R3B OR9, Canada. [5]Tanzanian Wildlife Research Institute, Box 661, Arusha, Tanzania. [6]Center for Biodiversity Research, University of British Columbia, Vancouver, BC VLT 1Z4, Canada.

*To whom correspondence should be addressed. E-mail: packer@cbs.umn.edu

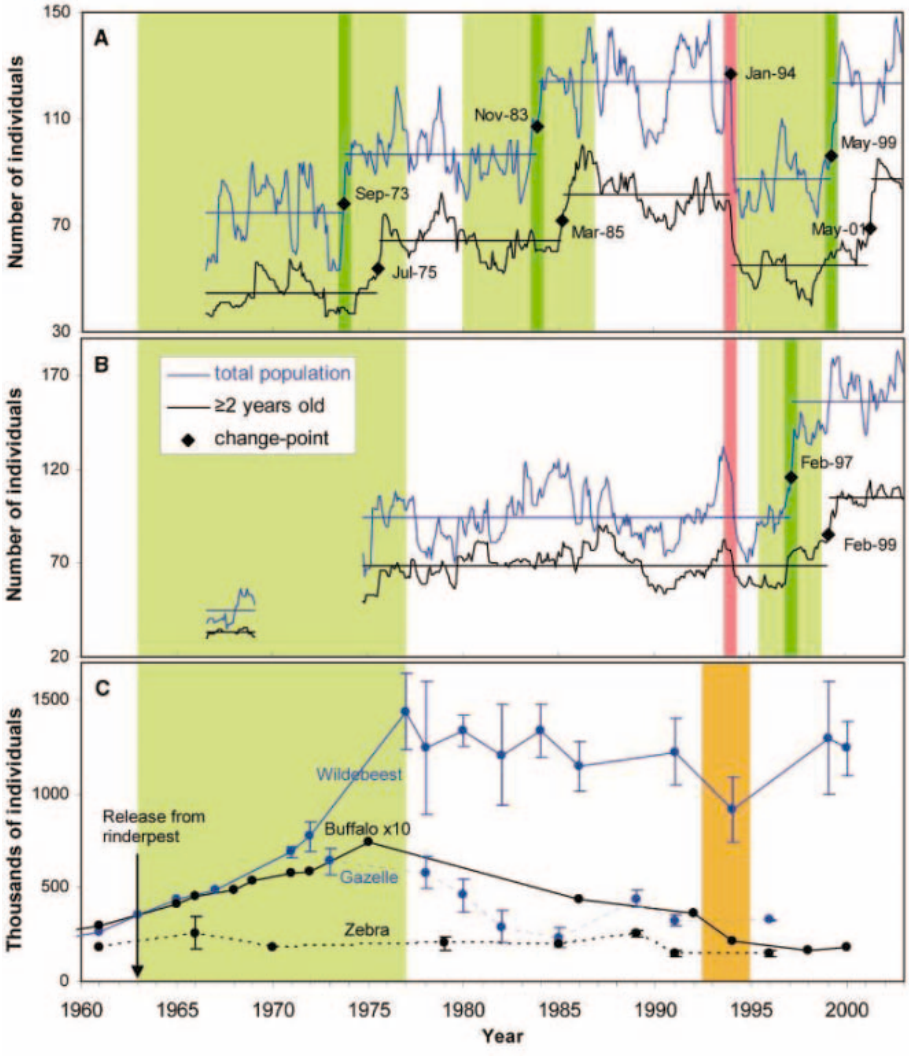

Fig. 1. Lion population sizes each month: (**A**) woodlands, (**B**) plains. Horizontal lines indicate periods where population sizes were statistically homogeneous but different from adjacent periods. Blue lines include all individuals; black lines indicate lions ≥2 years. Diamonds designate change points. Pale green blocks highlight times when the populations were below local equilibrium density; dark green lines demarcate years within these periods with favorable rainfall. Red line shows the CDV die-off in 1994. (**C**) Serengeti herbivore population sizes. Vertical bars show SE. Green box highlights recovery from rinderpest; brown box highlights drought-related die-off in the wildebeest.

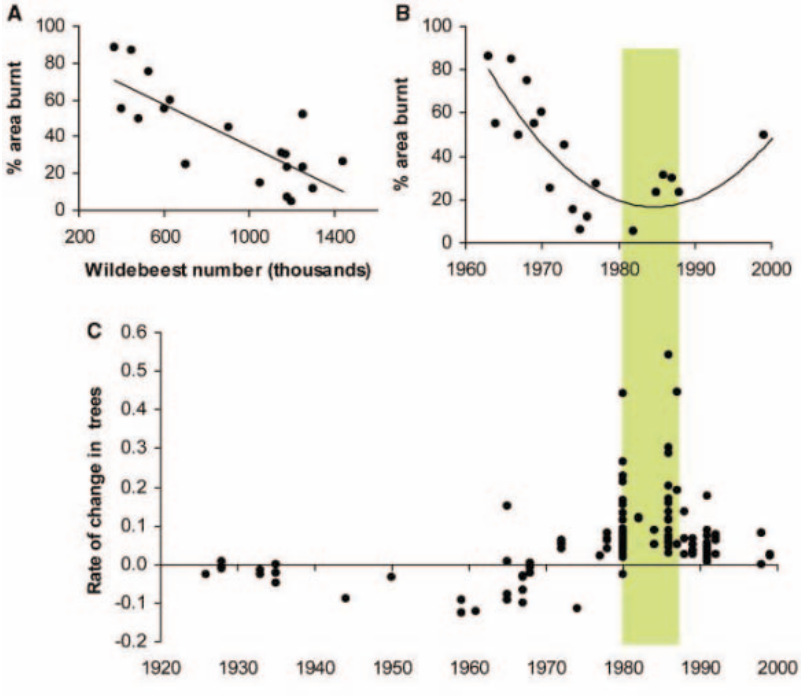

Fig. 2. Wildebeest, fire, and the regeneration of woody vegetation in the Serengeti woodlands. (**A**) The extent of wildfire is inversely related to the size of the wildebeest population. (**B**) Wildfire reached a low point in the late 1970s and early 1980s. (**C**) Population growth rates of acacias in the Serengeti woodlands as measured from fixed-point photography; woodland recovery peaked in the early 1980s. Green band indicates time period when the woodlands lions experienced the greatest increase in prey accessibility.

(*16*)], 1983 and 1999 were followed by the two driest wet seasons in more than 40 years, and the increase in the plains population occurred during the extreme El Niño rainfalls of 1997–1998, which were the heaviest since 1962. (Migrant herbivores spend less time on the plains in "dry" wet seasons and more time on the plains in "wet" wet seasons.)

Thus, the background of long-term change in prey availability is overlain with a stochastic year-to-year pattern of prey distribution, and the first "good year" permitted rapid recruitment in the lion population. Across all significant population increases, the primary demographic response was increased cub survival ($P < 0.01$) rather than larger litter size or shorter interbirth intervals. All the population "leaps" involved successful reproduction in an exceptional number of prides. Five of six woodlands prides successfully raised cohorts of cubs in 1973 and 1983 (four of six was the prior record) and six of seven in 1999. There had never been more than six successful prides in any single year on the plains until 1997, when 11 of 12 prides successfully fledged offspring.

Our data clearly reveal the impact of the wildebeest on the Serengeti lions. Buffalo and gazelle both returned to 1960s levels by 2002 (Fig. 1C) without a concomitant decline in lion numbers, whereas the wildebeest population has remained at about 1.2 million for the past 25 years. The wildebeest were also responsible for two indirect effects on the lions. Increased levels of grazing led to extensive regeneration of woody vegetation, permitting an increase in the woodlands lion population, whereas a temporary decline in the wildebeest population increased the average height of grasses in the intermediate grass community, enabling an expansion of the lion population on the plains. The first significant improvement in local wildebeest abundance during a period of persistent ecological change also permits the simultaneous establishment of viable new prides (with ≥4 females), thus triggering the sudden increase of the population as a whole (*13*). In contrast, the herbivore community in the nearby Ngorongoro Crater is nonmigratory, and the Crater lion population fell to one-eighth of its local equilibrium density after a disease outbreak in 1962 (*19*) but subsequently showed a continuous period of exponential growth, doubling every 4 years for 12 years (*20*).

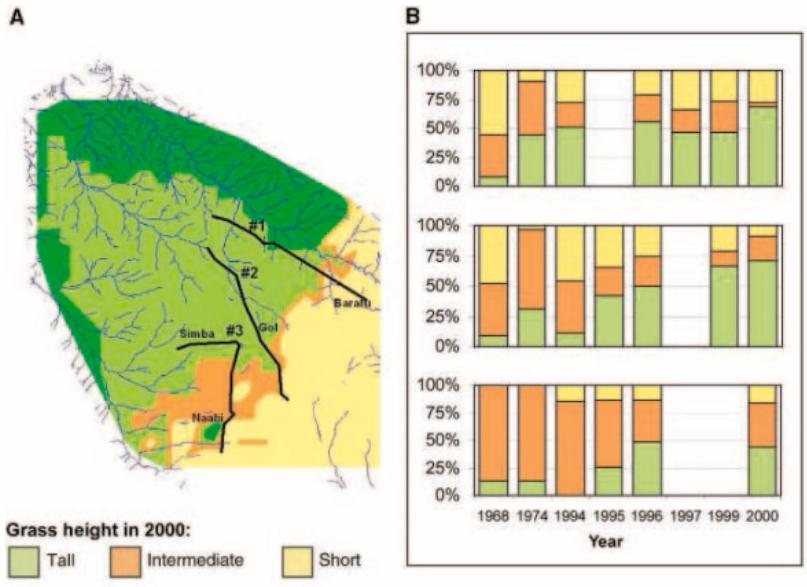

Fig. 3. Long-term changes in grass height. (**A**) Grasslands map for the Serengeti plains. (**B**) Bar graphs indicate percentage of each grass type along the three transects in (A). The extent of tall grass has increased since 1994 ($P < 0.01$).

Impact of social structure. To evaluate the importance of group living on population changes in the Serengeti, we developed a detailed simulation model that incorporated long-term data on cub productivity, pride splitting, and adult survival as functions of annual rainfall, pride size, and dispersal status. We modeled the impact of large-scale ecological change as an increase in the number of potential territories in each study area (the magnitude being set by the observed change in equilibrial population size); rainfall followed the observed sequence over the past 40 years, and the simulated population suffered the observed level of disease mortality in 1994. Pride formation was a stochastic process that depended on the number of available territories, the size of the maternal pride, and cub recruitment. Key parameters were varied first to mimic an asocial species. In this initial case, all offspring dispersed and females were solitary (thus the model was deterministic rather than stochastic). In the second scenario, lions lived in stochastically created prides and new prides were only viable if they contained ≥4 females, but there was no within-group den-

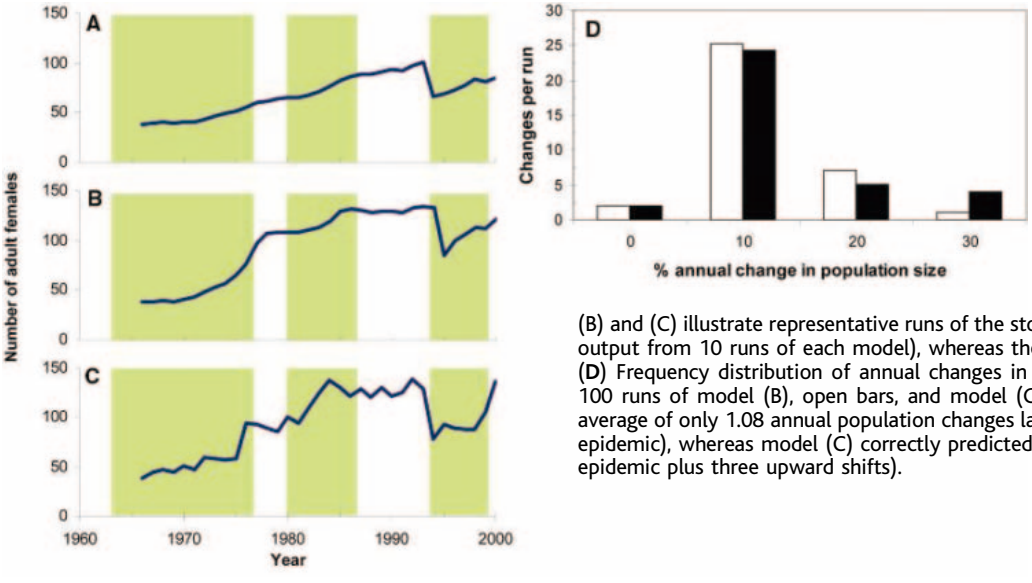

Fig. 4. Number of adult females predicted by simulation models of the Serengeti woodlands population under three different scenarios. (**A**) Each territory is occupied by only one adult female; all adult daughters disperse. (**B**) Lions live in prides that must contain ≥3 females to be viable, but cubs do not suffer higher mortality in excessively large prides. (**C**) Prides must be ≥3 females to be viable, and cubs born in large prides suffer higher mortality. (B) and (C) illustrate representative runs of the stochastic models (see figs. S1 and S2 for output from 10 runs of each model), whereas the model shown in (A) is deterministic. (**D**) Frequency distribution of annual changes in female population size averaged over 100 runs of model (B), open bars, and model (C), black bars. Model (B) generated an average of only 1.08 annual population changes larger than 30% (because of the disease epidemic), whereas model (C) correctly predicted an average of 4.08 such changes (the epidemic plus three upward shifts).

sity dependence: Cubs in large prides had similar mortality as those in medium-sized prides. The final model imposed both a threshold minimum viable pride size and the observed levels of cub mortality in excessively large prides.

In a solitary species, gradual changes in the environment in the Serengeti woodlands produce a continuous response in adult population size (Fig. 4A), because females can be added one at a time as the number of potential territories increases. In a social species with a threshold minimum group size but lacking within-group density dependence, adult population growth is less continuous, but the shifts between equilibria are still gradual because daughters can always be added to preexisting prides (Fig. 4B). With both a threshold minimum pride size and within-group density dependence, however, adult population growth is abrupt, and the model often generates the kind of saltatory equilibrium observed in the empirical data (Fig. 4, C and D). With an upper limit on pride size, moderate-sized prides require exceptional circumstances to rear large cohorts of daughters, and this is the only scenario that accurately predicts a delayed (but abrupt) recovery from the 1994 CDV outbreak (see also figs. S1 and S2).

Lion social structure imposes a coarse-grained tempo on population change that is further amplified by synchronous recruitment of large cohorts by multiple prides and stabilized by within-group density dependence. Until now, population models have assumed that population trends could be predicted by extrapolation from the survival and reproduction of individuals. However, a more complete understanding of population dynamics can only be achieved by incorporating the impact of social organization and family structure on the population as a whole.

References and Notes

1. V. C. Wynne-Edwards, *Animal Dispersion in Relation to Social Behaviour* (Oliver & Boyd, Edinburgh, 1962).
2. J. R. Krebs, *Ecology* **52**, 2 (1971).
3. C. J. Krebs, *Ecology: The Experimental Analysis of Distribution and Abundance* (Harper & Row, New York, 1972).
4. A. R. E. Sinclair, in *Serengeti: Dynamics of an Ecosystem*, A. R. E. Sinclair, M. Norton-Griffiths, Eds. (Univ. of Chicago Press, Chicago, 1979), pp. 82–103.
5. C. Packer, A. E. Pusey, L. Eberly, *Science* **293**, 690 (2001).
6. K. E. McComb, C. Packer, A. E. Pusey, *Anim. Behav.* **47**, 379 (1994).
7. R. Heinsohn, C. Packer, *Science* **269**, 1260 (1995).
8. C. Packer *et al.*, in *Reproductive Success*, T. H. Clutton-Brock, Ed. (Univ. of Chicago Press, Chicago, 1988), pp. 363–383.
9. C. Packer, D. Gilbert, A. E. Pusey, S. J. O'Brien, *Nature* **351**, 562 (1991).
10. K. G. Van Orsdol, J. P. Hanby, J. D. Bygott, *J. Zool.* **206**, 97 (1985).
11. H. Kruuk, D. W. MacDonald, in *Behavioural Ecology*, R. M. Sibley, R. H. Smith, Eds. (Blackwell, Oxford, 1985), pp. 521–536.
12. J. P. Hanby, J. D. Bygott, C. Packer, in *Serengeti II: Research, Management and Conservation of an Ecosystem*, P. Arcese, A. R. E. Sinclair, Eds. (Univ. of Chicago Press, Chicago, 1995), pp. 315–331.
13. Time-series correlations between the change in the number of adults (age ≥2 years) in a given month and the change in the number of prides during that same month were highest when "prides" were defined as groups containing four adult females. Plains: $N = 369$ pride months, $r = 0.374$, $P < 0.0001$; woodlands: $N = 437$ pride months, $r = 0.249$, $P < 0.0001$. Autocorrelations within each time series were not significant; best fits were found with a zero time lag between the number of adults and the number of prides.
14. R. Heinsohn, C. Packer, A. E. Pusey, *Proc. R. Soc. London Ser. B* **263**, 475 (1996).
15. An optimal segmentation method (*21*) determined the number of segments and the date of the change points for each population. This method segments a data series so as to minimize the total sum-of-squares deviations by using the mean and sum of squares for each segment (and assuming a normal distribution and constant variance). The minimum number of equilibria for each habitat was determined by a dynamic programming algorithm that measured the improvement in the sum of squares with each additional segment. A cumulative sum (CUSUM) technique (*22*) confirmed the number and date of the change points by detecting persistent shifts from a known mean in a time series (table S1).
16. J. P. Hanby, J. D. Bygott, in *Serengeti: Dynamics of an Ecosystem*, A. R. E. Sinclair, M. Norton-Griffiths, Eds. (Univ. of Chicago Press, Chicago, 1979), pp. 249–262.
17. J. G. C. Hopcraft, A. R. E. Sinclair, C. Packer, *J. Anim. Ecol.*, in press.
18. M. E. Roelke-Parker *et al.*, *Nature* **379**, 441 (1996).
19. B. Kissui, C. Packer, *Proc. R. Soc. London Ser. B* **271**, 1867 (2004).
20. C. Packer *et al.*, *Conserv. Biol.* **5**, 219 (1991).
21. D. M. Hawkins, *Stat. Med.* **21**, 1913 (2002).
22. D. M. Hawkins, D. Olwell, *Cumulative Sum Control Charts and Charting for Quality Improvement* (Springer, New York, 1998).

23. Supported by NSF Long-Term Research in Environmental Biology grants DEB-9903416 and DEB-0343960, NSF Biocomplexity grant BE-0308486, the Canadian Natural Sciences and Engineering Research Council, and the Frankfurt Zoological Society. We thank H. Brink, J. Fryxell, D. M. Hawkins, G. Sharam, K. Skinner, I. Taylor, P. West, and K. Whitman for advice and assistance and the Tanzanian Wildlife Research Institute and Tanzanian National Parks for permission to conduct research. This paper is the outcome of a working group on the Biocomplexity of the Serengeti hosted by the National Center for Ecological Analysis and Synthesis from 2001 to 2003.

Supporting Online Material
www.sciencemag.org/cgi/content/full/307/5708/390/DC1
SOM Text
Table S1
Figs. S1 and S2

10 September 2004; accepted 11 November 2004
10.1126/science.1105122

REPORTS

Grain Boundary Decohesion by Impurity Segregation in a Nickel-Sulfur System

Masatake Yamaguchi,* Motoyuki Shiga, Hideo Kaburaki

The sulfur-induced embrittlement of nickel has long been wrapped in mystery as to why and how sulfur weakens the grain boundaries of nickel and why a critical intergranular sulfur concentration is required. From first-principles calculations, we found that a large grain-boundary expansion is caused by a short-range overlap repulsion among densely segregated and neighboring sulfur atoms. This expansion results in a drastic grain-boundary decohesion that reduces the grain-boundary tensile strength by one order of magnitude. This decohesion may directly cause the embrittlement, because the critical sulfur concentration of this decohesion agrees well with experimental data on the embrittlement.

The incorporation of a small quantity of impurities can drastically change the mechanical strength of metals. Auger electron spectroscopy studies, together with various tensile tests, show that the sulfur (S)–induced embrittlement of nickel (Ni) is clearly associated with S segregation to grain boundaries (GBs) and that the transition from ductile to brittle behavior requires a critical intergranular concentration of S (*1*, *2*). However, why and how S weakens the GBs and the significance of the critical intergranular concentration remain unclear. One hypothesis assumes that the embrittlement arises from S-induced changes in the electronic structure that lead to weakening of the Ni-Ni bonds holding the GB (*3*, *4*). A second assumes that the magnitude of the embrittling effect can be estimated by the binding energy difference for S at a GB and at a fractured free surface according to the Rice-Wang model (*5*, *6*). These hypotheses, however, do not directly explain the existence of a critical

Center for Promotion of Computational Science and Engineering, Japan Atomic Energy Research Institute, Tokai-mura, Ibaraki 319-1195, Japan.

*To whom correspondence should be addressed. E-mail: yamagu@popsvr.tokai.jaeri.go.jp

concentration of S. In other words, what is the correlation between S concentration and GB weakening?

By tensile test calculations from first principles, we show here that the tensile (cohesive) strength of a Ni GB decreases by one order of magnitude, owing to a large GB expansion caused by a dense S segregation. We clarify that such a dense segregation of S is energetically possible, considering the calculated segregation energies with McLean's model (*7*) for equilibrium segregation. Furthermore, the estimated intergranular concentration of S to induce the strong decohesion (9 to 14 atomic % S, 1.5 to 2.0 monolayers, 10.8 to 14.4 atoms/nm^2) is in agreement with the experimentally observed critical concentration for the embrittlement of Ni (10 to 16 atomic % S) by Heuer *et al.* (*1*, *2*).

In contrast to the hypotheses that focus on S-induced changes in the electronic structure of Ni-Ni and/or Ni-S bonds, we found that a short-range repulsive interaction among S atoms in the GB region plays a crucial role. This repulsion is based on the fact that S makes stronger bonds with Ni than with S. Therefore, the covalent bondings among S atoms do not form in the situation where S atoms are surrounded by many Ni atoms. As a result, the attractive term disappears and only the repulsive term remains in the S-S interatomic potential. Owing to this repulsion, S atoms cannot neighbor with each other on Ni surfaces and in some Ni-S ordered alloys. In the GB region, however, S atoms can get close and neighbor with each other, because an energy gain by the segregation is much larger than an energy loss by the repulsive interaction. Consequently, the nearest neighbor Ni-Ni or Ni-S pair is replaced with the S-S pair, and the interaction in the pair reverses from attraction to repulsion. Furthermore, the elongation of the S-S distance occurs up to ~3.3 Å, because the Ni-Ni or Ni-S distance (~2.5 Å) is too short for the repulsive S-S pair. This elongation has the side effect of expanding adjacent Ni-Ni and Ni-S bonds that hold the GB structure. Therefore, this results in the large GB expansion that causes the strong GB decohesion.

It is necessary for later discussion to understand the atomic structure of a GB. Figure 1A shows the unit cell modeling for a NiΣ5(012) symmetrical tilt GB, which we use for calculations (*8*) [supporting online material (SOM)]. This unit cell includes 80 Ni atoms. The Ni sites and GB vacancy sites are indicated by numbers. We refer to this unit cell as the GB unit cell and to the atomic sites as GB0, GB1, GB2, etc. In this unit cell, there are two GB planes, one of which includes GB1 sites and the other includes the GB11 site. The GB0 site is a GB vacancy site, which is shown in one of the two GB planes, because the other will be kept clean (no segregation) in our calculations. In Fig. 1B, the structure of fractured free surface at the GB plane is shown. We can see that there are four equivalent sites in the same *ab* plane for each site.

The calculated binding energies per one S atom depending on the site and its occupation, $-E_b$(site,occ.) as in Table 1, indicate to what extent the S atom is energetically stabilized with respect to the atomic gas state of S. For the GB case, this is the energy difference among the total energies of the GB unit cell that includes S atoms, the clean GB unit cell, and the isolated S atom. These (inherently negative) total energies are calculated with atomic geometry relaxation by force minimization and c-axis optimization by total energy minimization (*8*) using the Vienna ab initio Simulation Package (VASP) (*9*, *10*) with projector-augmented plane wave (PAW) potentials (*11*).

First, we show which site in the GB region is occupied by S segregation, in consideration of the calculated binding energies per one S atom as in Table 1. When one S atom is inserted into the GB vacancy site (GB0) or substituted for a Ni atom at the other sites (GB1 to GB6), the binding energies at GB0 and GB±2 sites show values of 4.69 and 4.67 eV per atom of S (eV/S), respectively. On the other hand, those at GB±*i* (*i* = 1, 3 to 6) sites show smaller values of 3.11 to 3.51 eV/S. From these binding energies, we can estimate the impurity occupation of each site under equilibrium segregation using McLean's (*7*) equation as follows: $\Delta E_{seg} = E_b(\text{site,occ.}) - E_b(\text{bulk})$, $C_{GB} = [C_{bulk}\exp(-\Delta E_{seg}/RT)]/[1 + C_{bulk}\exp(-\Delta E_{seg}/RT)]$. Here, $-E_b$(site,occ.) is the binding energy as stated above, and $-E_b$(bulk) is the binding energy when one S atom is in the inner bulk environment. We calculated $-E_b$(bulk) (2.96 eV/S) using a unit cell in which a part of the atomic geometries in the GB unit cell is modified to recover bulk face-centered cubic (fcc) symmetry in the whole cell. The difference between the two energies, ΔE_{seg}, is segregation energy (SOM). T is the aging temperature for the segregation process, and C_{GB} and C_{bulk} are the occupation of impurity in the GB region and inner bulk, respectively. The im-

Table 1. Calculated binding energies $-E_b$ (eV/S) per S atom with respect to the atomic gas state of S. S is in GBs and bulk unit cells. The binding energies depend on occupation.

Site	Occ.	$-E_b$ (eV/S)	Site	Occ.	$-E_b$ (eV/S)
GB0	1/4	4.69	GB0*	4/4	4.75
GB2	1/4	4.67	GB2	4/4	4.66
GB1	1/4	3.47			
GB3	1/4	3.51	GB4	1/4	3.50
GB5	1/4	3.44	GB6	1/4	3.11
Bulk	1/4	2.96	(Exp. 2.76§)		
In addition to GB0 4/4, …					
GB2	1/4	4.49	GB2†	2/4	4.33
GB2	3/4	4.24	GB2‡	4/4	4.23
In addition to GB0 4/4, and GB2 4/4, …					
GB-2	4/4	3.84			

*Fig. 2B. †Fig. 2C. ‡Fig. 2D. §(*17*, *18*).

Table 2. Calculated binding energies $-E_b$ (eV/S) per S atom with respect to the atomic gas state of S. S is in the solid α-S, S_2 molecule and in some ordered alloys. For the ordered alloys, the energies are calculated with respect to the atomic S and bulk fcc Ni.

Material	Type	S-S (Å)	$-E_b$ (eV/S)	Exp. (eV/S)
α-S	A16	2.05	2.88	2.88*
S_2	–	1.91	2.17	2.20*
Ni_3S_2	$D5_e$	3.49	4.06	4.50†
NiS	B4	3.58	3.71	
NiS	$B8_1$	3.21	3.60	
NiS	B13	3.14	3.82	
Ni_3S_4	$D7_2$	3.12	3.72	
NiS_2	C2	2.08	3.43	

*(*19*). †(*20*).

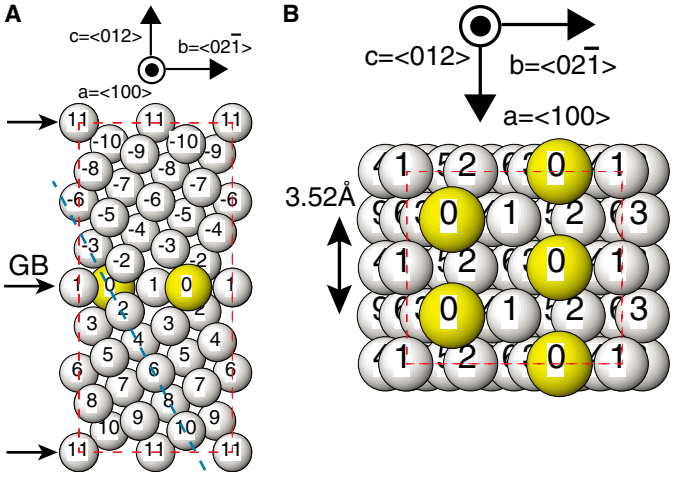

Fig. 1. Modeling of Σ5(012) symmetrical tilt GB. Gray balls indicate Ni atoms; yellow balls indicate S atoms. 80 Ni atoms are included for the clean GB case. The red dashed lines indicate a two-dimensional unit cell. Because the GB plane is a mirror plane, GB*i* and GB-*i* (*i* = 2 to 10) are crystallographically equivalent sites. (**A**) Side view of the unit cell. The blue dashed line indicates the cross-sectional plane on which valence electron density is shown in Fig. 2, B to D. (**B**) Top view of the fractured free surface at the GB. The distance between two GB0 sites is 3.52 Å, which is equal to the lattice constant of fcc Ni.

purity occupation (concentration) in the inner bulk, C_{bulk}, should be far less than 1.0 in this equation. In Fig. 2A, we show the occupation curves calculated from the above equation for some conditions of aging temperatures and bulk S concentrations. Here we focus on the middle line for 918 K and 25 atomic parts per million (ppm), because this condition was chosen by Heuer *et al.* (*1*, *2*) for their experimental determination of the critical S concentration. From this figure, we can see that the occupations of both the GB0 and GB2 sites are very close to 1.0, whereas those of the others (GB1 and GB3 to GB6) are under 0.1 (SOM).

Next, we assume that more than one S atom segregates in the GB unit cell. When we insert S atoms one by one at four GB0 sites, the average binding energy per one S atom does not change appreciably, as in Table 1. This indicates that the GB0-GB0 distance (3.52 Å) is so long that any appreciable interaction does not begin. Similar results are also obtained for the GB±2 site. On the other hand, the distance between the GB0 and GB±2 sites is 2.2 Å in the clean GB case, which is even shorter than Ni-Ni nearest-neighbor distance (2.49 Å) in fcc Ni. Although there are many choices for how to insert or substitute S atoms at GB0, GB2, and GB-2 sites, we show here only one example for simplicity, which gives the largest average binding energies. We substitute S atoms for Ni atoms one by one at four GB2 sites, in addition to four GB0 sites occupied by S. The average binding energy reduces from 4.75 to 4.23 eV/S, as in Table 1. This clearly shows that there is a strong repulsive interaction between S atoms (SOM). Although in McLean's model the binding energy of impurity is assumed not to depend on the site and the occupation of impurity in the GB region, we estimate the occupation as a first approximation by substituting the average binding energy for the fixed one in McLean's equation. Despite the large energy loss, the average binding energy, 4.23 eV/S, is still sufficiently large for the eight S atoms to segregate fully at all GB0 and GB2 sites, as in Fig. 2A. If we insert or substitute 12 S atoms fully at GB0, GB2, and GB-2 sites, however, the average binding energy reduces to 3.84 eV/S. In the conditions for segregation (918 K, 25 atomic ppm) chosen by Heuer *et al*., it is thought to be difficult for all 12 sites to be fully occupied by S atoms as in Fig. 2A. Experimentally, it is reported that elemental S is removed from GBs by the formation of Ni_3S_2 precipitates after 120 hours of annealing at 918 K and 20 weight ppm of S (*12*). This fact is consistent with our results, in which the binding energy of S for Ni_3S_2 (4.06 eV/S) is larger than the above binding energy (3.84 eV/S) and is the largest among those for some Ni-S ordered alloys, as in Table 2 (SOM).

Along with the increase of occupation at GB0 and GB2 sites, the distance between adjacent GB0 and GB2 sites increases greatly. Figure 2, B to D, shows valence electron density maps when S atoms are gradually substituted for Ni atoms at all four GB2 sites in addition to fully occupied four GB0 sites by S. These figures clearly show that S atoms do not bond with each other, whereas they bond strongly with Ni atoms. The valence electron density at the middle point between two neighboring S atoms is close to zero. The distance between adjacent GB0 and GB2 sites when they are fully occupied by S is 3.3 Å, which is large when compared with its original distance (2.2 Å) for the clean GB case and the

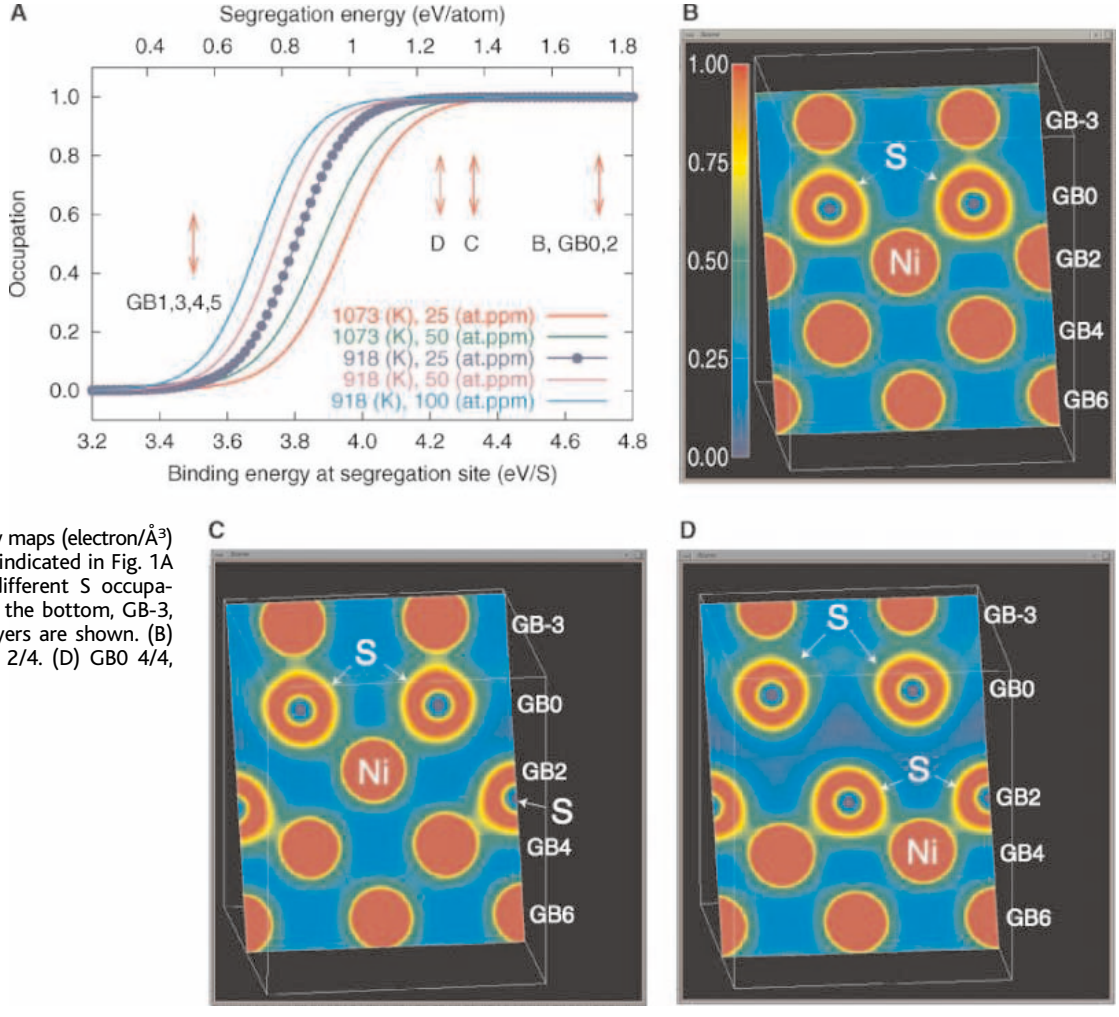

Fig. 2. (**A**) Occupation versus binding energy, $-E_b$ (eV/S), at a segregation site calculated from McLean's equation with respect to the aging temperature (K) and bulk S concentration (atomic ppm, 10^{-4} atomic % S). The blue line with circles indicates the occupation under the conditions chosen by Heuer *et al.* (*1*, *2*) to determine a critical intergranular concentration of S. Both binding energies and segregation energies of S are roughly indicated by arrows for each single site (GB0 to GB5) and for cases [(B) to (D)] in which S atoms interact with each other. (**B** to **D**) Valence electron density maps (electron/Å^3) on the cross-sectional plane indicated in Fig. 1A for three cases that have different S occupations. From the top layer to the bottom, GB-3, GB0, GB2, GB4, and GB6 layers are shown. (B) GB0 4/4. (C) GB0 4/4, GB2 2/4. (D) GB0 4/4, GB2 4/4.

Ni(GB2)-S(GB0) distance (2.27 Å) after all GB0 sites are occupied by S. From the S-S distance, the radius of the S atom is estimated to be 1.65 Å. This radius is about 60% longer than the radius of S (1.03 Å) estimated from the above Ni-S distance by subtracting the half length (1.25 Å) of the nearest-neighbor Ni-Ni distance in fcc Ni. This indicates that the GB expansion in this case cannot be explained by an atomic "size effect" that is often used to explain some phenomena such as solid solubility (SOM).

From the above argument, it is evident that a short-range repulsive interaction occurs between S atoms in Ni when S atoms come sufficiently close to each other, within 3 or 4 Å (SOM). We think that this force has a common origin with the well-known phenomena that Ni and S form ordered alloys, and adsorbed S atoms on Ni surfaces form ordered structures (*13*). These phenomena are usually explained by assuming the repulsive interaction between S atoms in Ni and on Ni surfaces. The origin of this force is based on the fact that S atoms prefer to bond with Ni atoms instead of with other S atoms. In fact, the binding energy per one S atom in an S_2 molecule is 2.2 eV/S, which is appreciably smaller than those in some Ni-S ordered alloys and in the GBs and bulk unit cells as in Tables 1 and 2. In addition, the S-S distance is over 3.0 Å for some Ni-S ordered alloys, except for NiS_2 as in Table 2. This indicates that distances of about 2.2 to 2.5 Å between neighboring sites in the GB region are too short for the repulsive S-S pair to be stable. For these reasons, the repulsive S atoms expand the GB region. Only in the NiS_2 case, where S forms an S_2 dimer in which the S-S distance is 2.08 Å, is it close to the S-S distance in the S_2 molecule, 1.91 Å. However, this is an exceptional case in which S is richer than Ni.

The physical origin of this repulsive interaction (force) can be explained in the following way. The Ni-S bond has larger binding energies than the S-S bond. This indicates that the electronic levels of Ni-S bondings are formed in an energetically deeper range than those of S-S bondings (fig. S1). In this case, most electrons of S are thought to contribute to Ni-S bonds rather than S-S bonds. This results in the situation where among S atoms, the attractive interaction due to covalency does not work. Generally speaking, an interatomic potential is a superposition of the attractive term and a short-range repulsive term. As a result, only the short-range repulsive term remains in the S-S interatomic potential.

To measure the tensile (cohesive) strength of a GB, we performed simple tensile test calculations from first principles as in Fig. 3 (SOM). The results of these tests reveal a dramatic reduction of the maximum tensile stress (tensile strength) of the GB with the increase in S segregation. First, we see the result for the bulk unit cell that does not include the GB. As in Fig. 3A, the calculated tensile strength for the bulk case in the ⟨012⟩ direction is 30 GPa, which is close to the ideal tensile strength in the ⟨100⟩ direction (37 GPa) that is estimated from experimental data (*14*). Second, we see the result for a clean GB case. In this case, the c-axis length is already expanded by 0.4 Å, which is the GB expansion (SOM). The resulting tensile strength of a clean GB is 26 GPa, which is slightly smaller than that of the bulk case. For the GB that includes four S atoms at four GB0 sites (GB0 4/4), the GB is already expanded by 0.9 Å. The resulting tensile strength reduces to 22 GPa (*15*). Further tensile tests were performed by substituting S atoms one by one for Ni atoms at the four GB2 sites. The GB expansion further increased and the resulting tensile strength decreased. The decrease of the tensile strength was clearly in proportion to the increase in GB expansion. The final tensile strength was 2.5 GPa, which is only 10% of the clean GB case. This is comparable to the ideal shear strength of Ni, 2.4 to 7.1 GPa, estimated by Mackenzie's method (*14*) (SOM), and is only five times larger than the experimental tensile strength of Ni, 493 MPa (*16*). Although these tensile tests are within the limits of only one kind of Σ5(012) GB, the strong decohesion can occur for any kind of GB that includes a sufficient number of segregation sites having large segregation (binding) energies and neighboring each other within a distance about 2.5 Å. As for the other impurity elements, the calculated results for Ni-P (phosphorous) and Ni-B (boron) systems are in agreement with experimental facts (SOM).

The estimated critical concentration of S for the strong GB decohesion agrees well with the experimental data. In Heuer *et al.* (*1*, *2*), the GB region is assumed to be within about 5 Å depth from the GB plane, from analysis of Auger electron spectroscopy. Similarly, we assume the GB region from the GB0 site plane to the GB±7 or GB±8 site plane within about 5 Å from the GB, in which 56 or 64 atomic sites are included. Then we assume that this strong decohesion begins in a range of S occupations from (GB0 4/4, GB2 2/4) to (GB0 4/4, GB2 4/4). In this region, the tensile strength of GB is less than half of that for the clean GB case. Thus, the critical S concentration is estimated to be 9 to 14 atomic % S (6 out of 64 to 8 out of 56), which is in agreement with the experimentally determined concentration (10 to 16 atomic % S) (*1*, *2*).

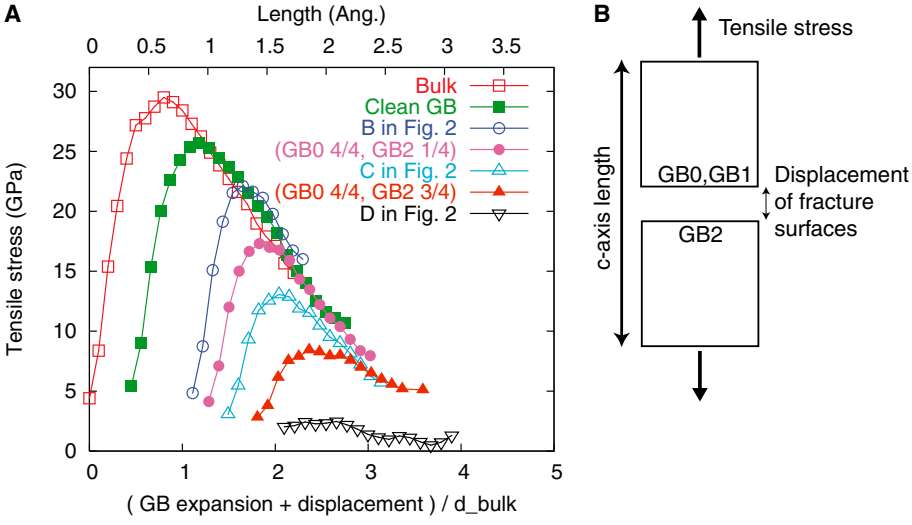

Fig. 3. (**A**) Stress displacement curves calculated from first principles. The first point of each line indicates the GB expansion with respect to the bulk interlayer distance in the ⟨012⟩ direction (*d*_bulk = 0.785 Å). The relative GB expansion from the first point of each line indicates the displacement between fracture surfaces. The curves are plotted for the following cases: bulk (open squares), clean GB (solid squares), GB0 4/4 (open circles), GB0 4/4, GB2 1/4 (solid circles), GB0 4/4, GB2 2/4 (open upward triangles), GB0 4/4, GB2 3/4 (solid upward triangles), and GB0 4/4, GB2 4/4 (open downward triangles). (**B**) These tensile tests were performed in such a way that two crystals divided by a fracture plane were gradually separated in the direction of the *c* axis, with no relaxation for atomic positions and *ab* axes' lengths. The tensile stress (GPa) perpendicular to the GB(012) plane is calculated from the derivative of total energies. Here, the fracture plane lies between the GB0(GB1) and GB2 plane in order to measure the tensile stress between the two fractured surfaces.

References and Notes

1. J. K. Heuer, P. R. Okamoto, N. Q. Lam, J. F. Stubbins, *J. Nucl. Mater.* **301**, 129 (2002).
2. J. K. Heuer, thesis, Univ. of Illinois at Urbana-Champaign (2000).
3. R. P. Messmer, C. L. Briant, *Acta Metall.* **30**, 457 (1982).
4. M. E. Eberhart, K. H. Johnson, R. M. Latanision, *Acta Metall.* **32**, 955 (1984).

5. J. R. Rice, J.-S. Wang, *Mater. Sci. Eng. A* **107**, 23 (1989).
6. R. Wu, A. J. Freeman, G. B. Olson, *Science* **265**, 376 (1994).
7. D. McLean, *Grain Boundaries in Metals* (Oxford Univ. Press, London, 1957).
8. Materials and methods are available as supporting material on *Science* Online.
9. G. Kresse, J. Hafner, *Phys. Rev. B* **47**, R558 (1993).
10. G. Kresse, J. Furthmüller, *Phys. Rev. B* **54**, 11169 (1996).
11. G. Kresse, D. Joubert, *Phys. Rev. B* **59**, 1758 (1999).
12. A. Larere, M. Guttmann, P. Dumoulin, C. Roques-Carmes, *Acta Metall.* **30**, 685 (1982).
13. J. Oudar, *Mater. Sci. Eng.* **42**, 101 (1980).
14. A. Kelly, N. H. Macmillan, *Strong Solids* (Clarendon Press, Oxford, ed. 3, 1986).
15. G. S. Painter, F. W. Averill, *Phys. Rev. Lett.* **58**, 234 (1987). (They pointed out the importance of lattice expansion for the embrittlement of Ni due to expanded valence orbitals of S.)
16. A. Buch, *Pure Metals Properties* (ASM International, Materials Park, OH, 1999).
17. T. Miyahara, K. Stolt, D. A. Reed, H. K. Birnbaum, *Scr. Metall.* **19**, 117 (1985).
18. N. Barbouth, J. Oudar, *C. R. Acad. Sci. Ser. C* **269**, 1618 (1969).
19. B. Meyer, *Chem. Rev.* **76**, 367 (1976).
20. G. M. Mehrotra, V. B. Tare, J. B. Wagner Jr., *J. Electrochem. Soc.* **132**, 247 (1985).
21. We thank J. K. Heuer, P. R. Okamoto, N. Q. Lam, and J. F. Stubbins for their fundamental and precise experiments for S-induced embrittlement of Ni. Part of this research is supported by ACT-JST.

Supporting Online Material
www.sciencemag.org/cgi/content/full/1104624/DC1
Materials and Methods
SOM Text
Figs. S1 to S3
Tables S1 to S3
References and Notes

30 August 2004; accepted 07 December 2004
Published online 6 January 2005;
10.1126/science.1104624
Include this information when citing this paper.

Porous Semiconductor Chalcogenide Aerogels

Jaya L. Mohanan, Indika U. Arachchige, Stephanie L. Brock*

Chalcogenide aerogels based entirely on semiconducting II-VI or IV-VI frameworks have been prepared from a general strategy that involves oxidative aggregation of metal chalcogenide nanoparticle building blocks followed by supercritical solvent removal. The resultant materials are mesoporous, exhibit high surface areas, can be prepared as monoliths, and demonstrate the characteristic quantum-confined optical properties of their nanoparticle components. These materials can be synthesized from a variety of building blocks by chemical or photochemical oxidation, and the properties can be further tuned by heat treatment. Aerogel formation represents a powerful yet facile method for metal chalcogenide nanoparticle assembly and the creation of mesoporous semiconductors.

Porous solids, such as zeolites, ordered mesoporous materials (M41S type), aerogels, and photonic crystals, find applications in such technologies as catalysis, sorption, filtration, thermal and acoustic insulation, and optical switches. Their distinctive properties are a function of the high internal surface area; the size, shape, and degree of interconnectedness of the pores; and the chemical nature of the framework. The pore structure can act as either a thoroughfare or a trap, or can even modulate the optical properties (as in photonic crystals), whereas the chemical interface is where catalysis, sensing, and sorption take place. The vast majority of porous solids are oxide based, thereby limiting the range of chemical functionality and physical properties that can be engineered into these materials. Recently, there has been sustained effort to prepare metal chalcogenide (sulfide, selenide, and telluride) analogs that are semiconducting substitutes for traditional oxide materials, the majority of which are electrically insulating.

There has been considerable success with the creation of microporous (<2 nm pores) zeolitic chalcogenide structures (*1*–*3*), as well as macroporous (>50 nm) materials created by sphere-templating strategies (photonic crystals) (*4*–*6*). In contrast, attempts to prepare similarly ordered mesoporous (2 to 50 nm) materials of metal chalcogenides have met with less success. Efforts have largely emphasized surfactant templating methodologies, originally developed for M41S-type materials, that employ metal chalcogenide building blocks and transition metal ion linkers. The resulting materials demonstrate long-range ordering of the surfactant/chalcogenide framework; however, attempts to remove the surfactants to access the pores invariably result in structure collapse (*7*–*12*).

We have developed a strategy for the production of mesoporous nanostructured metal chalcogenides based on the assembly of discrete nanoparticles to produce aerogel-type frameworks. Aerogels are highly porous architectures that arise when the solvent in a wet polymeric gel is replaced by air while the structural integrity of the framework is maintained (*13*). They are defined by a nanonetwork of particles, each with a low degree of connectivity, resulting in porosity that is intrinsic to an aerogel (regardless of whether a monolith is produced) and not to a precipitate. Aerogels are typically produced by supercritical drying because other routine techniques for drying gels (e.g., vacuum extraction or heating) result in collapse of the pore structure due to capillary forces and, ultimately, in the formation of dense aggregates (xerogels). Unlike the mesostructured materials reported to date, there is no long-range order in aerogels; however, the range of pore sizes and interconnectedness should be optimal for properties dependent on facile transport of small molecules through the interior space, such as photocatalysis and sensing (*14*). Such properties have only begun to be exploited in aerogels and are usually achieved through the incorporation of conductive or fluorescent moieties into conventional silica aerogels (*15*, *16*). In contrast, the semiconducting and luminescent nature of the aerogels presented herein is a consequence of the intrinsic properties of the metal chalcogenide aerogel framework.

The methodology for chalcogenide aerogel formation is simple, comprising three steps: (i) Nanoparticle formation/thiolate capping, (ii) gelation through controlled surface-group loss, and (iii) supercritical CO_2 drying to maintain the pore architecture (*17*–*19*). Both room-temperature reverse-micellar strategies (CdS, ZnS, PbS, and CdSe) and high-temperature arrested-precipitation techniques (CdSe) can be employed for nanoparticle production. The controlled loss of surface groups to reveal reactive sites for nanoparticle condensation is achieved by chemical oxidation of thiolate capping groups (*17*) or, in the case of CdSe, by photo-oxidation of the capping groups (*20*). This step is pivotal for the preparation of porous gel frameworks, because rapid surface-group loss leads to the formation of dense aggregates and precipitation. The resultant gels are exchanged multiple times with acetone to remove the oxidized disulfide by-product and then are dried at ~40°C by using supercritical CO_2. For comparison, samples were also permitted to air dry on the benchtop, producing xerogels.

The chalcogenide aerogels appear to be morphologically similar to base-catalyzed silica aerogels, as depicted for CdS and CdSe (Fig. 1, A and B). The nanoparticle building blocks that make up the pearl-necklace morphology are visible, as is the presence of mesopores (2 to 50 nm). Unlike traditional silica aerogels, the building blocks appear to be crystalline, as evidenced by the presence of lattice fringes (Fig. 1C), which

Department of Chemistry, Wayne State University, Detroit, MI 48202, USA.

*To whom correspondence should be addressed. E-mail: sbrock@chem.wayne.edu

correspond to the (102) planes of the hexagonal wurtzite (CdS) structure. This is also in contrast to what is observed in the surfactant-templated mesostructured materials where the framework itself was amorphous, despite the presence of long-range order due to the surfactant substructure. Electron diffraction patterns of CdS aerogels confirm the crystallinity, revealing four rings. These could likewise be indexed to the wurtzite structure (fig. S1).

Notably, monoliths can be achieved for CdS and ZnS with bulk densities as low as 0.07 g/cm^3 and 0.35 g/cm^3, respectively, representing 1.4 to 8.7% of the density of a single crystal (CdS, 4.83 g/cm^3; ZnS, 4.04 g/cm^3). Figure 1D shows a representative CdS aerogel monolith (right) compared with the wet gel (center). Only a small volume loss is observed upon aerogel formation, in contrast to a sample dried on the benchtop (xerogel) (Fig. 1D, left). If the wet gels are washed before benchtop drying, xerogel monoliths cannot be obtained at all, because fragmentation occurs upon drying.

An assessment of the porosity of the chalcogenide aerogels and xerogels is achieved by using N_2 adsorption/desorption analysis (Table 1). All samples exhibit a type IV isotherm with H3-type hysteresis loop attributed to an interconnected mesoporous system with a broad pore-size distribution (fig. S2) (*19*, *21*, *22*). The small upward hysteresis exhibited by the isotherms suggests a cylindrical pore geometry (*23*). Pore-size distribution plots of the aerogels confirm the presence of a range of pores extending from the meso to the macro regime, with averages of 15 to 45 nm (fig. S2 and Table 1). The xerogels (washed) have a considerably narrower size distribution, with average pore diameters in the lower mesoporous range (CdS is 5 to 7 nm for a xerogel versus 29 to 30 nm for an aerogel).

The surface areas achieved for the chalcogenide aerogels range from 120 to 250 m^2/g and are comparable to those obtained for many oxide-based aerogels. For example, aerogels of vanadia (*24*) are reported to have surface areas of 150 to 280 m^2/g, whereas those of manganese oxide (*25*) have surface areas of up to 210 m^2/g. Silica sets the benchmark, with surface areas of up to 1600 m^2/g (600 m^2/g is a typical value) (*13*). When compared on a per mole basis, our CdS aerogels with mean surface area of 245 m^2/g are equivalent to a silica aerogel of surface area 590 m^2/g. In contrast, the washed xerogels exhibit considerably lower surface area (47 m^2/g), not unlike values obtained for precipitated CdS nanoparticles (56 m^2/g) (*26*).

Despite these aerogels having a three-dimensional connected chalcogenide network, they nevertheless retain the optical features of the nanoparticle building blocks. As illustrated in Fig. 2, all of the aerogel materials examined exhibit a sharp absorption onset at an energy far greater than the bandgap for bulk solids (Fig. 2, tabular inset), consistent with retention of quantum-confinement effects in the solids (*19*). This strongly suggests that the nanoparticle chromophore remains effectively isolated, which can be attributed to the fractal connectivity of the network or to the presence of grain interfaces. These chromophores can be ripened by heating, resulting in a systematic red shift of the absorption onset that is nearly linear with temperature (Fig. 3). This also correlates with a growth in the average crystallite size, as probed by x-ray powder diffraction (Fig. 3). Thus, the sharp absorption onset in these materials can effectively be tuned. In addition to the growth of particles, there is a systematic transformation from the cubic crystal structure (as observed for as-prepared aerogels produced from room-temperature reverse-micelle nanoparticles) to the more thermodynamically stable hexagonal modification (dominant phase at 500°C) (fig. S3). Even at conditions where the x-ray data suggest a dominant cubic structure (100°C), nanocrystallites with hexagonal features can clearly be seen with transmission electron microscopy (TEM), and indexing of lattice fringes and electron diffraction patterns are consistent with some degree of cubic-to-hexagonal transformation (Fig. 1 and fig. S1).

Photoluminescence studies on as-prepared CdS aerogels reveal only broad, trap-state emission near 600 nm (fig. S4). Upon heating at 100°C, some of the band-edge emission apparent in the nanoparticle precursors is

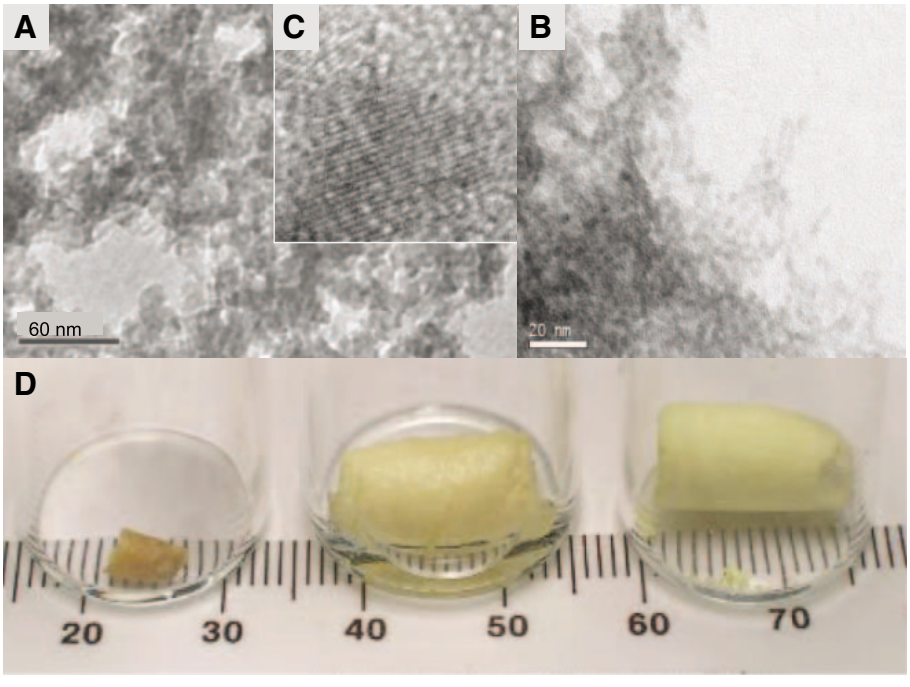

Fig. 1. Electron microscope images of (**A**) CdS aerogels and (**B**) CdSe aerogels, illustrating the colloidal nature of the aerogel aggregates. The presence of mesopores (2 to 50 nm) can be clearly seen. (**C**) A high-magnification image of a CdS aerogel heated in vacuo at 100°C, illustrating the crystalline nature of the nanoparticle architecture. The lattice fringe separation is 2.5 Å, corresponding to the (102) reflection of hexagonal CdS. (**D**) A photograph provides a comparison of a wet CdS gel (center) with an unwashed CdS xerogel (left) and a monolithic CdS aerogel (right). In contrast to xerogel formation, minimal volume loss is observed in the conversion of wet gels to aerogels. The scale is in millimeters.

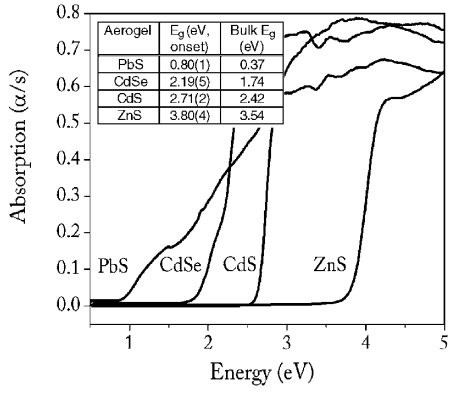

Fig. 2. Diffuse reflectance data for as-prepared aerogels of PbS, CdSe, CdS, and ZnS and comparative values for bulk crystalline samples. Data were acquired on a Shimadzu (Columbia, MD) model UV-3101PC double-beam, double-monochromator spectrophotometer equipped with an integrating sphere, using $BaSO_4$ as a 100% reflectance standard. The bandgaps of the samples were estimated from the low-energy onset in the absorbance data (converted from reflectance).

recovered. This is coincident with the beginning of the transformation from cubic to hexagonal and an increase in crystallinity as evidenced by x-ray powder diffraction. It is well documented that the highly crystalline hexagonal nanoparticles produced from high-temperature (~200°C to 300°C) routes exhibit greater photoluminescence quantum yields than the cubic nanoparticles produced at room temperature with reverse-micellar strategies (*27*). Thus, we sought to test whether nanoparticles produced from high-temperature routes would give rise to as-prepared aerogels demonstrating strong band-edge photoluminescence.

CdSe nanoparticles were prepared in trioctylphosphine oxide at elevated temperatures and capped with mercaptoundecanoic acid (MUA) to form hexagonal CdSe nanoparticles of ~5.1 nm in diameter, as estimated from the absorbance onset according to the mass approximation model (*20*, *28*, *29*). The CdSe nanoparticles exhibit a sharp band-edge emission near 540 nm, along with a broad shoulder centered near 610 nm, attributable to trap states near the surface (Fig. 4). These nanoparticles transform into opaque orange gels upon standard treatment with tetranitromethane. However, gels were also observed to form in alcohol solutions after standing in ambient light over several days, likely as a result of photooxidation of the MUA capping groups from the surface, representing an alternate method of condensation (*20*). Aerogels formed from supercritical drying of these gels demonstrate slightly lower surface areas than those prepared from reverse-micellar strategies (*30*). However, the sharp band-edge emission characteristic of the quantum-confined nanoparticles is retained, with no further processing required (*19*). The appreciable change in the chromophore environment is evidenced by the shift in the broad trap-state emission peak to near 650 nm (Fig. 4), which suggests very different surface characteristics after condensation and drying than is present in the pristine CdSe nanoparticles in solution.

Together, these data suggest that the controlled removal of surface groups under conditions that lead to the formation of lacunar aggregates and eventually gelation is quite general for metal chalcogenide nanoparticles. This is consistent with a previously reported study by Kotov in which CdSe nanoparticle samples stripped of excess thioglycolic acid spontaneously assembled first into chainlike aggregates and subsequently into wires (*31*). Likewise, Peng found that photooxidation of surface thiolate ligands from CdSe nanoparticles resulted in aggregate formation, and this was reversible upon introduction of more capping agent (*20*). We find that by adjusting the conditions under which capping groups are removed, robust gels can be produced, and the characteristic pore structure of these colloidal gels can be maintained by supercritical drying. The generality of this method should lend itself to a number of new aerogel materials if the surface chemistry can be appropriately tailored. Because the resulting aerogels retain the photophysical properties of the quantum-confined building blocks, gelation and aerogel formation represents an excellent strategy for the assembly of nanoparticles from solution into solid state devices where exploitation of size-dependent properties is desired.

The aerogels presented here based on PbS, CdSe, CdS, and ZnS cover the optical spectrum from the infrared through the ultraviolet, and the optical features of each material can be effectively "tuned" over a substantial range by adjusting the heating profile employed. The aerogel structure effectively preserves the integrity of the quantum dots by locking them into a network while providing a pore structure through which chemical species can be introduced, either as analytes or as secondary components for composite formation. Current efforts are devoted to preparing these materials in thin-film form and evaluating their potential for photovoltaic and sensing applications.

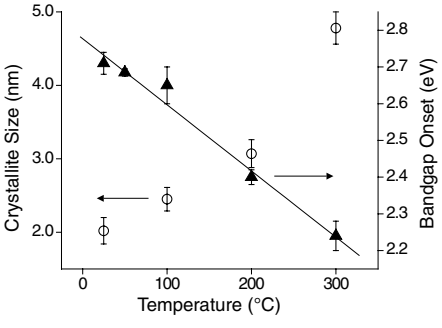

Fig. 3. Influence of temperature on crystallite size of the primary particle components in CdS aerogels (open circles, x-ray powder diffraction data) and on absorption onset (filled triangles, diffuse reflectance data).

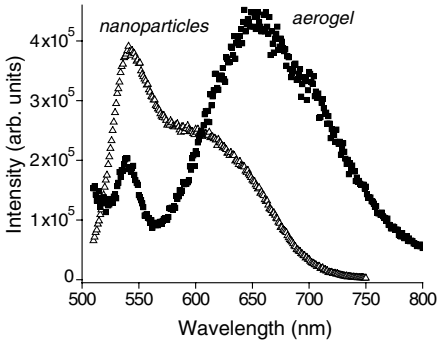

Fig. 4. Photoluminescence data for MUA-capped CdSe nanoparticles (open triangles) and an as-prepared aerogel (filled squares), acquired by using an excitation wavelength of 480 nm. Data were collected at 77 K on a SPEX Fluorolog model spectrometer (Jobin Yvon Horiba, Edison, NJ) with 1681 Spex 0.22 m excitation module and 0.34 m emission module. Powdered aerogel samples were placed in evacuated quartz tubes for measurement.

Table 1. Surface area and porosity data for metal chalcogenide xerogels and aerogels. All samples were treated with H_2O_2 to induce gelation, with the exception of CdSe, which was treated with tetranitromethane. Data were acquired on a Micromeritics (Norcross, GA) ASAP 2010 Surface Area Analyzer. Samples were degassed for a minimum of 24 hours at 100°C before analysis. In an effort to extract the full pore volume of the aerogels, long equilibrium intervals were used and granular specimens were evaluated in lieu of monoliths (*32*). Surface areas were computed with the Brunauer, Emmett, and Teller (BET) multimolecular layer adsorption model, and average pore size and cumulative pore volumes were computed with the Barrett, Joyner, and Halenda (BJH) model. The range of values reflects data from two or more samples prepared and measured under similar conditions.

Metal chalcogenide xerogel/aerogel	BET surface area (m^2/g)	Mean BET surface area (m^2/g)	BJH adsorption average pore diameter (nm)	BJH adsorption cumulative pore volume (cm^3/g)
CdS xerogel	38–55	47	5–7	0.05–0.11
CdS aerogel	239–250	245	29–30	1.90–2.02
CdSe aerogel	128–161	143	16–29	0.53–0.98
ZnS aerogel	182–202	192	15–30	0.40–0.86
PbS aerogel	119–141	130	21–45	0.79–0.94

References and Notes

1. H. Li, A. Laine, M. O'Keeffe, O. M. Yahgi, *Science* **283**, 1145 (1999).
2. N. Zheng, X. Bu, P. Feng, *Nature* **426**, 428 (2003).
3. N. Zheng, X. Bu, B. Wang, P. Feng, *Science* **298**, 2366 (2002).
4. W. Park, J. S. King, C. W. Neff, C. Liddell, C. J. Summers, *Phys. Status Solidi B* **229**, 949 (2002).
5. P. V. Braun, P. Wiltzius, *Nature* **402**, 603 (1999).
6. Y. A. Vlasov, N. Yao, D. J. Norris, *Adv. Mater.* **11**, 165 (1999).
7. P. V. Braun, P. Osenar, V. Tohver, S. B. Kennedy, S. I. Stupp, *J. Am. Chem. Soc.* **121**, 7302 (1999).
8. B. M. Rabatic, M. U. Pralle, G. N. Tew, S. I. Stupp, *Chem. Mater.* **15**, 1249 (2003).
9. P. N. Trikalitis, K. K. Rangan, T. Bakas, M. G. Kanatzidis, *Nature* **410**, 671 (2001).
10. P. N. Trikalitis, K. K. Rangan, M. G. Kanatzidis, *J. Am. Chem. Soc.* **124**, 2604 (2002).
11. K. K. Rangan *et al.*, *Nano Lett.* **2**, 513 (2002).
12. A. E. Riley, S. H. Tolbert, *J. Am. Chem. Soc.* **125**, 4551 (2003).
13. N. Hüsing, U. Schubert, *Angew. Chem. Int. Ed. Engl.* **37**, 22 (1998).

14. D. R. Rolison, *Science* **299**, 1698 (2003).
15. J. V. Ryan *et al.*, *Nature* **406**, 169 (2000).
16. D. R. Rolison, B. Dunn, *J. Mater. Chem.* **11**, 963 (2001).
17. T. Gacoin, K. Lahlil, P. Larregaray, J.-P. Boilot, *J. Phys. Chem. B* **105**, 10228 (2001).
18. 4-fluorophenylthiolate–capped nanoparticles of cubic CdS, CdSe, ZnS, and PbS were prepared by a modified literature synthesis (*17*) and dispersed in acetone to a concentration of ~0.05 to 0.5 M. Samples of 2 to 4 mL of the sols in polyethylene vials were treated with 0.1 to 0.2 mL of 3% H_2O_2 (CdS, ZnS, PbS) or 3% tetranitromethane (CdSe) to induce gelation. Gels were aged for several days to a week, exchanged multiple times with acetone, and dried in a SPI-Dry (Structure Probe, Inc., West Chester, PA) critical-point dryer using CO_2.
19. Materials and methods are available as supporting material on *Science* Online.
20. J. Aldana, Y. A. Wang, X. Peng, *J. Am. Chem. Soc.* **123**, 8844 (2001).
21. P. A. Webb, C. Orr, *Analytical Methods in Fine Particle Technology* (Micromeritics Instrument Corp., Norcross, GA, ed. 1, 1997).
22. Z. Zhang, T. J. Pinnavaia, *J. Am. Chem. Soc.* **124**, 12294 (2002).
23. A. H. Janssen, A. J. Koster, K. P. de Jong, *J. Phys. Chem. B* **106**, 11905 (2002).
24. W. Dong, D. R. Rolison, B. Dunn, *Electrochem. Solid State Lett.* **3**, 457 (2000).
25. J. W. Long, K. E. Swider-Lyons, R. M. Stroud, D. R. Rolison, *Electrochem. Solid-State Lett.* **3**, 453 (2000).
26. W.-W. So, J.-S. Jang, Y.-S. Rhee, K.-J. Kim, S.-J. Moon, *J. Coll. Inter. Sci.* **237**, 136 (2001).
27. C. B. Murray, D. J. Norris, M. G. Bawendi, *J. Am. Chem. Soc.* **115**, 8706 (1993).
28. Z. A. Peng, X. Peng, *J. Am. Chem. Soc.* **123**, 183 (2001).
29. M. L. Steigerwald, L. E. Brus, *Acc. Chem. Res.* **23**, 183 (1990).
30. Surface area (BET), 106 to 124 m^2/g (mean 115 m^2/g); adsorption average pore diameter (BJH), 23 to 28 nm; adsorption cumulative pore volume (BJH), 0.70 to 0.73 cm^3/g.
31. Z. Tang, N. A. Kotov, M. Giersig, *Science* **297**, 237 (2002).
32. G. Reichenauer, G. W. Scherer, *J. Non-Cryst. Solids* **285**, 167 (2001).
33. Financial support was provided by NSF (IGERT award DEG-9870720 and CAREER award DMR-0094273) and Research Corporation (Research Innovation Award-R10617). We thank M. Kanatzidis (Michigan State University) for the use of solid-state optical bandgap and luminescence equipment, C. Wauchope and J. Mansfield (University of Michigan) for assistance with TEM analyses, and S. L. Suib (University of Connecticut) for critical reading of this manuscript. The microscopy in this publication was performed in the University of Michigan Electron Microbeam Analysis Laboratory on a JEOL 2010EX (JEOL-USA, Peabody, MA) purchased under NSF grant DMR-9871177.

Supporting Online Material
www.sciencemag.org/cgi/content/full/307/5708/397/DC1
Materials and Methods
Figs. S1 to S4
References and Notes

19 October 2004; accepted 15 December 2004
10.1126/science.1106525

Deep-Ultraviolet Quantum Interference Metrology with Ultrashort Laser Pulses

Stefan Witte,* Roel Th. Zinkstok,* Wim Ubachs, Wim Hogervorst, Kjeld S. E. Eikema†

Precision spectroscopy at ultraviolet and shorter wavelengths has been hindered by the poor access of narrow-band lasers to that spectral region. We demonstrate high-accuracy quantum interference metrology on atomic transitions with the use of an amplified train of phase-controlled pulses from a femtosecond frequency comb laser. The peak power of these pulses allows for efficient harmonic upconversion, paving the way for extension of frequency comb metrology in atoms and ions to the extreme ultraviolet and soft x-ray spectral regions. A proof-of-principle experiment was performed on a deep-ultraviolet (2 × 212.55 nanometers) two-photon transition in krypton; relative to measurement with single nanosecond laser pulses, the accuracy of the absolute transition frequency and isotope shifts was improved by more than an order of magnitude.

In recent years, the invention of the femtosecond frequency comb laser (*1*–*3*) has brought about a revolution in metrology. A frequency comb acts as a bridge between the radio frequency (RF) domain (typically tens of MHz) and the optical frequency domain (typically hundreds of THz). Thus, in precision spectroscopy, the optical cycles of a continuous wave (CW) ultrastable laser can be phase-locked and counted directly with respect to an absolute frequency standard such as an atomic clock (*4*, *5*). The resultant frequency measurements approach a precision of 1 part in 10^{15} in certain cases, potentially enabling the detection of possible drift in the fundamental constants (*6*, *7*), among other quantum mechanical applications.

Laser Centre, Vrije Universiteit, De Boelelaan 1081, 1081 HV Amsterdam, Netherlands.

*These authors contributed equally to this work.
†To whom correspondence should be addressed. E-mail: kjeld@nat.vu.nl

Here, we perform precision metrology without the use of a CW laser. Instead, an atomic transition is excited directly with amplified and frequency-converted pulses from a femtosecond frequency comb laser. As a result of quantum interference effects in the atomic excitation process, we can achieve an accuracy that is about six orders of magnitude higher than the optical bandwidth of the individual laser pulses.

The method used is related to Ramsey's principle of separated oscillatory fields (*8*), which probes the phase evolution of an atom in spatially separated interaction zones. This technique is widely used in the RF domain for atomic fountain clocks (*9*). By extension, in the optical domain, excitation can be performed by pulses separated in time (rather than in space) to maintain phase coherence between the excitation contributions. Several experiments have been performed to investigate Ramsey-type quantum interference fringes in the optical domain (*10*–*14*) and phase-stable amplification of single pulses (*15*). Actual quantitative spectroscopy with phase-coherent oscillator pulses has been limited to a few relative frequency measurements on fine and hyperfine structure of atoms (*13*, *14*, *16*) and relative and absolute measurements on rubidium (*17*); absolute frequency measurements with amplified pulses have been frustrated by an unknown phase difference between the pulses or by limited resolution.

We generate powerful laser pulses with a precise phase relationship by amplifying a selected pulse train from a frequency comb laser. This amplified frequency comb can be used to measure absolute optical frequencies directly. The advantage of amplified laser pulses is that the high peak power allows for efficient frequency upconversion in crystals and gases. It has been shown that harmonic generation in gases can preserve the coherence properties of the driving laser pulse (*18*, *19*). Therefore, the present experiment paves the way for precision metrology with frequency combs at optical frequencies that are very difficult or almost impossible to reach with CW lasers, such as vacuum-ultraviolet and even shorter wavelengths (e.g., x-rays). Possible applications are precision spectroscopy of hydrogen-like ions and helium to test quantum electrodynamics and nuclear size effects. The technique may also lead to more accurate atomic clocks that operate on resonances with ultrahigh frequencies.

In quantum interference metrology (Fig. 1), an atom is excited by a train of N phase-locked laser pulses separated by a time T. Assuming a two-level system, the resulting excited-state population after the pulse train can be written as

$$|b_N|^2 = \left| \sum_{n=1}^{N} a_n \exp[i(n-1)(\omega_0 T + \varphi)] \right|^2 \quad (1)$$

where φ is the phase difference between subsequent laser pulses, and a_n is the

excitation amplitude for the nth pulse. Thus, $|b_N|^2$ is a periodic function of both the pulse delay T and the phase difference φ. The resonance frequency ω_0 is encoded not just in the amplitude a_n, as with conventional spectroscopy, but also in the phase of the oscillating population signal. The first pulse creates an atomic superposition with a well-defined initial phase. The maxima of the excited-state population occur when subsequent laser pulses arrive in phase with this superposition. If the time delay and the pulse-to-pulse phase shift are known, the exact transition frequency can be derived from the position of these maxima. The more pulses are used, the narrower the resulting interference fringes. Therefore, multiple-level contributions can be resolved by the use of a sufficient number of pulses.

This method to measure the transition frequency is largely insensitive to the laser pulse spectral shape, which only influences the global signal amplitude. Therefore, spectral distortions of the laser pulses due to amplification or harmonic generation have little influence on the measurement, provided the distortion is identical from pulse to pulse. In contrast, traditional single-pulse spectroscopy is strongly affected by chirp (*20*, *21*). However, the periodicity of the signal with respect to T leads to an inherent ambiguity in the determination of the transition frequency. This ambiguity can be resolved if a previous measurement with an accuracy much better than the repetition frequency exists; otherwise, the measurement can be repeated with different repetition rates, as shown below.

The frequency comb used in our experiment is based on a mode-locked Ti:sapphire oscillator. It emits 7-nJ pulses with a bandwidth (full width at half maximum) of ~90 nm, centered at 800 nm, and with an adjustable repetition rate between 60.9 and 79 MHz. For frequency accuracy, both the repetition rate and the phase of the pulses are locked to a Global Positioning System–disciplined Rb atomic clock (*1*, *2*, *22*, *23*). An electro-optic modulator (EOM) is used to select up to three consecutive pulses from the mode-locked pulse train. These pulses are amplified in a six-pass Ti:sapphire nonsaturating amplifier to an energy of about 15 μJ per pulse (*24*). Spectral filtering is applied in the amplifier to limit the bandwidth of the amplified pulses to <0.5 nm. This filtering reduces the complexity of the signal, as only a single transition will be excited (see below). The amplification process gives rise to a small phase shift (~100 to 200 mrad) between the pulses, which is measured with a 1σ accuracy of 25 mrad (<1/250 of an optical cycle). These measurements are performed by placing the amplifier in one arm of a Mach-Zehnder interferometer and recording spatial interferograms on a charge-coupled device (CCD) camera, from which this phase shift can be extracted (*25*).

To demonstrate the potential of high-frequency quantum interference metrology, we selected the $4p^6 \rightarrow 4p^5 5p[1/2]_0$ two-photon transition in krypton at a frequency of $\omega_0/2\pi$ = 2821 THz. Because both the ground state and the excited state of this transition are $J = 0$ states, the atoms can be considered two-level systems. The required wavelength of 212.55 nm for the two-photon krypton resonance was obtained by fourth-harmonic generation of the amplifier output at 850.2 nm through sequential frequency doubling in two beta–barium borate (BBO) crystals. The resultant 212.55-nm pulses (1.6 μJ) were focused in a highly collimated atomic beam of krypton (Fig. 2). The excited-state population was probed by a delayed 532-nm ionization pulse (1.5 mJ, 100 ps) from a Nd:yttrium-aluminum-garnet laser-amplifier system, and the experiment was repeated at 1 kHz.

The isotope shift and the absolute transition measurements described below can be influenced by a possible systematic Doppler shift as a result of nonperpendicular excitation. Therefore, all measurements were

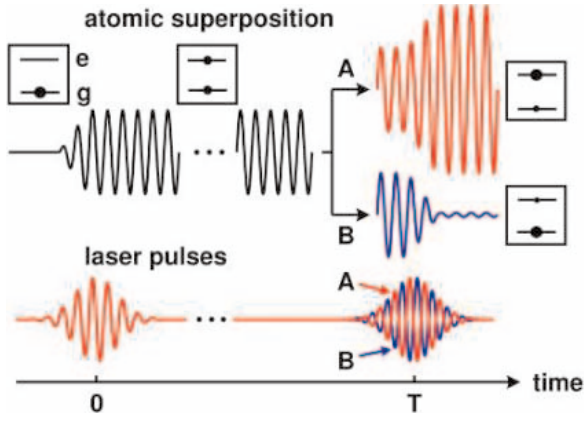

Fig. 1. The principle of quantum interference metrology. An atom in the ground state $|g\rangle$ is resonantly excited by a broadband laser pulse. This pulse creates a coherent superposition of the ground state and the excited state, with an initial phase difference between the states determined by the laser pulse. After the initial excitation, the superposition will evolve freely with a phase velocity $\omega_0 = (E_e - E_g)/\hbar$, where $E_e - E_g$ is the energy difference between the states and $\hbar$ is Planck's constant divided by 2π. After a time T, a second pulse with a controlled phase illuminates the atom, interfering with the atomic superposition. Depending on the phase and the time delay T, the total $|g\rangle \rightarrow |e\rangle$ excitation probability can be either enhanced (case A, red pulse) or suppressed (case B, blue pulse). By measuring the amplitude of the superposition (i.e., the population of the excited state) after the second pulse (with, e.g., an ionizing laser pulse), the energy difference between the states can be deduced.

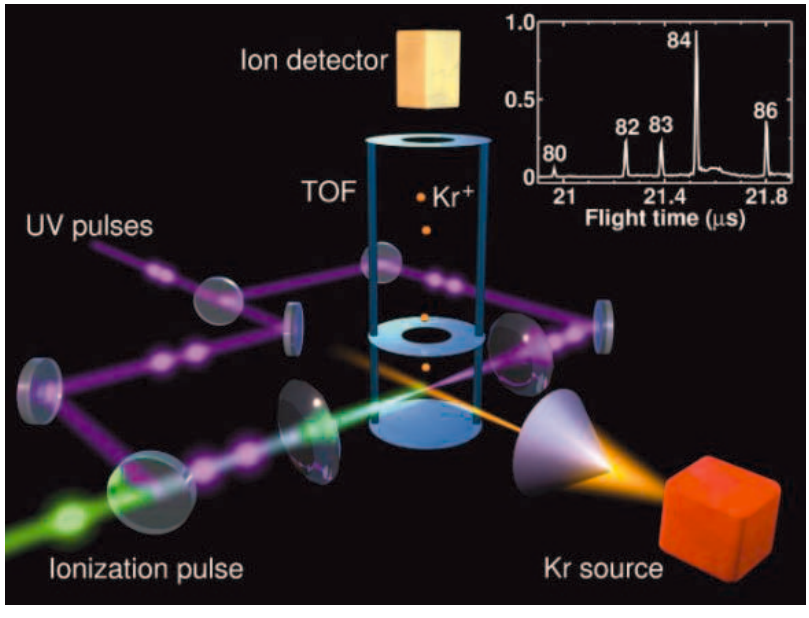

Fig. 2. Schematic of the experimental setup. The ultraviolet pulses (beam diameter 1 mm) are focused with an f = 30 cm lens in a collimated 0.3-mm-wide krypton beam (double skimmer arrangement, Doppler width <10 MHz) from both sides, crossing the beam perpendicularly. Measurements are performed with light from one side at a time. After the ultraviolet excitation, a delayed 532-nm pulse is used for ionization, and the resulting krypton ions are accelerated into a 60-cm time-of-flight mass spectrometer (TOF) by a pulsed electric field. Here the isotopes are separated in time (see inset) and counted with a channeltron detector.

performed from two opposite sides, with the average taken to determine the Doppler-free signal (*26*).

The data depend on the number of phase-locked pulses used to excite the transition (Fig. 3A). The pulse delay T was scanned by changing the comb laser repetition frequency, which is near 75 MHz. With a single pulse, the excitation probability is constant. With two pulses, a clear cosine oscillation is observed, with a contrast reaching 93%. Three-pulse excitation gives the pulse-like structure predicted by Eq. 1 ($N = 3$) as well as an expected narrowing by 3/2 relative to two-pulse excitation. The solid lines are fits using Eq. 1, including an additional amplitude scaling factor to account for signal strength variations between the traces. In the three-pulse case, we took into account that the amplitude contribution of the pulses is not exactly equal because of spontaneous emission of the 5p state (lifetime 23 ns) and differences in energy between the three pulses (*27*). For all other measurements, we used two-pulse excitation, as this minimizes the complexity of the experiment without sacrificing accuracy in this two-level case. The first of these measurements concerns the dependence on the pulse-to-pulse (carrier envelope) phase shift φ_{CE} (Fig. 3B), which is in complete agreement with expectations: The interference signal moves by one fringe when φ_{CE} of the comb laser is scanned through one-eighth of a cycle (due to the frequency conversion and two-photon transition).

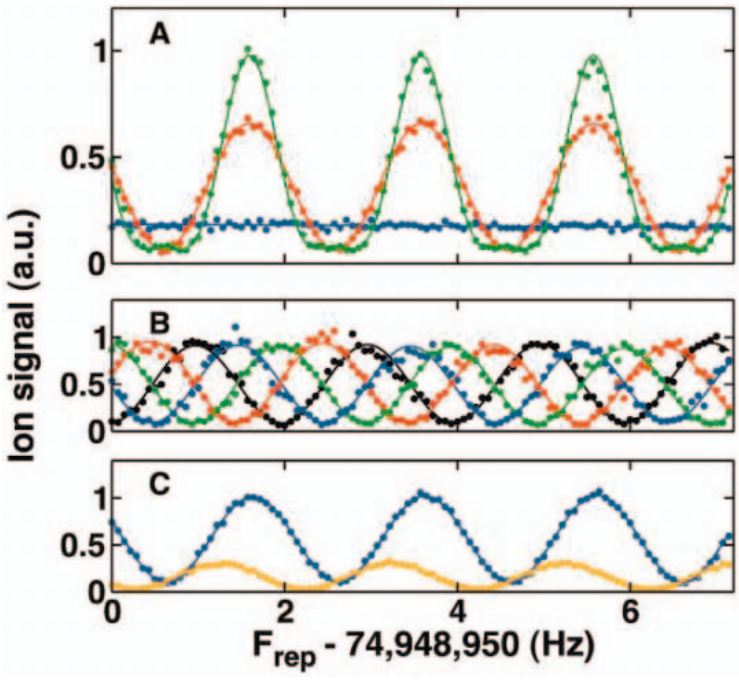

Fig. 3. Demonstration of quantum interference metrology. (**A**) ^{84}Kr signal as a function of the repetition rate of the comb laser for one (blue), two (red), and three (green) pulses 13.3 ns apart. The solid lines are fits to the theory (see text). (**B**) Measurement of the quantum interference signal for various phase differences between two excitation pulses, with the pulse-to-pulse phase shift (as seen by the atom) set to 0 (green), $\pi/2$ (blue), π (black), and $3\pi/2$ (red), respectively. (**C**) Measurement of the isotope shift between ^{84}Kr (blue trace) and ^{86}Kr (orange trace). The isotope shift can be determined from the phase shift between these two simultaneously recorded scans. The counter gate time is 10 s for each data point.

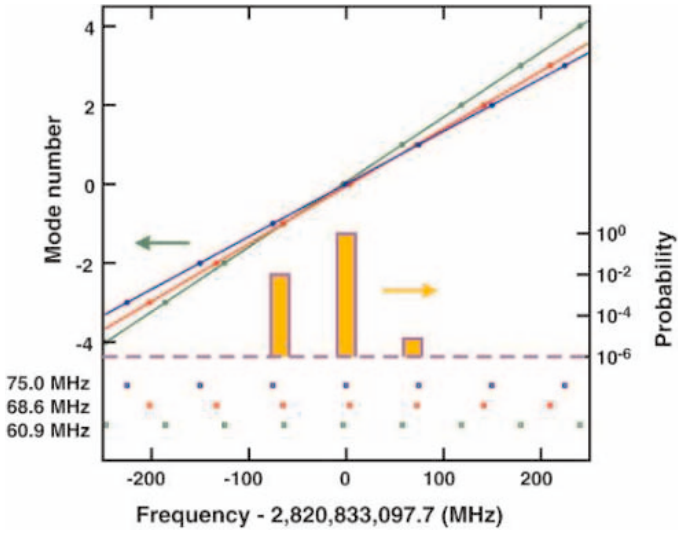

Fig. 4. Absolute calibration of the $4p^6 \rightarrow 4p^5 5p[1/2]_0$ transition in krypton is performed by finding the coincidence of three separate measurement series with repetition rates of 60.9 MHz (green), 68.6 MHz (red), and 75.0 MHz (blue). The orange bars (logarithmic scale) show the normalized statistical probability per mode for each measured mode position, revealing the location of the most probable coincidence.

Isotope shifts can be measured straightforwardly. The broad spectrum of the pulses places a frequency ruler on all isotopes simultaneously, so that spectra of ^{80}Kr through ^{86}Kr could be acquired at the same time (Fig. 3C). The measurements of Kaufman (*28*) were used for identification of the proper comb line for each isotope. The resulting shifts (^{84}Kr – ^{X}Kr), based on at least six measurements per isotope, are 302.02 ± 0.28 MHz (^{80}Kr), 152.41 ± 0.15 MHz (^{82}Kr), 98.54 ± 0.17 MHz (^{83}Kr), and –135.99 ± 0.17 MHz (^{86}Kr). The stated uncertainties (1σ) are smaller than the 6-MHz uncertainty reported by Kaufman (*28*) by a factor of 20 to 40.

In the measurement of the absolute transition frequency, an additional issue is the determination of the mode that corresponds to the true position of the resonance. The most accurate measurement to date (*29*) has an uncertainty of 45 MHz, which is not sufficient to assign the mode with confidence. Therefore, measurements were repeated at repetition rates near 60.9 MHz, 68.6 MHz, and 75.0 MHz to find the point at which the measurements coincide (four to nine measurements were performed at each repetition rate). After correction of the data for the phase shifts and systematic effects (*30*), there were three sets of possible positions for the 5p resonance transition (Fig. 4). The measurements have one clear coincidence (with an estimated probability of 98%, based on a statistical uncertainty of 2.5 MHz for each data point) near the literature value. Combining the three sets leads to an absolute frequency of 2,820,833,097.7 MHz with a 1σ uncertainty of 3.5 MHz (statistical and systematic errors combined), which is an order of magnitude smaller than the previous determination using single nanosecond laser pulses (*29*).

We envision several extensions of the above technique. One possibility is the use of a regenerative amplifier to amplify pulses to the μJ level at a repetition rate of 100 kHz. For high-frequency metrology, the resolution is ultimately limited by the comb laser and the interaction time of the atom with the pulses. This interaction time can be increased almost indefinitely if cooled ions in a trap are used in place of an atomic beam,

opening the prospect of atomic optical clocks operating at vacuum-ultraviolet or extreme-ultraviolet frequencies. Outside frequency metrology, amplified frequency combs could be used to perform quantum control experiments on a time scale much longer than is currently possible, because phase coherence can be maintained for many consecutive laser pulses.

References and Notes

1. R. Holzwarth *et al.*, *Phys. Rev. Lett.* **85**, 2264 (2000).
2. D. J. Jones *et al.*, *Science* **288**, 635 (2000).
3. Th. Udem, R. Holzwarth, T. W. Hänsch, *Nature* **416**, 233 (2002).
4. M. Niering *et al.*, *Phys. Rev. Lett.* **84**, 5496 (2000).
5. Th. Udem *et al.*, *Phys. Rev. Lett.* **86**, 4996 (2001).
6. M. Fischer *et al.*, *Phys. Rev. Lett.* **92**, 230002 (2004).
7. J. P. Uzan, *Rev. Mod. Phys.* **75**, 403 (2003).
8. N. F. Ramsey, *Phys. Rev.* **76**, 996 (1949).
9. A. Clairon, C. Salomon, S. Guellati, W. D. Phillips, *Europhys. Lett.* **16**, 165 (1991).
10. M. M. Salour, C. Cohen-Tannoudji, *Phys. Rev. Lett.* **38**, 757 (1977).
11. M. M. Salour, *Rev. Mod. Phys.* **50**, 667 (1978).
12. R. Teets, J. N. Eckstein, T. W. Hänsch, *Phys. Rev. Lett.* **38**, 760 (1977).
13. M. Bellini, A. Bartoli, T. W. Hänsch, *Opt. Lett.* **22**, 540 (1997).
14. M. J. Snadden, A. S. Bell, E. Riis, A. I. Ferguson, *Opt. Commun.* **125**, 70 (1996).
15. A. Baltuška *et al.*, *Nature* **421**, 611 (2003).
16. J. N. Eckstein, A. I. Ferguson, T. W. Hänsch, *Phys. Rev. Lett.* **40**, 847 (1978).
17. A. Marian, M. C. Stowe, J. R. Lawall, D. Felinto, J. Ye, *Science* **306**, 2063 (2004); published online 18 November 2004 (10.1126/science.1105660).
18. R. Zerne *et al.*, *Phys. Rev. Lett.* **79**, 1006 (1997).
19. S. Cavalieri, R. Eramo, M. Materazzi, C. Corsi, M. Bellini, *Phys. Rev. Lett.* **89**, 133002 (2002).
20. K. S. E. Eikema, W. Ubachs, W. Vassen, W. Hogervorst, *Phys. Rev. A* **55**, 1866 (1997).
21. S. D. Bergeson *et al.*, *Phys. Rev. Lett.* **80**, 3475 (1998).
22. A. Apolonski *et al.*, *Phys. Rev. Lett.* **85**, 740 (2000).
23. S. Witte, R. Th. Zinkstok, W. Hogervorst, K. S. E. Eikema, *Appl. Phys. B* **78**, 5 (2004).
24. Standard amplifiers operate in saturated mode to reduce output power fluctuations and can therefore amplify only one pulse. In the present experiment, the number of pulses that can be amplified is limited to three by the EOM, which must be switched off before any backreflections from the amplifier lead to uncontrolled extra pulses. An additional Faraday isolator in the setup would lift this limitation.
25. An EOM and polarizing optics were used to project the interference patterns for two consecutive pulses simultaneously and vertically displaced from one another on a CCD camera. The relative positions on the CCD (up or down) were alternated by switching the EOM; the relative phase shift to the comb laser was then determined by looking at the phase difference in both projection situations, so as to cancel out any alignment effects.
26. The Doppler shift can in principle be reduced on a two-photon transition by measuring with colliding pulses from opposite sides. This arrangement also enhances the signal, as was seen experimentally. However, contrary to CW spectroscopy, Doppler-free signal (photons absorbed from opposite sides) and Doppler-shifted signal (two photons from one side) cannot be distinguished properly in the case of excitation with two ultrashort pulses, because the large bandwidth always contains a resonant frequency. This situation might lead to a calibration error when there is an imbalance in signal strength from opposite sides. Another aspect is that the total Doppler shift has an ambiguity due to the periodicity of the signal. The difference in Doppler shift for the isotopes, which is on the order of a few hundred kHz, therefore provides a valuable initial estimate of about 25 MHz for this shift. From the measurement of the absolute positions, one can then determine the Doppler shift to be 29 MHz for each of the counterpropagating beams.
27. The energy ratio of pulses 1, 2, and 3 is 1.0:0.91:0.6. In all measurements with two pulses, the pulse energies have been kept equal to within about 5%.
28. V. Kaufman, *J. Res. Natl. Inst. Stand. Technol.* **98**, 717 (1993).
29. F. Brandi, W. Hogervorst, W. Ubachs, *J. Phys. B* **35**, 1071 (2002).
30. Two systematic effects dominate the determination of the resonance frequency: the phase shifts induced by the amplifier (100 to 200 mrad in the infrared), and the residual Doppler shift (2 MHz) due to possible misalignment of the counterpropagating beams. Other effects include light-shifts (0.47 ± 0.44 MHz), static field effects ($\ll$100 kHz), the second-order Doppler shift ($\sim$1 kHz), and a recoil shift (209 kHz). The phase shift due to the pulse-picker EOM is negligible ($<$5 mrad) when it is aligned such that it acts as a pure polarization rotator, as verified experimentally. The phase shift due to frequency doubling is negligible as well, on the order of 1 mrad in the ultraviolet, as estimated from the model of (*31*).
31. R. DeSalvo *et al.*, *Opt. Lett.* **17**, 28 (1992).

32. Supported by the Foundation for Fundamental Research on Matter (FOM), the Netherlands Organization for Scientific Research (NWO), the EU Integrated Initiative FP6 program, and the Vrije Universiteit Amsterdam.

21 October 2004; accepted 30 November 2004
10.1126/science.1106612

Charging Effects on Bonding and Catalyzed Oxidation of CO on Au_8 Clusters on MgO

Bokwon Yoon,[1] Hannu Häkkinen,[1]* Uzi Landman,[1]† Anke S. Wörz,[2] Jean-Marie Antonietti,[2] Stéphane Abbet,[2] Ken Judai,[2] Ueli Heiz[2]†

Gold octamers (Au_8) bound to oxygen-vacancy F-center defects on Mg(001) are the smallest clusters to catalyze the low-temperature oxidation of CO to CO_2, whereas clusters deposited on close-to-perfect magnesia surfaces remain chemically inert. Charging of the supported clusters plays a key role in promoting their chemical activity. Infrared measurements of the stretch vibration of CO adsorbed on mass-selected gold octamers soft-landed on MgO(001) with coadsorbed O_2 show a red shift on an F-center–rich surface with respect to the perfect surface. The experiments agree with quantum ab initio calculations that predict that a red shift of the C–O vibration should arise via electron back-donation to the CO antibonding orbital.

The exceptional catalytic properties of small gold aggregates (*1*, *2*) have motivated research (*3*–*17*) aimed at providing insights into the molecular origins of this unexpected reactivity of gold. Investigations on size-selected small gold clusters, $Au_n (2 \leq n \leq 20)$, soft-landed on a well-characterized metal oxide support [specifically, a MgO(001) surface with and without oxygen vacancies or F centers], revealed (*4*) that gold octamers bound to F centers of the magnesia surface are the smallest known gold heterogeneous catalysts that can oxidize CO into CO_2 at temperatures as low as 140 K. The same cluster bound to a MgO surface without oxygen vacancies is catalytically inactive for CO combustion (*4*).

Quantum-mechanical ab initio simulations, in juxtaposition with laboratory experiments, led us to conclude (*4*, *5*) that the key for low-temperature gold catalysis in CO oxidation is the binding of O_2 and CO to the supported gold nanocluster, which activates the O–O bond to a peroxo-like (or superoxo-like) adsorbate state. This process is enabled by resonances between the cluster's electronic states and the $2\pi^*$ antibonding states of O_2, which are pulled below the Fermi level (E_F). Charging of the metal cluster, caused by partial transfer of charge from the substrate F center into the deposited cluster, underlies the catalytic activity of the gold octamers (Au_8), as well as that of other small gold clusters (Au_n, $8 \leq n \leq 20$) (*4*). These investigations predicted that (i) the F centers on the metal oxide support surface play the role of active sites (a concept that has been central to the development of heterogeneous catalysis); (ii) these sites serve to anchor the deposited clusters more strongly than sites on the undefective surface (thus inhibiting their migration and coalescence); and, most important, (iii) these active sites control the charge state of the gold clusters, thus promoting the activation of adsorbed reactant molecules (that is, formation of the aforementioned peroxo or superoxo species) (*18*).

We have studied the cluster-charging propensity of the F-center active sites, both exper-

[1]School of Physics, Georgia Institute of Technology, Atlanta, GA 30332–0430, USA. [2]Departement Chemie, Lehrstuhl für Physikalische Chemie I, Technische Universität München, Lichtenbergstraße 4, 85747 Garching, Germany.

*Present address: Department of Physics, Nanoscience Center, Box 35, FIN-40014, University of Jyväskyla, Finland.

†To whom correspondence should be addressed. E-mail: uzi.landman@physics.gatech.edu (U.L.); ulrich.heiz@ch.tum.de (U.H.)

imentally and theoretically, by examining the vibrational properties of adsorbed CO. The internal CO stretch frequency ν(CO), measured in the presence of coadsorbed O_2 for the octamer bound to the F center of the magnesia substrate [Au_8/CO/O_2/MgO(FC)], shifted to lower frequency by about 25 to 50 cm^{-1} compared to the ν(CO) frequency recorded for the gold octamer bound to the F-center–free MgO(001) surface (Au_8/CO/O_2/MgO). Systematic ab initio calculations (*4*, *5*) reveal that this shift is caused by enhanced back-donation (from the gold nanocluster) into the antibonding 2π* orbital of the CO adsorbed on the cluster anchored to a surface F center. In addition, calculations addressing free Au_8/O_2/CO coadsorption complexes provide further evidence that the bonding characteristics and spectral shifts are related to each other and that they are correlated with, and sensitive to, the charge state of the cluster (*18*).

We reproduced experimentally the results of our earlier investigations pertaining to the enhanced catalytic activity of Au_8 clusters deposited on F-center–defective MgO surfaces, and then went beyond those measurements by recording (under the same conditions as for the reactivity studies) the infrared (IR) spectra of the reactants as a function of the annealing temperature (Fig. 1). Size-selected Au_8 cations were deposited at 90 K, with low kinetic energy, onto MgO(FC) thin films at low coverages (8×10^{12} clusters/cm^2). Several experimental studies [such as the synthesis of monodispersed model catalysts by using soft-landing cluster deposition (*19*)] have shown that, in general, upon deposition, the clusters are neutralized, maintain their nuclearity, and stay well isolated at defect sites. These model catalysts were then saturated with isotopicaly labeled $^{18}O_2$ and $^{13}C^{16}O$; the order of the exposure of the reactants (0.2 Langmuir) did not change the activity (unlike the case for other metals). Upon heating, $^{13}C^{16}O^{18}O$ was produced at 140 and 280 K, as shown in Fig. 1A. No other isotopomer was detected, indicating that only the adsorbed O_2 and CO participate in the reaction. We attribute the reaction at 140 K to an ensemble of Au_8 clusters, with O_2 bound to the top facet of the cluster; and the reaction at 280 K to an Au_8 ensemble, with O_2 bound to the perimeter of the cluster at the cluster-to-substrate interface (Fig. 2B). These assignments were made by us previously (*4*) on the basis of calculated activation barriers for the CO oxidation. Specifically for small gold clusters, only a single O_2 molecule can be adsorbed, and thus the two ensembles are saturated with O_2 via either direct adsorption or reverse spillover.

The corresponding IR study reveals absorption bands of the two reactants. In Fig. 1, C and D, we show only the spectra for adsorbed CO, with the decrease in intensity correlating with the formation of CO_2 (Fig. 1C). The IR band corresponding to adsorbed O_2 occurs around 1300 cm^{-1} for both the F-center–rich and perfect MgO surfaces. The IR frequencies (2049 and 2077 cm^{-1}) are typical for on-top adsorbed ^{13}CO on gold. In this context, we recall that the band at 2127 cm^{-1} originates from ^{13}CO adsorbed directly on defect sites of the MgO(001) surface (*20*). On Au single crystals (*21*–*23*), as well as on oxide-supported Au particles (*9*, *24*, *25*), sharp ^{13}CO absorption bands occur at a single frequency around 2060 cm^{-1}. We infer that the detection of two absorption features reveals the presence of (at least) two types of adsorbed CO molecules, which differ somewhat in how they bind to the Au_8 cluster (Fig. 2C and discussion below).

Upon heating, the population of the three bands changes. At an annealing temperature of 220 K (subsequent to the 140 K combustion reaction), a small single absorption band at 2055 cm^{-1} was observed (Fig. 1C). Earlier studies (*26*) detected such a band for ^{13}CO adsorbed to Au_8/MgO(FC).

In contrast to the above, gold octamers adsorbed on an F-center–free MgO(001) surface were essentially inactive for the combustion reaction (Fig. 1B). In fact, even under quasi–steady-state conditions with pulsed molecular beams, no CO_2 formation was observed. The absorption band of ^{13}CO in this case (2102 cm^{-1}) was shifted to a higher frequency (by 25 to 50 cm^{-1}), as compared to the case of ^{13}CO adsorbed on a gold octamer deposited on MgO(FC).

The above-noted red shift of the CO stretch when the molecule is adsorbed on Au_8 supported on MgO(001)(FC) is a key for elucidating the change in the charge state of the gold octamer bound to F-center defects on the MgO surface. The absorption frequency of CO adsorbed on metal surfaces depends strongly on the population of the 2π* orbital, because occupation of this antibonding orbital weakens the C–O bond. Furthermore, results from extensive ab initio calculations, using the method developed in

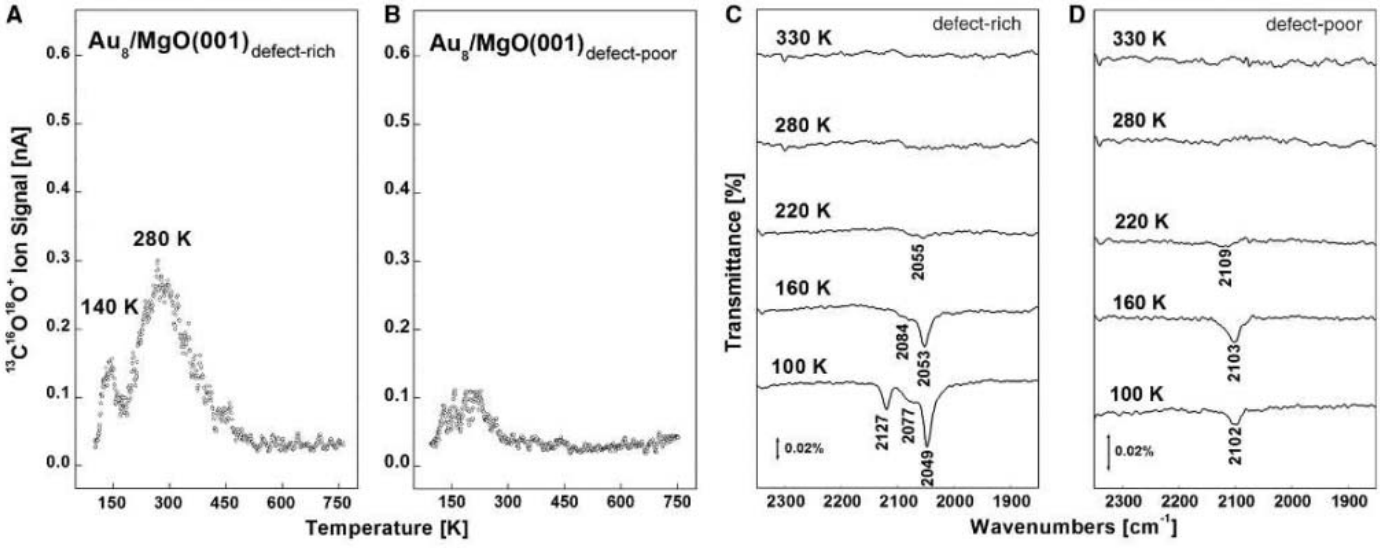

Fig. 1. Mass spectrometric signals pertaining to the formation of CO_2 on Au_8 deposited on (**A**) F-center–rich and (**B**) F-center–free MgO(001) thin films. To unambiguously show that both CO and O_2 are involved in the reaction, isotopically labeled ^{13}CO and $^{18}O_2$ were used. [(**C**) and (**D**)] Fourier-transform IR spectra measured for the same surfaces (defect-rich and defect-poor) and with the same CO and O_2 exposures as in (A) and (B), respectively, at various annealing temperatures. The indicated temperatures cannot be compared directly with the ones in the temperature-programmed reaction spectrum but are lower limits. We have also observed an IR absorption band at 1300 cm^{-1}, which we attribute to superoxo/peroxo-type O_2. In order to better disentangle the vibrational band of ^{13}CO adsorbed on Au_8 deposited on defect-poor films (B) from that of the CO weakly bound to the support material, the sample was annealed to 120 K. In this way, the ^{13}CO frequency from MgO-adsorbed CO disappears, otherwise observed at 2127 cm^{-1}.

(*27*) [see also (*18*)], given in Table 1 for the isolated $Au_8/O_2/^{13}CO$ complex (which we present first in order to allow a clear distinction between charging and other support-related effects), reveal that the ^{13}CO stretch vibration shifts to lower frequency in a manner that is correlated with increased charging of the complex (given by Q_c in Table 1), as well as with the estimated increase in the population of the antibonding state [given by δQ(CO) in Table 1]. For a neutral free complex with zero spin [$Q_c = 0$ and $S = 0$ in Table 1; see the corresponding atomic configuration shown in the inset of Fig. 2], a vibrational frequency of 2009 cm^{-1} was obtained for the adsorbed ^{13}CO molecule. We attribute the calculated decrease in frequency (61 cm^{-1}) in comparison to the value calculated for the free molecule (2070 cm^{-1}) to a net excess charge [$\delta Q(CO) = 0.28e$, where e is the electron charge] on the adsorbed molecule. The excess charge on the molecule results from back-donation into the CO($2\pi^*$) antibonding state.

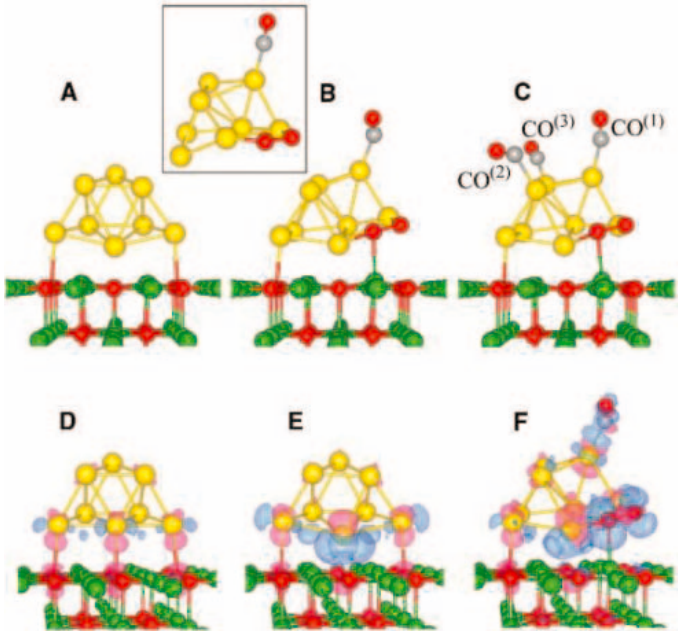

Fig. 2. Optimized configurations of (**A**) a bare Au_8 cluster (yellow spheres) adsorbed on an F center of a MgO(001) surface (O atoms are in red and Mg atoms in green) and (**B**) a surface-supported gold octamer with O_2 adsorbed at the interface between the Au_8 cluster and the magnesia surface and a CO molecule adsorbed on the top triangular facet (the C atom is depicted in gray). There is a significant change in the geometry of Au_8 compared to the one shown in (A). The inset between (A) and (B) shows a local-energy-minimum structure of the free Au_8 cluster in the three-dimensional (3D) isomeric form with coadsorbed O_2 and CO molecules. Although in the global ground state of the free $Au_8/O_2/CO$ complex the gold octamer is characterized by a higher degree of 2D character (*14*), we chose to display here an isomer that closely resembles the structure of the surface-adsorbed complex: Compare the structure in the inset with that shown in (B). (**C**) Au_8 on the magnesia surface [MgO(FC)] with three CO molecules adsorbed on the top facet of the cluster and an O_2 molecule preadsorbed at the interface between the cluster and the magnesia surface. The molecule marked $CO^{(2)}$ lies parallel to the surface and is thus not IR-active in the experimental configuration used here. The C–O bond length $d(CO^{(i)})$, the charge transferred to the $CO^{(i)}$ molecule $\Delta Q^{(i)}$, and the calculated C–O vibrational frequency $\nu^{(i)}$ (i =1, 2, and 3), as well as the corresponding values for the O_2 molecule, are as follows: $d(CO^{(i)})$ [Å] = 1.151, 1.158, 1.153; $d(O_2)$ = 1.422; $\delta Q^{(i)}$ [e] = 0.31, 035, 0.32; $\delta Q(O_2)$ [e] = 1.12; $\nu^{(i)}$ [cm^{-1}] = 1993, 1896, 1979. Isosurfaces of charge differences are as follows: (**D**) Au_8 cluster adsorbed on defect-free MgO, $\delta\rho = \rho_{tot} - (\rho_{Au8} + \rho_{MgO})$, where $\rho_{tot} = \rho[Au_8/MgO]$; (**E**) Au_8 cluster anchored to a surface F center of MgO, $\delta\rho = \rho_{tot} - (\rho_{Au8} + \rho_{MgO(FC)})$, where $\rho_{tot} = \rho[Au_8/MgO(FC)]$; (**F**) same as (E) but with O_2 and CO molecules adsorbed on the gold cluster, $\delta\rho = \rho_{tot} - (\rho_{Au8} + \rho_{O2} + \rho_{CO} + \rho_{MgO(FC)})$, where $\rho_{tot} = \rho[Au_8/O_2/CO/MgO(FC)]$. Pink isosurfaces represent $\delta\rho < 0$ (depletion) and blue ones correspond to $\delta\rho > 0$ (excess). All of the isosurfaces are plotted for the same (absolute) value of the density difference ($\delta\rho$) in order to allow direct comparison between the different cases.

Table 1. Results for free $Au_8/O_2/^{13}CO$ complexes as a function of the amount of excess electron charging Q_c, shown for various values of the spin. For the neutral cluster ($Q_c = 0$), we show the triplet ($S = 1$) and singlet ($S = 0$) states. The quantities that we display are: $\nu(^{13}CO)$, the ^{13}CO vibrational frequency; the calculated excess electronic charge on the adsorbed molecules δQ(CO) and $\delta Q(O_2)$, with the procedure used for achieving these estimates described in (*18*); and the bond distances d(CO) and $d(O_2)$. The calculated values for the isolated molecules are d(CO) = 1.14 Å and $d(O_2)$ = 1.24 Å, compared to the gas-phase experimental values of 1.13 and 1.21 Å, respectively. The calculated vibrational frequency of gas-phase ^{13}CO is 2070 cm^{-1}, which is 25 cm^{-1} smaller than the experimental value $\nu_{exp}(^{13}CO)$ = 2095 cm^{-1}.

Q_c (e)	S	ν (cm^{-1})	$d(^{13}CO)$ (Å)	δQ(CO) (e)	$d(O_2)$ (Å)	$\delta Q(O_2)$ (e)
0	1	2005	1.149	0.29	1.336	0.71
0.25	0.875	1987	1.150	0.32	1.344	0.75
0.5	0.75	1968	1.154	0.35	1.350	0.77
1.0	0.5	1926	1.160	0.43	1.364	0.86
0	0	2009	1.148	0.28	1.378	0.88
0.25	0	1990	1.150	0.31	1.381	0.89
0.5	0	1975	1.153	0.34	1.385	0.92
1.0	0	1920	1.158	0.41	1.398	1.00

As expected, such donation of charge from occupied orbitals of the metal to unoccupied states of the adsorbed molecule is even more pronounced (0.88e) for the more electronegative O_2 molecule. Upon charging the complex with up to 1.0e, the net excess charge on the ^{13}CO molecule increases to 0.41e, and the CO stretch redshifts by 89 cm^{-1} to 1920 cm^{-1}. The increased degree of charging of the metal cluster with back-donation, and the consequent decrease of ν(CO), increase the C–O bond length from 1.148 Å for Q_c = 0 to 1.158 Å for Q_c = 1.0e. Similar changes were seen starting from the triplet state of the neutral complex (Table 1).

We next focused on the adsorption of CO to gold complexes surface-supported on perfect or defective magnesia [with an oxygen molecule preadsorbed at the interface between the cluster periphery and the MgO surface (Fig. 2B)]; that is, $Au_8/O_2/MgO$ or $Au_8/O_2/MgO(FC)$. Three energy-optimized deposited cluster configurations pertinent to the experimental work are displayed in the top row of Fig. 2, A to C. The bare adsorbed Au_8 cluster (Fig. 2A) exhibits only a slight distortion from the structure of the corresponding gas-phase neutral cluster (*4*, *5*), consisting mainly of a displacement of the gold atom of the cluster closest to the surface oxygen vacancy. The cluster is anchored strongly to the defective MgO surface (with a binding energy of 3.44 eV) compared to a significantly weaker binding to the defect-free surface (1.22 eV). From examination of the charge-difference isosurfaces displayed in Fig. 2, we observe that bonding of the Au_8 cluster to the MgO(FC) surface is accompanied by a significantly larger degree of charge transfer from the magnesia surface to the gold cluster (Fig. 2E) as compared to the case of adsorption on an F-center–free surface (Fig. 2D).

Optimal geometries with a single adsorbed CO molecule, $Au_8/O_2/CO/MgO(FC)$, and at saturation coverage of the cluster [that is, with three adsorbed CO molecules, $Au_8/O_2/(CO)_3/MgO(FC)$] are shown in Fig. 2, B and C, respectively. Comparison between the bare-cluster geometry in Fig. 2A with those shown in Fig. 2, B and C, reveals a significant change

in the geometry of the gold cluster caused by the adsorption of the reactant molecules, mainly the peripherially adsorbed O_2. This structural change, occurring during adsorption (or in the course of reaction), is a manifestation of the "structural fluxtionality" of clusters (*5*). The system shown in Fig. 2C possesses two IR-active ^{13}CO molecules ($CO^{(1)}$ and $CO^{(3)}$), as we had seen experimentally (*18*).

Because the bonding characteristics, and other properties of the system, with a single adsorbed CO molecule (Fig. 2B) are similar to the ones associated with the CO-saturated cluster (Fig. 2C), we focus next on the former (which is more convenient to analyze and illustrate). The energetics of the adsorption of the O_2 and CO molecules to the defect-free and F-center clusters, corresponding in each case to two possible spin states (S = 0 or 1), together with the calculated amount of charge transferred to the deposited complex (gold cluster and adsorbed molecules), the bond length d(CO), and the calculated vibrational frequency are given in Table 2. Stronger binding of O_2 to the cluster occurs in the presence of the F center (A and B in Table 2).

Adsorption is accompanied by a significant degree of charge transfer, which in the case of the defective surface is directed from the oxygen vacancy into the deposited gold cluster and adsorbed molecules. Comparison of the charge-difference isosurfaces for the bare cluster (Fig. 2E) and for the cluster with adsorbed O_2 and CO molecules (Fig. 2F), bonded to MgO(FC), reveals a significant amount of charge excess on the adsorbed molecules. The consequent weakening of intramolecular bonds manifests itself in increased bond lengths and lower vibrational frequencies of the adsorbed molecules (Table 2) (*28*).

The correlation diagram (Fig. 3, A to C) depicts the local density of states (LDOS) for the two reactants, CO (Fig. 3A) and the Au_8/O_2/MgO(FC) complex (Fig. 3C), as well as for the product complex Au_8/O_2/CO/MgO(FC) with the CO adsorbed on the deposited cluster (Fig. 3B). The LDOS of Au_8/O_2/CO/MgO(FC) is reproduced in Fig. 4 along with images of the corresponding molecular orbitals, which aid visualization of the bonding mechanism discussed below. As expected, the 3σ and the nonbonding 4σ (oxygen lone-pair) molecular orbitals of the isolated CO are not involved in the bonding to the cluster complex, and the nonbonding 5σ (carbon lone-pair) orbital is stabilized by the interaction (by about 3eV) and thus it contributes to CO chemisorption (*29*). The 1π level is slightly pushed upward in energy (<1eV).

The LDOS of the complex projected on the adsorbed CO also reveals contributions of the 2π* orbitals that are spread over the entire energy range of the cluster's electronically occupied spectrum (Fig. 3B, the black-shaded LDOS for energies between about –10eV and E_F). The 2π* orbitals of the CO molecule are pushed below E_F, which populates this state via back-donation [that is,

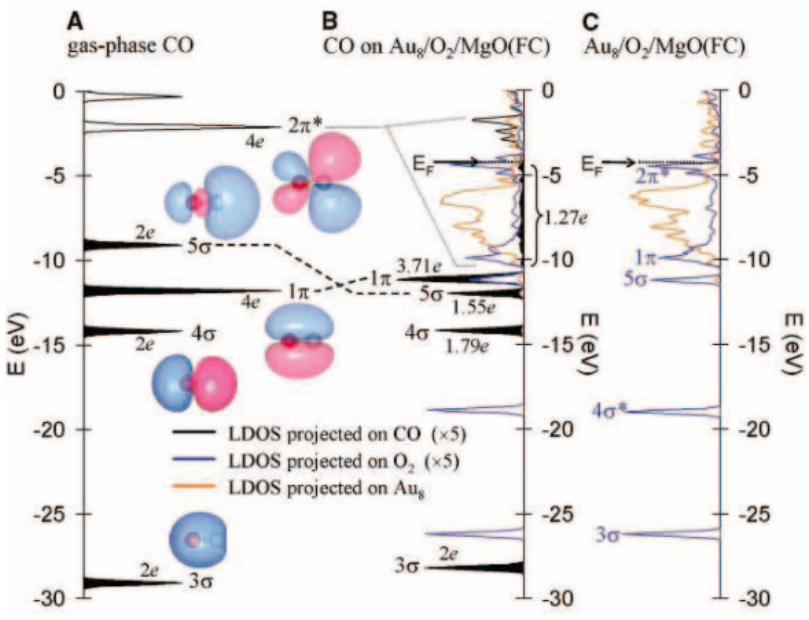

Fig. 3. LDOS correlation diagram of (**A**) free CO, (**C**) Au_8/O_2/MgO(FC), and (**B**) after adsorption of a CO molecule, resulting in the complex Au_8/O_2/CO/MgO(FC). The results correspond to the spin singlet (S = 0) case. The electron populations of the various levels of the free and adsorbed CO molecule are given as 2*e*, 4*e*, etc., and isosurface images of the orbitals of the free CO molecules are also shown in (A). Black dashed lines indicate orbital shifts and redistribution caused by the adsorption of the CO molecule.

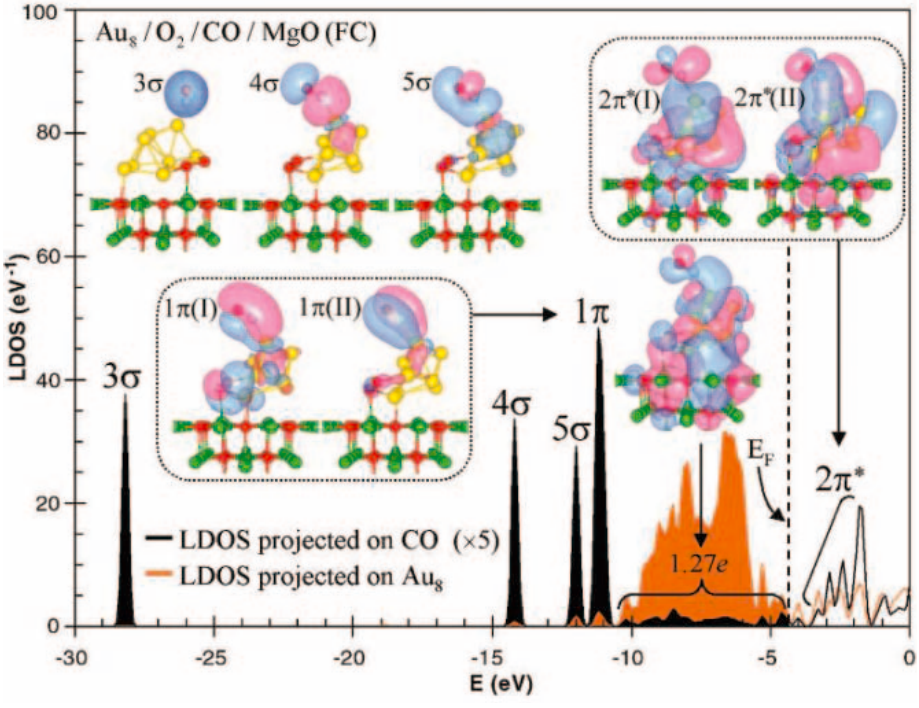

Fig. 4. LDOS and orbitals of the Au_8/O_2/CO complex adsorbed on MgO(FC). Results are shown for the spin singlet S = 0 case. The LDOS projected on the CO molecule is shown in black and that projected on the gold cluster is colored orange. E_F is indicated by a dashed line. The electronic population of the orbitals of the CO molecule (found to be mainly of 2π* character), with energies in the range that overlaps the gold cluster states, provides an estimate of the back-donated charge (1.27*e*). Included also are isosurface images of the wave functions of the Au_8/O_2/CO/MgO(FC) complex, which may be identified with the indicated orbitals of CO (compare to the orbital images of the free CO molecule in Fig. 3A).

Table 2. Binding energies: BE(O_2), binding energy of O_2 to Au_8/MgO; BE(CO), binding energy of CO to Au_8/O_2/MgO. Excess electronic charge $\Delta Q(Au_8/O_2/CO)$ on the complex adsorbed on the (001) surface of magnesia is shown. The C–O bond length d(CO) and the C–O stretch vibrational frequency $\nu(^{13}CO)$ are shown. Results are given for the gold octamer adsorbed on a MgO(001) surface with (F center), or without (F-center–free), a surface F center, and in each case we give results calculated for two spin states, S. The calculated amount of charge transferred to a bare gold octamer cluster adsorbed on the defect-free surface is $\Delta Q(Au_8/MgO) = 0.82e$, and it is significantly larger for the cluster adsorbed on a surface F center; that is, $\Delta Q(Au_8/MgO(FC)) = 1.44e$. The excess charge ΔQ is calculated as described in (*18*).

	S	BE(O_2) (eV)	BE(CO) (eV)	$\Delta Q(Au_8/O_2/CO)$ (e)	d(CO) (Å)	ν (^{13}CO) (cm^{-1})
				F center		
A	1	0.33	0.79	1.52	1.155	1937
B	0	0.47	0.65	1.58	1.156	1931
				F-center–free		
C	1	0.30	0.79	0.87	1.152	1965
D	0	0.15	0.91	1.01	1.150	1994

hybridization and population of the initially unoccupied antibonding orbitals of the CO molecule through interaction with occupied surface orbitals (*30*–*32*)]. All of these features are also present in the correlation diagram of the cluster complex bound to the defect-free MgO surface (not shown here), where back-donation, however, is less pronounced. We can estimate the amount of back-donated electronic charge by integrating over the squared amplitude of the $2\pi^*$ orbital located below E_F. For the Au_8/O_2/CO bound to the F center of the MgO support, 1.27e are back-donated into the $2\pi^*$ orbital, whereas a smaller degree of back-donation (1.18e) occurs for the complex bound to the undefective surface.

The above-noted difference in the degree of back-donation is manifested in a variation of the stretch frequencies of the adsorbed CO molecules, and these correlate with the aforementioned variation in the degrees of substrate-induced charging of the gold octamer deposited on magnesia surfaces with or without F-center defects (*33*). Indeed, ν(CO) for the complex bound to an F-center–rich surface is measured to be redshifted by 25 to 53 cm^{-1} with respect to the frequency of a CO molecule bonded to the complex deposited on an F-center–free support (Fig. 1). This compares favorably with the corresponding calculated red shift; for example, from Table 2, a value of 34 cm^{-1} is estimated when comparing ν(CO) for the C(FC-free) and B(FC) states [both corresponding to the complexes exhibiting the largest binding energy of the oxygen molecule (Table 2)].

We conclude that partial electron transfer from the F centers to the adsorbed cluster complex correlates with frequency shifts of the intramolecular vibration of adsorbed CO. In addition, these sites serve to strongly anchor the deposited clusters, thereby inhibiting their coalescence into larger inert ones. Understanding of such issues pertaining to the interactions between deposited clusters and the support surfaces, and investigations of the dependencies of such interactions on the materials' identity, their size, and their chemical and physical properties, promise to enhance progress toward the design and use of specific nanocatalytic systems.

References and Notes

1. M. Haruta, T. Kobayashi, H. Sano, N. Yamada, *Chem. Lett.* **34**, 405 (1987).
2. M. Haruta, *Catal. Today* **36**, 153 (1997).
3. M. Valden, X. Lai, D. W. Goodman, *Science* **281**, 1647 (1998).
4. A. Sanchez *et al.*, *J. Phys. Chem. A* **103**, 9573 (1999).
5. H. Häkkinen, S. Abbet, A. Sanchez, U. Heiz, U. Landman, *Angew. Chem. Int. Ed. Engl.* **42**, 1297 (2003).
6. M. Mavrikakis, P. Stoltze, J. K. Norskov, *Catal. Lett.* **64**, 101 (2000).
7. N. Lopez, J. K. Norskov, *J. Am. Chem. Soc.* **124**, 11262 (2002).
8. A. Cho, *Science* **299**, 1684 (2003).
9. C. Lemire, R. Meyer, S. Shaikhutdinov, H.-J. Freund, *Angew. Chem. Int. Ed. Engl.* **43**, 118 (2004).
10. J. Guzman, B. C. Gates, *J. Am. Chem. Soc.* **126**, 2672 (2004).
11. D. M. Cox, R. Brickman, K. Creegan, A. Kaldor, *Z. Phys. D* **19**, 353 (1991).
12. W. T. Wallace, R. L. Whetten, *J. Am. Chem. Soc.* **124**, 7499 (2002).
13. G. Mills, M. S. Gordon, H. Metiu, *Chem. Phys. Lett.* **359**, 493 (2002).
14. B. Yoon, H. Häkkinen, U. Landman, *J. Phys. Chem. A* **107**, 4066 (2003).
15. L. D. Socaciu *et al.*, *J. Am. Chem. Soc.* **125**, 10437 (2003).
16. D. Stolcic *et al.*, *J. Am. Chem. Soc.* **125**, 2848 (2003).
17. Y. D. Kim, M. Fischer, G. Ganteför, *Chem. Phys. Lett.* **377**, 170 (2003).
18. Details of the calculation methodology and comments about calculated vibrational frequencies are available on *Science* Online. The aforementioned theoretical ab initio predictions that charging plays a key role in the catalytic reactivity of gold clusters that are a few atoms in size has been clearly demonstrated recently through gas-phase studies. These investigations showed that only negatively charged even-numbered gold clusters bind a single O_2 molecule in a superoxo-like configuration (*16*, *17*) and that negatively charged free gold clusters are catalytically active for the CO-combustion reaction (*15*), whereas positively charged clusters are inert for the reaction, because oxygen cannot be adsorbed (*11*).
19. S. Abbet, K Judai, L Klinger, U. Heiz, *Pure Appl. Chem.* **74**, 1527 (2002).
20. A. S. Wörz, K. Judai, S. Abbet, U. Heiz, *J. Am. Chem. Soc.* **125**, 7964 (2003).
21. C. Ruggiero, P. Hollins, *J. Chem. Soc. Faraday Trans. 1* **92**, 4829 (1996).
22. P. Dumas, R. G. Tobin, P. L. Richards, *Surf. Sci.* **171**, 579 (1986).
23. Y. Jugnet, F. J. Cadete Santos Aires, C. Deranlot, L. Piccolo, J. C. Bertolini, *Surf. Sci.* **521**, L639 (2002).
24. D. R. Rainer, C. Xu, P. M. Holmblad, D. W. Goodman, *J. Vac. Sci. Technol. A* **15**, 1653 (1997).
25. C. Winkler, A. J. Carew, S. Haq, R. Raval, *Langmuir* **19**, 717 (2003).
26. U. Heiz, A. Sanchez, S. Abbet, W.-D. Schneider, *Chem. Phys.* **262**, 189 (2000).
27. R. N. Barnett, U. Landman, *Phys. Rev. B* **48**, 2081 (1993).
28. As discussed by us previously (*4*, *5*), for the adsorbed oxygen molecule, the transferred charge partially populates the antibonding orbital of the molecule, resulting for the systems studied here in increased interatomic distance $d(O_2)$, exhibiting characteristic superoxo (about 1.35 Å for $S = 1$; A and C in Table 2) and peroxo (about 1.42 Å for $S = 0$; B and D in Table 2) O–O distances, compared to a distance of 1.24 Å for the free molecule. The calculated stretch frequencies for the adsorbed O_2 molecule corresponding to the stronger binding states [B (for the F-center–rich surface) and C (for the F-center–free surface) (Table 2)] are 966 and 1084 cm^{-1}, respectively. For reference, we note that for free O_2 we obtained a frequency of 1485 cm^{-1} as compared to the experimental value of 1580 cm^{-1}. Because the peripherially adsorbed O_2 is oriented parallel to the surface (Fig. 2F), it is IR-inactive. The aforementioned measured IR absorption band (at 1300 cm^{-1}) originates from IR-active configurations of O_2 molecules [for example, the ensemble of supported Au_8 clusters with the molecule adsorbed on the top facet of the cluster (*4*)].
29. The consequent depletion of the 5σ frontier orbital is often referred to in surface science studies as (forward) donation from CO to the metal (*30*, *31*).
30. G. Blyholder, *J. Phys. Chem.* **68**, 2772 (1964).
31. R. Hoffmann, *Rev. Mod. Phys.* **60**, 601 (1988).
32. L. Lian, P. A. Hackett, D. M. Rainer, *J. Chem. Phys.* **99**, 2583 (1993).
33. The binding energy of the molecule to the gold cluster is the result of several factors that manifest themselves simultaneously (the aforementioned hybridizations of the CO 5σ and 1π orbitals with the *s*-*d* wavefunctions of the gold cluster, in addition to the contribution to the binding associated with population of the $2\pi^*$ orbital). Consequently, although the C–O bond length and the CO vibrational frequency are sensitive to and correlate with the degree of back-donation into the hybridized antibonding $2\pi^*$ orbital, the adsorption energy of CO to the gold cluster may not exhibit such correlation (for example, results in Table 2).

34. U.L., B.Y., and H.H. acknowledge support by the U.S. Air Force Office of Scientific Research and the U.S. Department of Energy (DOE). The computer simulations were performed on U.S. Department of Defense computers supported by the High Performance Computing Modernization Program and at DOE's National Energy Research Scientific Computing Center at the Lawrence Berkeley National Laboratory. The experiments were carried out at the University of Ulm. Support for the experiments was also obtained from the Deutsche Forschungsgemeinschaft, the Sonderforschungsbereich 569, and the Landesstiftung Baden-Württemberg. K.J. thanks the Alexander v. Humboldt foundation and the Japan Society for the Promotion of Science foundation for financial support, J.-M.A. thanks the Swiss National Science foundation, and S.A. thanks the Alexander v. Humboldt foundation for financial support. A.S.W. acknowledges support from the Graduiertenkolleg Molekulare Organisation und Dynamik an Grenz- und Oberflächen.

Supporting Online Material

www.sciencemag.org/cgi/content/full/307/5708/403/DC1
SOM Text
References

17 August 2004; accepted 30 November 2004
10.1126/science.1104168

Creating Order from Random Fluctuations in Small Spin Ensembles

R. Budakian,* H. J. Mamin, B. W. Chui, D. Rugar

We demonstrate the ability to create spin order by using a magnetic resonance force microscope to harness the naturally occurring statistical fluctuations in small ensembles of electron spins. In one method, we hyperpolarized the spin system by selectively capturing the transient spin order created by the statistical fluctuations. In a second method, we took a more active approach and rectified the spin fluctuations by applying real-time feedback to the entire spin ensemble. The created spin order can be stored in the laboratory frame for a period on the order of the longitudinal relaxation time of 30 seconds and then read out.

Creating order from random thermal fluctuations has been of interest to physicists since the development of statistical mechanics in the 19th century (*1*). In a more modern context, creating order in microscopic physical systems is an essential part of quantum information processing and quantum computation (*2*–*4*), where the ability to set the state of a collection of quantum objects to a desired configuration is required. The device used to perform this operation must be capable of controlling the microscopic degrees of freedom of the system while being subjected to environmental fluctuations.

Here, we take advantage of the outstanding sensitivity of magnetic resonance force microscopy (MRFM) to follow statistical $\sqrt{N}$ fluctuations in small ensembles of electron spins (*5*, *6*) with a real-time sensitivity corresponding to $1.3\mu_B$, where μ_B is the Bohr magneton. The spin manipulation protocols we have developed allow us to monitor and respond to the instantaneous spin imbalance in the rotating frame. By monitoring the spin system and selectively capturing the large positive fluctuations, we have created a mean polarization corresponding to $\sim 6\mu_B$ in an ensemble of $N \approx 70$ spins. We also used real-time feedback to effectively cool the spin system and create a mean polarization corresponding to $\sim 7\mu_B$. The spin order was then transferred to the laboratory frame, stored, and later read out.

In MRFM detection, spins are manipulated by using magnetic resonance, and the longitudinal component of the magnetization is detected mechanically by measuring the interaction between the spins and a small permanent magnet attached to the end of a sensitive silicon cantilever. Typically, the force generated by a spin on the cantilever is quite small. An electron spin will produce a force of only 2×10^{-18} N when subjected to a magnetic field gradient from the tip as large as 2×10^5 T m^{-1}. Sensitivity to such small forces requires the ability to coherently manipulate spins for many cycles of the cantilever. Recently, through the use of specially engineered cantilevers that reduce disturbance to the spins (*7*–*9*), we observed longitudinal relaxation times in the rotating frame (i.e., during measurement) of up to several seconds. This has allowed us to realize a single-shot detection sensitivity approaching the single spin level (*5*) and the detection of an isolated electron spin by signal averaging (*6*).

In the experimental setup of the MRFM apparatus (Fig. 1A), a custom-fabricated mass-loaded silicon cantilever with a submicrometer SmCo magnetic particle attached to the tip is used as the force-sensing element (*5*, *6*). The sample consists of vitreous silica (Suprasil W2, Heraeus Quarzglas GmbH and Company KG, Hanau, Germany) that has been irradiated by gamma rays from a ^{60}Co source to produce spin-1/2 paramagnetic defects or E' centers (unpaired electron spins on Si) (*10*). Experiments were performed with two different cantilever and sample combinations. In setup 1, a cantilever having a fundamental resonance frequency $f_c = 8.7$ kHz and stiffness $k = 0.6$ mN m^{-1} with a 250-nm-wide SmCo tip was used with a sample that had a spin concentration of $\sim 10^{15}$ cm^{-3}. In setup 2, a cantilever with $f_c = 5.5$ kHz, $k = 0.11$ mN m^{-1}, and a 150-nm-wide SmCo tip was used with a $\sim 10^{14}$ cm^{-3} concentration sample. The MRFM apparatus was operated in vacuum and cooled to 300 mK to reduce the thermal vibrations of the cantilever.

Electron spin resonance was excited at $\omega_{rf}/2\pi = 2.96$ GHz with the use of a microwave field with amplitude $B_1 \approx 0.3$ mT. In the presence of the inhomogeneous field from the tip, only those spins within a thin resonant slice satisfying the resonance condition given by $B_0(x,y,z) \equiv |\mathbf{B}_{tip}(x,y,z) + B_{ext}\hat{\mathbf{z}}| = \omega_{rf}/\gamma$ will interact with the microwave field. Here, $B_0(x, y, z)$ is the sum of the tip field, $\mathbf{B}_{tip}(x, y, z)$, and a uniform external field, $B_{ext}\hat{\mathbf{z}}$, produced by a superconducting magnet, and γ is the gyromagnetic ratio ($\gamma/2\pi = 2.8 \times 10^{10}$ Hz T^{-1}). For the vertical orientation of the cantilever shown in Fig. 1A, only those spins that are slightly to the left or right of the tip contribute to the signal. Furthermore, because of symmetry, the cantilever will respond only to the left-right imbalance of spin polarization.

To detect spins, we use the recently developed spin manipulation protocol OSCAR (oscillating cantilever-driven adiabatic reversal), which measures the shift in the fundamental frequency of the cantilever in response to tip-spin interactions (*5*, *6*, *11*). The cantilever is self-oscillated at its fundamental resonance frequency by using a piezoelectric transducer that drives the cantilever to a fixed amplitude x_{pk} (*11*, *12*). As the cantilever position oscillates according to $x_c(t) =$

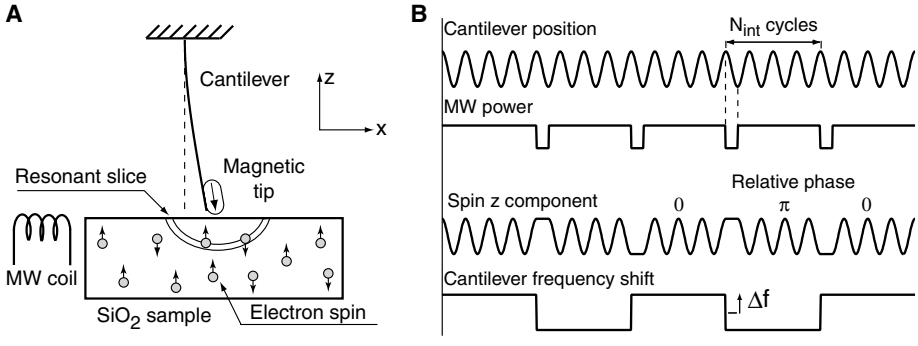

Fig. 1. (**A**) Schematic of the MRFM apparatus. The cantilever with the attached magnetic tip is oriented vertically about 140 nm away from the surface of a sample containing a low concentration of E' centers. A small coil placed near the sample generates microwaves at 2.96 GHz to excite electron spin resonance. At 2.96 GHz, the resonance condition for electrons is met for $B_0 = 106$ mT. For $B_{ext} = 30$ mT, the resonant slice is a paraboloidal shell that extends about 250 nm below the tip. (**B**) Timing diagram for the interrupted OSCAR protocol. For setups 1 and 2, the microwave (MW) power is interrupted every 88 cycles ($f_{sig} \approx 50$ Hz) and 64 cycles ($f_{sig} \approx 43$ Hz), respectively.

IBM Research Division, Almaden Research Center, 650 Harry Road, San Jose, CA 95120, USA.

*To whom correspondence should be addressed. E-mail: budakian@us.ibm.com

$x_{pk}\sin(2\pi f_c t)$, the field experienced by a spin near the tip is modulated sinusoidally at the cantilever frequency with peak amplitude $\Delta B = Gx_{pk}$, where $G = \partial B_0/\partial x$ is the lateral gradient from the tip. For typical experimental parameters of $x_{pk} \approx 20$ nm and $G \approx 2 \times 10^5$ T m^{-1}, the external field experienced by spins within the resonant slice is modulated by $\Delta B = 4$ mT. In the presence of the microwave field, the slow variation of the static field at the cantilever frequency causes each spin within the resonant slice to be adiabatically inverted synchronously with the cantilever motion. The back action of the spin on the cantilever in turn shifts the fundamental frequency of the cantilever by a small amount

$$\delta f_i = \frac{2 f_c G_i \mu_B}{\pi k x_{pk}} \alpha_i$$

where G_i is the gradient at the position of the ith spin and α_i is a random variable that takes values +1 or –1, depending on whether the spin moment is aligned or anti-aligned with respect to the effective field in the rotating frame (*5*, *13*, *14*). The two-level nature of α_i reflects the quantum measurement characteristic of MRFM spin detection (i.e., a rotating frame Stern-Gerlach behavior) (*15*–*17*). For an ensemble of N spins, we define the instantaneous statistical spin imbalance in the rotating frame to be $\Delta N = \sum_{i=1}^{N} \alpha_i$ and the corresponding magnetic moment to be $\Delta m = \Delta N \mu_B$. The cantilever frequency shift for the ensemble is given by $\Delta f = \sum_{i=1}^{N} \delta f_i$.

Near the surface of the sample, the cantilever frequency is affected not only by the presence of the spins but also by the more dominant electrostatic and van der Waals forces. In order to make the spin component of the signal distinctive, we periodically reversed the sign of the frequency shift by interrupting the microwave power for 1/2 cycle of the cantilever vibration every N_{int} cycles (Fig. 1B). The periodic interruptions encode the spin signal with a characteristic frequency $f_{sig} = f_c/2N_{int}$. A lock-in amplifier referenced to f_{sig} is used to demodulate the frequency shift and determine Δf (*5*, *6*).

A 200-s record of the cantilever frequency shift, recorded from the in-phase channel of the lock-in amplifier, is shown (Fig. 2A). A histogram of the frequency fluctuations (Fig. 2B) reveals a Gaussian shape with variance $\sigma_I^2 = 69$ mHz^2. We note that the distribution has a zero mean, indicating that the spin ensemble does not have a preferred direction with respect to the effective field. To show that the measured frequency shift is dominated by the spin signal rather than measurement noise, we show the histogram of the measurement noise recorded from the quadrature channel of the lock-in amplifier ($\sigma_Q^2 = 5$ mHz^2) (Fig. 2C). The variance of the spin signal without measurement noise is simply related to the in-phase and quadrature variances by $\sigma_{spin}^2 = \sigma_I^2 - \sigma_Q^2$ (*6*). From the measured variance σ_{spin}^2 and a model of the field produced by the tip (*18*), we estimate the total number of spins contained within the resonant slice to be $N \approx 70$.

The power spectrum of the frequency fluctuations (Fig. 2D) fits well to a Lorentzian with spectral width $\Delta\nu_s = 21$ mHz, corresponding to a correlation time $\tau_m = 1/2\pi\Delta\nu_s = 7.6$ s. This long correlation time, closely related to the rotating frame longitudinal relaxation time, allows us to measure real-time fluctuations of the spin ensemble with a lock-in time constant of up to 3 s.

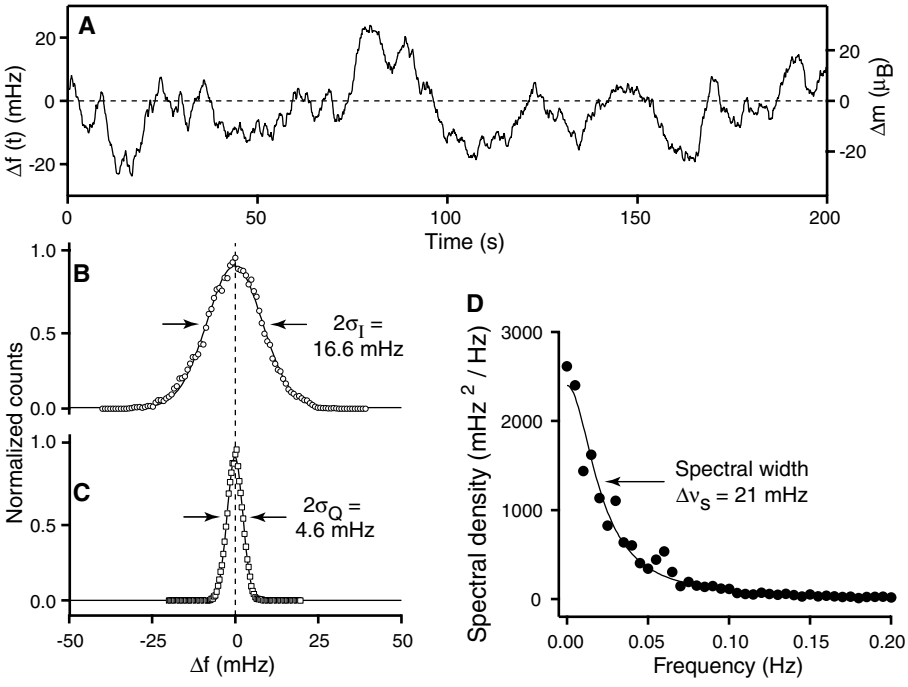

Fig. 2. (**A**) Trace showing a time record of the statistical fluctuations recorded in a 83-mHz bandwidth with the use of setup 1. The frequency shift is converted to equivalent number of spins (right-hand axis) by dividing Δf by the average frequency shift per spin ($|\overline{\delta f}| = 0.8$ mHz/spin). (**B**) Histogram of a 1-hour continuous record of the in-phase lock-in output signal. The Gaussian distributed spin fluctuations have a zero mean, indicating that the time-averaged spin imbalance does not point in a preferred direction with respect to the effective field. This observation is consistent with the fact that the spin temperature in the rotating frame approaches $T_s = \infty$ for measurement times $t_{meas} \gg \tau_m$. (**C**) Histogram of the quadrature channel showing the detection noise. (**D**) Power spectrum of a 1-hour record of the fluctuations.

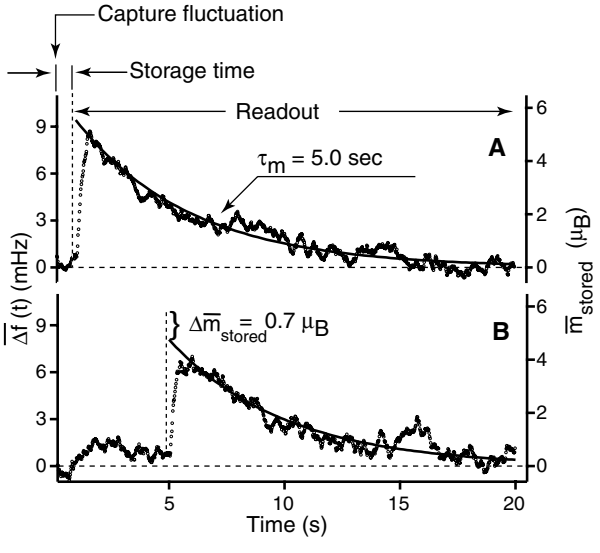

Fig. 3. (**A**) Trace showing the average of 2800 individual capture-store-readout sequences with a storage time of 1.0 s, taken with use of setup 2. The average frequency shift, $\overline{\Delta f}(t)$, and stored magnetization, $\overline{m}_{stored}$, are shown on the left- and right-hand axes, respectively. Equivalent spins are calculated by using $|\overline{\delta f}| = 1.7$ mHz/spin. (**B**) Data taken under the same conditions as (A), except the storage time was increased to 5.0 s. The decaying magnetization observed during readout in (A) and (B) fits well to an exponential indicating a $\tau_m = 5.0$ s spin relaxation time during measurement.

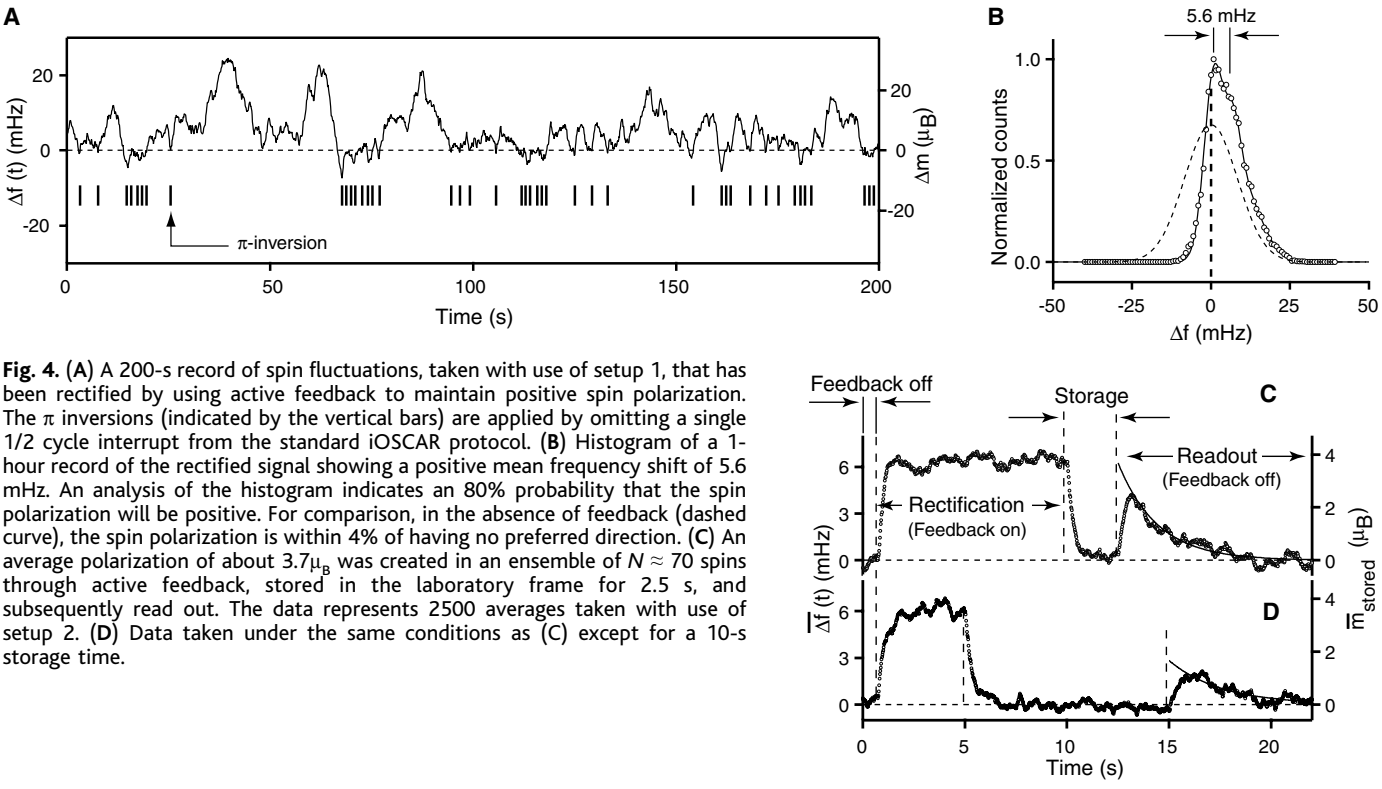

Fig. 4. (**A**) A 200-s record of spin fluctuations, taken with use of setup 1, that has been rectified by using active feedback to maintain positive spin polarization. The π inversions (indicated by the vertical bars) are applied by omitting a single 1/2 cycle interrupt from the standard iOSCAR protocol. (**B**) Histogram of a 1-hour record of the rectified signal showing a positive mean frequency shift of 5.6 mHz. An analysis of the histogram indicates an 80% probability that the spin polarization will be positive. For comparison, in the absence of feedback (dashed curve), the spin polarization is within 4% of having no preferred direction. (**C**) An average polarization of about $3.7\mu_B$ was created in an ensemble of $N \approx 70$ spins through active feedback, stored in the laboratory frame for 2.5 s, and subsequently read out. The data represents 2500 averages taken with use of setup 2. (**D**) Data taken under the same conditions as (C) except for a 10-s storage time.

As an initial demonstration of harnessing spin fluctuations, we created a hyperpolarized spin state by selectively capturing and storing the especially large statistical fluctuations. To do this, we continuously monitor the spin signal and wait until a fluctuation exceeds a predetermined threshold value $\Delta f_{\mathrm{threshold}}$ (*19*). Upon registering a suitable fluctuation, the microwave power is turned off at a maximum of the cantilever motion, which leaves the instantaneous spin polarization pointing along $\mathbf{B}_0$. In the absence of the microwave field, the spins no longer respond to the cantilever motion, and the nonequilibrium state of the spin ensemble can be stored in the laboratory frame for as long as a spin-lattice relaxation time, T_1. The stored magnetization can then be read out by reapplying the microwave field at a maximum of the cantilever motion and using the standard interrupted OSCAR (iOSCAR) protocol.

The average of 2800 individual capture-store-readout sequences, taken with use of setup 2, is shown (Fig. 3). For the data in Fig. 3A, the captured magnetization was stored for 1 s in the laboratory frame (i.e., with the microwave field off) and then read out with use of the iOSCAR protocol. The readout signal had a peak amplitude of 9.4 mHz, which we estimate corresponds to an average magnetization of $\overline{m}_{\mathrm{stored}} = 5.5\mu_B$. When the storage time was increased to 5 s (Fig. 3B), the peak stored magnetization decreased by 14% to $\overline{m}_{\mathrm{stored}} = 4.8\mu_B$. This drop in $\overline{m}_{\mathrm{stored}}$ is the result of depolarization due to longitudinal relaxation, indicating $T_1 \sim 30$ s. The observed T_1 includes the contribution from the lattice as well as tip-induced relaxation (*11*).

In addition to simply selecting and capturing desired fluctuations, we can also take a more active approach by applying real-time feedback to the spin system in order to continuously guide its evolution. As a demonstration of feedback control, we have rectified the spin fluctuations by monitoring the spin signal and applying a π inversion to the entire spin ensemble whenever $\Delta f < 0$ (*19*). The π inversions, accomplished with the use of adiabatic inversion, flip the sign of the spin imbalance so as to always keep Δm positive in the iOSCAR reference frame. Figure 4A shows a 200-s record of the iOSCAR signal, taken with the use of setup 1, along with vertical bars indicating times when π inversions were applied. In contrast to Fig. 2B, the histogram of the signal with feedback control (Fig. 4B, solid curve) now shows a nonzero mean value of 5.6 mHz corresponding to $\sim 7.0\mu_B$. Thus, through the use of feedback, we have essentially hyperpolarized the spins in the rotating frame of the iOSCAR measurement. This spin order can once again be transferred to the laboratory frame, stored, and then read out (Fig. 4, C and D).

We have demonstrated real-time control of electron spins in small ensembles using two spin manipulation protocols: fluctuation capture and fluctuation rectification. Because the present single-shot detection sensitivity is already approaching the single spin level, relatively modest improvements in detection signal-to-noise ratio should allow real-time quantum state detection and control of individual electron spins.

References and Notes

1. J. C. Maxwell, *Theory of Heat* (Longmans, London, ed. 6, 1880).
2. D. P. Divincenzo, *Science* **270**, 255 (1995).
3. B. E. Kane, *Nature* **393**, 133 (1998).
4. A. Steane, *Rep. Prog. Phys.* **61**, 117 (1998).
5. H. J. Mamin, R. Budakian, B. W. Chui, D. Rugar, *Phys. Rev. Lett.* **91**, 207604 (2003).
6. D. Rugar, R. Budakian, H. J. Mamin, B. W. Chui, *Nature* **430**, 329 (2004).
7. G. P. Berman, V. N. Gorshkov, D. Rugar, V. I. Tsifrinovich, *Phys. Rev. B* **68**, 094402 (2003).
8. B. W. Chui *et al.*, in *Technical Digest of the 12th International Conference on Solid-State Sensors and Actuators (Transducers '03)*, IEEE, Boston, MA, 8 to 12 June 2003 (IEEE, Piscataway, NJ, 2003), pp. 1120–1123.
9. D. Mozyrsky, I. Martin, D. Pelekhov, P. C. Hammel, *Appl. Phys. Lett.* **82**, 1278 (2003).
10. J. G. Castle, D. W. Feldman, P. G. Klemens, R. A. Weeks, *Phys. Rev.* **130**, 577 (1963).
11. B. C. Stipe *et al.*, *Phys. Rev. Lett.* **87**, 277602 (2001).
12. T. R. Albrecht, P. Grutter, D. Horne, D. Rugar, *J. Appl. Phys.* **69**, 668 (1991).
13. G. P. Berman, D. I. Kamenev, V. I. Tsifrinovich, *Phys. Rev. A* **66**, 023405 (2002).
14. C. P. Slichter, *Principles of Magnetic Resonance* (Springer-Verlag, Heidelberg, ed. 3, 1996).
15. G. P. Berman, F. Borgonovi, H. S. Goan, S. A. Gurvitz, V. I. Tsifrinovich, *Phys. Rev. B* **67**, 094425 (2003).
16. T. A. Brun, H. S. Goan, *Phys. Rev. A* **68**, 032301 (2003).
17. H. Gassmann, M. S. Choi, H. Yi, C. Bruder, *Phys. Rev. B* **69**, 115419 (2004).
18. For measurement setups 1 and 2, we estimate the average magnitude of the lateral gradient to be $\sim 1.7 \times 10^5$ T m^{-1}.

19. Materials and methods are available as supporting material on *Science* Online.
20. We thank J. Sidles, K. Holczer, and A. Hero for discussions and D. Pearson and M. Sherwood for technical assistance. This work was supported by the Defense Advanced Research Projects Agency Three-Dimensional Atomic-Scale Imaging program administered through the U.S. Army Research Office.

Supporting Online Material
www.sciencemag.org/cgi/content/full/307/5708/408/DC1
Materials and Methods
Figs. S1 and S2
References

25 October 2004; accepted 15 December 2004
10.1126/science.1106718

Slip-Rate Measurements on the Karakorum Fault May Imply Secular Variations in Fault Motion

M.-L. Chevalier,[1,2] F. J. Ryerson,[2]* P. Tapponnier,[1] R. C. Finkel,[2] J. Van Der Woerd,[3] Li Haibing,[4] Liu Qing[5]

Beryllium-10 surface exposure dating of offset moraines on one branch of the Karakorum Fault west of the Gar basin yields a long-term (140- to 20-thousand-year) right-lateral slip rate of ~10.7 ± 0.7 millimeters per year. This rate is 10 times larger than that inferred from recent InSAR analyses (~1 ± 3 millimeters per year) that span ~8 years and sample all branches of the fault. The difference in slip-rate determinations suggests that large rate fluctuations may exist over centennial or millennial time scales. Such fluctuations would be consistent with mechanical coupling between the seismogenic, brittle-creep, and ductile shear sections of faults that reach deep into the crust.

The Karakorum Fault in Tibet is the main Quaternary right-lateral fault north of the Himalayas. Determining its past and present motion is critical to understanding the kinematics of Asian continental deformation and the rheology of the continental lithosphere (*1*, *2*). The fault trends roughly parallel to the western Himalayan range, extending from at least Kailas to the Pamirs, a length of >1200 km (Fig. 1). Its Quaternary slip rate remains poorly constrained, compared to that of other large faults in Asia such as Kunlun, Haiyuan, and Altyn Tagh (*3*–*5*). Previous attempts to determine the rate have produced disparate values ranging from 1 to 30 mm/year (*2*, *6*–*11*). Such disparities may result from the different techniques applied and time periods observed, the part of the fault investigated, or its complex geometry, which displays multiple splays with oblique slip (*12*). We present measurements of the Mid- to Late Pleistocene slip rate on the southern stretch of the fault, based on ^{10}Be surface exposure dating of two moraine crests displaced by the fault at the Manikala glacial valley terminus (32°2.529′N, 80°1.212′E, 4365 to 4760 m above sea level) (Figs. 1 and 2).

[1]Laboratoire de Tectonique, Mécanique de la Lithosphère, Unité Mixte de Recherche (UMR) 7578, CNRS, Institut de Physique du Globe de Paris, 75252 Paris Cedex 05, France. [2]Insitute of Geophysics and Planetary Physics, Lawrence Livermore National Laboratory, Livermore, CA 94550, USA. [3]Institut de Physique du Globe de Strasbourg, UMR 7516, CNRS, Strasbourg, France. [4]Laboratory of Continental Dynamics, Institute of Geology, Chinese Academy of Geological Sciences, Beijing 100037, China. [5]Total Exploration China, Total-Fina-Elf, Beijing, 100004, China.

*To whom correspondence should be addressed. E-mail: ryerson@llnl.gov

The Manikala moraine complex lies at the base of the faulted Ayilari range front, which bounds the west side of the Gar valley, a large pull-apart basin floored by marshland that hides other strands of the Karakorum Fault system (*13*) (Fig. 1). The moraines, M1 and M2, lie southeast of the U-shaped Manikala Valley, a glacial trough deeply entrenched into the range's igneous basement (Fig. 2 and fig. S1). The range front is marked by triangular facets as high as 800 m that testify to a normal component of slip on the fault. The principal strand of the fault shows discrete right-lateral offsets (10 ± 2 m, 35 ± 5 m, and 75 ± 5 m) of young rills of different depths, incised into postglacial colluvium (fig. S1). Within the till complex, two main groups of moraines are recognized (Fig. 2 and fig. S2). All were emplaced by the Manikala Daer glacier, whose terminus is today ~7 km upstream. The morphology of the moraines indicates that they correspond to major advances of the glacier and were later abandoned when the glacier retreated upstream (fig. S3).

The relative ages of the moraine groups can be qualitatively assessed from their surface characteristics (Fig. 2 and fig. S2). The M1 surface is rough and composed of chaotically distributed, imbricate blocks (as large as 3 m in diameter) surrounded by coarse debris. The smoother surface of M2 appears older, with blocks (tens of centimeters to a meter in diameter) protruding above a mantle of smaller debris (Fig. 2 and fig. S2). The morainic ridges thus appear to become younger from east to west, consistent with right-lateral motion on the fault.

The M2 moraine complex is divided into eastern and western sections (M2E and M2W, respectively) by a deep, beheaded, flat-floored paleovalley that is truncated by the fault and flanked by well-defined lateral moraines (Fig. 2). The crest of the lateral moraine east of the paleovalley is well preserved, and its eastern edge extends to the base of the faceted range front. There is no catchment on the mountain slope facing this valley, indicating that it must correspond to a former channel of the Manikala glacier (Fig. 2 and fig. S3). The youngest moraine group, M1 (Fig. 2), is the only one present on both sides of the Manikala outwash valley and displays well-preserved terminal lobes and sharply defined ridge crests.

Upstream from the fault, the limits of glacial incision reach the base of the triangular facets that border the Manikala valley. Downstream, the M1 and M2E moraine ridge crests extend linearly to the fault and, when realigned with the sharp edge of glacial bedrock incision south of the fault, provide the only piercing points accurate enough to obtain offset estimates (*14*) (Fig. 2 and fig. S4). Once restored from satellite images, the M1 and M2E offsets are 220 ± 10 m and 1520 ± 50 m, respectively. Another moraine complex with morphologically similar surfaces and offsets is found at the terminus of the Tajiang Daer glacial valley ~10 km to the west (fig. S3), lending additional support to this reconstruction (fig. S4).

^{10}Be model ages for samples collected along the moraine ridge crests (Fig. 2B) define consistent age clusters that can be used to date their abandonment (*15*). Ages on the two M2 ridges (Fig. 3) fall mostly between 103 and 204 thousand years (ky) (15 samples; mean age, 152 ± 28 ky), with a subset of seven samples between 132 and 150 ky old (mean age, 140 ± 5.5 ky). Samples WG-3, WG-4, and WG-7, on the eastern moraine (M2E), are more than 55 ky older than the main M2E population (132 to 150 ky old). We consider these three samples to be outliers, probably originating from more ancient till upstream. Examination of the M2 population with the outliers excluded reveals two distinct subgroups: a younger cluster of nine samples with ages of 103 to 149 ky (mean age, 133 ± 15 ky) and an older group of six samples of 160 to 204 ky (mean age, 181 ± 14 ky). The nine samples from the M1 moraine yield a younger mean age of 35 ± 9 ky. Seven samples fall between 36 and 45 ky (mean age, 40 ± 3 ky), and two distinctly younger samples have ages of 21 ± 1.0 ky.

The peaks in the overall M1-M2 age distribution correspond to the coldest periods (~19, 36, 151, and 182 ka) as derived from proxy paleotemperature records, such as the SPECMAP $\partial^{18}O$ curve (*16*) (Fig. 3B), and hence to maximal glacial advances. In particular, 140 ± 5.5 ky (the younger M2 age group) corresponds roughly to the glacial maximum at the end of Marine Isotope Stage (MIS) 6 [150 to 140 ky ago (ka)], 40 ± 3 ky (the older M1 subgroup) to the cold period at the end of MIS 3 (~40 ka), and 21 ± 1.0 ky (WG-14 and WG-16 on M1) to the Last Glacial Maximum (LGM) (19 ka). The ~20- and ~40-ka advances are documented in the western Himalayas and Pakistan (*17*, *18*). The correlation implies that the mean ages obtained for the M1 and M2 moraines are not affected by erosion or snow cover. Cosmic-ray exposure before deposition and surface processes, coupled with the right-lateral fault motion of the till surfaces north of the fault (M2W, in particular) relative to the glaciers to the south, may contribute to the dispersion of the ages on M2. The oldest ^{10}Be ages on M2E suggest that it was emplaced during the major glacial advance at the beginning of MIS 6, whereas the youngest ages on M2E are consistent with abandonment ~140 ka, at the beginning of the Eemian interglacial (Fig. 3). The bulk of the ages on the younger M1 moraine are consistent with emplacement at ~40 ka. However, the younger ages on this surface suggest that it was not abandoned until the onset of post-LGM warming after ~20 ka.

Matching the 1520 ± 50 m offset of the M2E lateral moraine with the sample ages that approximate the end of the MIS 6 glacial maximum (140 ± 5.5 ka) yields an average slip rate of 10.9 ± 0.6 mm/year. Likewise, matching the 220 ± 10 m offset of M1 with the age of the M1 LGM samples (21 ± 1.0 ky) yields a rate of 10.5 ± 0.5 mm/year. In contrast, if we associate the measured offsets with the older ages for samples on the M2E and M1 moraines (181 ± 14 and 40 ± 3 ky, respectively), we obtain disparate rates of 8.4 ± 0.8 and 5.5 ± 0.5 mm/year, respectively (fig. S5). Reconciling these rates would imply a rate of ~9.2 mm/year between 181 and 40 ka and a factor of two recent velocity decreases without any plausible, independent tectonic justification. We conclude, therefore, that a Mid- to Late Pleistocene right-lateral slip rate of 10.7 ± 0.7 mm/year on this segment of the Karakorum Fault is most probable. The total rate of displacement between southwest-

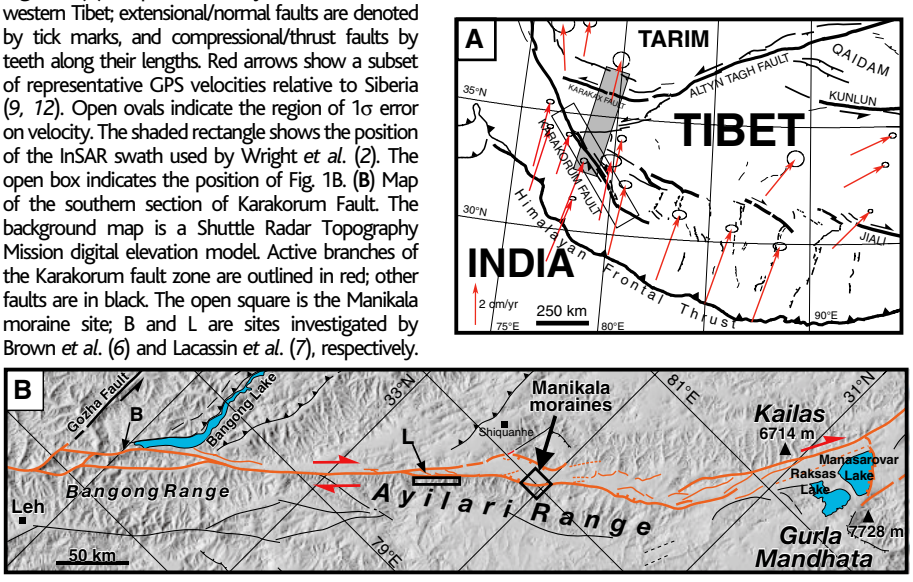

Fig. 1. (**A**) Map of the major active faults of western Tibet; extensional/normal faults are denoted by tick marks, and compressional/thrust faults by teeth along their lengths. Red arrows show a subset of representative GPS velocities relative to Siberia (*9*, *12*). Open ovals indicate the region of 1σ error on velocity. The shaded rectangle shows the position of the InSAR swath used by Wright *et al.* (*2*). The open box indicates the position of Fig. 1B. (**B**) Map of the southern section of Karakorum Fault. The background map is a Shuttle Radar Topography Mission digital elevation model. Active branches of the Karakorum fault zone are outlined in red; other faults are in black. The open square is the Manikala moraine site; B and L are sites investigated by Brown *et al.* (*6*) and Lacassin *et al.* (*7*), respectively.

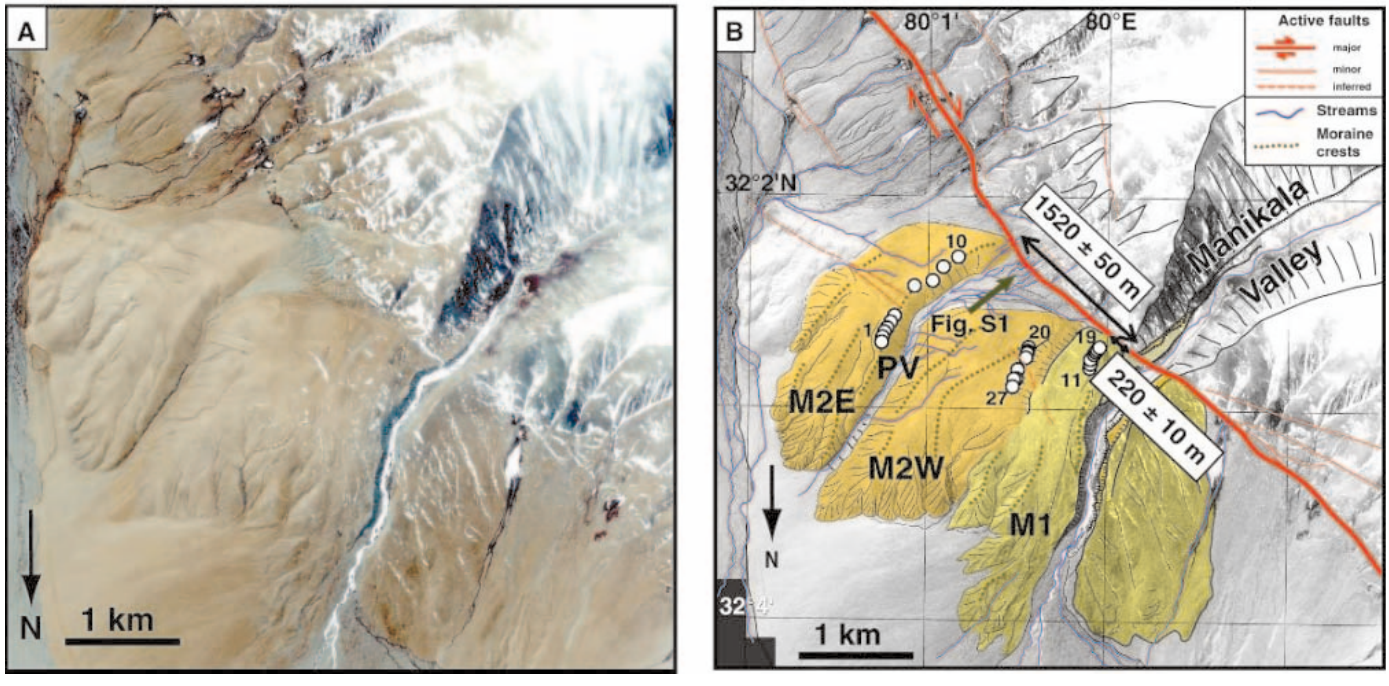

Fig. 2. (**A**) IKONOS satellite image of abandoned Manikala glacier moraines offset by Karakorum Fault. Present-day Manikala glacier outwash is represented by the frozen stream (narrow white feature) cutting across the moraines north of the fault. The abandoned glacial channel (PV, the paleovalley of Manikala glacier) is east of the Manikala outwash. (**B**) Map of offset moraines (yellow, M1; orange, M2) and sample locations (circles with numbers). Thin lines outline main geomorphic features. Moraines M1 and M2E are offset ~220 and 1520 m, respectively (offset restorations are given in figs. S3 and S4).

ern Tibet and the western Himalayas ought to be greater, because the normal component of throw on the main fault must be taken into account, along with slip accommodated on other active fault strands within and on the opposite side of the Gar pull-apart basin. These features have not been reported on at present.

At the 2σ level, the millennial slip rate (10.7 ± 1.4 mm/year) derived from the Manikala moraines is larger than that (1 ± 6 mm/year) inferred from the latest interferometric synthetic aperture radar (InSAR) study of western Tibet (*2*) (table S2). It is also almost three times larger than the morphochronologic rate of 4 ± 1 mm/year determined north of Bangong Lake (*6*), which also must be considered a minimum value because it only samples the northern of the two strands of the fault at this longitude (Fig. 1).

The slip-rate determinations at the Manikala glacial site sample many earthquake cycles. Hence, the effects of interseismic strain or postseismic relaxation on this measurement are largely restricted to the time interval since the last major earthquake and are therefore minimized. Two offsets of different ages yield a result consistent with eastsoutheastwards motion of western Tibet at an average long-term rate of at least ~10 mm/year relative to the western Himalayas over the past 150 ky. The extent to which such motion reflects slip partitioning in the western Himalaya–Karakorum Fault system or extrusion of Tibet between the converging India and Tarim plates cannot be decided without additional kinematic constraints from the region between the Karakorum and Karakax faults (Fig. 1).

For the time being, we cannot rule out the possibility that the lack of a decadal InSAR displacement signal across the Karakorum Fault results from tropospheric effects, which, because of the strong Asian monsoon and exceptional topography, have been shown to be markedly seasonal in northern Tibet (*19*) and which remain poorly understood over the rest of the plateau. In this connection, the Global Positioning System (GPS) geodetic rate found by Banerjee *et al.* (*10*), although based on only one station 20 km north of the fault (Shiquanhe station), is 11 ± 4 mm/year (table S2), which is compatible with our millennial geomorphic rate and agrees with the geological rate of Lacassin *et al.* (*7*), 10 ± 3 mm/year averaged over 25 to 35 million years (Fig. 1).

If the observed disparity is real, the variation in rate must be related to fault zone mechanics and measurement interval. Deformation profiles across strike-slip faults measured geodetically can vary through the earthquake cycle depending on the rheology of the crust and mantle below the seismogenic zone (*20–22*). Geodetic rates derived from standard dislocation models (*2*, *10*) are sensitive to these variations and may underestimate slip rates, particularly if the fault is late in its earthquake cycle. Kinematic compatibility constraints and recent observations suggest that strike-slip faults that intersect, such as the Garlock/San Andreas (*23*) and East/North Anatolian (*24*), might be prone to slip-rate fluctuations over time scales longer than the typical seismic cycle. The Karakorum and Altyn Tagh faults also intersect and have not ruptured in large earthquakes since the inception of instrumental seismology; the decadal and millennial slip rates on the central Altyn Tagh fault differ by a factor of three (*5*, *25–27*). On the basis of three-dimensional paleoseismology at Wrightwood, California, Weldon *et al.* (*28*) show that the slip rate on the San Andreas Fault varied between 8.9 and 2.4 cm/year over the past 2,000 years, spanning 14 seismic cycles. Complementary, long-term variations in slip rates appear to have existed between the San Andreas and San Jacinto faults since 1.5 million years ago (*29*). On the basis of emerging data, we thus conclude that secular variations in slip rate may be the rule, rather than the exception, on most faults, and that geodetic and geologic data need not be in agreement.

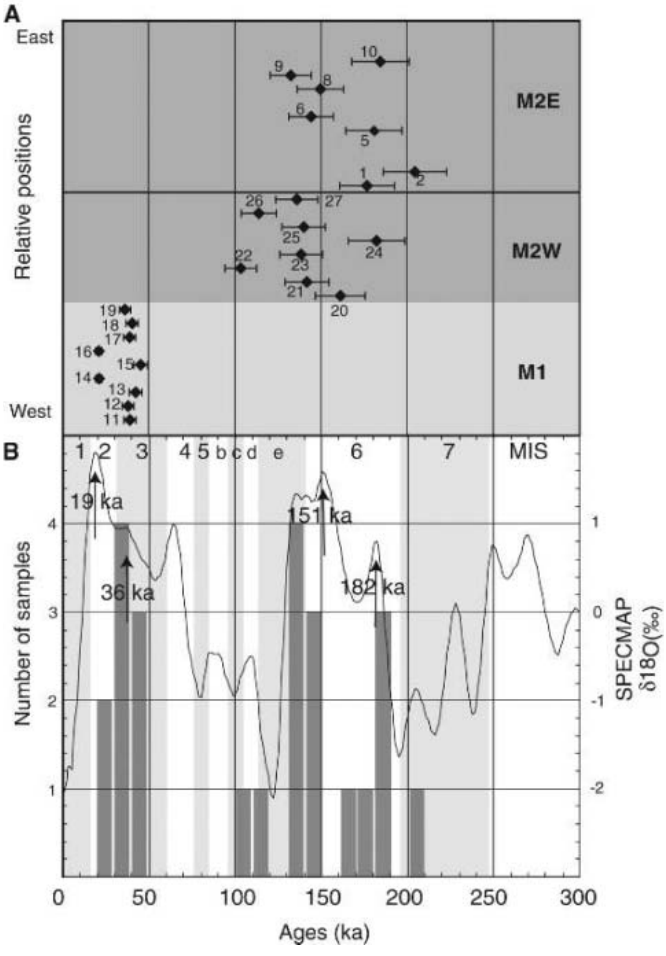

Fig. 3. (**A**) ^{10}Be exposure ages of blocks sampled along the M1 and M2 moraine crests (numbers refer to Fig. 2B and table S1). (**B**) Comparison of the distribution of sample ages (10-ky bins) with the SPECMAP δ^{18}O proxy climate curve (*16*) shows a simple correlation of main moraine emplacement periods with MIS 2 (the LGM), MIS 3, and the coldest parts of MIS 6. (δ^{18}O increases during glacial advances as ^{16}O is preferentially sequestered in the polar ice caps.)

References and Notes

1. J. P. Avouac, P. Tapponnier, *Geophys. Res. Lett.* **20**, 895 (1993).
2. T. J. Wright, B. Parsons, P. C. England, E. J. Fielding, *Science* **305**, 236 (2004).
3. J. Van der Woerd *et al.*, *Geophys. J. Int.* **148**, 356 (2002).
4. C. Lasserre *et al.*, *J. Geophys. Res.* **107**, art. no. 2276 (2002).
5. A. Mériaux *et al.*, *J. Geophys. Res.* **109**, art. no. B06401 (2004).
6. E. T. Brown *et al.*, *J. Geophys. Res.* **107**, art. no. 2192 (2002).
7. R. Lacassin *et al.*, *Earth Planet. Sci. Lett.* **219**, 255 (2004).
8. Q. Liu, thesis, Université Paris VII (1993).
9. Q. Wang *et al.*, *Science* **294**, 574 (2001).
10. P. Banerjee, R. Burgmann, *Geophys. Res. Lett.* **29**, art. no. 1652 (2002).
11. M. A. Murphy *et al.*, *Geol. Soc. Am. Bull.* **114**, 428 (2002).
12. P. Zhang *et al.*, *Geology* **32**, 809 (2004).
13. R. Armijo, P. Tapponnier, H. Tonglin, *J. Geophys. Res.* **94**, 2787 (1989).
14. A piercing point is the intersection of a fault with linear landscape features such as abandoned stream channels, terrace risers, or morainic ridges that have been cut and offset by fault motion. We estimated the errors on the offset determinations by translating the opposing sides of the fault until an obvious visual mismatch of the relevant piercing points was observed. Because the spatial resolution of the IKONOS satellite imagery used in this study is 1 m,

the resulting error estimates are dominated by the width of the features used and become larger (in absolute terms) as the features become older. The crests of M1 and M2 are 10 m and 50 m wide, respectively, at their widest in the field and on the satellite images.
15. Sampling was performed in September 2001. Samples were typically well-embedded blocks of vein quartz ~20 cm in diameter or, occasionally, chips removed from exposed parts of larger samples. Beryllium extraction procedures and production rate calculations follow those described by Mériaux *et al*. (*5, 30*). The ratios of cosmogenic ^{10}Be to stable isotope ^{9}Be were determined by accelerator mass spectrometry at the Lawrence Livermore National Laboratory Center for Accelerator Mass Spectrometry.
16. J. Imbrie *et al.*, in *Milankovitch and Climate, Part I*, A. Berger, J. Imbrie, J. Hays, G. Kukla, B. Saltzman, Eds. (Reidel, Boston, 1984), pp. 269–305.
17. R. C. Finkel, L. A. Owen, P. L. Barnard, M. W. Caffee, *Geology* **31**, 561 (2003).
18. L. A. Owen *et al.*, *Geol. Soc. Am. Bull.* **115**, 1356 (2003).
19. C. Lasserre, G. Peltzer, F. Crampe, *Eos* **42**, F271 (2001).
20. P. Segall, *Int. Geol. Rev.* **44**, 62 (2002).
21. J. C. Savage, W. H. Prescott, *J. Geophys. Res.* **83**, 3369 (1978).
22. H. Perfettini, J. P. Avouac, *J. Geophys. Res.* **109**, art. no. B06402 (2004).
23. G. Peltzer, F. Crampe, S. Hensley, P. Rosen, *Geology* **29**, 975 (2001).
24. A. Hubert-Ferrari *et al.*, *Geophys. J. Int.* **153**, 111 (2003).
25. R. Bendick, R. Bilham, J. Freymueller, K. Larson, G. H. Yin, *Nature* **404**, 69 (2000).
26. K. Wallace, G. H. Yin, R. Bilham, *Geophys. Res. Lett.* **31**, art. no. L09613 (2004).
27. A. Mériaux *et al.*, *J. Geophys. Res.*, in press.
28. R. Weldon, K. Scharer, T. Fumal, G. Biasi, *GSA Today* **14**, 4 (2004).
29. R. A. Bennett, A. M. Friedrich, K. P. Furlong, *Geology* **32**, 961 (2004).
30. Materials and methods are available as supporting material on *Science* Online.
31. This work was performed under the auspices of the U.S. Department of Energy by University of California Lawrence Livermore National Laboratory under contract W-7405-Eng-48 under the sponsorship of the Laboratory Directed Research and Development program (report no. UCRL-JRNL-206541). Also supported by the Institut National des Sciences de l'Univers, Centre National de la Recherche Scientifique (Paris, France), through programs Imagerie et Dynamique de la Lithosphère and Intérieur de la Terre, and by the China Earthquake Administration and the Ministry of Lands and Resources (Beijing, China).

Supporting Online Material
www.sciencemag.org/cgi/content/full/307/5708/411/DC1
Materials and Methods
Figs. S1 to S5
Tables S1 to S2
References and Notes

21 September 2004; accepted 15 December 2004
10.1126/science.1105466

Speciation by Distance in a Ring Species

Darren E. Irwin,[1]* Staffan Bensch,[2] Jessica H. Irwin,[1] Trevor D. Price[3]

Ring species, which consist of two reproductively isolated forms connected by a chain of intergrading populations, have often been described as examples of speciation despite gene flow between populations, but this has never been demonstrated. We used amplified fragment length polymorphism (AFLP) markers to study gene flow in greenish warblers (*Phylloscopus trochiloides*). These genetic markers show distinct differences between two reproductively isolated forms but gradual change through the ring connecting these forms. These findings provide the strongest evidence yet for "speciation by force of distance" in the face of ongoing gene flow.

Traditional models emphasize geographic separation as a necessary prerequisite to speciation (*1*, *2*). Although experiments and theory indicate that species can form despite ongoing gene flow (*3–5*), there are very few known examples in nature (*2*). Some studies have demonstrated divergence despite gene flow (*6*, *7*), but they do not enable an assessment of reproductive isolation because the divergent forms remain geographically separated. Species are usually defined as groups of interbreeding populations reproductively isolated from other such groups (*1*, *2*), and this can only be critically examined if different populations regularly come into contact in nature.

There are a few examples where reproductively isolated populations coexist while being connected by apparently gradual variation around geographic barriers ["ring species"; reviewed in (*8*)]. In theory, ring species enable us to trace the process by which one species diverges into two. They also potentially show that reproductive isolation can arise in the face of gene flow (*1*, *8–10*). However, a clear pattern of a gradual genetic variation has not previously been observed in a ring species. Here, we use molecular markers to show that two reproductively isolated forms of greenish warbler (*Phylloscopus trochiloides*) are connected by gene flow through a ring of populations, providing the strongest empirical evidence yet for "speciation by force of distance" (*1*, *9*).

Two forms of greenish warbler, one in west Siberia (*P. t. viridanus*) and one in east Siberia (*P. t. plumbeitarsus*; Fig. 1), coexist without interbreeding in central Siberia and can therefore be considered separate species (*10*). These forms are connected by a chain of populations to the south that encircles the high-altitude desert of the Tibetan Plateau, which is not inhabited by the warblers. Through this chain of populations, traits such as color patterns, morphology, and behaviors (song and song recognition), change gradually, demonstrating a smooth gradient in forms between two species (*10*, *11*). There is evidence that all of these traits are under selection in the *Phylloscopus* warblers (*10–15*); it is therefore unclear that such traits can be used to infer gene flow. To directly measure genome-wide genetic relationships, we used amplified fragment length polymorphism (AFLP) markers (*16*).

From 105 greenish warblers at 26 sites throughout the breeding range we obtained 62 AFLP markers that were variable and could be scored unambiguously as present or absent in each individual (*17*). West Siberian *viridanus* and east Siberian *plumbeitarsus* are clearly separated in AFLP genotypes, which confirms that the two taxa are genetically distinct. In contrast, AFLP genotypes change gradually through the ring of populations to the south (Fig. 1). The genetic gradient in the AFLP genotypes around the southern ring of populations is best seen in a plot of pairwise AFLP distances versus pairwise geographic distance (Fig. 2). Geographic distances were measured under the assumption that no genes flow across the uninhabited area in the center of the ring or between *viridanus* and *plumbeitarsus* in central Siberia. Thus, "corrected" distances between west Siberian (*viridanus*) and east Siberian (*plumbeitarsus*) populations were measured through the long chain of populations running to the south of Tibet, through the Himalayas. Genetic distance and corrected geographic distance are strongly correlated (Mantel's $r = 0.782$, $P = 0.0003$), consistent with a pattern of isolation by distance (*18*) around the ring. An alternative analysis based on pairwise F_{ST} distances between populations produces similar results (Mantel's $r = 0.677$, $P = 0.0012$; table S1 and fig. S3).

On the basis of these results, we conclude that there is no break in gene flow through the ring of populations, except between the divergent forms *viridanus* and *plumbeitarsus* in central Siberia. Thus all populations have been recently connected by at least some gene

[1]Department of Zoology, University of British Columbia, 6270 University Boulevard, Vancouver, BC, Canada V6T 1Z4. [2]Department of Animal Ecology, Lund University, S-223 62 Lund, Sweden. [3]Department of Ecology and Evolution, University of Chicago, 1101 E. 57th Street, Chicago, IL 60637, USA.

*To whom correspondence should be addressed. E-mail: irwin@zoology.ubc.ca

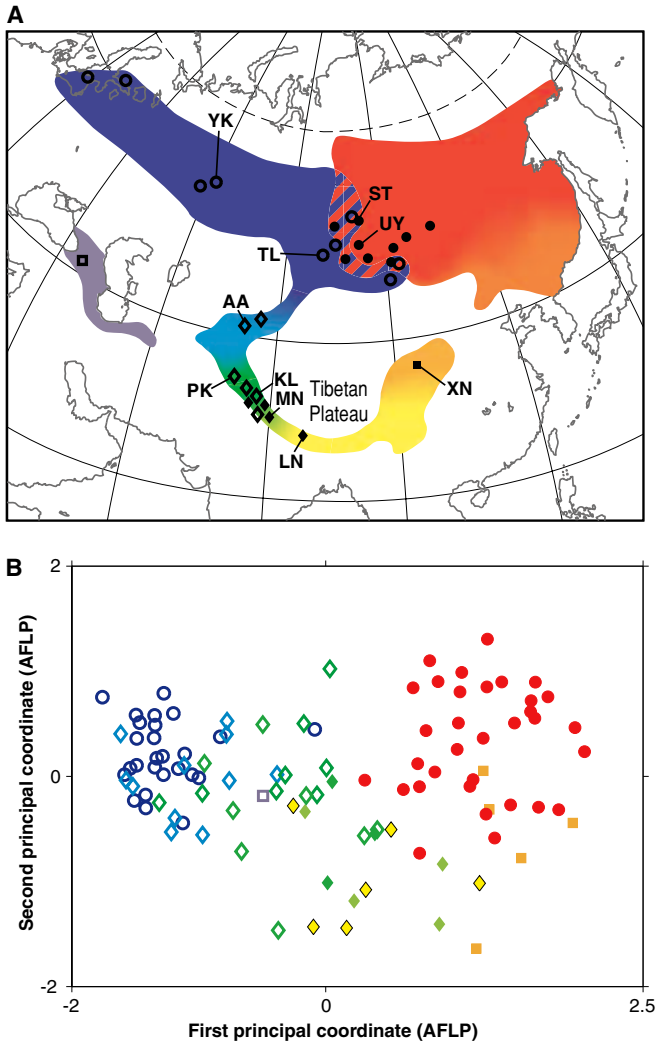

Fig. 1. (A) Map of Asia showing the range of greenish warblers in the breeding season. Different colors represent different subspecies as designated by Ticehurst (*20*) (*P. t. viridanus*, blue; *ludlowi*, green; *trochiloides*, yellow; *obscuratus*, orange; *plumbeitarsus*, red; and *nitidus*, violet). Colors grade together in areas where Ticehurst described gradual morphological change. The hatched area in central Siberia indicates the overlap zone between *viridanus* and *plumbeitarsus*. The gap in the ring in northern China is likely due to recent habitat destruction (*10*). Sampling sites are indicated by symbols corresponding to major mitochondrial clades [open symbols indicate western clade, and closed symbols eastern, see fig. S1 and (*10*)], with the most important sites indicated by two-letter codes. (B) Geographic variation in 62 AFLP markers as summarized by principal coordinates analysis. Each symbol represents a single individual, and distance between symbols corresponds roughly to genetic distance. Colors and symbols correspond to (A). Although the northern subspecies *viridanus* and *plumbeitarsus* differ distinctly in their genetic characteristics, there is gradual genetic change through the southern chain of populations. PC1 explains 19.4% of the variance, PC2 5.6%.

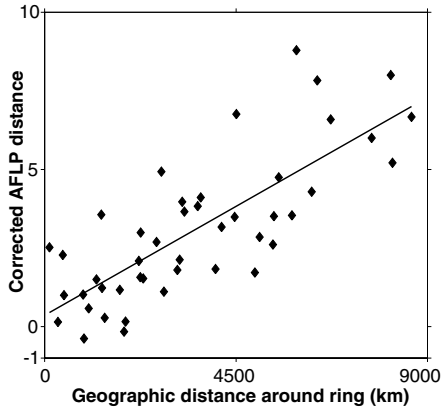

Fig. 2. Genetic distance based on AFLP markers increases with geographic distance measured around the southern ring (that is, if one assumes no direct gene flow between *viridanus* and *plumbeitarsus* or across the uninhabited area in the center of the ring). Corrected average pairwise distances between populations were calculated as the mean number of pairwise differences between two populations minus the average distance between individuals within those populations. For purposes of illustration, a least-squares regression line is fit to all points.

flow. The simplest historical scenario for this result is that short-distance dispersal in a continuously distributed species has resulted in a pattern of isolation by distance (*18*).

This interpretation may at first seem inconsistent with previously published patterns of variation in mitochondrial DNA (mtDNA) (*10*) (fig. S1), in which there are several deep phylogeographic breaks around the ring, the deepest of which is in the western Himalayas. In fact, the mtDNA and AFLP patterns are compatible. Short-distance dispersal in a continuously distributed species is expected to cause phylogeographic structuring in mtDNA clades (*19*) and a pattern of isolation by distance in AFLP markers (*18*). The shape of the greenish warbler range is particularly suited to creating this pattern; the birds breed in a narrow string of treeline habitat through the Himalayas, where dispersal distances are likely shorter than in more broadly distributed forest habitat further north. Ticehurst (*20*) hypothesized that the greenish warblers were at one time confined to the Himalayas and then expanded northward along two pathways into Siberia. Theory predicts that the pattern of isolation by distance should be weaker in regions of recent range expansion compared with regions that have been inhabited over a long period of time (*18*). The steeper genetic change seen in AFLPs (figs. S2 and S3), mtDNA, and two microsatellite loci (*10*) through the Himalayas than through regions to the north is consistent with this prediction. It is also possible that these patterns were influenced by temporary breaks in gene flow due to geographic barriers in the Himalayas; however, such barriers, if they existed, did not cause reproductive isolation to evolve in that region.

Greenish warblers provide the only known example of a smooth genetic gradient between two genetically differentiated and reproductively isolated forms, providing rare insight into how speciation can occur. Patterns of variation in ecologically and sexually selected traits of greenish warblers suggest that latitudinal gradients in environmental characteristics, such as forest density and seasonal migration distance, during the two northward expansions into Siberia have resulted in rapid evolutionary adaptation, divergence, and reproductive isolation (*8*, *10*, *11*).

Several authors (*4*, *21*) have suggested on theoretical grounds that ring species or "sexual continua" are unstable and will fairly quickly break into two or more species that do not exchange genes. The two models that show this effect do not apply well to the greenish warbler, because one (*4*) does not include local adaptation throughout a continuous geographic range and the other (*21*) does not include different geographic locations for different populations. We suggest that ring species such as the greenish warbler, in which local adaptation occurs along a long and nearly continuous ring of populations, could be stable indefinitely. This stability could be interrupted by processes such as habitat change, which could increase the likelihood of parapatric speciation (*5*), or habitat destruction, which could divide the continuous range and thereby increase the likelihood of additional species boundaries forming.

References and Notes

1. E. Mayr, *Systematics and the Origin of Species* (Dover Publications, New York, 1942).
2. J. A. Coyne, H. A. Orr, *Speciation* (Sinauer Associates, Sunderland, MA, 2004).
3. W. R. Rice, E. E. Hostert, *Evolution* **47**, 1637 (1993).
4. S. Gavrilets, H. Li, M. D. Vose, *Proc. R. Soc. London B Biol. Sci.* **265**, 1483 (1998).
5. M. Doebeli, U. Dieckmann, *Nature* **421**, 259 (2003).
6. T. B. Smith, R. K. Wayne, D. J. Girman, M. W. Bruford, *Science* **276**, 1855 (1997).

7. C. J. Schneider, T. B. Smith, B. Larison, C. Moritz, *Proc. Natl. Acad. Sci. U.S.A.* **96**, 13869 (1999).
8. D. E. Irwin, J. H. Irwin, T. D. Price, *Genetica* **112-113**, 223 (2001).
9. T. Dobzhansky, in *A Century of Darwin*, S. A. Barnett, Ed. (Heinemann, London, 1958), pp. 19–55.
10. D. E. Irwin, S. Bensch, T. D. Price, *Nature* **409**, 333 (2001).
11. D. E. Irwin, *Evolution* **54**, 998 (2000).
12. A. D. Richman, T. Price, *Nature* **355**, 817 (1992).
13. K. Marchetti, *Nature* **362**, 149 (1993).
14. A. V. Badyaev, E. S. Leaf, *Auk* **114**, 40 (1997).
15. K. Marchetti, T. Price, *Oikos* **79**, 410 (1997).
16. U. G. Mueller, L. L. Wolfenbarger, *Trends Ecol. Evol.* **14**, 389 (1999).
17. Materials and methods are available as supporting material on *Science* Online.
18. M. Slatkin, *Evolution* **47**, 264 (1993).
19. D. E. Irwin, *Evolution* **56**, 2383 (2002).
20. C. B. Ticehurst, *A Systematic Review of the Genus* Phylloscopus (Johnson Reprint Corp., New York, 1938).
21. A. J. Noest, *Proc. R. Soc. London B. Biol. Sci.* **264**, 1389 (1997).
22. Supported by an International Research Fellowship grant from the National Science Foundation (to D.E.I.) and the Swedish Research Council (to S.B.) plus grants for fieldwork by the National Geographic Society and National Science Foundation (to T.D.P.). We thank Z. Benowitz-Fredericks, J. Gibson, S. Gross, G. Kelberg, A. Knorre, K. Marchetti, and B. Sheldon for assistance in the field, and P. Alström, K. Marchetti, U. Olsson, A. Richman, J. Tiainen, and the Burke Museum for additional samples. R. Calsbeek, M. Whitlock, and several anonymous reviewers provided helpful comments.

Supporting Online Material
www.sciencemag.org/cgi/content/full/307/5708/414/DC1
Materials and Methods
Figs. S1 to S3
Table S1
References

14 September 2004; accepted 17 November 2004
10.1126/science.1105201

Large Sulfur Bacteria and the Formation of Phosphorite

Heide N. Schulz[1]* and Horst D. Schulz[2]

Phosphorite deposits in marine sediments are a long-term sink for an essential nutrient, phosphorus. Here we show that apatite abundance in sediments on the Namibian shelf correlates with the abundance and activity of the giant sulfur bacterium *Thiomargarita namibiensis*, which suggests that sulfur bacteria drive phosphogenesis. Sediments populated by *Thiomargarita* showed sharp peaks of pore water phosphate (≤300 micromolar) and massive phosphorite accumulations (≥50 grams of phosphorus per kilogram). Laboratory experiments revealed that under anoxic conditions, *Thiomargarita* released enough phosphate to account for the precipitation of hydroxyapatite observed in the environment.

The formation of phosphorites in marine sediments is a major long-term sink for phosphorus, removing it from the biosphere. The initial step in phosphorite formation is the precipitation of phosphate-containing minerals, for example, hydroxyapatite, followed by many other processes such as sediment transport, winnowing, and re-crystallization (*1*, *2*). A fundamental problem in explaining massive phosphorite deposits has been identifying mechanisms that can concentrate pore water phosphate enough to drive spontaneous precipitation of phosphorus minerals. Here we suggest a new mechanism, the episodic release of phosphate into the anoxic sediment by an abundant benthic bacterium that is specially adapted to survive under both oxic and anoxic conditions. *Thiomargarita* periodically contacts oxic bottom water in order to take up nitrate, and it survives long intervals of anoxia with nitrate stored internally (*3*). The phosphate uptake from different sources occurs when *Thiomargarita* forms thick mats at the sediment surface or is suspended in the oxic water column.

The giant sulfur bacterium *Thiomargarita namibiensis* occurs in high biomass in surface sediments off the coast of Namibia (*3*). Like its close relatives *Beggiatoa* spp. and *Thioploca* spp., this bacterium gains energy by oxidizing sulfide, which accumulates in anoxic marine sediments as a result of the degradation of organic matter by sulfate-reducing bacteria. The production of sulfide is directly proportional to the amount of organic carbon in the sediment, thus these large sulfide-oxidizing bacteria are abundant in highly productive upwelling areas, where the flux of organic material to the sea floor is high. *Thiomargarita* and *Beggiatoa* dominate sediments beneath the Benguela upwelling area off Namibia (*3*), whereas *Thioploca* dominates sediments off the South American west coast (*4*) and in the Arabian Sea (*5*). In all of these areas, modern phosphorite formation has been reported (*1*, *6*). All of these sulfur bacteria species contain large amounts of intracellular polyphosphates, which we found by staining cells specifically for polyphosphate with toluidine blue (*7*, *8*). Also, these bacteria show electron-dense inclusions (*3*, *9*, *10*), which is a typical appearance of polyphosphate.

During an expedition with the German research vessel *Meteor* off the coast of Namibia in March 2003, we found high pore water phosphate concentrations (*7*) of up to 300 μM in sediments that were densely populated by *T. namibiensis* (Fig. 1A). The sharp phosphate peaks that were observed in sediments were restricted to a narrow sediment horizon (about 3 cm thick), which corresponded to the depths where *T. namibiensis* was most abundant (Fig. 1C). Because of the high phosphate concentrations, active formation of phosphorite occurred in this thin zone as indicated by the large amounts of phosphorus-containing minerals in the sediment (*7*) (>50 g kg^{-1} of dry sediment or 5% P) (Fig. 1B). The predominant phosphorus mineral phase was hydroxyapatite [$Ca_5OH(PO_4)_3$], which was determined by x-ray diffraction (XRD) analysis (*7*). Fifty grams of P per kg of sediment is equivalent to 270 g of hydroxyapatite per kg of sediment. Therefore, more than 25% of the solid phase in this layer was hydroxyapatite, which is one of the major

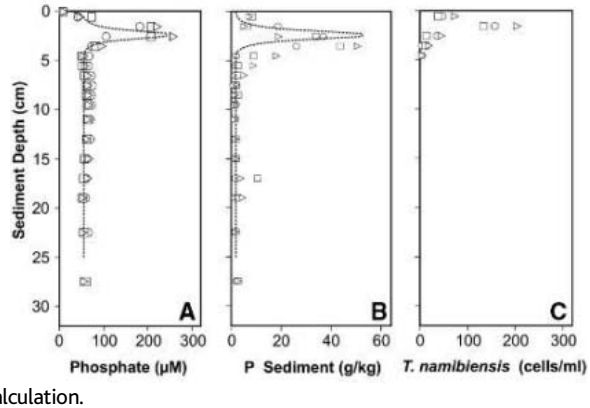

Fig. 1. Sediment profiles from the Namibian shelf (22°10′S, 14°03′E; water depth 70 m). (**A**) Phosphate concentrations in the pore water (μM) at different sediment depths (cm). (**B**) Phosphorus content of dried sediment (g kg^{-1}) at different sediment depths. (**C**) Biomass of *T. namibiensis* (cells ml^{-1}) at different sediment depths. Three parallel measurements are shown as indicated by the different symbols. The dashed lines show the steady-state concentration of pore water phosphate and the amount of phosphorus accumulating as predicted by the model calculation.

[1]Institute for Microbiology, University of Hannover, Schneiderberg 50, D-30167 Hannover, Germany. [2]Department of Geosciences, University of Bremen, Klagenfurter Strasse, D-28359 Bremen, Germany.

*To whom correspondence should be addressed. E-mail: schulz@ifmb.uni-hannover.de

mineral precursors in the formation of phosphorite deposits.

To gain a quantitative understanding of the measured pore water and solid phase-concentration profiles, we used a spreadsheet model similar to that of Schulz (*11*). Diffusive transport of phosphate [diffusion coefficient in sediment $D_{sed} = 4.1 \times 10^{-10}$ m^2 s^{-1} with a temperature of 11°C and a porosity of 0.9 for HPO_4^{2-} as a major species, following thermodynamic calculations (*12*)] was calculated for a one-dimensional (1D) column of 100 cells using an explicit numerical solution of Fick's laws of diffusion (*7*). Boundary conditions were 5 μM phosphate in the bottom water and precipitation of hydroxyapatite when concentrations exceeded 40 μM, which reflects saturation with respect to hydroxyapatite. Thus, the measured pore water profile of Fig. 1A reflects a steady-state situation for production of dissolved phosphate by the bacteria and simultaneous precipitation of hydroxyapatite. Fitting the model to the measured pore water concentration (Fig. 1A, dashed line) resulted in pairs of values; fast phosphate release and fast precipitation, or slow phosphate release and slow precipitation. Laboratory experiments on apatite precipitation as well as the calculation of the necessary diffusive calcium supply for this precipitation confined the range of plausible values for simultaneous release and precipitation of phosphate. As long as a near steady-state condition persisted for ~3 to 14 months, phosphate release rates between 20 (at 3 months) and 6 (at 14 months) nmol liter^{-1} s^{-1} would lead to the observed amounts of precipitated phosphorus in the sediment. (Fig. 1B). The shape of the curve of Fig. 1A, is matched by a phosphate release between 20 and 6 nmol liter^{-1} s^{-1}. Under these circumstances, 3 to 14 months of constant phosphate release would lead to the observed amounts of hydroxyapatite in the sediment (Fig. 1B, dashed line). In contrast, the dissolution of hydroxyapatite after a periodic release of phosphate would be much slower because it is controlled only by diffusion (*7*). *Thiomargarita* cells picked manually and incubated in artificial media in the laboratory (*7*) showed an increase in concentration between 0.011 and 0.028 pmol of phosphate liter^{-1} s^{-1} cell^{-1} with a mean value of 0.018 pmol of phosphate liter^{-1} s^{-1} cell^{-1} (Fig. 2). In comparison, the predicted phosphate release of 6 to 20 nmol of phosphate liter^{-1} s^{-1}, produced by 250 cells ml^{-1} counted in the field, equals an increase in concentration of 0.024 to 0.08 pmol liter^{-1} s^{-1} cell^{-1}. These data confirm that *T. namibiensis* alone could be responsible for the observed pore water phosphate peak and the resulting precipitation of hydroxyapatite.

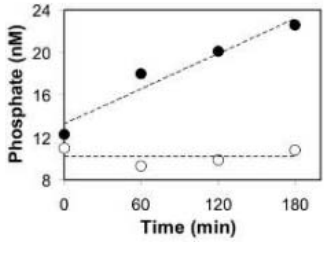

Fig. 2. Phosphate release under anoxic conditions from 50 cells of *T. namibiensis* after 24 hours of anaerobic preincubation, compared to a control (open circles) not containing *T. namibiensis*. Solid circles show mean values of three independent measurements. The single measurements are available in (*7*).

Polyphosphate occurs in nearly all living organisms (*13*), but only some bacteria and yeasts are capable of accumulating large amounts. Bacterial phosphate accumulation has been most thoroughly studied in wastewater treatment plants, where bacteria are used to remove phosphate. To initiate luxury uptake of phosphate by bacteria in a wastewater treatment plant, it is necessary to introduce an anaerobic phase whereby phosphate is released and acetate is taken up and stored, for example, in the form of polyhydroxyalkanoate (PHA). Acetate uptake and storage require energy which, in the absence of an electron acceptor, the bacteria can gain from the breakdown of polyphosphate and consequent release of phosphate. In the aerobic phase that follows, the polyphosphate-accumulating bacteria gain energy by oxidizing the stored carbon using oxygen as the electron acceptor, and they take up an excess of phosphate, which they store as polyphosphate (*14*, *15*). This results in a sludge rich in bacterial polyphosphate, which can be removed from the system.

Based on our incubation experiments, we hypothesize that the mechanisms of phosphate uptake and release in *T. namibiensis* are similar to that of polyphosphate-accumulating bacteria in wastewater, even though their main energy source is considered to be the oxidation of sulfide with nitrate or oxygen as the electron acceptor (*3*, *16*). In vitro, enhanced rates of phosphate release were induced under anaerobic conditions only when acetate was added to the medium. In addition to the many large sulfur globules that were observed in the cells, smaller inclusions were visible in differing amounts (Fig. 3, A and B). Specific staining (*7*) demonstrated that most of the smaller inclusions were polyphosphate (Fig. 3C). The remaining small inclusions did not stain with Nile red, a specific stain for PHA, but were stained dark brown with iodine (*17*) (Fig. 3D) suggesting that they consisted of glycogen or another polyglucose.

T. namibiensis appears to have a life mode that is unusual for marine bacteria. Under anoxic conditions, it takes up sulfide and, presumably, acetate, which appears to be stored as glycogen. Because there is an insufficient supply of a suitable external electron acceptor, internally stored nitrate and polyphosphate are sacrificed and sulfide is oxidized to elemental sulfur to gain energy. Under oxic conditions, the bacterium can gain energy from the oxidation of both sulfur and, presumably, glycogen. At the same time, it invests energy in the accumulation of polyphosphate and nitrate, the latter of which is stored in a central vacuole at concentrations of up to 0.8 M (*3*). Thus, *T. namibiensis* is able to take up each of these chemical compounds under conditions where the chemicals are readily available and use them under different redox conditions, when they are a valuable energy source that would otherwise be impossible to obtain at that time. The observation

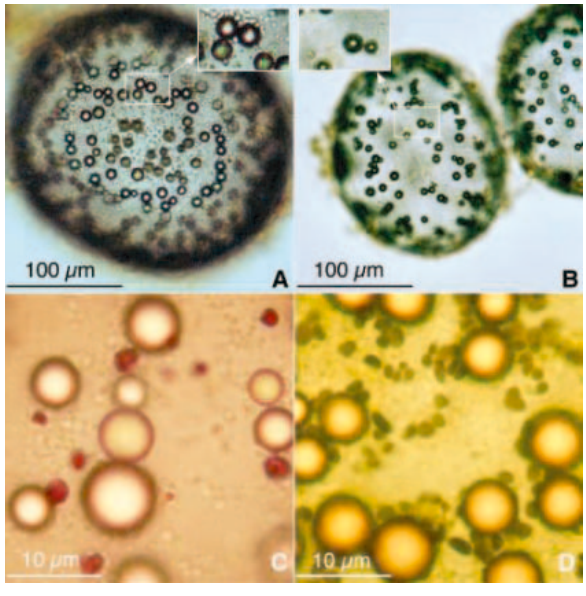

Fig. 3. *T. namibiensis*. (**A**) A single cell of *T. namibiensis* with many smaller inclusions apart from the large sulfur globules. Inset: higher magnification image of the inclusions. (**B**) A single cell of *T. namibiensis* with few smaller inclusions. Inset: higher magnification image of the inclusions. (**C**) Small inclusions stained dark red for polyphosphate with toluidine blue. Many unstained inclusions can be seen. (**D**) Small inclusions stained with iodine, showing a dark brown color typical for glycogen.

that phosphate release could be induced only when acetate was added to the medium shows that the breakdown of polyphosphate is an auxiliary metabolism, which explains why it occurs only episodically and why phosphorus does not continuously accumulate with increased depth.

A connection between polyphosphate-accumulating bacteria and phosphorite formation was proposed two decades ago (*2*, *18–20*). The main arguments in favor of a bacterial involvement were microfossils resembling sulfur bacteria enclosed in phosphorite deposits, for example, in the Miocene Monterey Formation (*18*), and the finding of low C:P ratios in recent *Beggiatoa* mats (*20*). Early diagenetic precipitation of phosphorite minerals has also been reported from the Santa Barbara Basin, where elevated pore water nitrate concentrations after sediment centrifugation suggest an involvement of large sulfur bacteria (*21*). There are also reports of phosphatized bacteria from the Namibian shelf (*22*), which seem to resemble *Thiomargarita*. Because recent phosphorite formation and high biomass of large sulfur bacteria largely occur in the same areas, phosphorite formation through the activity of large sulfur bacteria could be a widespread phenomenon and is likely to also have been important in the past.

References and Notes

1. K. B. Föllmi, *Earth Sci. Rev.* **40**, 55 (1996).
2. K. P. Krajewski *et al.*, *Eclogae Geol. Helv.* **87**, 701 (1994).
3. H. N. Schulz *et al.*, *Science* **284**, 493 (1999).
4. V. A. Gallardo, *Nature* **268**, 331 (1977).
5. R. Schmaljohann *et al.*, *Mar. Ecol. Prog. Ser.* **220**, 295 (2001).
6. S. J. Schenau, C. P. Slomp, G. J. DeLange, *Mar. Geol.* **169**, 1 (2000).
7. Materials and methods are available as supporting material on *Science* Online.
8. H. N. Schulz, data not shown.
9. S. Maier, H. Volker, M. Beese, V. A. Gallardo, *Can. J. Microbiol.* **36**, 438 (1990).
10. J. M. Larkin, M. C. Henk, *Microsc. Res. Tech.* **33**, 23 (1996).
11. H. D. Schulz, in *Marine Geochemistry*, H. D. Schulz, M. Zabel, Eds. (Springer-Verlag, Heidelberg, New York, 2000), pp. 417–442.
12. D. L. Parkhurst, C. A. J. Appelo, "User's guide to PHREEQC (Version 2)—A computer program for speciation, batch-reaction, one-dimensional transport, and inverse geochemical calculations" (U.S. Geological Survey, 1999); available at http://wwwbrr.cr.usgs.gov/projects/GWC_coupled/phreeqc/html/final.html.
13. A. Kornberg, *J. Bacteriol.* **177**, 491 (1995).
14. T. Mino, *Biochemistry* (*Mosc.*) **65**, 341 (2000).
15. M. C. M. van Loosdrecht, G. J. Smolders, T. Kuba, J. J. Heijnen, *Antonie Leeuwenhoek* **71**, 109 (1997).
16. H. N. Schulz, D. de Beer, *Appl. Environ. Microbiol.* **68**, 5746 (2002).
17. Lugol's stain: 40 g KI and 20 g I_2 per liter.
18. L. A. Williams, C. Reimers, *Geology* **11**, 267 (1983).
19. Y. Nathan, J. M. Bremner, R. E. Loewenthal, P. Monteiro, *Geomicrobiol. J.* **11**, 69 (1993).
20. C. E. Reimers, M. Kastner, R. E. Garrison, in *Phosphate Deposits of the World*, W. C. Burnett, S. R. Riggs, Eds. (Cambridge Univ. Press, Cambridge, 1990), vol. 3, p. 300.
21. C. E. Reimers, K. C. Ruttenberg, D. E. Canfield, M. B. Christiansen, J. B. Martin, *Geochim. Cosmochim. Acta* **60**, 4037 (1996).
22. G. N. Baturin, in *Coastal Upwelling*, J. Thiede, E. Suess, Eds. (Plenum, New York, 1983), vol. B, p. 11.

23. We thank the crew of the research vessel *Meteor* and the participants of the expedition, especially V. Brüchert. We also thank K. Enneking, S. Hessler, K. Wien, J. Birkenstock, C. D. Fraley, and M. Wendschuh for technical and scientific assistance, and B. B. Jørgensen, S. B. Joye, J. Peckmann, M. Zabel, and an anonymous reviewer for comments. The study was supported by the Deutsche Forschungsgemeinschaft. This is publication no. 0240 of the Research Center Ocean Margins of the University of Bremen (Germany). The data are electronically available through the database PANGAEA.

Supporting Online Material
www.sciencemag.org/cgi/content/full/307/5708/416/DC1
Materials and Methods
Figs. S1 to S3
Table S1
References
Models S1 to S4

22 July 2004; accepted 24 November 2004
10.1126/science.1103096

Cardiovascular Risk Factors Emerge After Artificial Selection for Low Aerobic Capacity

Ulrik Wisløff,[1,2]*† Sonia M. Najjar,[3]* Øyvind Ellingsen,[1,2] Per Magnus Haram,[1] Steven Swoap,[4] Qusai Al-Share,[3] Mats Fernström,[3] Khadijeh Rezaei,[3] Sang Jun Lee,[3] Lauren Gerard Koch,[5] Steven L. Britton[5]

In humans, the strong statistical association between fitness and survival suggests a link between impaired oxygen metabolism and disease. We hypothesized that artificial selection of rats based on low and high intrinsic exercise capacity would yield models that also contrast for disease risk. After 11 generations, rats with low aerobic capacity scored high on cardiovascular risk factors that constitute the metabolic syndrome. The decrease in aerobic capacity was associated with decreases in the amounts of transcription factors required for mitochondrial biogenesis and in the amounts of oxidative enzymes in skeletal muscle. Impairment of mitochondrial function may link reduced fitness to cardiovascular and metabolic disease.

Several investigations link aerobic metabolism to the pathogenesis of cardiovascular disease. Large-scale epidemiological studies of subjects with and without cardiovascular disease demonstrate that low aerobic exercise capacity is a stronger predictor of mortality than other established risk factors (*1–4*). In patients with type 2 diabetes, low aerobic capacity is associated with reduced expression of genes involved in oxidative phosphorylation (*5*). In insulin-resistant elders, there is a 40% reduction in mitochondrial oxidative and phosphorylation activity, largely attributable to impaired skeletal muscle glucose metabolism (*6*). These observations are consistent with impaired regulation of mitochondrial function as an important mechanism for low aerobic capacity and cardiovascular risk factors linked to the metabolic syndrome. These risk factors include weight gain, high blood pressure, reduced endothelial function, hyperinsulinemia, and increased triglyceride concentration in blood. The working hypothesis of the present study was that rats selected on the basis of low versus high intrinsic exercise performance would also differ in maximal oxygen uptake, mitochondrial oxidative pathways, and cardiovascular risk factors linked to the metabolic syndrome.

In previous work, we began large-scale artificial selection for low and high aerobic treadmill-running capacity with the genetically heterogeneous N:NIH stock of rats as the founder population (*7*). Eleven generations of selection produced low-capacity runners (LCRs) and high-capacity runners (HCRs) that differed in running capacity by 347% (Fig. 1A). The founder population had a capacity to run for 355 ± 144 m (23.1 min) until exhausted. On average, the treadmill-running capacity decreased 16 m per generation in LCRs and increased 41 m per generation in HCRs in response to selection. At generation 11, the LCRs averaged 191 ± 70 m (14.3 min), and the HCRs ran for 853 ± 315 m (41.6 min). For this study, we used young adult rats (ages 16 to 24 weeks) derived from generations 10 and 11 to test our hypothesis that risk factors for common dis-

[1]Department of Circulation and Medical Imaging, Norwegian University of Science and Technology, Olav Kyrres gt. 3, 7489 Trondheim, Norway. [2]Department of Cardiology, St. Olavs Hospital, 7006 Trondheim, Norway. [3]Department of Pharmacology, Cardiovascular Biology, and Metabolic Diseases, Medical College of Ohio, 3035 Arlington Avenue, Toledo, OH 43614–5804, USA. [4]Department of Biology, Williams College, Williamstown, MA 01267, USA. [5]Department of Physical Medicine and Rehabilitation, University of Michigan, 1500 East Medical Center Drive, Ann Arbor, MI 48109–0718, USA.

*These authors contributed equally to this work.
†To whom correspondence should be addressed. E-mail: ulrik.wisloff@medisin.ntnu.no

eases segregate with variation in intrinsic aerobic capacity (*8*).

High blood pressure is associated with increased risk for stroke and ischemic heart disease (*9*). We found that, relative to the HCRs, the LCR rats had higher mean blood pressures during the day (105 ± 13 mm Hg compared with 89 ± 8 mm Hg), at night (98 ± 3 mm Hg compared with 91 ± 7 mm Hg), and for the combined 24-hour period (102 ± 6 mm Hg compared with 90 ± 7 mm Hg) (Fig. 1B). Extrapolating from human data (*9*), this 13% higher 24-hour blood pressure suggests that the LCRs are twice as likely to develop cardiovascular disease as the HCRs.

Endothelial dysfunction is an independent predictor of long-term cardiovascular disease progression and cardiovascular event rates (*10*). To assess endothelial function in the two strains of rats, we assayed nitric oxide–mediated (acetylcholine) vascular relaxation in isolated ring segments of carotid arteries. In this assay, higher vessel relaxation is interpreted as better endothelial function. For maximal absolute relaxation, the HCR rats demonstrated a 48% increase compared with the LCR rats. Furthermore, the concentration of acetylcholine that provoked a half-maximal response [median effective concentration (EC_{50})] was 7.8-fold greater in LCR than HCR rats (Fig. 1C and fig. S1).

LCR rats were insulin-resistant compared with the HCR rats, as demonstrated by higher fasting insulin levels and impaired glucose tolerance (Table 1 and fig. S2). Insulin C-peptide levels were normal in LCR rats, indicating that insulin secretion was preserved. However, insulin clearance was reduced in the LCR rats, as indicated by lower steady-state C-peptide/insulin molar ratios. These data indicate that hyperinsulinemia results mainly from reduced insulin clearance. Consistent with the clinical scenario of the metabolic syndrome, the LCR rats also had more visceral adiposity, higher plasma triglycerides, and elevated plasma free fatty acids compared with the HCR rats (Table 1).

Because individuals with cardiovascular disease often show diminished capacity for adaptation to exercise training (*11*), we measured 12 variables to assess the general exercise capacity and left ventricular function both in sedentary control (C) and in exercise-trained (T) LCR and HCR rats (Table 2). Each rat was trained for 6 weeks on a treadmill at an intensity relative to its own individual maximal oxygen consumption (VO_{2max}) (*12*). Consistent with a low tolerance for exercise, the C-LCR rats had a 58% lower VO_{2max}, a 17% lower economy of running (i.e., higher oxygen cost of running), 23% less left ventricular weight, and a trend ($P = 0.07$) toward shorter left ventricular cell length compared with the C-HCR rats. Isolated left ventricular cells from C-HCR rats had better systolic and diastolic function relative to the C-LCR rats (Table 2). In response to training, both T-LCR and T-HCR rats showed significant improvement in all 12 of the measures of capacity (Table 2), with a uniformly greater training response in the T-HCR relative to the T-LCR rats for each measure except cell width.

Mitochondrial dysfunction is associated with a wide range of human diseases (*5*). In view of the lower aerobic capacity and reduced cardiovascular function of LCR rats, we hypothesized that they have compromised mitochondrial oxidative function relative to the HCR rats. To test this hypothesis, we measured the cellular content of proteins required for mitochondrial biogenesis and function (*5*, *13*) in soleus muscle, which is composed largely of highly oxidative fibers. The amounts of peroxisome proliferative activated receptor γ (PPAR-γ), PPAR-γ coactivator 1 α (PGC-1α), ubiquinol-cytochrome c oxidoreductase core 2 subunit (UQCRC2), cytochrome c oxidase subunit I (COXI), uncoupling protein 2 (UCP2), and ATP synthase H^+-transporting mitochondrial F1 complex (F_1-ATP synthase) were markedly reduced in the LCR rats in comparison with the HCRs. The uniform decline in these proteins is consistent with the hypothesis that reduced aerobic metabolism

Table 1. LCR and HCR rats differed significantly for carbohydrate and lipid metabolic measures. Measurements were taken from male LCR ($n = 8$) and HCR ($n = 8$) rats. Blood was drawn at 0900 hours with food and water ad libitum to measure random blood sugar. Other metabolic measures were made on blood drawn after 12 hours of food and water deprivation.

	LCR	HCR	% Difference LCR vs. HCR	*P* value
Random glucose (mg/dl)	86 ± 6	75 ± 12	15%	0.036
Fasting glucose (mg/dl)	110 ± 9	92 ± 5	20%	0.0007
Insulin (pM)	684 ± 195	296 ± 172	131%	0.002
C-peptide (pM)	1590 ± 338	1077 ± 565	48%	0.061
C-peptide/insulin	2.4 ± 0.4	3.8 ± 1.2	–58%	0.013
Visceral adiposity/body weight (%)	1.55 ± 0.39	0.95 ± 0.32	63%	0.005
Triglycerides (mg/dl)	67 ± 24	25 ± 4	168%	0.013
Free fatty acids (meq/l)	0.64 ± 0.22	0.33 ± 0.04	94%	0.031

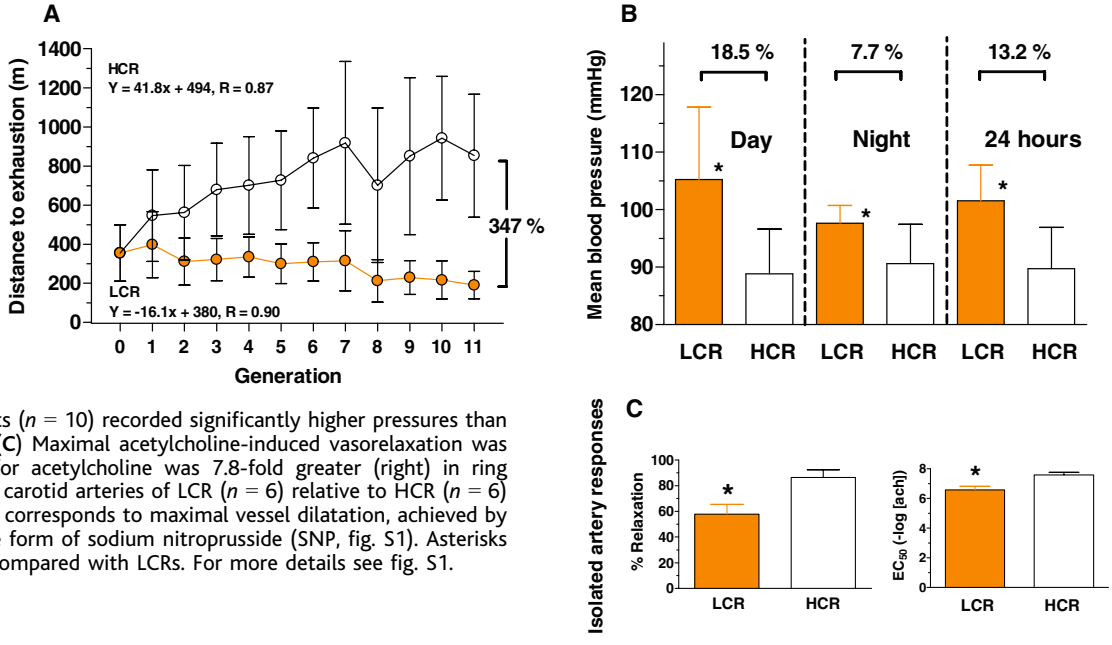

Fig. 1. Eleven generations of selective breeding in rats resulted in two divergent strains. Values are mean ± 1 SD. (**A**) Response to selection for aerobic treadmill-running capacity across 11 generations (n = 2912 rats). On average, the LCR rats decreased 16 m per generation and the HCR rats gained 42 m per generation in distance run to exhaustion. (**B**) Mean blood pressures from sedentary female rats recorded via telemetry. For both day and night values, the LCR rats ($n = 10$) recorded significantly higher pressures than did the HCR rats ($n = 10$). (**C**) Maximal acetylcholine-induced vasorelaxation was lower (left) and the EC_{50} for acetylcholine was 7.8-fold greater (right) in ring segments from the common carotid arteries of LCR ($n = 6$) relative to HCR ($n = 6$) female rats. 100% dilatation corresponds to maximal vessel dilatation, achieved by adding exogenous NO in the form of sodium nitroprusside (SNP, fig. S1). Asterisks indicate $P < 0.01$ for HCRs compared with LCRs. For more details see fig. S1.

plays a causal role in the development of the differences between the LCR and HCR rats (Fig. 2). PGC-1α, particularly because it interacts with PPAR-γ, seems to be centrally positioned for influencing both energy metabolism and the progression of complex diseases. PGC-1α is a transcriptional coactivator involved in energy transfer pathways and mitochondrial biogenesis and permits PPAR-γ to interact with many transcription factors (*14*). PPAR-γ, a regulator of adipocyte differentiation, has been implicated in the pathology of numerous diseases including obesity and diabetes. Thiazolidinediones are selective ligands of PPAR-γ and effective for the treatment of type 2 diabetes, suggesting a pivotal role for PPAR-γ in complex diseases (*15*).

Body weight can have a substantial influence on both aerobic running capacity and the emergence of disease (*16*). Eleven generations of selective breeding for running capacity produced a correlated change in body weight. By generation 11, male LCR rats weighed 92 g more (39%) than HCR males, and similarly the LCR female rats weighed 44 g more (24%) than HCR females (fig. S3). Multiple regression analysis using weight and generation as predictors of running capacity revealed that changes in body weight explained 7% of the variation in distance run in HCR females, 7% in LCR females, 20% in HCR males, and 14% in LCR males. Thus, factors other than body weight account for the majority of the variation in distance run across the 11 generations of selection in both strains.

Because risk factors for complex diseases often emerge with aging (*17*), we measured indices of metabolic risk in 5-week-old male pups (fig. S4). At this age, the HCR and LCR lines had essentially identical body and visceral fat weights, with a 25% greater VO_{2max} in the HCR relative to the LCR. The LCR pups showed 12% higher plasma glucose ($P < 0.001$) and plasma triglyceride values ($P < 0.04$) compared with the HCR pups. Thus, in our contrasting strains, metabolic changes preceded the increase in body weight (fig. S4), a result that is consistent with a role for hyperinsulinemia in weight gain. Although mechanistic arguments have been put forward for either pattern in humans, clinical studies have not resolved whether obesity precedes or follows the development of insulin resistance in type 2 diabetes (*18*).

In summary, the present study demonstrated that selection for low versus high intrinsic aerobic exercise capacity simultaneously generated a differential load of metabolic and cardiovascular risk factors. Rats with low aerobic capacity expressed low amounts of key proteins required for mitochondrial function in skeletal muscle, suggesting a mechanistic association. Although a direct cause-effect relationship has not been proven, our observations support the notion that impaired regulation of oxidative pathways in mitochondria may be a common factor linking reduced total-body aerobic capacity to cardiovascular and metabolic disease. This is in concert with previous epidemiological and clinical studies (*1*–*6*, *19*).

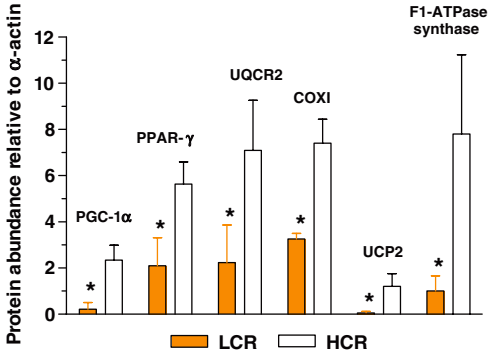

Fig. 2. Proteins known to be integral for mitochondrial function and hypothesized to be inversely associated with diseases were more abundant in soleus skeletal muscles from HCR male rats relative to LCR male rats ($n = 6$ of each strain). Asterisks indicate $P < 0.01$ for HCRs compared with LCRs. Bars show mean ± 1 SD.

Table 2. Exercise capacity and isolated left ventricular cell variables for LCR and HCR rats separated in groups of sedentary control (C) and exercise-trained (T). Before exercise, the C-LCR and C-HCR rats differed significantly (indicated by asterisks for $P < 0.01$) for all variables except left ventricular cell length and width. Six weeks of exercise training significantly improved each of these 11 variables in both T-LCR and T-HCR rats (indicated by ‡ for $P < 0.01$). In each case except cell width, T-HCR rats improved more than T-LCR rats with training († for $P < 0.05$). PS, percentage cell shortening. Values are means ± 1 SD from six LCR and six HCR female rats.

	C-LCR	C-HCR	% Difference	% Change with training	
			C-LCR vs. C-HCR	C-LCR vs. T-LCR	C-HCR vs. T-HCR
	Whole animal variables				
VO_{2max} (ml kg$^{-0.75}$ min^{-1})	43 ± 2	68 ± 3	–58%*	38%‡	44%‡†
Economy of running (ml O_2 kg$^{-0.75}$ m^{-1})	4.9 ± 0.1	4.2 ± 0.2	17%*	–7%‡	–17%‡†
Left ventricular weight (mg kg$^{-0.75}$)	1561 ± 176	1917 ± 88	–23%*	22%‡	27%‡†
	Left ventricular cell variables				
Cell length (μm)	118 ± 2	124 ± 2	–5%	6%‡	14%‡†
Cell width (μm)	23 ± 3	19 ± 3	20%	2%	2%
	Systolic cell function				
Cell shortening (%)	14.0 ± 1.2	17.1 ± 1.1	–22%*	30%‡	39%‡†
Relative time to peak shortening (ms PS^{-1})	2.7 ± 0.2	2.3 ± 0.2	17%*	–24%‡	–32%‡†
Systolic [Ca^{2+}] (μM)	1.61 ± 0.03	1.73 ± 0.04	–7%*	–16%‡	–23%‡†
Amplitude of [Ca^{2+}] transient (μM)	1.20 ± 0.03	1.38 ± 0.05	–15%*	–19%‡	–24%‡†
	Diastolic cell function				
Time to 50% relengthening (ms)	39.9 ± 1.2	35.2 ± 1.3	13%*	–14%‡	–16%‡†
Diastolic [Ca^{2+}] (μM)	0.41 ± 0.02	0.35 ± 0.02	17%*	–7%‡	–20%‡†
Time to 50% decay of [Ca^{2+}] transient (ms)	55.3 ± 1.4	45.9 ± 1.3	20%*	–11%‡	–13%‡†

References and Notes

1. S. Yusuf *et al.*, *Lancet* **364**, 937 (2004).
2. J. Myers *et al.*, *N. Engl. J. Med.* **346**, 793 (2002).
3. T. Kavanagh *et al.*, *J. Am. Coll. Cardiol.* **42**, 2139 (2003).
4. T. Kavanagh *et al.*, *Circulation* **106**, 666 (2002).
5. V. K. Mootha *et al.*, *Nat. Genet.* **34**, 267 (2003).
6. K. F. Petersen *et al.*, *Science* **300**, 1140 (2003).
7. L. G. Koch, S. L. Britton, *Physiol. Genomics* **5**, 45 (2001).
8. Materials and methods are available as supporting material on *Science* Online.
9. Prospective Studies Collaboration, *Lancet* **360**, 1903 (2002).
10. V. Schächinger, M. B. Britten, A. M. Zeiher, *Circulation* **101**, 1899 (2000).
11. R. Hambrecht *et al.*, *JAMA* **283**, 3095 (2000).
12. U. Wisloff, J. Helgerud, O. J. Kemi, O. Ellingsen, *Am. J. Physiol.* **280**, H1302 (2001).
13. P. Puigserver, B. M. Spiegelman, *Endocr. Rev.* **24**, 78 (2003).
14. M. E. Patti *et al.*, *Proc. Natl. Acad. Sci. U.S.A.* **100**, 8466 (2003).
15. H. Yki-Järvinen, *N. Engl. J. Med.* **351**, 1106 (2004).
16. S. Kenchaiah *et al.*, *N. Engl. J. Med.* **347**, 305 (2002).
17. A. A. Yousef, R. Valdez, A. Elkasabany, S. R. Srinivsan, G. S. Berenson, *Ann. Epidemiol.* **12**, 553 (2002).
18. S. R. Srinivasan, M. G. Frontini, G. S. Berenson, *Metabolism* **52**, 443 (2003).
19. F. H. Wilson *et al.*, *Science* **306**, 1190 (2004); published online 21 October 2004 (10.1126/science.1102521).

20. We thank M. Nelson, K. Pettee, A. Gilbert, M. Kaufmann, T. Kennedy, O. J. Kemi, L. Gilligan, and A. Duvall for technical assistance and J. W. Britton for helpful discussions. Supported by NIH grants HL 64270 and RR 17718 (S.L.B. and L.G.K.) and DK 54254 and DK 57497 (S.M.N.), the American Diabetes Association (S.M.N.), NSF grant IBN 9984170 (S.S.), and the Norwegian Council on Cardiovascular Research (U.W. and O.E.).

Supporting Online Material

www.sciencemag.org/cgi/content/full/307/5708/418/DC1
Materials and Methods
Figs. S1 to S4
References and Notes

28 May 2004; accepted 13 December 2004
10.1126/science.1108177

Mechanism of *hsp70i* Gene Bookmarking

Hongyan Xing,[1] Donald C. Wilkerson,[1] Christopher N. Mayhew,[1,3] Eric J. Lubert,[1,4] Hollie S. Skaggs,[1] Michael L. Goodson,[1,5] Yiling Hong,[1,3] Ok-Kyong Park-Sarge,[2] Kevin D. Sarge[1]*

In contrast to most genomic DNA in mitotic cells, the promoter regions of some genes, such as the stress-inducible *hsp70i* gene that codes for a heat shock protein, remain uncompacted, a phenomenon called bookmarking. Here we show that *hsp70i* bookmarking is mediated by a transcription factor called HSF2, which binds this promoter in mitotic cells, recruits protein phosphatase 2A, and interacts with the CAP-G subunit of the condensin enzyme to promote efficient dephosphorylation and inactivation of condensin complexes in the vicinity, thereby preventing compaction at this site. Blocking HSF2-mediated bookmarking by HSF2 RNA interference decreases *hsp70i* induction and survival of stressed cells in the G_1 phase, which demonstrates the biological importance of gene bookmarking.

During mitosis, the genome must be compacted in order for chromosomes to be segregated during cytokinesis. An enzyme called condensin, which is composed of five subunits, plays an important role in this compaction process and is activated at the onset of mitosis by phosphorylation of the CAP-G, CAP-H, and CAP-D2 subunits by the Cdc2–cyclin B kinase (*1*–*5*). However, a number of gene promoters, including those of the *hsp70i* and c-*myc* genes, do not appear to be tightly compacted in mitotic cells (*6*–*9*). The mechanism responsible for preventing compaction of specific gene regions during mitosis, called bookmarking, is unknown.

HSF2 is a transcription factor that can bind heat shock elements (HSEs) in the *hsp70i* promoter. But unlike the related HSF1 factor, which mediates stress-induced transcription of this gene, the function of HSF2 has remained unclear (*10*–*15*). To better understand HSF2 function, we performed a yeast two-hybrid screen to identify HSF2-interacting proteins. One of the isolated clones contains a segment of the CAP-G protein, which is a subunit of the condensin enzyme (fig. S1A). The HSF2-interacting sequence is in the C-terminal region of CAP-G, and consists of amino acids 811 to 957 (fig. S1B). Immunoprecipitation analysis demonstrated that endogenous HSF2 and CAP-G interact and that more of the complex is detected in mitotic than asynchronous cells (Fig. 1A). Our previous work demonstrated that HSF2 is covalently modified at lysine 82 by the 97–amino acid small ubiquitin-related modifier (SUMO)–1 protein (*16*). Transfection of HeLa cells with *myc*-tagged wild-type HSF2 or a sumoylation-deficient K82R HSF2 mutant (in which Lys^{82} is replaced by Arg), followed by CAP-G immunoprecipitation analysis, revealed that sumoylation of HSF2 positively regulates its association with CAP-G (Fig. 1B). We postulated that sumoylation of HSF2 might be regulated in a cell-cycle–dependent manner to control HSF2 interaction with CAP-G. Consistent with this, Western blot analysis of extracts of cells that were obtained by fluorescence-activated cell sorting (FACS) indicated that G_2/M-phase extracts displayed a band whose size was consistent with SUMO-modified HSF2, which was also detected in asynchronous cell extracts but displayed lower intensity in G_0/G_1- or S-phase cell extracts (Fig. 1C). Immunoprecipitation analysis of HSF2 from extracts of each cell population followed by SUMO-1 Western blot confirms that higher levels of sumoylated HSF2 are found in G_2/M cells than in G_0/G_1 or S cells (Fig. 1D).

The results above suggested that HSF2 may bind to the *hsp70i* promoter in a mitotic-dependent manner as part of a mechanism for preventing compaction of this promoter. This suggestion was tested by chromatin immunoprecipitation (ChIP) assay, which demonstrated that HSF2 does bind to the *hsp70i*

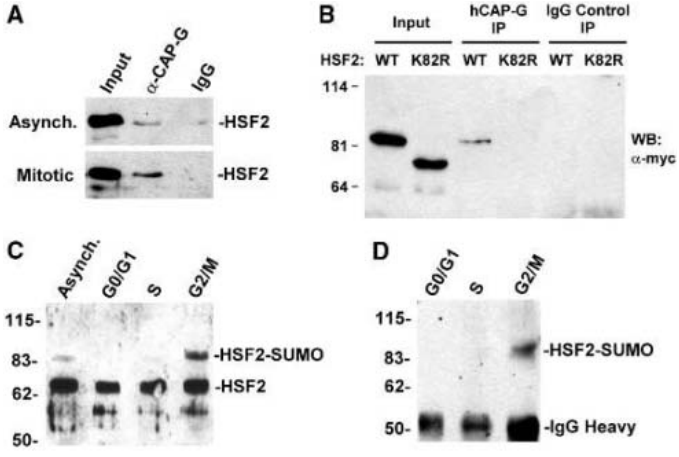

Fig. 1. HSF2 interacts with the condensin subunit CAP-G in mitotic cells. (**A**) Extracts of asynchronous or mitotic (nocodazole-blocked) cells were immunoprecipitated with antibodies to CAP-G or nonspecific immunoglobulin (IgG), and the immunoprecipitates were subjected to Western blot with HSF2 antibodies. (**B**) HSF2 sumoylation stimulates CAP-G interaction. Extracts of HeLa cells transfected with *myc*-tagged wild-type HSF2 or nonsumoylatable K82R HSF2 were immunoprecipitated with CAP-G antibodies or nonspecific IgG followed by Western blot with *myc* antibodies. (**C**) HSF2 exhibits modification associated with G_2/M cells. Extracts of equal numbers of G_0/G_1, S, and G_2/M populations of human K562 cells obtained by FACS and asynchronous cells were subjected to HSF2 Western blot. (**D**) HSF2 exhibits increased sumoylation in G_2/M cells. Extracts of equal numbers of FACS-sorted G_0/G_1, S, and G_2/M populations of K562 cells were immunoprecipitated with HSF2 antibodies followed by Western blot with SUMO-1 antibodies.

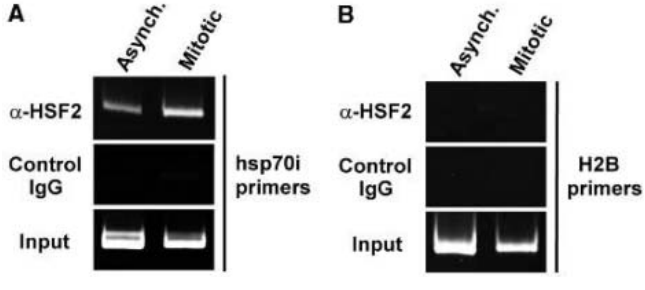

Fig. 2. HSF2 binds to the *hsp70i* promoter in mitotic cells. (**A**) ChIP assay was performed on asynchronous or mitotic (nocodazole-blocked) Jurkat cells by using HSF2 antibodies or control IgG antibodies and polymerase chain reaction (PCR) primers specific to the *hsp70i* gene. (**B**) Asynchronous and mitotic Jurkat cells were analyzed by ChIP assay by using HSF2 antibodies or control IgG, followed by PCR with primers specific to the histone H2B gene.

[1]Department of Molecular and Cellular Biochemistry, [2]Department of Physiology, Chandler Medical Center, University of Kentucky, Lexington, KY 40536, USA. [3]Department of Cell Biology, Neurobiology, and Anatomy, University of Cincinnati, Cincinnati, OH 45267, USA. [4]Battelle Memorial Institute, Columbus, OH 43201, USA. [5]Section of Microbiology, University of California at Davis, Davis, CA 95616, USA.

*To whom correspondence should be addressed. E-mail: kdsarge@uky.edu

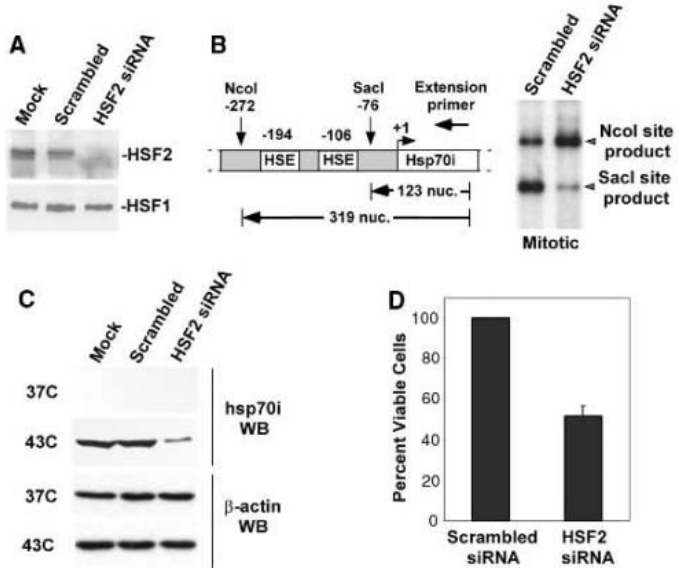

Fig. 3. Reducing cellular HSF2 levels decreases *hsp70i* promoter bookmarking in mitotic cells and *hsp70i* inducibility and survival of stressed G_1 cells. (**A**) Reduction of cellular HSF2 levels by RNAi. HeLa cells were transfected with no siRNA (mock), scrambled siRNA, or HSF2-specific siRNA, and extracts analyzed by HSF2 and HSF1 Western blot. (**B**) Lowering cellular HSF2 levels decreased accessibility of the *hsp70i* promoter in mitotic cells. (Left) An accessibility assay of *hsp70i* promoter in intact chromatin, indicating positions of the Sac I test site, the Nco I complete digestion site, the primer binding site, and the expected sizes of extension products. (Right) Chromatin of HeLa cells that were treated with scrambled siRNA or HSF2-specific siRNA, then blocked in mitosis by nocodazole treatment, was incubated with Sac I for 30 min at 37°C. Genomic DNA was extracted, digested to completion with Nco I, then subjected to primer extension analysis with an *hsp70i*-specific primer. (**C**) Reducing HSF2 levels decreased the ability of G_1 cells to induce *hsp70i* expression in response to stress. HeLa cells were transfected with scrambled siRNA or HSF2 siRNA, then blocked with nocodazole before being released from blockage for 2 hours to allow entry into the G_1 phase. The HeLa cells were next subjected to heat treatment at 43°C for 30 min (or kept at 37°C) followed by recovery at 37°C for 3 hours, then analyzed by Western blot with *hsp70i* antibody or β-actin antibody (loading control). (**D**) Reducing HSF2 levels increased stress-induced killing of G_1 cells. HSF2 RNAi-treated HeLa cells that were nocodazole-blocked and released for 2 hours as in (C) were then subjected to thermo-tolerance–inducing treatment of 43°C for 30 min. Cells were then recovered at 37°C for 4 hours to allow *hsp70i* expression, followed by severe 45°C 30-min heat stress. After 40 hours back at 37°C, cell viability was measured by trypan blue exclusion.

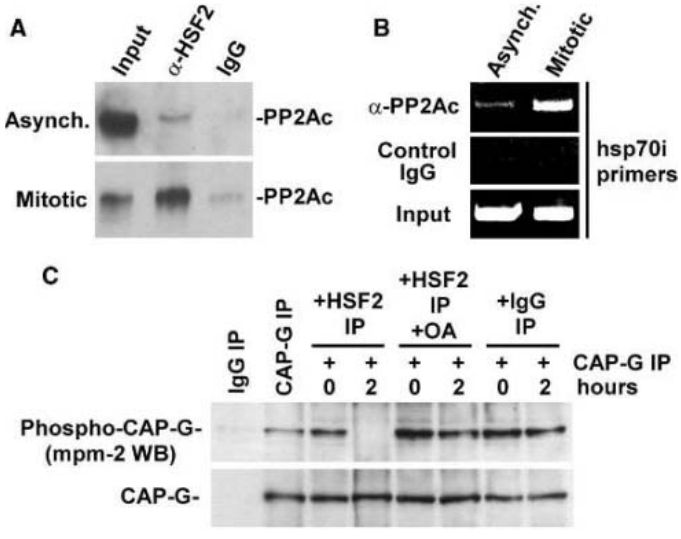

Fig. 4. PP2A associates with HSF2 and the *hsp70i* promoter in mitotic cells and dephosphorylates mitotic CAP-G. (**A**) HSF2 complexes with PP2A in mitotic cells. HSF2 was immunoprecipitated from extracts of asynchronous or mitotic HeLa cells (with nonspecific IgG as negative control) followed by Western blot with PP2A catalytic subunit antibodies. (**B**) PP2A is associated with the *hsp70i* promoter in mitotic cells. ChIPAssay was performed on asynchronous or mitotic (nocodazole-blocked) Jurkat cells by using PP2A catalytic subunit antibodies or control IgG antibodies and *hsp70i* promoter primers. (**C**) Endogenous mitotic HSF2 associates with okadaic acid–inhibitable phosphatase activity that dephosphorylates mitotic CAP-G. The first two lanes show immunoprecipitates pulled down by non-specific IgG or CAP-G antibody subjected to Western blot with either Mpm2 (detects phosphoCAP-G) or CAP-G antibodies (loading and degradation control). The next lanes show reactions containing CAP-G immunoprecipitates from mitotic cell extracts resuspended in phosphatase reaction buffer (NEB) and incubated with HSF2 immunoprecipitates (± 200 nM okadaic acid) or nonspecific IgG immunoprecipitates from mitotic cell extracts for 2 hours or no time.

promoter in mitotic cells, and more binding was observed in these cells as compared with asynchronous cells (Fig. 2A). HSF2 interaction was not observed for the histone H2B promoter gene in mitotic cells, demonstrating specificity (Fig. 2B).

To assess directly the importance of HSF2 for *hsp70i* promoter bookmarking, we tested the effect of decreasing cellular HSF2 levels on the accessibility of this promoter in mitotic cells. HSF2 levels were reduced by using RNA interference (RNAi) methods, which decreased cellular HSF2 protein levels without affecting levels of the related HSF1 protein (Fig. 3A). Chromatin of the HSF2 RNAi-treated mitotic HeLa cells was subjected to a restriction enzyme accessibility assay, which measures the accessibility of a specific DNA region within intact chromatin (*17–20*). In this assay, chromatin from HSF2 small interfering RNA (siRNA)–treated nocodazole-blocked (mitotic) cells was incubated with the restriction enzyme Sac I, which cleaves at nucleotide –76 near the proximal HSE of the *hsp70i* promoter (Fig. 3B, left side). Genomic DNA was then extracted, cut to completion with Nco I to yield a defined end beyond this Sac I site, and subjected to primer extension by using an *hsp70i* gene-specific primer. The intensity of the 123-nucleotide extension product was taken as a measure of the accessibility of the *hsp70i* promoter Sac I site within intact chromatin. The initial Sac I digestion of DNA within the chromatin was not anticipated to be completely efficient, even if the DNA target site was completely accessible. Therefore, some fragments that were not digested by Sac I (319-nucleotide products) were always expected. HSF2 siRNA treatment resulted in decreased accessibility of this Sac I site, as compared with the scrambled siRNA control (Fig. 3B, right side), which indicates a critical role for HSF2 in bookmarking the *hsp70i* promoter. Performing the same experiment with S cells suggests that the effect of lowered HSF2 levels on *hsp70i* promoter accessibility is more pronounced in G_1 cells, which is consistent with the bookmarking hypothesis (fig. S2A). HSF2 reduction does not affect accessibility of another promoter accessible in mitotic cells, the histone H2B gene promoter (*7*), which indicates specificity (fig. S2B).

It has been postulated that *hsp70i* bookmarking maintains the gene in a transcription-competent state so that induction could occur even in early G_1 phase if stress were to arise. To test this hypothesis, HSF2 siRNA-treated cells blocked in mitosis with nocodazole but released from the block for 2 hours to permit entry into the G_1 phase were subjected to 43°C treatment for 30 min followed by recovery at 37°C for 3 hours. Western blot indicated that *hsp70i* protein induction was significantly lower in HSF2 RNAi-treated cells compared with

cells treated with scrambled siRNA (Fig. 3C). Furthermore, this reduced ability to induce *hsp70i* protein was correlated with a significant increase in cell death after stress treatment (Fig. 3D), which indicates the critical importance of HSF2-mediated *hsp70i* bookmarking for cell stress survival.

The results above show that in mitotic cells, HSF2 binds the *hsp70i* promoter, interacts with the CAP-G subunit of condensin, and is critical for the bookmarking of this promoter. But how does HSF2 mediate inhibition of condensin activity at this locus? Condensin activity requires phosphorylation of the CAP-G, CAP-D2, and CAP-H subunits by the mitotic kinase Cdc2–cyclin B (*21*, *22*). We previously showed that HSF2 interacts with the serine-threonine protein phosphatase 2A (PP2A) (*23*), and other studies have suggested that a member of the PPP family of serine-threonine phosphatases, which includes PP2A, is involved in dephosphorylating the condensin subunits that are phosphorylated by Cdc2 (*24*). On the basis of these data, we hypothesized that HSF2 mediates *hsp70i* promoter bookmarking by recruiting PP2A to this promoter. When condensin interacts with HSF2 via CAP-G, it could be dephosphorylated and inactivated by the HSF2-associated PP2A to prevent compaction of this region of DNA. Supporting this hypothesis, immunoprecipitation experiments demonstrate that HSF2 does associate with PP2A in mitotic cells, and that more of the complex is observed in mitotic than in asynchronous cells, suggesting mitosis-dependent regulation of this interaction (Fig. 4A). Furthermore, ChIP assays show that PP2A exists within cross-linking distances of the *hsp70i* promoter in mitotic cells and that more association is observed in mitotic cells than in asynchronous cells (Fig. 4B). To confirm the function of PP2A as a condensin phosphatase, we isolated condensin by immunoprecipitation with CAP-G antibodies, phosphorylated it with purified Cdc2–cyclin B and [γ-^{32}P]adenosine triphosphate (ATP) in vitro, and then incubated the phosphorylated condensin with purified PP2A. The results show that PP2A can dephosphorylate CAP-G, CAP-D2, and CAP-H (fig. S3A). Finally, we took advantage of the ability of the Mpm2 antibody to detect the phosphorylated forms of Cdc2–cyclin B substrates, including CAP-G (*25*), to show that HSF2 immunoprecipitates from mitotic cells contain an okadaic acid–inhibitable phosphatase activity that can efficiently dephosphorylate phosphorylated CAP-G that was immunoprecipitated from mitotic cells (Fig. 4C). This activity is not detected in HSF1 immunoprecipitates from mitotic cells (fig. S3B).

The results in this paper suggest that HSF2 mediates *hsp70i* promoter bookmarking by binding to this promoter in mitotic cells, recruiting PP2A, and interacting with condensin enzyme by binding to the CAP-G subunit to allow the PP2A to dephosphorylate efficiently and to inactivate this condensin, thereby preventing compaction of this region of chromosomal DNA. The results also demonstrate the biological importance of bookmarking by showing that the loss of HSF2-mediated bookmarking significantly reduces the ability of cells to induce *hsp70i* gene expression and to survive stress. This knowledge opens the door to investigating the mechanisms and biological roles of other gene bookmarking events, toward understanding the full biological ramifications of bookmarking for cell function.

References and Notes

1. T. Hirano, *Cell Cycle* **3**, 26 (2004).
2. A. V. Strunnikov, *Prog. Cell Cycle Res.* **5**, 361 (2003).
3. K. A. Hagstrom, B. J. Meyer, *Nature Rev. Genet.* **4**, 520 (2003).
4. J. R. Swedlow, T. Hirano, *Mol. Cell* **11**, 557 (2003).
5. K. Yokomori, *Curr. Top. Microbiol. Immunol.* **274**, 79 (2003).
6. E. F. Michelotti, S. Sanford, D. Levens, *Nature* **388**, 895 (1997).
7. R. Christova, T. Oelgeschlager, *Nature Cell Biol.* **4**, 79 (2002).
8. S. John, J. L. Workman, *Bioessays* **20**, 275 (1998).
9. M. A. Martinez-Balbas, A. Dey, S. K. Rabindran, K. Ozato, C. Wu, *Cell* **83**, 29 (1995).
10. E. S. Christians, L. J. Yan, I. J. Benjamin, *Crit. Care Med.* **30**, S43 (2002).
11. L. Pirkkala, P. Nykanen, L. Sistonen, *FASEB J.* **15**, 1118 (2001).
12. C. Jolly, R. I. Morimoto, *J. Natl. Cancer Inst.* **92**, 1564 (2000).
13. K. A. Morano, D. J. Thiele, *Gene Expr.* **7**, 271 (1999).
14. T. J. Schuetz, G. J. Gallo, L. Sheldon, P. Tempst, R. E. Kingston, *Proc. Natl. Acad. Sci. U.S.A.* **88**, 6911 (1991).
15. K. D. Sarge, V. Zimarino, K. Holm, C. Wu, R. I. Morimoto, *Genes Dev.* **5**, 1902 (1991).
16. M. L. Goodson *et al.*, *J. Biol. Chem.* **276**, 18513 (2001).
17. F. L. Sun *et al.*, *Proc. Natl. Acad. Sci. U.S.A.* **97**, 5340 (2000).
18. T. H. Li, C. Kim, C. M. Rubin, C. W. Schmid, *Nucleic Acids Res.* **28**, 3031 (2000).
19. B. J. Deroo, T. K. Archer, *Mol. Biol. Cell* **12**, 3365 (2001).
20. T. Wang, W. P. Lafuse, K. Takeda, S. Akira, B. S. Zwilling, *J. Immunol.* **169**, 795 (2002).
21. K. Kimura, M. Hirano, R. Kobayashi, T. Hirano, *Science* **282**, 487 (1998).
22. K. Kimura, O. Cuvier, T. Hirano, *J. Biol. Chem.* **276**, 5417 (2001).
23. Y. Hong, K. D. Sarge, *J. Biol. Chem.* **274**, 12967 (1999).
24. T. Hirano, R. Kobayashi, M. Hirano, *Cell* **89**, 511 (1997).
25. A. Takemoto, K. Kimura, S. Yokoyama, F. Hanaoka, *J. Biol. Chem.* **279**, 4551 (2004).

26. We are grateful to K. Yokomori and M. Matunis for generously providing antibodies and to R. Hilgarth and L. Murphy for insightful discussions. This research was supported by NIH grants GM61053, GM64606 (K.D.S.), and HD36879, HD41609 (O.-K.P.-S.).

Supporting Online Material

www.sciencemag.org/cgi/content/full/307/5708/421/DC1
Materials and Methods
Figs. S1 to S3
References and Notes

18 October 2004; accepted 24 November 2004
10.1126/science.1106478

Mathematical Modeling of Planar Cell Polarity to Understand Domineering Nonautonomy

Keith Amonlirdviman,[1] Narmada A. Khare,[2] David R. P. Tree,[2] Wei-Shen Chen,[2] Jeffrey D. Axelrod,[2]*† Claire J. Tomlin[1]*†

Planar cell polarity (PCP) signaling generates subcellular asymmetry along an axis orthogonal to the epithelial apical-basal axis. Through a poorly understood mechanism, cell clones that have mutations in some PCP signaling components, including some, but not all, alleles of the receptor *frizzled*, cause polarity disruptions of neighboring wild-type cells, a phenomenon referred to as domineering nonautonomy. Here, a contact-dependent signaling hypothesis, derived from experimental results, is shown by reaction-diffusion, partial differential equation modeling and simulation to fully reproduce PCP phenotypes, including domineering nonautonomy, in the *Drosophila* wing. The sufficiency of this model and the experimental validation of model predictions reveal how specific protein-protein interactions produce autonomy or domineering nonautonomy.

As the understanding of cellular regulatory networks grows, system behaviors resulting from feedback effects have proven sufficiently complex so as to preclude intuitive understanding. The challenge now is to show that enough of a network is understood to explain such behaviors. Using mathematical modeling, we show the sufficiency of a proposed biological model and study its properties, to demonstrate that it can explain complex PCP phenotypes and to provide insight into the system dynamics that govern them.

Many epithelia are polarized along an axis orthogonal to the apical-basal axis. On the *Drosophila* adult cuticle, each hexagonally packed cell elaborates an actin-rich hair that develops from the distal vertex and points distally (Fig. 1A). Genetic analyses have identified a group of PCP proteins whose activities are required to correctly polarize

these arrays (*1*, *2*). The domineering nonautonomy adjacent to cell clones mutant for some, but not other, PCP genes has not yet been adequately explained (*1*). For example, in the *Drosophila* wing, *Van Gogh/strabismus* (*Vang*; encoding a four-pass transmembrane protein) (*3*, *4*) clones disrupt polarity proximal to the mutant tissue (*3*), whereas null *frizzled* (*fz*; encoding a seven-pass transmembrane protein) alleles disrupt polarity distal to the clone (*5*, *6*). Models to explain this phenomenon have often invoked diffusible factors, referred to as factor X or Z, because they have not yet been identified (*1*, *7*–*15*). We propose instead that the observed behaviors of known PCP proteins are sufficient to explain domineering nonautonomy.

Fz and other PCP signaling components accumulate selectively on the distal or proximal side of wing cells (Fig. 1A). Evidence has been provided that these proteins function in a feedback loop that amplifies an asymmetry cue, which converts uniform distributions of PCP proteins into highly polarized distributions (*11*, *16*–*18*) (Fig. 1B). The proposed feedback mechanism depends on several functional relationships (*18*). Fz recruits Dishevelled (Dsh; a cytoplasmic protein) to the cell membrane (*16*, *19*). In addition, Fz promotes the recruitment of Prickle-spinylegs (Pk; a LIM domain protein) (*5*, *18*, *20*) and Vang (*21*) to the cell membrane of the adjacent cell. Feedback is provided by the ability of Pk [and Vang; supporting online material (SOM)] to cell-autonomously block Fz-dependent recruitment of Dsh (*18*). This feedback loop functions strictly locally, between adjacent cells. Global directionality is imposed through the agency of the novel transmembrane protein Four-jointed and the cadherins Dachsous and Fat (Ft) (*22*–*24*). Widerborst, a regulatory subunit of protein phosphatase 2A, accumulates asymmetrically within each cell and is required to bias the feedback loop (*25*). Although the mechanism by which Ft biases the direction of the feedback loop is unknown, one possibility is that Ft may direct Widerborst distribution.

However, it is not readily apparent that this biological model does not readily explain the complex patterns observed in fields of cells containing mutant clones, and others have argued that it cannot account for some of the observed phenotypes (*1*, *26*). Indeed, progress in understanding PCP signaling has been hampered by an inability to deduce, given a particular signaling network hypothesis, definitive links between molecular genetic interventions and tissue patterning effects. For example, although it is apparent that removing Dsh or Fz would disrupt the feedback loop, it is not obvious how the feedback loop in adjacent wild-type cells responds, such that *dsh* mutant clones behave autonomously, whereas for most *fz* alleles, mutant clones behave nonautonomously. Interestingly, though, for some *fz* alleles, mutant clones produce an almost cell-autonomous phenotype (*5*, *6*, *27*). As another example, Pk overexpression promotes the asymmetric accumulation of Dsh and Fz (*18*), despite the role of Pk in the feedback loop as an inhibitor of Dsh membrane recruitment.

We have developed a mathematical model based on the described feedback loop and an initial asymmetry input representing the global directional cue (*18*, *22*, *23*). Although mathematical modeling cannot prove the correctness of the underlying biological model, the ability of the mathematical model to capture the known behaviors of the system proves the feasibility of the biological model, provides testable

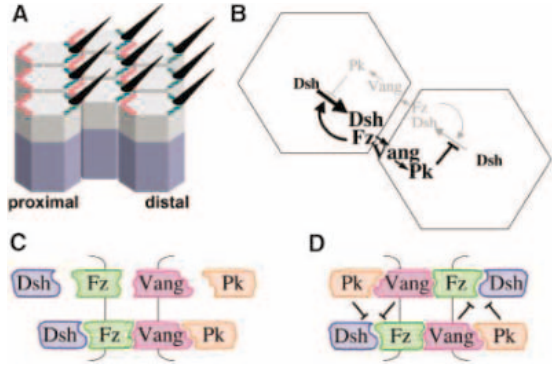

Fig. 1. Illustrations of PCP. (**A**) Hexagonally packed wing cells accumulate Fz and Dsh distally (blue/green) and Pk and Vang proximally (pink/orange). A hair is elaborated from the distal vertex of each cell. (**B**) A local feedback loop model for a PCP signaling mechanism. Black lettering indicates protein accumulation. Gray lettering indicates proteins whose concentrations are decreased. (**C**) Representation of proposed binding interactions. (**D**) Inhibition model representing disruption of the Dsh-Fz interaction by Pk and Vang.

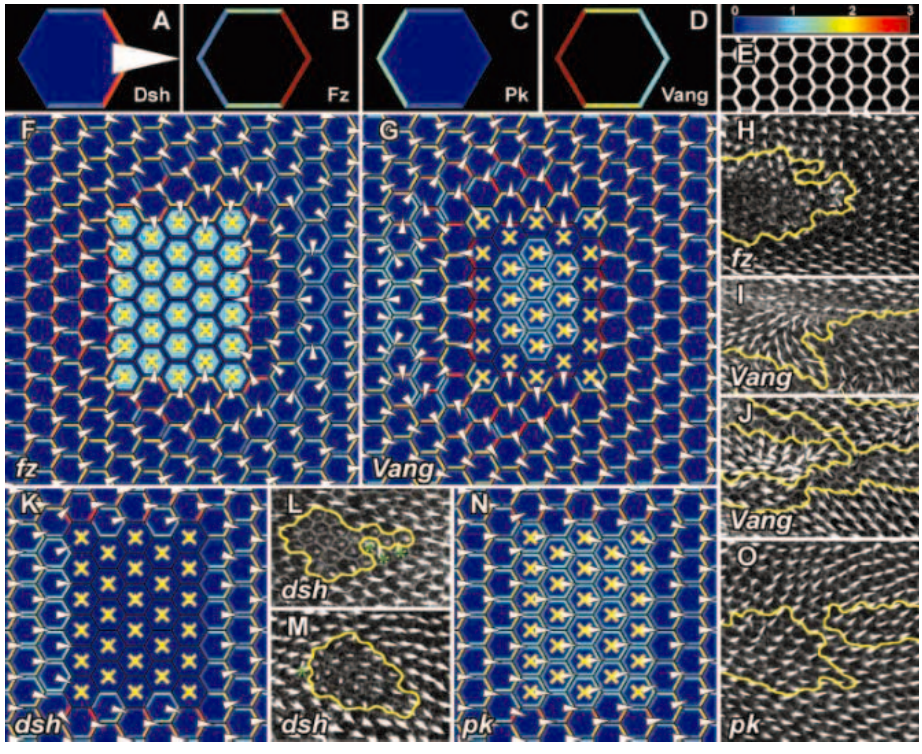

Fig. 2. Simulation results. Wild-type results showing the final distributions of Dsh (**A**), Fz (**B**), Pk (**C**), and Vang (**D**). The same color scale is used in all figures, where 1 is scaled to the initial uniform concentration of Dsh and the scale is truncated so that concentrations greater than 3 are shown in red. (**E**) Simulated distribution of Dsh displayed as an intensity representing total Dsh concentrations, corresponding to the appearance of Dsh::GFP in wild-type experiments. Simulation results of several PCP phenotypes showing the final distribution of Dsh with predicted hair growth directions derived from the vector sum of Dsh (**F**, **G**, **K**, and **N**) and corresponding pupal wings (**H** to **J**, **L**, **M**, and **O**). Greater Dsh asymmetry is represented by hair placement at increasing distances from the cell center. When Dsh asymmetry does not exceed the threshold value, the hair is depicted at the center of the cell. Mutant cells are designated with yellow. (H) fz^{R52} null clones. (**I**) and (J) $Vang^{A3}$ mutant clones. (L and M) dsh^{V26} mutant clones. (O) $pk\text{-}sple^{13}$ mutant clones. Asterisks mark nonautonomous effects near *dsh* clones.

[1]Department of Aeronautics and Astronautics, Stanford University, Stanford, CA 94305–4035, USA. [2]Department of Pathology, Stanford University School of Medicine, Stanford, CA 94305–5324, USA.

*These authors contributed equally to this work.
†To whom correspondence should be addressed. E-mail: tomlin@stanford.edu (C.J.T.); jaxelrod@stanford.edu (J.D.A.)

hypotheses, and yields insight into the factors contributing to autonomy and nonautonomy.

We have represented the features of the biological feedback loop model as a mathematical reaction-diffusion model (*28*) that describes the concentrations of Dsh, Fz, Vang, and Pk throughout a network of cells. Although the mechanisms that underlie the local feedback loop are not fully understood, the essential logic of this feedback loop is preserved by representing these interactions as binding to form protein complexes (Fig. 1, C and D).

Inhibition of Dsh membrane recruitment by Pk and Vang (Fig. 1, C and D, SOM) is represented in the mathematical model as an increase in the backward reaction rate of reactions in which Dsh binds Fz (or Fz complexes) by a factor dependent on the local concentration of Pk and Vang. The specific mechanism for the introduction of the directional bias into the feedback loop network is not known. Two forms of a global biasing signal were therefore implemented, and the results using either of these models were similar (SOM). The resulting mathematical model consists of a system of 10 nonlinear partial differential equations. With a given set of model parameters, an array of cells could then be simulated, and the resulting hair pattern assigned on the basis of the final distribution of Dsh.

The model parameters, including the initial protein concentrations, reaction rates, and diffusion constants, were not known, and so these parameters were identified by constraining them to result in specific qualitative features of the hair pattern phenotypes. A sensitivity analysis showed that the model results are not highly sensitive to the precise parameter values and suggests that our conclusions regarding the feasibility of the model are valid for considerable ranges of parameters. The full development and discussion of assumptions for the mathematical model are in the SOM text.

In simulated wild-type cells (Fig. 2, A to E), Dsh and Fz localize to the distal membrane, and Vang and Pk localize to the proximal membrane, as is seen in vivo (*16*–*18*, *21*). Simulated clones of cells lacking *fz* function disrupt polarity in wild-type cells distal to the clones [Fig. 2F, compare with 2H (*5*, *6*)], whereas simulated clones lacking *Vang* function disrupt polarity on the proximal side of the clones [Fig. 2G, compare with 2, I and J; (*3*)]. Simulated clones lacking *dsh* function result in the disruption of polarity within the mutant cells, but only show a mild effect outside of the clones (Fig. 2K). The nearly, though not fully cell autonomous, phenotype is similar to that which we observed experimentally [Fig. 2, L and M; and (*29*)]. Clones lacking all *pk* function show only a subtle phenotype [Fig. 2, N and O; (*20*)]. Examination of protein distributions (Fig. 2; fig. S7) shows that the results are highly concordant with published observations (table S2). Similarly, simulated overexpression clones produce results closely mimicking observed experimental results (fig. S8). In simulations and in wings, relatively small clones lacking a global biasing signal show no phenotype, demonstrating that not all cells need to respond to the global directional signal for the feedback loop to cooperatively align all of the cells (*23*, *30*).

Previously, we found that Pk overexpression in the posterior wing domain enhanced the accumulation of Fz and Dsh at cell boundaries, despite the observed ability of Pk and Vang to block Dsh recruitment (*18*). Consistent with these results, Dsh and Fz are seen in a simulation of this experiment to accumulate to higher levels in the region overexpressing *pk* than in the wild-type region, and they accumulate perpendicular to the wild-type orientation near the anterior-posterior boundary (Fig. 3).

Our results suggested a mechanistic explanation for the difference between autonomous and nonautonomous *fz* alleles. Because the nearly autonomous *fz* alleles [fz^{J22} and fz^{F31}; (*27*)] have phenotypes similar to *dsh* clones, we hypothesized that these alleles may be selectively deficient in complexing with Dsh, but normal in their ability to complex with Vang (Fig. 4A). Simulations of clones in which we disrupted the interaction between Dsh and Fz by reducing the corresponding forward reaction rates produced nearly cell autonomous polarity phenotypes (Fig. 4B and fig. S9).

This hypothesis makes two easily testable predictions. First, Fz autonomous proteins should be present in the membrane and should recruit Vang to the adjacent membrane, whereas Fz nonautonomous protein should not recruit Vang. It has previously been shown that GFP-tagged Fz^{J22}, expressed in a wild-type background, is present at the apical cell cortex, but remains symmetrically distributed (*17*), a distribution in accordance with our simulation of this condition (fig. S11). Examining this further, we found that in cells adjoining clones of the autonomous fz^{F31} al-

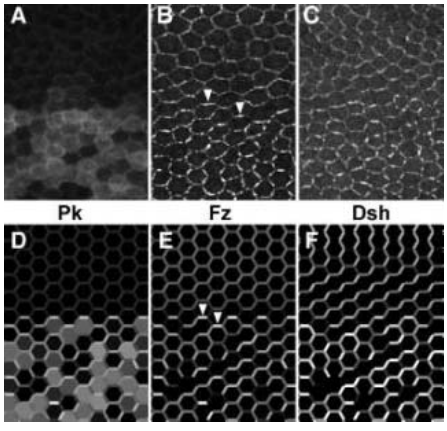

Fig. 3. *pk* overexpression. Pk (**A**), Fz::GFP (**B**) and Dsh::GFP (**C**) near the anterior-posterior boundary of pupal wings overexpressing *pk* in the *engrailed* domain. (**D** to **F**) Simulation of a periodic horizontal band of random 1x – 11.58x *pk* overexpression, showing Pk (D), Fz (E) and Dsh (F). Reorientation of Fz accumulation is denoted with arrowheads. (A to C) are different wings.

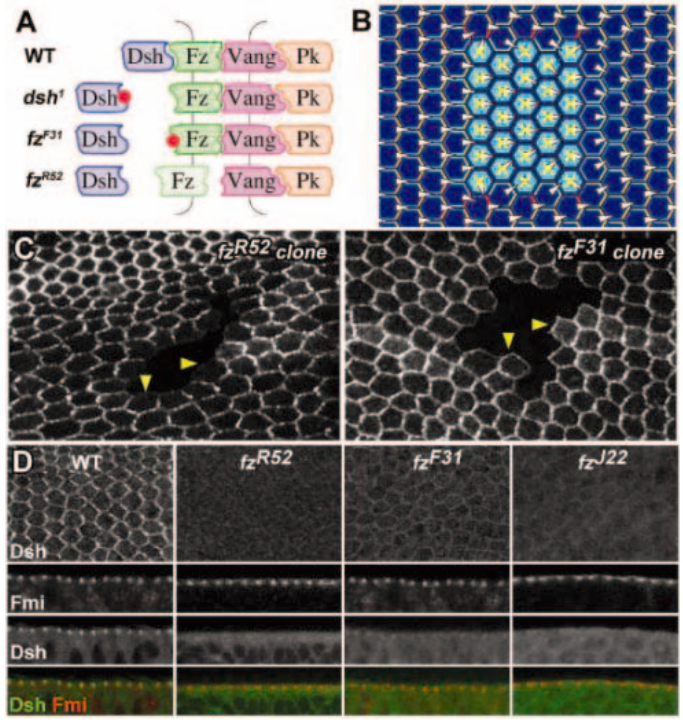

Fig. 4. Cell autonomy. (**A**) Interactions for wild-type, Dsh^1, Fz autonomous, and Fz nonautonomous alleles. Red dots indicate point mutations, and the faded Fz indicates absent protein in some null alleles. Spaces between proteins indicate loss of interaction. (**B**) Simulation of a Fz autonomous clone in which Fz has 0.01% of wild-type interaction with Dsh. (**C**) fz^{R52} (nonautonomous) and fz^{F31} (autonomous) clones with Vang::YFP in nonmutant cells. Vang accumulates at all boundaries of the fz^{F31} but not the fz^{R52} clones (arrowheads). (**D**) Dsh::GFP and Flamingo (Fmi) localization in wild-type, fz^{R52} (null), as well as fz^{F31} and fz^{J22} (autonomous) wings, viewed on the apical surface (top) or in edge cells (bottom three rows). Fmi staining identifies the correct focal plane.

lele, Vang is recruited to the boundary between wild-type and mutant cells, whereas substantially less Vang is recruited to those boundaries in cells adjoining clones of the nonautonomous fz^{R52} allele (Fig. 4C, arrowheads). Thus, $Fz^{autonomous}$ proteins recruit Vang to the opposing cell surface, whereas nonautonomous alleles do not. The second prediction is that autonomous Fz proteins should fail to recruit Dsh. Indeed, we find that both are substantially impaired in Dsh recruitment, though somewhat less impaired than the very strong, nonautonomous fz^{R52} allele (Fig. 4D). Thus, strong *fz* alleles, many of which fail to accumulate Fz protein (*27*), display no or severely impaired interaction with Dsh and Vang, whereas autonomous alleles have impaired interaction with Dsh, but retain substantial ability to recruit Vang to the adjacent membrane. Notably, simulated overexpression of Fz with impaired Dsh interaction also produced the correct polarity disruption in cells proximal to the clones [fig. 9; (*17*)].

The Dsh^1 protein produces nearly autonomous clones, and it carries a mutation in its DEP domain, which is required for membrane localization (*16*, *19*); autonomous *fz* alleles bear point mutations in the first cytoplasmic loop (*27*), suggesting these mutations may affect the same interaction. A low affinity interaction between the Dsh PDZ domain and a sequence in the cytoplasmic tail of Fz has been demonstrated (*31*). Our data suggest that sequences in the Dsh DEP domain, and in the Fz first intracellular loop, are also important for Dsh membrane association. Thus, a regulated, bipartite, high affinity association of Dsh with Fz may be selectively disrupted in $fz^{autonomous}$ alleles.

The ability of our mathematical model to simultaneously reproduce all of the most characteristic PCP phenotypes (table S2) demonstrates the feasibility of the underlying biological model as a PCP signaling mechanism. Further, the mathematical model demonstrates how the overall scheme of the model—a local feedback loop between adjacent cells amplifying an initial asymmetry—can explain the autonomous and nonautonomous behavior of PCP mutant clones. Alternative models invoking diffusible factors have not been supported by the identification of such factors (*12*), and the contact-dependent intercellular signaling model more readily accounts for the slight nonautonomy of *dsh* and $fz^{autonomous}$ clones than do the diffusible factor models.

The ability of the mathematical model to make predictions and provide a detailed picture of PCP signaling is limited by the lack of complete biological understanding. Although the validity of quantitative model predictions is subject to its assumptions and the set of features used in parameter identification (SOM text), the model has allowed us to directly connect a biological model to the complex behaviors it was hypothesized to explain and to explore the implications of variations in the model.

References and Notes

1. P. N. Adler, *Dev. Cell* **2**, 525 (2002).
2. D. R. P. Tree, D. Ma, J. D. Axelrod, *Semin. Cell Dev. Biol.* **13**, 217 (2002).
3. J. Taylor, N. Abramova, J. Charlton, P. N. Adler, *Genetics* **150**, 199 (1998).
4. T. Wolff, G. M. Rubin, *Development* **125**, 1149 (1998).
5. D. Gubb, A. Garcia-Bellido, *J. Embryol. Exp. Morphol.* **68**, 37 (1982).
6. C. R. Vinson, P. N. Adler, *Nature* **329**, 549 (1987).
7. G. Struhl, D. A. Barbash, P. A. Lawrence, *Development* **124**, 2155 (1997).
8. M. Wehrli, A. Tomlinson, *Development* **125**, 1421 (1998).
9. P. A. Lawrence, J. Casal, G. Struhl, *Development* **126**, 2441 (1999).
10. P. N. Adler, J. Taylor, J. Charlton, *Mech. Dev.* **96**, 197 (2000).
11. D. Strutt, R. Johnson, K. Cooper, S. Bray, *Curr. Biol.* **12**, 813 (2002).
12. P. A. Lawrence, J. Casal, G. Struhl, *Development* **129**, 2749 (2002).
13. M. Fanto *et al.*, *Development* **130**, 763 (2003).
14. M. P. Zeidler, N. Perrimon, D. I. Strutt, *Genes Dev.* **13**, 1342 (1999).
15. P. A. Lawrence, J. Casal, G. Struhl, *Development* **131**, 4651 (2004).
16. J. D. Axelrod, *Genes Dev.* **15**, 1182 (2001).
17. D. I. Strutt, *Mol. Cell* **7**, 367 (2001).
18. D. R. P. Tree *et al.*, *Cell* **109**, 371 (2002).
19. J. D. Axelrod, J. R. Miller, J. M. Shulman, R. T. Moon, N. Perrimon, *Genes Dev.* **12**, 2610 (1998).
20. D. Gubb *et al.*, *Genes Dev.* **13**, 2315 (1999).
21. R. Bastock, H. Strutt, D. Strutt, *Development* **130**, 3007 (2003).
22. C. Yang, J. D. Axelrod, M. A. Simon, *Cell* **108**, 675 (2002).
23. D. Ma, C. H. Yang, H. McNeill, M. A. Simon, J. D. Axelrod, *Nature* **421**, 543 (2003).
24. J. Casal, G. Struhl, P. Lawrence, *Curr. Biol.* **12**, 1189 (2002).
25. M. Hannus, F. Feiguin, C. P. Heisenberg, S. Eaton, *Development* **129**, 3493 (2002).
26. H. Strutt, D. Strutt, *Dev. Cell* **3**, 851 (2002).
27. K. H. Jones, J. Liu, P. N. Adler, *Genetics* **142**, 205 (1996).
28. A. M. Turing, *Philos. Trans. R. Soc. London B Biol. Sci.* **237**, 37 (1952).
29. P. N. Adler, personal communication.
30. K. Amonlirdviman, unpublished observations.
31. H. C. Wong *et al.*, *Mol. Cell* **12**, 1251 (2003).

32. This work was supported by the Defense Advanced Research Projects Agency BioInfoMicro (C.J.T.) and BioComp (C.J.T. and J.D.A.) Programs, Stanford's Bio-X IIP (J.D.A. and C.J.T.), NIH R01-GM59823 (J.D.A.), a National Defense Science and Engineering Graduate fellowship (K.A.), a Burt and Deedee McMurtry Stanford Graduate Fellowship (K.A.) and a PHS grant awarded by the National Cancer Institute, DHHS (W.-S.C.). We thank H. McAdams for the initial suggestion of the problem and R. Ghosh for contributions to the mathematical model.

Supporting Online Material

www.sciencemag.org/cgi/content/full/307/5708/423/DC1
Materials and Methods
SOM Text
Figs. S1 to S16
Tables S1 and S2
References and Notes

21 September 2004; accepted 29 November 2004
10.1126/science.1105471

Visfatin: A Protein Secreted by Visceral Fat That Mimics the Effects of Insulin

Atsunori Fukuhara,[1,2*] Morihiro Matsuda,[1*] Masako Nishizawa,[3*] Katsumori Segawa,[1] Masaki Tanaka,[1] Kae Kishimoto,[3] Yasushi Matsuki,[3] Mirei Murakami,[4] Tomoko Ichisaka,[4] Hiroko Murakami,[3] Eijiro Watanabe,[3] Toshiyuki Takagi,[1] Megumi Akiyoshi,[3] Tsuguteru Ohtsubo,[3] Shinji Kihara,[5] Shizuya Yamashita,[5] Makoto Makishima,[1] Tohru Funahashi,[5] Shinya Yamanaka,[4] Ryuji Hiramatsu,[3] Yuji Matsuzawa,[6] Iichiro Shimomura[1,5,7]†

Fat tissue produces a variety of secreted proteins (adipocytokines) with important roles in metabolism. We isolated a newly identified adipocytokine, visfatin, that is highly enriched in the visceral fat of both humans and mice and whose expression level in plasma increases during the development of obesity. Visfatin corresponds to a protein identified previously as pre–B cell colony-enhancing factor (PBEF), a 52-kilodalton cytokine expressed in lymphocytes. Visfatin exerted insulin-mimetic effects in cultured cells and lowered plasma glucose levels in mice. Mice heterozygous for a targeted mutation in the visfatin gene had modestly higher levels of plasma glucose relative to wild-type littermates. Surprisingly, visfatin binds to and activates the insulin receptor. Further study of visfatin's physiological role may lead to new insights into glucose homeostasis and/or new therapies for metabolic disorders such as diabetes.

Recent work in obesity research has revealed that adipose tissue functions as an endocrine organ, producing a variety of secreted factors including leptin (*1*), adiponectin/ACRP30/AdipoQ (*2*–*4*), tumor necrosis factor–α (TNF-α) (*5*), resistin (*6*), and plasminogen

activator inhibitor–1 (*7*). These so-called adipocytokines play important roles in metabolic homeostasis, and when their production is not properly regulated, they can contribute to metabolic diseases and atherosclerosis (*8*, *9*).

We sought to identify new adipocytokine(s) that are preferentially produced by human abdominal visceral fat, the accumulation of which has been linked to metabolic syndrome (*10*–*12*). Using a differential display method, we compared 8800 polymerase chain reaction (PCR) products from cDNAs derived from paired samples of subcutaneous fat and visceral fat, obtained from two female volunteers. A total of 31 bands were detected exclusively in the visceral fat samples (Fig. 1A). When used as a probe on Northern blots, one of these cDNAs detected mRNA that was more abundantly expressed in visceral fat than in subcutaneous fat (Fig. 1B). Sequencing revealed that this cDNA fragment corresponds to the 5′-untranslated region of the gene encoding pre-B cell colony-enhancing factor (PBEF) (GenBank accession number U02020) (*13*). PBEF is a growth factor for early-stage B cells and is a secreted protein mainly expressed in bone marrow, liver, and muscle (*13*). Recently, Marshall and colleagues reported that PBEF inhibits neutrophil apoptosis in clinical and experimental sepsis (*14*). A rabbit polyclonal antibody to human PBEF detected a 52-kD protein in the medium as well as the lysate of COS-1 cells transfected with the gene encoding PBEF. The same antibody detected a protein of similar size in human and mouse plasma (Fig. 1C). During differentiation of 3T3-L1 adipocytes in vitro, PBEF mRNA expression increased markedly (Fig. 1D, top), and this was accompanied by secretion of PBEF protein into the medium (Fig. 1D, bottom).

To investigate the relationship between serum levels of PBEF and adiposity, we studied both humans and mice. In 101 male and female human subjects, plasma PBEF concentrations correlated strongly with the amount of visceral fat as estimated by computed tomography ($r = 0.68$, $P < 0.001$) but only weakly with the amount of subcutaneous fat ($r = 0.22$, $P < 0.05$) (Fig. 1E). We also analyzed KKAy mice, a model for obese type II diabetes. KKAy mice rapidly become obese between 6 and 12 weeks of age (Fig. 1F). We found that during this time period, plasma PBEF levels increased significantly (Fig. 1G), as did PBEF mRNA levels in visceral fat (Fig. 1H). In contrast, PBEF mRNA levels in subcutaneous fat and liver changed very little. Finally, we measured plasma PBEF levels in c57BL/6J mice fed a normal chow diet or a high-fat/high-sucrose diet. Mice on the high-fat diet had higher plasma PBEF concentrations relative to mice fed normal chow (9.94 ± 1.70 pM versus 6.86 ± 1.35 pM, mean ± SD; $P < 0.05$), and this was accompanied by a significant increase in PBEF mRNA levels in visceral mesenteric fat (*15*). These results suggest that PBEF is a secreted factor produced abundantly by visceral fat; we therefore refer to it as visfatin.

Assessment of the biological function of visfatin revealed that it has a glucose-lowering effect. Acute administration of recombinant visfatin to c57BL/6J mice by intravenous injection resulted in a statistically significant fall in plasma glucose levels within 30 min (Fig. 2A). This effect was dose-dependent and was not due to changes in plasma insulin levels (Fig. 2B). We next injected visfatin into insulin-resistant obese KKAy mice. Visfatin significantly reduced plasma glucose concentrations, and the effect was similar to that induced by insulin injection (Fig. 2C). Similar results were seen with streptozotocin (STZ)–treated insulin-deficient mice (Fig. 2D). To investigate the effects of chronic administration of visfatin, we infected c57BL/6J and KKAy mice with an adenovirus vector encoding visfatin or LacZ (Fig. 2, E and F). Plasma visfatin

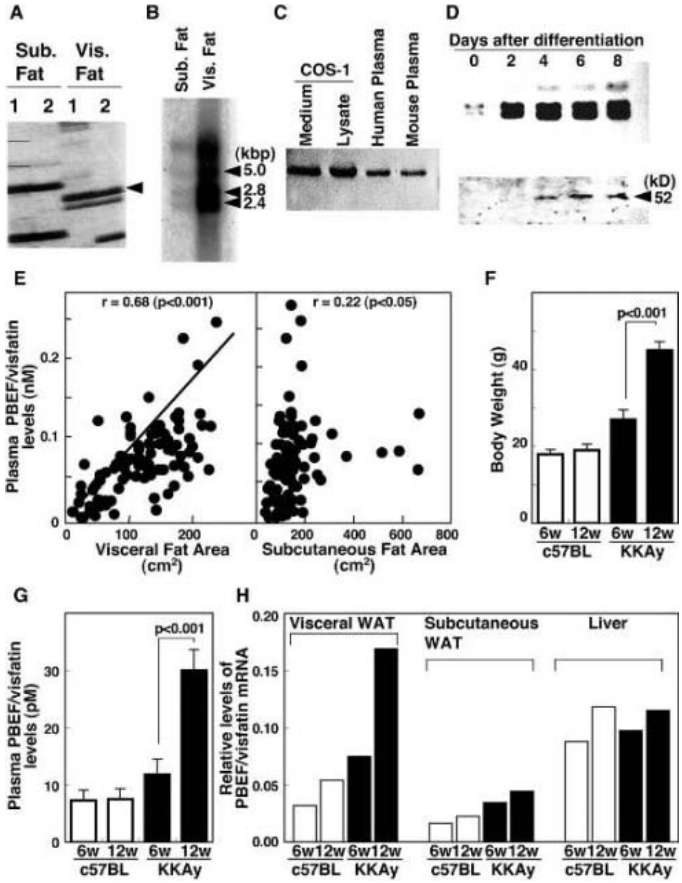

Fig. 1. Identification, expression, and secretion of PBEF/visfatin. (**A**) Differential display using paired samples of human visceral and subcutaneous fat from two female volunteers. Arrowhead indicates PCR fragment equivalent to PBEF/visfatin. (**B**) Northern blotting of PBEF/visfatin mRNA in human visceral and subcutaneous fat, using the cDNA fragment in (A) as a probe. (**C**) Immunoblotting of PBEF/visfatin protein in cell culture medium, cell lysate, and plasma from humans and mice. COS-1 cells were transfected with PBEF/visfatin expression vector. (**D**) Northern blotting of PBEF/visfatin mRNA in vitro (top) and immunoblotting of PBEF/visfatin protein secreted into the culture medium during this process (bottom). (**E**) Correlation between plasma PBEF/visfatin levels and visceral fat area (left) or subcutaneous fat area (right) in 101 male and female human subjects. (**F**) Body weight of male c57BL/6J and KKAy mice at 6 and 12 weeks of age (six mice per group). (**G**) Plasma PBEF/visfatin levels in male c57BL/6J and KKAy mice at 6 and 12 weeks of age (six mice per group). (**H**) Relative abundance of PBEF/visfatin mRNA in visceral fat, subcutaneous fat, and liver of 6- and 12-week-old male c57BL/6J and KKAy mice. Pooled total RNA from six mice per group was subjected to real-time reverse transcription PCR. The expression level of PBEF/visfatin mRNA was compared with that of cyclophilin mRNA. WAT, white adipose tissue. All data are expressed as means ± SD. Differences between groups were examined for statistical significance with Student's *t* test.

[1]Department of Medicine and Pathophysiology, Graduate School of Medicine, and Department of Organismal Biosystems, Graduate School of Frontier Biosciences, Osaka University, 2-2 Yamadaoka, Suita, Osaka 565-0871, Japan. [2]Japan Society for the Promotion of Science, Ichibancho, Chiyoda-ku, Tokyo 102-8471, Japan. [3]Genomic Science Laboratories, Sumitomo Pharmaceuticals Co. Ltd., 2-1, Takatsukasa 4-Chome, Takarazuka, Hyogo 665-0051, Japan. [4]CREST, JST, Laboratory of Animal Molecular Technology, Research and Education Center for Genetic Information, Nara Institute of Science and Technology, Ikoma, Nara 630-0192, Japan. [5]Department of Internal Medicine and Molecular Science, Graduate School of Medicine, Osaka University, 2-2 Yamadaoka, Suita, Osaka 565-0871, Japan. [6]Sumitomo Hospital, 5-3-20 Nakanoshima, Kita-Ku, Osaka, 530-0005, Japan. [7]PRESTO, Japan Science and Technology Agency, 4-1-8 Honcho, Kawaguchi, Saitama 332-0012, Japan.

*These authors contributed equally to this work.
†To whom correspondence should be addressed. E-mail: ichi@imed2.med.osaka-u.ac.jp

levels almost doubled upon adenoviral infection (*15*). Chronic production of visfatin via the adenovirus significantly attenuated plasma glucose and insulin levels in both strains of mice (Fig. 2, E and F).

To explore the physiological function of visfatin, we generated visfatin-deficient (visfatin$^{-/-}$) mice. The visfatin$^{-/-}$ mice died during early embryogenesis, so we analyzed heterozygous (visfatin$^{+/-}$) mice. These mice were viable, and their plasma visfatin levels were about two-thirds those of wild-type mice (wild type, 7.2 ± 0.5 pM; visfatin$^{+/-}$, 4.8 ± 0.3 pM). There were no differences in growth rate, food intake, total body weight, and tissue weight of epididymal fat, brown fat, liver, gastrocnemius muscle, and heart between wild-type and visfatin$^{+/-}$ mice. Plasma insulin levels did not differ significantly between these mice (wild type, 0.9 ± 0.2 ng/ml; visfatin$^{+/-}$, 1.0 ± 0.3 ng/ml). However, plasma glucose levels were higher in the visfatin$^{+/-}$ mice under both fasting and feeding conditions. This effect was modest but statistically significant (Fig. 2G). Glucose tolerance tests showed that the plasma glucose levels of visfatin$^{+/-}$ mice were modestly higher than those of wild-type mice at 60 and 120 min after glucose overload (Fig. 2H). Insulin tolerance tests showed similar insulin sensitivity in visfatin$^{+/-}$ and wild-type mice (*15*). These analyses indicate that, like insulin, visfatin has a physiological role in lowering plasma glucose levels.

To examine the insulin-mimetic effects of visfatin in more detail, we studied a variety of cultured cells. Visfatin treatment enhanced glucose uptake in 3T3-L1 adipocytes (Fig. 3A) and L6 myocytes (Fig. 3B) and suppressed glucose release in H4IIEC3 hepatocytes (Fig. 3C). These effects were similar to those of insulin (Fig. 3, A to C). We also examined the effect of visfatin on adipocyte differentiation. Primary-cultured preadipocytes from visceral mesenteric (Fig. 3D, left) and subcutaneous (Fig. 3D, right) fat depots of control ICR (Institute for Cancer Research) mice were treated with phosphate-buffered saline (PBS), visfatin, or insulin. Like insulin, visfatin induced triglyceride accumulation in preadipocytes from both fat depots and accelerated triglyceride synthesis from glucose (Fig. 3E) (fig. S1). Visfatin treatment also markedly induced the expression of genes encoding adipose markers such as peroxisome proliferator-activated receptor–γ (PPAR-γ), CCAAT-enhancer binding protein–α (C/EBP-α), fatty acid synthase (FAS), diacylglycerol *O*-acyltransferase–1 (DGAT-1), adipose P2 (aP2), and adiponectin (fig. S2). Similar adipogenesis-inducing effects of visfatin were observed in 3T3-L1 and 3T3-F442A cells (*15*).

We next investigated whether visfatin had an effect on insulin signaling. Intravenous injection of visfatin into mice induced tyrosine phosphorylation of the insulin receptor (IR), insulin receptor substrate–1 (IRS-1), and IRS-2 in the liver, similar to the effects of insulin injection (Fig. 4A). Visfatin treatment of 3T3-F442A adipocytes in culture induced the phosphorylation of IR, IRS-1, and IRS-2; binding of phosphatidylinositol 3-kinase (PI3K) to IRS-1 and IRS-2; and phosphorylation of Akt and mitogen-activated protein kinase (MAPK), again resembling the effects of insulin (Fig. 4B). Similar activation of the insulin signal transduction pathway was observed in L6 myocytes (Fig. 4C) and H4IIEC3 hepatocytes (Fig. 4D). Visfatin also enhanced IRS-1–associated PI3K activity in epididymal fat–derived primary adipocytes, and the effect of visfatin and insulin was additive in this assay (Fig. 4E).

We also analyzed the binding affinity of visfatin to IR. Expression of IR at the cell surface in human embryonic kidney (HEK) 293 cells enhanced the binding of both visfatin and insulin to cells (Fig. 4F). The binding equilibrium dissociation constant (K_D) of visfatin to IR (4.4 nM) was similar to that of insulin (6.1 nM). However, binding of visfatin to insulin-like growth factor I receptor (IGF-IR) was very weak (fig. S3). We also found that visfatin binds to immunoprecipitated IR protein from HEK-293 cells transfected with the gene encoding IR (Fig. 4G).

To determine whether insulin and visfatin share a common binding site in IR, we used a competitive inhibition assay. Unlabeled insulin displaced radiolabeled insulin binding to IR expressed in intact HEK-293 cells, but unlabeled visfatin did not (Fig. 4H, top). Similarly, unlabeled visfatin displaced radiolabeled visfatin binding to IR, but unlabeled insulin did not (Fig. 4H, bottom). We also investigated whether visfatin bound to IR with an Asn^{15} → Lys mutation in the α-subunit (IR-N15K). Insulin binds to the extracellular α-subunit of IR, and N15K mutant was reported to cause loss of binding affinity of insulin (*16*). As previously described, the binding affinity of IR-N15K to insulin (K_D = 69.7 nM) was blunted relative to that of wild-type IR (IR-

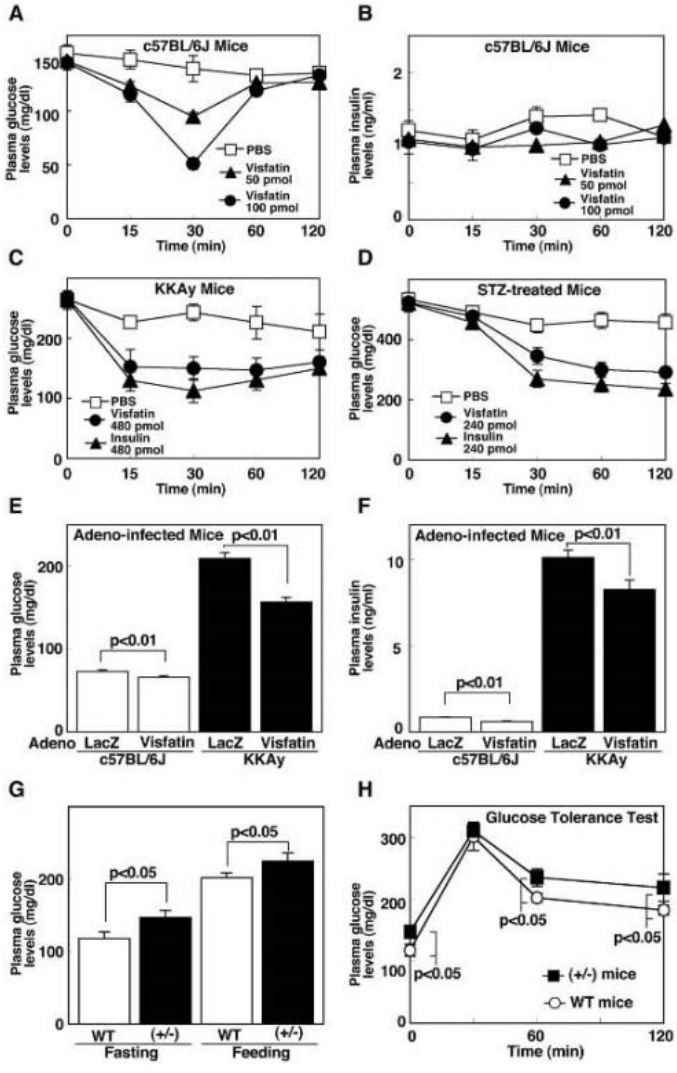

Fig. 2. Glucose-lowering effects of visfatin in mouse models. (**A** and **B**) Plasma glucose (A) and insulin (B) concentrations in male c57BL/6J mice after a single-bolus injection of PBS or visfatin (five mice per group). (**C** and **D**) Plasma glucose concentrations in male KKAy mice (C) and STZ-treated male c57BL/6J mice (D) after a single-bolus injection of PBS, visfatin, or insulin (five mice per group). (**E** and **F**) Fasting plasma glucose (E) and insulin levels (F) in male c57BL/6J and KKAy mice at day 7 after infection with an adenovirus vector expressing the LacZ gene product or visfatin (10 mice per group). (**G**) Plasma glucose levels in male wild-type and visfatin$^{+/-}$ mice in 12-hour fasting or feeding conditions (seven mice per group). (**H**) Glucose tolerance test in male wild-type and visfatin$^{+/-}$ mice (seven mice per group). All data are expressed as means ± SD. Differences between groups were examined for statistical significance with Student's *t* test.

WT) to insulin (K_D = 2.5 nM) (Fig. 4I, top). However, visfatin potently bound to IR-N15K (K_D = 6.6 nM), comparable to the binding of visfatin to IR-WT (K_D = 3.0 nM) (Fig. 4I, bottom). Indeed, we also observed visfatin-dependent autophosphorylation of IR-N15K in intact CHO cells expressing IR-N15K (*15*). These results suggest that visfatin directly activates IR but in a manner distinct from insulin.

In summary, several lines of evidence indicate that visfatin shares properties with insulin both in vivo and in vitro. First, administration of high doses of recombinant visfatin lowered plasma glucose levels in both

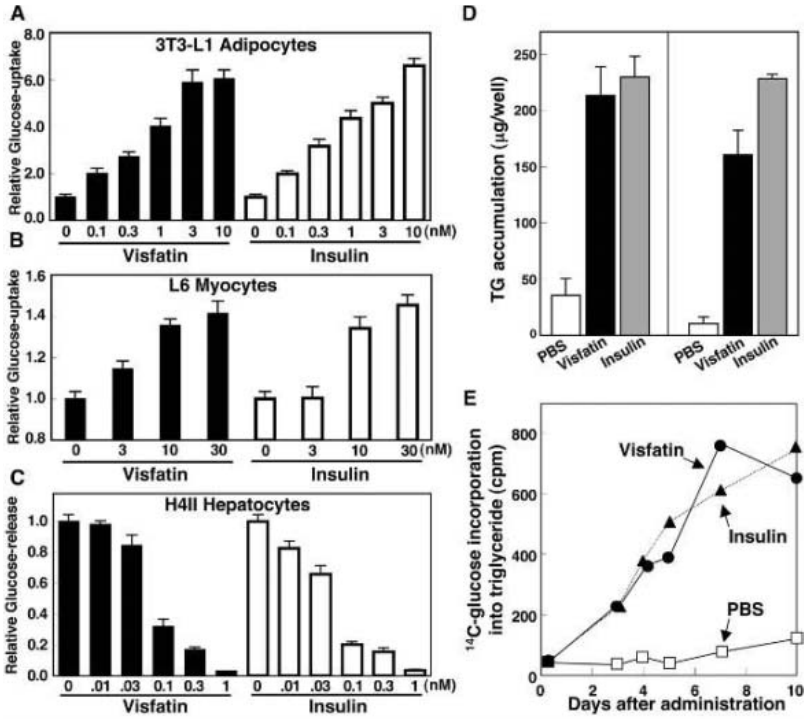

Fig. 3. Effects of visfatin in cultured cells. (**A** to **C**) Effects of visfatin and insulin on glucose uptake in 3T3-L1 adipocytes (A) and L6 myocytes (B) and on glucose release into medium in H4IIEC3 hepatocytes (C). Data are expressed as means ± SD of three experiments performed in duplicate. (**D** and **E**) Effects of visfatin and insulin on triglyceride accumulation. Preadipocytes obtained from visceral mesenteric [(D), left] or subcutaneous [(D), right] fat depots of control male ICR mice were cultured with visfatin or insulin (10 ng/ml each) for 6 days. Accumulated triglyceride (TG) was measured. (E) ^{14}C-glucose incorporation into triglycerides. All data shown are means ± SD.

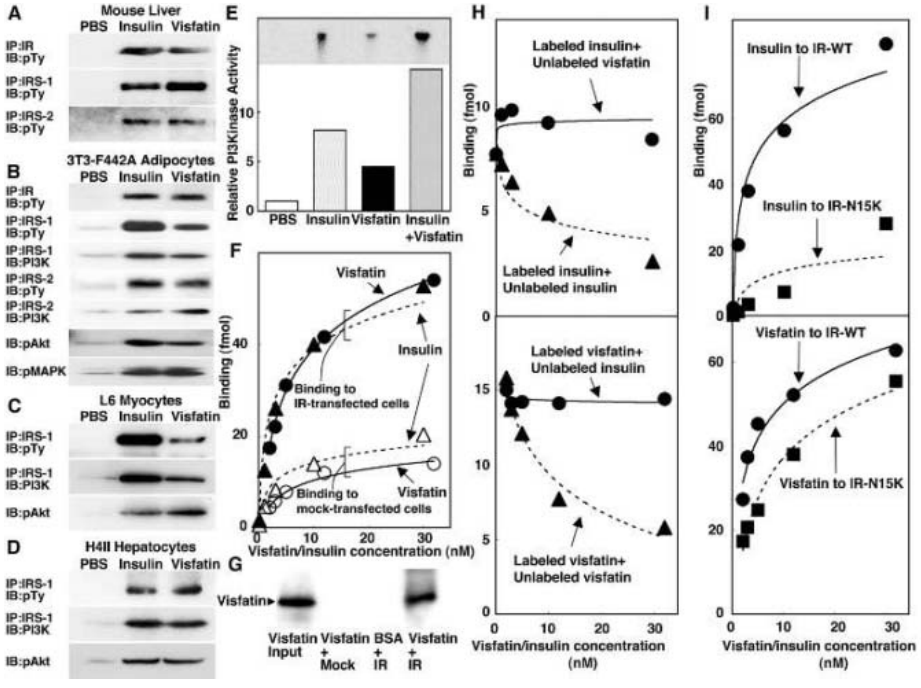

Fig. 4. Effects of visfatin on insulin signal transduction. (**A**) Tyrosine phosphorylation of IR, IRS-1, and IRS-2 in mouse liver after delivery of 240 pmol of insulin or visfatin by injection into the jugular vein. The liver was removed 10 min after injection, and the protein extract was analyzed by immunoprecipitation (IP) with antibodies to IR, IRS-1, and IRS-2 after immunoblotting (IB) with antibody to phosphotyrosine (pTy). (**B**) Tyrosine phosphorylation of IR, IRS-1, and IRS-2 and serine phosphorylation of Akt and MAPK in cultured 3T3-F442A adipocytes after treatment with PBS, insulin (100 ng/ml), or visfatin (100 ng/ml). (**C** and **D**) Tyrosine phosphorylation of IRS-1, serine phosphorylation of Akt, and amounts of PI3K bound to IRS-1 in L6 myocytes (C) or H4IIEC3 hepatocytes (D). Cells were treated with PBS, insulin (100 ng/ml), or visfatin (100 ng/ml). For measurement of serine phosphorylation of Akt and MAPK, proteins were separated by electrophoresis, blotted onto a membrane, and detected with antibodies to phospho-Akt and phospho-MAPK. For measurement of IRS-1 and IRS-2, the protein extracts were analyzed by immunoprecipitation with antibodies to IRS-1 and IRS-2 and detected with antibodies to phosphotyrosine and PI3K. (**E**) IRS-1–associated PI3K activity in primary adipocytes from epididymal fat depots of c57BL/6J mice treated as in (B). (Inset) ^{32}P-labeled 3-phosphatidylinositides. (**F**) Binding of ^{125}I-labeled insulin (triangles) or visfatin (circles) to intact HEK-293 cells transfected with plasmid alone or plasmid encoding IR. (**G**) Direct binding of visfatin to human IR in vitro. Purified visfatin or bovine serum albumin (BSA) was incubated with Flag-IR or Flag alone immobilized on anti-Flag beads. The beads were extensively washed and subjected to SDS–polyacrylamide gel electrophoresis followed by Western blotting with antibody to visfatin. (**H**) (Top) Competitive inhibition of binding of ^{125}I-labeled insulin by unlabeled visfatin or insulin to intact HEK-293 cells transfected with IR. (Bottom) Competitive inhibition of binding of ^{125}I-labeled visfatin by unlabeled insulin or visfatin to intact HEK-293 cells transfected with IR. (**I**) Binding of ^{125}I-labeled insulin (top) or visfatin (bottom) to intact HEK-293 cells transfected with IR-WT or IR-N15K vector.

insulin-resistant and insulin-deficient mice. Second, in obese KKAy mice, a doubling of plasma visfatin levels achieved by an adenovirus vector also led to a reduction of plasma glucose and insulin concentrations. Finally, our biochemical studies indicate that visfatin activates insulin signaling through IR but in a different fashion from insulin.

There are important differences between visfatin and insulin, however. Plasma visfatin levels did not change significantly upon fasting or feeding in mice (fig. S4), whereas plasma insulin levels increased in the fed state and decreased in the fasting state. The plasma concentration of visfatin was 10% that of insulin in the fasting condition and only 3% in the fed condition. These low concentrations of visfatin may account for the modest effect of visfatin on plasma glucose levels relative to that of insulin, as shown by our analysis of visfatin$^{+/-}$ mice. Our biochemical studies showed that at similar concentrations, visfatin and insulin have a comparable ability to activate insulin signaling and glucose uptake and to inhibit glucose release. Moreover, in visfatin$^{+/-}$ mice, a 3 pM reduction in plasma visfatin levels leads to a 10 to 20 mg/dl elevation in plasma glucose concentrations. Taken together, these data suggest that visfatin plays a physiological role in lowering plasma glucose concentrations, but its contribution is small because of its low concentration.

The previously reported function of PBEF/visfatin was enhancement of the effect of interleukin-7 (IL-7) on pre-B cell colony formation (*13*). Insulin and IGFs were also reported to potentiate pre-B cell colony formation (*17*). Thus, this function of PBEF/visfatin may be attributed to another insulin-like effect. Relative to adipose tissue of lean mice, adipose tissue of obese mice contains increased amounts of proinflammatory cytokines such as TNF-α or IL-6. Both of these cytokines increase mRNA levels of PBEF/visfatin (*18*) and thus may be responsible for the increased mRNA levels of PBEF/visfatin in visceral fat.

The discovery of the insulin-mimetic function of visfatin may shed new light on glucose and lipid homeostasis, adipocyte proliferation and differentiation, and other aspects of insulin-related biology. The potential relationship between visfatin and metabolic syndrome also merits further investigation, because plasma visfatin levels increase in proportion to visceral fat accumulation. Finally, our results raise the possibility that visfatin may be a useful target for the development of drug therapies for diabetes.

References and Notes

1. J. M. Friedman, J. L. Halaas, *Nature* **395**, 763 (1998).
2. K. Maeda *et al.*, *Biochem. Biophys. Res. Commun.* **221**, 286 (1996).
3. P. E. Scherer, S. Williams, M. Fogliano, G. Baldini, H. F. Lodish, *J. Biol. Chem.* **270**, 26746 (1995).
4. E. Hu, P. Liang, B. M. Spiegelman, *J. Biol. Chem.* **271**, 10697 (1996).
5. G. S. Hotamisligil, N. S. Shargill, B. M. Spiegelman, *Science* **259**, 87 (1993).
6. C. M. Steppan *et al.*, *Nature* **409**, 307 (2001).
7. I. Shimomura *et al.*, *Nature Med.* **2**, 800 (1996).
8. I. Shimomura, R. E. Hammer, S. Ikemoto, M. S. Brown, J. L. Goldstein, *Nature* **401**, 73 (1999).
9. N. Maeda *et al.*, *Nature Med.* **8**, 731 (2002).
10. A. H. Kissebah, A. N. Peiris, *Diabetes Metab. Rev.* **5**, 83 (1989).
11. Y. Matsuzawa, I. Shimomura, T. Nakamura, Y. Keno, K. Tokunaga, *Ann. N. Y. Acad. Sci.* **676**, 270 (1993).
12. S. Fujioka, Y. Matsuzawa, K. Tokunaga, S. Tarui, *Metabolism* **36**, 54 (1987).
13. B. Samal *et al.*, *Mol. Cell. Biol.* **14**, 1431 (1994).
14. S. H. Jia *et al.*, *J. Clin. Invest.* **113**, 1318 (2004).
15. A. Fukuhara *et al.*, unpublished data.
16. T. Kadowaki, H. Kadowaki, D. Accili, S. I. Taylor, *J. Biol. Chem.* **265**, 19143 (1990).
17. K. S. Landreth, R. Narayanan, K. Dorshkind, *Blood* **80**, 1207 (1992).
18. S. Ognjanovic *et al.*, *J. Mol. Endocrinol.* **26**, 107 (2001).

19. We thank the members of the Shimomura laboratory for helpful discussions, D. Accili and S. Takahashi for the IGF-IR expression vector, and H. Kondo for the visfatin-producing adenovirus. Supported by the 21st Century Center of Excellence Program; the Japan Research Foundation for Clinical Pharmacology; the Ministry of Health, Labor and Welfare, Japan; and the Ministry of Education, Culture, Sports, Science and Technology, Japan.

Supporting Online Material

www.sciencemag.org/cgi/content/full/1097243/DC1
Materials and Methods
Figs. S1 to S4

26 February 2004; accepted 29 October 2004
Published online 16 December 2004;
10.1126/science.1097243
Include this information when citing this paper.

T Helper Cell Fate Specified by Kinase-Mediated Interaction of T-bet with GATA-3

Eun Sook Hwang,[1] Susanne J. Szabo,[1]* Pamela L. Schwartzberg,[3] Laurie H. Glimcher[1,2]†

Cell lineage specification depends on both gene activation and gene silencing, and in the differentiation of T helper progenitors to Th1 or Th2 effector cells, this requires the action of two opposing transcription factors, T-bet and GATA-3. T-bet is essential for the development of Th1 cells, and GATA-3 performs an equivalent role in Th2 development. We report that T-bet represses Th2 lineage commitment through tyrosine kinase–mediated interaction between the two transcription factors that interferes with the binding of GATA-3 to its target DNA. These results provide a novel function for tyrosine phosphorylation of a transcription factor in specifying alternate fates of a common progenitor cell.

The immune system T-box protein T-bet controls lineage commitment of the two subsets of cytokine-producing helper T cells, Type 1 (Th1) and Type 2 (Th2) (*1*–*3*) by simultaneously driving Th1 genetic programs and repressing the development of the opposing Th2 subset. T-bet is principally required for expression of the potent inflammatory cytokine interferon-γ (IFN-γ), the hallmark of Type 1 immunity, and simultaneous repression of the signature Th2 cytokines interleukin-4 (IL-4) and IL-5 (*1*, *4*). As a consequence, mice lacking T-bet fail to develop a Th1 compartment but possess an overexpanded Th2 compartment, which leads to a spontaneous asthma-related phenotype (*2*, *5*). Although it is established that T-bet accomplishes Th1 programs partly through direct induction of IFN-γ– and IL-12Rβ2–chain gene transcription (*6*), the mechanism by which it represses Th2 programs is unclear.

To determine whether T cell receptor (TCR) signaling induced alterations in T-bet, a Th1 clone and control Th2 clone were tested after polyclonal TCR engagement. Western blotting revealed a specific phosphorylated species in a Th1 clone that was not present in Th2 cells (fig. S1A). T-bet was rapidly induced in early Th1 differentiation, gradually decreasing at later stages (Fig. 1A). We also observed T-bet tyrosine phosphorylation to occur primarily in Thp cells upon TCR engagement, being most pronounced early in differentiation (day 2), declining by day 4, and being undetectable upon secondary stimulation (Fig. 1A). Tyrosine phosphorylation of T-bet was also enhanced in the presence of the phosphatase inhibitor pervanadate (fig. S1B). Thus, T-bet becomes tyrosine phosphorylated at the earliest stages of Thp dif-

[1]Department of Immunology and Infectious Diseases, Harvard School of Public Health, and [2]Department of Medicine, Harvard Medical School, Boston, MA 02115, USA. [3]National Human Genome Research Institute, National Institutes of Health, Bethesda, MD 20892, USA.

*Present address: Novartis Pharmaceuticals, Cambridge, MA 02115, USA.

†To whom correspondence should be addressed. E-mail: lglimche@hsph.harvard.edu

ferentiation, consistent with its involvement at the initial stages of lineage commitment.

T-bet is constitutively nuclear (*7*), which indicates that its phosphorylation is mediated by one of the few nuclear tyrosine kinases identified in T cells (*8*, *9*). Using the Scansite program (*10*), we identified an ITK phosphorylation motif at the C terminus of T-bet (Y525), as well as three conserved c-Abl sites (Y76, Y107, and Y117). Although phosphorylation of T-bet was restricted to the Tec kinases ITK and RLK (fig. S1C), coexpression studies demonstrated that this was most efficiently performed by ITK (Fig. 1B). In primary CD4 T cells isolated from ITK-, RLK-, or double ITK/RLK-deficient mice (*11*), the greatest diminution of T-bet tyrosine phosphorylation was seen in the absence of ITK (*7*) (Fig. 1C). Furthermore, mutation of T-bet at tyrosine residue 525, but not control tyrosine residue 437, resulted in greatly reduced phosphorylation by ITK (Fig. 1D), revealing that ITK phosphorylates T-bet at residue Y525 after TCR stimulation.

To assess the functional relevance of ITK-induced T-bet phosphorylation, CD4+ T-bet$^{-/-}$ Thp cells were transduced with mutant green fluorescent protein (GFP) retroviruses expressing T-bet wild-type (RV-T-bet) and Y525F (RV-T-bet Y525F), with assessment of cytokine production after secondary stimulation. Both RV-T-bet and Y525F T-bet could restore T-bet function, demonstrated by the repression of IL-2 and the increased induction of IFN-γ (by a factor of >100) (Fig. 1E). However, Y525F T-bet was much less effective in repressing the expression of Th2 cytokines IL-4, IL-5, and IL-13. Similar results were obtained in T-bet$^{-/-}$ × IFN-γ$^{-/-}$ CD4+ Th cells (fig. S1F), revealing that the role of T-bet tyrosine phosphorylation in repressing Th2 cytokines is independent of IFN-γ.

The multidomain protein ITK, an important mediator of TCR signaling in lymphocytes (*9*, *12*, *13*), resides in both nucleus and cytosol, which suggests that it physically associates with T-bet. Selective association of ITK with T-bet in coexpression studies correlated with its ability to phosphorylate T-bet (Fig. 2A). Using a series of ITK mutants, we also revealed that this occurred via the ITK SH1 kinase domain (Fig. 2B). Additionally, this interaction depended largely on the presence of tyrosine 525 within T-bet, as ITK coimmunoprecipitated less well with the Y525F T-bet mutant (Fig. 2C). To look for association under endogenous conditions, T-bet was immunoprecipitated from nuclear extracts of BALB/c wild-type, T-bet$^{-/-}$, and Itk$^{-/-}$ thymocytes followed by Western blotting with antibody (Ab) to ITK. In these experiments, the presence of ITK was apparent in immune complexes from wild-type, but not T-bet$^{-/-}$ or Itk$^{-/-}$, thymocytes (Fig. 2D).

Because T-bet is known to be coregulated with GATA-3, we tested whether this might take place through a physical association. Coexpression of FLAG-tagged GATA-3 or GATA-3 mutants bearing truncations with wild-type or Y525F T-bet did suggest a physical interaction of the two proteins that was diminished by the Y525F mutation (Fig. 3A) and mapped to the GATA-3 N-terminal (amino acids 1–257) domain (fig. S2D). Coimmu-

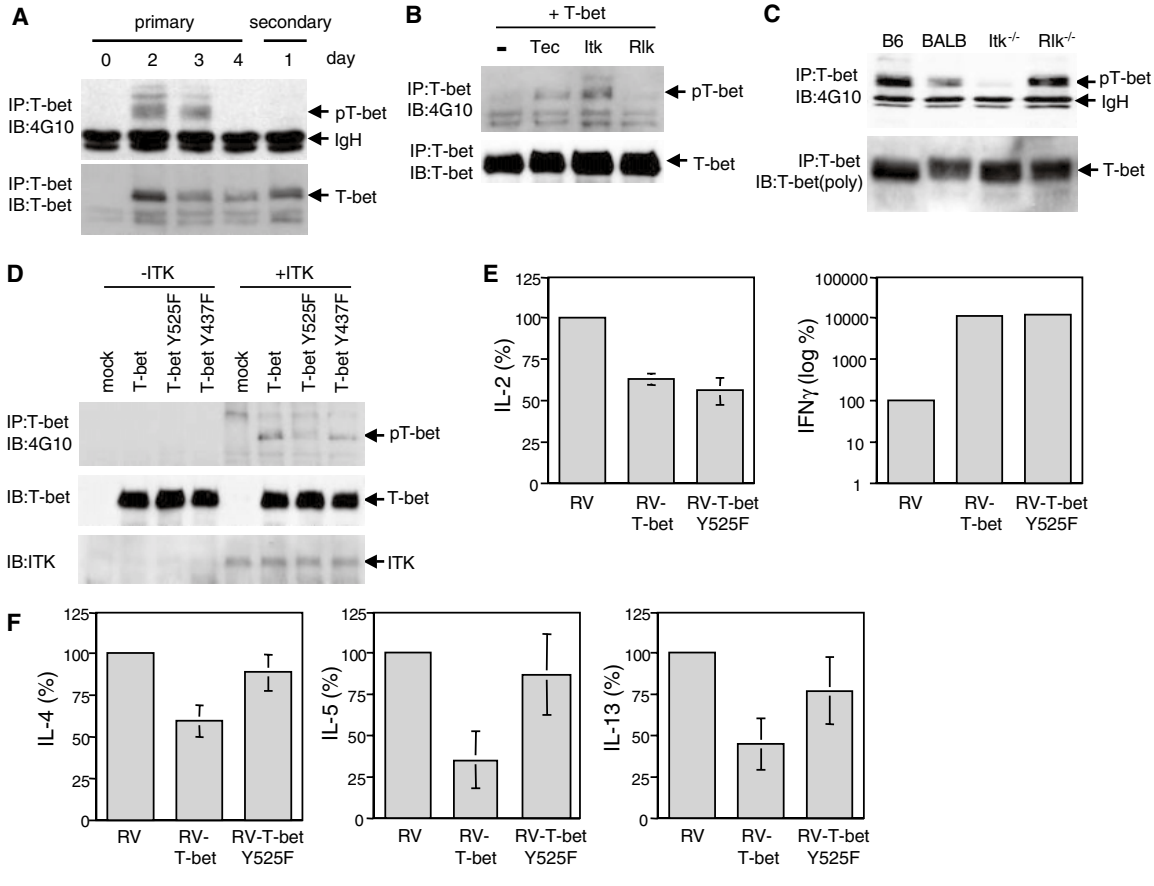

Fig. 1. (**A**) T-bet tyrosine phosphorylation in primary Th1 cells. CD4+ lymph node and spleen Thp cells were stimulated with plate-bound Ab to CD3 (2 μg/ml), Ab to CD28 (1 μg/ml), and IL-2 (100 U/ml) with IL-12 (1 ng/ml) and Ab to IL-4 (10 μg/ml). Total cell extracts were prepared on days 0, 2, 3, and 4 after primary stimulation and on day 1 after secondary stimulation. Pervanadate (100 μM) was added 15 min before cell lysis. (**B**) ITK phosphorylates T-bet. T-bet was cotransfected with Tec kinases TEC, ITK, or RLK in 293T cells, and total cell lysates were prepared after incubation with pervanadate for 15 min. (**C**) Diminished tyrosine phosphorylation of T-bet in Itk$^{-/-}$ CD4+ T cells. CD4+ T cells isolated from the indicated strains were stimulated with plate-bound Ab to CD3 and Ab to CD28 under Th1-skewing condition for 2 days. (**D**) ITK phosphorylates tyrosine 525 residue of T-bet. Wild-type (WT) or tyrosine mutants of T-bet (Y525F and Y437F) were cotransfected with either control vector or ITK into 293T cells. Expression of T-bet or ITK was detected by Western blot using total cell lysates. [(A) to (D)] Tyrosine phosphorylation of T-bet was performed by immunoprecipitation with monoclonal antibody (mAb) to T-bet and by immunoblot with mAb to phosphotyrosine, 4G10, as in fig. S1A. (**E**) WT and Y525F T-bet both restore T-bet function in regulating IL-2 and IFN-γ. Data represent mean ± SD. (**F**) The optimal repression of Th2 cytokines by T-bet requires Y525. *P* value of 0.0002 for IL-4, 0.0074 for IL-5, and 0.002 for IL-13. CD4+ T cells purified from T-bet$^{-/-}$ or T-bet$^{-/-}$ × IFN-γ$^{-/-}$ (fig. S1F) mice were stimulated for 24 hours under Th2-skewing conditions and then transduced with RV, RV-T-bet, or RV-T-bet Y525F. Cells sorted for GFP were expanded for 6 days and restimulated with Ab to CD3 for 24 hours, and cytokines were measured by enzyme-linked immunosorbent assay. Data represent mean ± SD.

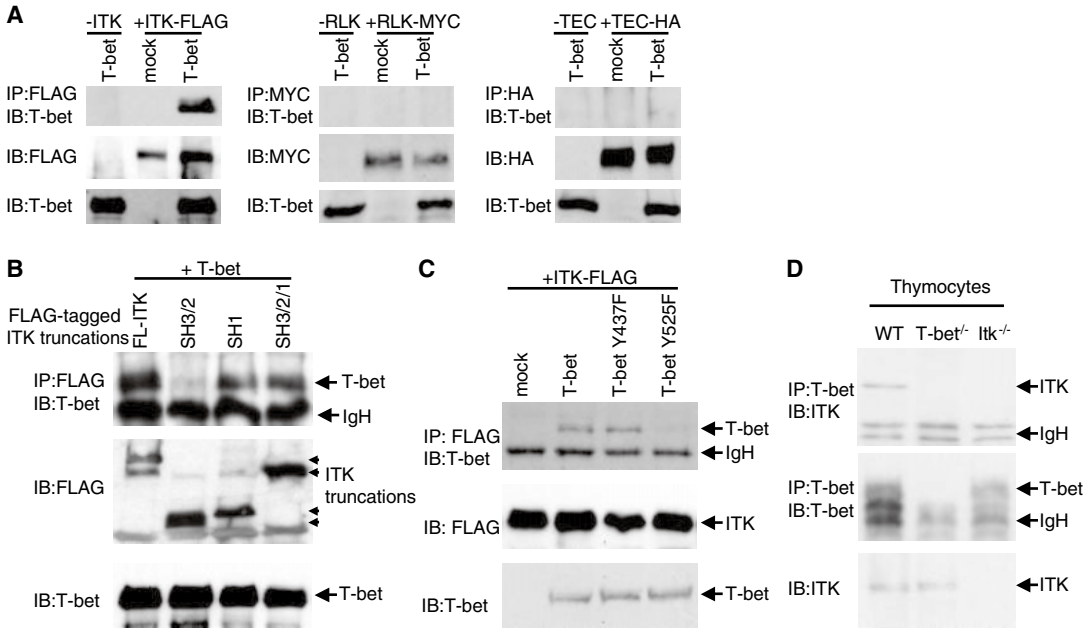

Fig. 2. T-bet physically interacts with ITK. (**A**) T-bet was cotransfected into 293T cells with peptide-tagged TEC kinases ITK-FLAG, RLK-MYC, or TEC-hemagglutinin (TEC-HA). Total cell extracts were incubated with Abs to FLAG, MYC, or HA, and immunocomplexes were resolved by 7.5% Tris-Glycine (Tris-HCl Gel, BIO-RAD, Hercules, CA) gel and probed with Ab to T-bet. Expression of T-bet or TEC kinases was assayed by Western blot using total cell lysates. (**B**) ITK interacts with T-bet through its SH1 domain. The FLAG-tagged ITK truncations were cotransfected with T-bet into 293T cells and immunoprecipitated with Ab to FLAG followed by Western blot with Ab to T-bet. Expression of ITK truncations and T-bet was detected with Abs to FLAG T-bet. (**C**) ITK interacts with the tyrosine Y525 residue of T-bet. FLAG-tagged ITK was coexpressed with WT or tyrosine mutants (Y525F or Y437F) of T-bet, immunoprecipitated with FLAG-M2 agarose, and the protein blot was probed with Ab to T-bet. Similar expression levels of T-bet proteins and ITK were detected in 30 μg of total cell lysates. (**D**) T-bet interacts with ITK in vivo in thymus. Nuclear extracts were prepared from BALB/c WT, T-bet$^{-/-}$, and Itk$^{-/-}$ thymi with NE-PER (Pierce, Rockford, IL). Two mg of nuclear extracts were incubated with 4B10 in 150 mM NaCl, and immune complexes were resolved and probed with mAb to ITK (2F12) and then sequentially with 4B10 after stripping. ITK expression was assayed in 30 μg of nuclear extracts.

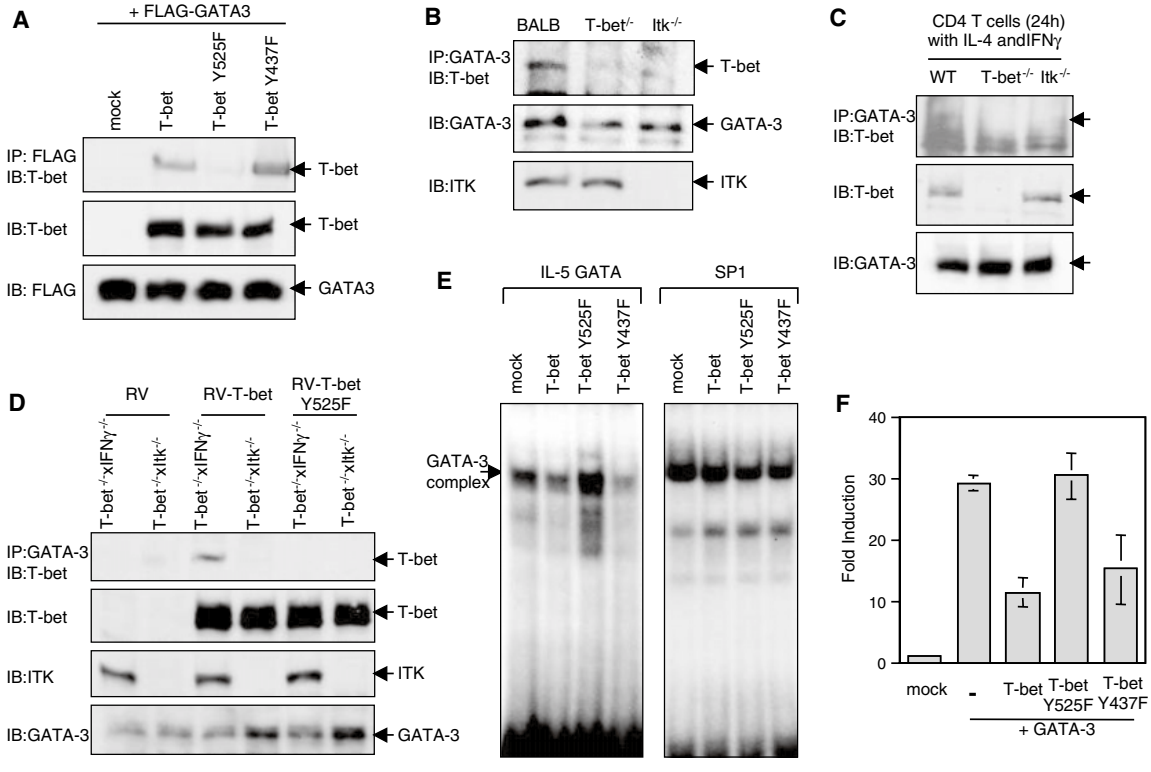

Fig. 3. T-bet interacts with GATA-3 and sequesters it away from binding to target DNA. (**A**) FLAG-tagged GATA-3 was cotransfected into 293T cells with WT, Y525F, or Y437F T-bet and immunoprecipitated with FLAG-M2 agarose, and protein blots were probed with 4B10. Expression of T-bet and GATA-3 was analyzed by Western blot of total cell lysates. (**B**) T-bet interacts with GATA-3 in thymocytes in an ITK-dependent manner. Thymocyte nuclear extracts (3 mg) isolated in Fig. 2D were used for immunoprecipitation and immunoblot analyses as described in fig. S2A. (**C**) Naive Thp from BALB/c WT, T-bet$^{-/-}$, and Itk$^{-/-}$ mice were cultured for 24 hours with Ab to CD3 plus Ab to CD28 and IL-2 in the presence of rIL-4 and rIFN-γ, nuclear extracts were prepared, and immunoprecipitation and immunoblot analyses were performed as in fig. S2A. (**D**) T-bet interacts with GATA-3 in vivo, in an ITK-dependent manner. CD4+ T cells isolated from T-bet$^{-/-}$ × IFN-γ$^{-/-}$ or T-bet$^{-/-}$ × Itk$^{-/-}$ mice were activated and transduced with retroviruses as described (Fig. 1, E and F). Nuclear extracts were prepared for immunoprecipitation with Ab to GATA-3 and for immunoblot analyses of T-bet, GATA-3, and ITK. We observed comparable expression of GATA-3 in Th cells transduced with control, WT, or Y525F T-bet (fig. S2E). (**E**) DNA binding activity of GATA-3 is blocked by T-bet but not by T-bet Y525F. EL4 cells were transfected with WT, Y525F, or Y437F T-bet and nuclear extracts were incubated with radiolabeled GATA-3 binding sites from the IL-5 promoter, or with SP1 binding sites, resolved in native 6% polyacrylamide gel, and subjected to autoradiography. (**F**) WT but not Y525F T-bet inhibits GATA-3 driven IL-5 promoter activation. EL4 cells were cotransfected with an IL-5 promoter reporter gene with GATA-3 and T-bet cDNAs and a β-gal reporter gene. Relative luciferase activity was assayed, standardized with β-galactosidase activity, and shown as fold induction. There was comparable expression of GATA-3 and T-bet (fig. S2F). Data represent mean ± SD.

noprecipitation experiments further confirmed that the two proteins directly associate in vivo (Fig. 3B and fig. S2A). Notably, this was facilitated by ITK, because it was not detected in Itk$^{-/-}$ thymus (Fig. 3B). We also detected endogenous association of T-bet and GATA-3 in Thp cells treated in culture for 24 hours with Ab to CD3/CD28 and recombinant IL-2 (rIL-2) alone (fig. S2B) or in the presence of IL-4 and IFN-γ to induce higher expression of T-bet and GATA-3 (Fig. 3C). Again, this was dependent on Y525 phosphorylation by ITK (Fig. 3D). T-bet and GATA-3 were also observed to associate in the human natural killer cell line YT (fig. S2C). Reconstitution of T-bet$^{-/-}$, T-bet$^{-/-}$ × IFN-γ$^{-/-}$, and T-bet$^{-/-}$ × Itk$^{-/-}$ Thp with wild-type or Y525F mutant T-bet confirmed that the T-bet/GATA-2 interaction required Y525 and ITK (Fig. 3D).

We reasoned that the physical interaction between T-bet and GATA-3 might act to sequester GATA-3 away from its binding sites in the Th2 cytokine locus. Indeed, electrophoretic mobility shift assay with nuclear extracts from EL4 cells transfected with wild-type or Y437F T-bet revealed diminished binding of GATA-3 to its target sequence in the IL-5 promoter (Fig. 3E). In contrast, expression of the T-bet Y525F mutant did not affect GATA-3/DNA complex formation (Fig. 3E), nor did it repress GATA-3–dependent IL-5 promoter activity (Fig. 3F) despite all proteins being expressed at equivalent levels in these experiments (fig. S2, E and F).

Considerable work has implicated ITK and RLK in directing CD4+ T helper cell differentiation. However, integrating the various studies and model systems into a single unified model has been complex and controversial (*11*, *14–17*). ITK$^{-/-}$ mice display a range of impaired and expanded Th2 phenotypes. Thus, although the exact relation to our studies is not yet resolved, the evidence suggests a pivotal modulation of T helper differentiation by this kinase.

Our studies show that tyrosine phosphorylation of T-bet by this and possibly other kinases is required for the repression of Th2 genetic programs rather than the activation of Th1 genetic programs, which reveals that the two major functions of T-bet in directing Th lineage commitment, gene activation and gene silencing, are physically distinct. Few transcription factors are known to be tyrosine phosphoproteins (*18–21*), and although there is precedent for transcription factors that cross-regulate one another in cell lineage commitment, no structural basis for such repression has been established (*22*). Our studies reveal one such mechanism, whereby tyrosine phosphorylation activity of a nuclear kinase controls the interaction of two opposing transcription factors, T-bet and GATA-3, in the repression of Th2 lineage development. The in vivo importance of this observation in the full context of normal immune responses requires further exploration.

References and Notes

1. S. J. Szabo *et al.*, *Cell* **100**, 655 (2000).
2. S. J. Szabo *et al.*, *Science* **295**, 338 (2002).
3. S. J. Szabo, B. M. Sullivan, S. L. Peng, L. H. Glimcher, *Annu. Rev. Immunol.* **21**, 713 (2003).
4. B. M. Sullivan, A. Juedes, S. J. Szabo, M. von Herrath, L. H. Glimcher, *Proc. Natl. Acad. Sci. U.S.A.* **100**, 15818 (2003).
5. S. Finotto *et al.*, *Science* **295**, 336 (2002).
6. A. C. Mullen *et al.*, *Nature Immunol.* **3**, 652 (2002).
7. E. S. Hwang, L. H. Glimcher, unpublished data.
8. A. Takesone, L. D. Finkelstein, P. L. Schwartzberg, *J. Cell Sci.* **115**, 3039 (2002).
9. J. A. Lucas, A. T. Miller, L. O. Atherly, L. J. Berg, *Immunol. Rev.* **191**, 119 (2003).
10. M. B. Yaffe *et al.*, *Nature Biotechnol.* **19**, 348 (2001).
11. E. M. Schaeffer *et al.*, *Nature Immunol.* **2**, 1183 (2001).
12. S. C. Bunnell *et al.*, *J. Biol. Chem.* **275**, 2219 (2000).
13. Y. W. Su *et al.*, *Eur. J. Immunol.* **29**, 3702 (1999).
14. E. M. Schaeffer *et al.*, *Science* **284**, 638 (1999).
15. E. M. Schaeffer *et al.*, *J. Exp. Med.* **192**, 987 (2000).
16. D. J. Fowell *et al.*, *Immunity* **11**, 399 (1999).
17. C. Mueller, A. August, *J. Immunol.* **170**, 5056 (2003).
18. E. Ktistaki, N. T. Ktistakis, E. Papadogeorgaki, I. Talianidis, *Proc. Natl. Acad. Sci. U.S.A.* **92**, 9876 (1995).
19. A. E. Reifel-Miller, D. S. Calnek, B. W. Grinnell, *J. Biol. Chem.* **269**, 23861 (1994).
20. C. D. Novina, V. Cheriyath, A. L. Roy, *J. Biol. Chem.* **273**, 33443 (1998).
21. R. Scully *et al.*, *Cell* **90**, 425 (1997).
22. A. M. Pulichino *et al.*, *Genes Dev.* **17**, 738 (2003).

23. We thank B. Sullivan for data contribution; N. Iwakoshi, M. Townsend, G. Koretzky, B. Sullivan, and G. Lord for thoughtful manuscript review; B. Sullivan, B. Neel, and A. Lee for helpful suggestions on experimental approaches; L. Berg for Itk constructs; and D. Littman for the Itk$^{-/-}$ strain. Supported by NIH grants AI48126 and AI56296 (L.H.G.) and an Arthritis Foundation Postdoctoral Fellowship (E.S.H.). L.G.H. has equity in and is on the corporate board of Bristol-Myers Squibb Company and has equity in and is a paid consultant for HealthCare Ventures LLC Scientific Advisory Board and Mannkind Corporation, a biopharmaceutical company focused on the development and commercialization of treatments for diseases including cancer and autoimmune diseases.

Supporting Online Material

www.sciencemag.org/cgi/content/full/307/5708/430/DC1
SOM Text
Figs. S1 and S2
References

28 July 2004; accepted 12 November 2004
10.1126/science.1103336

Carotenoid Cation Formation and the Regulation of Photosynthetic Light Harvesting

Nancy E. Holt,[1,3]* Donatas Zigmantas,[1,3]* Leonas Valkunas,[1]† Xiao-Ping Li,[2] Krishna K. Niyogi,[2,3] Graham R. Fleming[1,3]‡

Photosynthetic light harvesting in excess light is regulated by a process known as feedback deexcitation. Femtosecond transient absorption measurements on thylakoid membranes show selective formation of a carotenoid radical cation upon excitation of chlorophyll under conditions of maximum, steady-state feedback deexcitation. Studies on transgenic *Arabidopsis thaliana* plants confirmed that this carotenoid radical cation formation is correlated with feedback deexcitation and requires the presence of zeaxanthin, the specific carotenoid synthesized during high light exposure. These results indicate that energy transfer from chlorophyll molecules to a chlorophyll-zeaxanthin heterodimer, which then undergoes charge separation, is the mechanism for excess energy dissipation during feedback deexcitation.

The regulation of photosynthetic light harvesting through a feedback deexcitation quenching mechanism (qE) is one physiologically important strategy used by plants to minimize the deleterious effects of short-term high light exposure (*1–3*). qE involves harmless thermal dissipation of excess energy in the chlorophyll (Chl) singlet excited states (^{1}Chl*) in photosystem II (PSII) of green plants and algae so as to minimize alternative reaction pathways that generate toxic photo-oxidative intermediates (*4–6*). Elucidation of the biophysical mechanism of this vital regulatory process is fundamental for understanding photosynthesis on a molecular scale. In addition, because qE has been shown to be important for plant fitness (*3*), it is a requirement for engineering natural and artificial photosynthetic systems to be more robust when exposed to fluctuations in light intensity.

In excess light, a low thylakoid lumen pH (*7*, *8*) has two effects: It activates formation of the carotenoid (Car) zeaxanthin (Zea) from violaxanthin via the xanthophyll cycle (*9*) (Fig. 1A), and it drives protonation of

[1]Department of Chemistry, [2]Department of Plant and Microbial Biology, University of California, Berkeley, CA 94720, USA. [3]Physical Biosciences Division, Lawrence Berkeley National Laboratory, Berkeley, CA 94720, USA.

*These authors contributed equally to this work.
†Present address: Institute of Physics, Savanoriu Ave. 231, 02300 Vilnius, Lithuania, and Theoretical Department, Faculty of Physics, Vilnius University, Sauletekio Ave. 9, Building 3, 10222 Vilnius, Lithuania.
‡To whom correspondence should be addressed. E-mail: grfleming@lbl.gov

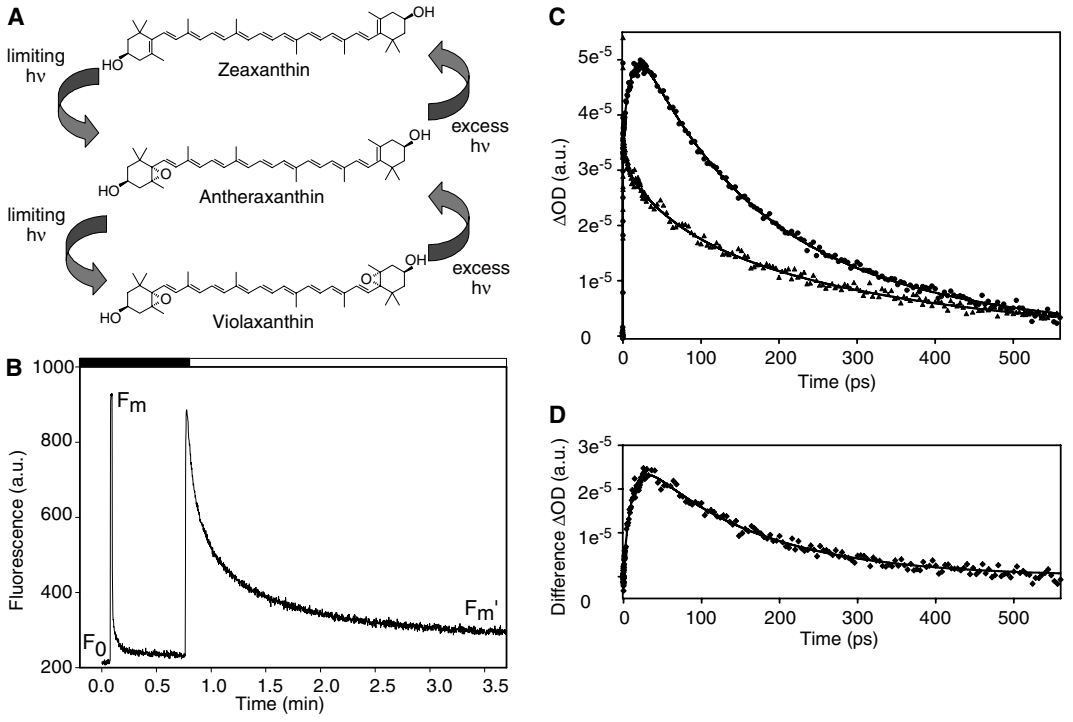

Fig. 1. (**A**) Xanthophyll cycle. (**B**) Chlorophyll fluorescence in isolated spinach thylakoid membranes without (black bar above the graph) and with (white bar) continuous high light illumination. F_0 is the fluorescence with open reaction centers in the absence of high light; F_m and F_m' denote fluorescence with closed reaction centers (achieved with a saturating pulse, ~2200 μmol photons m^{-2} s^{-1}, 1 s) in the absence and presence of continuous high light, respectively. (**C**) TA data for spinach thylakoids upon excitation at 664 nm and detection at 1000 nm under quenched (circles) and unquenched (triangles) conditions and their corresponding fits (solid lines). (**D**) Difference between quenched and unquenched TA curves detected at 1000 nm upon excitation at 664 nm (diamonds) and the corresponding fit (solid line). OD, optical density; a.u., arbitrary units.

PsbS (*10*, *11*), a PSII subunit that is necessary for qE in vivo (*12*). Determining why Zea is necessary for complete qE induction is central to an understanding of the mechanism(s) of ^{1}Chl* deactivation during qE. Transient absorption (TA) kinetics recorded previously in the spectral region from 530 to 580 nm upon selective excitation of Chl indicated direct Car excitation during qE (*13*).

We performed ultrafast TA measurements upon excitation of the first excited singlet state of Chl (Q_y) at 664 nm under conditions where no qE was present (unquenched) or where maximum, steady-state qE (quenched) was induced and maintained with constant illumination from the high light source (*14*), as determined by the Chl fluorescence (Fig. 1B). We recorded the kinetics in the region from 900 to 1080 nm where the carotenoid radical cation ($Car^{+\bullet}$) absorbs (*15*–*17*). The traces for spinach thylakoids upon excitation at 664 nm and detection at 1000 nm (the probe wavelength where the largest amplitude differences were observed) showed an additional rise-and-decay component in the quenched case relative to the unquenched case (Fig. 1C). Subtraction of the quenched trace from the unquenched trace and a corresponding fit of the data produced a single exponential rise and decay of ~11 ps and ~150 ps, respectively (Fig. 1D). The reconstructed kinetic difference spectrum from kinetic traces measured in the 900- to 1080-nm region upon excitation at 664 nm and a delay time of 20 ps, which corresponds to the maximal difference between the quenched and unquenched traces at 1000 nm, is shown in Fig. 2.

Additional experiments were performed on thylakoids from two *Arabidopsis thaliana* mutants in addition to the wild type (WT): (i) *WT + psbS*, which overexpresses PsbS and thus has ~2.5 times the qE of the wild type (*2*), and (ii) *npq4-1*, which lacks the *psbS* gene and is therefore completely qE-deficient (*12*). Despite the lack of qE capacity, *npq4-1* carries out light-induced photochemistry at the same rate as the wild type (*12*). The TA measurements for the three genotypes upon excitation at 664 nm and detection at 1000 nm showed kinetic differences with time constants similar to those observed in spinach only for the wild type and *WT + psbS*, with larger amplitude differences in the latter (Fig. 3). Hence, the kinetic differences we observe are correlated with qE.

TA measurements were also performed on wild-type *A. thaliana* thylakoids and three mutants with distinct Car composition. The wild-type plant has all of the components necessary to form Zea in high light and has the highest amount of qE of the four plants. The *npq2* and *npq2lut2* mutants lack activity of the Zea epoxidase enzyme, resulting in constitutively high levels of Zea in all light conditions (*18*, *19*). The *npq2* mutant contains the xanthophylls Zea and lutein (Lut), whereas the only xanthophyll pigment in *npq2lut2* is Zea (*19*). qE studies on these two mutants have shown that Zea is dominantly responsible for qE in *A. thaliana*, whereas Lut has a minor role in affecting the rate of qE induction and the net amount of quenching (*18*). As a result, both *npq2* and *npq2lut2* have qE levels comparable to those of the wild type. The *npq1* mutant lacks Zea in low light and cannot form it in high light, making it severely qE-deficient (*6*). The TA studies upon excitation at 664 nm and detection at 1000 nm for *npq2* and *npq2lut2* (*20*) showed an additional rise-and-decay component in the quenched case relative to the unquenched case, with time constants similar to those obtained for spinach and the wild-type and *WT + psbS A. thaliana* plants. The kinetics observed for *npq1* with and without high light illumination were very similar, displaying only minor differences in the decay component, but neither signal included a rise component (*20*). The magnitude of the differences varied as follows: wild type ≥ *npq2* ≥ *npq2lut2* ≫ *npq1*. These findings demonstrate that Zea is necessary to produce the kinetic differences.

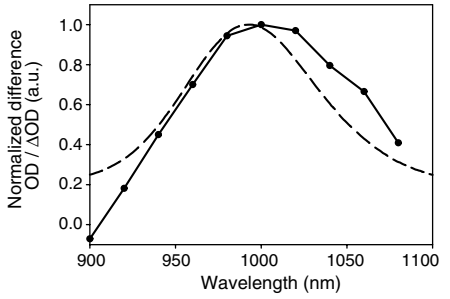

Fig. 2. Near-IR reconstructed quenched minus unquenched difference spectrum (solid line with circles) for the kinetics measured upon excitation at 664 nm at a time delay of 20 ps in isolated spinach thylakoid membranes. The estimated error for all spectral points is ±30%. The spectrum of β-$Car^{+\bullet}$ (dashed line) from O_2-evolving *Synechocystis* PSII core complexes at 20 K is also shown (*16*).

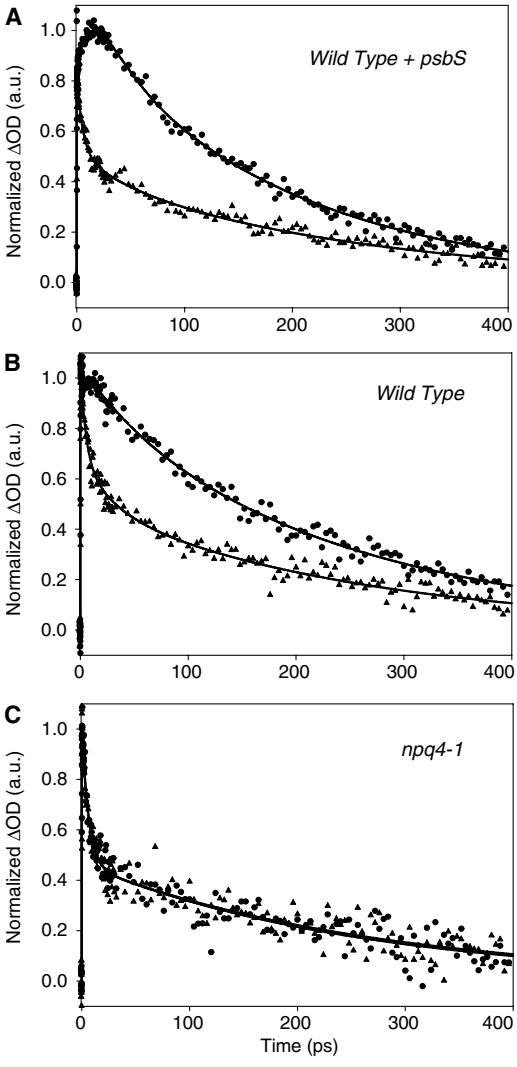

Fig. 3. TA data (circles) detected at 1000 nm upon excitation at 664 nm for (**A**) *WT* + *psbS*, (**B**) wild-type, and (**C**) *npq4-1 A. thaliana* plants. Quenched (circles) and unquenched (triangles) kinetic data are shown with their corresponding fits (solid lines). All kinetics were normalized with respect to the maximum ΔOD of the quenched trace.

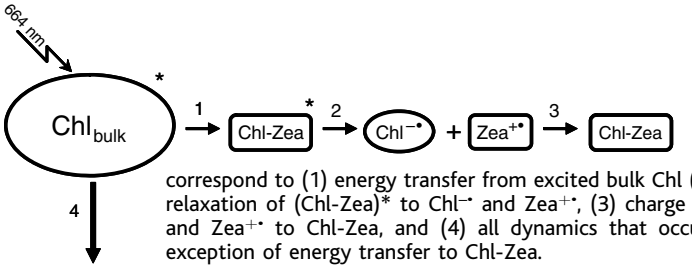

Fig. 4. Scheme of the qE quenching mechanism, showing generation of $Zea^{+\bullet}$ after selective excitation of the Chl Q_y band at 664 nm. The numbers correspond to (1) energy transfer from excited bulk Chl (Chl^*_{bulk}) to Chl-Zea, (2) relaxation of (Chl-Zea)* to $Chl^{-\bullet}$ and $Zea^{+\bullet}$, (3) charge recombination of $Chl^{-\bullet}$ and $Zea^{+\bullet}$ to Chl-Zea, and (4) all dynamics that occur in Chl^*_{bulk}, with the exception of energy transfer to Chl-Zea.

On the basis of the similarity in absorption maxima and spectral widths between the kinetic difference spectrum (Fig. 2) and the ground-state absorption spectra of the β-carotene (*16*) and spheroidene (*15*) radical cations, we conclude that the changes observed are due to the formation of $Car^{+\bullet}$ selectively under quenched conditions. Identification of the species as a $Car^{+\bullet}$ is consistent with the large amplitude of the differences probed in the near-infrared (near-IR) because the absorption cross section of $Car^{+\bullet}$ is similar to the value for the Car $S_0 \rightarrow S_2$ transition (*21*), which is substantially larger than the excited-state absorption cross section of Chl, the transition that dominates the signal detected at 1000 nm under unquenched conditions (*22*). Moreover, the lack of additional strongly allowed transitions from other photosynthetic chromophores in the probe region supports the assignment of the species as a $Car^{+\bullet}$. The demonstrated necessity of Zea for the generation of the kinetic changes enables specific assignment of the species observed during qE as a zeaxanthin radical cation ($Zea^{+\bullet}$).

The observation of $Car^{+\bullet}$ formation upon selective excitation of Chl is in agreement with previous experimental findings in model systems comprising Cars and molecules that are structurally and spectroscopically similar to Chl (*23*, *24*), as well as theoretical studies (*25*). However, our work shows that $Zea^{+\bullet}$ formation is correlated with qE. The result is in line with calculations that showed Zea to have the lowest ionization potential of the three xanthophyll-cycle Cars (Fig. 1A) (*25*). A model that is consistent with all our data (*13*) involves three species: a bulk Chl pool (Chl_{bulk}), a Chl-Zea heterodimer that quenches excited Chl_{bulk} molecules, and a charge-separated ground state consisting of $Chl^{-\bullet}$ and $Zea^{+\bullet}$ (Fig. 4). The charge-separated state is formed from relaxation of the Chl-Zea excited state, (Chl-Zea)*, which is probably a charge-transfer state (*25*). In this scheme, the ~11-ps component corresponds to the net dynamics of the Chl_{bulk} molecules that transfer to Chl-Zea. Simulations of the kinetics, including Chl_{bulk} annihilation dynamics, show that energy transfer from Chl_{bulk} to Chl-Zea occurs in ~15 to 200 ps and the relaxation time scale of (Chl-Zea)* to form $Chl^{-\bullet}$ and $Zea^{+\bullet}$ is on the order of 0.1 to 1 ps. Such a fast heterodimer relaxation time scale would ensure efficient quenching because it would prevent the energy that is transferred to the heterodimer from returning to Chl_{bulk}. The $Zea^{+\bullet}$ signal decays on a time scale of ~150 ps, which corresponds to charge recombination between $Chl^{-\bullet}$ and $Zea^{+\bullet}$. Integration of the photophysical quenching pathways uncovered in this work with the currently emerging spatial and dynamical picture of the entire PSII complex (*26*), including high-resolution crystal structure information on the major light-harvesting protein LHCII (*27*), is necessary for precise determination of the time scales that generate efficient regulation of photosynthetic light harvesting.

The detection of selective formation of $Zea^{+\bullet}$ under conditions of maximum, steady-state qE identifies the key molecular component involved in energy dissipation in PSII. Our results strongly suggest that the mechanism of nonradiative deactivation of $^1Chl^*$ during excess light occurs by excitation transfer to a Chl-Zea heterodimer, followed by ultrafast $Car^{+\bullet}$ formation.

References and Notes

1. B. Demmig-Adams, *Biochim. Biophys. Acta* **1020**, 1 (1990).
2. X.-P. Li, P. Müller-Moulé, A. M. Gilmore, K. K. Niyogi, *Proc. Natl. Acad. Sci. U.S.A.* **99**, 15222 (2002).
3. C. Külheim, J. Ågren, S. Jansson, *Science* **297**, 91 (2002).
4. J. Barber, B. Andersson, *Trends Biochem. Sci.* **17**, 61 (1992).
5. K. K. Niyogi, *Annu. Rev. Plant Physiol. Plant Mol. Biol.* **50**, 333 (1999).
6. M. Havaux, K. K. Niyogi, *Proc. Natl. Acad. Sci. U.S.A.* **96**, 8762 (1999).
7. P. Horton, A. V. Ruban, R. G. Walters, *Annu. Rev. Plant Physiol.* **47**, 655 (1996).
8. P. Müller, X.-P. Li, K. K. Niyogi, *Plant Physiol.* **125**, 1558 (2001).

9. B. Demmig-Adams, W. W. Adams III, *Trends Plant Sci.* **1**, 21 (1996).
10. X.-P. Li, A. Phippard, J. Pasari, K. K. Niyogi, *Funct. Plant Biol.* **29**, 1131 (2002).
11. X.-P. Li *et al.*, *J. Biol. Chem.* **279**, 22866 (2004).
12. X.-P. Li *et al.*, *Nature* **403**, 391 (2000).
13. Y.-Z. Ma, N. E. Holt, X.-P. Li, K. K. Niyogi, G. R. Fleming, *Proc. Natl. Acad. Sci. U.S.A.* **100**, 4377 (2003).
14. See supporting data on *Science* Online.
15. T. Polívka *et al.*, *J. Phys. Chem. B* **106**, 11016 (2002).
16. C. A. Tracewell, G. W. Brudvig, *Biochemistry* **42**, 9127 (2003).
17. T. Polívka, T. Pullerits, H. A. Frank, R. J. Cogdell, V. Sundström, *J. Phys. Chem. B* **108**, 15398 (2004).
18. B. J. Pogson, K. K. Niyogi, O. Björkman, D. DellaPenna, *Proc. Natl. Acad. Sci. U.S.A.* **95**, 13324 (1998).
19. K. K. Niyogi, A. R. Grossman, O. Björkman, *Plant Cell* **10**, 1121 (1998).
20. N. E. Holt *et al.*, data not shown.
21. J. A. Jeevarajan, C. C. Wei, A. S. Jeevarajan, L. D. Kispert, *J. Phys. Chem.* **100**, 5637 (1996).
22. D. Zigmantas, R. G. Hiller, V. Sundström, T. Polívka, *Proc. Natl. Acad. Sci. U.S.A.* **99**, 16760 (2002).
23. G. Kodis *et al.*, *J. Phys. Chem. B* **108**, 414 (2004).
24. J. Pan, Y. Xu, L. Sun, V. Sundström, T. Polívka, *J. Am. Chem. Soc.* **126**, 3066 (2004).
25. A. Dreuw, G. R. Fleming, M. Head-Gordon, *Phys. Chem. Chem. Phys.* **5**, 3247 (2003).
26. J. Nield, C. Funk, J. Barber, *Philos. Trans. R. Soc. London Ser. B* **355**, 1337 (2000).
27. Z. Liu *et al.*, *Nature* **428**, 287 (2004).
28. We thank M. Kobayashi and S. McCarthy for assistance with thylakoid preparations, and G. Brudwig for the β-carotene radical cation absorption spectrum. Supported by the Fulbright Program (L.V.) and by the Office of Basic Energy Sciences, Chemical Sciences Division, U.S. Department of Energy (contract DE-AC03-76SF00098).

Supporting Online Material
www.sciencemag.org/cgi/content/full/307/5708/433/DC1
Materials and Methods
References

29 September 2004; accepted 15 November 2004
10.1126/science.1105833

Cryo–Electron Tomography Reveals the Cytoskeletal Structure of *Spiroplasma melliferum*

Julia Kürner,[1] Achilleas S. Frangakis,[2]* Wolfgang Baumeister[1]*

Evidence has accumulated recently that not only eukaryotes but also bacteria can have a cytoskeleton. We used cryo–electron tomography to study the three-dimensional structure of *Spiroplasma melliferum* cells in a close-to-native state at ~4-nanometer resolution. We showed that these cells possess two types of filaments arranged in three parallel ribbons underneath the cell membrane. These two filamentous structures are built of the fibril protein and possibly the actin-like protein MreB. On the basis of our structural data, we could model the motility modes of these cells and explain how helical Mollicutes can propel themselves by means of coordinated length changes of their cytoskeletal ribbons.

One of the key functions of a cytoskeleton is to determine and maintain the shape of cells. In bacteria, the cell wall is generally considered to be the primary determinant of cell shape. However, this has been called into question, most recently by the discovery of the Mollicutes (*Mycoplasma*, *Acholeplasma*, and *Spiroplasma*) (*1*). Mollicutes are the smallest and simplest free-living and self-replicating cells within prokaryotes, and they are enveloped only by a cholesterol-containing cell membrane. Despite the lack of a cell wall, these cells have distinct morphologies, and their peculiar mode of movement that occurs in the absence of appendages normally implicated in motility (e.g., flagella or secretion organelles) makes the existence of an internal cytoskeleton likely.

Williamson (*2*) first reported the isolation of a cytoskeleton upon cell lysis and sodium deoxycholate extraction of *Spiroplasma* isolated from *Drosophila*. Cytoskeletal elements have also been released from *Spiroplasma* cells by repeated freezing and thawing (*3*). Townsend *et al.* (*3*) also developed methods for purification of the membrane-associated fibrils from *S. citri* and suggested that they may be involved in motility. Electron microscopy and SDS gel electrophoresis have shown that *S. melliferum* possesses a cytoskeletal ribbon comprosed of ~4- to 5-nm-wide fibrils with an axial repeat of ~9 nm; these fibrils form pairs within the ribbon and are composed of the 55-kD fibril protein (*3*, *4*). Townsend and Plaskitt (*5*) further used immunogold staining of thin sections with an antibody to p55 to localize the ribbon built of the fibril protein within *S. melliferum* cells. More recently, the structure and localization of this cytoskeleton was described as a flat, monolayered, membrane-bound ribbon composed of six or seven pairs of fibrils following the inner, shortest helical path of the cell (*6*, *7*). The fibril protein, which is completely unrelated to any other eukaryotic or prokaryotic protein and has been found exclusively in the genome of *Spiroplasma* (*8*), was identified as the only component of this ribbon (*7*). Because this protein would have a diameter of about 5 nm, assuming a spherical shape, it was proposed that the subunit of the fibrils is a tetramer and that the filaments form pairs to give the 10-nm axial and lateral spacings in the cytoskeletal ribbon (*9*).

Our tomographic studies (*10*, *11*) of intact vitrified *S. melliferum* cells, however, reveal a more complex pattern of filamentous structures

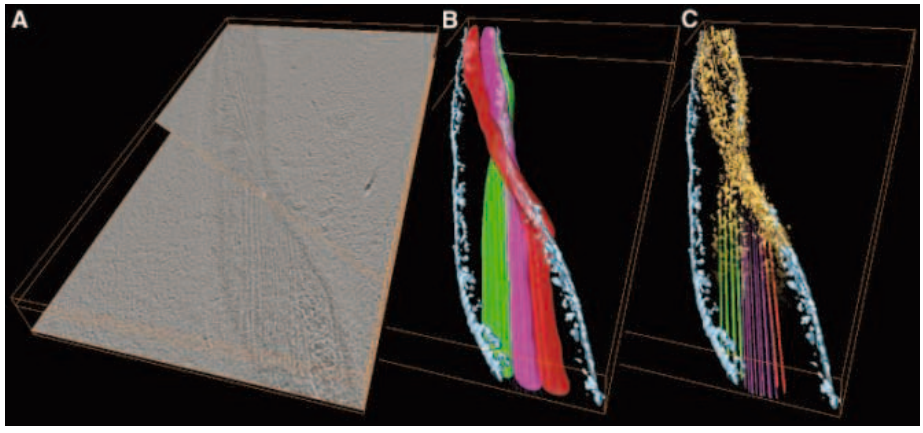

Fig. 1. Superimposed slices from different *z* heights of a tomogram (**A**) (*z* heights indicated by bounding box) and two corresponding 3D visualizations (**B** and **C**) of part of a *S. melliferum* cell showing the arrangement and course of the cytoskeleton. (A) The cytoskeleton is composed of two outer ribbons of thick filaments and a ribbon of thin filaments sandwiched in between. (B) Simplified 3D representation of the filament ribbons (green, purple, and red) that wind in parallel helically around the cell just underneath the cell membrane (blue), showing, in this case, the left-handed course of the cytoskeleton. (C) Idealized visualization of the filaments with smooth transition to the original data (yellow).

[1]Department of Structural Biology, Max Planck Institute of Biochemistry, Am Klopferspitz 18, D-82152 Martinsried, Germany. [2]Structural and Computational Biology, European Molecular Biology Laboratory (EMBL), Meyerhofstrasse 1, D-69117 Heidelberg, Germany.

*To whom correspondence should be addressed. E-mail: baumeist@biochem.mpg.de (W.B.); frangak@embl.de (A.S.F.)

just underneath the cell membrane (Fig. 1). Two types of filaments (thin and thick) are arranged in parallel, anchored to each other and to the cell membrane, and jointly form three ribbons that span the entire cell from the blunt to the tapered end. By calculating the Hough transformation (*12*) of the filament regions in several tomograms and finding the position of the highest contrast, we determined the number and spacings of the individual filaments (Fig. 2). The two outer ribbons consist of five thick filaments with a spacing of ~11 nm. These two ribbons are joined together by nine thinner filaments with a spacing of ~4 nm. Depending on the extent of twisting of the cell and the position of the filaments with regard to the direction of the electron beam during data acquisition, five or locally fewer than five thick filaments are visible in the tomograms. Using three-dimensional (3D) visualization (*11*), we were able to illustrate the arrangement and path of the two outer ribbons underneath the cell membrane through the entire cell body (Fig. 3 and movie S1). Although the ribbons cannot be visualized as continuous bands along the cell membrane of the whole cell because of the "missing wedge" problem (*13*), it becomes clear that the ribbons follow, in parallel, a helical path from one end of the cell to the other. By calculating the geodetic line (*14*) (i.e., the fastest connection between two arbitrary points on the 3D cell membrane), we could also show that one of the two outer ribbons is locally shorter; indicating differential length changes of the two ribbons (Fig. 3 and movie S1).

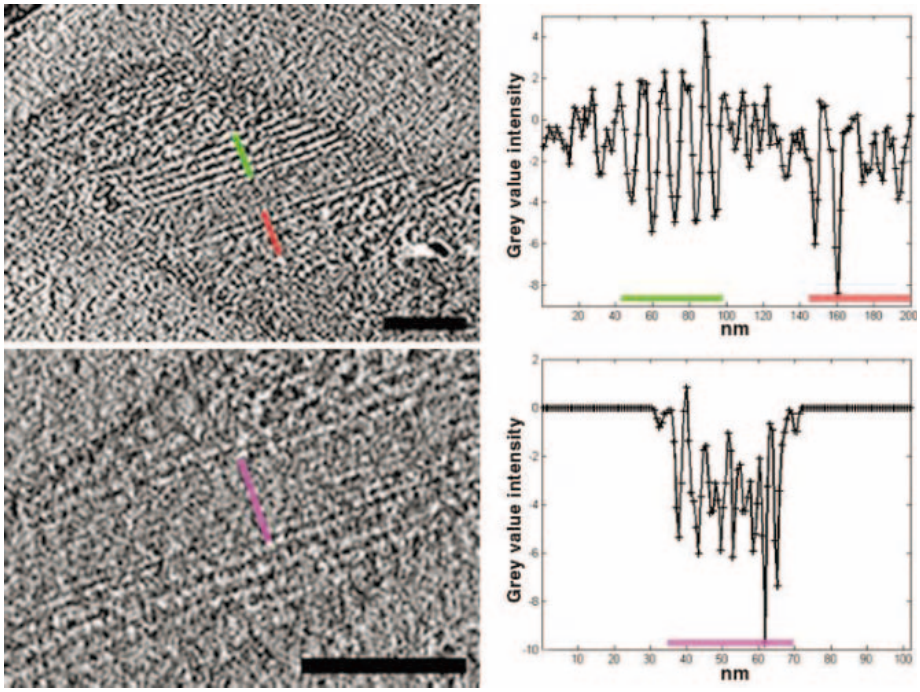

Fig. 2. Sections (2.7-nm thick) of parts of *S. melliferum* cells derived from the tomograms (left) and corresponding profiles of the filament grey values (right) showing the number and spacings of the individual filaments. (**Top**) The two outer ribbons are composed of five thick filaments with a spacing of about 11 nm (highlighted in green and red). Depending on the extent of twisting of the cell, five or locally fewer than five thick filaments are visible in the tomogram. (**Bottom**) The region in between is composed of nine thin filaments with a spacing of about 4 nm (highlighted in purple). Each cross in the graphs corresponds to one pixel (pixel size: top, 1.72 nm; bottom, 0.68 nm). (In the bottom graph, the values on each side of the inner ribbon were set to zero.) Scale bars, 100 nm.

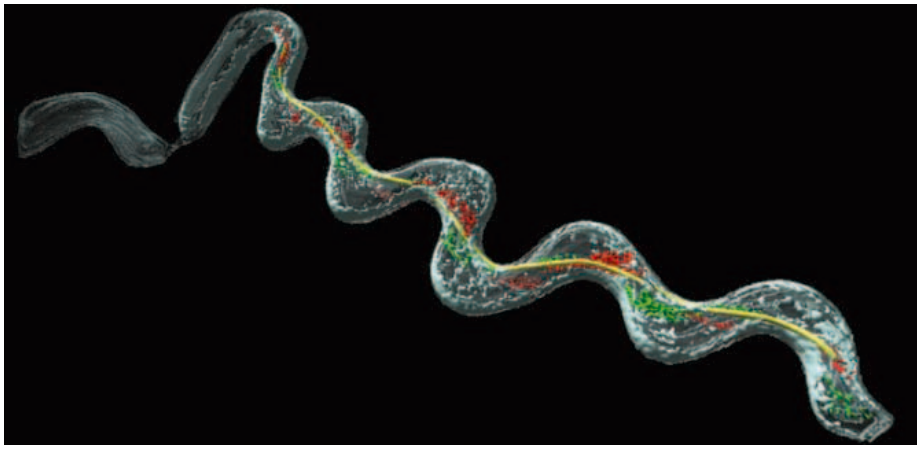

Fig. 3. Three-dimensional visualization of a *S. melliferum* cell. The localization and course of the two outer ribbons within the cell are illustrated in red and green. The position of the geodetic line is shown in yellow. The red ribbon is locally overlapping with the geodetic line, which indicates that, in this case, it is shorter than the green one. This is most probably accomplished by simultaneous conformational changes of adjacent subunits of the five filaments. The length differences explain the helicity of the cell, as well as the ability to alternate handedness between left- and right-handed (movie S1).

What is the protein composition of the ribbons? We have been able to show that isolated and purified filaments (*11*) composed of the fibril protein exist in pairs with a total thickness of about 10 nm; hence, we suppose that the two outer ribbons of the *S. melliferum* cytoskeleton are made of the fibril protein. Our structural data showing two different filaments in the cytoskeleton of *S. melliferum* raises the question of the identity of the second protein. Until recently, there has been an ongoing controversy about the existence of actin or actin-like proteins in prokaryotes, including Mollicutes [for a review, see (*15*)]. Bacterial homologs of actin were first identified when the cell-shape determinants MreB and Mbl (MreB-like) were shown to assemble into helical filamentous structures that run in spirals around the periphery of the cell under the cytoplasmic membrane in *Bacillus subtilis* (*16*). Depletion of MreB induced the formation of rounded inflated cells that was ultimately lethal. This phenomenon was also reported for *Escherichia coli* (*17*, *18*). MreB has been found only in bacterial species with rod-shaped, filamentous, or helical cells (*16*). Consistent with this, the helical cells of *S. citri* have five MreB homologs (*19*). Using Western blot and sequence analysis (*11*), we showed that both the fibril protein and MreB exist in *S. melliferum* cells and both are homologous to the sequenced fibril and MreB proteins of *S. citri* (supporting online material text). Hence, we suggest that the inner ribbon of the *S. melliferum* cytoskeleton is composed of MreB. Because of the instability of MreB filaments, the isolation of intact triple ribbons proved difficult and therefore, direct and unambiguous proof for this assignment by immunolabeling was not possible. Nevertheless, there is evidence supporting our assumption about the protein composition of the cytoskeleton. Purified MreB from *Thermotoga maritima* has been shown to form ~4-nm-wide protofilaments in vitro (*20*), and a link-

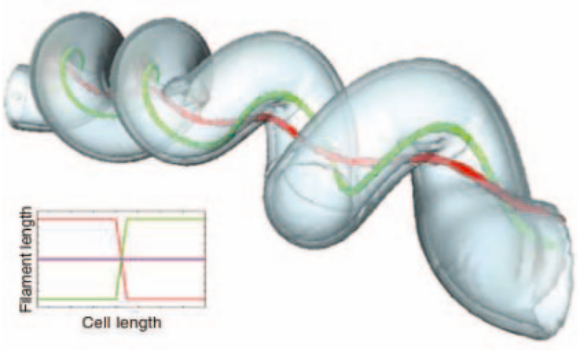

Fig. 4. Computer simulation explaining the change of handedness from left-handed (right) to right-handed (left). If the cell has a certain handedness over its entire length, then one of the two outer ribbons (red and green) is tense, and the other one is relaxed. If the tense, short ribbon gradually lengthens while the other one concurrently shortens its length (inset), the handedness switches, and the point of transition between the two states travels through the whole cell, producing a thrust in the opposite direction. The inset shows the length differences between the two outer filament ribbons (red and green) on each side of the point of transition (cross-over point). The inner ribbon, which does not change its length, is shown in purple (movie S2).

age between an actin-like protein and the fibrils in *Spiroplasma* cells was already proposed by Williamson *et al*. (*4*) but has not yet been proven.

How does this cytoskeleton enable the movements of *S. melliferum* cells? Trachtenberg and Gilad (*7*) suggested that the filaments can change their length in a coordinated manner, driven by conformational changes of their tetrameric subunits from nearly circular to elliptical. In this regard, the assumptions for our computer simulations (*11*), which are based on light microscopy experiments (*21*) and the existence of three ribbons, are (i) the ribbons are connected to each other, (ii) the inner thin filament ribbon functions elastically during cell movement, and (iii) length changes of the five filaments of the outer two ribbons occur simultaneously by switching between two conformational states of the filament subunits. Hence, we can simulate on a molecular level how the different motility modes are generated. If length changes in the two outer ribbons are coordinated such that one ribbon becomes gradually tense by shortening while the second one concurrently relaxes, the cell would alternate handedness between left- and right-handed, with handedness switching at the position where the state of tension and relaxation of the ribbons reverses (Fig. 4 and movie S2). This point of transition between left- and right-handedness travels throughout the whole cell, leading to a motion that resembles that of a bacterial flagellar bundle or of a single eukaryotic flagellum or cilium. A similar motion can be generated if the distance between the two outer ribbons is changed locally, thereby creating a deformation or kink, which propagates throughout the cell body. Thus, the whole *Spiroplasma* cell functions as a dynamic helical propeller. Coupling of a biochemical cycle (e.g., adenosine 5′-triphosphate hydrolysis) to the dynamics of the filaments could enable these filaments to propagate deformations that generate propulsive forces which, in turn, can drive cell motion (*22*). We assume that MreB filaments give the cell a rodlike shape by forming the inner, elastic ribbon, whereas the outer filaments composed of the fibril protein enable the formation of a helix, as well as movement, by interaction with the MreB ribbon.

In the future, it will be necessary to elucidate in more detail the nature of the interaction between the individual filaments, as well as between the cytoskeleton and the cell membrane. Finally, the fine structure of the filaments and the mechanisms underlying changes in filament length and distance, as well as their driving force, remain to be clarified.

References and Notes

1. J. G. Tully, in *Encyclopedia of Microbiology*, J. Lederberg, Ed. (Academic Press, New York, 1992), vol. 3, pp. 181–191.
2. D. L. Williamson, *J. Bacteriol.* **117**, 904 (1974).
3. R. Townsend, D. B. Archer, K. A. Plaskitt, *J. Bacteriol.* **142**, 694 (1980).
4. D. L. Williamson, J. Renaudin, J.-M. Bové, *J. Bacteriol.* **173**, 4353 (1991).
5. R. Townsend, K. A. Plaskitt, *J. Gen. Microbiol.* **131**, 983 (1985).
6. S. Trachtenberg, *J. Struct. Biol.* **124**, 244 (1998).
7. S. Trachtenberg, R. Gilad, *Mol. Microbiol.* **41**, 827 (2001).
8. R. Townsend, D. B. Archer, *J. Gen. Microbiol.* **129**, 199 (1983).
9. S. Trachtenberg, S. B. Andrews, R. D. Leapman, *J. Bacteriol.* **185**, 1987 (2003).
10. W. Baumeister, R. Grimm, J. Walz, *Trends Cell Biol.* **9**, 81 (1999).
11. Materials and methods are available as supporting material on *Science* Online.
12. J. C. Russ, *The Image Processing Handbook* (CRC Press, Florida, ed. 4, 2002), pp. 496–500.
13. A. J. Koster *et al.*, *J. Struct. Biol.* **120**, 276 (1997).
14. R. Kimmel, J. A. Sethian, *Proc. Natl. Acad. Sci. U.S.A.* **95**, 8431 (1998).
15. H. Neimark, *Yale J. Biol. Med.* **56**, 419 (1983).
16. L. J. F. Jones, R. Carballido-López, J. Errington, *Cell* **104**, 913 (2001).
17. M. Doi *et al.*, *J. Bacteriol.* **170**, 4619 (1988).
18. M. Wachi *et al.*, *J. Bacteriol.* **169**, 4935 (1987).
19. Information about the five MreB homologs is available in the Expert Protein Analysis System (ExPASy) available at www.expasy.org (SWISS-PROT accession codes Q8VP64, Q8VQG1, Q8VQG2, Q8VQG3, and Q8VQG4).
20. F. van den Ent, L. A. Amos, J. Löwe, *Nature* **413**, 39 (2001).
21. J. Kürner, A. S. Frangakis, W. Baumeister, unpublished data.
22. C. W. Wolgemuth, O. Igoshin, G. Oster, *Biophys. J.* **85**, 828 (2003).

23. This work was supported financially by the Fonds der Chemie and the Max-Planck-Forschungspreis. We thank J. Errington (University of Oxford, Oxford) for providing the MreB antibody, O. Mihalache (Max Planck Institute (MPI) of Biochemistry, Martinsried) for assistance with biochemical experiments, R. Mentele (MPI of Biochemistry, Martinsried) for carrying out sequence analyses, J. Ellenberg (EMBL, Heidelberg) for assistance with light microscopy experiments and A. Leis for critical reading of the manuscript.

Supporting Online Materials

www.sciencemag.org/cgi/content/full/307/5708/436/DC1
Materials and Methods
SOM Text
Movies S1 and S2
References

13 August 2004; accepted 1 December 2004
10.1126/science.1104031

New Products

http://science.labvelocity.com

High Sample Recovery Plate

A new 384-well High Sample Recovery plate is suitable for applications such as drug discovery when samples are either precious or available only in limited volumes. The unique conical well profile and polypropylene composition combine to provide a dead volume of less than 0.2 μl and a working volume of up to 65 μl. Designed for high-throughput automation, the exceptionally flat profile of the new plates maximizes robotic stack capacity and leads to real gains in storage capacity.

Genetix For information +44 1425 624600 www.genetix.com

Gas Chromatograph/TOF Mass Spectrometer

The JEOL AccuTOF-GC is a high-speed, high-resolution gas chromatograph/time-of-flight mass spectrometer that combines fast data acquisition speeds with high resolution/exact mass measurements and a high dynamic range for both qualitative and quantitative analysis. The AccuTOF-GC provides a solution for determination of exact mass, target compound identification in trace analysis with no sensitivity loss. In general, systems designed for high-speed data acquisition offer only low resolution while those designed for high resolution operate at lower data acquisition rates. With the AccuTOF-GC, no trade-off is required between speed and resolution. It also provides a high linear dynamic range for analysis of both low and high concentrations.

JEOL For information 978-535-5900 www.jeol.com

Sequence Analysis Software

Lasergene version 6, a major upgrade of a sequence analysis software package, introduces a new module, SeqBuilder, that allows sequence editing, creation of plasmid maps, and exporting of presentation-quality graphics into a variety of graphical and presentation software applications. Along with SeqBuilder comes the ability to share data among other Lasergene modules. This new capability can greatly enhance researchers' efficiency in the lab. Lasergene is a comprehensive, easy-to-use suite of tools for the analysis of DNA and protein sequences used by molecular biologists and geneticists in more than 65 countries.

DNASTAR For information 608-258-7420 www.dnastar.com

FT-IR Microscopy System

The Spectrum Spotlight 200 Fourier transform-infrared microscopy system takes infrared microscopy to new levels of performance, speed, and applications capability. The exclusive detector design offers superior signal-to-noise ratios and a wide spectral range to enable the most information to be obtained from challenging samples in the quickest time possible. The system allows samples to be measured in either transmission or reflectance mode. For thick, non-reflective samples, micro-attenuated total reflection (ATR) measurement is suitable for obtaining high-quality surface spectra. The unique micro-ATR design does not require a separate objective and therefore no realignment is required—the user simply lowers the ATR objective onto the sample.

Perkin Elmer For information 800-762-4000 www.perkinelmer.com

High-Quality Fosmid DNA

The FosmidMAX DNA Purification Kit provides easy, reliable isolation of high-quality fosmid and cosmid DNA. The scalable protocol is based on a modified alkaline-lysis procedure that typically yields 0.6 to 25 μg of fosmid DNA from 1.5 to 100 ml of a single-copy fosmid culture. Selective precipitation steps and the incorporation of the RiboShredder RNase Blend effectively remove contaminants that degrade DNA and interfere with downstream applications. FosmidMAX DNA provides consistent results in sequencing, fingerprinting, shotgun libraries, and polymerase chain reaction.

Epicentre Biotechnologies For information 800-284-8474 www.EpiBio.com

Inverted Microscope

The Leica DMI 6000 B combines Leica's traditional expertise in high-performance optics with unparalleled flexibility in an inverted microscope platform. Multiple cameras, detectors, and light sources can be attached for individual or simultaneous use. Excitation wavelengths can be quickly switched with an internal high-speed filter wheel. In addition, a wide range of accessories for live cell experiments support the DMI 6000 B, including environmental control and objectives designed for optimal performance at physiological conditions. Realizing the importance of working at low expression levels, Leica has optimized the fluorescence axis to be optically efficient as well as to reduce background levels from stray light, which results in brilliant fluorescence. In combination with the fluorescence intensity management system, excitation light levels can be precisely controlled to increase cell viability during long measurements. A new excitation manager allows the microscopist to precisely balance light levels coming from dual-labeled specimens.

Leica For information 847-405-7026 www.leica-microsystems.com

Literature

Aquacounter Karl Fisher Titrators is a 12-page catalog on this line. The AQV-2000S volumetric titrator, the AQ-2000S coulometric titrator, and the AQV-2000C combination volumetric and coulometric titrator all display real-time curves and store up to 50 results. The AQ-200 and AQV-200 offer the same specifications at very low prices. Solid evaporators and automated evaporator/sample changer titration systems are also described.

JM Science For information 716-774-8706 www.jmscience.com

Newly offered instrumentation, apparatus, and laboratory materials of interest to researchers in all disciplines in academic, industrial, and government organizations are featured in this space. Emphasis is given to purpose, chief characteristics, and availability of products and materials. Endorsement by *Science* or AAAS of any products or materials mentioned is not implied. Additional information may be obtained from the manufacturer or supplier by visiting www.science.labvelocity.com on the Web, where you can request that the information be sent to you by e-mail, fax, mail, or telephone.

ScienceCareers.org

Classified Advertising

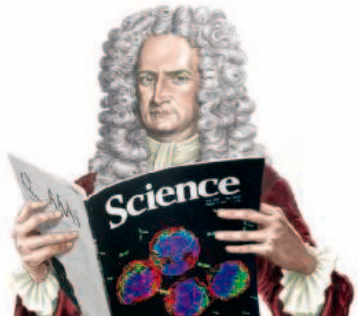

For full details on advertising rates, deadlines, mechanical requirements, and editorial calendar go to **www.sciencecareers.org** and click on **How to Advertise** or call one of our representatives.

United States & Canada

E-mail: advertise@sciencecareers.org
Fax: 202-289-6742

JILL DOWNING
(CT, DE, DC, FL, GA, MD, ME, MA, NH, NJ, NY, NC, PA, RI, SC, VT, VA)
Phone: 631-580-2445

KRISTINE VON ZEDLITZ
(AK, AR, CA, CO, HI, ID, IL, IA, KS, LA, MN, MO, MT, NE, NV, NM, ND, OK, OR, SD, TX, UT, WA, WI, WY)
Phone: 415-956-2531

BETH DWYER
(AL, IN, KY, MI, MS, OH, TN, WV and Internet Sales)
Phone: 202-326-6534

EMNET TESFAYE
(Line Advertising)
Phone: 202-326-6740

DARYL ANDERSON
(Canada and Meetings and Announcements)
Phone: 202-326-6543

Europe & International

E-mail: ads@science-int.co.uk
Fax: +44 (0) 1223-326-532

TRACY HOLMES
Phone: +44 (0) 1223-326-525

EMILIE STOTT
Phone: +44 (0) 1223-326-527

CLAIRE GRIFFITHS
Phone: +44 (0) 1223-326-528

CHRISTINA HARRISON
Phone: +44 (0) 1223-326-510

JASON HANNAFORD
Phone: +81 (0) 52-777-9777

To subscribe to *Science*:
In U.S./Canada call 202-326-6417 or 1-800-731-4939
In the rest of the world call +44 (0) 1223-326-515

Science makes every effort to screen its ads for offensive and/or discriminatory language in accordance with U.S. and non-U.S. law. Since we are an international journal, you may see ads from non-U.S. countries that request applications from specific demographic groups. Since U.S. law does not apply to other countries we try to accommodate recruiting practices of other countries. However, we encourage our readers to alert us to any ads that they feel are discriminatory or offensive.

POSITIONS OPEN

FACULTY POSITION
SYSTEMS NEUROSCIENCE
California Institute of Technology

The California Institute of Technology offers a position at the **ASSISTANT PROFESSOR** level in the Division of Biology working in systems neuroscience to study neural processes underlying high-level brain functions such as perception, attention, decision-making, and action. The position is tenure track, with an initial appointment of four years. The successful candidate is expected to maintain an active research program and to teach. Facilities include the Caltech Brain Imaging Center with a 3 Tesla magnet for imaging humans, a 4.7 Tesla vertical bore magnet for nonhuman primates, and a 9.4 Tesla magnet for small mammals.

The candidate must have a Ph.D. degree or equivalent degree. Caltech is especially interested in candidates who combine research in systems neuroscience with functional imaging in nonhuman primates.

Applications should include curriculum vitae, a statement of research plan, and three letters of recommendation. This material should be sent to: **Tessa Yao, Systems Neuroscience Faculty Search Committee, California Institute of Technology, MC 216-76, 1200 E. California Boulevard, Pasadena, CA 91125,** or by **e-mail: tessa@vis.caltech.edu.**

Caltech is an Equal Opportunity/Affirmative Action Employer. Women, minorities, veterans, and disabled persons are encouraged to apply.

SENIOR INVESTIGATORS
(PROFESSOR RANK)
Statistics, Bioinformatics, or Complex Network Analysis

The National Center for Genome Resources (NCGR) invites applications for three Senior Investigator positions in statistics, bioinformatics, and complex network analysis. Ideal candidates will have expertise in the development of algorithms for a systems biology approach to human health and nutrition. Senior Investigators will be scholars of national distinction who will bring established, funded, research programs and a strong desire to participate in a dynamic leadership team.

NCGR is a leading, independent bioinformatics research institute **(website: http://www.ncgr.org)**. We are committed to the translation of large-scale, collaborative research into improved health and nutrition. We have an entrepreneurial, team-based, multidisciplinary environment.

Nestled in the foothills of the Rocky Mountains, Santa Fe boasts an unparalleled quality of life. America's oldest capital city, Santa Fe features a rich cultural heritage, extraordinary fine arts, and unlimited outdoor activities. Senior Investigators will enjoy a generous salary and benefits package. Please e-mail curriculum vitae, description of research, and a list of three references to **e-mail: resumes@ncgr.org.** *Equal Opportunity Employer.*

POSITION #ALH 370
Department of Microbiology
University of Manitoba, Winnipeg, Manitoba, Canada

The Department of Microbiology invites applications for a full-time, tenure-track position, subject to final budgetary approval, at the **ASSISTANT PROFESSOR** level, commencing September 1, 2005, or on a date mutually agreed upon. The successful candidate must have a Ph.D. and postdoctoral experience in molecular microbiology and evidence of a strong research potential. The closing date for receipt of applications and letters of reference is March 1, 2005. Further information may be obtained from **website: http://www.umanitoba.ca/admin/human_resources.**

POSITIONS OPEN

TENURE-TRACK POSITION
Coastal Watershed Science

The Marine Science Institute (MSI, **website: http://www.utmsi.utexas.edu**) and Environmental Science Institute (ESI, **website: http://www.geo.utexas.edu/esi**) at The University of Texas at Austin invite applications for a faculty position in coastal watershed science. This position will further a growing program at UT-Austin in marine and environmental science that is focussed on coastal issues, including a current faculty search in ecological modeling and a proposed National Estuarine Research Reserve at MSI (**website: http://www.utmsi.utexas.edu/txnerr**). We seek an individual with broad interests in integrated field, laboratory, and modeling studies of the physical, geochemical, and biological processes that occur in coastal watersheds. The position is at the rank of **ASSISTANT PROFESSOR** in the Department of Marine Science and **RESEARCH ASSISTANT PROFESSOR** in MSI. The successful candidate will be based at the Marine Science Institute in Port Aransas and will be expected to build a vigorous and interdisciplinary research program with one or more affiliated ESI departments in Austin, including integrative biology, geological sciences, geography, engineering, and social sciences. Candidates must have a Ph.D. degree at the time of appointment; postdoctoral experience and a strong research and publication record are preferred. Primary teaching responsibilities will be participation in a developing Integrated Watershed Science graduate program that will train students in science, engineering, and policy aspects of water resources, and a graduate course (likely team taught) in one of the following: coastal oceanography, time series analysis, or microbial ecology. Applicants should send a statement of research and teaching interests (three pages maximum), curriculum vitae, and five letters of recommendation to: **MSI-ESI Search Committee Chair, The University of Texas Marine Science Institute, 750 Channel View Drive, Port Aransas, TX 78373-5015.** The statement of research interests should mention how the program would incorporate coastal watershed science. Review of applications will start February 15, 2005, and will continue until the position is filled. Background check conducted on applicant selected. *The University of Texas at Austin is an Affirmative Action/Equal Opportunity Employer.*

CHAIR
Department of Biomedical Sciences
University of Guelph

Applications and nominations are invited for the position of Chair, Department of Biomedical Sciences, Ontario Veterinary College, University of Guelph. Candidates must hold the Ph.D. degree (or equivalent), have an established research reputation in a discipline compatible with the mission of the Department, leadership skills, administrative experience, and devotion to excellence in education and research in biomedical sciences. The Department takes part in B.Sc. (bio-med), B.Sc. (toxicology), D.V.M., M.Sc., Ph.D., and D.V.Sc. programs. Graduate training involves multidisciplinary investigations on topics basic to our understanding of health and disease in human beings and animals. More information may be obtained at **website: http://www.ovc.uoguelph.ca/biomed/posting/shtml.** Applications should be accompanied by detailed curriculum vitae, names of at least three references, and a statement of interest in the position. The deadline for applications and nominations is March 31, 2005, or until a suitable applicant is identified, and should be sent to: **Dr. Carlton Gyles, Interim Dean, Ontario Veterinary College, University of Guelph, Guelph, Ontario N1G 2W1, Canada.**

The University of Guelph is committed to an Employment Equity program that includes special measures to achieve diversity among its faculty and staff. We therefore particularly encourage applications from qualified Aboriginal Canadians, persons with disabilities, members of visible minorities, and women. All qualified candidates are encouraged to apply; however, Canadians and permanent residents will be given priority.

OPEN TO

DISCOVER

Within each discovery is a new future. That future begins with you.

Inside our cutting-edge research facilities in Cambridge, MA, world-class scientists have all the resources they need to carry out the mission of lifesaving drug discovery.

We now have opportunities for all functional specialties in addition to the following disease areas: cardiovascular, diabetes, oncology, and infectious diseases.

To view descriptions of all open positions and to apply, visit www.nibr.novartis.com and follow the links to Careers and Job Opportunities.

Novartis is committed to embracing and leveraging diverse backgrounds, cultures, and talents to achieve competitive advantage.
Novartis is an equal opportunity employer. M/F/D/V

NOVARTIS
NOVARTIS INSTITUTES
FOR BIOMEDICAL RESEARCH

Think what's possible.

www.nibr.novartis.com

USC UNIVERSITY OF SOUTHERN CALIFORNIA

ChildrensHospitalLosAngeles
International Leader in Pediatrics

Developmental Therapeutics Program

THE USC-CHLA INSTITUTE FOR PEDIATRIC CLINICAL RESEARCH

Faculty Positions

Childrens Hospital Los Angeles and The University of Southern California are expanding their translational research efforts to develop new agents for the treatment of childhood cancers. Investigators with M.D., M.D.,/Ph.D., or Ph.D. degrees are invited to apply for the following positions in the USC-CHLA Institute for Pediatric Clinical Research (IPCR) Developmental Therapeutics Program. All faculty positions have outstanding start-up packages. Successful candidates will be eligible for appointment to an appropriate academic rank in the Dept of Pediatrics, Keck School of Medicine, USC, according to their level of professional qualifications. USC is an equal opportunity/affirmative action employer.

Assistant, Associate, or Full Professor, Pediatric Pharmacology: Conduct independent research, and work with an integrated team, conducting pre-clinical and clinical studies of new anticancer agents in children. Postdoctoral experience and publications in pharmacology required, experience in cancer preferred.

Assistant or Associate Professor, Pharmacodynamics: Establish a state-of-the art pharmacodynamics laboratory, especially of sphingolipids, to study new agents for treating childhood cancers.

Assistant or Associate Professor, Pre-Clinical Models of Leukemia: Conduct independent research establishing and validating cell culture and animal models for identifying new agents for clinical testing with a focus on childhood acute lymphoblastic leukemias.

Assistant Professor or Associate Professor, Antibody Therapy: Conduct independent research leading to the development and clinical testing of antibodies for therapy of childhood cancers with a focus on childhood acute lymphoblastic leukemias.

Assistant or Associate Professor, Leukemia Clinical Investigations: Develop and chair clinical trials in pediatric leukemias, and assist in managing the Therapeutic Advances for Childhood Leukemia (TACL) consortium Operations Office. BC/BE in Pediatric Hematology-Oncology required.

Postdoctoral Fellowship Positions Available: Retinoid pharmacology or mechanism of action; ceramide/sphingolipid metabolism; pre-clinical testing models of anti-cancer agents. Good command of written and spoken English required. Excellent salaries commensurate with training.

Other Positions: Clinical Research Associate, and Research Specialist positions are available.

Applicants should forward (via email only, indicating position desired) a copy of their C.V., a statement of current and future research interests, and three references to :

C. Patrick Reynolds, M.D., Ph.D.
Director, Developmental Therapeutics Program
USC-CHLA Institute for Pediatric Clinical Research MS 55
Childrens Hospital Los Angeles
4650 Sunset Blvd., Los Angeles, CA 90027

Please apply by email only to: recruiting@ipcr.us

Further information on these positions can be found online at:
www.ipcr.us

Assistant/Associate Professor
UCSF Program in Craniofacial and Mesenchymal Biology

The Program of Craniofacial and Mesenchymal Biology, a new research program at UCSF, seeks faculty members to be appointed at the Assistant or Associate Professor level. An appointment in the new Department of Cell and Tissue Biology and membership in the Biomedical Sciences Graduate Program and Oral and Craniofacial Sciences Graduate Program will be offered. Candidates are expected to establish a dynamic research program and to contribute to teaching and training programs.

Candidates are expected to hold a Ph.D., M.D., or D.D.S. degree and to have demonstrated achievements in cell and/or developmental biology in one of the following areas: mesenchymal stem cell biology, mesenchymal cell proliferation or differentiation, mesenchymal-epithelial interactions, muscle, bone, fat and/or cartilage biology, skeletal development and biology, including craniofacial development and skeletal immunology, or tissue repair. The positions remain open until filled, but review of the applications will start on **March 1, 2005**.

Applications should include a curriculum vitae, a brief description of research accomplishments and a statement (maximum two pages) of future research plans and teaching interests. Supporting reference letters should be sent under separate cover. Submit curriculum vitae and supporting documents to: **Dr. Rik Derynck, Craniofacial and Mesenchymal Biology Search, Department of Cell and Tissue Biology, University of California at San Francisco, 513 Parnassus Avenue, Room HSW-613, Box 0512, San Francisco, CA 94143-0512.**

UCSF is an Affirmative Action/ Equal Opportunity Employer. The University undertakes affirmative action to assure equal employment opportunity for underutilized minorities and women, for persons with disabilities, and for Vietnam-era veterans and special disabled veterans.

University of California San Francisco
UCSF
School of Dentistry

Assistant/Associate Professor
UCSF Developmental and Stem Cell Biology Program

The Developmental and Stem Cell Biology (DSCB) Program at the University of California, San Francisco is seeking to recruit new faculty members whose research is focused on stem cell biology and its application. The DSCB Program, located on the Parnassus Campus, is an interactive and collaborative research environment for research spanning basic principles to bedside practice. The program emphasizes neuronal, pancreatic, liver, blood, cardiac developmental and stem cell biology to complement our strong basic research and clinical programs. Members of faculty in this program are expected to further their understanding of stem cell biology and develop better ways to treat and prevent diseases. The successful candidates are expected to have a research plan relevant to Stem Cell biology, and to be committed to active participation in the affairs of the DSCB Program. The appointees will be members of the Biomedical Sciences Graduate Program and an appropriate academic department. Candidates are expected to hold a Ph.D or M.D degree, and to have demonstrated achievement in their field. Applicants should submit curriculum vitae, a 1-2 page summary of research accomplishments, 3 letters of reference, a 1-2 page perspective on future research plans, and reprints of major publications.

Review will commence by **March 1, 2005**. Please submit curriculum vitae and supporting documents to: **Arnold R. Kriegstein, M.D., Ph.D., Director, Developmental and Stem Cell Biology Program, Chair, Search Committee, School of Medicine, 513 Parnassus Avenue, Campus Box 0525, San Francisco, CA 94143-0525.** Or via email in a Microsoft Word compatible format to: **stidhame@stemcell.ucsf.edu**.

UCSF is an Affirmative Action/ Equal Opportunity Employer. The University undertakes affirmative action to assure equal employment opportunity for underutilized minorities and women, for persons with disabilities, and for Vietnam-era veterans and special disabled veterans.

University of California San Francisco
UCSF
School of Medicine

CHIRON




Creating products that transform human health worldwide.

At Chiron, our aim is to prevent and treat diseases, and improve people's lives. A global biopharmaceutical leader with over 5500 employees worldwide, Chiron, headquartered in Emeryville, California, in the San Francisco Bay Area, continues to grow, and we are currently seeking experienced professionals to join us. ***Come make a difference!***

ASSOCIATE II, RESEARCH

BS or MS level synthetic organic chemist for the discovery and development of novel compounds for new therapeutic applications. Requires BS or MS in Organic Chemistry. Proficiency with operation of common laboratory and analytical equipment and ability to interpret NMR, IR, GC, HPLC and MS reports is essential. **44002997-RK**

ASSOCIATE DIRECTOR, RESEARCH

Currently seeking PhD medicinal chemist responsible for directing a team of PhD and BS/MS level chemists performing research and development of small molecule therapeutics in a highly collaborative multi-disciplinary team environment. Experience in the design of therapeutics for oncology indications and in structure-guided drug design a plus. Requires PhD in Organic or Medicinal Chemistry with 8+ years of small molecule medicinal chemistry drug discovery experience. **44002996-RK**

DIRECTOR, RESEARCH

Candidate will lead projects in oncology from the antibody discovery phase up to IND-enabling studies. Requirements for this position include MD/PhD in Immunology or Oncology, along with 10 years of post-graduate experience, including 5 years in biotech or pharmaceuticals. **44002909-RK**

PRINCIPAL SCIENTIST, RESEARCH

Develop projects in immunohistochemistry, and design, implement and interpret scientific research projects between Experimental Pathology and Molecular and Cell Biology. Requires PhD in a biological scientific discipline, postdoctoral work, and 5-8 years of related experience. **44003007-RK**

PRINCIPAL SCIENTIST, RESEARCH

Support oncology drug discovery and development. Successful candidate will sit on late stage research and early development project teams for small molecule oncology drugs. Design, implement, analyze and interpret toxicology studies in-house and at CROs, write and review regulatory documents, and sit on project teams. Experience with in vitro toxicity screening useful. Requires PhD in Toxicology or related field with 5-8 years pharmaceutical industry experience. American Board of Toxicology certification desirable. **44003008-RK**

PRINCIPAL SCIENTIST, RESEARCH

Play a central role in target validation and the preclinical evaluation of antibody therapeutics for cancer. Design, plan and perform experiments to validate targets for anti-cancer therapeutic antibodies. Requires PhD in Cell Biology or related field with more than 5 years of postgraduate experience in cancer cell biology and antibody therapeutics. **44003039-RK**

SCIENTIST II, RESEARCH

Participate in and perform the design, development, execution, and interpretation of scientific research projects pertaining to the bioassays department. Contribute to small molecule drug discovery in the field of Oncology. Requires PhD in Applied Cell Biology or Biochemistry, with postdoctoral work and 3-5 years of related experience. **44003011-RK**

SPECIALIST I, RESEARCH

Support research projects in therapeutic antibodies and small molecule drug discovery. Develop purification processes and produce proteins for efficacy studies, X-ray crystallography, and high-throughput screening. Requires BS/MS in Biochemistry or a related scientific discipline, with a minimum of 5 years related experience. **44003009-RK**

SENIOR SCIENTIST, RESEARCH

Provide expertise in preclinical models, PK/PD understanding, in vivo biomarker discovery and assay development in support of projects that span from research to clinical development. Broad scientific experience in cancer biology is essential. Prior research experience with pharmacodynamic investigations using in vivo tumor models required. The candidate should also have a clear understanding of new research methodologies, as well as prior experience in identification and implementation of these technologies to support their research. **44002910-RK**

SPECIALIST I, RESEARCH

Develop and perform cell-based assays as part of the hit evaluation. Employ a variety of automation instruments, signal detection technologies, and analysis techniques in this process. Ideal candidate would have experience with FACS and High-Throughput Imaging Instruments and familiarity with spreadsheet/curve-fit/graphic software. Requires BS or MS in Cell Biology, Biochemistry or related field, with minimum of 5 years work experience. **44003012-RK**

We offer an outstanding compensation/benefits package and actively promote a work-life balance.

For complete job descriptions, and to apply, please visit:

www.chiron.com

Chiron welcomes candidates from diverse backgrounds.

Entry-Level And Senior Scientists

Molecular Biology

The Departments of Head and Neck Surgery and Molecular Biology at The University of Texas M. D. Anderson Cancer Center are accepting applications for Assistant, Associate, and Full-Professor scientists. Candidates must have a Ph.D. or equivalent and a track record in publications and peer-reviewed funding. The positions are responsible for supervising and performing investigations in the molecular biology of head and neck cancer. The candidates will supervise research technical staff and develop and maintain independent research programs in an academic setting.

Celebrating six decades of Making Cancer History®, The University of Texas M. D. Anderson Cancer Center is located in Houston, Texas, on the sprawling campus of the Texas Medical Center. It is one of the world's most respected centers devoted exclusively to cancer patient care, research, education and prevention. Competitive salary and exceptional benefits are offered.

Please send a current curriculum vitae to:

Gary L. Clayman, D.M.D., M.D.
Director of Research
UT M. D. Anderson Cancer Center
Department of Head and Neck Surgery
1515 Holcombe Blvd. – Unit 441
Houston, TX 77030-4009

THE UNIVERSITY OF TEXAS
MD ANDERSON
CANCER CENTER
Making Cancer History®

M. D. Anderson Cancer Center is an EOE employer and does not discriminate on the basis of race, color, national origin, gender, sexual orientation, age, religion, disability or veteran status, except where such distinction is required by law. All positions at M. D. Anderson are considered security sensitive; drug screening and thorough background checks will be conducted. The University of Texas M. D. Anderson Cancer Center values diversity in its broadest sense. Diversity works at M. D. Anderson. Smoke-free environment.

Senior Scientist/Group Leader in Protein Chemistry

Novo Nordisk China R&D Center
Zhongguancun Life Science Park, Beijing, China

Novo Nordisk is the world leader in diabetes care and is headquartered in Copenhagen, Denmark. Novo Nordisk China R&D is an integrated part of Novo Nordisk Global R&D, and is a dedicated center of excellence in protein expression and purification. The center is now recruiting a senior scientist to head a protein chemistry group working on purification and characterization of proteins in support of therapeutic protein research. The group has been established during the last 2 years and is fully equipped with state-of-the-art instrumentation and technology.

Requirements:

- Ph.D. in protein chemistry or biochemistry
- A solid theoretical background and a good track record in protein chemistry including e.g., protein purification, characterization and refolding
- >2-5 years (post doc.) hands-on experience with several purification protocols for a large variety of proteins, especially proteins expressed in *E. coli*
- Excellent communication skills in both English and Chinese
- Knowledge within up-scaling processes and protein drug development programs
- Industrial experience outside of China is preferred
- Management experience is preferred

The successful candidate must have a dynamic personality and look forward to work in an ambitious project team in Beijing. Please send your CV and a cover letter by e-mail to: **NNCPRD@novonordisk.com**

Vice Chancellor for Research
North Carolina Central University

North Carolina Central University (NCCU) invites applications and nominations for the position of Vice Chancellor for Research. The primary responsibility for the Vice Chancellor for Research is to support the University's research mission. As the chief research officer of the University, the Vice Chancellor will provide administrative support for research activities through the Office of Sponsored Research, the Office of Technology Transfer, and the Office of Contracts and Grants. The Vice Chancellor will also play an important role in promoting interdisciplinary collaborations and coordinating the University's relationships with federal agencies, corporations, foundations, and state and local governments. The Vice Chancellor for Research is also responsible for developing and coordinating NCCU's Chairs and Faculty searches; faculty development activities/awards; post-doctoral trainee and graduate research policies/programs. Reporting to the Chancellor of the University, the Vice Chancellor for Research is a senior administrative officer charged with the growth and development of the University's research endeavors.

Located in Durham, North Carolina, the University is in the heart of the Research Triangle region, an area with a robust infrastructure for Biotech and Life Sciences. In fact North Carolina is ranked third in the Nation for its concentration in Biotech and Life Sciences (ref: Ernst & Young "America's Biotechnology Report") and brings together over 500 research organizations. NCCU, a comprehensive university that offers programs at the undergraduate, graduate, and first-professional degree levels to over 7,700 students, is a constituent campus of the University of North Carolina.

The University seeks an individual with a proven record of excellence in research in the basic sciences; documented success in securing peer-reviewed extramural funding for research; significant administrative experience; and demonstrated leadership abilities. Applicants must have an earned doctorate. Candidate screening will begin immediately and will continue until the position is filled. All materials should be sent to: **North Carolina Central University Vice Chancellor for Research, c/o Heidrick & Struggles, Inc., 303 Peachtree Street, Suite 4300, Atlanta, GA 30308; Fax: 404-577-4048; Phone: 404-577-2410; Email: nccuresearch@heidrick.com**.

NCCU is an Equal Opportunity, Affirmative Action Employer and is an institution that is committed to, and proudly values diversity. Candidates of all backgrounds are encouraged to apply.

MICHIGAN STATE
UNIVERSITY

ASSISTANT/ASSOCIATE PROFESSOR
ENVIRONMENTAL POLICY

The Environmental Science and Policy Program (ESPP) at Michigan State University seeks two tenure-system faculty in the area of environmental policy. We are looking for dynamic researchers who are comfortable with interdisciplinary work. We have a special interest in risk as an organizing concept in policy for at least one of these positions. Substantive areas of interest should complement MSU's environmental strengths (see **environment.msu.edu**). Some preference will be given to applicants with international experience and skills in languages other than English. Ph.D. or equivalent is required at the time of the appointment.

The positions are academic-year appointments at the rank of Assistant Professor although in some cases a more senior appointment would be considered. The initial appointment would be joint between ESPP and a tenure-granting department or school. The positions will be structured to allow development of a significant research program, and the faculty are expected to develop nationally and internationally renowned research programs with extramural support.

Questions can be e-mailed to the Search Committee at **esppsrch@msu.edu**. Letters of application should be accompanied by a curriculum vitae, short statement of professional goals, and writing sample. Three letters of reference should also be arranged and mailed separately.

Applications will be reviewed starting on **February 24, 2005**, and will be accepted until suitable candidates are found. Applications and letters of reference can be mailed to:

Jack Liu and Saundra Schneider, Co-Chairs
ESPP Search Committee
Environmental Science & Policy Program
Michigan State University
274 Giltner Hall
East Lansing, MI 48824-1101

Women and minorities are encouraged to apply.
MSU is an Affirmative Action/Equal Opportunity Institution.

International Aspirin® Award

Young Researchers' Aspirin® Award

The objective of the Young Researchers' Aspirin® Award is to encourage scientific research into the mechanism of action and clinical use of acetylsalicylic acid, the active ingredient of Aspirin®. Scientists who have contributed to the knowledge of Aspirin® through original independent scientific research in the field of theoretical (experimental) and/or clinical medicine are invited to compete for the Award. The results of their work should have a direct effect on the knowledge or use of Aspirin® and be based on a peer-reviewed publication, accepted and/or published. The publication should not be older than two years. The age limit of the Young Researchers' Aspirin® Award in the year of candidature is 40.

The Young Researchers' Aspirin® Award is valued at Euro 10,000.

Entries will be judged by an international scientific committee representing basic and clinical research.

The application documents are available on the internet at http://www.aspirin.com

Young researchers are invited to either download the complete application documents from the internet or to order a hardcopy from the following address:

International Aspirin® Award
c/o Bayer HealthCare
Consumer Care Europe
Research and Development
Medical Affairs
Dr. Gisela Latta
Building C 151
D-51368 Leverkusen/Germany
Fax: ++49-214-30-55184
E-mail: gisela.latta@bayerhealthcare.com

The deadline for submission is April 30, 2005
(Date of receipt of documents by Bayer HealthCare)

THE ORIGINAL ASPIRIN

BAYER Bayer HealthCare

Exhibit at the AAAS/*Science* Career Fair, 21 February 2005.

Postdoctoral Careers 1

A *Science* Advertising Supplement

Great scientists don't just fall from the sky.

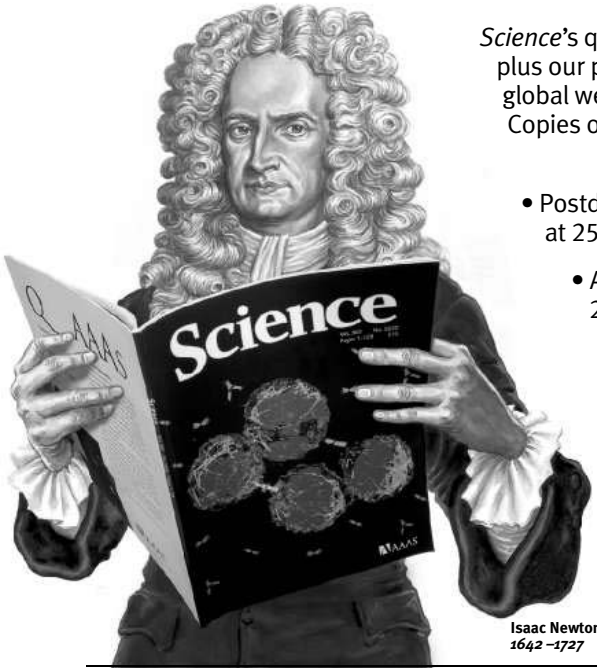

Isaac Newton
1642 –1727

Science's qualified circulation of 129,590[1] plus our pass-along readers brings total global weekly readership to over 710,000.[2] Copies of this issue will be distributed to:

- Postdoctoral organizations at 25 top universities
- AAAS/*Science* Career Fair 21 February, Washington, DC
- AAAS Annual Meeting 17–21 February, Washington, DC

1 *Science* June 2004 BPA Publisher's Statement.
2 *Science* June 2004 circulation as applied to 14 January 2000 Harvey Readership Survey and 2002 Harvey Cumulative Report, publisher's own data.

Issue date 11 February 2005

Reserve ad space by 25 January 2005

For more information, contact:
Daryl Anderson – 202-326-6543
advertise@sciencecareers.org

ScienceCareers.org
We know science AAAS

UNIVERSITY OF CALIFORNIA, IRVINE
COLLEGE OF MEDICINE
Department of Anatomy and Neurobiology and the UCI Epilepsy Research Training Program

Positions: Postdoctoral Researcher/Scholar

Multidisciplinary Postdoctoral Training program in Epilepsy Research has multiple openings for non-tenured, academic term appointments as Postdoctoral Scholar. The program supports diverse approaches to the understanding of the fundamental neurobiological processes leading to epilepsy and /or holding promise for its cure. Participating laboratories include:

Nancy L Allbritton, MD, PhD: Cellular machinery
Tallie Z. Baram, MD, PhD: Neuroplasticity, mechanisms of epileptogenesis, febrile seizure models, hyperpolarization activated channels
Christine M. Gall, PhD: Neurotrophins, integrins, activity-dependent plasticity
Alan L. Goldin, MD, PhD: Sodium channels, transgenic approaches, electrophysiology
Robert E. Moyzis, PhD: Genomic approaches
Charles E. Ribak, PhD: Granule cell plasticity, neuroanatomy
M. Anne Spence, PhD: Population genetics, complex/multigene interactions
Ivan Soltesz, PhD: Electrophysiology, computational neurobiology, interneurons and inhibition
Oswald Steward, PhD: Mechanisms of vulnerability to excitotoxicity
John Weiss, MD, PhD: Excitotoxicity, calcium and zinc trafficking
See: **http://www.ucihs.uci.edu/epilepsyresearch/**

These positions are funded by an NIH training grant; eligible candidates must be U.S. citizens or non-citizen nationals or must be lawfully admitted for permanent residence. An MD or PhD degree is required. All qualified candidates, including minorities and women, are highly encouraged to apply. Salary is commensurate with experience and based on the Kirschstein-NRSA postdoctoral stipend levels for 2005. Candidates should submit resume and references to **Postdoctoral Search/Epilepsy, c/o Dept. of Anatomy and Neurobiology; University of California, Irvine; Irvine, CA 92697-1275** and contact also their preferred laboratory.

UCI is an Equal Opportunity Employer committed to excellence through diversity.

UCI
University of California, Irvine

ERNA OCH VICTOR HASSELBLADS STIFTELSE
HASSELBLAD FOUNDATION

Hasselblad Professor in Public Understanding of Science

The Erna and Victor Hasselblad Foundation, in collaboration with Chalmers University of Technology and Göteborg University, will fund a chair in *Public Understanding of Science,* a subject that may include studies of public understanding and attitudes towards science and technology, science in schools, science and media, science and gender. The position will be affiliated with either or both of the two universities and will offer opportunities to collaborate closely with the National Science Centre, Universeum.

A preferred research direction is to identify structural and methodological bottlenecks in communication between the professional scientist and the public and to devise and implement ways to ameliorate these bottlenecks.

For further information: **www.hasselbladfoundation.org**

For inquiries:
Professor Bengt Nordén, Chalmers. Phone: Int +46 31 772 3041, e-mail **norden@chembio.chalmers.se**
Mrs Margareta Wallin Peterson, Pro Vice-Chancellor, Göteborg University. Phone: Int + 46 31 773 1145, e-mail **m.wallin@zool.gu.se**

Applications should be addressed to The Registrar, Chalmers, SE-412 96 Göteborg, Sweden.
Deadline: February 28, 2005.

PIONEER.
A DuPont Company

RESEARCH POSITIONS

Pioneer Hi-Bred International, Inc is the world leader in the discovery, development and delivery of elite crop genetics.

VISITING SCIENTIST in MOLECULAR NUTRITION - Penn State University, PA: Together with Penn State University's Center of Excellence in Nutrigenomics within the Huck Institute of Life Sciences, we are offering a Visiting Scientist position. This individual will focus on the molecular nutrition of long-chain polyunsaturated fatty acids as they relate to cardio-inflammatory disorders such as metabolic syndrome and obesity. A doctorate in molecular nutrition, genomics, biochemistry, or medical sciences is required. In addition, a technical background in nutrition, molecular biology, cell culture, and lipid metabolism is highly desirable. Information about the Center of Excellence in Nutrigenomics can be found at **www.nutrigenomics.psu.edu**. **Requisition ID** for this position is **RW24**.

ASSOCIATE REGISTRATION MANAGER - Johnston, IA: This individual will obtain government approvals of regulated products. This requires that the manager analyze data, plan, organize and write complex technical reports and submissions, interact with internal and external contacts to address technical biosafety questions from reviewers and work with collaborators to gain regulatory approvals. Ph.D. in biological sciences preferred with at least 3 years of experience in product registration or equivalent technical experience. **Requisition ID** for this position is **RP522**.

RESEARCH ASSOCIATE - Newark, DE: The Insect Control Group based in Newark, DE is seeking a qualified candidate to work in a multidisciplinary team to isolate and characterize novel insecticidal leads against various target pests. The candidate must have at least a B.S. degree with 2-4 years of experience in biochemistry or a related field. Prior experience in protein fractionation is preferred. **Requisition ID** for this position is **RP385**.

For a complete job description and to apply, go to **www.pioneer.com/employment**. Enter the Requisition number in the keyword search.

EOE

Ivy Chair in Morphogenesis in the Biology Department University of Virginia

The Department of Biology is searching for a distinguished scientist to fill the endowed Ivy Chair in Morphogenesis. The University of Virginia has recently established the Morphogenesis and Regenerative Medicine Institute and chosen this area as one of 4 at the University for growth over the next decade. The Ivy chair was established in part to promote the development of the Institute and we expect the holder of the chair to be an intellectual leader in both the Biology Department and the Institute. The area is open although preference will be given to candidates who will interact productively with and complement the University-wide Morphogenesis group and the Biology Department as a whole. The position will be filled at the Full Professor level. The Biology Department is broad based with particular strengths in Developmental Biology, Cell Biology, Neurobiology and Evolution. Biology Department faculty use animal, plant and microbial systems in their research and we encourage candidates using any of these systems to apply. The University of Virginia is consistently ranked among the best public universities in the United States. In addition to being a distinguished research scientist the successful candidate will have the interest and ability to provide outstanding instruction to our talented undergraduate and graduate students.

Please send curriculum vitae, statement of research and teaching interests, and the names of three references to: **Ivy Chair Search Committee, Department of Biology, Gilmer Hall, P.O. Box 400328, University of Virginia, Charlottesville, VA 22904-4328.**

Candidates are encouraged to apply by **February 28, 2005**. The search will continue until the position is filled. Additional information about the Biology Department and the Morphogenesis and Regenerative Medicine Institute can be found at **www.virginia.edu/biology** and **www.morphogenesis.virginia.edu** respectively. Inquiries can be sent to **bio-ivy@virginia.edu**.

The University of Virginia is an Equal Opportunity/ Affirmative Action Employer.

AAAS Annual Meeting and *Science* Career Fair

The 2005 AAAS Annual Meeting is the perfect place to explore your career options and attend the *Science* Career Fair. Both the career fair and the career-related workshops are FREE to attend.

AAAS Annual Meeting

DATES: **17–21 February 2005**

PLACE: **Marriott Wardman Park Hotel Washington, DC**

CAREER WORKSHOPS (see website for complete listing of workshops):

- Strategic Networking
- Pathways to Multiple Career Opportunities
- AAAS Fellowship Program in Public Policy and Mass Media
- Research Training at the NIH
- How to Fire Up your Presentation

AAAS/*Science* Career Fair

DATE: **21 February 2005**

PLACE: **Marriott Wardman Park Hotel Washington, DC**

TIME: **11:00 am – 4:00 pm**

Science Careers offers you the chance to meet employers.

Exhibiting employers are typically from biotechnology, pharmaceutical, government, and manufacturing organizations.

For more information and updates to our exhibitor list, please visit www.sciencecareers.org and click on Career Fairs.

▶ **Registration is required to attend the career workshops. Visit www.sciencecareers.org and click on Career Fairs for instructions on how to register for free.**

ScienceCareers.org

We know science AAAS

Evolution, Ecology, Behavior, Conservation
Systematics Director,
Mountain Lake Biological Station
The University of Virginia

The University of Virginia is seeking an outstanding biologist as Director of Mountain Lake Biological Station. He or she will have a record of accomplishment and the expectation of continued excellence in research and teaching. The Director will be a resident tenured member of the Department of Biology in Charlottesville during the academic year.

Mountain Lake Biological Station is located 3 hours southwest of Charlottesville in the Alleghenies Mountains surrounded by the Mountain Lake Wilderness Area and the Jefferson National Forest. The station is a center for research in population biology and community ecology and is now in its 75th year of offering summer courses in field biology.

Applicants should submit a curriculum vitae, research and teaching statements, a letter explaining their anticipated contribution to the field station, and names and addresses of four references to: **Dr. Janis Antonovics, MLBS Search Committee Chair, Department of Biology, PO Box 400328, Charlottesville, VA 22904-0328**. Applications are encouraged by **February 15, 2005**, but the search will remain open until the position is filled. Additional information can be found at **www.mlbs.virginia.edu** or by e-mail to **antonovics@virginia.edu**.

The University of Virginia is an Equal Opportunity/Affirmative Action Employer.

ROBERT C. BYRD HEALTH SCIENCES CENTER
West Virginia University

Faculty Positions
Center for Interdisciplinary Research in Cardiovascular Sciences

As part of a major interdisciplinary initiative in cardiovascular research, the West Virginia University Health Sciences Center invites applications from outstanding scientists for multiple tenure-track positions, available July 1, 2005. This recruitment is open to all ranks, but we are especially interested in individuals with established research programs, to be hired at the Associate or Full Professor level. We seek investigators across broad areas of the cardiovascular sciences, whose research programs relate to atherosclerosis and metabolic syndrome. Areas of interest include:

- lipid and lipoprotein metabolism
- signal transduction and hormone action
- endothelial cell biology
- vessel/vascular network remodeling

Individuals incorporating analytical biochemistry and molecular biology in their experimental approach are especially encouraged to apply. Appointees for Assistant Professor will be expected to develop an innovative, NIH-funded, independent research program; appointees for Associate or Full Professor will be expected to have current NIH funding. Appointees will also be expected to participate in the teaching mission of the institution. The successful candidate will receive a generous startup package, competitive salary, and renovated laboratory space commensurate with experience and qualifications. An appointment in the most suitable basic science or clinical department will be provided.

A major goal of this interdisciplinary center (website: **http://www.hsc.wvu.edu/circs**) is to develop collaborations among basic, translational and clinical research in cardiovascular health and disease. The Health Sciences Center supports excellent core facilities that include proteomics and protein mass spectrometry, confocal microscopy, functional imaging, flow cytometry, and mouse transgenics. West Virginia University is a comprehensive, Carnegie designated Doctoral Research-Extensive, public institution. Morgantown is rated as one of the best small towns in the U.S., with affordable housing, excellent schools, a picturesque countryside, and many outdoor activities.

Qualifications: A Ph.D. or M.D., two or more years of postdoctoral training, and evidence of significant research accomplishments. Interested individuals should submit a complete curriculum vitae, a brief description of research interests, and the names and addresses (including e-mail) of three references to: **Matthew A. Boegehold, Ph.D., Director, Center for Interdisciplinary Research in Cardiovascular Sciences, PO Box 9105, West Virginia University, Morgantown, WV 26506-9105**. Review of applications will begin **February 1, 2005**, and continue until positions are filled.

West Virginia University is an Affirmative Action/ Equal Opportunity Employer.

UNIVERSITY of VIRGINIA

PROFESSOR & CHAIR

Department of Internal Medicine

The University of Virginia School of Medicine invites applications for the position of Professor and Chair of the Department of Internal Medicine. The Department has a long tradition of excellence in basic and clinical research, education and clinical practice.

We are seeking candidates with highly developed leadership, collaborative communication and interpersonal skills. The successful candidate will be expected to have an outstanding academic record in clinical care, research and education. The candidate must be able to define and communicate a vision and strategic direction for the department, as well as provide important input into the academic direction of the School of Medicine and Medical Center. In addition, the candidate must be able to shape annual departmental objectives and plans and manage the support of these goals.

This position will have a five-year appointment. Full review commences February 1, 2005. Position is open until filled. Candidates must meet the criteria for appointment to senior faculty ranks and be Board Certified in Internal Medicine.

Please submit electronically and in hard copy a letter of interest, a curriculum vitae, and the names and addresses of three referees to:

Search Committee for Professor and Chair of
Department of Internal Medicine
University of Virginia - School of Medicine Dean's Office
PO Box 800793, Charlottesville, VA 22908
Attention: Shirley Rothlisberger

srr8w@virginia.edu

The University of Virginia is an Equal Opportunity/Affirmative Action Employer.

Tenure-Track Investigator Position in Immunology and Related Fields
National Institute of Allergy and Infectious Diseases
National Institutes of Health (NIH)

The National Institute of Allergy and Infectious Diseases (NIAID), Division of Intramural Research (DIR) is recruiting for a Tenure-Track Investigator in the Laboratory of Cellular and Molecular Immunology (LCMI). The NIAID is a major research component of the NIH and the Department of Health and Human Services (DHHS).

The Laboratory of Cellular and Molecular Immunology (LCMI) is seeking a M.D., Ph.D., D.V.M., or an equivalent degree for a tenure track position. Candidates with a strong record of creative, scientific accomplishments, and those with a novel, progressive approach to the discipline are particularly encouraged to apply.

The successful candidate will have a unique opportunity to establish an independent research program at the NIH main campus in Bethesda, Maryland. This facility houses one of the largest immunological research communities in the world, with access to flow cytometry, confocal microscopy, mass spectrometry and microarray production. This position will have committed resources for space, a technician and two postdoctoral fellows, as well as an allocated budget to cover service, supplies, animals and salaries.

Salary will be commensurate with research experience and accomplishments. A full Civil Service package of benefits is available, including retirement, health, life, long term insurance care and Thrift Savings Plan.

To apply, candidates must submit a curriculum vitae and bibliography, three letters of recommendation, and a 2-3 page description of a proposed research program to: Dr. Jack Bennink, Chair, Search Committee, Attn: Jennifer Walker, Executive Secretary, NIAID, NIH, 6700B Rockledge Dr., Rm. 1134, Suite 1230, MSC-7617, Bethesda, MD 20892-7617. All applications must be received by February 7, 2005. All applicants will be notified by e-mail or phone when their applications are complete.

DHHS and the NIH are Equal Opportunity Employers.

POSITIONS OPEN

ASSISTANT PROFESSOR POSITIONS
Oregon State University

Assistant Professor in Pathogenic Microbiology. The Department of Microbiology at Oregon State University (OSU) invites applications for a full-time (1.0 FTE), nine-month, tenure-track appointment. The successful candidate is expected to establish a competitive research program focused on the molecular biology of bacterial or viral pathogens of health relevance. Areas of particular interest include, but are not limited to, research on pathogenesis, evasion of host defenses, use of animal models, and interaction with the immune system. The candidate will be expected to contribute to undergraduate and graduate teaching. A Ph.D. and two years of relevant postdoctoral research are required.

Assistant Professor in Immunology. The Department of Microbiology and the Linus Pauling Institute at Oregon State University invite applications for a full-time (1.0 FTE), nine-month, tenure-track appointment. The successful candidate is expected to establish a competitive research program focused on studying the involvement of the immune response in bacterial or viral pathogenesis; research on the interactive effects of inflammation, nutritional factors, or aging are of particular interest. The candidate will be expected to contribute to undergraduate and graduate teaching. A Ph.D. and two years of relevant postdoctoral research are required.

Send or e-mail a letter of application with research and teaching goals, curriculum vitae, and names and contact information of three references by March 15, 2005, to either: **Pathogenic Microbiology Search Committee, or Immunologist Search Committee, c/o Mary Fulton, Department of Microbiology, 220 Nash Hall, Oregon State University, Corvallis, OR 97331. E-mail: mary.fulton@oregonstate.edu.**

For full position announcements see **website: http://oregonstate.edu/admin/hr/jobs/ADept.html.** *OSU is an Affirmative Action/Equal Opportunity Employer.*

INFORMATION TECHNOLOGY WEB DEVELOPER

The Institute of Marine and Coastal Sciences, an international leader in marine science, wishes to hire an experienced Web Developer to handle all aspects of the technological development, advancement, and implementation of its Ocean Biodiversity Information System (**website: http://www.iobis.org**) to its next generation.

Requires at least three years of web server-side development experience using Java/JSP, JDBC, and Oracle PL/SQL. Plone, Phython, and environmental systems research institute geographic information system experience desirable. Master's degree in computer science is preferred.

Please send resume to: **Attn: Ken Eng, Institute of Marine and Coastal Sciences, Rutgers, The State University of New Jersey, 71 Dudley Road, New Brunswick, NJ 08901-8521.** Applications must be postmarked by January 31, 2005. *Rutgers is an Affirmative Action/Equal Opportunity Employer. Employment eligibility verification required.*

RESEARCH ASSISTANT PROFESSOR: The Department of Obstetrics and Gynecology at The University of Alabama at Birmingham has a vacant nontenure-track research faculty position open in the Division of Gynecologic Oncology. The applicant should have a Ph.D. in one of the health sciences with postdoctoral training in the area of gene therapy and ovarian cancer. The successful applicant will have demonstrated ability to develop a research program that advances gene therapy methodologies, especially those involving recombinant adenovirus and in vivo imaging. Send curriculum vitae and a statement of research interests to: **Kathy B. Minor, Executive Director, The University of Alabama at Birmingham, Department of Obstetrics and Gynecology, Old Hillman Building 246, 618 South 20th Street, Birmingham, AL 35233.** Application deadline is January 31, 2005.

The University of Alabama at Birmingham is an Affirmative Action/Equal Employment Opportunity Employer.

TENURE-TRACK FACULTY POSITIONS, CANCER RESEARCH
Case Western Reserve University
School of Medicine
Case Comprehensive Cancer Center

The Case Comprehensive Cancer Center, a National Cancer Institute designated comprehensive cancer center, invites applications for tenure-track faculty positions both at **JUNIOR** and **SENIOR** levels (open rank). Candidates should have a Doctorate and postdoctoral experience with an outstanding record of cancer research achievement, preferably in targeted areas of: cell proliferation and apoptosis, tumor suppressors, angiogenesis, signal transduction, cell cycle regulation, stem cells, DNA damage and repair, cancer genetics, and breast or prostate cancer. The successful candidate is expected to have, or develop, an independent and externally funded research program, and contribute to graduate and postgraduate teaching. These positions offer outstanding opportunities for multidisciplinary research collaborations in a supportive research environment. Please send curriculum vitae, a list of three or more references, and a cover letter outlining research focus and interests to: **Stanton L. Gerson, M.D., Director, Case Comprehensive Cancer Center, 10900 Euclid Avenue, Wearn 151, Cleveland, OH 44106-5065. E-mail: cancer@case.edu.**

Case is an Affirmative Action/Equal Opportunity Employer. Minorities and women are encouraged to apply.

POSTDOCTORAL RESEARCH ASSOCIATE POSITION
Biochemistry and Biophysics

The Chemical Sciences Division, Oak Ridge National Laboratory (ORNL) (**website: http://www.ornl.gov**) has an immediate opening for a Postdoctoral Research Associate to perform biochemistry and biophysics studies in support of U.S. Department of Energy's Photobiological (algal) Hydrogen Production Research and Development Program. Applications are sought from highly motivated individuals with a strong background in biochemistry, biophysics, and/or plant physiology. Qualified candidates must have skills in protein structural and functional determination, biochemistry, and/or physiology assays. Experience in algal (such as Chlamydomonas reinhardtti) molecular genetics or molecular biology is a plus. Salary (around $38,000 per year, plus medical benefits) will be determined according to the research skills and experience of qualified candidates.

To apply, please send curriculum vitae, a brief description of research interest, and contact information for three references to: **Dr. James W. Lee, Oak Ridge National Laboratory, Chemical Sciences Division, 4500N, A16, MS-6194, Oak Ridge, TN 37831-6194. E-mail: Leejw@ornl.gov.**

Please reference the position title and number (ORNL05-12-CSD), when corresponding about this position.

These appointments are offered through the ORNL Postdoctoral Research Associates Program (**website: http://www.orau.gov/orise/edu/ornl/ornl-pd/ornlpdoc.htm**) and are administered by the Oak Ridge Institute for Science in Education (ORISE).

The postdoctoral program is open to all qualified individuals without regard to race, color, age, religion, sex, national origin, physical or mental disability, or status as a Vietnam-era veteran or disabled veteran. ORNL, a multi-program research facility managed by UT-Battelle, LLC, for the U.S. Department of Energy, is an Equal Opportunity Employer committed to building and maintaining a diverse work force.

ASSISTANT PROFESSOR MICROBIAL GENOMICS
Department of Botany and Plant Pathology
Oregon State University

The Department of Botany and Plant Pathology (**website: http://www.science.oregonstate.edu/bpp/**), Oregon State University (OSU) invites applications from individuals with outstanding research accomplishments who will establish a vigorous, innovative program in genomics (functional, structural, computational, or environmental) or systems biology of prokaryotic or eukaryotic microbes. We encourage applications from candidates whose research complements existing Departmental strengths, including plant biology, plant-microbe interactions, comparative biology, bacterial genomics, and fungal biology. Centralized facilities supporting genomics, proteomics, imaging, and computational research are provided by the Center for Gene Research and Biotechnology (**website: http://www.cgrb.orst.edu**). The successful candidate will contribute to the undergraduate and graduate teaching missions of the Department. Ph.D. in molecular biology or related area and relevant experience is required. Experience with or understanding techniques used by educators to ensure educational equity and excellence in a multicultural setting required. Research accomplishment in microbial genomics preferred. Position is a 12-month, 0.75 FTE tenure-track appointment. For full consideration, apply by March 1, 2005, by sending resume, a brief summary of research accomplishments and future research plans, reprints of up to five publications, and names/phone numbers of three professional references to: **Microbial Genomics Search Committee, Department of Botany and Plant Pathology, Oregon State University, 2082 Cordley Hall, Corvallis, OR 97331-2902.** Send applications by **e-mail: birkye@science.oregonstate.edu** or **fax: 541-737-3573.** Full position announcement at **website: http://oregonstate.edu/jobs.** *OSU is an Affirmative Action/Equal Opportunity Employer, and has a policy of being responsive to dual-career needs.*

TIER I CANADA RESEARCH CHAIR IN ADVANCED MATERIALS
Faculty of Science, University of Manitoba

The Faculty of Science invites applications for a Tier I Canada Research Chair in Advanced Materials to be appointed at the **ASSOCIATE** or **FULL PROFESSOR** level, and tenured or tenure-track as appropriate. The successful candidate will be expected to pursue a vigorous research program in a field of experimental or theoretical materials science based in the Faculty of Science, and will have the opportunity to take a leadership role in the development of an internationally recognized Materials Research Centre. The review of applications will begin in March 2005 and will continue until the position is filled. Detailed information about the position and application procedure may be obtained from **website: http://www.umanitoba.ca/faculties/science** or **e-mail: mark_whitmore@umanitoba.ca.** Applications including a brief description of a research plan, curriculum vitae, and the names of three references should be sent to: **Dr. M. Whitmore, Dean of the Faculty of Science, University of Manitoba, Winnipeg MB, Canada R3T 2N2.** *The University of Manitoba encourages applications from qualified women and men, including members of visible minorities, Aboriginal peoples, and persons with disabilities. All qualified candidates are encouraged to apply; however, Canadians and permanent residents will be given priority.*

Applications are invited for a faculty position at the rank of **ASSISTANT PROFESSOR** in research and Extension on environmental issues related to nursery production as well as biotic or abiotic factors limiting plant production or quality, with emphasis on integrated container production systems. Appointment to the position will become effective as early as July 1, 2005. For a complete announcement, visit the website of the Department of Horticulture at **website: http://oregonstate.edu/dept/hort/.** *Oregon State University is an Affirmative Action/Equal Opportunity Employer.*

UNMC Eppley Cancer Center
Associate Director, Cancer Prevention and Control

The University of Nebraska Medical Center (UNMC) Eppley Cancer Center, a National Cancer Institute-designated Clinical Cancer Center, seeks outstanding candidates for the position of Associate Director, Cancer Control and Prevention. The position may be tenured or tenure-leading with academic rank commensurate with experience.

Applicants should have a Ph.D., M.D. or other doctoral level degree, with appropriate post-doctoral training and a track record of funding in cancer epidemiology and/or cancer prevention and control. The successful applicant will be expected to develop comprehensive, extramurally funded cancer epidemiology, cancer control and prevention research programs and to collaborate with other Cancer Center Investigators including our NCI SPORE program in pancreatic cancer and our NCI-funded Cancer Research Training Program. The Cancer Center has active multidisciplinary research programs in lymphoma, breast, prostate, pancreas, GI, and aero digestive cancers.

Resources to build population sciences research in the Cancer Center, including funds to recruit several cancer epidemiology, and cancer control and cancer prevention faculty, is expected to be part of the successful candidate's recruitment package.

Applicants should send their CV and a statement outlining their vision for the development of cancer epidemiology, and cancer and prevention programs to: **Dr. Ken Cowan, Director UNMC Eppley Cancer Center, University of Nebraska Medical Center, 986805 Nebraska Medical Center, Omaha, NE 68198-6805**. Applicants are encouraged to apply online to position **# 0013** at **https://jobs.unmc.edu**. Additional information about the UNMC Eppley Cancer Center is available at **www.unmc.edu/cancercenter/**.

Department of Health and Human Services
National Institutes of Health
National Heart Lung and Blood Institute
Division of Intramural Research
Laboratory of Molecular Immunology
Bethesda, MD

A post-doctoral fellowship is available in the area of immunology/molecular biology. The focus of the lab is to elucidate mechanisms by which the immune system is regulated by cytokines (IL-2, IL-4, IL-7, IL-9, IL-15, and IL-21) that share the common cytokine receptor gamma chain, a protein which when mutated in humans results in X-linked severe combined immunodeficiency. Exciting projects range from studying biology of these cytokines to investigating aspects of signal transduction and gene regulation, using state of the art in vitro techniques and transgenic/knockout/knock-in in vivo methodologies. Exciting results are emerging in multiple areas. The successful candidate should have a Ph.D. and/or M.D. with strong background in immunology, biochemistry, or molecular and cell biology. The candidate will be supported through an excellent intramural NIH fellowship in a stimulating and interactive research environment at NIH.

Send curriculum vitae and names and addresses of 3 references:

Dr. Warren Leonard
Chief, Laboratory of Molecular Immunology
NHLBI/NIH
10 Center Drive, MSC 1674
Bldg. 10, Rm. 7N252
Bethesda, MD 20892-1674
Fax: 301-402-0971
Email: wjl@helix.nih.gov

Applications from women, minorities, and persons with disabilities are strongly encouraged. The NHLBI/NIH is a smoke-free workplace.

DHHS and NIH are Equal Opportunity Employers

Chief, Division of Rheumatology and Immunology

The Keck School of Medicine of the University of Southern California (Department of Medicine) is seeking applications for the position of Chief, Division of Rheumatology and Immunology. Candidates must hold M.D. or M.D./Ph.D. degrees and qualify for tenure or tenure-track appointment at the Associate or Full Professor level at the University of Southern California (USC). Candidates should be nationally/internationally recognized for scholarly achievements in basic and/or translational research in immunology. The Division Chief must have a strong commitment to research, patient care and education, and promote the growth and development of the Division and its faculty.

The Division has been ranked in the top 20 national rheumatology programs by U.S. News and World Report. It affords broad research, educational and clinical opportunities supported by exceptional resources on the USC Health Sciences Campus. Affiliated hospitals include LAC+USC Medical Center, Rancho Los Amigos National Rehabilitation Center and USC University Hospital. Established research programs in systemic lupus erythematosus, rheumatoid arthritis, organ transplantation, other immune diseases and immune-based therapeutics provide a vibrant laboratory and clinical research environment. Applicants should send a letter of interest and CV to: **Search Committee for Rheumatology/Immunology, Department of Medicine, Keck School of Medicine, University of Southern California, 2020 Zonal Ave., IRD 620, Los Angeles, CA 90033-9520, Attn: Linda Forman, lforman@usc.edu.**

The Keck School of Medicine of USC is an Equal Opportunity Employer.

POSTDOCTORAL POSITION

Developing Novel RNA Aptamers to Block HIV-1 Replication

A post-doctoral position is available immediately to work on an exciting program of developing RNA aptamers directed to HIV-1 RT, Tat, Rev and other targets. This basic research is aimed at measuring efficacy, understanding resistance, delineating the mechanism of action and is ultimately geared towards bringing the aptamers to the clinic.

Individuals interested in learning more about the research program can visit the laboratory website at: **http://www.aecom.yu.edu/prasadlab**

Candidates with experience in the areas of Virology, Nucleic Acid Biochemistry, Protein Chemistry, DNA/RNA Polymerase Biology and Cell Biology should directly email their curriculum vitae and names of three references to: **Prasad@aecom.yu.edu, Albert Einstein College of Medicine, Jack and Pearl Resnick Campus, 1300 Morris Park Avenue, Bronx NY 10461.** EOE

ALBERT EINSTEIN COLLEGE OF MEDICINE
Advancing science, building careers

UNIVERSITY OF MASSACHUSETTS ASSISTANT PROFESSOR IMMUNOLOGY/ PATHOGENESIS

The Department of Veterinary and Animal Sciences at the University of Massachusetts, Amherst invites applications for a Tenure-Track faculty position at the Assistant Professor level. Applicants are required to have a Ph.D., or Ph.D./DVM, or a Ph.D./MD, post-doctoral training and to have developed an independent creative research program in immunology and/or pathogenesis. A focus on equine, bovine, ovine, or porcine systems is considered advantageous. The candidate will be expected to co-teach undergraduate courses in Research Animal Management and laboratory aspects of Veterinary Microbiology, and a graduate course in Immunology. Applicants should send a letter of intent, statement of research interests, current curriculum vita and the names and contact information of three references to: **Dr. Samuel J. Black, Department of Veterinary and Animal Sciences, 314 Paige Lab, University of Massachusetts, Amherst, MA 01003.**

Review of applications will begin on 15th March 2005 and continue until the position is filled. A profile of the Department can be viewed at: http://www.umass.edu/vasci

The University of Massachusetts is located in a college town in Western Massachusetts within 3 hours drive of New York and 2 hours drive of Boston. The region houses Amherst, Smith, Hampshire and Mount Holyoke Colleges and is recognized nationally as both a center of higher education and a scenic treasure offering extensive opportunities for summer and winter recreation.

The University of Massachusetts is an Affirmative Action/Equal Opportunity Employer. Women and members of minority groups are encouraged to apply.

POSITIONS OPEN

VANDERBILT School of Medicine

MANAGING DIRECTOR
Vanderbilt Transgenic Mouse/Embryonic Stem Cell Core Facility

Applications are invited for a Ph.D. level scientist to manage a full-service production facility for the generation of genetically altered mice. This resource, which is based in the Center for Stem Cell Biology, has been in operation for over 10 years and provides a full range of services for the production and cryopreservation of gene altered mice to the Vanderbilt community. Please see **website: http://vcscb.mc.vanderbilt.edu.** The successful candidate will have previous managerial experience of high-level research staff and first-hand knowledge about gene targeting vector design, embryonic stem cell culture, and transgenic mouse generation. Strong organizational and communication skills are essential. Qualified candidates will be eligible for appointment as faculty on the research, nontenure track. Applications will be accepted until the position is filled.

Applicants should submit their curriculum vitae and names of three references to: **Pamela Uttz, Senior Executive Secretary, 744 Light Hall, 21st Avenue South at Garland, Nashville, TN 37232-0615.**

Vanderbilt University is an Equal Opportunity/Affirmative Action Employer with a strong institutional commitment to diversity.

FACULTY POSITION
SENIOR SEARCH, DIRECTOR
UCSB BRAIN IMAGING CENTER
Department of Psychology
University of California, Santa Barbara

The Department of Psychology at the University of California, Santa Barbara (UCSB), invites applications for a senior Cognitive Neuroscientist (**ASSOCIATE** or **FULL PROFESSOR**) and Director of the UCSB Brain Imaging Center to begin on or after July 1, 2005. The Department is especially interested in candidates who can contribute to the diversity and excellence of the academic community through research, teaching, and service. Preference will be given to applicants whose research builds on strengths of the Department's existing faculty (see **website: http://www.psych.ucsb.edu**). The Director of the new UCSB Brain Imaging Center will manage overall operations of this research-dedicated facility that focuses on functional magnetic resonance imaging. The Center is allocated approximately 3,000 assignable square feet in the basement of the new addition to the Psychology Building. Ph.D. in psychology or related field and a strong record of funded research is required at time of appointment. Please send curriculum vitae, statement of teaching and research interests, representative publications, and names of three references to: **Chair, Cognitive Neuroscience Search Committee, Department of Psychology, University of California Santa Barbara, Santa Barbara, CA 93106-9660.**

Review of applications will begin on April 1, 2005, and will continue until filled.

The University of California is an Equal Opportunity/Affirmative Action Employer.

TECHNOLOGY TRANSFER SCIENTIFIC OFFICER wanted to perform and conduct research and technology management as well as valuation of scientific projects for commercialization. Apply commercializing technologies in the areas of oncology, cardiovascular systems, metabolic diseases, endocrinology, neurology, gene therapy, and medical devices. Ph.D., M.D., V.M.D., or D.D.S. in biochemistry engineering, medicine laboratory research, or related field required. Send resume to: **Attn: William McKinney, Cedars-Sinai Medical Center, 8723 Alden Drive, SSB-130, Los Angeles, CA 90048.** *Equal Opportunity Employer.*

POSITIONS OPEN

FACULTY POSITIONS
Baylor College of Medicine
Department of Molecular Physiology and Biophysics

The Department of Molecular Physiology and Biophysics at Baylor College of Medicine is seeking to recruit several new faculty members at the **ASSISTANT, ASSOCIATE,** or **FULL PROFESSOR** levels. We are looking for faculty whose research interests are in cardiovascular, skeletal muscle, or renal physiology. Other research areas will also be considered. The Department has a strong commitment to both basic and translational biomedical research. The Department has state-of-the-art facilities for confocal microscopy, mouse magnetic resonance imaging, multiphoton imaging, and facilities for the creation and analysis of new mouse models. Baylor College of Medicine is a world-renowned research institution with strengths in mouse genetics, cardiovascular sciences, and neuroscience. Ample opportunities exist for scientific interaction and collaborations within the Department, throughout the College, and within the Texas Medical Center. Located in the heart of the Texas Medical Center, Baylor College of Medicine is just across the street from many institutions, including the University of Texas Medical School at Houston and the M.D. Anderson Cancer Center.

Candidates should send a brief research description, curriculum vitae, and the names of three references to:

Ms. Lynda Attaway
Department of Molecular Physiology and Biophysics
Baylor College of Medicine
One Baylor Plaza
Houston, TX 77030

Screening of applicants will begin immediately and continue until all positions are filled.

DIRECTOR
Department of Physiology
The Johns Hopkins University
School of Medicine

The Johns Hopkins University School of Medicine is seeking an eminent academician to Chair our Department of Physiology. Applicants should have demonstrated leadership qualities, administrative experience, and outstanding abilities in research and teaching. Please send letter of application, curriculum vitae, and bibliography no later than April 18, 2005, to:

Randall Reed, Ph.D.
Chair, Physiology Search
Johns Hopkins University
School of Medicine
733 North Broadway, SOM 100
Baltimore, MD 21205
Fax: 410-955-0889
E-mail: kparkent@jhmi.edu

An Affirmative Action/Equal Opportunity Employer.

BIOCHEMIST/MOLECULAR BIOLOGIST

The Division of Pharmacogenomics and Molecular Epidemiology at the National Center for Toxicological Research (NCTR) seeks an individual with biochemistry and molecular biology training to carry out both independent and collaborative studies aimed at assessment of human exposure and individual susceptibility to carcinogens, organ toxicity, and adverse drug reactions that are of regulatory or public health concern to the U.S. Food and Drug Administration. The position is at the AD-12 level (**STAFF FELLOW**; salary is $60,718 per year). Appropriate technical support and startup funding will be provided. Interested applicants should submit curriculum vitae and the names and addresses of at least three references to: **Fred F. Kadlubar, Ph.D. E-mail: fkadlubar@nctr.fda.gov.**

NCTR is an Equal Opportunity/Affirmative Action Employer.

POSITIONS OPEN

The Department of Anatomy at the Kirksville College of Osteopathic Medicine of the A. T. Still University of Health Sciences invites applications for a 12-month, tenure-track faculty position at the **ASSISTANT PROFESSOR** level or above. The successful candidate shall have demonstrated experience in teaching human gross anatomy and shall develop and sustain an extramurally funded independent research program. Applicants must have a Doctorate degree and significant postdoctoral research experience. Details on this position are found at **website: http://www.kcom.edu/academia/anatomy.htm**. Send letter of application, curriculum vitae with research interests, and contact information for three references to: **Lex C. Towns, Ph.D., Chairperson, Department of Anatomy, Kirksville College of Osteopathic Medicine, 800 West Jefferson Street, Kirksville, MO 63501.** Review of applications will begin March 15, 2005, and continue until the position is filled. *The A. T. Still University of Health Sciences is an Equal Opportunity Employer.*

FACULTY POSITION
JUNIOR OR SENIOR LEVEL
Department of Cellular and Molecular Physiology
Yale University
School of Medicine

The Department of Cellular and Molecular Physiology seeks applicants for a Faculty Position at the junior or senior level. Candidates must hold a Ph.D., M.D., or equivalent degree. The candidate's research interest should be in the general area of cellular and molecular physiology with particular emphasis in any of the following: integrative or translational research in genetic model systems; functional genomics of ion channels, exchangers, or transporters; and/or molecular probes or computational methods. Outstanding candidates working in other areas of cellular, molecular, and systems physiology are also encouraged to apply. Excellent opportunities are available for collaborative research as well as for graduate and medical student teaching.

Applicants should include curriculum vitae, a statement of research interests and goals, and three letters of reference. Applications should be sent by **e-mail: leisa.strohmaier@yale.edu** in PDF format or sent to:

Dr. Steven C. Hebert, Chair
Department of Cellular and Molecular Physiology
Yale University
School of Medicine
333 Cedar Street
P.O. Box 3333
New Haven, CT 06510

Application deadline: March 31, 2005.

Yale University is an Affirmative Action/Equal Opportunity Employer.

ASSOCIATE/PROFESSOR
BIOCHEMISTRY
Emmanuel College
Boston, Massachusetts

Emmanuel College seeks a Biochemist to teach upper-level courses and develop a biochemistry major. Teaching at the introductory level will be expected. This is a full-time, tenure-track appointment at the rank of Associate Professor or Professor. The position requires a Ph.D. in biochemistry, evidence of successful college-level teaching, and research that engages undergraduate students. The College's location in the Longwood Medical Area and the presence of a major pharmaceutical research facility on the college campus offer opportunities to both students and faculty. Applications will be reviewed beginning in January 2005, and will continue to be considered until the position is filled. Please visit our **website: http://www.emmanuel.edu** for more details.

MUSC
MEDICAL UNIVERSITY OF SOUTH CAROLINA

Endowed Chairs in the Center for Drug Discovery in Cancer

Endowed Chair in Chemical Biology/Medicinal Chemistry
Endowed Chair in Advanced Cellular Technologies

The Medical University of South Carolina is seeking outstanding applicants for endowed chairs in the Center for Drug Discovery in Cancer. Two endowed chairs in Chemical Biology/Medicinal Chemistry and Advanced Cellular Technologies are available. The successful candidates will play key roles in the growth of the Center for Drug Discovery. New faculty will have space in the new Hollings Cancer Research Building. The endowed chairs are expected to participate in professional and graduate education, and maintain a nationally recognized, funded research program. Candidates should be eligible for appointment as Full Professor.

The Medical University of South Carolina is a rapidly growing research environment. Extramural research support has consistently increased over the past 10 years, topping $170 million last fiscal year. State-of-the-art research facilities include x-ray crystallography, NMR and mass spectrometry, molecular modeling, proteomics, and lipidomics.

The Charleston area provides an outstanding quality of life in a historic coastal city offering excellent opportunities to enjoy the beach, arts, sports, and excellent cuisine.

Interested candidates should submit their curriculum vitae, statement of research interests, and the names of three references to: **Rick G. Schnellmann, PhD, Department of Pharmaceutical Sciences, Medical University of South Carolina, PO Box 250140, 280 Calhoun St., Charleston, SC 29425** or email **spencesj@musc.edu**. Review of applications begins on **February 1, 2005** and will continue until the positions are filled.

The Medical University of South Carolina is an Affirmative Action/ Equal Opportunity Employer.

The Jackson Laboratory

Director of Research

We are seeking a senior level scientist who is enthusiastic about the promise of mouse genetics and its application to diverse fields of biomedical research, and enjoys mentoring others to reach their full scientific potential. In this position he/she will devote approximately half time to their own, competitively funded, research project(s). The other half will be focused on leadership, mentoring and assisting the scientific staff to fully meet their professional and scientific goals. In this capacity, the responsibilities will include: recruitment, promotions and general oversight of the scientific staff; scientific oversight of institutional research support grants and program projects; functioning as liaison to our Board of Scientific Overseers; providing input for scientific strategic planning. The individual hired to fill this position will report to the Director of The Jackson Laboratory.

Applications should include a CV, a 2–3 page statement of research interests and plans, and the names of at least three references.

Interested applicants should apply on-line at www.jax.org. Click on the Careers link and go to "Search Job Listings."

Please direct any questions to: Hook Wheeler, Human Resources Manager at: hrw@jax.org

The Jackson Laboratory is an EOE/AA employer.

www.jax.org

The University of North Carolina at Wilmington
RESEARCH ASSOCIATE PROFESSOR
(Derived Products Research Group Leader)

As part of a new initiative in Marine Biotechnology at the University of North Carolina Wilmington, Center for Marine Science (CMS), there is a requirement for an energetic Research Associate Professor to manage an expanding research effort in the generation, isolation, and identification of bioactive natural products from culturable marine organisms. The position will be available immediately. The successful candidate will have the responsibility of assisting the Biotechnology Research director in the development and management of a team of researchers composed of postdoctoral researchers, research analysts, and graduate students. This work will involve bioassay-guided isolation and structure elucidation of bioactive natural products, and the application of molecular genetics to identify biosynthetic genes of natural products and generate new compounds by modification of these genes. Applicants must have received a Ph.D. degree in natural products, biochemistry, or a related field, with a minimum of two years postdoctoral experience in an established school or institute, or equivalent experience in an appropriate industrial (pharmaceutical) setting. Successful candidates must have experience in one or both of these fields, and published examples of their research work related to these areas of natural products discovery are also required. The UNCW Center for Marine Science is a modern facility and is well equipped with a Bruker Avance 500 MHz NMR (1mm, 5mm, and flow-through probes), FTIR, and LC/MS, LC/MS/MS and JEOL high-resolution mass spectrometry facilities. CMS also has elaborate culture facilities for the production of photosynthetic and non-photosynthetic marine microbes, and a DNA sequencing facility equipped with two automated genetic analyzers and a QPCR instrument.

Interested candidates are encouraged to submit a letter of application, a current curriculum vitae, and the names of three referees to: **Professor Jeffrey Wright, UNCW Center for Marine Science, 5600 Marvin Moss Lane, Wilmington NC 28409**. Submissions can also be communicated electronically to **wrightj@uncw.edu**. Applications received by **February 14, 2005** will receive priority consideration.

UNCW is an Equal Opportunity, Affirmative Action Employer. Women and minorities are encouraged to apply.

UNIVERSITY OF FLORIDA

Assistant Professor
Environmental Microbiology

The Department of Microbiology and Cell Science at the University of Florida invites applications and nominations for a 12-month tenure-track position as **Assistant Professor** to develop an internationally recognized environmental microbiology research program in an area related to space life sciences such as the origin of life, microbial evolution, the study of extremophiles, or stress responses.

Applicants must have a Ph.D., postdoctoral experience, and a strong publication record in relevant areas. The successful candidate is expected to develop an outstanding research program supported with extramural funding, to supervise Ph.D. students, and to be an innovative instructor of undergraduate and graduate students in microbiology and related areas in molecular biological sciences.

The successful candidate will join a group of faculty with similar research interests located at the new Space Life Sciences Laboratory, Kennedy Space Center. Details of the Department and the position may be found at **http://microcell.ufl.edu**.

Electronic applications only will be accepted (submit as a single pdf file). Applications should be sent to Prof. Wayne Nicholson (**WLN@ufl.edu**) and include a cover letter, curriculum vitae, and description of research interests. Applicants should also arrange to have three letters of reference sent directly to **Prof. Nicholson** by email. Review of applications will begin **February 15, 2005** and continue until the position is filled.

The University of Florida is an Equal Opportunity Employer.

POSITIONS OPEN

HEAD
Department of Physiological Sciences
Center for Veterinary Health Sciences
Oklahoma State University

The Department of Physiological Sciences invites applications and nominations for the position of Head, Department of Physiological Sciences, to be filled at the rank of tenured **PROFESSOR** effective July 1, 2005.

The Department of Physiological Sciences is part of the Oklahoma State University College of Veterinary Medicine and encompasses the disciplines of physiology, anatomical sciences, pharmacology, and toxicology. The Department has broad research interests in these disciplines as well as a significant commitment to teaching in both the graduate and D.V.M. professional curricula.

The Department Head is the chief administrative officer with responsibility for the instructional programs of the Department; administrative, budgetary, and promotion decisions; and for providing strong leadership in the development of research, teaching, and public service. The position is 50 percent administration and 50 percent flexible based on research and/or teaching interests. Candidates must have an earned Doctorate; achieved national and international recognition for their scholarship appropriate to the rank of Professor; and have a distinguished scholarly record. Desirable qualifications include, but are not limited to, documented leadership skills, previous administrative experience in a doctoral-granting program, a history of external funding, experience with program development in research and education, evidence of strong communication and organizational skills, and evidence of commitment to working with and supporting a diverse student and faculty population. Applicants possessing the credentials for such a position should submit a full resume including a list of publications and the names, addresses, and telephone numbers of at least five references. Salary is commensurate with experience. A starting date of July 1, 2005, is desirable. To ensure full consideration, applications should be received by February 28, 2005. Applications will be accepted until the position has been filled. Interviews may take place prior to the application deadline; however, no final decision will be made until after that date. Send applications and nominations to:

Jerry R. Malayer, Ph.D.
Professor and Associate Dean
for Research and Graduate Education
Center for Veterinary Health Sciences
Oklahoma State University
222 McElroy Hall
Stillwater, OK 74078
Telephone: 405-744-8085
E-mail: malayer@cvm.okstate.edu

Oklahoma State University is an Affirmative Action/Equal Employment Opportunity Employer, committed to multicultural diversity.

Highly motivated **POSTDOCTORAL FELLOWS/RESEARCH ASSOCIATES** are sought to join our laboratory, which is funded by multiple NIH grants to study the virology of adeno-associated virus and its use as a vector system for gene therapy of cardiomyopathy, muscular dystrophy, diabetes, and orthopedic diseases. Candidates with a Ph.D. degree and expertise in molecular virology, immunology, muscle physiology, cardiology, or orthopedic research are encouraged to apply. The salary will be highly competitive. Please send your curriculum vitae to: **Dr. Xiao Xiao** at **e-mail: xiaox@mgb.pitt.edu.**

POSTDOCTORAL POSITIONS in molecular evolution at the University of Colorado at Boulder. Openings in several projects to study evolution of proteins to serve new functions in the research group of **Dr. Shelley D. Copley** (molecular, cellular, and developmental biology). Skills in molecular biology and/or mechanistic enzymology required. Please send curriculum vitae and names of three references to **e-mail: copley@cires.colorado.edu.**

POSITIONS OPEN

SCIENTIST
High Throughput Drug Screening

Scientist needed to program and run a Biomek & Orca robotic system for Reno-based biotechnology company. Minimum qualifications are a life sciences related degree and experience with high throughput screening robotic techniques and processes. Resume to: **Sierra Sciences, Inc., e-mail: tmcafee@sierrasci.com.**

VICE PRESIDENT RESEARCH

The Leukemia and Lymphoma Society is the world's largest voluntary health organization dedicated to funding blood cancer research. The Society's mission: cure leukemia, lymphoma, Hodgkin's disease and myeloma, and improve the quality of life of patients. The Vice President for Research, located in our White Plains, New York, home office, will supervise administration of all research grant programs and grant review, including grant receipt and award, and update guidelines, applications, and contracts. The candidate will be responsible for supervising review and approval of grantee annual progress and completion of institutional contracts and intellectual property agreements. He/she will also maintain familiarity with grantee research to coordinate with marketing and public affairs acknowledgement of scientific accomplishments.

Potential candidates must possess knowledge of the grant application and review process; an advanced degree in the biological sciences is required and familiarity with cancer biology. You must be able to travel as necessary to attend Society Board and scientific meetings. Please send your resume and salary history to: **The Leukemia and Lymphoma Society, Human Resources Manager, 1311 Mamaroneck Avenue, White Plains, NY 10605. Fax: 914-821-8948** or **e-mail: hr@lls.org; website: http://www.lls.org.** *Equal Opportunity Employer.*

The Department of Physiology, Louisiana State University Health Sciences Center (LSUHSC), New Orleans seeks outstanding candidates for up to four tenure-track faculty positions at the **ASSISTANT** to **FULL PROFESSOR** level. The successful candidate must have a Ph.D. and/or M.D. degree with a strong record of research accomplishments in one or more of the following research areas: pathophysiology of the host defense response to oral, lung, or systemic inflammation and infection; renal physiology; obesity and diabetes; angiogenesis.

There are excellent opportunities for collaboration at molecular, cellular, or systems levels of integration. Successful candidates will be expected to complement the existing research strengths of the Department, rapidly develop an extramurally funded research program, and participate in the Department's graduate and undergraduate teaching programs. An excellent startup package, competitive salary, and state-of-the-art instrumentation are available for each position. Applicants should send curriculum vitae that includes previous and current research funding, a statement of research plans, and the names of at least three references to: **Dr. Gregory Bagby (e-mail: gbagby@lsuhsc.edu), Department of Physiology, Louisiana State University Health Sciences Center, 1901 Perdido Street, New Orleans, LA 70112-1393.** *LSUHSC is an Affirmative Action/Equal Opportunity Employer.*

POSTDOCTORAL POSITIONS in retinal angiogenesis/vascular biology-funded positions are available to M.D.s or Ph.D.s to study angiogenesis and vascular biology in retinopathy addressing basic science questions relevant to clinical problems. The laboratory of **Dr. Lois Smith** is located in the new research building at Children's Hospital, Boston, and Harvard Medical School. Experience in molecular biology and mouse surgery is preferable. Please send curriculum vitae and three references to **e-mail: Lois.Smith@tch.harvard.edu.**

POSITIONS OPEN

UNIVERSITY OF MISSOURI

The Department of Veterinary Pathobiology is announcing their search for one full-time, tenure-track **FACULTY** position in molecular and/or immuno-parasitology to include the **ASSOCIATE PROFESSOR** level. Candidate will be expected to develop a vigorous, externally funded research program, direct Ph.D. students and participate in teaching professional veterinary students, graduate and undergraduate students.

ASSISTANT/ASSOCIATE PROFESSOR: Candidate should have a Ph.D. degree with a minimum of three years relevant postdoctoral or equivalent experience, significant publications, and evidence of potential to sustain high-quality research. Candidate should have expertise in molecular parasitology, immuno-parasitology, parasitic pathogenesis, clinical parasitology, and/or related areas.

The candidate should complement one or more research areas of focus in the Department. Departmental focus areas include infectious diseases, molecular biology, genomics, reproductive biology, and laboratory animal medicine. The candidate would be expected to be involved in the instruction of professional students in parasitology and participate in graduate instruction in their specialty.

Candidates with advanced training and active research programs are particularly encouraged to apply. The Department encourages the development of intra- and interdisciplinary research teams. There is opportunity to collaborate with faculty in our Veterinary Teaching Hospital, Veterinary Diagnostic Laboratory, and Veterinary Clinical Pathology Laboratory as well as faculty in our School of Medicine and our Animal Science Departments. Candidates with a Ph.D. and D.V.M. degree are especially desired. The successful candidate would be located in state-of-the-art laboratories.

Salary for this position is competitive and commensurate with experience. Interested candidates should submit curriculum vitae, statement of research interests and goals, and the names, addresses, telephone numbers, and e-mail addresses of at least three references to: **Parasitology Search Committee, Attn: Anne Chegwidden, Department of Veterinary Pathobiology, 201 Connaway Hall, University of Missouri, Columbia, MO 65211.** Screening of applications will start February 1, 2005, and will continue until the position is filled. To request ADA accommodations, please contact the above individual at **telephone: 573-884-2444.** *The University of Missouri is an Equal Opportunity/Affirmative Action Employer.*

POSTDOCTORAL TRAINING MOLECULAR THERAPY
Children's Hospital of Philadelphia/
University of Pennsylvania

National Hearth, Lung, and Blood Institute Training Grant, "Training in Molecular Therapeutics for Pediatric Cardiology," supporting studies of cardiovascular disease mechanisms and molecular therapies. Project fields include: heart valve disease, nanotechnology, biomaterials, gene-stents, gene delivery systems, cardiac, and pulmonary development, vascular injury, drug delivery, regenerative medicine, stem cell biology, and pharmacology. Competitive salary and full benefits. Only applicants with Ph.D. and/or M.D. (*who must be a resident alien or U.S. citizen status*) should send their curriculum vitae and the names of three references to:

Robert J. Levy, M.D.
William J. Rashkind Endowed Chair
University of Pennsylvania
School of Medicine
Training Program Director
The Children's Hospital of Philadelphia, 702 ARC
3615 Civic Center Boulevard
Philadelphia, PA 19104
Fax: 215-590-5454
E-mail: levyr@e-mail.chop.edu.

Equal Opportunity Employer. Minorities/Females/Persons with Disabilities/Veterans.

McGill

Bioinformatics (Faculty Position)

The Institute of Parasitology is seeking to appoint a tenure track faculty member with experience and research interests in bioinformatics. The appointee will hold a PhD, have an interest in the application of bioinformatics to parasite systems, will become a member of the McGill Centre for Bioinformatics, a multi-disciplinary group bringing together expertise from several Faculties across the University, and the FQRNT Centre for Host-Parasite Interactions (**http://www.mcgill.ca/chpi/**).We are seeking applicants with demonstrated research experience in modeling protein structures/folding or genome mining, and their application in parasite biology. The successful applicant is expected to develop a research program supported by external funding and to teach in the undergraduate and graduate programs. McGill has a dynamic research community with a commitment to develop research and teaching in the Life Sciences, Genomics and Proteomics.

Forward a CV, a summary of your proposed research plans and the names of 3 referees by **28 February 2005** to: **Professor Terry Spithill, Director, Institute of Parasitology, McGill University, 21111 Lakeshore Rd, Ste. Anne de Bellevue, Quebec, Canada. H9X 3V9**. For further information, see **http://www.mcgill.ca/parasitology/** or call **(514) 398-7954**.

All qualified candidates are encouraged to apply; however, Canadian citizens and permanent residents of Canada will be given priority. McGill University is committed to equity in employment.

EPFL
ÉCOLE POLYTECHNIQUE
FÉDÉRALE DE LAUSANNE

Swiss Federal Institute of Technology-Lausanne (EPFL)

POSTDOCTORAL FELLOWSHIP

A post-doctoral position is available immediately in the Laboratory of Molecular Neurobiology and Functional Neuroproteomics at the EPFL. Work in our laboratory will focus on understanding the role of protein aggregation in the pathogenesis of neurodegenerative diseases, including Alzheimer's disease, Parkinson's disease *in vitro*, cell cultures and animal models. The applicant must have a Ph.D. in Biochemistry or related fields and a strong background in molecular biology and protein biochemistry. Candidates with a strong background and demonstrated experience in molecular/cellular biology and are interested in gaining more experience in protein biochemistry and biophysics are encouraged to apply. Applicant should submit their letter of interest, curriculum vitae and the names and addresses of three references to:

Prof. Hilal A. Lashuel, Swiss Federal Institute of Technology (EPFL)- SV-IGBB-AAB045, Station 15 Ecublens, CH-1015 Lausanne, Switzerland. Email: hilal.lashuel@epfl.ch

Cellular and Developmental Biology

The Department of Zoology at Michigan State University (www.zoology.msu.edu) has openings for two tenure track Assistant Professors beginning Fall 2005. We are particularly interested in individuals whose research focuses on cellular or developmental processes underlying morphology, physiology, behavior, ecology, or evolution of animals. Examples of research topics for each position include, but are not limited to:

- Cellular basis for learning, sensory reception and processing, hormone action and reproduction, or physiological adaptations.
- Developmental mechanisms underlying pattern formation and nervous system function; evolution of development.

Applicants should have postdoctoral research experience, the clear potential to compete successfully for external research funding, and an interest in undergraduate and graduate teaching. Applications should include a vita, and statements of research goals and teaching interests. Please arrange for letters of support from three referees. Review of applications will begin **February 15, 2004**. For information contact **Fred Dyer** at **zoology@msu.edu** or **517-353-9864**. All materials should be sent to: **Integrative Biology Search, Department of Zoology, 203 Natural Science Building, Michigan State University, East Lansing, MI 48824**.

MICHIGAN STATE UNIVERSITY IS AN AFFIRMATIVE ACTION/EQUAL OPPORTUNITY INSTITUTION.

Manager for Transgenic and Knockout Mouse Core Facility

Institute of Molecular Biology (IMB) Academia Sinica, Taipei, Taiwan

The Institute of Molecular Biology (IMB) of Academia Sinica, Taipei, is seeking a manager to direct the Transgenic and Knockout Mouse Core Facility. The appointment will be at the rank of Assistant, Associate, or Full Research Specialist, depending on the candidate's qualifications. Applicants should have general familiarity and actual experience on most aspects of transgenic and knockout technologies. Candidate is expected to have a Ph.D. degree or equivalent, but highly qualified individual without Ph.D. will also be considered. The manager will supervise 5 research technicians and provide transgenic/knockout mouse services to IMB and other institutes at Academia Sinica. Adoption and development of new technologies and research collaboration with IMB investigators will be highly encouraged.

Please send curriculum vitae, a description of research experience, and three letters of reference, preferably before **February 28, 2005**, to Search Committee, c/o Fei Chen, Institute of Molecular Biology, Taipei, Taiwan 11529. The interview process will start from March 1, 2005, until the position is filled.

Further information can be obtained from **http://www.imb.sinica.edu.tw/imb/index.html** or **http://www.imb.sinica.edu.tw/TCF/index.html** or Ms. Fei Chen at: **feichen@imb.sinica.edu.tw**

POSITIONS OPEN

GRADUATE RESEARCH FELLOWSHIPS BIOMEDICAL SCIENCE Florida Atlantic University

The Department of Biomedical Sciences at the Florida Atlantic University (FAU) has Graduate Research Fellowships available for well-qualified doctoral students. These renewable positions provide full financial and tuition support for students pursuing dissertation research in neuroscience, cancer, immunology, cardiovascular disease, aging, endocrinology, infectious diseases, and eye diseases. Specific research interests of faculty of biomedical science can be found at **website: http://bioserv.biomed.fau.edu/biomedical/.** Qualified students must apply and be admitted to the Ph.D. program in integrative biology at FAU. The Department of Biomedical Science is housed in a brand new 93,000 square foot facility, the Schmidt Biomedical Science Center. The Department works in close association with other research centers in the University, area medical centers, and the University of Miami School of Medicine. Interested students should submit a statement of intent, transcripts, two letters of recommendation, and GRE scores to: **Dr. Keith Brew, Director of Graduate Studies, c/o Kathy Jurewicz, Florida Atlantic University, Biomedical Sciences, 777 Glades Road, Boca Raton, FL 33431. Telephone: 561-297-2216; e-mail: kbrew@fau.edu.**

POSTDOCTORAL POSITIONS: CANCER GENETICS AND DNA CHIPS

Positions available as part of a Cornell University Medical Center–Memorial Sloan Kettering Cancer Center–international's National Cancer Institute–funded program project grant for (i) the development of comprehensive genetic and epigenetic DNA chips for the profiling of human tumors, i.e., expression analysis, point mutations, loss of heterozygocity/gene amplification, Taqman assays, DNA methylation status; (ii) use of single nucleotide polymorphism DNA chips for identification of new cancer genes; and (iii) identification of inherited mutations associated with increased risk for cancer development. Applicant should have a Ph.D., with substantial recent research experience, preferably in cancer genetics, molecular biology, genomics, bioinformatics, protein-DNA interactions, DNA arrays, single-molecule Quantum Dot and fluorescence based assays, liquid-handling robotics, and/or automation in DNA and polymerase chain reaction technology. Competitive salary commensurate with experience. Send curriculum vitae and names of three references to: **Professor Francis Barany, Program Director, Programs of Biochemistry, Structural Biology, and Molecular Biology, Box 62, Cornell University Medical Center, 1300 York Avenue, New York, NY 10021. Fax: 212-746-7983; e-mail: barany@med.cornell.edu.** *Equal Opportunity Employer.*

VISITING BIOLOGIST

The Department of Biology invites applications for a one-year **ASSISTANT PROFESSOR** position to begin August 2005. Teaching responsibilities include introductory courses for non-majors, participation in the biology core, and upper-level elective courses. Preference will be given to biologists capable of teaching courses in developmental biology and comparative/human anatomy or physiology. Applicants should have or expect a Ph.D. before the starting date.

To apply, please submit a cover letter, curriculum vitae (including e-mail address), and three letters of reference to: **Biology Search Committee, 18952 E. Fisher Road, St. Mary's College of Maryland, St. Mary's City, MD 20686-3001.** Review of applications will begin immediately and continue until the position is filled. Visit our **website: http://www.smcm.edu.** *St. Mary's College of Maryland is an Affirmative Action/Equal Opportunity Employer.*

Ecophysiology: The Department of Zoology at Southern Illinois University Carbondale (SIUC) invites applications for a tenure-track position in ecological physiology at the **ASSISTANT PROFESSOR** level with a start date of August 16, 2005. Postdoctoral experience is preferred. The applicant should demonstrate the existence of, or potential for developing, an externally funded research program. We prefer an Ecophysiologist who can contribute to our existing strengths in ecology, environmental biology, conservation, biodiversity, evolution, environmental toxicology, and ecosystem modeling with the potential to collaborate with faculty in other departments, such as an isotope geochemist currently being sought by the Department of Geology. The successful applicant is expected to teach a course in introductory zoology and undergraduate and graduate courses in their area of expertise. Applicants must hold a Ph.D. or show that they will complete all degree requirements by the time of appointment.

Review of applications will begin February 21, 2005, and continue until the position is filled. Applicants should submit curriculum vitae, a statement of teaching and research interests, and the names and addresses of at least three references to: **Search Committee Chair, Department of Zoology, Mailcode 6501, Southern Illinois University Carbondale, Carbondale, IL 62901-4324. E-mail: muhlach@zoology.siu.edu.**

Southern Illinois University Carbondale is a large, research-oriented institution situated in a pleasant small-town setting southeast of St. Louis. SIUC is seeking to enhance interdisciplinary research as it strives to be a top 75 public research university (**website: http://news.siu.edu/s150/**). The Department of Zoology has a full-time faculty of 24 with about 240 undergraduate and 85 M.S. and Ph.D. graduate students. For further information, please visit our **website: http://www.science.siu.edu/zoology.**

SIUC is an Affirmative Action/Equal Opportunity Employer that strives to enhance its ability to develop a diverse faculty and staff and to increase its potential to serve a diverse student population. All applications are welcomed and encouraged and will receive consideration.

BACTERIAL PATHOGENESIS/ IMMUNOLOGY

Postdoctoral positions are available to study the membrane biology of the syphilis bacterium, *Treponema pallidum,* and its relationship to the immunology of syphilis. The research will focus on (1) discerning the locations (topologies) of selected membrane proteins within the dual-membrane system of *T. pallidum* and (2) utilizing the rabbit model of infection/immunity to probe, dissect, and manipulate the development of protective immunity against selected target antigens. Candidates with a Ph.D. and relevant backgrounds in one or more of prokaryotic membrane biology, molecular biology, immunology, and/or contemporary vaccinology are highly desired. The position offers the opportunity to carry out research in one of the premier U.S. medical centers, under the co-direction of **Drs. Michael V. Norgard** and **Kayla E. Hagman.** Please provide curriculum vitae and the names and addresses of three references to: **Dr. Michael V. Norgard, Chair, Department of Microbiology, The University of Texas Southwestern Medical Center, 6000 Harry Hines Boulevard, Dallas, TX 75390-9048. Fax: 214-648-5905; e-mail: michael.norgard@utsouthwestern.edu.** *The University of Texas Southwestern Medical Center is an Equal Opportunity/Affirmative Action Employer.*

BIOANALYTICAL/BIOPHYSICAL/POLYMER POSTDOCDOCTORAL(S). (1). Gylcosaminoglycan-protein interactions. Immediately available. Techniques applicable: capillary electrophoresis, mass spectrometry, light scattering, and protein modeling. (2). Colloid-polyelectrolyte coacervates. Techniques: dynamic light scattering, fluorescence photobleaching, rheology. Salary commensurate with experience. **website: http://www.chem.iupui.edu/~dubin/research.html** or **e-mail: dubin@chem.iupui.edu.**

The University of Georgia

EMINENT SCHOLAR FOREST BIOTECHNOLOGY

Readvertisement. The Daniel B. Warnell School of Forest Resources invites applications for a senior-level position at the rank of **PROFESSOR AND EMINENT SCHOLAR.** Applicants are expected to have demonstrated creativity in applying advanced biotechnological applications, such as genomics/proteomics, marker-assisted breeding, and/or genetic engineering, to plant biology problems. Experience with commercial forest tree species would be advantageous, but is not required. Recognized international leadership and demonstrated capacity for vigorous interactions with the private sector are highly desired. Applications should include curriculum vitae, statement of research goals and interests, and the names and contact information for four references. Applications received by March 31, 2005, guaranteed full consideration. Send application packages to: **Dr. Jeffrey Dean, Eminent Scholar Search Committee Chair, Warnell School of Forest Resources, University of Georgia, Athens, GA 30602-2152.** *An Affirmative Action/Equal Employment Opportunity Institution.*

ECOLOGIST, Department of Biology, DePauw University. Tenure-track position beginning August 2005. Ph.D. required for tenure. Rank and salary commensurate with experience. Commitment to undergraduate teaching in liberal arts setting essential. Teaching responsibilities include: general education and advanced biology courses in ecology and environmental biology, introductory biology classes in organismal biology, ecology, and evolution. Successful candidate is expected to develop a research program involving undergraduate students. Preference will be given to individuals who have expertise that complements that of existing faculty members. For information about Department, visit **website: http://www.depauw.edu/acad/biology/.** DePauw has exceptional programs for supporting its faculty members, including a pretenure leave and funding for professional and curriculum development activities (see **website: http://www.depauw.edu/admin/acadaffairs/facdev.htm**). Submit letter of application, curriculum vitae, three letters of recommendation, transcripts, statements of teaching philosophy, teaching and research interests, and evidence of teaching effectiveness to: **Ecology Search Committee, Department of Biology, DePauw University, Greencastle, IN 46135.** Review of applications begins February 1, 2005, and continues until position is filled. *DePauw University is an Equal Opportunity/Affirmative Action Employer. Women and members of underrepresented groups are encouraged to apply.*

Interested candidates are invited to apply for a new **POSTDOCTORAL POSITION** at the Microarray Core Laboratory of the National Institute of Diabetes and Digestive and Kidney Diseases (NIDDK) at NIH campus in Bethesda, Maryland. Our work will focus on the analysis of data gathered from different microarray platforms and related gene expression technologies, and the combined use of existing and novel bioinformatics tools to understand gene expression in studies related to Type 1 and Type 2 diabetes. This postdoctoral **RESEARCH ASSOCIATE** position is a one-year appointment with the possibility of renewal, and salary is negotiable depending on years of experience and programming skills. Our current team is composed of biologists and bioinformatics/scientific programmers. We would welcome the addition of candidates experienced in any of these areas. Our research interests can be found on our **website: http://microarray.niddk.nih.gov.** If you would like more information or are interested in applying for this position, please contact or send your curriculum vitae to: **Dr. Margaret Cam** at **e-mail: maggie_cam@nih.gov.**

AWARDS

ANNOUNCEMENTS

POSITIONS OPEN

The University of Washington (UW) seeks to appoint a **DIRECTOR** for the Institute for Nuclear Theory (INT), the Department of Energy's national visitor center in this field (see **website: http://www.int.washington.edu/overview.html**). The successful applicant will also be appointed as a tenured professor in the UW Department of Physics. We seek an outstanding researcher with a record of leadership and innovation in nuclear physics, who can maintain and enhance the vitality of the INT's programs and local research efforts. The individual should have wide interests and a broad perspective on nuclear physics, and a commitment to building ties with related subfields, including astrophysics and particle, atomic, and condensed matter physics. Applicants must have a Ph.D. degree and a strong record of published research. Opportunities are available for teaching and advising graduate students. Please provide curriculum vitae and the names of at least three references that the Committee could consult. Applications should be sent to: **Professor R. G. Hamish Robertson, Search Committee Chair, c/o Cynthia Wythe, Office of Research, Box 351202, University of Washington, Seattle, WA 98195-1202.** Consideration of applications will begin March 1, 2005. *The University of Washington is building a culturally diverse faculty and strongly encourages applications from women and minority candidates. Affirmative Action/Equal Opportunity Employer.*

VETERINARY PHYSIOLOGIST

The Oklahoma State University (OSU) Center for Veterinary Health Sciences invites applications for a tenure-track **FACULTY** position in veterinary physiology. Applicants must have a Ph.D. (D.V.M. preferred). Responsibilities include instruction in the D.V.M. and graduate programs and development of an extramurally funded research program. Applications, including curriculum vitae, statement of professional goals, and names of three references should be submitted to: **Dr. Cyril Clarke, Interim Head, Department of Physiological Sciences, 205 McElroy Hall, Stillwater, OK 74078 (telephone: 405-744-8093; e-mail: clarke@okstate.edu).** To ensure full consideration, applications should be received by February 28, 2005, and review of applications will continue until a suitable candidate is identified.

OSU is an Equal Opportunity/Affirmative Action Employer that encourages applications from members of minority groups.

The United States Geological Survey invites applications for **UNIT LEADER** for the Montana Cooperative Wildlife Research Unit (MCWRU) in Missoula, Montana. The Unit Leader will: (1) conduct wildlife research; (2) educate graduate students; (3) provide technical assistance to parties who have interests in natural resource issues; and (4) maintain close working relationships with cooperators. Applicants must have: (1) a doctoral degree in wildlife biology or related field; (2) worked as a permanent employee for the U. S. Government; and (3) a strong publication record and demonstrated leadership in wildlife research. Candidates who use quantitative techniques, including biometrics and vital rate parameter estimation, are encouraged to apply. Screening of applicants will begin on 18 February 2005. For additional information, see full job description at **website: http://www.forestry.umt.edu/academics/wildlife.** To apply, go to **website: http://jobsearch.usajobs.opm.gov/getjob.asp?JobID=25788944.**

POSTDOCTORAL POSITIONS available to study Plasmodium falciparum proteins involved in placental cytoadherence. Strong background in purification and characterization of proteins is required. Additional experience in cell culture, gene cloning, and expression is desirable. Please e-mail curriculum vitae to: **Dr. Channe Gowda, Biochemisty and Molecular Biology, Penn State College of Medicine, Hershey, PA,** at **e-mail: gowda@psu.edu.** *Penn State is committed to Affirmative Action/Equal Opportunity and to the diversity of its work force.*

POSITIONS OPEN

POSTDOCTORAL AND CLINICAL FELLOWSHIPS
at the
National Institutes of Health
U.S. Department of Health and Human Services

Website: http://www.training.nih.gov

NIH is dedicated to building a diverse community in its training and employment programs.

Brown University, Division of Biology and Medicine, Neuroscience: Responsible for assisting with preparation, writing, and submission of multidisciplinary grant proposals, assisting in transfer of technology through patent disclosures, participate in development efforts for private/foundation support, coordinate media interaction for faculty, and promote public awareness of the Brain Science Program and its research/educational activities. Requirements include Ph.D. in a science-related field or equivalent combination of education/experience. Excellent communication skills (verbal/written); demonstrated skills as a science writer in a medical school environment preferred. Experience with federal funding mechanisms (NIH/National Science Foundation/DOD grants). Demonstrated ability to manage a complex work environment and meet deadlines. Knowledge of health care and biomedical sciences required; neuroscience knowledge desired. Knowledge of technology transfer and intellectual property issues helpful; knowledge of University or foundation fund-raising mechanisms helpful.

To apply please visit us at **website: http://careers.brown.edu** and reference Job# M01490 to submit an application and resume. *Equal Opportunity Employer/Affirmative Action.*

The interdepartmental Computational Biology Program of the University of Colorado School of Medicine is soliciting applications for computational biology and bioinformatics **FACULTY** at the junior and senior levels. The recruitment spans all departments, and is open to scientists doing outstanding computational research relevant to any aspect of human health. Topics of interest include (but are not limited to): whole genome comparison, polymorphism analysis, informatics related to Type 1 diabetes or autoimmune diseases, cancer informatics, neuroinformatics, and mass spectrometry informatics. Recruitment packages include substantial startup resources and extensive space at the new Fitzsimons campus. To apply, please send your curriculum vitae, names of at least three references, and a statement of teaching and research interests to: **Bioinformatics Search Committee, c/o Kathy Thomas, University of Colorado Health Sciences Center at Fitzsimons, Mail Stop 8303, P.O. Box 6511, Aurora, CO 80045-0511,** or by **e-mail: kathy.r.thomas@uchsc.edu.** Review of applications will begin immediately and continue until the position is filled. *The University of Colorado is committed to Diversity and Equality in education and employment.*

ASSISTANT DIRECTOR
Center for Sleep and Circadian Biology
Northwestern University

The Center for Sleep and Circadian Biology invites applications for a full-time administrator with research experience in neurobiology and/or molecular biology. The Assistant Director will be responsible for the coordination of a variety of research and training programs focused on sleep and circadian rhythms in animal models as well as in humans. Applicants should hold a Ph.D. or equivalent degree and have strong writing, personal, organizational, and management skills. Please submit curriculum vitae and three reference letters to: **Dr. Fred W. Turek, Center for Sleep and Circadian Biology, 2205 Tech Drive, Northwestern University, Evanston, IL 60208.** Or **e-mail: fturek@northwestern.edu.**

Northwestern University is an Affirmative Action/Equal Opportunity Employer.

POSITIONS OPEN

SENIOR POSTDOCTORAL RESEARCH ASSOCIATES

Two positions are available for studying NIH funded projects on signaling pathways controlling cholesterol homeostasis and atherosclerosis. A Ph.D. in biological sciences with postdoctoral experience is required. Experience with molecular biology, biochemistry, transgenic, and mammalian cell culture will be advantageous. Applications with contact information of three references should be sent to: **Dr. Kamal D. Mehta** at **e-mail: mehta.80@osu.edu. Telephone: 614-688-8451.**

SYMPOSIA

THE CHARLES RODOLPHE BRUPBACHER FOUNDATION

announces its 7th Scientific Symposium in conjunction with the Charles Rodolphe Brupbacher Cancer Research Award 2005
Advances in Oncology: From Model Systems to the Clinic
March 16–19, 2005
Zurich, Switzerland

Symposium organizers:
Michel Aguet and Josef Jiricny

Speakers: **Alitalo, Kari** (Helsinki, Finland), **Barbacid, Mariano** (Madrid, Spain), **Basler, Konrad** (Zurich, Switzerland), **Beachy, Phil** (Baltimore, Maryland, U.S.A.), **Berns, Anton** (Amsterdam, The Netherlands), **Christofori, Gerhard** (Basel, Switzerland), **Clevers, Hans** (Utrecht, The Netherlands), **Cunha, Gerald** (San Francisco, California, U.S.A.), **DePinho, Ronald** (Boston, Massachusetts, U.S.A.) **Friedl, Peter** (Würzburg, Germany), **Jackson, Stephen** (Cambridge, United Kingdom), **Krek, Wilhelm** (Zurich, Switzerland), **Lane, David** (Dundee, United Kingdom), **Matter, Alex** (Singapore, Asia), **Polyak, Kornelia** (Boston, Massachusetts, U.S.A.), **Radtke, Freddy** (Lausanne, Switzerland), **Rajewsky, Klaus** (Boston, Massachusetts, U.S.A.), **Stamenkovic, Ivan** (Lausanne, Switzerland), **Tuveson, David** (Philadelphia, Pennsylvania, U.S.A.), **Yancopoulos, George** (New York, New York, U.S.A.)

For registration and more information see **website: http://www.brupbacher-stiftung.ch.**

FELLOWSHIPS

RESEARCH FELLOWSHIPS in cell and molecular biology and molecular medicine at the University of Pennsylvania Institute for Environmental Medicine. Programs are available for qualified Ph.D., M.D., *or equivalent U.S. citizens/permanent residents* in an NIH-funded program. Candidates have a choice of 10 established laboratories in several departments. The focus of the research is protein and lipid trafficking, exo/endocytosis, developmental biology, cell membrane receptors, cell signaling, immunotargeting, oxidant injury, lung phospholipids, mechanotransduction, endothelial cell biology, transcription/translational control, gene therapy, and related areas. We provide full benefits and stipend supplementation. **Website: http://www.med.upenn.edu/ifem/pep.htm.**

Applications may be submitted to: **S. Turbitt** via **fax: 215-898-0868** or via **e-mail: turbitt@mail.med.upenn.edu.**

Qualified women and minority candidates are especially encouraged to apply. Affirmative Action/Equal Opportunity Employer.

GRANTS

BRAIN TUMOR RESEARCH GRANTS
One-Year $100,000 Grants
Two-Year $200,000 Grants
Available Nationwide
Application Deadline: March 16, 2005

The Brain Tumor Society (TBTS) is awarding grants to fund basic scientific research directed at finding a cure for brain tumors. Grants are awarded annually at a maximum of $100,000 per year. Grants may be used for startup projects or supplementary funding. Funds cannot be used for indirect costs.

For research guidelines and application visit TBTS's **website: http://www.tbts.org.**

Johnson & Johnson
PHARMACEUTICAL RESEARCH & DEVELOPMENT
DIVISION OF JANSSEN PHARMACEUTICA N.V.

Johnson & Johnson
Pharmaceutical Research & Development announces:

"In memory of Dr Paul Janssen" (1926 - 2003)

4th Symposium on Drug Discovery

April 7-8, 2005, Antwerp, Belgium

Speakers

Keynote Speaker:

Professor Adam Smith Editor, Nature Reviews, Drug Discovery

Plenary Lectures:

Professor Jean-Marie Lehn
Université Louis Pasteur, France

Professor Camille G. Wermuth
President, CSO Prestwick Chemicals, France

Professor Antonello Mai
Università degli Studi di Roma, "La Sapienza", Italy

Dr Duane Burnett
Schering-Plough Research Institute, U.S.A.

Professor Giuseppe Campiani
Università degli Studi di Siena, Italy

Dr Jürg Zimmerman
Novartis, Switserland

Professor Bernard Testa
University Hospital Centre, Switserland

Dr Christopher A. Lipinski
(retired) Pfizer Global R&D, Groton New London Labs U.S.A.

Professor Eddy Arnold
Center for Advanced Biotechnology & Medicine Rutgers State University, U.S.A.

Professor Tom L. Blundell
University of Cambridge, UK

Short Communications:

Dr Paul Lewi
J&JPRD, Belgium

Dr Koen Andries
J&JPRD, Belgium

Dr Mark Macielag
J&JPRD, U.S.A.

Dr Jose Maria Cid
J&JPRD, Spain

Dr Patrick Angibaud
J&JPRD, France

Dr Bruce Maryanoff
J&JPRD, U.S.A.

Registration:
www.jjprddrugdiscoverysymposium.com
Registration deadline: March 1st, 2005

For further information contact:
prdglobal@prdbe.jnj.com
Tel.: +32(0)14.60.33.45

Venue:
Aula Major
University of Antwerp
Universiteitsplein 1
B-2610 Antwerp
Belgium

Call for poster abstracts:
Deadline: March 1st, 2005
Submission on website

There will be Best Poster Awards

Biological Dark Matter

Illuminate the mystery of microRNAs with innovative research solutions

MicroRNAs (miRNAs) are small, highly conserved RNA molecules that act as key regulators of development, cell proliferation, differentiation, and cell cycle. miRNAs have been implicated in oncogenesis and viral infection. Explore this emerging field with a complete portfolio of advanced products specifically designed for miRNA investigation.

miRNA Isolation—collect small RNAs that other kits neglect

- *mir*Vana™ RNA Isolation Kit (for miRNA)
- *mir*Vana™ PARIS™ Kit (for miRNA and protein)

miRNA Expression Profiling—miRNA arrays

- *mir*Vana™ miRNA Probe Set (includes probes to all known human and mouse miRNAs)
- *mir*Vana™ miRNA Labeling Kit (for universal labeling of miRNAs)

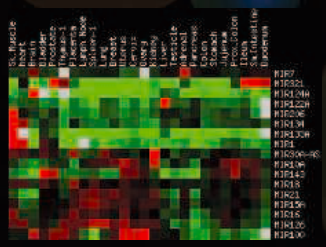

Experiment
Differential expression of miRNAs between normal human tissues.

Functional Analysis—discover regulatory pathways

- Up regulation with Pre-miR™ miRNA Precursor Molecules
- Down regulation with Anti-miR™ miRNA Inhibitors
- Monitor expression with pMIR-REPORT™ miRNA Reporter Vector

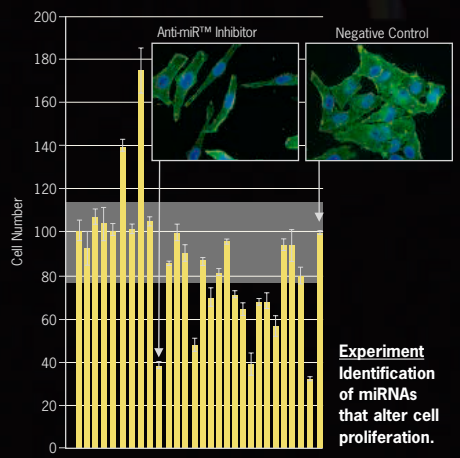

Experiment
Identification of miRNAs that alter cell proliferation.

Uncover the mystery of miRNA function at

www.ambion.com/miRNA

THE COMPLETE miRNA SOLUTION PROVIDER™

Ambion®
THE RNA COMPANY®

Ambion, Inc.
tel +1-512-651-0200 toll free in the U.S. 800-888-8804
fax +1-512-651-0201 toll free in Canada 800-445-1161

Ambion (Europe) Ltd
tel +44 (0) 1480 373 020
fax +44 (0) 1480 373 010

For a list of Ambion direct free phone numbers and distributors in your country, go to www.ambion.com